SYNTHETIC LIPIDS FOR THE STUDY OF MEMBRANE DYNAMICS

JONATHAN ANDREW PURDIE

SYNTHETIC LIPIDS FOR THE STUDY OF MEMBRANE DYNAMICS

A thesis submitted in partial fulfilment of requirements for the degree of Doctor of Philosophy

At the Department of Chemistry, Durham University

Submitted by

Jonathan Andrew Purdie

Under the supervision of

Dr John M. Sanderson

Supported by EPSRC grant EP/J017566/1

2017

Declaration

The work described in this thesis was carried out between October 2013 and January 2017 under the supervision of Dr John Sanderson at Durham University (UK). The content is original work and has not been previously submitted for another degree at any institution. The research was primarily carried out by the author; small pieces of work were performed by undergraduate students with their contributions clearly acknowledged.

Statement of copyright

Abstract

This thesis describes the production of lipids and sterols which can be used as tools to promote or probe membrane asymmetry, both transverse and lateral.

The first section of this work will detail efforts to synthesise the molecular recognition lipids, BAR and TAP lipid for incorporation into liposomes, in order to produce transversely asymmetric vesicles. The synthesis of TAP lipid proceeded as expected, whilst the production of BAR lipid proved challenging. Efforts to produce BAR lipid by conventional means were met with frustration, low conversion was observed due to residual H_2O promoting by-product formation. BAR lipid was resolved chromatographically, but low conversion led to alternative strategies being explored which ultimately proved unsuccessful. An alternative strategy involving a one pot Knoevenagel condensation proved promising on a test substrate, but the aldehyde precursor required for BAR lipid formation was not producible.

Development of a methodology to synthesise dialkyl phosphates and lipids on a solid support is reported. The methodology employs the use of a β-hydroxysulfone linker, which was produced and quantitatively bound to Merrifield resin. The β-hydroxysulfone linker proved successful for the attachment of substrates *via* the phosphate. In practice the use of a β-hydroxythioether linker, with the desired transformations taking place, followed by on resin oxidation to the sulfone in a penultimate step produced the desired linker in a 'safety catch' approach. Development of linker binding, phosphitylation and oxidation through both solid phase and solution phase mimic studies are described. The developed methodology was implemented to synthesise didecyl phosphate in high purity as a proof of concept. The production of this symmetric didecyl phosphate is envisaged to be the first step in producing a solid phase methodology for the production of glycerophospholipids.

Syntheses for the production of heavy oxygen labelled cholesterol, 6-ketocholestanol, 25-hydroxycholesterol, 5α-cholestanol and lanosterol are reported. The

compounds were obtained through two routes using ^{17}O and ^{18}O-water as the enrichment source. Sterols were enriched by the hydration of 3,5-cyclosterols and by one pot enrichment and reduction of ketone precursors. Use of expensive labelled H_2O was minimised, by optimisation of the reaction conditions, with 5 and 10 equivalents for the 3,5-cyclosterol and direct enrichment routes respectively. Enrichments of 28-38% and 79-94% were obtained for enrichment by ^{17}O and ^{18}O respectively, representing > 77% of the maximum theoretical enrichment. Enrichments were verified by both ^{13}C NMR and GC-MS. In most cases GC-MS and NMR data correlated well, the exception being 6-ketocholestanol, wherein a discrepancy was observed with lower enrichments reported by NMR. A unique keto-enol tautomerism leading to exchange of the label through a 3,5-cyclosterol intermediate was observed in $CDCl_3$, diminishing enrichment. This tautomerism was not observed for samples in DCM by GC-MS.

Publication list

Peer reviewed publications produced from this thesis:

- *"Optimised conditions for the synthesis of ^{17}O and ^{18}O labelled cholesterol"*. C. de la Calle Aregui, J. A. Purdie, C. Haslam, R. V. Law and J. M. Sanderson, *Chem. Phys. Lipids*, 2016, **195**. 58-62.
- *"Synthetic approaches to produce ^{17}O and ^{18}O labelled sterols"*. J. A. Purdie, D. Yufit and J. M. Sanderson, *manuscript in preparation.*

Acknowledgements

I would like to start by expressing my gratitude to my supervisor Dr John Sanderson for all of his insights, support and guidance in developing these projects. I am thankful to Dr Elizabeth Grayson for her help and advice in the lab when I first began working in GC216. I am grateful to Prof Andy Whiting for all of his advice and making me feel a part of his group. I thank Dr Jackie Mosely for all of help in resolving my mass spec issues as well as her general advice during group meetings. I would also like to thank Celia de la Calle Arregui and Catherine Haslam for their hard work and contributions to the sterol Chapter. I am appreciative for the assistance of Lei Xia with the HPLC-MS experiments.

I thank the numerous services throughout the department for their support during my studies, especially to the groups of Dr Jackie Mosely, Dr Alan Kenwirght and Dr David Apperley. I would like to especially thank Dr Dmitry Yufit for his patience and eagerness to test the diffraction of even the poorest quality crystals. I am also grateful to Dr Darren Gröcke for his assistance with isotopic water enrichment analysis.

I am thankful to all of the past and presents members of CG214 for being excellent colleagues, supporting me through my PhD and making the experience more enjoyable. Special mention must go to Sergey Arkhipenko, Dr Mona al Batal, Hannah Britt, Yihao ‘Eric’ Du, Dr Enrico La Cascia, David Chisholm, Dr Ludovic Eberlin, Dr Alexander Gehre, Dr Wade Leu, Kate Madden, and of course Alba Pujol Santiago.

I am grateful to the EPSRC for funding this project (EP/J017566/1) and allowing me to carry out a project I have thoroughly enjoyed (for the most part).

I am indebted to my family for all of their patience, understanding and unfaltering support over the course of my studies.

Una menció especial a Alba Pujol Santiago per tot el seu suport a través d'aquests anys, hagués estat molt més difícil sense ella al meu costat.

Abbreviations

Å	Angstrom
∫	Fixed frequency
Δ^n	Unsaturation starting at the nth carbon
25-HC	25-hydroxycholesterol
6-KC	6-ketocholestanol
Ac	Acetyl
AFM	Atomic force microscopy
Aq	Aqueous
ASAP	Atmospheric solids analysis probe
Atm	Atmosphere
ATP	Adenosine triphosphate
BAR	Barbituric acid
Bn	Benzyl
CLC	Cholesterol loaded cyclodextrins
Cp	Cyclopentyl
CryAA	αA-Crystallin
CryAB	αB-crystallin
d	doublet (NMR)
d.e	Diastereomeric excess
Da	Dalton
DCE	Dichloroethane
DCM	Dichloromethane
DHP	3,4-Dihydro-2-pyran
DIB	Droplet interface bilayer
DIBAL	Diisobutylaluminium hydride
DIC	N, N-Diisopropylcarbodiimide
DIPEA	N, N-Diisopropylethylamine
DMAP	4-Dimethylaminopyridine
DMF	Dimethylformamide
DMP	Dess-Martin Periodinane
DMSO	Dimethyl sulfoxide
DNA	Deoxyribonucleic acid
DOPC	1, 2-dioleoyl-sn-glycero-3-phospho-choline
DOPS	1, 2-dioleoyl-sn-glycero-3-phospho-L-serine
DPhPC	1,2-diphytanoyl-sn-glycero-3-phosphocholine
DPPC	1, 2-dipalmitoyl-sn-glycero-3-phosphocholine
DRM	Detergent resistant membrane
DVB	Divinylbenzene
E_{max}	Energy maxima
EPC	Egg phosphatidylcholine
Eq	Equivalent
ESI	Electrospray ionisation
Et	Ethyl

FRET	Förster resonance energy transfer
GC	Gas chromatography
GUV	Giant unilamellar vesicle
HP	High performance
HPαCD	2-Hydroxypropyl-α-cyclodextrin
HR	High resolution
IPA	Isopropanol
IR	Infrared
J	Coupling constant (NMR)
l	Large (IR)
L_α	Fluid phase
L_β	Gel phase
LB	Langmuir-Blodgett
LC	Liquid chromatography
L_d	Liquid disordered phase
L_o	Liquid ordered phase
LR	Low resolution
LS	Langmuir-Schaeffer
LUV	Large unilamellar vesicle
m	Medium (IR); multiplet (NMR)
M.S	Molecular sieves
m/*z*	mass to charge ratio
MβCD	Methyl-β-cyclodextrin
MALDI	Matrix assisted laser desorption ionisation
MLV	Multi-layered vesicle
mCPBA	meta-chloroperbenzoic acid
Me	Methyl
MEK	Methyl ethyl ketone
mp	Melting point
mRNA	Messenger ribonucleic acid
MS	Mass spectrometry
NBD-PE	2-dipalmitoyl-sn-glycero-3-phosphoethanolamine-N-(7-nitro-2-1,3benzoxadiazol-4-yl)
NHS	N-hydroxysuccinimide
NMI	N-methylimidazole
NMR	Nuclear magnetic resonance spectroscopy
PA	Phosphatidyl acid
PC	Phosphatidylcholine
PCC	Pyridinium chlorochromate
PC-TP	Phosphatidylcholine transfer protein
PE	Phosphatidylethanolamine
PEG	Polyethylene glycol
PG	Phosphatidylglycerol
PI	Phosphatidylinositol
PMA	phosphomolybdic acid
POPC	1-palmitoyl-2-oleoyl-sn-glycero-3-phosphocholine

POPS	1-palmitoyl-2-oleoyl-sn-glycero-3-phospho-L-serine
ppb	Parts per billion
ppm	Parts per million
PPTS	Pyridinium p-toluenesulfonate
PS	Phosphatidylserine
PSI	Pounds per square inch
PSt	Polystyrene
Py	Pyridine
PyBOP	benzotriazol-1-yl-oxytripyrrolidinophosphonium hexafluorophosphate
q	Quartet (NMR)
REV	Reverse phase evaporation
R_f	Retention factor
Rh-PE	Glycero-3-phosphoethanolamine-N-(lissamine rhodamine B sulfonyl)
rpm	Revolutions per minute
RSE	Rapid solvent evaporation
s	Small (IR); Singlet (NMR)
SFVS	Sum frequency vibrational spectroscopy
SIMS	Secondary ionisation mass spectrometry
siRNA	Small interfering ribonucleic acid
SLB	Supported lipid bilayer
SM	Sphingomyelin
ssNMR	Solid state nuclear magnetic resonance spectroscopy
SUV	Small unilamellar vesicle
t	Triplet (NMR)
$t_{1/2}$	Half-life of transverse diffusion
TAP	Triaminopyrimidine
TBDMS	tert-Butyldimethylsilyl
TEMPO	(2, 2, 6, 6-tetramethylpiperidin-1-yl) oxidanyl
TFDO	Trifluoromethyl(methyl)dioxirane
TFP	Trifluoropropanone
THF	Tetrahydrofuran
THP	Tetrahydropyran
TIC	Total ion chromatogram
TLC	Thin layer chromatography
T_m	Phase transition temperature.
t_R	Retention time
Ts	Tosyl
w/o	Water in oil
wt	weight
v	volume
VF	Vesicle fusion

Contents

Chapter 1. Production of Transversely Asymmetric Lipid Bilayer Systems

1.1. Structure of membranes

The fluid mosaic model of cell membranes proposed by Singer and Nicholson states that cell membranes typically have three main constituents; phospholipids, sterols and proteins arranged into bilayers as shown in Figure 1.1.[1] Lipids in the proximal and distal monolayers are orientated so that the hydrophilic head groups interact with the cytosolic and extra-cellular aqueous medium respectively. The lipophilic tails will become buried away from the aqueous environments, forming a bilayer. The bilayer components are not static and are 'fluid'; however the scale of the fluidity was not fully appreciated, components are now known to constantly rotate and diffuse, both laterally and transversely.[2] The Singer-Nicholson model was a remarkable step forward in elucidating the organisation of membrane components, however one vital aspect was omitted, asymmetry. Aside from a few examples such as the endoplasmic reticulum,[3] membranes lipids are asymmetrically distributed both within a leaflet (lateral asymmetry) and between leaflets (transverse asymmetry).[4]

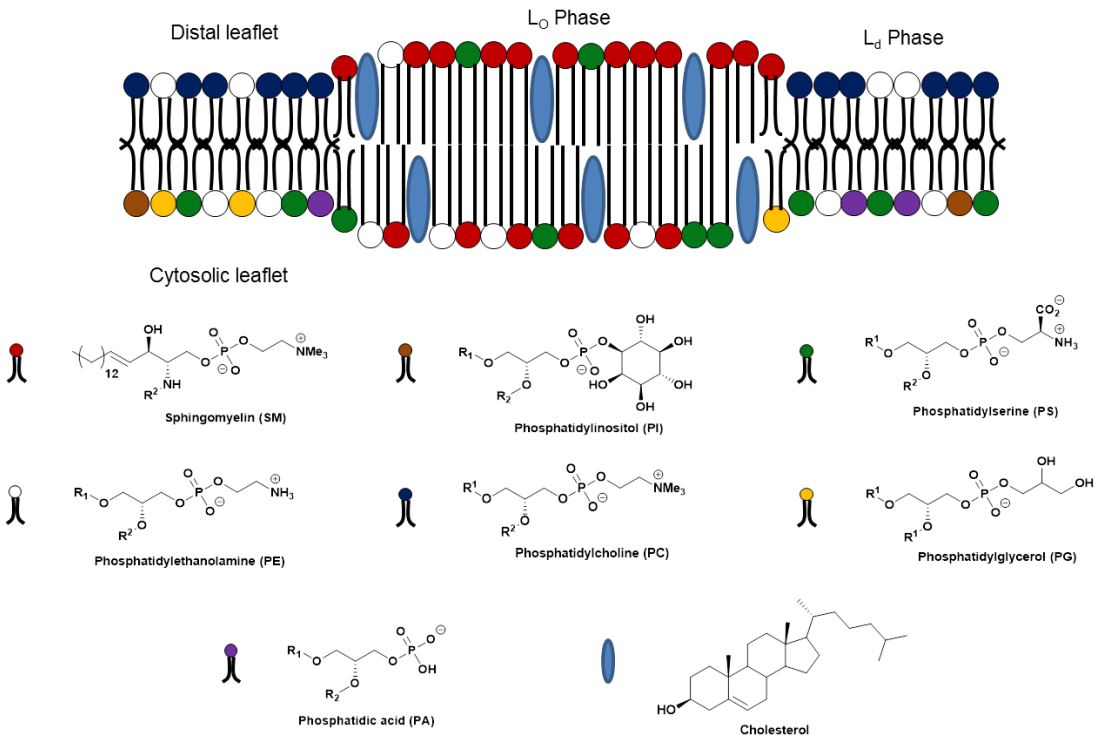

Figure 1.1. Image showing both transverse and lateral asymmetry of phospholipids bilayer within a membrane. PC and SM reside predominately within the extra-cellular leaflet. Whilst PE, PG, PA, PI and PS largely make up the cytosolic leaflet. Proteins are omitted for simplicity. R^1 and R^2 typically represent C_{14}-C_{22} fatty acids that can be saturated, unsaturated or polyunsaturated (up to 6 cis π-bonds).

1.2. Lateral bilayer asymmetry

1.2.1. Origin of lateral asymmetry

Within artificial lipid bilayers, the propensity of certain components to preferentially interact with each other has been observed;[5-7] these associations lead to macroscopic segregation of components or phase separation,[5] resulting in lateral asymmetry. Bilayers composed solely of phospholipids typically exist in two states depending on the main gel to liquid crystalline phase transition temperature (T_m) of the lipids composing the bilayer. When $T_m > T$, the bilayer is in the gel phase (L_β), when $T > T_m$, the bilayer exists in the fluid phase (L_α). The L_α phase is the required state for biological processes to occur and hence is observed under physiological conditions, therefore it is vital that $T_m < 38$ °C. This results in natural bilayers typically containing lipids with one saturated and one unsaturated aliphatic chain.[8]

When artificial bilayers consists of certain sterols (most notably cholesterol), a third intermediate phase is observed, the liquid ordered state (L_o).[9] Bilayer heterogeneity is present within bilayers by L_o regions forming within the bulk liquid disordered (L_d) phase. The L_o phase is witnessed in the presence of certain sterols which associate with rigid saturated chains allowing tighter packing and thickening of the bilayer.[3] Typically, L_o regions consist largely of sphingomyelin (SM), cholesterol and lipid anchored proteins, whilst unsaturated glycerophospholipids and transmembrane proteins mainly remain with the L_d phase.[9] The phases into which certain sterols are known to partition and hence, whether they drive phase separation, are displayed in Figure 1.2.[5,10] The criteria for whether a sterol will drive phase separation is somewhat ambiguous, however a good approximation is presented by Barenholz.[11] Sterols must process a small hydrophilic head group in the *3-C* position, a flat fused ring system, cholesterol like tail, and a small surface area (< 40 $Å^2$ when assembled at the air-surface interface at a surface pressure of 12 mN/ m).

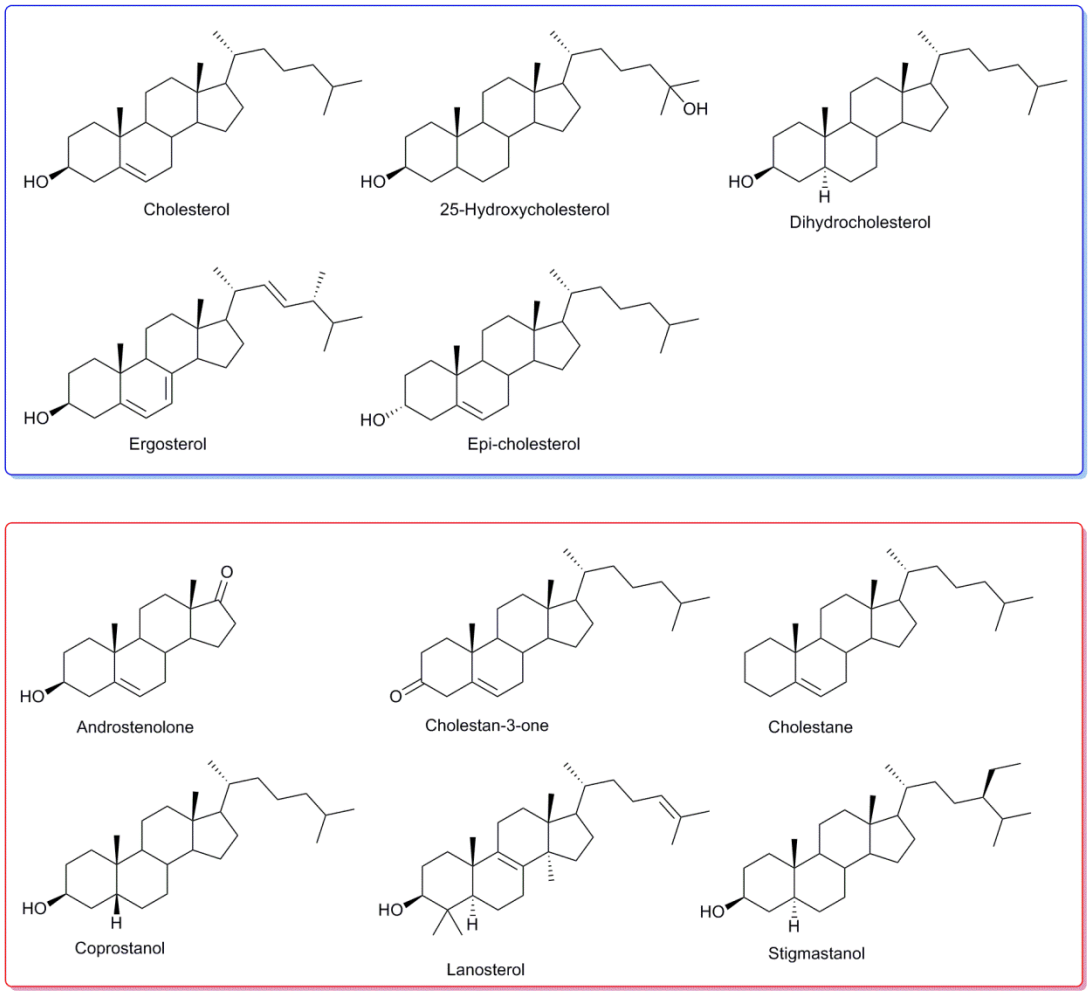

Figure 1.2. Top: sterols that drive phase separation (partition into L_o phase). Bottom: sterols that do not induce phase separation (partition into L_d phase).

The formation of a L_o phase within a bulk L_d phase *in vitro* has led to speculation that analogous structures are present within natural membranes *in vivo*, where the L_o regions are referred to as lipid rafts.[9] The existence of lipid rafts is controversial, in part, due to being poorly defined. It has been postulated that whilst the L_d and L_β phases possesses well-defined parameters with minimal deviation, the L_o phase encompasses much wider variations in structure.[12] The general consensus on lipid rafts is that they are highly dynamic, having the ability to form larger platforms *via* protein-protein and protein-lipid interactions.[13] There is a discrepancy between some of the basic properties of the L_o phase in artificial bilayers and membranes in natural systems. The L_o phase is typically reported in the macroscopic level, hundreds of nanometres long, whilst more conservative values of tens

of nanometres have been reported for lipid rafts.[6] Some authors report values as low as 5-20 nm,[14] putting the size well below the limit of optical resolution; techniques of higher spatial resolution such as atomic force microscopy (AFM) and nuclear magnetic resonance spectroscopy (NMR) are required.[15,16]

1.2.2. Analytical methods to study rafts

Classically, the existence of rafts structures *in vivo* has been demonstrated by isolation of detergent resistant membranes (DRMs), associations of lipids and proteins which remain intact following solubilisation of animal cells by a non-ionic detergent at 4 °C.[17] The structure of the DRM was speculated to correspond to the lipid raft in the cell prior to treatment by detergent.[18] For a more comprehensive description see Lingwood and Simons.[19] The difficulty in observing these rafts *in vivo* has led to debate as to whether these structures only exist *in vitro*. Some argue that rafts are produced by artefacts from the extraction procedure and are not representative of the *in vivo* structures if they even exist at all.[9] This is based on obtaining DRMs from homogeneous lipid mixtures and detergent solubilisation conditions can result in changes to the local lipid composition, causing rafts to break down or even the association of lipids to form DRMs which do not associate *in vivo.*[20] The use of different detergents has shown to give rise to different DRMs; if DRMs are truly representative of lipid rafts formed by spontaneous lateral phase separation, then rafts should be identical regardless of detergent used.[21] Alternative, more convincing methods of measuring lateral domain segregation in model membranes and *in vivo* have emerged including fluorescence microscopy,[22] AFM,[23] NMR[24] and secondary ionisation mass spectrometry (SIMS).[25] Each method, whilst improving upon the DRM approach, has its own unique flaws, addressed in a recent review by Klymchenko.[26] Fluorescence microscopy requires modification of natural lipids, the marker used must be carefully chosen as the addition of bulky fluorophores can alter the phase behaviour of the membrane components.[27] AFM requires that cell extracts be removed and immobilised on a surface, which again may affect inherent properties of the bilayer. NMR techniques are restricted to simple artificial

membrane mimics, due to poor resolution. SIMS and other mass spectrometric techniques require harsh manipulation of the membrane through application of vacuum and freeze drying. The benefits and disadvantages of these techniques are displayed in Figure 1.3.

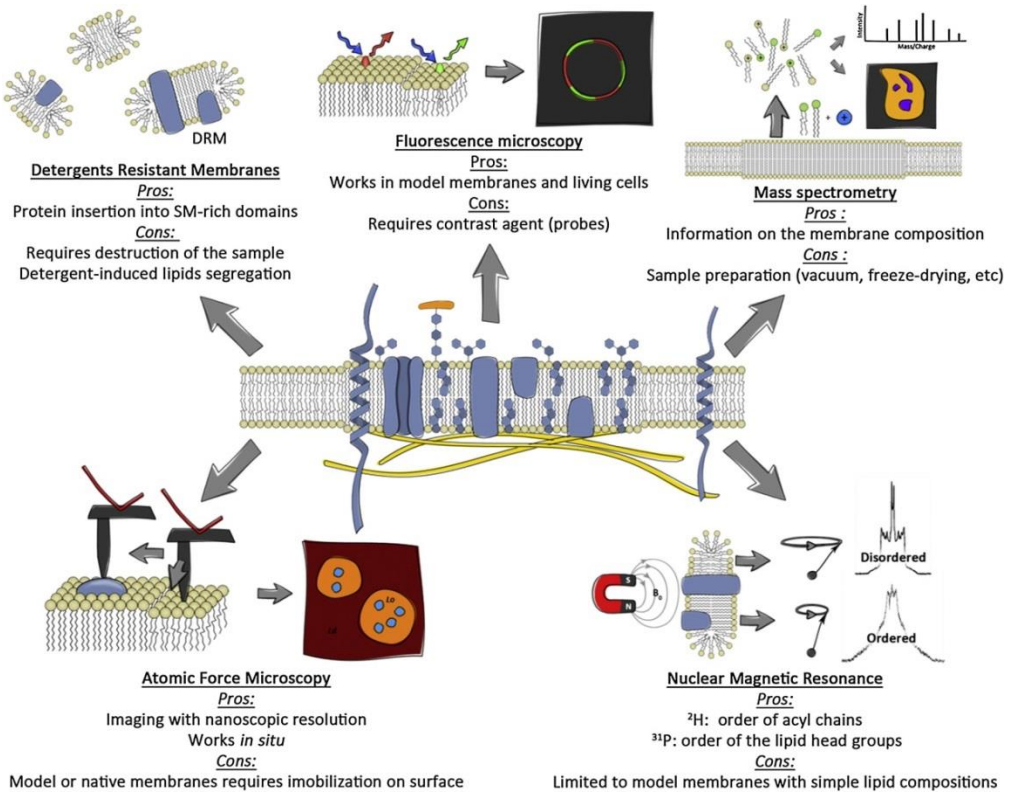

Figure 1.3. Methods of observing later phase segregation in model membrane and *in vivo* along with the advantage and flaws in each technique. Reprinted from Ref. 9, copyright 2014, with permission from Elsevier.

1.3. Transverse bilayer asymmetry

1.3.1. Transverse distribution of bilayer components

Transverse bilayer symmetry is the equilibrium state, where the ratio of lipid components within each leaflet is equal; deviations from this value indicate an asymmetric bilayer. The vast majority of bilayers within nature are asymmetric.[4] The cytosolic (inner) leaflet of cell membranes are rich in anionic phosphatidylserine (PS), phosphatidic acid (PA), phosphatidylgylcerol (PG), phosphatidylinositol (PI) and zwitterionic phosphatidylethanolamine (PE). Larger zwitterionic lipids, sphnigomyelin (SM), phosphatidylcholine (PC) and glycosphingolipids are largely confined to the extra-cellular

(outer) leaflet as seen in Figure 1.1.[28] A salient example is PS which largely occupies the inner leaflet. Appearance of PS on the outer leaflet has been implicated in a number of biological processes including blood coagulation,[3] phagocytosis,[29,30] and inhibition of membrane fusion.[31] PS had also been discovered to play a role in disease states including heart disease, stroke[32] and sickle cell anaemia.[33] An abundance of PS on the outer leaflet of cells infected by various viruses has also been observed, with PS being a potential target of broad spectrum anti-virals.[34]

1.3.2. Monitoring transverse diffusion

Classically, the ability to mimic asymmetry *in vitro* has been a limitation of many methods of bilayer synthesis due to the short lifetime of the asymmetric composition. The lifetime of the asymmetric state is dependent on lipid diffusion across the bilayer known as translocation (or 'flip-flop' colloquially). The rate of translocation determines asymmetry, with fast flip-flop eliminating asymmetry. The rate of flip-flop is defined by the half-life ($t_{1/2}$) of a species to undergo inter-leaflet exchange.[2] In *vivo*, flip-flop occurs both passively and with the aid of enzymes.[35] These enzymes can be broken down into three classes; flippases transport lipids from the outer to inner leaflet, whilst floppases mediate lipid transfer from the inner to outer leaflet, both of these enzymes are ATP dependent and maintain lipid asymmetry.[36] In contrast, ATP independent scramblase catalyses bidirectional translocation of lipids and eliminates bilayer asymmetry.[32]

The rate of translocation in the absence of enzymes is widely disputed owing to a number of parameters that are not standardised when testing flip-flop. It is generally agreed to be slower than lateral diffusion due to the enthalpic cost of the hydrophilic head group diffusing through the hydrophobic core of the bilayer.[37] Some estimates put the rate of flip-flop being up to 10^9 slower than lateral diffusion, with estimates typically in the range of several hours for gylcerophospholipids.[38] Sterols are generally thought of as having faster flip-flop, however the exact values reported for $t_{1/2}$ range from hours down to the ms timescale.[39,40] A number of variables are not standardised between studies including

composition, size (curvature), bilayer type (vesicle *vs.* supported lipid bilayer), temperature and analysis technique which all make comparison of data difficult.[41,42] Different techniques employed include fluorescence quenching,[43] spin label quenching,[44] NMR[45] and sum frequency vibrational spectroscopy (SFVS).[46]

Fluorescence quenching techniques are very limited with bilayers composed solely of natural lipid, requiring bilayer doping by fluorescing or spin labelled analogues. Flip-flop measurements determined *via* these probes are inaccurate; bulky groups slow diffusion through the bilayer.[47] A salient example is comparison of unlabelled DPPC with spin and fluorescently labelled analogues, TEMPO-DPPC (1,2-dipalmitoyl-sn-glycero-3-phosphoethanolamine-n,n-Dimethyl-n-(29,29,69,69-tetramethyl-49-piperidyl)) and NBD-DPPE (7-nitrobenz-2-oxa-1,3-diazol-4-yl phosphatidylethanolamine) respectively. The presence of a bulky spin labelled head group was determined to result in a 27 fold decrease in $t_{1/2}$ from 813 ± 92 minutes at 33.1 ± 0.3 °C to 30.5 ± 0.1 minutes at 32.3 ± 0.1 °C for TEMPO and natural DPPC respectively in supported lipid bilayers (SLBs) composed of DPPC (see Section 1.4).[46] Interestingly, the $t_{1/2}$ of TEMPO-DPPC is double that originally reported by McConnell at a similar temperature (390 minutes, 30 °C),[44] this discrepancy may be due to McConnell reporting this value by monitoring TEMPO-DPPC 'flop' from the inner to outer leaflet by electron paramagnetic resonance in SUVs composed of DPPC. Steric repulsion of the bulky probe in the highly curved SUV inner leaflet may have potentially accelerated $t_{1/2}$.[48] The rate of flip-flop has shown to be in excess of 4200 minutes for fluorescing NBD-PE in DPPC LUVs; however this measurement was taken at a lower temperature of 25 °C.[49] The rate of flip-flop has been shown to follow T_m temperature > above T_m > below T_m,[41] although all measurements were taken below the T_m of DPPC, the measurements at 33 °C are expected to have a lower $t_{1/2}$ than those recorded at 25 °C. This very large discrepancy cannot solely be attributed to temperature and has to be attributed to alteration of the head group. Additionally, fluorescently labelled probes can change fundamental properties of the natural compound changing attributes such as which phase the

compound occupies, affecting the $t_{1/2}$ relative to native lipid.[27] Whilst SFVS can be applied to minimally perturbed deuterated lipids, the experimental set-up is niche and expensive in addition to only being applicable to SLBs. Likewise no alteration of lipids is required for NMR, but the systems are typically simpler due to poor resolution and a shift reagent is required to distinguish between the leaflets. A recent comprehensive review by Sanderson details factors affecting flip-flop and typical rates.[2]

Fluorescence quenching is one of the most popular methods for determining asymmetry due to the use of non-specialist equipment,[50,51] cheaper cost and applicability with free floating vesicles, displayed in Figure 1.4. Asymmetry is determined by loss of labelled lipid fluorescence upon addition of membrane impermeable quencher (*e.g.* sodium hydrosulfite). Addition of surfactant results in vesicle lysing and micelle formation, exposing all fluorophores to the quencher and reducing fluorescence to background levels. The degree of asymmetry was deduced by the relative tagged lipid abundance in each leaflet. Determining the degree of asymmetry by florescence quenching assumes the asymmetric distribution of labelled lipid is representative of their natural analogues. Ideally, asymmetry should be corroborated by additional methods, preferably with minimal or no lipid modification.

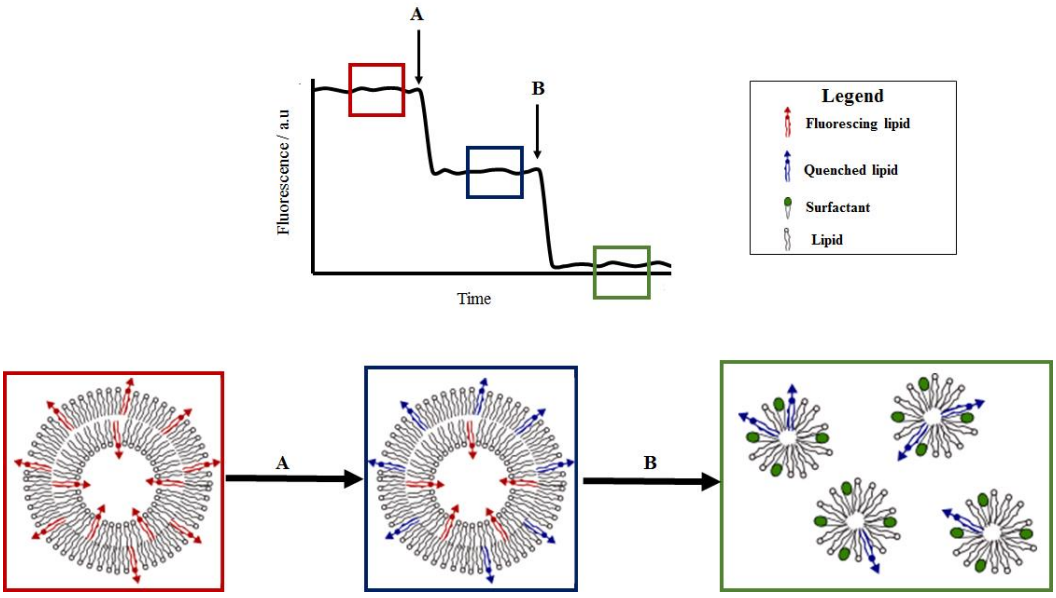

Figure 1.4. A Table showing fluorescence intensity of a liposome doped by a fluorescing lipid (red box) over time. Arrow A indicates the time at which a quencher was introduced into the liposome suspension resulting in outer leaflet fluorescing lipids becoming quenched (blue box). Arrow B shows the point at which surfactant is added leading to formation of micelles and total extinguishing of lipid fluorescence (green box).

1.4. Artificial membrane mimics

Bilayer mimics can be broadly broken down into two types, the first class are lipid SLBs in which the bilayer is adsorbed onto a solid support. The second class are free floating vesicles of which the most common are known as liposomes, liposomes are spontaneously formed vesicles produced when lipids are introduced into an aqueous environment due to entropic factors.[52] The first liposomes were initially large, polydisperse and contained many bilayers (multilamellar vesicles or MLVs),[53] and half a century of investigation has established new liposome production methods, producing several classes of vesicles, varying in size and number of layers (lamellae) as shown in Figure 1.5.[54] The amphiphilic nature of liposomes allows incorporation of a wide range of hydrophilic and hydrophobic guest compounds. *In vivo* applications include encapsulation of DNA,[55] SiRNA,[56] contrasting agents for magnetic resonance imaging[57,58] and various therapeutic compounds.[59,60] Further to these biological roles, liposomes can be exploited as micro

reactors in the synthesis of mRNA,[61] sugars[62] and proteins[63] as well as nano reactors in the synthesis of inorganic nanoparticles.[64,65]

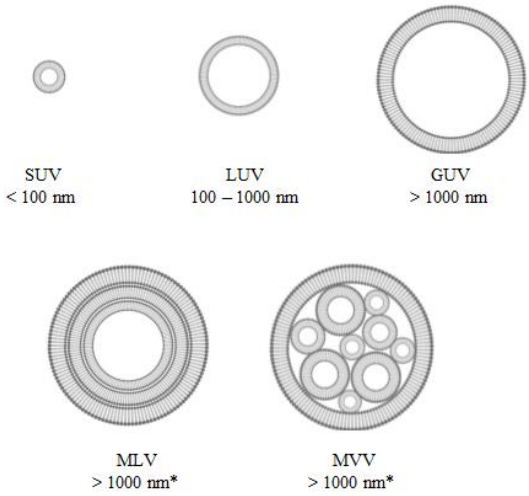

Figure 1.5. Pictorial representation of SUVs (small unilamellar vesicles), LUV (large unilamellar vesicles, GUVs (giant unilamellar vesicles), MLVs (multi lamellar vesicles and MVV (multivesicular vesicles) including their diameter. Sizes given are only typical values for MLV and MVVs, as these structures are defined by structure and not size. Republished with permission of the Royal Society of Chemistry, from Ref. 54, copyright 2013; permission conveyed through Copyright Clearance Center, Inc.

1.5. Classic methods for the production of symmetric lipid bilayers

There are many classic preparations of liposomes, with each technique continually being developed looking to improve on size, monodispersity, protein incorporation and repeatability. The following sections will detail some of the most prominent examples of bilayer synthesis developed. Whilst these methods have been polished since their inception the reader should note a distinct void in the field; the ability to repeatedly produce asymmetric liposomes with well-defined parameters. With few exceptions conventional liposome synthesis can be broken down into four distinct stages;[66]

1. Drying down lipids from organic solvent.
2. Dispersion of the lipid in aqueous solvent.
3. Purification of the liposome mixture.
4. Analysis of the final solution.

The initial step of the majority of liposome preparation techniques is solvation of the lipid components and lipophilic guest to be encapsulated in an organic solvent usually $CHCl_3$. The lipid solution is well mixed and concentrated *in vacuo* producing a thin lipid film, with further drying under high *vacuo* for several hours to remove trace solvent. Residual solvent will impact bilayer properties and is undesirable for liposomes with *in vivo* applications where the leakage of residual solvent is undesirable in the host organism.[67] Aqueous buffer is then introduced to the dried down lipid mixture and the lipids dispersed. Several techniques can be utilised, with the most common being mechanical dispersion (vortexing and gentle agitation both hand and non-hand shaken). These techniques result in MLV formation with little control over lamellarity and size.[68] These parameters can be adjusted to desirable levels by mechanical methods, such as extrusion. Finally the resultant liposomes are examined to confirm the desired lamellarity and size is met prior to being used.[69]

1.5.1. Sonication

Further processing of the obtained MLV can be achieved through sonication, which reduces the size of MLVs by using acoustic energy to break down liposomes into SUVs.[70] Cavitation, where gas bubbles contract and expand in response to an ultrasonic wave is believed to be responsible. Stable cavitation, where bubble oscillations occur without implosion, is capable of applying large shearing forces to phospholipid bilayers reducing their size.[71] Although one of the oldest methods that emerged in the late 1960s[70] sonication is still a popular tool in forming SUVs today.[72,73] Sonication is a high energy process resulting in homogeneous liposome distribution at the lower size limit, typically 5-50 nm. The size of liposomes has been shown to be dependent on the time as well as the frequency and power of ultrasonic radiation.[74,75] Longer irradiation times at lower frequency and higher power produce smaller liposomes. Interestingly the dominant factor determining vesicle size is ultrasound strength with stronger radiation at shorter times yielding smaller vesicles than weak irradiation for a longer time.[74]

There are predominately two types of sonicators, probe tip and bath. Probe sonication is the higher energy approach, in which the tip of a titanium probe is submerged into the solution and applies sonic energy with stirring of the liposome mixture to produce SUVs. Probe sonication has 3 fundamental drawbacks;[66] titanium can come off the tip contaminating the liposome solution which must be filtered (although silica glass probes have been developed to circumvent this issue). The process may leave residual MLVs. Finally the high energy nature of this technique has consequence with respect to degrading both lipid and encapsulated guests.[76] Oxidation of unsaturated lipid is a particular problem which may be reduced by using an inert atmosphere,[69] although this can be challenging to achieve.

Bath sonication involves placing a vessel containing the lipid mixture into a water bath which supplied with sonic energy. Bath sonication is a far milder method than probe sonication (at least a 100 times less ultrasonic power),[77] reducing lipid degradation, allowing an inert atmosphere and eliminating contamination by titanium particles. However bath sonication produces less consistent crops of liposomes, due to the increased variables which must be controlled such as sample position in the water bath, depth of water, number of samples in the bath and any contaminants in the bath.[78]

1.5.2. Extrusion through a membrane filter

Extrusion is an alternative method for processing MLVs, producing liposomes typically in the LUV range of hundreds of nanometres. Larger MLVs prepared by conventional methods are reduced in size by pressing the liposomes through a polycarbonate membrane under pressure several times to give a more homogeneous distribution of unilamellar vesicles of approximately the diameter of the filter pores.[79] For high T_m lipids such as DPPC, the solution must be kept above this temperature by utilising a water bath to prevent gel phase lipid blocking the instrument.[69] Surprisingly, whilst extrusion produces vesicles averaging just below the size of the pore, a small proportion of liposomes may be larger than the filter utilised. This is due to liposomes slightly larger than the pore being able

to squeeze through the membrane without breaking if the liposome is comprised of less rigid lipids.[80] This was demonstrated using liposomes comprised of detergent and lipid passing through filters of up to half the size of the liposome. Such experiments have been used as mimics to explain why large dermatologically applied liposomes can pass through pores in the skin of much smaller diameter, although this mechanism of action is contested.[81]

Since the development of the technique by Papahadjopoulos *et al*.,[82] extrusion has become widespread and is one of the major routes to preparing LUVs today.[83,84] The adoption of this method by the wider community is largely due to the ease and speed of preparation making bulk preparation of liposomes feasible with no residual solvent.[79] Another great strength of extrusion is repeatability of liposome size obtained, increasing confidence in comparing different liposome formulations.[85] Although extrusion appears an enticing method of generating liposomes some problems persist, namely that extrusion is a time intensive manual technique. LUVs produced by this method typically have low encapsulation efficiency.[86] Whilst these problems may be overlooked, potential loss of asymmetry upon extrusion due to the lysis and reannealing of liposomes being forced through the membrane filter and leakage of encapsulated guests remove this technique from contention in preparing asymmetric liposomes.[87]

1.5.3. Rapid Solvent exchange

Buboltz and Feigenson claim conventional methods of producing liposomes may result in formation of vesicles with a different concentration of components than anticipated due to solid state demixing of cholesterol monohydrate at high cholesterol concentrations.[88] In response to demixing, rapid solvent exchange (RSE) was developed in which the lipid mixture is precipitated into the aqueous buffer directly from the organic solution, bypassing the need for a lipid film. Cholesterol demixing was shown to increase heterogeneity of the final hydrated liposomes.[89] The typical RSE setup utilised by Buboltz and Feigenson is displayed in Figure 1.6. In short, the lipid mixture in an organic solvent is injected into a manifold containing an aqueous buffer fitted with a vortexer. The manifold is under negative

pressure (23 mmHg at room temperature) causing evaporation of organic solvent, producing liposomes in the remaining aqueous buffer. There will be presumably some loss of water, making the liposome concentration greater than anticipated.

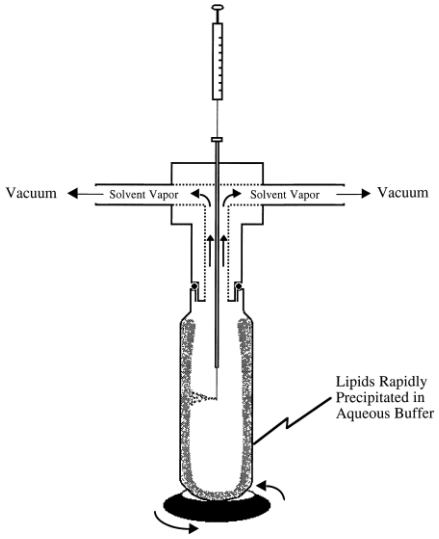

Figure 1.6. The cross section of the Buboltz and Feigenson RSE apparatus, image republished from ref. 88 and used with permission from Elsvier.

This methodology presents improvements over conventional methods such as the rapid removal of bulk and residual solvent (dichloromethane (DCM) and $CHCl_3$). Low boiling DCM is not commonly used to solvate lipids. Perhaps the time required for removal of residual MeOH may have been a more pertinent experiment as MeOH is a more common lipid co-solvent. The rapid preparation time is a vast improvement over methods requiring an intermediate solid state which is vacuum dried for hours. This significantly reduces the preparation time resulting in the ability to quickly produce liposomes, improving throughput. This resulted in a moderate adoption of this technique especially where preparation of liposomes with high levels of cholesterol is required.[90-92] Specialist equipment and long demixing times in low cholesterol concentration formulations have limited the wide spread use of RSE. Buboltz has since produced an improved device, further improving the methodology in an effort to cultivate more interest in the technique. Improvements include adding a biphasic, premixed organic and aqueous mixture directly to the vessel (opposed to organic phase injection) and use of an inert gas to drive residual solvent removal. These

adaptations have streamlined liposome preparation times by a factor of 2, although the total timeframe of liposome preparation is not quantified.[93]

1.5.4. Ethanol and ether injection

EtOH injection to form SUVs directly with high homogeneity and without the need for additional purification steps has been developed.[94] This method consists of lipid dissolved in EtOH being rapidly injected directly into the aqueous phase under an inert atmosphere. The solution is then concentrated by passing the solution through an ultrafiltration device with rapid stirring. The evident major drawback is retention of EtOH in the bilayer which can be difficult to remove due to EtOH forming an azeotrope with water.[66] EtOH can interfere with both hydrogen bonding between hydrophilic head groups and the aqueous medium and disrupt Van der Waal forces between acyl chains. Consequences of EtOH in the bilayer include an increased area per phospholipid in 1,2-dioleoyl-*sn*-glycero-3-phosphocholine (DOPC) and DPPC systems and a reduction in the bilayer thickness by forming an interdigitated phase, resulting in higher bilayer permeability to small molecules.[95] Additionally, L_o domains have also shown to be reduced in size by EtOH in bilayer systems.[96]

The strengths of the EtOH injection technique are that it is cheap, easy to use and rapid, resulting in a very low cost to scale up. Liposomes at 3 L scale have been reported in the range of 89-118 nm with a low polydispersity.[97] Near quantitative encapsulation efficiencies of lipophilic drugs such as α-tocopherol has been reported,[98] however much lower encapsulation efficiency of hydrophilic guests by passive loading owing to large solvent: lipid ratio is an issue, although guest containing aqueous solution can be collected and re-used. Active loading techniques can increase the encapsulation efficiency, exemplified by loading of anti-tuberculosis drug Kanamycin into soybean PC/ cholesterol liposomes. At lab scale, encapsulation efficiencies of 1% were achieved for passive loading *vs.* 63% for active loading. A value of 100% using active loading was also reported,[99]

however this required sacrificing the desired vesicle size with LUVs produced being 458 nm making *in vivo* delivery problematic.

An alternative method for producing LUVs utilises Et_2O as the organic solvent which is injected into the aqueous phase heated above the boiling point of Et_2O.[100] The method could also be used *in vacuo* at lower temperatures enabling encapsulation of heat sensitive compounds such as proteins. Ether has a tendency to form peroxides on storage, therefore the solvent must be tested regularly as unsaturated lipids may oxidatively degrade. Another drawback to solvent injection is the limited solubility of typical membrane components such as cholesterol and PE in EtOH and Et_2O.[101] Finally, repeatability of preparation gaining the same size of liposomes between experiments was not as reliable as other methods such as extrusion, reducing confidence in comparison of different lipid compositions.

1.5.5. Reverse Phase Evaporation

Reverse phase evaporation (REV) is a technique in which lipid mixtures are dried down onto a vessel wall and rehydrated in a biphasic mixture of organic solvent (usually Et_2O) and an aqueous buffer.[102] The solution is sonicated to produce a suspension that is stable for > 30 minutes. The solvent is removed *in vacuo* with additional buffer added to form the liposome. The preparation is then purified by dialysis, column, centrifugation or extrusion. LUVs within the range 200-1000 nm are typically formed; the exact size depends on lipid composition and solvent. REV was originally developed to address the poor encapsulation efficiencies of the sonication and EtOH injection techniques. Encapsulation efficiencies as high as 67% for Gemcitabine has been reported using REV.[103] This value was obtained for vesicles larger than 1000 nm, which is much larger that required for *in vivo* applications. Vesicles around 100 nm are generally preferred as larger vesicles are more rapidly cleared *in vivo*.[104] A follow up study similarly found 54% encapsulation efficiency for Gemcitabine in a 1000 nm liposome, once reduced to a size closer to that required for drug delivery (200 nm) the encapsulation efficiency dropped tenfold to 5%.[105]

A recent modification of this process to generate asymmetric vesicles was proposed by Mokhtarieh *et al* in which lipids constituting the inner and outer leaflet form micelles in solvent separately as shown in Figure 1.7.[106] Upon combination of the micelle solutions an asymmetric vesicle is produced, this method will only work with certain components. In this case the aqueous pool contains polyaninonic siRNA which will electrostatically interact with a cationic lipid, resulting in a higher proportion of this lipid in the inner leaflet. Asymmetry was not quantitatively proven and was only inferred from the high encapsulation (95%) of negatively charged siRNA using cationic inner leaflet composition. Even if a high degree of asymmetry is demonstrated, this methodology is not widely applicable to a range of liposome compositions and is limited to very niche combinations of lipids and encapsulated guests with a high affinity for each other.

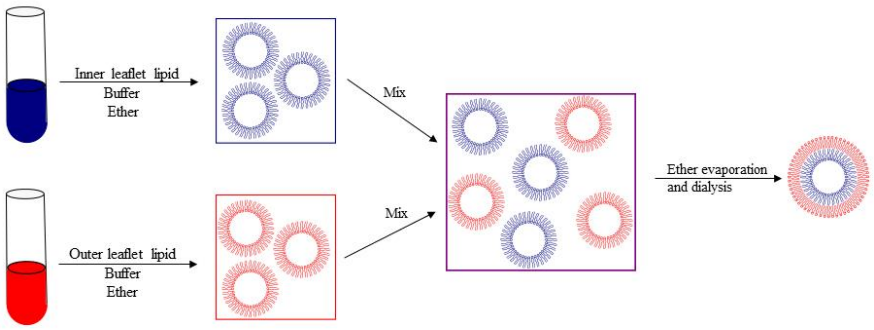

Figure 1.7. REV method to producing asymmetric liposomes. Separate inverse micelles composed of the inner and outer leaflet lipid are prepared in a biphasic mixture containing buffer and ether. The two mixtures were combined and concentrated, producing asymmetric liposomes which are purified by dialysis to remove residual unencapsulated guests.[106]

1.5.6. Electroformation

Electroformation is the most popular method for the production of GUVs,[107-109] entailing the production of lipid films on parallel platinum electrodes, a very small amount must be applied as unilamellar structures only form when the initial dried down film is 5-10 bilayer thick. The deposition is followed by rehydration in the presence of an electric field in the original protocol.[110] Initially direct current below 3 V was implemented although alternating current has since become more popular due to direct current causing electrolysis

of the water generating hydroxide anion leading to lysolipid formation.[111] Other popular modifications include obtaining the lipid deposit by drying down conventionally prepared SUVs onto the electrode as well as preparing the dried film on glass slides coated in conducting indium tin oxide.[112,113] Another improvement of the original electroformation technique avoids demixing in the solid state by coupling electroformation to the RSE technique, thereby bypassing drying of the lipid film.[114] The coupling of RSE and electroformation results in more homogeneous distributions of lipids between vesicles.

The process of electroformation can be broken into three stages;[112] the initial step is an increase in the field amplitude to the maximum value (E_{max}) at a fixed frequency (ʃ). The second step is the swelling process in which E_{max} and ʃ are kept constant to produce larger GUVs (this process may be omitted if E_{max} is reached quickly and GUVs of < 5 μm are desired). The final rebound stage is the reduction of ʃ to promote vesicle closing and electrode detachment.

Electroformation is the preferred choice in the production of GUVs due to the process speed and low number of defects compared to other methods such as gentle film hydration.[112] This is exemplified by Cribier *et al*,[115] who demonstrated that DOPC vesicles formed by electroformation took 15 hours and had 80% of the population free of defects whilst the population generated by the gentle hydration method took 24 hours and could only boast 40% free of defects. Low polydispersity of electroformed vesicles is another positive which can be achieved by patterning; polydimethylsiloxane is used to stamp a lipid layer onto the indium tin oxide slide. Liposomes of similar size grow on each patch which contact and coalesce, forming GUVs of a relatively monodisperse population.[116] Greater control of vesicle size was recently shown by Han *et al*,[117] who pioneered the use of an interdigitated co-planar electrode (opposed to parallel electrodes) increasing the number of controllable parameters and hence allowing great control of the final GUV produced. A range of frequencies and amplitudes were examined, larger vesicles can be generated at 5-8

V and 10^0-10^2 Hz whilst smaller vesicles are generated in 10^0-10^3 Hz at 1 V. Changes in amplitude bear a larger impact than frequency on GUV size.

In spite of these advantages it should be noted that vesicles only form by electroformation when $T > T_m$, or in low salt concentration buffer.[108] These factors may limit electroformation of protein containing liposomes (proteasomes), as a high salt buffer concentration is required to solubilise some proteins and higher temperature may denature the protein. Adaptations to the original method have resulted in the ability to generate GUVs under buffer conditions with an ionic strength mimicking that found *in vivo*. Alterations to the method include increasing the frequency used,[107,118] forming GUVs under low ionic strength and replacing the solution with a high salt concentration in a flow chamber.[119] An additional problem of electroformation is limitation of the amount of negatively charged lipid that can be incorporated into the vesicle. It was found that incorporation of 10 wt% 1,2-dioleoyl-*sn*-glycero-3-phospho-L-serine (DOPS) into DOPC vesicles resulted in a 10% increase in the number of defective liposomes found whilst 20% DOPS inhibited the formation of GUVs by electroformation completely.[115]

1.6. Methods for the production of asymmetric lipid bilayers

1.6.1. Synthesis of supported lipid bilayers

Supported lipid bilayers are distinct amongst conventional bilayer synthetic routes; they are the oldest, most reliable and widely utilised methodology for producing asymmetric bilayers.

1.6.1.1. Planar lipid bilayers

Painted or black lipid films are produced when two different lipid in oil solutions are ‘painted’ across an aperture in a hydrophobic surface, annealing and forming a bilayer.[120] However residual solvent perturbed membrane properties, such as low electrical capacity, and hampered the success of membrane protein reconstitution. Adaptation of this early technology, shown in Figure 1.8, utilises a volatile hydrophobic solvent which evaporates

prior to bilayer formation, significantly reducing solvent in the bilayer.[121] High encapsulation efficiency occurs due to low ratio of aqueous solution: organic solvent. The need for solvent during bilayer formation could be eliminated by doping preformed SUVs into the aqueous chambers, which subsequently form a monolayer. Different compositions of lipids within each population of SUVs results in asymmetric bilayer formation.[122]

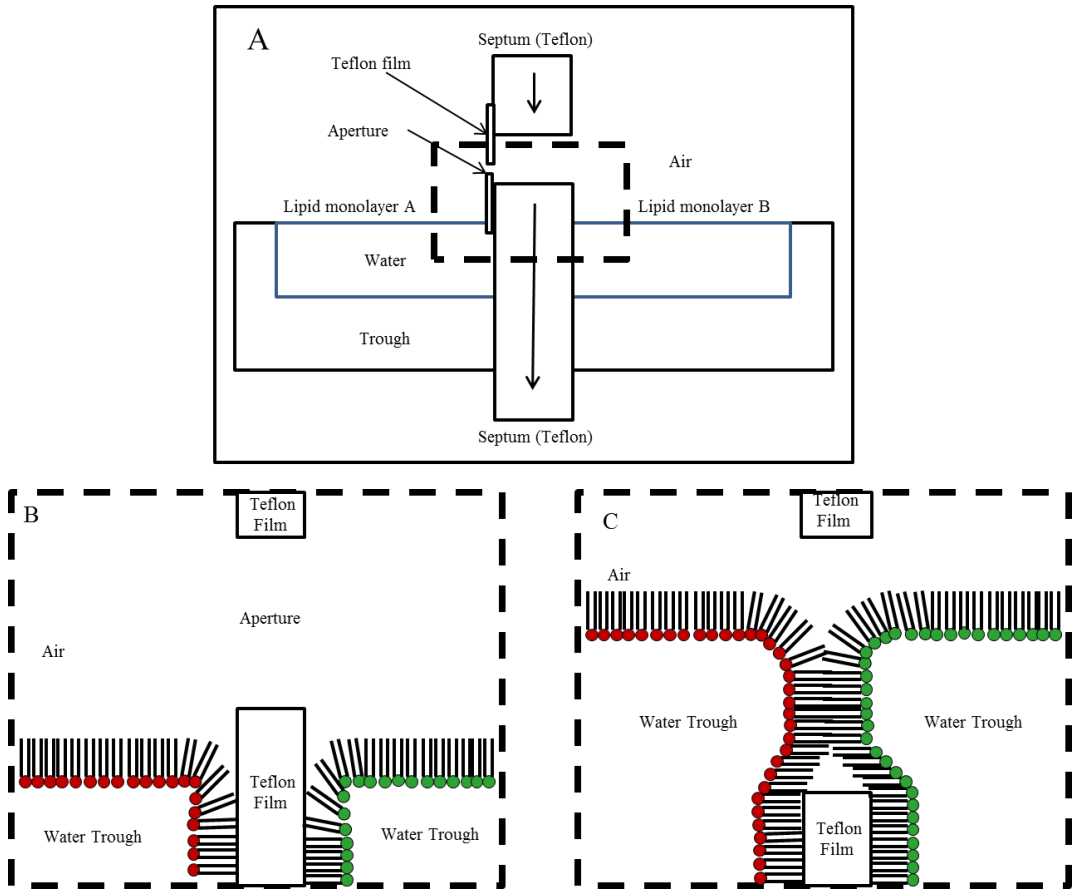

Figure 1.8. Visualisation of the Montal-Mueller apparatus. a) The experimental set up of the Montal-Mueller asymmetric vesicle formation. b) A closer look at bilayer formation. When the aperture is lowered below the water level the two monolayers at the surface of each trough contact in the hydrophobic Teflon cavity forming a bilayer. The red and green circles represent different lipids showing the formation of an asymmetric bilayer.[121]

1.6.1.2. Langmuir-Schaeffer and Langmuir-Blodgett SLBs

The Langmuir-Blodgett (LB) trough originally developed to allow deposition of fatty acid salt layers onto a glass substrate[123] was modified by Tamm and McConnell.[124] They deposited lipid bilayers onto hydrophilic substrates, including silicon, glass or quartz although gold,[125] mica[126] and even mercury[127] are suitable substrates. This was achieved

using a mixture of Langmuir-Blodgett and Langmuir-Schaeffer (LS) film formation in which a Langmuir trough was filled with a lipid mixture in water, with the lipid forming a monolayer at the water-air interface. Immersion and removal of a hydrophilic substrate from the trough results in formation of a monolayer on the substrate surface (LB deposition). Reduction of the trough surface area, followed by a second immersion of the monolayer bound substrate in the horizontal direction formed a bilayer (LS deposition). Whilst Tam and McConnell formed symmetric bilayers, asymmetric bilayers could be formed by changing the lipid monolayer at the air-water interface prior to the second immersion of the substrate.

1.6.1.3. Vesicle Fusion

The rupture of vesicles on to a solid support has been exploited to form lipid bilayers for over 30 years.[128] It is intuitive that rupture of symmetric vesicles will form a symmetric supported lipid bilayer; however asymmetric bilayers are also attainable by rupture of symmetric vesicles, albeit only with certain lipids and substrates. Asymmetric bilayers can form when using negatively charged lipids (PS) on silica with PS being deficient in the inner leaflet due to electrostatic repulsions of the support and anionic lipid.[129] Divalent cations can coordinate with the negatively charged lipid and support, increasing the quantity of anionic lipids in the proximal leaflet. Brisson reported using PS on mica in the presence of Ca^{2+} to form asymmetric bilayers;[130] however the degree of asymmetry was not quantified. Fusion of symmetric vesicles is not a suitable method to produce asymmetric SLBs, due to restriction of available lipids and supports, in addition to a lack of compositional control. Hybrid techniques combining LB deposition followed by vesicle fusion (VF) to produce an asymmetric SLB could be used to produce asymmetric vesicles.[125] This hybrid approach has been utilised in the production of SLBs which contain a linker between the proximal leaflet and support (tethered SLBs).[131]

1.6.1.4. Tethered supported bilayers

The solid support has been shown to have some degree of interaction with the proximal leaflet, reducing the rate of lateral diffusion and translocation of components.[132] Additionally, the small distance between the proximal leaflet and support is insufficient to allow peptides to fold into the right conformation for membrane insertion.[133] In order to use SLBs as cell mimics this issue must be circumvented. Tethered supported bilayers have come into fashion, granting a larger aqueous pool between the proximal leaflet and support enabling reconstitution of transmembrane proteins into the model cell bilayers. Tamm and Wagner proposed that such a tether should possess several qualities;[132] the linker must be hydrophilic and covalently bound at either terminus to the support and proximal leaflet of the bilayer. The linker must also be both chemically and physically inert with typical membrane components (aside from the binding site). Suitable linkers include proteins,[134] peptides,[135] polymers[132,133] and small molecules.[136]

Tethered SLBs are prepared by covalently binding a surface moiety to a reactive site on the linker. Common strategies include hydrosilylation between silicon wafer Si-H moieties and linker terminal alkynes[137] or addition of thiol spacers to gold substrates.[136] The linker usually terminates in an acid group which is converted to a succinimide ester. Lipids containing an amine functionality, such as PE, are then coupled to the spacer by amide bond formation. The distal leaflet is then able to be added by conventional methods such as VF, Figure 1.9 presents an example using mercaptoundecanoic acid linker and a gold substrate. A drawback of tethered SLBs is low coverage within the membrane, generating inhomogeneity during spontaneous bilayer self-assembly; μ-contact printing can be applied to promote a more homogeneous bilayer.[137,138]

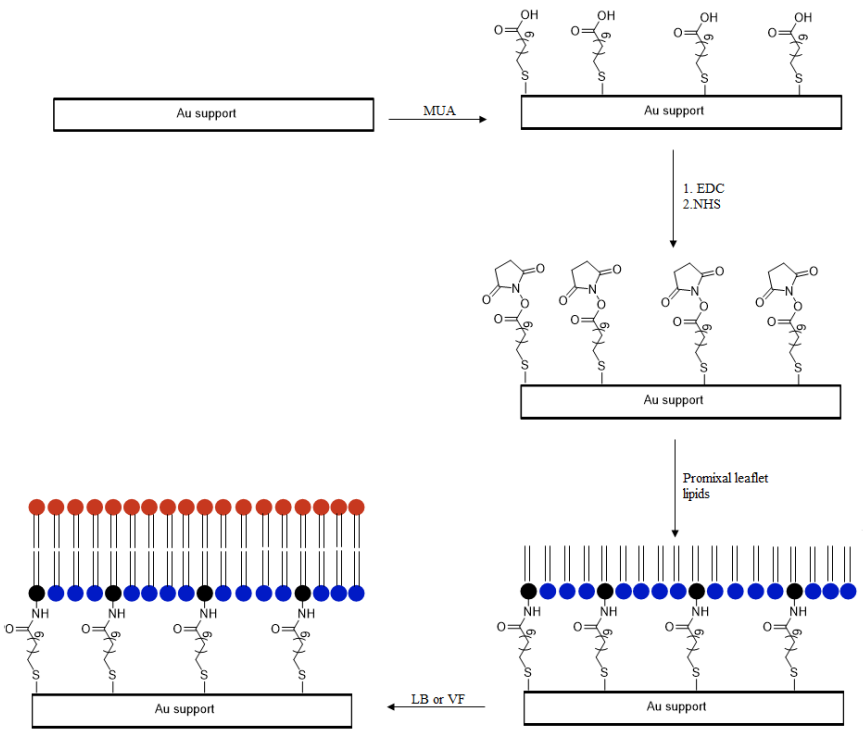

Figure 1.9. The preparation of a tethered asymmetric SLB on a gold support. Black lipid possesses an amine functionality capable of reacting with the succinimide ester (such as PE lipid). Blue lipid represents other lipids comprising the proximal leaflet. Red lipid represents lipid comprising the distal leaflet. MUA = mercaptoundecanoic acid.

1.6.2. Inverted emulsion technique

Weitz exploited phase exchange within a three phase system to produce asymmetric vesicles as seen in Figure 1.10.[139] The uppermost emulsion phase consisted of lipid stabilised water in oil (w/o) droplets; this lipid constituted the inner leaflet of the final asymmetric liposome. The size of the emulsion can be controlled by conventional methods, with extrusion proving the most popular.[51,140] The intermediate oil phase acts as a buffer sitting above the aqueous phase. A second compositionally distinct monolayer forms at the intermediate-aqueous phase interface. Sedimentation of the lipid stabilised w/o droplets through this lipid monolayer forms asymmetric vesicles.[141]

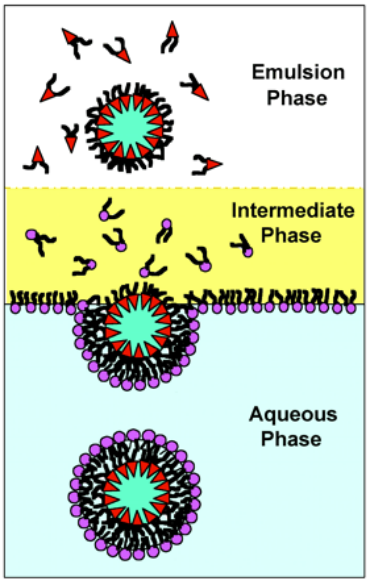

Figure 1.10. The Weitz method exploiting a three phase system to form asymmetric vesicles. Figure reproduced from Ref. 139, copyright 2003, National Academy of Sciences.

The preparation of liposomes displaying over 95% asymmetry, with POPC (1-palmitoyl-2-oleoyl-sn-glycero-3-phosphocholine) in the outer and POPS (1-palmitoyl-2-oleoyl-sn-glycero-3-phospho-L-serine) in the inner leaflet respectively (POPCo/POPSi) has been demonstrated.[139] Reversal of lipid composition, forming sterically unfavourable POPSo/POPCi, produced vesicles of 80% asymmetry which were stabile > 24 hours, indicating flip-flop was not prevalent over this time frame.[139] Asymmetry was determined by fluorescence quenching of 0.5% fluorescently labelled-lipid incorporated into the outer leaflet during vesicle synthesis. In addition to high asymmetry, encapsulation efficiencies of 91, 95 and 98% for fluorescein, 10 kDa dextran[43] and actin[51] respectively were recorded. High efficiency was expected as the initial w/o droplet was directly converted to the aqueous core of the final liposome. Whilst this is the expected outcome, the encapsulation efficiency can also be remarkably lower with reports of 14-18% encapsulation of AlexaFluor 350.[140] Low encapsulation was attributed to emulsion droplet breakage at the intermediate-water interface, or by spontaneous budding of lipid and bilayer formation at the aqueous-intermediate interface.[140] An additional positive aspect of the technique is the use of non-specialist equipment; most laboratories within the field have access to a centrifuge and extruder kit.

Several limitations of the technique are noted by Weitz,[51] primarily difficulty in controlling the size of the w/o droplet and hence final liposomes. The droplet size can be tailored by extrusion; however the unstable w/o emulsions require immediate use. Undesired liposomes form spontaneously and cannot be separated,[140] bimodal and trimodal vesicle populations were reported with recovery of more liposomes than initial emulsion particles used. Insufficient coverage of lipids at the intermediate-aqueous interface results in larger droplets breaking during sedimentation, resulting in no bilayer formation. The interface monolayer is slow to reform due to lipid diffusion in oil taking up to 90 minutes for zwitterionic species. Optimum conditions ensuring full coverage were found to be 2-3 hours since a longer equilibration period resulted in multilamellar structures forming at the interface.[139] Re-equilibration of the interface monolayer between batches requires 2 hours; this process is uneconomical and unsuitable for high throughput. Additionally not all proteins and lipids can tolerate high levels of oil, either denaturing or having poor solubility.[142] Oil trapped in the bilayer perturbing membrane properties was an initial concern, however GUVs formed by the inverted emulsion and electroformation techniques demonstrate similar properties such as bending rigidities.[143]

1.6.3. Microfluidic approaches to the inverted emulsion technique

The inverted emulsion approach can be applied to a microfluidic set up, producing asymmetric GUVs with increased throughput, greater reproducibility and bilayer formation efficiency.[144] The general concept is presented in Figure 1.11 and is analogous to painted bilayer formation.

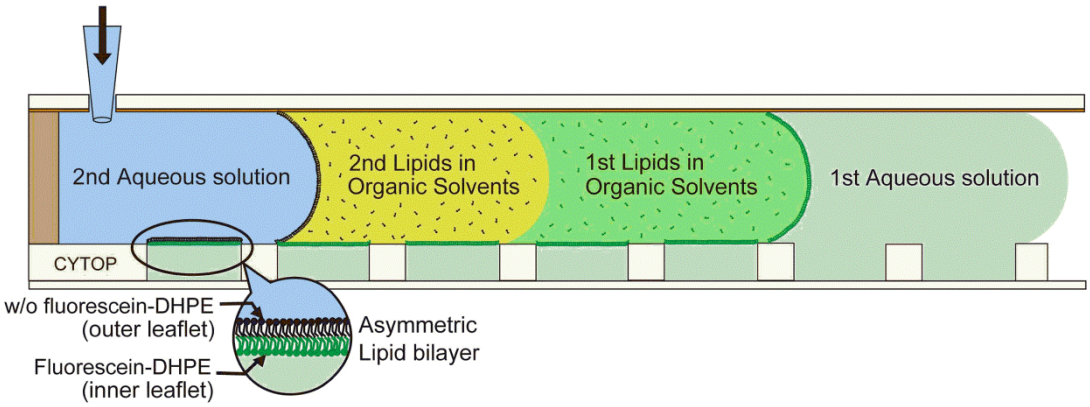

Figure 1.11. Microfluidic approach adopted by Noji, figure reprinted from Ref 144. The first aqueous (aq.) solution is introduced *via* the solvent inlet filling hydrophilic wells in the channel with aqueous solution. The first (green) lipid in organic solvent is passed through the channel forming monolayers in the channel; a second (black) lipid in solvent is passed through the channel producing an asymmetric bilayer which anneals upon a final aqueous wash through the column.

Initially an aqueous wash hydrates the hydrophilic wells; subsequent injection of lipid in solvent forms a monolayer at these surfaces. The lipid used at this stage will form the inner leaflet of the final bilayer. Injection of a different lipid in solvent through the channel followed by a final aqueous solution anneals the asymmetric bilayer and washes away excess solvent. Lipid used in the second solvent injection will form the outer leaflet of the bilayer. Further washes of lipid in oil and water can form asymmetric multilamellar structures, dubbed the layer by layer approach.[43] The batch inverted emulsion technique was performed with highly hydrophobic oil, whereas $CHCl_3$[144] and octanol[145] have been utilised in the microfluidic approach. Greater water miscibility of these solvents results in solvent being less likely to reside within in the final bilayer.

1.6.4. Cyclodextrin catalysed synthesis of asymmetric vesicles

Methyl-β-cyclodextrin (MβCD) has long been known to mediate cholesterol transfer both into and out of lipid bilayers.[146] Within the past decade, the effect of MβCD on lipid composition has been addressed with higher concentrations of MβCD having being shown to solubilise membranes.[147]

The observation that large concentrations of cyclodextrins (CDs) solubilise bilayers and bind gylcerophospholipids has been exploited to produce asymmetric SUVs,[148] LUVs,[149] GUVs,[150] in addition to asymmetric SLBs.[151] The initial production method consists of mixing 'donor' MLVs and MβCD forming MβCD saturated with lipid.[149,150] The MLV-MβCD mixture is added to 'acceptor' symmetric vesicles (containing 25% sucrose) or SLBs. The final bilayer exhibited asymmetry; the inner leaflet consisted of lipid from the acceptor bilayer (vesicle or SLB), whilst the outer leaflet was predominately composed of lipids from the donor vesicle (Figure 1.12). The exchanged vesicles were then separated using a Sepharose column or by centrifugation utilising a sucrose gradient. In the case of SLBs the remaining MLV-MβCD mix was washed.

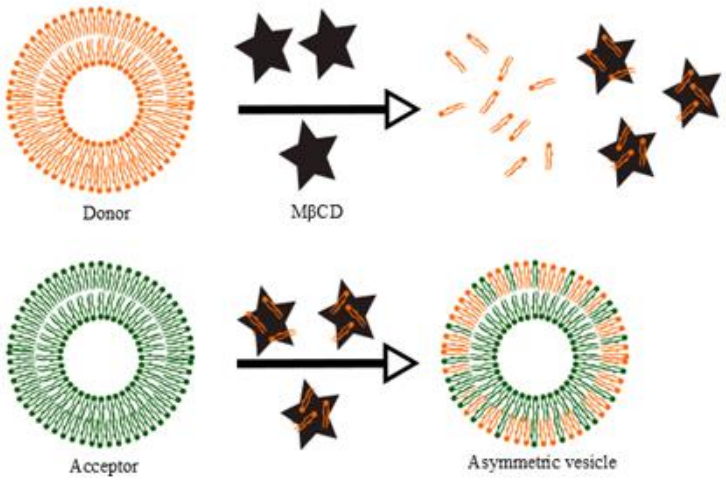

Figure 1.12. MβCD catalysed asymmetric vesicle synthesis. The donor vesicle is solubilised by MβCD which is added to the acceptor vesicle and incubated to produce an asymmetric vesicle.

High levels of lipid (SM) exchange into the outer leaflet of donor PC vesicles was achieved (62-96%), confirmed by a combination of high performance thin layer chromatography (HP-TLC) and 1-(4-trimethylammoniumphenyl)-6-phenyl-1,3,5-hexatriene p-toluenesulfonate (TMADPH) probe anisotropy.[152] Lower concentrations of cholesterol loaded cyclodextrins (CLCs) can be applied in a second step, adding cholesterol to the formed asymmetric vesicles.[148] Somerharju[153] demonstrated introduction of lipids into a biological cell from a donor liposome. Depletion of cholesterol from the membrane was

avoided by using donor vesicles containing 50 mol% cholesterol. This suggests that it would be possible to create acceptor vesicles containing the desired concentration of cholesterol without the need of a second step using CLCs. Balancing cholesterol influx and efflux from the bilayer, ensuring maintenance of cholesterol content in the donor vesicle would prove tedious across different vesicle compositions.

A more refined solution from London enabled a one-step synthesis of cholesterol containing asymmetric liposomes by replacing MβCD with (2-hydroxypropyl)-α-cyclodextrin (HPαCD).[50] Lipids but not cholesterol can bind in the smaller cavity of HPαCD. Generation of asymmetric liposomes utilising HPαCD for a small range of lipids has been achieved; however a lower efficiency for exchange using pure SM donor vesicles was observed. Higher HPαCD concentrations and longer incubation times were required to solubilise donor MLVs. Cyclodextrin (CD) cavity size played a minor role in MLV solubilisation, CD functionalisation has a more profound effect. These observations imply that MαCD may present the most efficient solubilisation of MLVs whilst also retaining lipid selectivity *vs.* cholesterol. This was found to be the case in a subsequent publication by London *et al*, with comparable volumes of MαCD used to solubilise MLVs as previously reported for MβCD.[154] The expense of commercial MαCD could act as a hindrance to adaptation of this CD for lipid exchange. Simple synthetic procedures are available to more cost effectively produce MαCD,[155] however the availability and cheap cost of MβCD and HPαCD will most likely favour the continued use of the latter CDs.

In vivo studies involving CD-mediated incorporation of lipids into cells found that the nature of the head group was of little consequence, showing no clear correlation to the amount of lipid transferred. This was attributed to the polar head groups limited interaction with the hydrophobic cavity of CD.[153] The nature of the acyl chain was found to be of more consequence; higher MβCD concentrations were required to solubilise donor MLVs composed of lipids with longer acyl chains.[156] The vast array of compositions possible for asymmetric vesicles may make it difficult to optimise the procedure for every possible

bilayer structure. It is unlikely that a general method will be established with factors such as CD concentration having to be fine-tuned for each lipid composition in order to yield maximum transfer and asymmetry.

Due to lipid flip-flop, vesicles composed of lipids possessing short or highly unsaturated aliphatic chains are unsuitable for use. This is corroborated by examination of the production of SMo/PCi vesicles with PCs of varying chain length. Exchanged vesicles composed of short or polyunsaturated chains allow translocation of SM into the inner leaflet, therefore SM never saturates the outer leaflet and can continue to be exchanged yielding a higher overall percentage of SM in the bilayer.[152] Whilst the author cites this as a drawback for this production method, any attempt to synthesise asymmetric liposomes will inherently have to contend with formation of a symmetric distribution of lipids by translocation.

A unique, unaddressed issue is encapsulation efficiency. Liposomes used as carriers of therapeutic agents require production methods of high guest encapsulation and low leakage. CD's removal of lipid from the bilayer could perturb the formed bilayer, resulting in leakage. Thus far, studies of leakage and encapsulation efficiency have been largely ignored, LUVs separated from residual MLVs by sucrose gradient centrifugation indicates some retention of cargo.[149] However, liposome yields are low and are variable with CD concentration (50%, 40 mM MβCD *vs.* 10%, 70 mM). The low yield afforded by higher CD concentrations may be rationalised by disruption of the bilayer and sucrose leakage lowering the yield.

1.6.5. Droplet interface bilayers

A novel route to forming bilayers was developed in parallel by Bayley[157] and Takeuchi[158] who pioneered the formation of droplet interface bilayers (DIBs). Lipid monolayer stabilised w/o emulsion droplets were brought into contact resulting in monolayer fusion, forming a bilayer. Bayley established the use of electrodes coated in a hydrophilic gel which are submerged in an oil-lipid bath. Water droplets pipetted down the electrodes

become anchored by the gel. A stabilisation period allows formation of lipid stabilised w/o droplets, which are brought into contact using micromanipulators forming a bilayer. (Figure 1.13) Takeuchi utilised both droplet and microfluidic approaches in the double well and cross channel chip methods.

Although a novel production method, modification of the procedure was necessary to produce asymmetric bilayers. DIB formation can be achieved by two basic methods, the lipid-in and lipid-out approach. In the lipid-out approach described above, lipid comprising the monolayers is dissolved in the oil medium; conversely the lipid-in method has lipid within the aqueous droplet which spontaneously forms a monolayer. The lipid-out approach is more costly, with longer stabilisation times (> 30 minutes) than the lipid-in method (5 minutes); additionally the lipid-out method only forms symmetric vesicles. Lipid is present in the oil; therefore identical monolayers form around all droplets. Hemifusion of two droplets results in symmetric bilayer formation. Bayley later utilised the lipid-in approach to generate asymmetric DIBs.[159]

Bayley's methods of DIB formation allow great control over the production of extended droplet networks using a micromanipulator; however the process is time consuming with low throughput. Additionally, DIBs produced were predominately composed of 1,2-diphytanoyl-sn-glycero-3-phosphocholine (DPhPC), a lipid not widely found in nature. DPhPC is an archaeal lipid that is known to form bilayers of high stability,[160] in order to demonstrate the robustness of DIBs, lipids of more widespread biological relevance need to be used. Both of these concerns have been addressed with a microfluidic process generating linear arrays[161] and extended 2D and 3D[162] asymmetric DIB networks comprised of biologically significant lipids.[163] Extended 3D DIB networks can be produced composed of 1600 DIBs in 30 minutes, with potential to act as simple tissue mimics. A promising application of such networks is use as protocells, a three DIB arrangement compartmentalised a four step reaction, with each step being carried out within a separate aqueous pool.[163] Additional applications include use as drug delivery vectors,[164]

electrical recording of ion channels,[159] light sensors and acting as biobatteries.[158] However, encapsulation of droplets in oil limits the applications of DIBs *in vivo*.

A subsequent publication by Ces *et al* combined the DIB and inverted emulsion approach to produce a w/o/w DIB (Figure 1.13).[165] In short, a DIB containing sucrose is formed at an oil-water boundary stabilised by a lipid monolayer. Sedimentation through the monolayer results in an external bilayer formation creating a w/o/w asymmetric DIB. Principally there is a lower size limit of each DIB compartment being 500 µm in order to pass through the interface, this value far exceeds that of a typical eukaryotic organism which are in the range of 20-30 µm.[166] This value may be reduced to more biologically relevant scale by varying the sugar concentration ratio between the aqueous phase and DIB droplets.[141] Interestingly, yields nearly double (83%) using the lipid-in *vs.* lipid-out approach (43%). The lipid-in approach was theorised as being more likely to form a stabilising monolayer and hence a bilayer passing through the interface.

Whilst w/o/w DIBs open up new potential applications, there are still some drawbacks that need addressing. Similar problems to those experienced using the inverted emulsion process (Section 1.6.2.) is expected, with spontaneous formation of liposomes at the interface and long re-equilibration of the interface monolayer. These systems are only stable for 1 hour before rupture due to osmotic pressure and have a lower size limit of 500 µm. Residual oil in the bilayer are also a concern; although insertion of the protein, α-haemolysin into DIBs has been shown to occur without disruption, the amount may still be sufficient to perturb other processes such as flip-flop.[165]

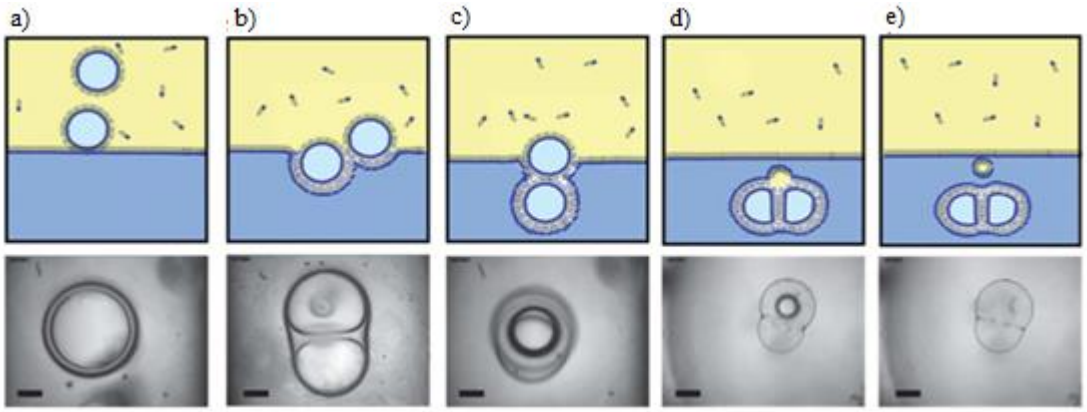

Figure 1.13. Stages in the formation of a two compartment DIB vesicle formation in the lipid in approach. a) Two droplets are introduced into the lipid in oil solution forming monolayer stabilised w/o droplets which begin to descend toward interface. b) The droplets reach the monolayer stabilised interface where they form a DIB. c) The DIB vesicles pass through the interface developing an external bilayer. d) Residual oil in the vesicle is accumulating at the external bilayer. e) The residual oil droplet buds (stabilised by a lipid monolayer). Republished with permission of the Royal Society of Chemistry, from Ref. 165, copyright 2013; permission conveyed through Copyright Clearance Center, Inc.

1.6.6. Microfluidic Jetting

Microfluidic jetting is a divergent technology from the DIB platform to form w/o/w droplets with sizes comparable to LUV and GUVs.[167,168] Early work applied the lipid-out technique limiting the method to production of symmetric bilayers, however asymmetric vesicles were produced by Fletcher applying the lipid-in approach.[142] In short, a piezoelectric inkjet nozzle in placed in one aqueous droplet of a standard double well set up. A microfluidic pulse from the nozzle resulted in the formation of a GUV in the adjacent aqueous droplet as shown in Figure 1.14.

The method produced relatively monodisperse vesicles varying in size by 3% between pulses. The size of the resultant vesicle is well defined, controlled by the diameter of the jet nozzle used and pulse time of the jet. High throughput is also possible for the lipid-in approach as the interface bilayer could quickly be replenished, possibly producing thousands of liposomes per minute.[168] Equilibration of an interface monolayer by lipid from the aqueous droplet occurred in 5 minutes.[159] Whilst this method is promising producing

asymmetric liposomes with the potential high throughput, reasonable control of vesicle size and ease of proteins incorporation compared to the electroformation technique, some questions over the technique remain.

As with all methods involving the exclusion of oil to form a bilayer, residual oil remains in the membrane which may affect bilayer properties. Asymmetry was only proven by coordination of fluorescently labelled histidine tagged protein (aqueous volume) to a bulky Ni chelating lipid incorporated into the bilayer by confocal microscopy. This large labelled lipid may not be represented of non-tagged analogues due to steric bulk. This procedure has only been demonstrated for asymmetric bilayers composed of robust, less biologically significant DPhPC and still needs to be expanded to form GUVs of more pertinent biological compositions to prove viability.

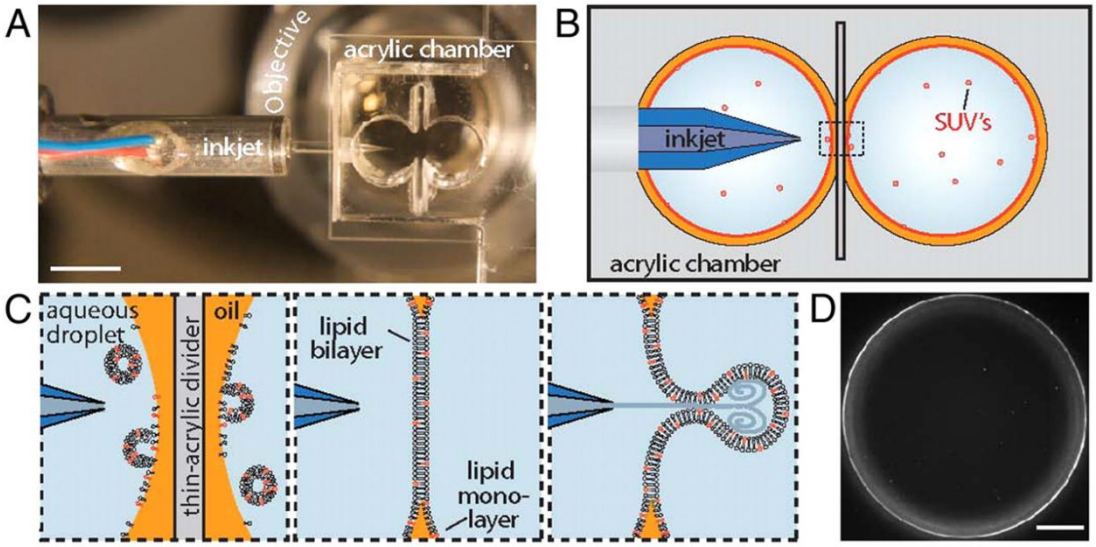

Figure 1.14. Overview of the microfluidic jetting process to form asymmetric vesicles. a) Picture of modified Takeuchi double well. b) Two monolayer stabilised water droplets in oil are separated by an acrylic divider. c) The divider is removed forming a DIB, application of an inkjet pulse results in the formation of GUVs. d) Produced GUV imaged by confocal microscopy. Figure reproduced from Ref 142, copyright 2011.

1.6.7. Enzyme catalysed lipid exchange

There are many proteins that catalyse phospholipid inter-bilayer exchange *in vivo* with examples being isolated from mammalian liver, fungi, and several varieties of plants.[169]

There are three classes of such proteins; phosphatidylcholine transfer protein, phosphatidylinositol transfer protein and nonspecific lipid transfer protein which is capable of transferring several types of phospholipids and sterols.[170] Lipid transfer proteins have long been used to exchange lipid between liposomes and biological membranes to elucidate the biological role of such proteins and probe mechanisms of *in vivo* lipid redistribution.[171] Exchanged lipid is only delivered to the extra-cellular leaflet, therefore asymmetric vesicles can be generated using a lipid transfer protein provided the rate of protein catalysed exchange >> rate of flip-flop.

Asymmetric vesicles have been synthesised *in vitro*; however the asymmetry was not quantified, with the author focussing on inter-bilayer transfer rate.[172] Recently, Holzer *et al* incubated acceptor and donor vesicles with varying amounts of ns-LTP.[173] An optimum protein: lipid ratio of 19.5×10^{-5} was shown to produce acceptor vesicles with a mole fraction of 0.055 transferred lipid in the outer leaflet after 2-3 hours. Absence of ns-LTP showed slower rates of transfer, with a mole fraction of 0.02 after 216 hours.

The methodology still needs extensive work to generate a larger asymmetric distribution in addition to requiring further work to prove viability with a wider range of lipid systems. Isolation of the desired asymmetric vesicles was an initial concern; however separation of vesicles containing negatively charged lipids using free flow electrophoresis has been achieved. Addition of 4 mol% biotin to neutral donor liposomes allowed separation by addition of magnetic beads coated in streptavidin, followed by application of a magnetic field. Only the donor vesicles are tagged; therefore the acceptor vesicles of interest are only modified by the transfer lipid. Although extensive work is still required, the method is promising as there is no residual oil in the bilayer and allows utilisation of more refined conventional methods of liposome synthesis. This allows greater control of the size and monodispersity of the vesicles. Additionally, the method is likely to be widely applicable to a variety of systems due to large numbers of translocase proteins and is a bulk scalable method, indicating industrial applicability.

1.7. Conclusion

Preparation techniques of artificial bilayers have greatly improved over the last 50 years since the introduction of liposomes by Bangham; however, reliable methods to produce asymmetric systems have largely been absent until recently. Asymmetric bilayers are of vital importance in order to elucidate the role of asymmetry in biological processes. The need for asymmetric systems has led to a range of new methods of asymmetric bilayer production emerging over the last decade. These new asymmetric vesicles are promising; however, each production method has limitations. SLBs are simple and easy to produce but show poor mechanical stability, short lifetime and an inability to scale up as well as the inability to be used *in vivo* as delivery systems. The inverted emulsion technique gives largely excellent encapsulation efficiencies and allows the control of asymmetry for MLVs; however there is still a multitude of issues in producing monomodal distributions of liposomes and industrial scale up is not easy. DIBs are unique in allowing great control over extended networks mimicking artificial mutli-compartment cells; however, their formation in oil limits the scope of applications. Water soluble w/o/w droplets formed display limited stability, eliminating *in vivo* applications. Microfluidic jetting has thus far only been demonstrated for one system of little biological relevance and needs subsequent investigation to determine lifetime and viability for less robust lipid compositions. All three methods suggested suffer from initial formation from an oil phase leaving the question of residual oil perturbing the bilayer. The newest and perhaps the most promising technology is that of CD catalysed synthesis, which has shown to produce SUVs, LUVs and GUVs of a variety of compositions. Some questions remain however, including leakage of components and retention of CD within the bilayer after exchange.

The second chapter of this work will detail efforts towards the synthesis of two molecular recognition lipids which when incorporated into separate vesicles induce hemifusion. During hemifusion lipid diffusion occurs, generating transversely asymmetric hemifused vesicles, where upon cleavage produce asymmetric liposomes. This method

presents a potential alternative to producing transversely asymmetric liposomes. Chapter 3 will discuss progress on the solid phase synthesis of dialkyl phosphates. The optimisation of the process would be the first step in developing a solid support synthesis of phospholipids, both naturally occurring and synthetic. Production on the solid support could lead to a combinatorial approach where large libraries of phospholipids can become rapidly accessible. The final chapter of this thesis will focus on the synthesis of ^{17}O and ^{18}O labelled sterols, non-intrusive spectroscopic and spectrometric markers. These labelled sterols represent another tool to investigate membrane dynamics, such as lateral phase separation within bilayers.

Chapter 2. Synthesis of Complimentary Barbituric Acid (BAR) and Triaminopyrimidine (TAP) Lipid Analogues

2.1. Background and Aims

Whilst there are currently a plethora of methods to produce symmetric bilayer systems dating back 50 years, there has been a distinct lack of methods for producing asymmetric bilayers. Within the last decade this has begun to be remedied through the work of emulsion inversion,[51] DIBs[159] and MβCD catalysed methods[149] discussed previously (Sections 1.6.2, 1.6.5 and 1.6.4 respectively) however, there are still few methods for the bulk production of asymmetric liposomes, necessitating additional synthetic routes to be discovered.

A conceivable route to the formation of asymmetric vesicles is rate enhancement of lipid transfer between preformed symmetric vesicles. Typically this is a slow process, demonstrated by spontaneous transfer of 2 mol% egg PG taking 216 hours.[173] This value can be dramatically reduced to 2-3 hours with the use of proteins and high concentrations of MβCD.[152,173] A possible alternative route is the induction of hemifusion, in which the outer leaflet of two vesicles fuse whilst the inner leaflets and cytosolic aqueous pools remain separate. Lateral diffusion of lipids results in a mixed composition of the outer leaflet whilst each inner leaflet remains the same as the initial lipid composition, based on the rate of lateral diffusion being greater than $t_{1/2}$.[2] Splitting of the hemifused structure results in the formation of two populations of asymmetric vesicles. This concept is shown in Figure 2.1.

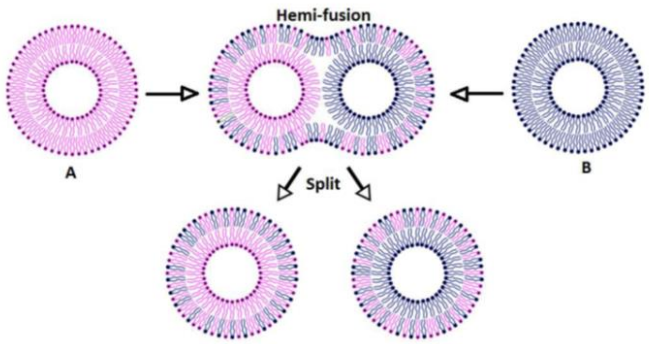

Figure 2.1. Proposed method of hemifusion induced asymmetric synthesis.

Hemifusion is believed to be an important intermediate in fusion between cell membranes *in vivo*[174] and has shown to be induced by the use of nucleic bases,[175] denatured protein,[176] oppositely charged vesicles[177] and surfactants at the surface of vesicles.[178] Another method to induce hemifusion was reported by Lehn *et al* where 10 mol% of complementary triaminopyrimidine (TAP, **1**) and barbituric acid (BAR, **2**) functionalised lipids shown in Figure 2.2 are incorporated into LUVs composed of egg phosphatidylcholine (EPC).[178]

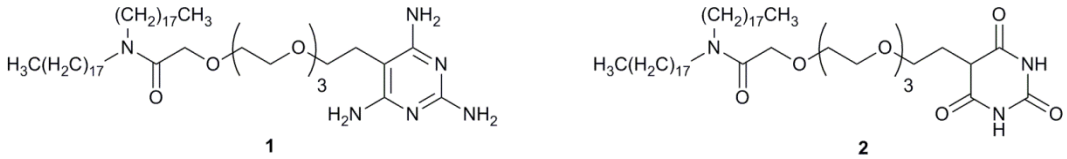

Figure 2.2. The structure of functionalised BAR and TAP lipids.

The ability of these complementary head groups to form extended structures has long been known, producing extended helical ribbon structures in the solid state.[179] The first instance of the use of these structures in lipid bilayers was the inclusion of BAR lipid into a Langmuir monolayer with the interaction of free TAP *in situ*. The complementary compounds were found to interact by forming an extended hydrogen bonded network (Figure 2.3) confirmed by X-ray diffraction.[180] In addition to hydrogen bonding there is also a strong electrostatic interaction with BAR (pK_a of 4.1) becoming negatively charged at neutral pH, whilst TAP is positively charged with a pK_a in the region of 6.8 (for the unsubstituted analogues).[181]

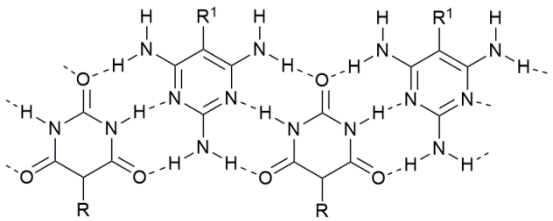

Figure 2.3. Hydrogen bonding network of BAR lipid and TAP lipid where R and R^1 represents the remaining lipid structure and associated vesicle.

Lehn demonstrated the ability of these systems to hemifuse, laying the foundation for the formation of asymmetric vesicle production; however several issues still need to be addressed. Dissociation of the hemifused state was not attempted by Lehn, as BAR and TAP associate by non-covalent interactions, introduction of a competitive inhibitor such as free BAR or TAP may induce dissociation of the fused vesicles. The inclusion of 1 mM BAR *in situ* has previously been shown to inhibit initial fusion.[182] The second issue is whether the BAR and TAP doped vesicles are truly hemifused or if the observed size increase in dynamic light scattering and changes in fluorescence observed by Förster Resonance energy transfer (FRET) are due to a prolonged interaction. The lifetime of this interaction may be manipulated by varying the mol% of BAR and TAP lipids within the vesicles. In LUVs composed of EPC, below 2 mol% of BAR and TAP lipids were found to not increase the size of the vesicles, whilst 10 mol% was shown to form fully fused vesicles. Therefore, varying the concentration of BAR and TAP lipids within vesicles (2-10 mol%) may identify the concentration at which prolonged association presents the ideal situation in terms of lipid exchange to from asymmetric vesicles followed by dissociation.

In addition to determining if dissociation is possible, the rate of lipid transfer in the vesicles must be deduced, a rate greater than that of translocation is required. The degree of asymmetry which can be obtained for different lipid compositions must be explored as currently the only hemifused system tested with BAR and TAP for vesicles composed of EPC. Finally, confirmation that the internal compartments do not mix and asymmetric vesicles are indeed produced, with retention of guests in the cytosolic aqueous pools.

The final asymmetric vesicle produced will be modified, containing > 2 mol% of BAR or TAP lipid at the extra-cellular leaflet. Methods to remove desired vesicle after modification include centrifugation,[148] removing negatively charged vesicles by free flow electrophoresis[173] and vesicle modification to include biotin.[172] The most likely method of separation would be centrifugation of differently sized vesicles or by flow cytometry, as the

internal aqueous pools remain distinct they can have different fluorescing guests incorporated into each vesicle population. The aims of this work were to;

- synthesise BAR and TAP lipids using a literature procedure,[183]
- incorporate these structures into a wide variety of liposome sizes and compositions, allowing determination of optimum conditions to observe the asymmetric hemifused liposomes,
- devise a strategy to dissociate the hemifused state and separate distinct populations of vesicles.

2.2. Results and Discussion

BAR and TAP lipids share some common structural motifs, they are amphiphilic, possessing two hydrophobic alkyl chains allowing incorporation into the lipid bilayer. They also contain a hydrophilic PEG spacer, with hydrophilic heterocyclic head groups, capable of hydrogen bonding. In the case of BAR lipid there are two possible synthetic approaches, to alkylate a malonic acid derivate and condense with urea, the second approach was modification of the *5-C* position of preformed barbituric acid.

Barbituric acid was first produced by von Baeyer in 1864 in a multistep procedure, starting from uric acid,[184] Grimaux streamlined the process by refluxing the corresponding malonic acid and urea in the presence of $POCl_3$ in a single step.[185] Fischer presented a slight modification utilising alkylated malonic ester and urea in the presence of NaOEt,[186] famously used in the preparation of 5,5-diethylbarbituric acid (Veronal). Veronal has been demonstrated to be a powerful hypnotic and sedative leading to the synthesis of thousands of 5,5-disubstituted barbituric acids derivatives and the development of over fifty clinical agents.[187] The popularity of barbitruic acid derivatives as therapeutic agents has been in decline since the late 20th century due to the relatively low dosage required for overdosing,[188] a fact reflected in the occasional use of barbiturates as the active component in capital punishment.[187] The early development of synthetic strategies to produce barbituric acid is

well presented by Carter.[189] Fischer's convenient synthesis was also widely used for the production of biologically inactive 5-alkylated barbituric acids.[190-192] Recently, novel methodologies are emerging to produce 5-alkylated barbituric acid. These approaches involve direct modification of preformed barbituric acid, by methods such as Knoevenagel condensation.[193] Potential routes are displayed in Scheme 2.1. The following section will details efforts to produce TAP lipid by an approach analogous to Fischer condensation (Route A, Scheme 2.1) using an alkylated malononitrile analogue. Attempts of BAR lipid production using Routes A-E will also be described.

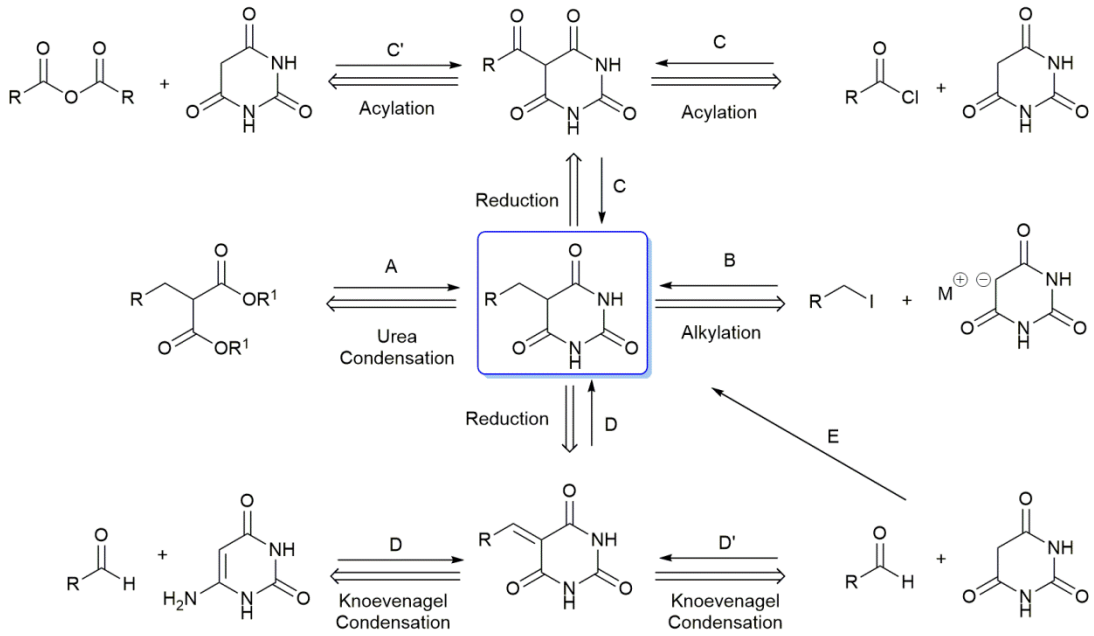

Scheme 2.1. Possible synthetic routes to produce 5-substituted barbituric acid (shown in the blue box). All routes aside from Route B have literature precedents.

2.2.1. Route A: Conventional Fischer synthesis of BAR and TAP lipids

Hydrophilic PEG linker was mono-functionalised, producing an asymmetric linker with a benzyl ester and alcohol on opposing termini. Route A (Scheme 2.2) was tested, building upon previous work within the group;[194] compound **5** was produced through a three step synthesis. Tetraethylene glycol was mono protected by a tetrahydropyranyl (THP) group, followed by addition of bromoacetic acid and benzyl bromide to produce **4**. Subsequent deprotection by pyridinium p-toluenesulfonate (PPTS) furnished the desired

product (**5**). The sequence produced a low overall yield (21%), was labour intensive (two chromatography purifications) and required a long overall reaction time (> 50 hours). In contrast, combining benzyl diazoacetate and an excess of tetraethylene gylocol (4 eq.) in the presence of a Lewis acid produced compound **5** in 62% yield as shown in route B (Scheme 2.2). A conversion of 83% was observed, with 5% benzyl alcohol produced by hydrolysis of diazoacetate and 12% conversion to the bis-benzylated by-product. In addition to an improvement in yield, Route B was much quicker (2 hours) and required a single purification by column chromatography which can be aided by the appropriate work-up procedure. A significant volume of tetraethylene glycol can be removed from the reaction mixture when using DCM as the organic phase and washing with H_2O. Use of EtOAc as the organic phase should be avoided, with near quantitative volumes of tetraethylene glycol recovered from the organic phase.

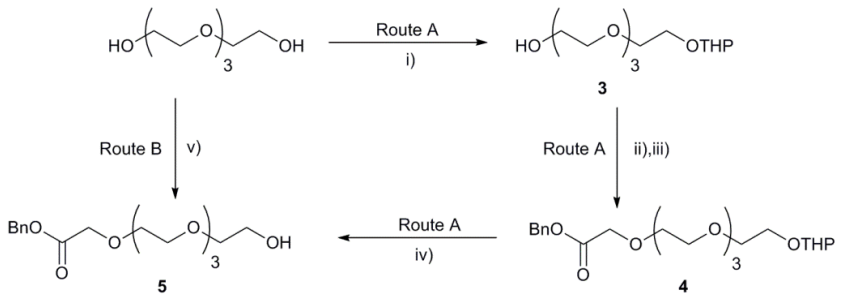

Scheme 2.2. Synthetic approaches to produce benzyl ester (**5**). i) DHP, TsOH, neat, 57%. ii) NaH, $BrCH_2CO_2H$, THF. iii) BnBr, NaH, THF, 41% (two steps). iv) PPTS, EtOH, 89%. v) $BF_3.OEt_2$, $C(CH_2N_2)O_2Bn$, DCM, 62%.

Tosylation of compound **5** shown in Scheme 2.3 initially utilised TsCl, *N*,*N*-diisopropylethylamine (DIPEA) and catalytic 4-dimethylaminopyridine (DMAP), producing 7% of product **6** after 16 hours. Increasing the reaction time to 69 hours resulted in no improvement. TsCl in anhydrous pyridine was found to significantly increase the yield to 92% after only 4 hours. Debenzylation of **6** was achieved using Pd/C (10 mol%) under a H_2 atmosphere at 50 PSI with a mechanical shaker, affording acid **7** in 95% yield. Alternatively, comparable yields (97%) can be obtained at atmospheric pressure, however a higher loading of catalyst (20 mol%) was found necessary to fully debenzylate in 16 hours.

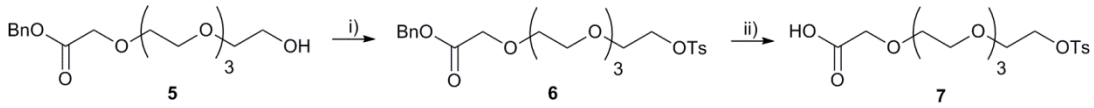

Scheme 2.3. Synthesis of acid (**7**). i) TsCl, Py, DCM, 92%. ii) Pd/C, H_2, DCE, 97%.

Introduction of two stearoyl groups *via* amidation imparts a large hydrophobic region allowing incorporation into lipid bilayers. The combination of hydrophobic steroyl groups and hydrophilic PEG linker mimics the amphiphilic nature of natural lipids. Literature procedures introduce the amide *via* the use of *N*-hydroxysuccinimide (NHS) to produce a succinimide ester intermediate (Scheme 2.4, Route A).[194] The yields reported were fairly low, with 22 and 49% total yield from compound **5** for the same substrate and a structural analogue respectively.[194,195] Alternative methods to synthesise amide (**9**) were explored; Route B involved the use of a well-known peptide coupling reagent benzotriazol-1-yl-oxytripyrrolidinophosphonium hexafluorophosphate (PyBOP).[196] The reaction showed a near quantitative conversion by ^{1}H NMR spectroscopy, however isolation was not possible, resulting in abandonment of the PyBOP route. Finally, Route C involved the use of oxalyl chloride producing acid chloride intermediate (**8C**), the reaction showed quantitative conversion by ^{1}H NMR spectroscopy after 2 hours. Excess, volatile oxalyl chloride and gaseous by-products were easily removed by concentration *in vacuo*, prior to addition of the acid chloride (**8C**) to a solution of dioctadecylamine in DCM, affording the desired amide (**9**) in 84% isolated yield.

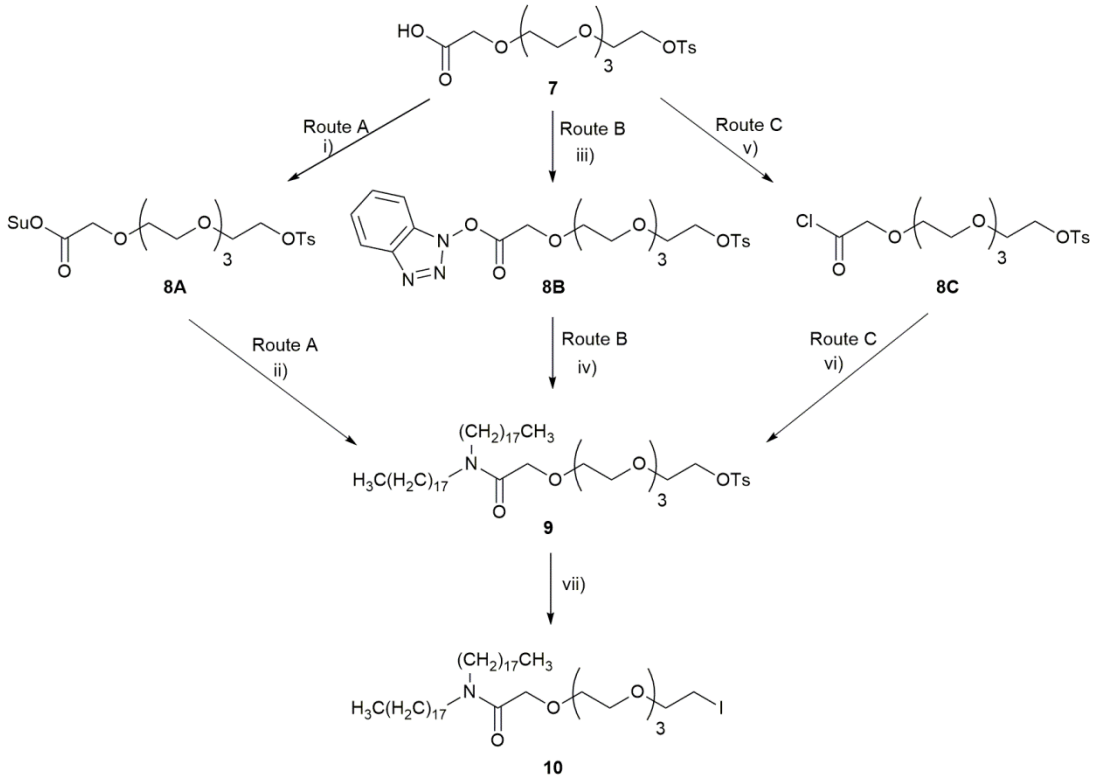

Scheme 2.4. Synthesis of iodinated amide (**10**) by 3 possible synthetic routes. i) NHS, DMAP, DCM. ii) DIC, DCM, $NH[(CH_2)_{17}CH_3]_2$, DCM, NEt_3, 22% (from **7**). iii) PyBOP, DIPEA, DCM. iv) $NH[(CH_2)_{17}CH_3]_2$, NEt_3, DCM, isolation not possible. v) $(COCl)_2$, DCM. vi) $NH[(CH_2)_{17}CH_3]_2$, NEt_3, DCM, 84% (from **7**). vii) NaI, MEK, 96%.

Compound **9** was refluxed with NaI in methyl ethyl ketone (MEK) producing iodinated compound (**10**) near quantitatively with negligible impurities by ^{1}H NMR spectroscopy, leading to the crude material being used without subsequent purification. Product **10** was split and simultaneously used in two subsequent pathways, producing direct precursors to TAP and BAR lipids, alkylated malononitrile (**11**), and alkylated dimethyl malonate (**12**) respectively as shown in Scheme 2.5. It was found necessary to produce the malonate ester (**12**) *via* the iodide (**10**), as direct alkylation of malonic esters using **9** did not produce the desired product. Complete consumption of **9** was observed, however, no formation of **12** was witnessed by ^{1}H NMR spectroscopy; a mixture was obtained with the components not being identified.

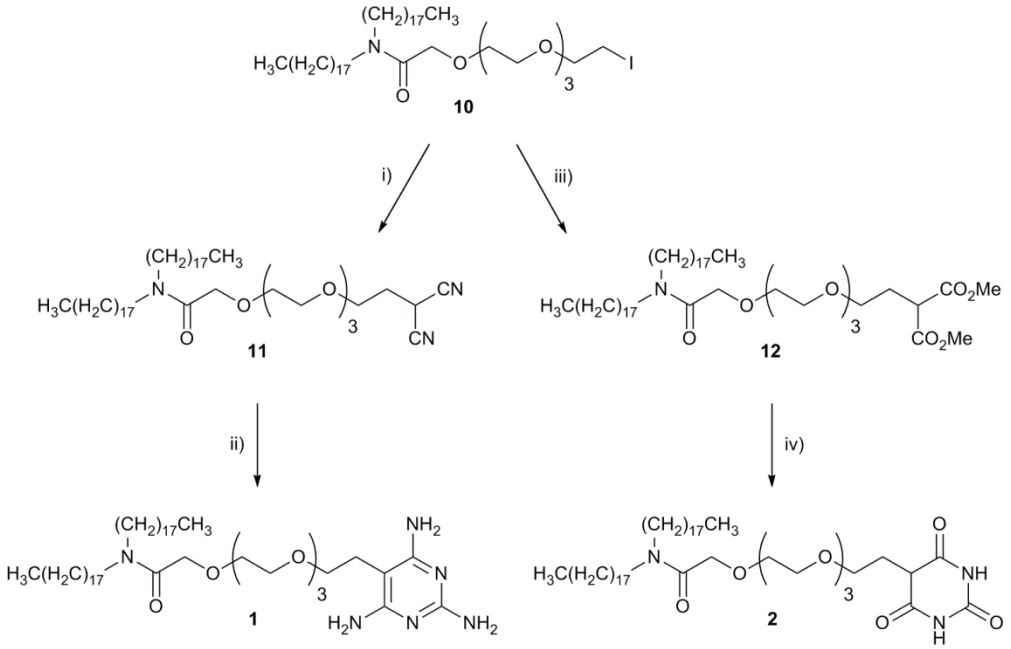

Scheme 2.5. Synthetic pathway to obtain the desired final products of TAP, **1**, and BAR, **2** lipids. i) $CH_2(CN)_2$, NaH, DMSO, 84%. ii) $C(NH2)_2NH$, NaOMe, MeOH, 58%. iii) $CH_2(CO_2Me)_2$, NaOMe, MeOH, 52%. iv) $CO(NH_2)_2$, NaOMe, MeOH, no product isolated.

Addition of excess malononitrile and NaH to **10** in DMSO produced TAP precursor (**11**). The substrate exhibits poor solubility in DMSO, compound **10** had to be fully suspended in the solvent to ensure complete conversion to **11**. Originally the target compound was isolated in 28% yield, despite quantitative conversion as assessed by ^{1}H NMR spectroscopy. The low yield was due to difficulties in separation of the compound from excess malononitrile and DMSO. The literature procedure purifies **11** by slow trituration from DCM: MeOH 95:5 using a rotary evaporator, comparable yields to those reported could not be obtained using this purification technique.[183] An alternative purification procedure was devised; the mixture was subjected to flask to flask (Kugelrohr) distillation removing both DMSO and excess malononitrile. Only pure, non-volatile **11** remained in the flask. The temperature used for the distillation was kept below 100 °C, and it is recommended to perform the distillation in a fume hood as there is some indication that exceeding this temperature may decompose malononitrile, producing highly toxic hydrogen cyanide gas.[197] The modified distillation procedure produced clean compound **11** without the need for further purification in a vastly improved yield of 84%. TAP lipid (**1**) was produced

in 58% yield by addition of guanidinium carbonate to **11** in the presence of NaOEt. Compound **12** was isolated in 52% yield by substitution of iodide by the relevant malonate diester. Neutralisation of the reaction mixture to pH 7 prior to work-up was carried out in order to avoid producing bis-acid by-product *via* ester hydrolysis. As well as the desired product around 10% of the elimination product was also observed, indicated by a double doublet at 6.33 ppm in the crude ^{1}H NMR spectrum.

The final reaction of the BAR synthetic pathway (Scheme 2.5), in which compound **12** was condensed with urea to produce the desired BAR lipid (**2**) proved challenging to isolate the product. The crude ^{1}H NMR specturm showed around 32% conversion to the desired product as displayed in Figure 2.4. The key peaks correlating to compounds *5-C* and *7-C* are visible and matched literature values.[183] Production of **2** was further confirmed by matrix assisted laser desorption ionisation mass spectrometry (MALDI-MS) in which the $[M+H]^+$, $[M+Na]^+$ and $[M+K]^+$ adducts were observed. Aside from the desired product several other by-products were visible in the ^{1}H NMR spectrum, as evidenced by the additional peaks at 2.3-2.5 ppm and at 4.2 ppm. The numerous signals at 4.2 ppm are particularly indicative of the purity as a singlet was expected corresponding to *15-C*.

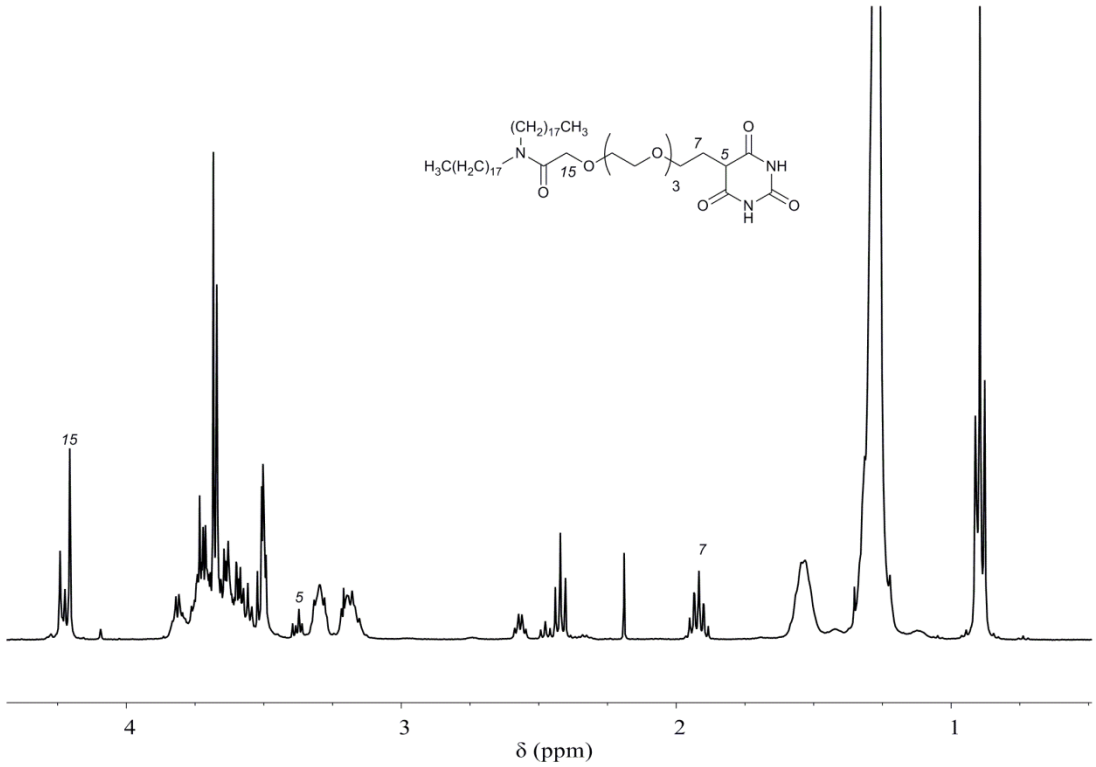

Figure 2.4. Crude ^{1}H NMR spectrum of BAR lipid (**2**) with key peaks identified.

Poor conversion was attributed to residual H_2O in the reaction mixture forming NaOH. The hydrophilic PEG linker in compound **12** was likely retaining H_2O making what is usually a trivial reaction frustrating for this particular substrate. Interestingly, the formation of NaOH potentially led to two separate decarboxylation by-products (shown in Figure 2.5) being detected by atmospheric solids analysis probe mass spectrometry (ASAP-MS). One decarboxylation product (**13**) was saponified converting the methyl group to the free acid (after acidic work-up), whilst the second decarboxylation product (**14**) curiously retains its methyl ester. It should be noted that the saponified decarboxylated product (**13**) may be only produced by fragmentation of the methyl ester decarboxylation product (**14**) during analysis and not a true component of the crude mixture. Subsequent analysis by high performance liquid chromatography mass spectrometry (HPLC-MS) identified both components in the mixture (Figure 2.6), with different t_R values indicating that compound **13** was a true component of the mixture and not merely a fragment of **14** produced in the mass spectrometer.

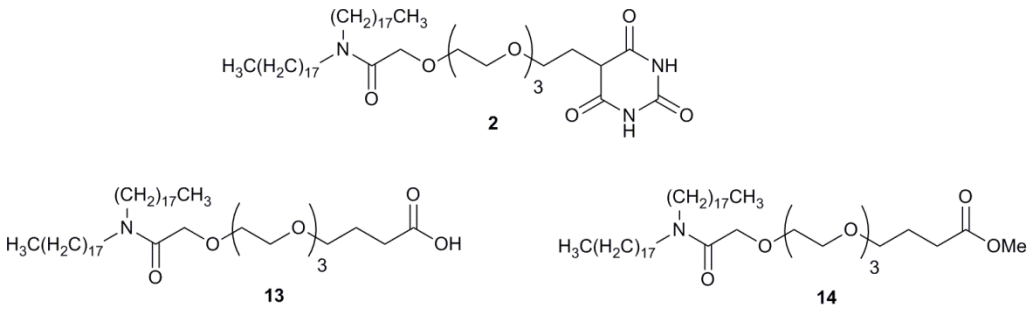

Figure 2.5. Compounds observed by mass spectrometry for the urea condensation of compound **12**.

Several precautions to remove residual H_2O were performed including varying the solvent source between commercial anhydrous solvent and freshly dried MeOH. MeOH was dried by refluxing with Mg & I_2 followed by storage over oven activated 3 Å molecular sieves (M.S) under an argon atmosphere. NaOMe solutions were freshly prepared just prior to use. Reactants were stirred over oven activated 3 Å M.S overnight prior to addition of NaOMe. All reagents were dried for 16 hours over P_2O_5 *in vacuo*. Due to its hygroscopic nature, urea was dried *in vacuo* (0.8 mmHg at 60 °C) for 2 hours, then stored overnight *in vacuo* over P_2O_5 as an additional precaution. These precautions unfortunately yielded little effect as decarboxylation product was observed in comparable amounts.

There are a number of sources from which the residual H_2O could potentially originate, due to precautions outlined previously, it was unlikely that the source of residual H_2O was from either the solvent or NaOMe. This leaves the likely remaining H_2O sources being urea and reagent **12**. In order to address this issue, dimethyl decylmalonate (**15**) was synthesised followed by urea condensation to produce decyl barbituric acid (**16**) as shown in Scheme 2.6. This will identify whether substrate **12** was especially problematic or the reagents are wet. Synthesis of **15** proceeded well, producing the desired compound in 87% yield, no elimination product was observed as in the synthesis of **12**. Urea condensation using the same batch of NaOMe and urea as previous experiments on **12** resulted in production of pure **16** in 64% yield. The successful production of **16** by the urea condensation pathway, indicates that the substrate was the problematic component of the

reaction, this was reflected by the low yield (30%) previously reported for multi-gram synthesis of compound **2** in the literature.[183]

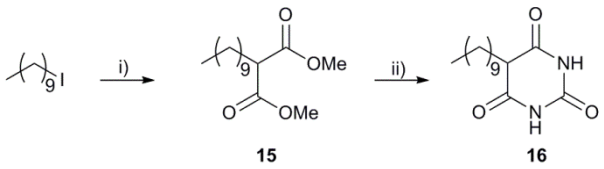

Scheme 2.6. Synthesis of 5-decyl barbituric acid. i) dimethylmalonate, NaOMe, MeOH, 87%. ii) NaOMe, urea, MeOH, 64%.

The classic isolation procedure for alkylated barbituric acids is acidification by HCl solution followed by filtration to remove H_2O miscible impurities. Recrystallisation from MeOH then returns the desired pure 5-alkylbarbituric acid. Isolation of the BAR lipid (**2**) was not possible by this method. Unfortunately, the by-products had low miscibility in both H_2O and MeOH and no solvent combination was found that solubilised just the by-products precluding recrystallisation. The highly polar nature of the substrate eliminated the use of column chromatography with a baseline R_f observed by TLC for both alumina and silica solid supports. Only polar solvent mixtures which also solubilise the solid support such as neat MeOH were sufficient to produce an $R_f > 0.00$.

The crude mixture was subject to reverse phase HPLC to determine if resolution of the mixture could be obtained; the sample had to be run in IPA with minimal H_2O to prevent precipitation. Although **2** has low miscibility in IPA, it may be feasible to recover a small amount of material by preparative HPLC. The amount of BAR lipid required for liposome incorporation is small (µmol), therefore even isolation of 1 mg of **2** would allow multiple hemifusion experiments to be performed. Optimisation of the mobile phase by applying different ratios of IPA: MeCN: H_2O, enabled identification of 3 peaks in the baseline chromatogram at t_R 7.3, 8.3 and 8.6 minutes, as shown in Figure 2.6. A gradient progressing from 63:25:12 to 90:10:0 IPA: MeCN: H_2O as detailed in Section 2.5.3, was found to give the best resolution. The peak with a t_R of 7.3 minutes was fully resolved whilst the remaining peaks were overlapping.

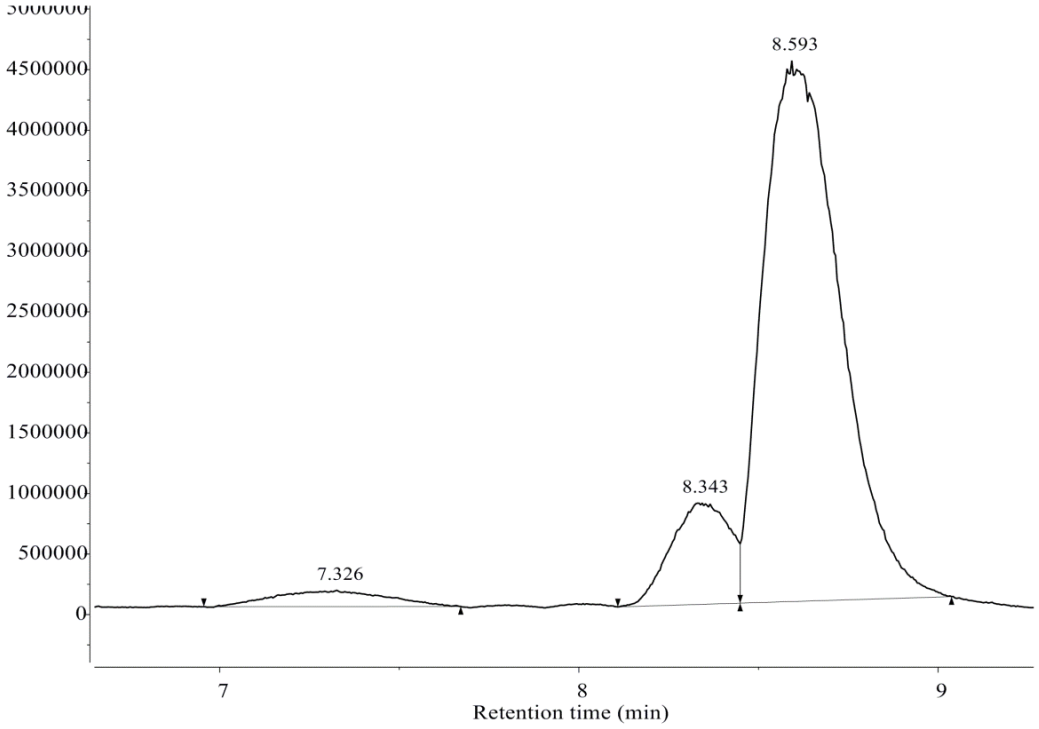

Figure 2.6. The base peak chromatogram from the separation of crude BAR lipid (**2**) by reverse phase HPLC.

An extracted ion mass chromatogram was applied searching for the anticipated *m*/*z* values for the $[M+H]^+$ adducts of BAR lipid (**2**), as well as the suspected decarboxylation by-products **13** and **14** are shown in Figure 2.7. The 3 peaks at t_R 7.3, 8.3 and 8.6 minutes were found to contain compounds with masses matching the $[M+H]^+$ adducts of compounds **2**, **13** and **14** respectively. In the base peak chromatogram, the $[M+H]^+$ adducts of the aforementioned compounds were the most abundant ions within each peak.

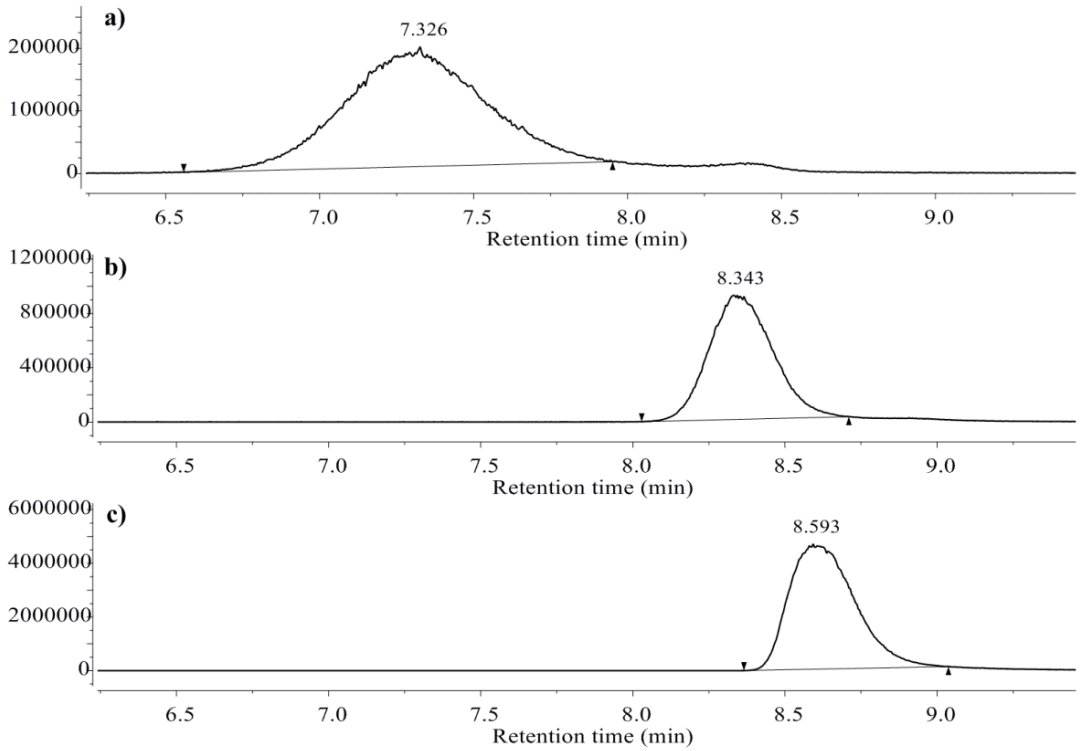

Figure 2.7. Extracted ion mass chromatograms for the sample of crude of **2**, the *m/z* values searched for were; a) 866, b) 798 and c) 812.

To further corroborate the assignment of the peaks, comparison of the accurate mass to the elemental mass of protonated compounds **2**, **13** and **14** was performed. The greatest deviation in the theoretical and experimental mass was found to be only 0.0008 as shown in Table 2.1. This demonstrates that BAR lipid (**2**) was synthesised and can be separated chromatographically from the crude mixture. Further efforts to separate **13** and **14** were not pursued as interconversion of these compounds could be achieved chemically. This will enable either by acquisition of a suitable preparative column or multiple injections through an analytical column to separate enough pure BAR lipid to perform hemifusion experiments.

Table 2.1. Accurate mass data and assignments for the extracted ion mass chromatograms shown in Figure 2.7.

Entry	t_R (minutes)	Theoretical *m/z*	Experimental *m/z*	Δ *m/z*	Assignment[a]
1	7.3	866.7179	866.7187	0.0008	**2**
2	8.3	798.7187	798.7183	0.0004	**13**
3	8.6	812.7343	812.7345	0.0002	**14**

[a]Numbering refers to compounds displayed in Figure 2.5.

2.2.2. Route B: Direct alkylation of barbituric acid

Ongoing problems in synthesising BAR lipid (**2**) led to exploration of new methodologies to produce 5-substituted barbituric acid. Scheme 2.1 depicts several possible synthetic routes to produce the desired substituted barbituric acid. The classic route for forming alkylated barbituric acid by condensing an alkylated malonate ester and urea (Route A, Scheme 2.1) proved problematic; therefore attention was turned to alternative syntheses. The following section will detail efforts to produce BAR lipid (**2**) using such methodologies.

Route B (Scheme 2.1.) consisted of exploring direct alkylation of barbituric acid by pegylated halide (**10**), using various approaches. Stirring **10** and barbituric acid in the presence of bases such as resin bound dimethylamine and pyridine was found to produce no reaction. An alternative was to form a barbiturate salt, which could be subsequently reacted with **10**. The tetrabutylammonium salt was a promising candidate, with the tetrabutylammonium counter ion improving the poor solubility of barbituric acid in organic solvents. Stirring tetrabutylammonium hydroxide in MeOH formed the desired barbituate salt (**17**) in less than 30 minutes, indicated by solubilisation of the suspension. It is worth noting that conventionally, barbituate salts such as sodium barbituate are depicted as having the NH moiety deprotonated with the negative charge residing on the oxygen of the enol tautomer. This is counter intuitive when considering that unsubstituted barbituric acid and 5,5-disubstitution barbiturates (veronal) possess pK_a values of 3.78 and 7.64 respectively in H_2O at 25 °C.[198] Although there will be an enol/ keto equilibrium with the charge residing on the OH and CH in the respective forms. Confirmation of the resulting tetrabutylammonium salt was achieved by ^1H NMR spectroscopy and X-ray diffraction of single crystals as seen in Figure 2.8. As expected, deprotonation of the NH functionality was not observed, with deprotonation of the *5-C* occurring. There was delocalisation of the charge shown by an average bond length of 1.392 Å between the *5-C* and *4-C*/ *6-C* centres. This value was more consistent with C=C bond lengths of other cyclic structures (see the crystal structure of compound **112** in Appendix A1.12), suggesting that the enol form dominates. The

misconception in deprotonation site may be attributed to the observation that the NH functionality deprotonates in 5,5-disubstituted barbitutric acids, which are more widely studied due to their sedative properties.[187]

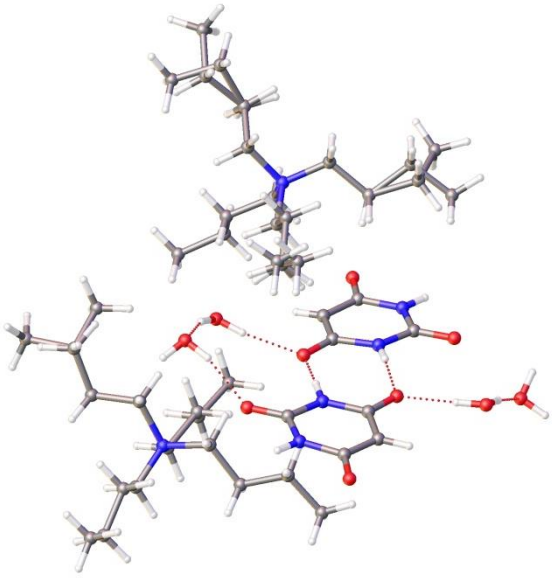

Figure 2.8. Structures from the unit cell of **17**, determined by X-ray diffraction of a single crystal, confirming the site of deprotonation as the *5-C* centre.

Refluxing **17** in MeCN with pegylated halide (**10**) as shown in Scheme 2.7 returned a complex mixture with BAR lipid (**2**), believed to be produced as evidenced by the crude ^{1}H NMR spectrum, however confirmation by HPLC-MS was not possible due to low compound solubility. Unfortunately, performing the reaction in MeOH, MeCN, DCM, 1,4-dioxane and DMF at room temperature returned only unreacted starting material, with application of heat producing the aforementioned complex mixture. The poor reactivity was attributed to the low nucleophilicity of the *5-C* centre due to charge delocalisation. Consequent bulk purification by recrystallisation or chromatography proved not viable. To combat this issue a structural analogue bearing benzyl ester and iodide moieties at opposite termini of the PEG chain, (**18**) was synthesised from alcohol (**5**). Compound **18** was used as an alkylating agent of barbituric acid, as shown in Scheme 2.7. The crude mixture was analysed by ESI-MS, although both the starting iodide (**18**) and pegylated barbituric acid (**19**) are isobaric, with the same *m*/*z* anticipated. A peak at *m*/*z*: 452 was identified in positive

mode; the corresponding $[M-H]^-$ was also observed in negative mode, suggesting the formation of **19**, which contains an acidic proton at *5-C* of the barbituric acid moiety. Compound **18** contains no immediately obvious acidic protons, further strengthening the argument for formation of **19**. This argument was further corroborated by accurate mass spectrometry, with the obtained experimental *m*/*z* peak being within 0.0012 of the theoretical value predicted for **19** (*vs.* a difference of 0.1099 for **18**). Combined, this evidence demonstrates that **19** was synthesised. Similar issues arose, restricting separation of **18** by chromatography and recrystallisation; this coupled with success in producing a structural analogue by acylation (see Section 2.2.3), led to other more promising routes being pursued.

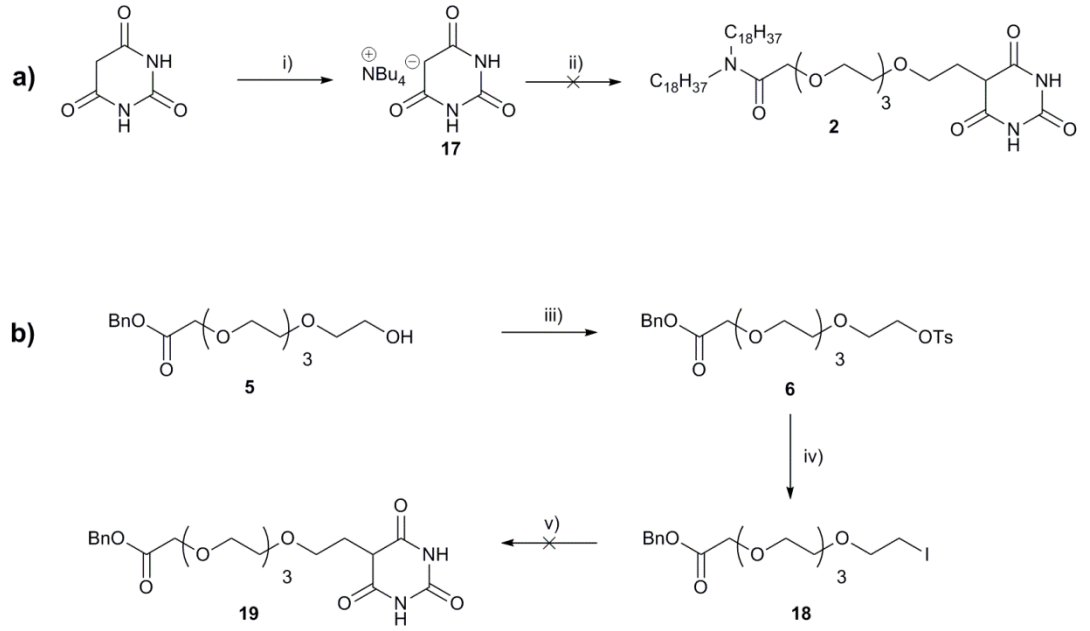

Scheme 2.7. a) Procedure for formation of BAR lipid (**2**) by alkylation using **10**. b) Procedure for alkylation of benzyl bearing pegylated iodide (**18**). i) NBu_4I, MeOH, quantitative conversion. ii) **10**, MeCN (product not isolated). iii) TsCl, Py, 92% iv) NaI, MEK, 83%. v) **17**, Py (product not isolated).

2.2.3. Route C: Acylation and reduction to produce 5-alkyl barbituric acid

In parallel to direct alkylation, alternative methodologies (Route C, Scheme 2.1) to produce 5-alkylated BAR were also explored using commercially available decyl derivatives. Acylation of barbituric acid by decanoyl chloride in anhydrous pyridine was found to be highly efficient with a near quantitative yield of **20** obtained in agreement with the literature (Scheme 2.8).[199] Reduction of the resultant carbonyl to an alkyl moiety was

explored using various methodologies, Clemmenson reduction generated no product, even with more forcing conditions than those utilised for barbituate analogues in the literature.[200] Wolff-Kishner reduction showed low conversion to the hydrazone intermediate (7%); the process was not further optimised due to alternative reducing conditions proving more promising. Reduction by various borohydrides proved superior. Cyanoborohydride in AcOH has shown to effectively reduce carbonyl groups adjacent to barbituric acid moieties,[201] utilising the same reaction conditions initially met little success as displayed in Table 2.2. Due to poor conversion and the evolution of HCN gas as a by-product, sodium triacetoxyborohydride and sodium borohydride were explored as alternative reductants, using decanoyl chloride as a model substrate.

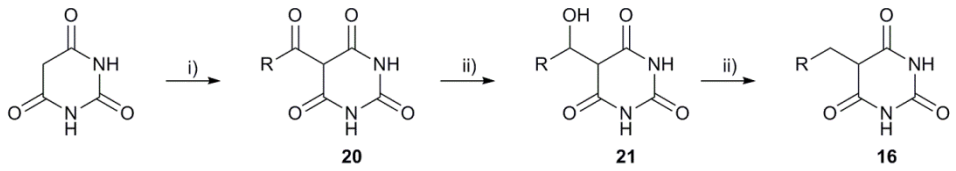

Scheme 2.8. Acylation and subsequent reduction of barbituric acid, R = C_9H_{19}. i) decanoyl chloride, Py, 98% ii) $NaBH(OAc)_3$, THF, 57%.

Use of sodium borohydride in the majority of cases completely converted the starting material to hydroxyl intermediate (**21**) or alkyl product (**16**). As anticipated, increasing the molar eq. of the borohydride resulted in a greater conversion to **16** (see entry 1 *vs.* 2). Batchwise addition of borohydride led to a slight improvement upon conversion (entry 8 *vs.* 1), which was attributed to quenching of $NaBH_4$ by H_2O produced by elimination from the hydroxyl intermediate (**21**). Replenishing $NaBH_4$ through batchwise addition ensured active reducing agent was always present, resulting in a higher conversion. It was theorised that additives that remove H_2O generated by elimination from **21** would drive the reaction to completion. However, the use of 3 Å M.S and Ac_2O within the reaction medium showed no improvement in conversion to **16** (entry 10 *vs.* 8 and entry 2 *vs.* 7). Quantitative conversion was obtained by employing a 4 fold excess of $NaBH(OAc)_3$ added batchwise (entry 11).

Table 2.2. Conditions and conversions to form product **16** or **21**, unless otherwise denoted, reactions were performed at 80 °C.

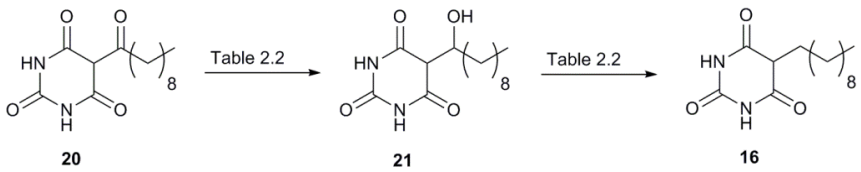

20 **21** **16**

Entry	Reductant (mol eq.)	Additive	Solvent	Addition	% Conversion[a]		
					20	**21**	**16**
1	$NaBH_4$ (5)	-	AcOH	One shot	0	52	48
2	$NaBH_4$ (2.5)	-	AcOH	One shot	0	68	32
3	$NaBH(OAc)_3$ (4)	-	AcOH	One shot	92	0	8
4	$NaBCN(OAc)_3$ (2.5)	-	AcOH	One shot	0	61	39
5	$NaBH(OAc)_3$ (8)	3 Å M.S	AcOH	One shot	75	0	25
6	$NaBH(OAc)_3$ (4)	-	DCE	One shot	5	43	52
7	$NaBH_4$ (2.5)	Ac_2O	AcOH	One shot	62	14	24
8	$NaBH_4$ (5)	-	AcOH	Batchwise[c]	0	39	61
9	$NaBH_4$ (5)	-	AcOH	Dropwise	0	79	21
10	$NaBH_4$ (5)	3 Å M.S	AcOH	Batchwise[c]	0	58	42
11[b]	$NaBH(OAc)_3$ (4)	-	THF	Batchwise[c]	0	0	100
12	$NaBH(OAc)_3$ (4)	-	THF	Batchwise[c]	0	0	100

[a]Conversions determined from the crude ^{1}H NMR spectrum. [b]Reaction performed at room temperature. [C]Additions of 1 eq. every 10 minutes until total eq. added.

The route optimised for the synthesis of **16** was next applied to the synthesis of BAR lipid (**2**). To that end, the pegylated barbiturate (**23**) was first synthesised as outlined in Scheme 2.9. A direct acid precursor (**25**) to BAR lipid was not initially used, as the amide functionality would be susceptible to immonium by-product formation during production of the acid chloride functionality by oxalyl chloride. Compound **23** was chosen as a desirable intermediate as the benzyl ester moiety should be stable to acid chloride formation. The subsequent debenzylation and amide formation steps were expected to proceed cleanly with minimal by-products. Oxidation of **5** using easily separable by-products was sought due to the high polarity of the resulting acid (**22**), complicating purification by chromatography. Initially, oxidation of alcohol **5** was attempted using TEMPO and diacetoxyiodobenzene in MeCN/ H_2O according to literature procedures.[202] A near equimolar mixture of aldehyde

intermediate and starting alcohol was obtained; the poor conversion was attributed to low solubility of the substrate in the solvent mixture. Performing the reaction in a vigorously stirred DCM/ H_2O mixture overnight produced the desired acid (**22**). Separation was relatively simple, a basic aqueous wash removed AcOH whilst application of high vacuum was sufficient to remove iodobenzene by-product, leaving behind non-volatile, pure acid (**22**) in 82% yield. A biphasic mixture was found to be necessary; performing the reaction solely in DCM resulted in a diminished conversion of 61% after 2 days, excess H_2O was required drive equilibrium to form the hydrate, enabling further oxidation.[203] Acid **22** was converted to the corresponding acid chloride quantitatively which was immediately added to a suspension of barbituric acid in pyridine. A conversion of 85% with the remainder being starting material (**22**), the incomplete conversion complicated recrystallisation. Uncharacteristically of alkylated barbituates, the product was found to be soluble in MeOH at room temperature typically used for recrystallisation. The improved MeOH solubility may be due to contaminant (**22**) acting as a co-solvent. Cold recrystallization from MeOH at -20 °C successfully obtained the desired product (**23**) in 49% yield.

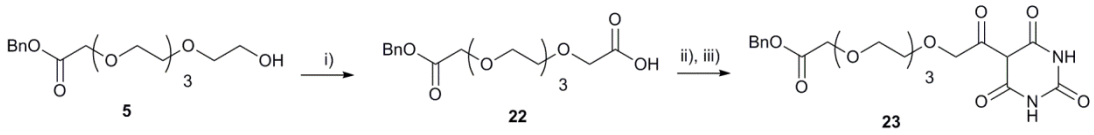

Scheme 2.9. Scheme showing the synthesis of alkylated barbituric acid. i) TEMPO, $PhI(OAc)_2$, DCM/H_2O, 82%. ii) $(COCl)_2$, DCM, v) Barbituric acid, pyridine, 49% (two steps).

Early attempts to reduce **23** using $NaBH(OAc)_3$ were frustrated, producing a mix of intermediate alcohol and desired alkyl product (35:65) even after 40 hours of subjecting the substrate (**23**) to multiple cycles of borohydride reduction. Direct displacement of the benzyl moiety to form the desired amide was also attempted by stirring **23** and dioctadecyalamine in DCM for 1 week. No amide was formed with imine exclusively produced instead. Pd/C catalysed reductions were also attempted, leading to elimination of the benzyl protecting group as anticipated. At least three other by-products were also formed indicated by the abundance of peaks in the 4.20 ppm region of the spectrum, where a singlet was expected.

The by-products could not be identified with high confidence although it was likely that the carbonyl moiety was at least partially reduced.

An alternative devised route, displayed in Scheme 2.10 would be direct acylation of barbituric acid by a direct acid precursor (**25**) already containing the amide functionality. Direct precursor (**25**) was produced by amidation of **22** *via* the acid chloride to produce **24** in 60% yield. Compound **24** was then debenzylated in 95% yield producing the direct acid precursor (**25**), which can be used to acylate barbituric acid, producing **26**. An obstacle to this approach would be production of immonium ion upon exposure of the amide to oxalyl chloride. Therefore, an alternative amide bond forming methodology was investigated. A model compound of decanoic acid was used to test whether it was feasible to acylate barbituric acid without progressing through an acid chloride intermediate. Production of 5-decanoyl barbitruic acid *via* the succinimide ester was first attempted. The succinimide ester was synthesised but proved too stable and did not react further with weakly nucleophilic barbituric acid. Condensation of barbituric acid and decanoic acid *via* a carbodiimide intermediate proceeded with 50% conversion. The desired product was obtained *via* recrystallisation from MeOH in 20% yield. Efforts to repeat the procedure with compound **25** resulted in a similar conversion, with isolation not being achievable and therefore, other avenues to produce BAR lipid were explored.

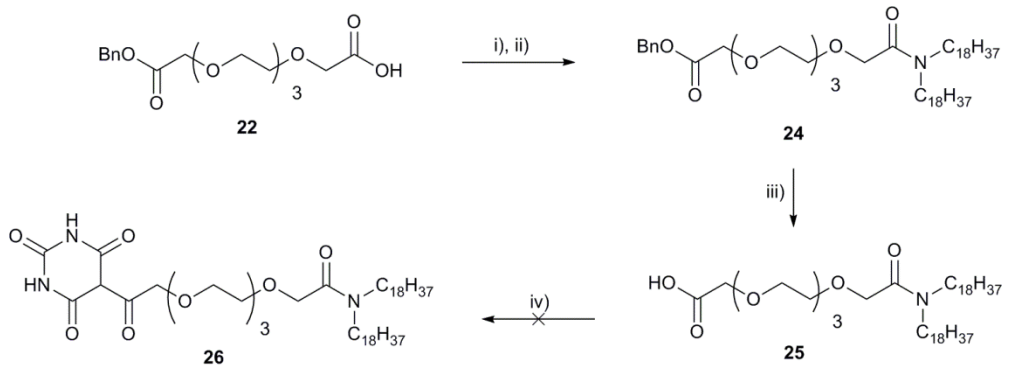

Scheme 2.10. Attempted synthesis of BAR lipid analogue (**26**). i) ($COCl_2$), DCM. ii) $NH[(CH_2)_{17}CH_3]_2$, DCM, 60%. iii) Pd/C, H_2, DCE, 95%. iv) NHS, DMAP, DIC, barbituric acid, Py, (product not isolated).

2.2.4. Route D: Knoevenagel condensation and reduction to produce 5-alkylated barbitruic acid

A possible alternative for the production of alklyated barbituric acid was by Knoevenagel condensation, involving condensation between 6-aminouracil or barbituric acid with various aldehydes having been reported, most recently for a green process using 6-aminouracil and $FeCl_3$ in H_2O (Scheme 2.11).[204] Replication of literature conditions showed no reaction, even when using a more H_2O soluble aldehyde, propionaldehyde. Refluxing for a longer period of time (16 hours) than previously reported in the literature (1 hour) also had no effect. It was unclear why the reaction did not proceed as previously reported. Knoevenagel condensations between aromatic aldehydes and barbituric acid have been shown to proceed with high yields, whilst aliphatic aldehydes have been reported to produce low yields for condensations performed in MeOH.[205] Initially, barbituric acid was stirred in excess neat decanal over several days; the large excess of aldehyde was anticipated to help drive the equilibrium toward product formation. Excess decanal was removed by Kugelrohr distillation, a gelatinous mixture was recovered with no product observed by ^{1}H NMR spectroscopy, interestingly a new pure crystalline form of decanoic acid was recovered from the distillate, confirmed by ^{1}H NMR spectroscopy and X-ray diffraction. Oxidation was favoured to condensation.

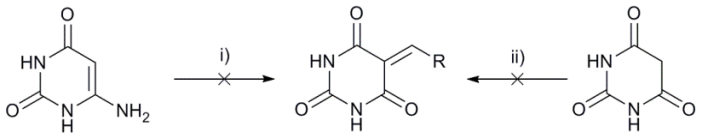

Scheme 2.11. Attempts to synthesise 5-akyl barbitruic acid from 6-aminouracil and barbituric acid. R = C_2H_5 or C_9H_{19}. i) RCHO, $FeCl_3$, H_2O. ii) RHCO, MeOH.

2.2.5. Route E: One pot Knoevenagel condensation and reduction to form 5-alkyl barbituric acid

Conditions for condensation solely between aliphatic aldehydes and barbituric acid were not found; an additive was required to drive the equilibrium promoting product

formation. A further attempt to condense decanal and barbituric acid was performed in boiling MeOH (to aid solubilisation of barbituric acid), in the presence of 3 Å M.S to drive the equilibrium by removing H_2O from the mixture. Unfortunately, the hemiacetal product was exclusively observed after 16 hours. Further work by Jursic and Neumann has shown that by addition of Pd/C, thereby performing Knoevenagel condensation and reduction in one-pot has generated yields > 80% for aliphatic substrates.[193] Repetition of the literature procedure with decanal in MeOH was shown to produce a mixture of products, with only 18% conversion to 5-decylbarbituric acid (by ^{1}H NMR spectroscopy). Replacement of the solvent to dichloroethane (DCE), a non-nucleophilic solvent that would more readily solvate lipophilic compounds was found to return a complex crude mixture with a 25% conversion to product. Addition of NEt_3 to the reaction mixture was found to produce the desired 5-decylbarbituric acid which could be recrystallised in a yield of 32% as shown in Scheme 2.12.

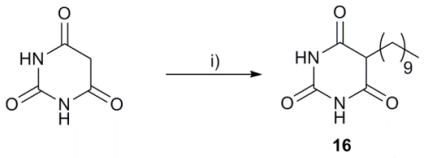

16

Scheme 2.12. *In situ* acylation and reduction of barbituric acid by decanal to produce **16**. i) Decanal, NEt_3, DCE, Pd/C, H_2, 32%.

In order to apply this methodology to obtain BAR lipid (**2**) aldehyde (**30**) was first synthesised as seen in Scheme 2.13. Alcohol (**5**) was silylated smoothly in 95% yield, debenzylation using Pd/C under a hydrogen atmosphere proved more challenging. Hydrogenation performed in DCE resulted in complete debenzylation, however partial desilylation (25%) was also observed by ^{1}H NMR spectroscopy. Although generally considered tolerant to Pd catalysed hydrogenation, catalytic cleavage of TBDMS groups has been reported in MeOH.[206] Evidence has suggested that catalytic TBDMS ether cleavage may be solvent dependent. Debenzylation with limited loss of TBDMS by catalytic hydrogenation in MeCN or EtOAc has been demonstrated.[207] Repeating the hydrogenation using MeCN as solvent exclusively produced **27**. Only debenzylation was promoted, with no

desilylation observed. The reason for this solvent selectivity is still unknown; although the ethylammonium salt was obtained indicating reduction of MeCN also occurs to a reasonable extent. Reduction presumably occurred at a rate intermediate to debenzylation and desilylation, with Pd catalyst being mildly poisoned either by MeCN or ethylamine by-product. This possibility was not entertained in the original publication; no ethylamine was observed due to its volatility and in a later publication when a similar selective benzyl deprotection was attempted, EtOAc was used as the solvent.[208] The resultant triethylammonium salt was acidified to produce the free acid in quantitative yield.

Initially amide formation was attempted through an acid chloride intermediate. Production of the desired acid chloride was not possible, with TBDMS cleavage observed due to acidic oxalic acid and HCl produced, even in the presence of an excess of DIPEA. The major by-product formed was believed to be carbonate, produced by the desilylated alcohol reacting with oxalic acid forming an oxalylic ester which was hydrolysed upon work up. Amide formation under neutral conditions was pursued and use of succinimide and carbodimide coupling agents led to formation of amide (**29**) in 72% yield. Desilylation through HCl solution in dioxane furnished the desired alcohol (**30**) in 96% yield.

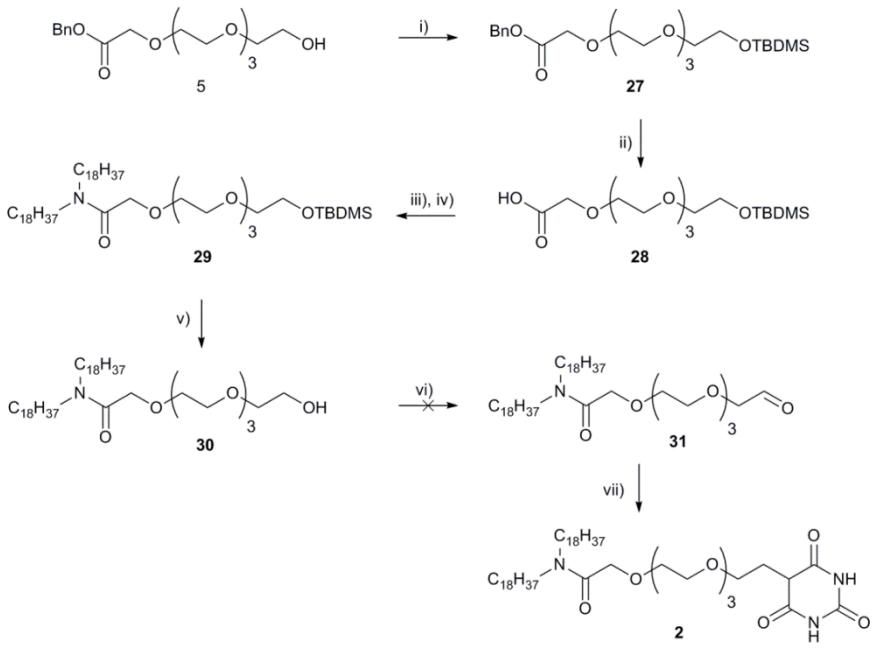

Scheme 2.13. Attempted synthetic route to BAR lipid by one-pot Knoevenagel condensation and reduction. i) TBDMS-Cl, NMI, I_2, THF, 95%. ii) Pd/C, H_2, MeCN, 94%. iii) NHS, DIC, DMAP, DCM. iv) $NH[(CH_2)_{17}CH_3]_2$, DCM, 72% (two steps), v) HCl, dioxane, 93%. vi) DMP, DCM, product not isolated. vii) barbituric acid, NEt_3, Pd/C, H_2, DCE, product not isolated.

Oxidation of alcohol (**30**) was carried out under Dess-Martin conditions using 2.5 eq. of Dess-Martin periodinane (DMP) and after 4 hours, 47% conversion to aldehyde (**31**) was observed. Although there was complete consumption of the starting material, a decrease in conversion to **31** was observed over time. The only new peaks which were not attributed to the product, DMP by-product or trace impurities of the previous step were broad singlets in the 4.2 ppm region, possibly indicating that a second oxidation process was occurring at a site relatively close to the amide functionality. Oxidation of the amide α position forming an imide has been previously reported for the use of DMP with secondary amides.[209] This reaction may be occurring to some extent with the tertiary amide, explaining the additional peaks at 4.2 ppm in the ^{1}H NMR spectrum. The amount of DMP was reduced to 1.2 eq. and monitored over time, conversion to **30** dropped from 63% after 25 minutes to 54% after 1 hour; in both cases starting material was still observed. To ensure that an impurity of the previous step was not responsible for the poor conversion to **31**, alcohol (**30**) was purified by column chromatography, followed by oxidation under Dess-Martin conditions; conversions

were comparable to oxidation on the unpurified alcohol. With oxidation proving more challenging than anticipated, TEMPO based oxidations were carried out. Alcohol (**30**) was stirred with TEMPO/ $PhI(OAc)_2$ under anhydrous conditions to prevent over oxidation producing the acid derivative. After stirring for 16 hours under the aforementioned conditions, a conversion of 48% was observed with the bulk of the remaining material being unreacted **30**. Further equivalents of TEMPO and $PhIOAc_2$ were added and allowed to stir for a further 6 hours, the remaining starting material was consumed but the conversion to desired aldehyde dropped to 29%. Use of a TEMPO/ Cu(I) system resulted in a conversion of 39% with complete consumption of starting material. Due to inability to purify crude aldehyde, a crude mixture containing 39% of **31** was condensed with barbituric acid under catalytic hydrogenation conditions. Only trace product was detected by ^{1}H NMR spectroscopy, the bulk of the mixture containing the starting alcohol (**30**). No aldehyde was observed in the mixture, it was unclear how this material was consumed, as there were not additional major signals which could not be assigned to either **30** or by-products of oxidation.

Difficulty in fully oxidising **30** to the corresponding aldehyde, led to an alternative method being sought as shown in Scheme 2.14. The principle of this new route was to produce the aldehyde moiety early in the reaction sequence and protect it, allowing purification. Compound **5** was oxidised under Swern conditions, the crude material was worked up and refluxed with ethylene glycol in the presence of TsOH and 4 Å M.S producing **32** in 31% yield over two steps. Dioxalane (**32**) was debenzylated in 94% yield with no deprotection of the acid sensitive dioxalane moiety being observed. Unfortunately, amide formation *via* the succinimide/carbodimide esters unexpectedly did not proceed cleanly. There was indication by ^{1}H NMR spectroscopy that ca 50% conversion was achieved when repeating the reaction twice with the same sample. The reason for the reaction preceding well to produce **29**, possessing a TBDMS ether but not for **34** containing a dioxalane group on the opposing terminus, was unclear. A possible explanation is the

hydrophilicity of the dioxalane was greater than that of the silyl ether, retaining H_2O more readily and poisoning the carbodimide reagent.

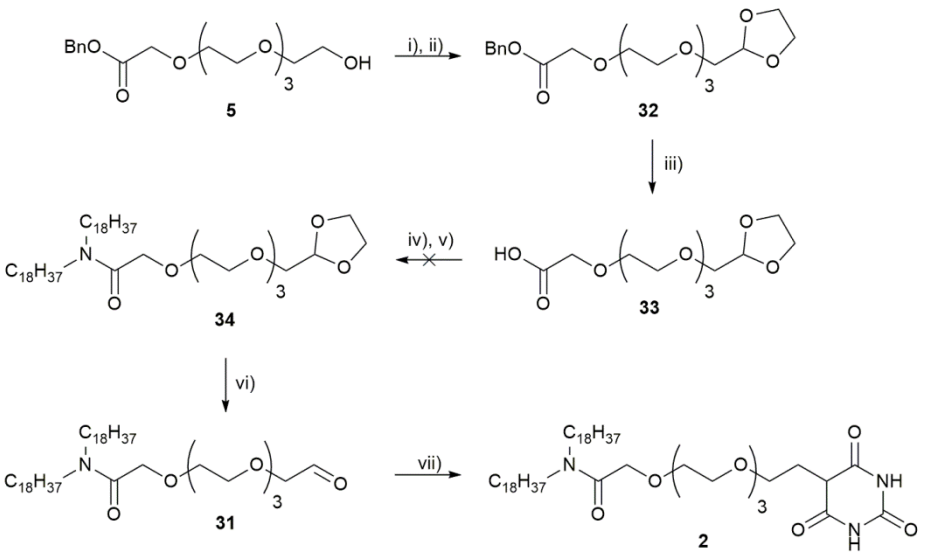

Scheme 2.14. Alternative synthetic pathway to production of BAR lipid (**2**). i) $(COCl)_2$, DMSO, DIPEA. ii) Ethylene glycol, 4 Å M.S., TsOH, toluene, 31% (two steps). iii) Pd/C, H_2, MeCN, 94%. iv) NHS, DIC, DMAP, DCM. v) $NH[(CH_2)_{17}CH_3]_2$, DCM. vi) HCl, dioxane. vii) Barbituric acid, Pd/C, H_2, NEt_3, DCE.

Time constraints prevented further investigation of the route outlined in Scheme 2.14. Synthesis of a test substrate (**16**) indicates that one pot Knoevenagel condensation and reduction would have a reasonable chance of returning BAR lipid (**2**); however, the unsuccessful synthesis the aldehyde precursor (**31**) rendered Route E unsuitable for the production of BAR lipid at this time.

2.3. Conclusion

TAP lipid (**1**) was synthesised by conventional means of condensation between guandinium carbonate and malononitrile with relative ease. The analogous Fischer condensation of an alkylated malonate ester and urea to produce BAR lipid (**2**) proved much more complex. A mixture containing the desired product and two decarboxylation by-products were obtained. Separation by literature procedures was not achievable. HPLC-MS was performed, achieving resolution and confirming the synthesis of **2** by accurate mass.

Conditions allowing full separation of **2** from the crude mixture are reported. Although an analogous preparative scale column was not readily available, prohibiting separation of the mixture by the author, conditions are detailed to enable future researchers with the appropriate apparatus to do so.

Problems associated with conventional Fischer synthesis, resulted in alternative methods being investigated. Direct alkylation of barbiturate salts by aliphatic iodides did not proceed at ambient temperature with complex mixtures obtained at elevated temperatures. Acylation followed by reduction proved to work well for a model substrate (5-decylbarbituric acid). Adaptation to produce BAR lipid (**2**) was troublesome, due to the inability to form a direct precursor to BAR lipid. The acid chloride derivative of compound **25** could not be produced owing to complications arising from the presence of the amide functionality. Alternatives to acylating barbituric acid using acid (**25**) and carbodimide coupling reagents did not proceed. Although a babrituric acid functionalised by a glycol linker (**26**) was produced, the opposing terminus was a benzyl ester and attempts to convert this functionality to the desired amide were again met with frustration.

Direct Knoevenagel condensation of barbituric acid and aliphatic aldehydes were found to not proceed directly, and an additive was required to drive equilibrium. Addition of Pd/C in a one pot condensation and reduction led to 5-decyl barbituric acid being synthesised, although a base was also found to be necessary to produce the desired product cleanly. Adaptation of the one pot Knoevenagel condensation/ reduction reaction to produce BAR lipid was unsuccessful due to an inability to produce the precursor aldehyde (**31**). Oxidation of alcohol (**30**) was found to not progress cleanly with the mixture being non-resolvable chromatographically and Knovevenagel condensation did not occur between the crude mixture and barbituric acid.

2.4. Future Work

2.4.1. Future syntheses

The priority would be continuation of the reaction sequence outlined in Scheme 2.14, looking at optimisation of the production of **34**, as subsequent acetal deprotection is expected to proceed well. Removal of H_2O would be the first concern, as well as trying alternative coupling reagents such as PyBOP. Alternative BAR lipid derivatives could also be synthesised and incorporated into vesicles to probe their ability to hemifuse. The amide functionality restricts acid chloride formation and reduction routes to produce aldehyde (**31**). Replacement of the amide functionality with a tertiary amine, may enable the production of alternative BAR lipids functionalised by a glycol spacer. From compound (**18**) two different potential alternative BAR lipids (**38** and **39**) could be synthesised as displayed in Scheme 2.15.

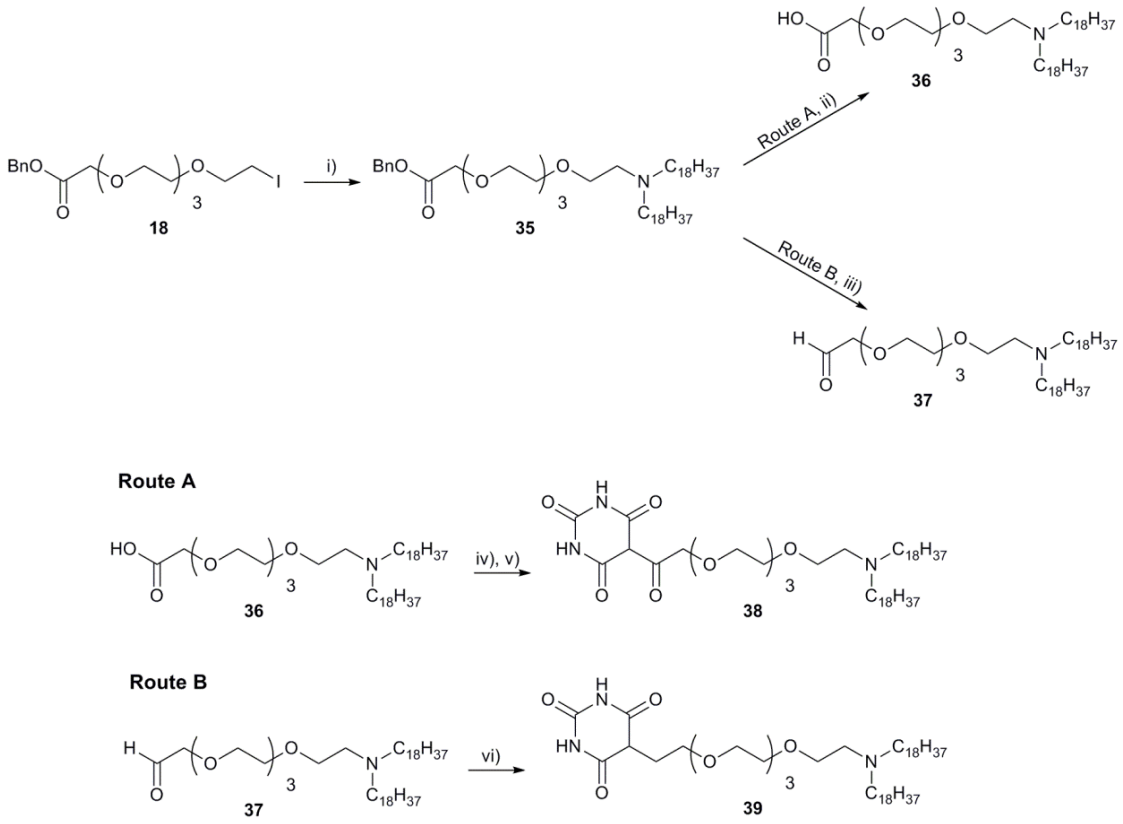

Scheme 2.15. Possible syntheses of alternative BAR lipids **38** and **39**. i) $NH[(CH2)_{17}CH_3]_2$, NEt_3, DCM. ii) Pd/C, H_2, DCE. iii) DIBAL, DCM. iv) $(COCl)_2$, DCM. v) Barbituric acid, Py. vi) Barbituric acid, Pd/C, H_2, NEt_3, DCE.

Compounds **36** and **37** are potentially simpler precursors to synthesise; **36** could be used to acylate barbituric acid producing **38**. It is uncertain how the conjugated carbonyl will contribute to the enol-keto tautomerism of the pyrimidine ring, if the enol form is more favoured than in BAR lipid (**2**), hemifusion with TAP incorporated vesicles may not proceed as anticipated, in which case **38** would have to undergo reduction. Compound **37** could undergo one pot Knoevenagel condensation and reduction to produce a BAR lipid analogue (**39**).

2.4.2. Hemifusion experiments

Upon synthesis of BAR lipid (**2**) or an analogue (**38** or **39**), the lipid could be incorporated into a vesicle containing 2 mol% NBD-PE and a simple gylcerophospholipid (such as POPC). TAP lipid could be incorporated into a separated population of vesicles containing 2 mol% Rh-PE (Glycero-3-phosphoethanolamine-N-(lissamine rhodamine B sulfonyl)) and a different simple lipid. These fluorescent lipids are a FRET pair, if a drop in the donor (NBD-PE) and an increase in acceptor (Rh-PE) fluorescence intensity is detected then a close association is known to occur, either fusion or hemifusion. Which process occurs could be detected in a second separate experiment by incorporating a fluorescing guest and quencher into the BAR and TAP vesicles internal aqueous compartments respectively, if no decrease in fluorescent intensity is observed, hemifusion would have taken place. Hemifusion may also be inferred by dynamic light scattering or by fluorescence microscopy so long as the size of the vesicles exceeds the optical detection limit.

If the vesicles are confirmed to hemifused, separation of the structures to form asymmetric liposomes will be attempted by the use of a competitive hydrogen bond inhibitor (free barbituric acid) or by physical forces such as vortexing. Alteration in the mol% of the complementary lipids in the vesicles could also be investigated. Separation of the two populations of vesicles could be carried out using flow cytometry or by centrifugation if the donor and acceptor vesicles are of differing sizes.

The degree of asymmetry and flip-flop will be monitored initially by observing the fluorescing intensity of NBD-PE. This could be performed by introducing a NBD-PE and BAR doped donor vesicle to a population of unlabelled TAP doped vesicles, incubation should result in NBD-PE doped TAP vesicle formation. The TAP vesicles could then be separated and the fluorescence measured. The intensity could be correlated to a calibration curve formed by measuring the intensity of different mol% of NBD-PE in vesicles of the same lipid composition as that initially used to determine degree of lipid transfer. The asymmetry could be determined by addition of a quencher, with the drop in intensity correlating to the amount of fluorescing lipid in the outer leaflet. Addition of a surfactant would then decrease the intensity to background levels, revealing the total incorporation of NBD-PE. Comparison of these values would indicate the degree of asymmetry obtained as described in Section 1.3.2 (Figure 1.4). The rate of flip-flop could be deduced in a similar manner by isolating the exchange NBD-PE TAP vesicles and monitoring the decrease of fluorescence over time, once a plateau is reached, surfactant addition would reveal the background intensity and the $t_{1/2}$ could be calculated.

Initially all the above experiments will be carried out on POPC vesicles doped with BAR or TAP lipids. Other liposome formulations will then be trialled in order to determine the effect of head group and acyl chain on the formation of the asymmetric vesicles. Mixtures of lipids would then be explored with incorporation of various amounts of cholesterol in POPC. The sizes of vesicles, temperature of exchange and mol% of recognition lipids are additional parameters which could be explored.

Alternative methods of detecting intervesicular transfer could also be investigated such as SFVS or Raman. Exchange between vesicles containing TAP and deuterated lipids with a SLB containing protonated lipids and BAR could also be explored. A decrease in the C-H band intensity of fatty acid chains in the SLB by Raman spectroscopy would be expected. Alternatively no signal would be observed by SFVS unless exchange occurred as the bilayer would be entirely composed of protonated lipids and would be symmetric.

Delivery of deuterated lipids to the external face would generate asymmetry and allow detection of transfer.

Chapter 3. A Combinatorial Approach Towards the Synthesis of Glycerophospholipids

3.1. Background and aims

3.1.1. Advantages and disadvantages of synthesis on a solid support

Solid phase synthesis, where organic transformations proceed on a substrate immobilised on a polymer resin prior to cleavage presents an attractive methodology for numerous reasons. Solid phase reactions are essentially one pot with isolation of intermediates achieved by simply washing with a range of solvents. This enables the synthesis of a large number of compounds quickly with no physical loss between steps as transfer and complex purifications are unnecessary.[210] Simple purification allows large excesses of reagents to be employed in order to drive each step to completion. Additionally once optimised, the same conditions can be employed to a number of substrates allowing a library to be produced with relative ease *via* a combinational approach.[211] Lipids which are anionic or zwitterionic can be difficult to handle due to their amphiphilic nature and limited solubility, immobilising these compounds on a solid support would mitigate these handling difficulties. Finally, safety concerns are reduced as hazardous intermediates are restricted to the solid phase.

Solid phase synthesis offers some excellent synthetic advantages, however there are also several drawbacks. Characterisation of intermediates is largely restricted; one option is cleavage from the resin followed by conventional analysis such as NMR spectroscopy, MS etc. This approach is time consuming and destructive, wasting potentially valuable material. This ‘cleave and analyse’ method may not be applicable to reaction sequences containing sensitive intermediates in which the cleavage conditions may alter the analyte liberated from the resin.[211] Another approach is solid state NMR (ssNMR) spectroscopy. Unlike solution phase NMR spectroscopy, ssNMR spectroscopy suffers from broad linewidths due to effects arising from homo and heteronuclear coupling as well as chemical shift anisotropy.[212] These effects are still present in solution phase NMR spectroscopy but are not observed. There is an orientational dependence on these effects that can be ignored in the solution phase due to

rapid motion of the nuclei in the sample, rendering the sample homogeneous on the NMR timescale. The analyte in ssNMR spectroscopy cannot relax *via* tumbling; anisotropic interactions that are usually averaged out are still observed, leading to broader peaks. Swelling the solvent to partially solvate the linker and significantly increasing the degree of rotational freedom in the 'gel phase method' can greatly reduce the broad line widths of the spectra.[213] Introducing artificial motions, namely rotating the sample around the magic angle of 54.74° relative to the external field magnetic field also reduces line broadening; spinning side bands may be present if the rate of rotation is less than the magnitude of broadening.[214] Within this thesis, ssNMR will be used to denote solid phase NMR in which the signal is spun about the magic angle. ^{1}H ssNMR spectra were recorded on samples in the gel phase whilst ^{31}P ssNMR spectra were recorded on solid (non-swollen) samples.

3.1.2. Methods of isolating or synthesising glycerophospholipids in the solution phase

Extraction of lipid requires that the desired lipid is synthesised *in vivo*, and is present in reasonable abundance within the tissue. The source of the lipid containing tissue must also be correctly stored and readily available as a prolonged storage period even at sub-zero temperatures can lead to degradation (oxidation) of sensitive components in the sample.[215] Phospholipids can be extracted from various natural sources, mainly animal or plant tissues. Typically, extraction methodologies are slight modifications of either the Bligh and Dyer,[216] or the Folch method.[217] In both methods the total lipid content was isolated by multiple homogenisation and filtration steps, as well as by phase separation. A biphasic mixture was achieved through the addition of a MeOH: $CHCl_3$ solution to the tissues aqueous phase. Slight modifications include the use of alternative solvents such as EtOAc, hexane or MEK.[218] These methods can be inefficient, when the Bligh and Dyer approach was used to extract lipid from various fillets of fishes over 100 g of tissue was required to recover between 0.50-7.85 g of total lipid.[216] These techniques have also been shown to be ineffective for recovery of certain lipid classes such as lysolipid.[219] These protocols are for

extraction of bulk lipid content, concerned with isolation of lipids from other cellular components, the lipid content was a wide distribution of lipid species. Isolation of individual lipid classes (defined phospholipid head groups) can be achieved by further separation using preparative TLC,[220] preparative HPLC,[221] solid phase extraction,[222] and supercritical CO_2,[223] usually a combination of techniques may be necessary for recovery of the desired lipid. Preparative LC techniques can be time consuming, and ineffective for separation of complex mixtures and have a higher possibility of polyunsaturated compound oxidation.[222] Solid phase extraction methodologies can also be ineffective at separating all lipid classes, with SM/PC and PS/PA proving difficult pairs to isolate.[224]

Although broad lipid classes (based on head group) can be isolated, purification to yield a specific glycerophospholipid containing a defined fatty acid is not trivial. Usually extraction methods are aimed at separation of broad classes of lipids, containing compounds with varied fatty acid chains.[225] There is variation in lipids extracted from different sources, necessitating in the need to use the same sources for comparable studies. For example, the source and exact composition of lipids can impact biological properties.[226]

Glycerophospholipids can also be produced synthetically; the most arduous step in gylcerophospholipid synthesis is production of the phosphate moiety, in the solution phase several approaches have been developed. Methods include direct phosphorylation,[227] use of a H-phosphonate and phosphoramidate intermediates.[228,229] Introduction of a phosphate moiety by use of a phosphoramidite intermediate, followed by oxidation and acid catalysed alcoholysis is reminiscent of work by Caruthers who utilised a similar approach to produce oligonucleotides on resin.[230] This methodology produces lipids in the range of 59-75% yield; additionally the dialkylphosphoramidate intermediates used are listed as schedule 2 under the chemical weapon convention.[231] Adsorbing these intermediates on the solid phase could increase yields and mitigate their potency.

3.1.3. Current solid phase syntheses of lipids

Solid phase synthesis is widely utilised for peptides[232-234] and nucleosides[235,236] and to a lesser extent saccharides.[237,238] Lipids are one of the few natural products for which solid phase methodologies are lacking. Few literature examples exist, revolving around the solid state synthesis of lipids bound to peptides[239] or polyamines[240,241] with these functionalised groups being responsible for binding to the resin. The former is *via* formation of a thioester composed of a fatty acid side chain bound to the cysteine residue of a peptide backbone. Whilst the latter is more relevant with regards to lipids, it is thus far targeted towards production of cationic lipids to be utilised in liposomes to carry genetic material. These structures are limited in scope, to the author's knowledge no methodology of glycerophospholipid synthesis on a polymer support currently exists. The closest example is perhaps provided by the polymer supported phosphorylation of carbohydrates.[242] A base labile β-ethoxythioester moiety was used to produce monophosphorylated sugars through a dialkoxychlorophosphine intermediate. In theory this methodology could be adapted to produce gyclerophospholipids, however, the methodology currently produces resin bound intermediates in low conversions, with several steps requiring harsh conditions (24 hour refluxes). Cleavage conditions require stirring with sodium methoxide for 24 hours, which would not be amenable to synthesis of glycerophospholipids due to transesterification of the fatty acid moieties.

A novel combinatorial approach to lipid synthesis was envisaged through the use of a β-hydroxysulfone linker, allowing rapid parallel syntheses, producing different lipid head and tail groups by way of a phosphoramidite intermediate as shown in Scheme 3.1.

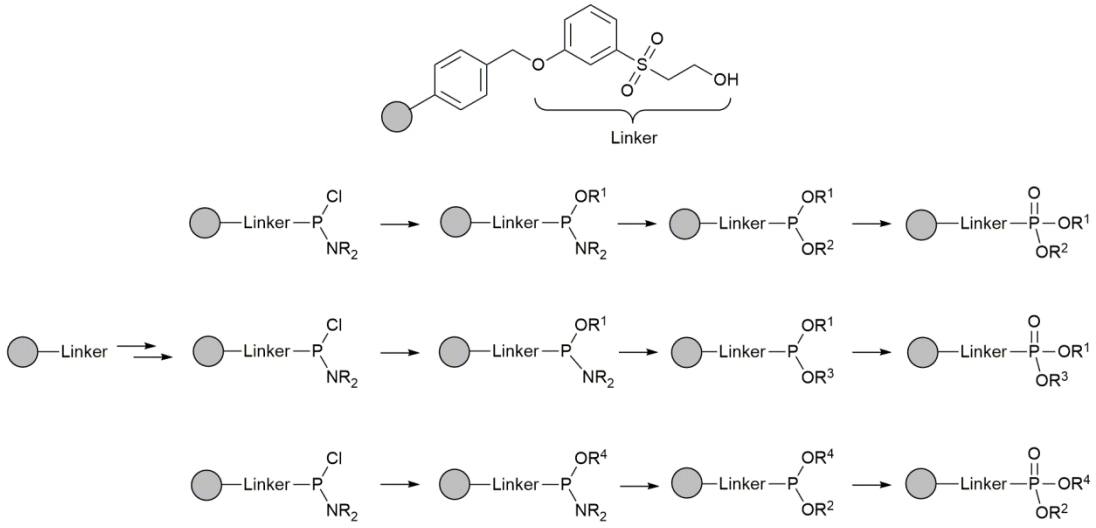

Scheme 3.1. Illustration of the combinatorial approach that potentially could be adopted in the solid phase synthesis of gylcerophospholipids.

The aims of the project were to;

- synthesise and bind the β-hydroxysulfone linker to a solid resin,
- use this resin to synthesise dialkyl phosphates on the solid state followed by cleavage,
- apply this methodology to produce a gylcerophospholipid,
- produce a penta-protected inositol building block that can be used in the polymer bound synthesis of phosphatidylinositol lipids.

3.1.4. Rationale for choice of resin and linker

The methodology revolves around the use of a β-hydroxysulfone linker shown in Figure 3.1, where application of a weak base results in elimination *via* a suspected E1cB mechanism. The cleavage mechanism is analogous to that employed in the solid phase synthesis of nucleotides, in which a β-cyanoethyl protecting group was cleaved by a weak base.[243-245] Similar β-hydroxysulfone linkers have been used in the production of peptides,[246] as well as a range of small molecules including cyclopentenones[247] and imidazopyridines.[248] Further examples are comprehensively detailed in a review by MacAllistar *et al*.[249] A similar sulfoxide linker has been utilised in the synthesis of aldehydes and alcohols, however, a

different deprotection mechanism was utilised with oxidation of a thioether to sulfoxide intermediate followed by cleavage *via* Pummerer rearrangement.[250]

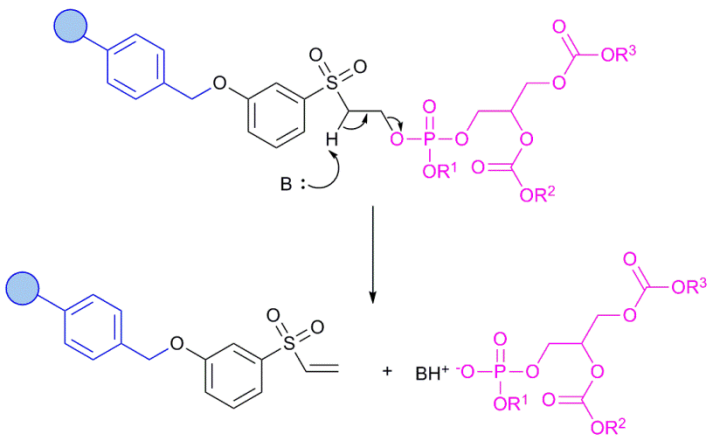

Figure 3.1. Structure and anticipated cleavage mechanism of a gyclerophospholid. The portion coloured blue is the polystyrene resin, black is the sulfone linker, whilst the magenta structure is the gyclerophospholipid to be cleaved. R^1 = hydrophilic head group e.g choline. R^2 and R^3 = fatty acid chains (may be the same or distinct).

The β-hydroxysulfone moiety was bound to the resin *via* a phenol ether moiety in the *meta* position. The β-hydroxysulfone and ether being *meta* to one another ensured that the ether had minimal electronic effects on the sulfone. If the E1cB cleavage mechanism proved undesirably fast, then the liability of the group could be reduced by moving the phenol linker to the *para* or *ortho* positions. The acidity of the sulfone α proton could be tuned by functionalisation of the ring. Incorporation of electron donating groups in the *ortho*/*para* positions could be used to reduce the acidity of the sulfone α-proton. There is also the possibility of performing all the desired transformations using a linker composed of a thioether precursor. The thioether could then be oxidised to the sulfone linker in a penultimate step, in a 'safety catch approach', followed by cleavage from the resin. In the case where the linker proved inert, the acidity of the α-proton could be increased by incorporation of electron withdrawing groups into the phenyl ring *meta* to the linker.

The resin chosen for these experiments was chloromethyl polystyrene (PSt) crosslinked by 2% divinyl benzene (DVB), the PSt/ DVB polymer is colloquially referred to as Merrifield resin, named for the pioneer of solid phase peptide synthesis.[234] Merrifield

resin was chosen due to its low cost, availability, chemical inertness and ability to swell under the envisaged reaction conditions. Although other resins such as PSt grafted by polyethylene glycol (Tentagel resin) swell better in a wider range of solvents,[251] the polyethylene glycol component will be more hydrophilic, making it more difficult to fully exclude H_2O from the resin, a problem with intermediates and reagents prone to hydrolysis. Tentagel resins are also more expensive with lower loadings. Low loadings are not as consequential in the synthesis of larger molecular weight structures (peptides), however for the synthesis of lower mass lipids and phosphoesters low loadings will require larger amounts of resin to return a reasonable quantity of product.

3.2. Results and discussion

3.2.1. Synthesis of β-hydroxysulfone linker

The sulfone linker (**43**) was synthesised in the solution phase, 3-hydroxybenzenethiol (**40**) was first synthesised in 85% yield. Interestingly, 3% of the recovered material was 3,3'-dithiobis-hydroxybenzene (**41**) confirmed by X-ray diffraction. Oxidation of **40** then furnished sulfone (**43**) as shown in Scheme 3.2.

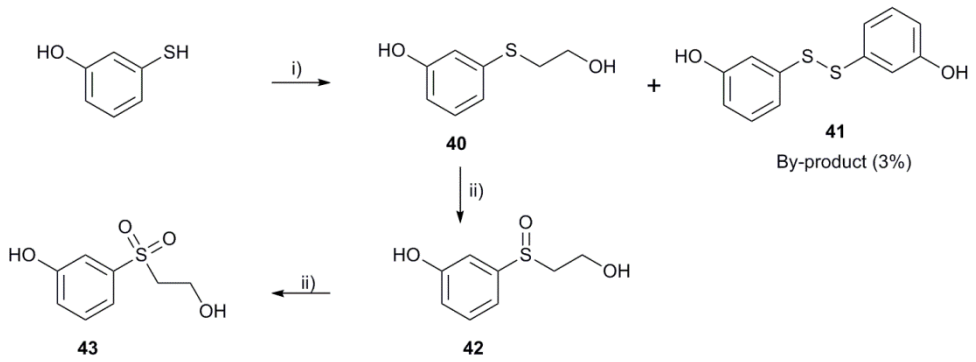

Scheme 3.2. Synthesis of sulfone linker. i) $BrCH_2CH_2OH$, NaOH, MeOH, 85%. ii) Oxone, MeOH, 89%.

Oxidation of thioether (**40**) was explored using three different conditions. The first attempt used trichlorotriazine (TCT) as the oxidant, a complex crude mixture was obtained, and isolation of the desired sulfone (**43**) was not achieved by column chromatography using silica or neutral alumina supports. The literature details a clean reaction in which only the

desired products obtained upon oxidation of various thioethers.[252] The literature cites one example of sulfone formation using a homologue of **40** with a phenyl *in lieu* of a phenol group. A possible side reaction was nucleophilic attack of the phenol moiety at the carbon centre of TCT in a S_NAr reaction.

The inability to obtain the desired sulfone led to exploration of a new methodology using H_2O_2 in acetic acid to form peracetic acid *in situ* which in turn oxidised **40**.[253] Initially, the reaction was performed for 1 hour with isolation of the sulfoxide intermediate (**42**) in 63% yield. No product was recovered due to the sulfones high affinity for the silica stationary phase precluding any product isolation. Allowing the reaction mixture to progress for 4 hours was also attempted with predominately sulfone being produced although the crude ^{1}H NMR spectrum showed the presence of sulfoxide and some other unidentified impurities. Despite formation of **43**, this route was discontinued due to emergence of unidentified by-products which were not possible to separate as the high polarity of **43** prohibited column chromatography.

Difficulty in purification again forced exploration for an alternative methodology. Stirring **40** with oxone in MeOH for 3 hours obtained a near quantitative conversion to **43**. Purification was simplified by the inorganic nature of the by-products, with filtration being sufficient to isolate **43** in 89% yield.

3.2.2. Functionalisation of Merrifield resin by sulfone linker

Production of resin bound sulfone linker (**44**) was achieved by Williams etherification of **43** and Merrifield resin. A range of conditions were examined to optimise the process, varying mild bases, solvents and additives as shown in Table 3.1. Systems used in the literature such as NaH in DMF were not employed due to the strong basicity of NaH.[250] Bases with pK_{aH} in the range 11-15 were trialled in order to promote chemeoselective etherification through the phenol moiety. This ensured that extra protection and deprotection steps could be forgone.

Table 3.1. Different conditions used for Williams etherification of sulfone (**43**) and Merrifield resin.

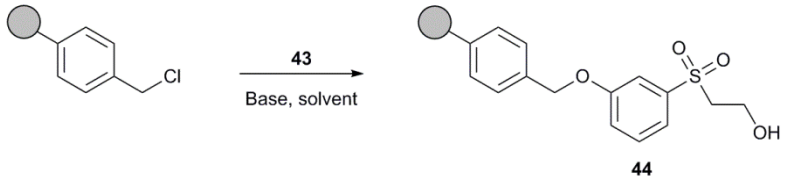

44

Entry	Base[a]	Additives[b]	Solvent	Reaction time (hours)	Temp (°C)	Conversion (%)
1	DIPEA	-	MeCN	16	25	0
2	DIPEA	-	MeCN	64	25	0
3	DIPEA	-	THF	20	25	0
4	K_2CO_3	-	DMF	40	25	7
5	K_2CO_3	NBu_4I	DMF	40	25	42
6	DIPEA	NBu_4I	DMF	40	25	8
7	DIPEA	NBu_4I	MeCN	40	25	0
8	DIPEA	NBu_4I	THF	40	25	0
9	K_2CO_3	NBu_4I	DMF	1	90	35
10	K_2CO_3	18-crown-6	DMF	40	25	32
11	K_2CO_3	NBu_4I	DMF	96	25	69
12	Cs_2CO_3	NBu_4I	DMF	40	25	77
13	Cs_2CO_3	NBu_4I	DMF	72	25	Quant. Con.
14	Cs_2CO_3	NBu_4I[c]	DMF	72	25	Quant. Con.

[a]Base unless stated otherwise was 5 molar equivalents relative to molar loading of resin. [b]Additives unless stated otherwise were in 1.1 molar equivalents relative to molar loading of resin. [c]NBu_4I for this entry was 0.3 molar equivalences relative to resin.

DIPEA was shown to be an ineffective base with no conversion in THF and MeCN (entries 1-3) even when the reaction was allowed to proceed for 64 hours. K_2CO_3 was employed, with the use of DMF to aid solvation of the base. The DMF/K_2CO_3 system produced a small improvement in conversion (7%), the addition of stoichiometric NBu_4I was found to dramatically increase conversion to 42% (entries 4 and 5 respectively). NBu_4I was believed to first react with the benzyl chloride moiety of the resin in a Finkelstein reaction, forming the more labile benzyl iodide, which subsequently underwent a Fisher etherification. It was believed that poor solubility of K_2CO_3 in DMF may limit conversion, to this end, phase transfer catalyst, 18-crown-6 ether was employed. The inclusion of the phase transfer catalyst did yield an improvement from 7 to 32% (entries 4 and 10

respectively), however, a greater benefit was observed when NBu_4I was used (entry 5). Frustratingly a conversion of only 69% was observed using NBu_4I, K_2CO_3 and DMF after 96 hours. Finally Cs_2CO_3 was probed as a base, due to its stronger basicity and higher solubility of cesium carboxylates in DMF,[254] quantitative conversion was obtained after 72 hours. Finally, it was determined that NBu_4I can be employed in a catalytic manner as 0.3 mol% was demonstrated to also yield quantitative conversion after 72 hours (entries 13 and 14) as shown by the ssNMR spectrum in Figure 3.2. Although 4 days appears impractical for a combinatorial approach, the resin could be prepared on a bulk multi-gram scale and stored for over a year at ambient temperature without degradation.

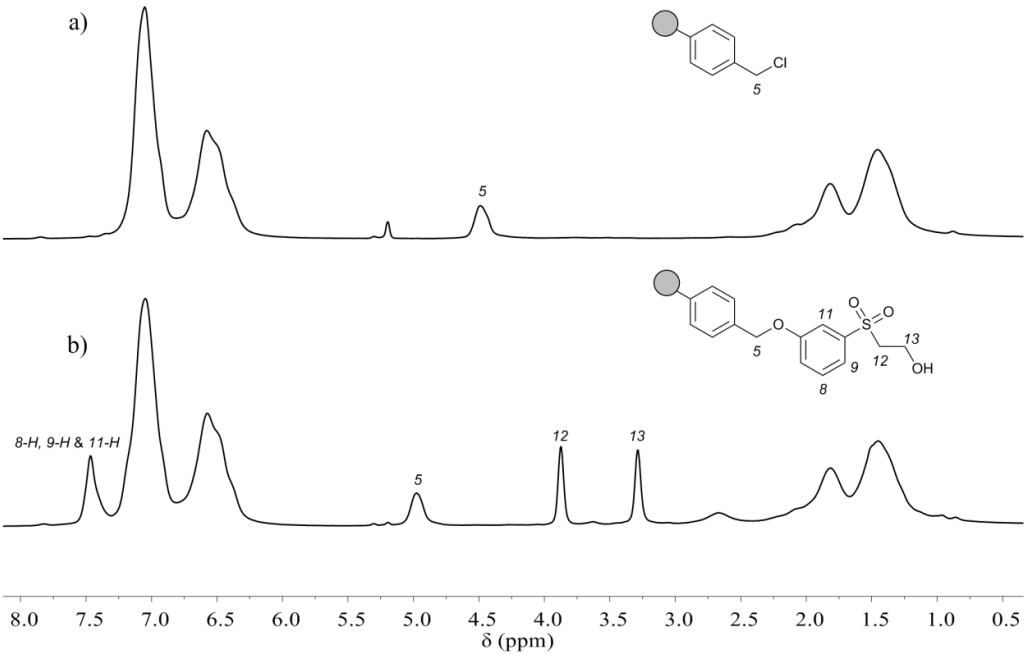

Figure 3.2. a) ^{1}H ssNMR spectrum showing unmodified Merrifield resin. b) The same resin after stirring for 4 days with **43** and Cs_2CO_3 in DMF to form resin bound sulfone linker (**44**). Comparison of the *5-H* signal, upfield shifted in compound **44** indicates complete conversion.

Following the synthesis of **44**, phosphorylation using $POCl_3$ and anhydrous DIPEA was explored. After 2 hours shaking in DCM, a resin was obtained deficient of a strong ^{31}P ssNMR signal and a modified ^{1}H ssNMR spectrum. The most likely side reactions are phosphorylation followed by E2 elimination producing alkene (**46**) or alternatively by an S_N2 reaction producing alkyl chloride (**47**) as depicted in Scheme 3.3.

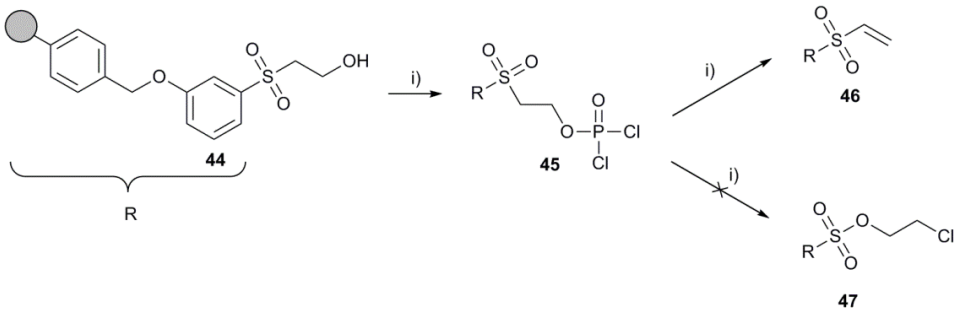

Scheme 3.3. Possible by-products of the phosphorylation of sulfone linked resin (**45**) by $POCl_3$. i) $POCl_3$, DIPEA, DCM.

The exact composition of the cleaved moiety was ambiguous with a complex solution phase ^{1}H NMR spectrum of the washings. The resultant resin bound structure was believed to consist of alkene (**46**) formed by elimination in an E1cB mechanism, this was corroborated by the appearance of a new signal at 6 ppm in a 1:2 ratio, relative to the benzylic CH_2 (signal *5-H*, Figure 3.3). Direct phosphorylation was found to not be applicable; however the cleavage mechanism from the resin was confirmed.

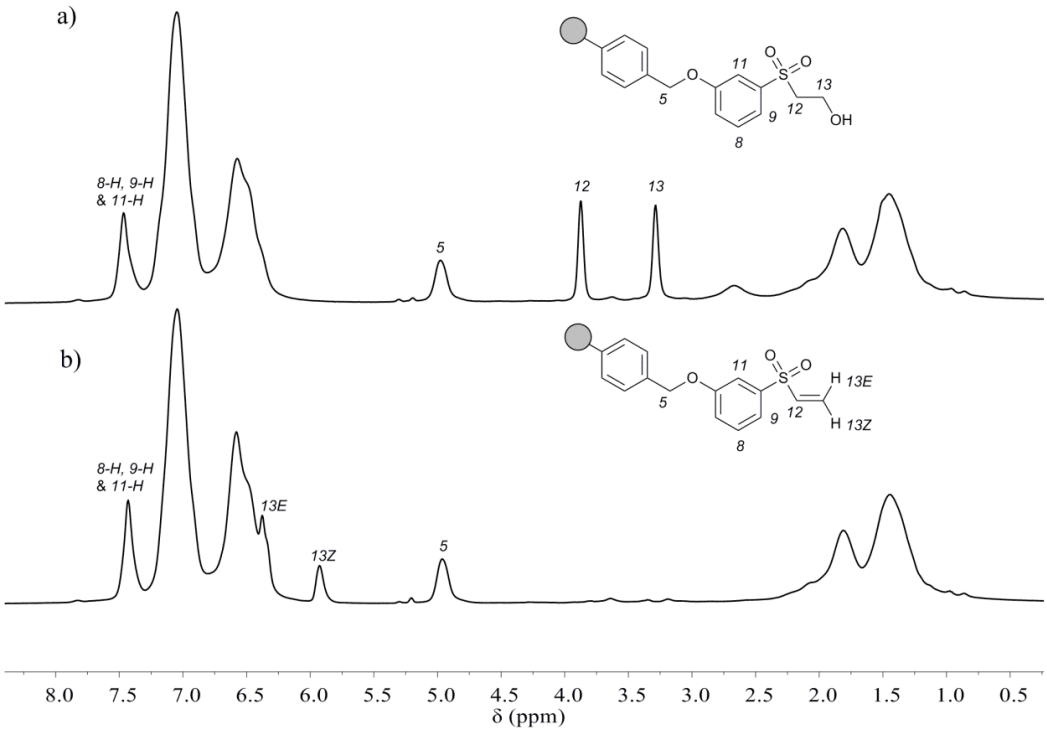

Figure 3.3. a) ^{1}H ssNMR spectrum showing resin bound sulfone (**44**) b) ^{1}H ssNMR spectrum of the same resin after being shaken overnight with $POCl_3$ and DIPEA in DCM, to produce resin bound alkene (**46**).

Although dehydration of similar β-hydroxysulfone moieties has been reported, the dehydrating agent was MsCl with the reaction occurring over 6 hours.[255] In order to further validate that elimination to produce **46** occurred, a solution phase analogue was produced as shown in Scheme 3.4. Thioether (**33**) was benzylated in 73% yield to obtain **48**, a simple solution phase mimic of **44**. The same conditions were used to benzylate **40** as those employed to bind the linker to Merrifield resin. The solution phase benzylation was found to be substantially faster, with complete conversion occurring within 16 hours in solution. Oxidation by oxone yielded the solution phase sulfone analogue (**49**) in 89% yield. Dehydration of the β-hydroxysulfone was achieved in 1 hour using $POCl_3$ and DIPEA producing alkene (**50**). Comparison of the solution and solid state NMR spectra of **50** and **46** respectively showed similarities, further supporting the argument for cleavage. Alkene (**50**) possesses a signal at 6.03 ppm corresponding to *13Z-H*, this correlates well to *13Z-H* at 6.02 ppm in the resin bound analogue (**46**). The other obvious signals for *13E-H* and *12-H* are at 6.44 and 6.65 ppm respectively which are buried beneath the PSt phenyl protons in compound (**46**), although it was likely that the shoulder at 6.47 ppm correlates to *13E-H* signal (E stereochemistry relative to *12-H*).

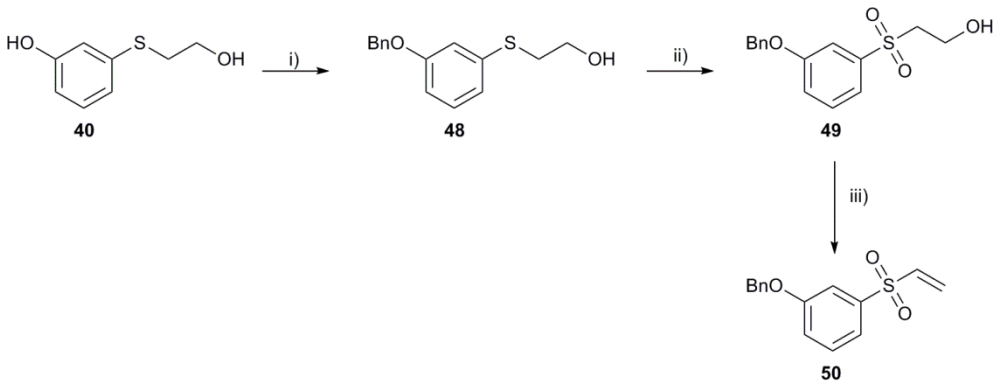

40 **48** **49** **50**

Scheme 3.4. Synthesis of a solution phase mimic of resin bound alkene produced by base catalysed elimination from a β-hydroxysulfone moiety. i) BnBr, Cs_2CO_3, DMF, 73%. ii) Oxone, MeOH, 89%. iii) $POCl_3$, DIPEA, DCM, 91%.

A small number of weak bases were considered, to determine if cleavage from the resin could be avoided, allowing direct phosphorylation as shown in Table 3.2. The control experiment of no base (entry 1) showed no elimination from the resin by ^{1}H ssNMR

spectroscopy and no signal in the ^{31}P ssNMR spectrum. NEt_3 and DIPEA were both shown to produce elimination product in the presence of $POCl_3$ (entries 2 and 3). The necessity of $POCl_3$ to convert the terminal alcohol to a more labile leaving group was demonstrated, NEt_3 alone was not sufficient to promote elimination from the resin (entry 5). It can be concluded by comparison of entries 1 and 5 that the resin was phosphorylated prior to elimination. The use of the weaker base, pyridine produced a more complex mixture, with partial elimination product observed (34%). There were trace peaks within the ^{1}H ssNMR spectrum which were not assigned to signals in compound **44** or **46**. The additional peaks can be observed within the aromatic region indicating addition of pyridine to the resin. It was unlikely that pyridine reacted with $POCl_3$ forming a pyridinium phosphate. Analogous solution phase compounds have been reported by ^{31}P NMR spectroscopy at -11.2 to -13.4 ppm,[256] although subsequent investigation indicates that these compounds are likely pyrophosphates which had been misidentified. Pyridinium phosphates are posited to exist but only transiently in amounts not detectable by spectroscopic means.[257] An alternative explanation was the elimination product was obtained, followed by partial addition of pyridine in a Michael reaction. The ^{31}P spectrum indicated a single peak at -0.2 ppm, this value was more consistent with trialkylphosphates.[258] The signal most likely corresponds to the resin bound dimethylphosphate, produced by the compound **5** reacting with MeOH during washing of the resin.

Table 3.2. Percentage of elimination product (**46**) produced by phosphorylation of **44** using various bases over 2 hours.

Entry	Base[a]	Additive[b]	Elimination Product[c] (%)
1	None	$POCl_3$	0
2	NEt_3	$POCl_3$	Quant.
3	DIPEA	$POCl_3$	Quant.
4	Pyridine	$POCl_3$	34
5	NEt_3	None	0

[a]all bases were used in a 5 molar eq. excess. [b]all additives were used in a 5 molar excess. [c]Percentage of elimination product determined from crude ^{1}H NMR spectrum.

3.2.3. Binding thioether linker to Merrifield resin

A more subtle approach to avoid base catalysed elimination from the linker was direct etherification of thioether (**40**) and Merrifield resin. The desired transformations such as phosphitylation and alcoholysis could then be carried out on the base stable linker. Oxidation on the solid support could then furnish a sulfone, which will undergo elimination under basic conditions producing the desired compound as demonstrated in Scheme 3.5. Merrifield resin was functionalised by **40** under the same conditions optimised for the etherification of **43**. It was rationalised that the phenolic moiety on the thioether and sulfone substrates should have comparable reactivity (acidity), due to the phenol being *meta* to these groups reducing the impact of the electronic effects. As expected, **40** was added to the Merrifield resin in quantitative yield after 4 days of shaking in anhydrous DMF. Curiously, reactions in the absence of NBu_4I gave comparable yields to reactions with NBu_4I, the reason for requiring NBu_4I to allow incorporation of the sulfone linker but not thioether was unknown. Again, although 4 days appears excessive for a combinatorial approach, thioether linked resin was also stable for > 1 year at ambient temperature with no oxidation of the thioether moiety observed.

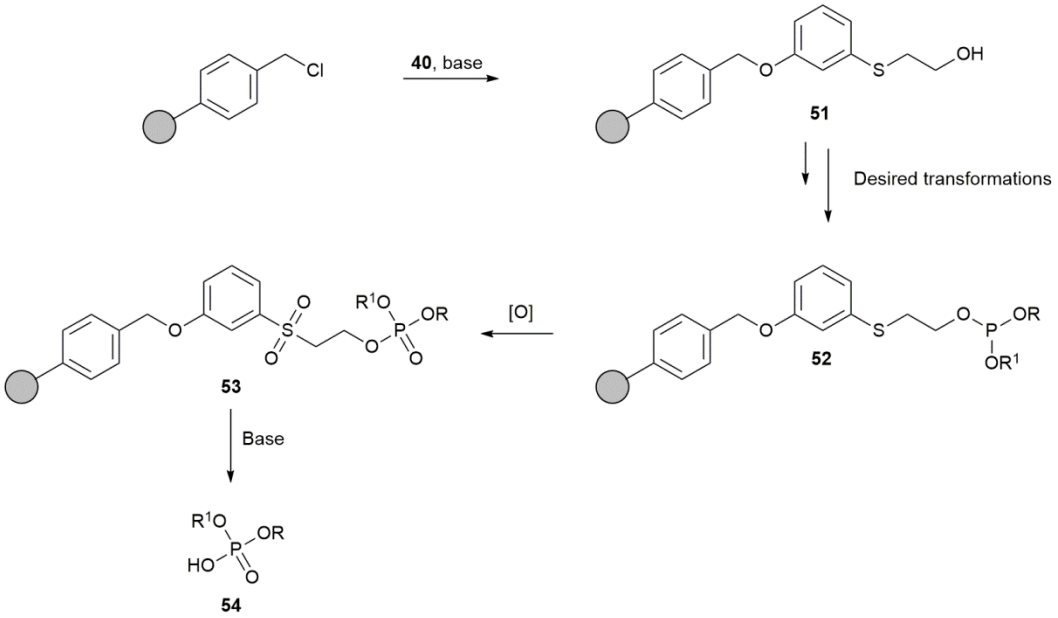

Scheme 3.5. A potential method for the solid phase production of gylcerophospholipids using a thioether linker. The linker could be activated towards basic elimination by oxidation of the linker to produce a β-hydroxysulfone moiety.

This 'safety catch' approach allows a wide range of harsh conditions to be applied to the system, followed by a transformation (oxidation) allowing cleavage under mild conditions. Several benefits are afforded, including greater flexibility in synthetic approaches to incorporation of a phosphate group. Phophitylation methodologies utilising P(III) reagents are now less cumbersome as an oxidation step was required to produce a sulfone moiety. Oxidation on the solid phase will result in simplified purification allowing a wider range of oxidants to be utilised. The thioether linker should have a higher base stability with cleavage not occurring until post oxidation, owing to the higher pK_a of the *α-H* of thioether (**40**) *vs*. sulfone (**43**).

In order for the safety catch methodology to be applicable, a suitable thioether oxidation strategy needed to be developed first. Oxidation of phosphite triesters during oligonucleotide synthesis is fairly routine in solid phase methodologies, with iodine: pyridine in a THF: H_2O mixture proving popular,[259,260] although other reagents such as peroxides and NBS-DMSO have been reported.[261-263] Oxidation of polymer supported

thioethers to sulfones favours mCPBA and oxone.[249] A range of oxidants were trialled as shown in Table 3.3 to determine the optimum conditions for production of the sulfone linker.

Table 3.3. Various oxidation conditions investigated for production of sulfone linked resin (**44**) from thioether linked resin (**51**)

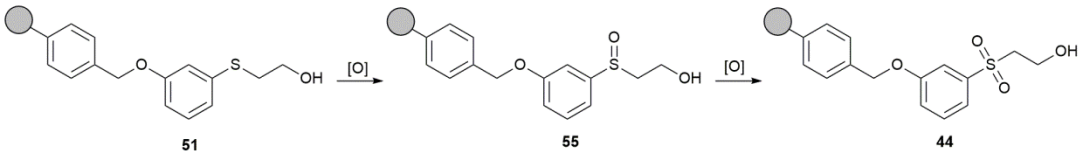

51 **55** **44**

Entry	Oxidant[a]	Solvent	Reaction time/ hours	% Conversion[b]		
				51	**55**	**44**
1	I_2	THF : H_2O (2:1)	16	69	31	0
2	$PhI(OAc)_2$	THF	16	89	11	0
3	I_2	THF : H_2O (2:1)	72	56	44	0
4	Oxone	MeOH	72	52	31	17
5	Oxone	DMF	72	0	0	100
6	mCPBA	DCM	16	0	0	100

[a]All oxidants used were 5 equiv. relevant to resin loading. [b]Conversion determined from crude ^1H ssNMR spectrum.

Iodine in THF/H_2O with added pyridine are standard conditions for oxidation of P(III) within solid phase nucleotide synthesis.[264] Similar conditions were first employed as seen in entry 1, although pyridine was omitted as partial elimination has been demonstrated in non-model systems (Table 3.2). Stirring for 16 hours was shown to produce low conversion and increasing the reaction time to 72 hours yielded no significant improvement. Oxone in MeOH was shown to effectively oxidise thioether (**40**) to the corresponding sulfone (**43**) in the solution phase. Employment of the same conditions for the solid phase produced only 17% of sulfone (**44**), with the bulk of the remaining material being unreacted thioether (**51**), whereas use of DMF as a solvent gave quantitative conversion. Merrifield resin has been shown to swell better in DMF than MeOH;[265] poor swelling rendered the bulk of the resin active sites within the matrix inaccessible to the oxidant. The optimum method appears to be oxidation by mCPBA in DCM which progressed quantitatively after 16 hours.

3.2.4. Phosphitylation of thioether resin

Addition of a fivefold excess of anhydrous NEt_3 and PCl_3 to the thioether linked resin (**51**) as shown in Scheme 3.6, was found to exclusively produce a compound containing a single peak in the ^{31}P ssNMR spectrum at 6.5 ppm, consistent with analogous solution phase P(V) dichlorides suggesting oxidation occured.[266] Exposure to oxygen could be either from the reaction or preparation of the sample for analysis. A possible source of oxygen could be during the DCM wash of the resin; however anhydrous DCM was obtained from distillation from CaH_2 under nitrogen atmosphere; it was ambiguous how oxidation of the sample during synthesis occurred. It was also possible that oxidation may have occurred at some stage during analysis despite storage of the sample under an argon atmosphere in a desiccator.

In order to investigate possible oxidation during synthesis, the sample was subjected directly to high vacuum in *lieu* of a washing step. The resin produced two major peaks in the ^{31}P ssNMR spectrum at 177.8 and 2.8/0.7 ppm (overlapping peaks) in a 1:6 ratio (14% conversion). The peak at 177.8 ppm was consistent with chemical shifts of compound **56** homologues in the solution phase,[267] whilst the latter broad peaks are more consistent with P(V) by-products which have been hydrolysed.[268] To further reduce the impact of moisture and oxygen on the system, a larger excess of base and PCl_3 (20 eq.) were used, ^{31}P ssNMR spectroscopy showed a mixture of products with a 25% conversion to product **56**. Residual PCl_3 was found to remain in the resin, therefore, washing with anhydrous DCM was found to be preferable for removal of excess reagents than by high vacuum. Replacing DCM for Et_2O was found to increase the conversion to 58 ± 8%. Repeating the ^{31}P ssNMR measurement with the sample at a later time was not reproducible. Obtaining P (III) or P (V) resin could not only be solely attributed to altering reaction conditions. Analysis of resin was not always immediate; times varied greatly depending upon demand upon the ssNMR service. Reasonable precautions were taken (storing under an argon atmosphere

atmosphere); however oxidation or hydrolysis during storage or preparation of analysis samples could not be ruled out.

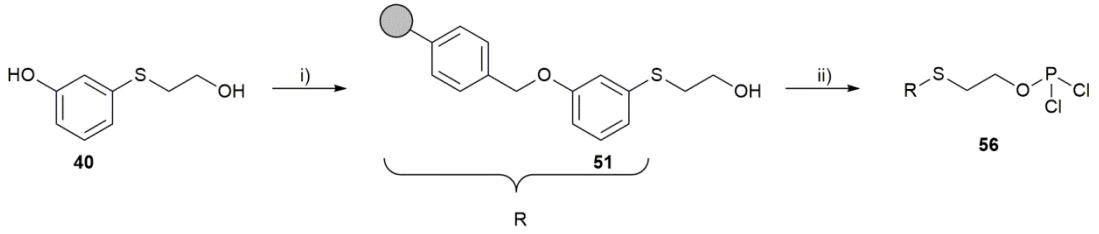

Scheme 3.6. Initial steps of a modified synthesis utilising a thioether linker.

3.2.4. Phosphorylation of thioether linker mimic

Inhomogeneity of the sample coupled with ambiguity surrounding the point of hydrolysis/ oxidation (reaction *vs.* analysis) led to two possible solutions. One possibility was to proceed with the reaction converting the resin bound phosphite dichloride moiety to a stable trialkyl phosphoester, however this would require a large degree of trial and error optimising reaction conditions. In order to determine appropriate conditions, a solution phase analogue was sought, where the reaction could be performed and analysed at each step with minimal exposure to H_2O. The use of solution phase analogues allow reaction times to be more closely approximated on the solid phase, in addition to obtaining NMR standards of intermediates for comparison to the polymer supported analogues.

Whilst direct phosphorylation of sulfone resin (**44**) was shown to lead to an elimination product (**46**), direct phosphorylation of the base stable thioether linked resin (**51**) was not explored. Phosphorylation of benzylated thioether (**48**) was attempted by $POCl_3$ followed by addition of excess decan-1-ol as shown in Scheme 3.7. A complex mixture was obtained containing dilauryl phosphate anhydride, tridecylphosphate as well as alkyl chloride (**59**) formed by S_N2 displacement of the phosphoester moiety by chloride anion liberated from formation of the phosphoester. A range of by-products were expected due to use of a large excess of PCl_3 and decan-1-ol, however formation of **59** was more troubling due to direct modification of the linker moiety. **59** was obtained in 40% yield; addition of Ag_2SO_4 proved ineffective at sequestering the chloride anion resulting in a comparable yield

of **59** obtained. Reduction of the reaction temperature to -78 °C was found to mitigate formation of **59**, however due to an abundance of peaks in the ^{31}P spectrum and a multitude of benzyl CH_2 peaks (ca. 5 ppm) in the ^{1}H NMR spectrum an alternative approach was adopted.

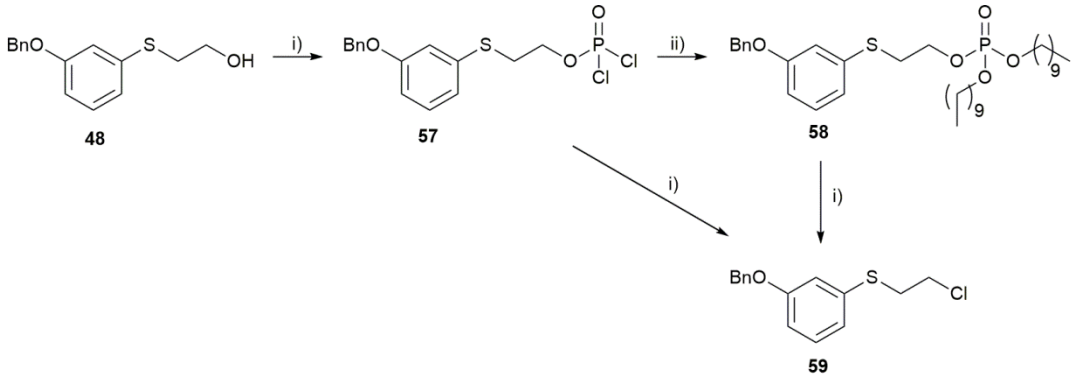

Scheme 3.7. Solution phase phosphorylation of thioether linker mimic (**48**) by $POCl_3$. i) $POCl_3$, DIPEA, DCM. ii) Decan-1-ol, DIPEA, DCM.

3.2.5. Solution phase NMR study of the phosphitylation of thioether linker analogue

Direct phosphorylation has been found to be incompatible with the linker, either producing an alkene in the presence of a sulfone linker where an E1cB mechanism is possible or an alkyl chloride in the presence of a thioether linker where an S_N2 mechanism dominates. Therefore, phosphorylation was abandoned in favour of phosphitylation, conversion to a phosphite triester followed by oxidation to produce a trialkyl phosphoester as seen in Scheme 3.8. The wide range of chemical shifts in ^{31}P NMR spectrum, absence of ^{31}P nuclei in conventional solvents and the reaction sequence occurring in one pot resulted in ^{31}P NMR spectroscopy being an attractive technique to monitor the progress of the reactions outlined in Scheme 3.8. The reaction sequence was performed in a Young's tap NMR tube sealed under an inert atmosphere, ensuring maximum exclusion of H_2O and air. Anhydrous and degassed protonated solvent was used, with a capillary containing D_2O added the tube to act as an external lock.

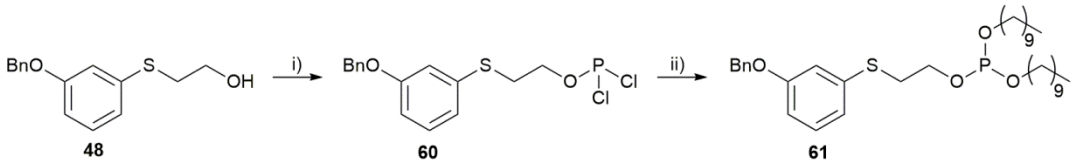

48 60 61

Scheme 3.8. Formation of thioether linker mimic bound didecyl phosphite (**61**). i) PCl_3, DIPEA, DCM. ii) decan-1-ol, DIPEA, DCM.

Addition of a fivefold excess of both PCl_3 and DIPEA to **48** in anhydrous ether was found to present two major peaks at 215.8 and 174.6 ppm indicating excess PCl_3 and **60** respectively with trace hydrolysis or oxidation products. Similarly when DCM or toluene were employed as solvent the same two peaks were observed in the ^{31}P NMR spectra, with spectra taken in 10 minute intervals for 10-80 minutes as displayed in Figure 3.4. Only two peaks were observed with constant integrations, the peaks at 215.8 and 174.6 ppm are indicative of excess starting material and product. There was no hydrolysis or oxidation product observed over 80 minutes and the reaction was complete prior to running the first measurement. This suggests that hydrolysis occurred during preparation of the sample for ssNMR and the conditions described above will yield only one phosphorous bearing moiety in the solid phase.

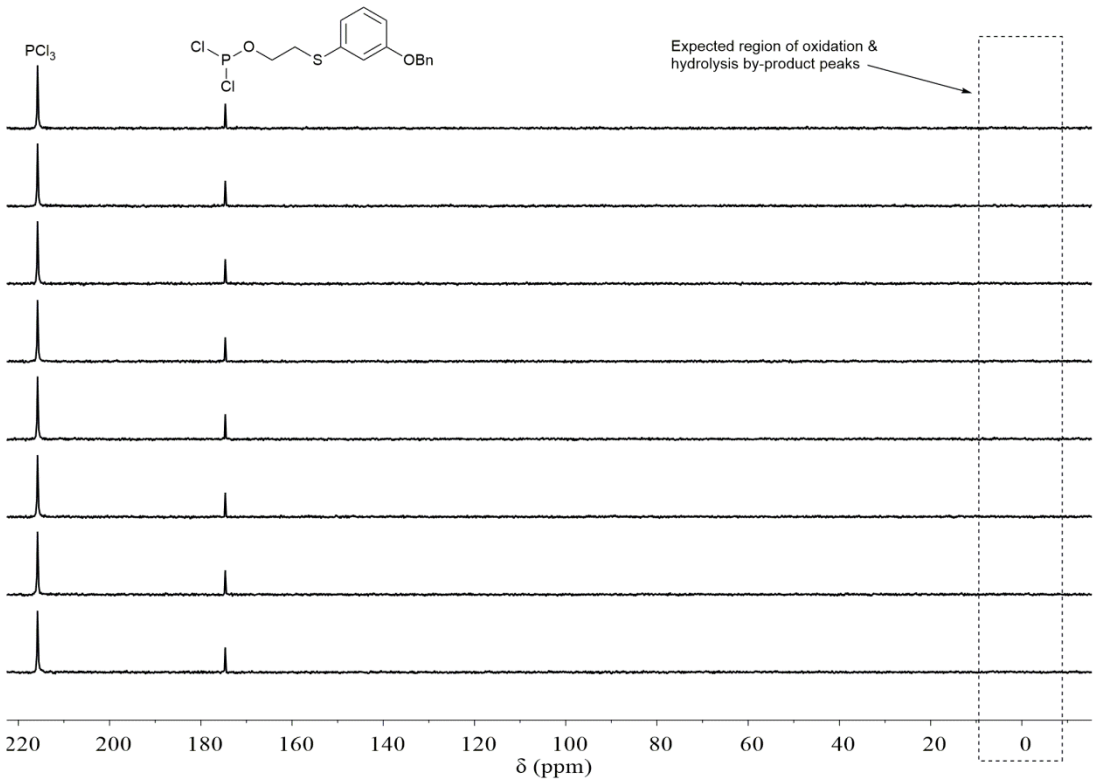

Figure 3.4. Plot showing the ^{31}P NMR spectrum of the reaction between compound **48** and PCl_3, no change was observed with no by-product formation detected over the course of the study. As the figure ascends time progresses from 10-80 minutes at 10 minute intervals.

A large excess of PCl_3 was required in order to prevent not only hydrolysis of the substrate but also to ensure only mono-substitution occurred. Using 1.3 eq. of PCl_3 was found to produce a mixture of mono, di and tri-substituted phosphite esters as well as minor amounts of pyrophosphate as seen in Figure 3.5. It was discovered that use of 3 eq. of PCl_3 predominately produced product with only traces of chlorophosphite diethers, as well as some by-products which had been both oxidised and hydrolysed. Although the rate of addition of **48** would have an impact on the degree of substitution, this was not explored by NMR spectroscopy as it would be difficult to add a solution of **48** to the NMR tube over a protracted period of time whilst maintaining an anaerobic and anhydrous atmosphere. Multiple substitutions should not be problematic for the analogous solid phase reaction due to the reduced mobility of the linker on the solid phase making it highly unlikely for two reactive sites to bind to the same PCl_3 moiety. To ensure mono-substitution however, an excess of > 3 eq. of PCl_3 will still be used in the solid phase. The excess can be easily

removed and the excess reagent will aid in driving the reaction to completion. Toluene, Et_2O and DCM are all solvents for which phosphitylations proceed effectively in the solution phase and are known to swell Merrifield resin to a reasonable extent.[265] DCM was chosen as the solvent to progress with due to its ability to solvate trialkylammonium salt by-products, allowing efficient mixing and preventing blockage of the NMR tube.

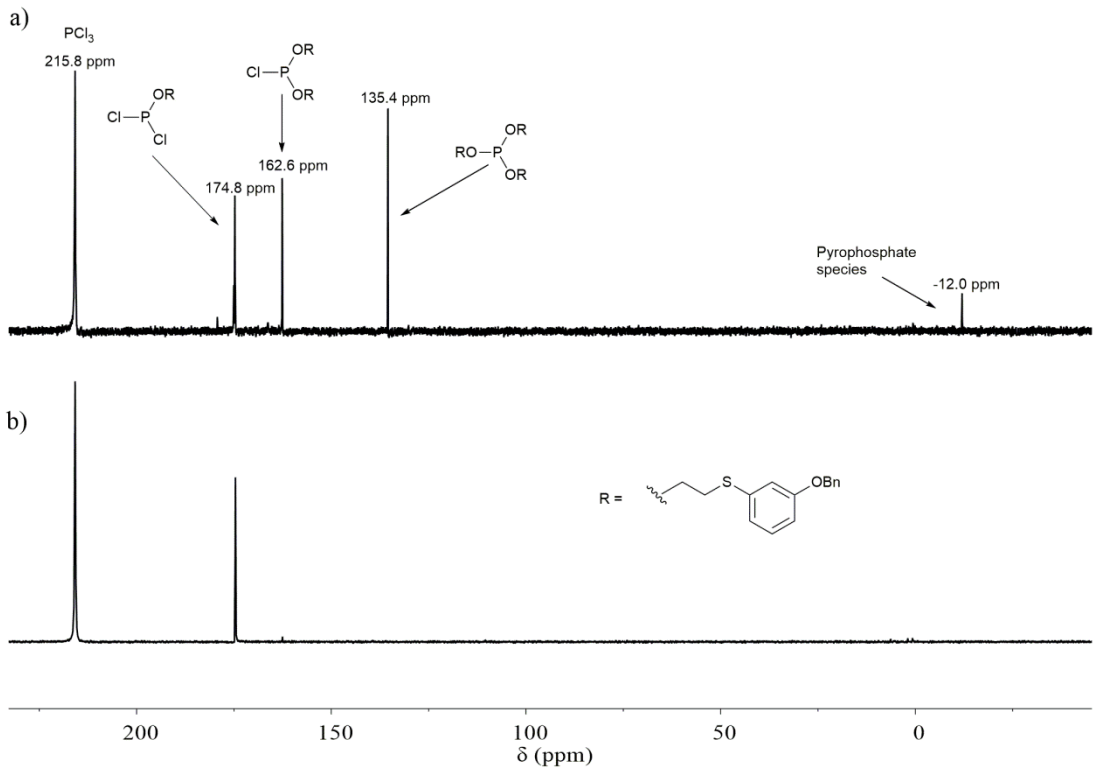

Figure 3.5. Plot showing the ^{31}P NMR spectrum of the reaction between compound **48** and PCl_3 in the presence of DIPEA. a) DIPEA and PCl_3 are in 1.3 molar excess of **48.** b) DIPEA and PCl_3 are in 3 molar excess of **48**.

Despite the large excess of PCl_3 required, an attempt to monitor the formation of linker mimic bound didecyl phosphite was attempted by ^{31}P NMR spectroscopy as seen in Figure 3.6. Whilst the spectrum was dominated by the formation of the tridecyl phosphite ester by-product, the results were still useful as they indicated the time frame for consumption of the dichloro imtermeditate (**60**). After 2.5 hours the majority of the crude material was converted to phosphite triesters with only minor traces of chloride intermediates remaining. (Figure 3.6, spectrum B). These traces did not disappear after 24 hours (spectrum C) indicating that the reaction was finished after 2.5 hours. It was unclear

why the trace material was not consumed, this may be attributed to ineffective mixing in the NMR tube by mechanical shaking. Alternatively a slightly larger excess of PCl_3 may have been added than intended, consuming decan-1-ol by forming tridecyl phosphite by-product, leaving unreacted chlorinated intermediates. In either case the solution phase NMR studies enabled a reasonable method for the production of resin bound didecyl phosphite to be devised.

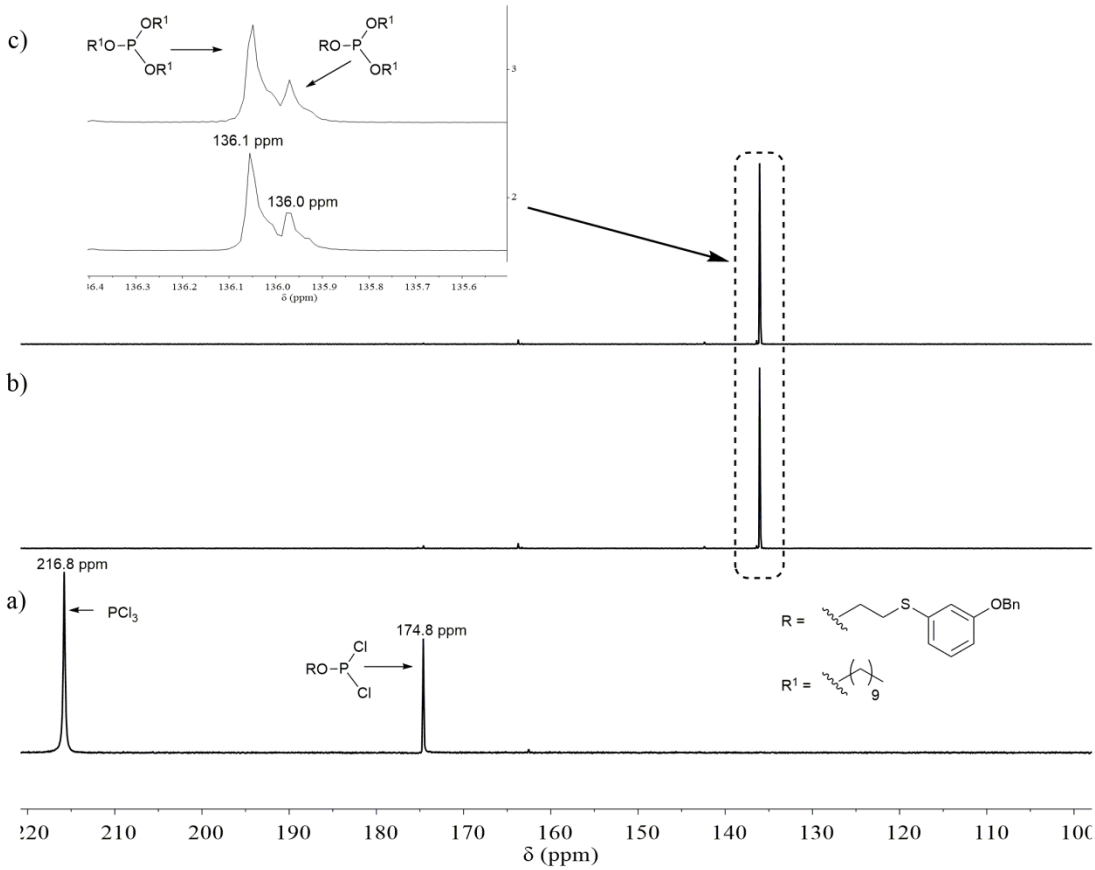

Figure 3.6. a) ^{31}P NMR spectrum of the addition of **48** to PCl_3 and DIPEA in anhydrous DCM after 5 minutes (capillary containing D_2O used as external lock). b) The same sample post addition of decan-1-ol and DIPEA after 2 hours. c) The same sample after shaking for 24 hours.

3.2.6. Formation of Resin bound didecyl phosphate

Observations from the solution phase NMR study enabled a method to be developed for the polymer supported synthesis of a dialkyl phosphate as displayed in Scheme 3.9. It was deduced that an excess of PCl_3 (5 molar eq.) was required in the initial phosphitylation step to reduce possible side reactions, although it was suspected a significantly shorter

reaction time would suffice, the reaction was left to shake for 1 hour to ensure complete conversion. After washing with anhydrous DCM to remove excess PCl_3, **56** was solvated followed by the addition of an excess of decan-1-ol and DIPEA. The reaction was left to stir for 6 hours, beyond that deemed necessary for the analogous solution phase reaction, producing resin bound didecyl phosphite ester (**62**). Both the thioether and P(III) moieties in Resin **62** were then oxidised by mCPBA over 16 hours which has shown to be sufficient to oxidise resin bound thioethers (Table 3.3). The resulting didecyl phosphate functionalised resin (**63**) was analysed by ssNMR spectroscopy.

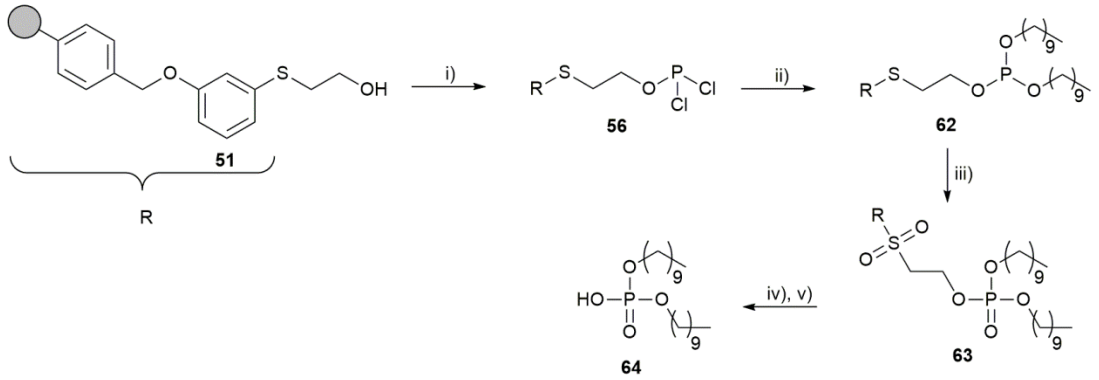

Scheme 3.9. Solid phase synthesis of didecyl phosphate (**64**). i) PCl_3, DIPEA, DCM. ii) Decan-1-ol, DIPEA, DCM. iii) mCPBA, DCM. iv) DIPEA, $CHCl_3$, v) HCl, $CHCl_3$, 26% (four steps).

Performing several steps to produce a compound devoid of easily hydrolysable or oxidisable functionalities prior to analysis by ssNMR spectroscopy allowed greater confidence in the returned spectra and conclusions to be more accurately drawn. From the obtained ^{1}H ssNMR spectrum (Figure 3.7) of compound **63** at the end of the resin bound reaction pathway, several conclusions could be drawn. The sulfone oxidation proceeded cleanly, evidenced by the signal at 7.6 ppm. Peaks at 3.94, 1.27, and 0.87 ppm are all consistent with signals of the decyl chain within didecyl phosphate which has corresponding signals at 4.02, 1.26 and 0.88 ppm (determined by analysis of authentic, commercially available material). There was a discrepancy between the anticipated integrations and the values observed when comparing signals corresponding *23-H* to the signal corresponding to *14-H*, with a 3:2 ratio anticipated, instead a 7:4 ratio was obtained. This was due to overlap

of the *23-H* signal with the broad signal corresponding to the resin and *16-22-H* contributing to the peak area of the *23-H* signal. Similarly, the anticipated 2:1 ratio of the *14-H*: *12-H* was not observed with a 2:1.5 ratio instead obtained. This discrepancy can be rationalised by the poor baseline and slight impurities under the signal at *12-H*, distorting the expected ratio. In the ^{31}P ssNMR spectrum, the appearance of a dominating single ^{31}P peak indicates that the addition of PCl_3 must have proceeded fairly cleanly with predominately one product formed, as no shoulder peaks are observed within the ^{31}P spectrum. The broad nature of the signal indicates that the signal belongs to a resin bound product, precluding retention of solution phase tridecyl phosphate by-product. Retention of solution phase by-products of this nature in general would be unlikely due to multiple resin washing steps prior to analysis. The chemical shift of -1.5 ppm was comparable to solution phase trialkyl phosphoesters.[269]

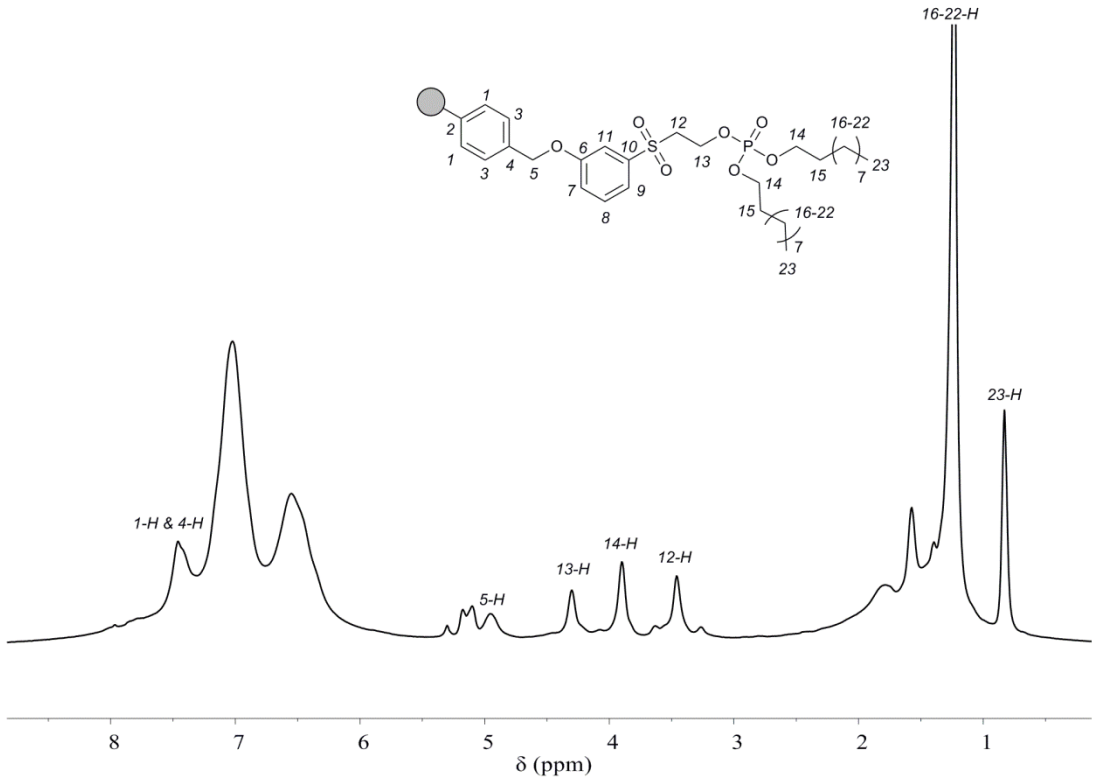

Figure 3.7. ^{1}H ssNMR spectrum of resin bound didecyl phosphoester (**63**).

After formation of resin **63**, cleavage by DIPEA in DCM for 2 hours was attempted; a small amount of material was recovered. To probe cleavage conditions, the same reaction conditions were applied but for 24 hours at room temperature. Analysis of the washings

showed that a small amount of product was recovered (by accurate mass); however the amount was too small to even return a reasonable ^{31}P NMR spectrum. Examination of the remaining resin showed that phosphate was resin bound even after 24 hours of stirring, there was a peak corresponding to protons of the resin bound elimination product. Exact quantification was difficult due to an uneven baseline; remaining phosphate was estimated to be in the region of > 70%. Stirring resin **63** with NH_4OH under conditions closer to those employed in the literature for similar resin based eliminations,[244] gave comparable results, with only minor traces of product detected. The decreased rate of elimination was in sharp contrast to the rapid elimination observed when resin **44** was mixed with $POCl_3$ (Table 3.2) under the same conditions. The difference in reactivity was attributed to the resulting PO_2Cl_2 being a better leaving group than the didecyl phosphate. The stronger negative inductive effect of the chloride substituents may be sufficient to increase the stability of the leaving group leading to a rate enhancement of the E1cB pathway relative to the didecyl phosphate. Alternatively, the inability of DCM to solvate the resulting phosphate salt may account for the diminished rate of cleavage, the elimination of a zwitterionic glycerophospholipid may actually be simplified by the higher solubility of the product in halogenated solvents.

In order to increase the rate of didecyl phosphate cleavage, microwave irradiation was employed. Didecyl phosphate functionalised resin (**63**) was irradiated with DIPEA in $CHCl_3$ at 100, 120 and 140 °C for 2 hours. The resin was initially washed using $CHCl_3$ and the filtrate was analysed by solution phase NMR spectroscopy, as expected, a complex crude ^{1}H NMR spectrum was returned, showing the mixture to be largely composed of DIPEA. Examination of the ^{31}P NMR spectrum showed three peaks, with a dominant signal at -1.0 ppm corresponding to *N'N*'-diisopropylethylammonium didecyl phosphate. Acidic work-up of the phosphate salt produced protonated didecyl phosphate, as well as significantly cleaning the mixture as displayed in Figure 3.8. In the case of reactions performed at 100 and 140 °C, other minor ^{31}P signals were present. Due to the absence of other peaks from the 120 °C reaction, the negligible impurities observed in the ^{31}P NMR spectrum would suggest

that the appearance of extra signals are likely due to efficiency of removing the by-products during the acid wash and are not directly correlated to temperature of the reaction.

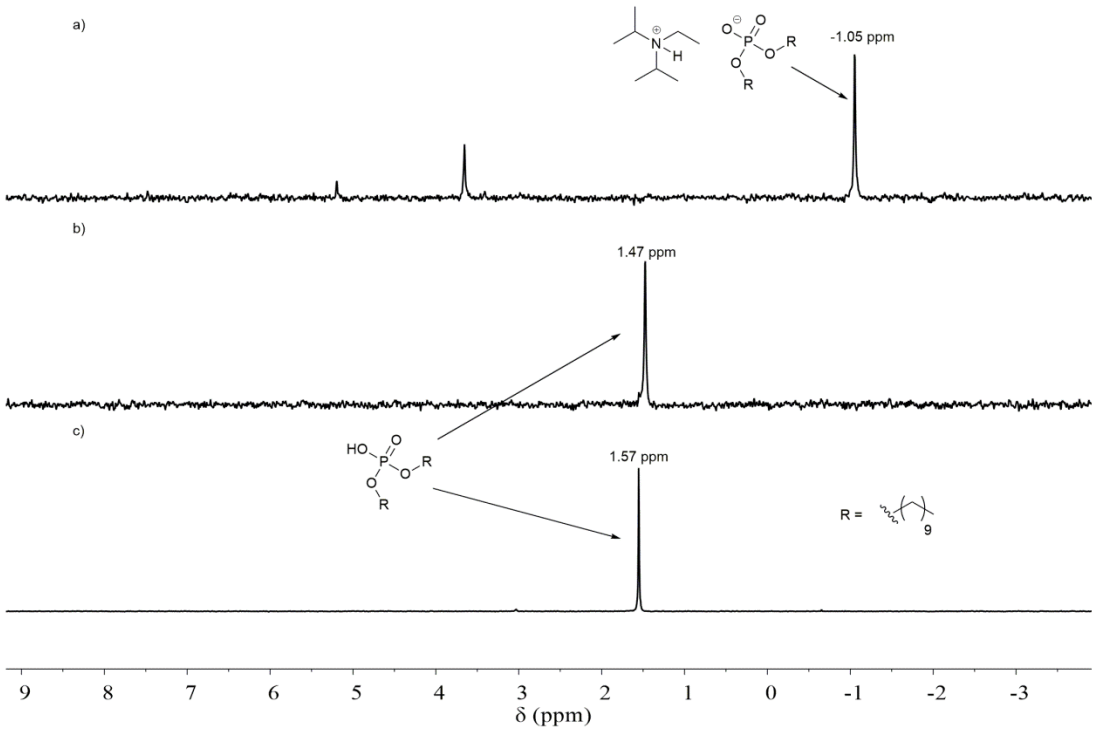

Figure 3.8. Solution phase ^{31}P NMR spectra of didecyl phosphate (**64**). a) Crude mixture of the salt after cleavage from resin **63** by stirring with DIPEA in $CHCl_3$ for 2 hours at 100 °C using microwave irradiation. b) The same crude mixture after an acidic work up. c) Didecyl phosphate authentic material acquired commercially.

Post acidification, the solution phase ^1H NMR spectrum of the crude material was compared to authentic commercially acquired material as shown in Figure 3.9. The recovered material matched the authentic sample, showing only minor by-products. The only appreciable difference between the spectra was the chemical shift associated with exchangeable protons such as the acidic proton of the phosphate and H_2O within the $CDCl_3$. The integration was not as anticipated, the integration of the *3-9-H* & *10-H* signals being higher than anticipated, corresponding to 40 and 8 protons opposed to 28 and 6 respectively. The higher values for these integrations may be partially due to the poor baseline and likely indicate that there may be impurities in the sample with their peaks being buried under the *3-9-H* and *10-H* signals. These impurities are more obvious for the *10-H* signal where a slight

shoulder can be observed. In addition, the ^{31}P NMR spectrum was remarkably clean matching the authentic material acquired commercially, with only one additional signal of negligible intensity. Confirmation of the structure was also achieved by high resolution mass spectrometry, the calculated accurate mass was within 0.0002 of that expected of the $[M-H]^-$ adduct of didecyl phosphate.

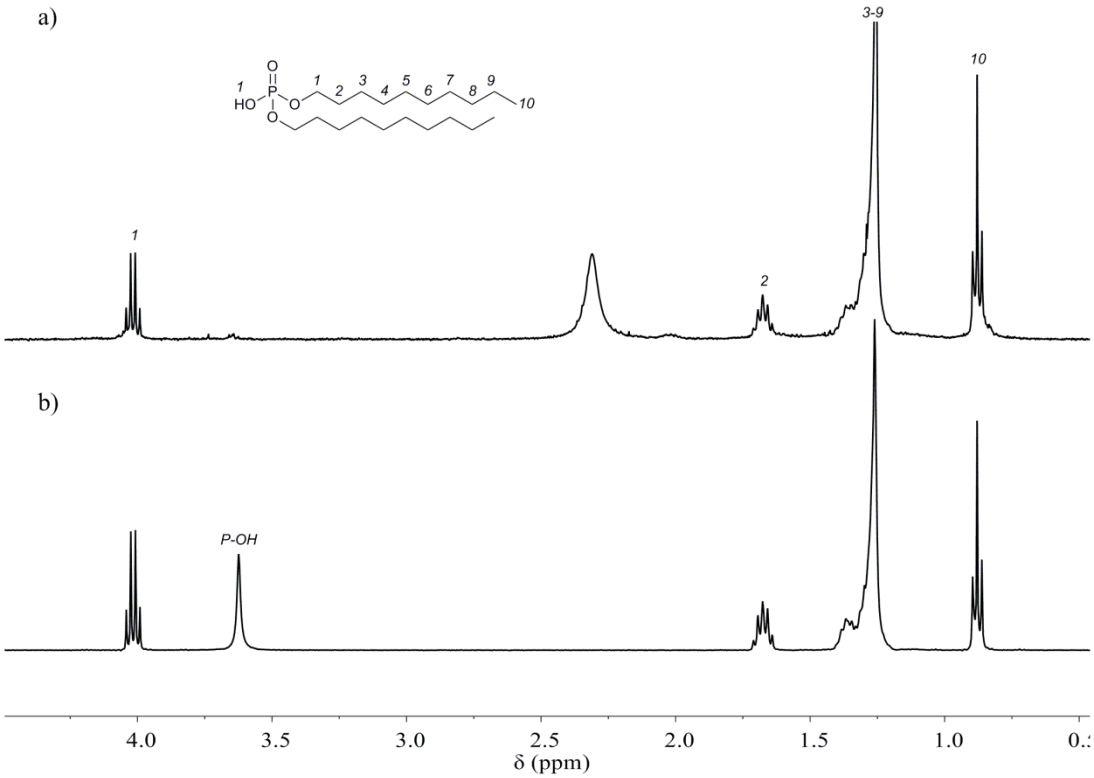

Figure 3.9. Solution phase ^1H NMR spectrum of didecyl phosphate (**64**). a) Spectrum of the crude washings of didceyl phosphate after acid work-up. b) Commercially bought, authentic didecyl phosphate.

The Merrifield resin was supplied with a loading in the range of 0.8-1.2 mmol g^{-1}, resulting in a yield of approximately 26-34% for the synthesis of didecyl phosphate. The stated loading was 1.2 mmol g^{-1}, however this was not substantiated by the supplier and was not analysed further by the author. Based upon Figure 3.2 and Table 3.3, attachment of the linker and oxidation were both determined to have progressed with near quantitative conversion. Poor yield may then be attributed to the remaining phosphitylation/alcoholysis and cleavage steps. From the NMR study shown in Figure 3.6, near quantitative conversion to the phosphotriether was observed, it was possible that the reaction did not proceed as well

as anticipated after 6 hours, with a longer reaction time required on the resin. Alternatively, other phosphitylating agents could be explored. Cleavage from the resin appears to be the greatest contributing factor to the poor recovered yield. A study employing microwave irradiation to cleave the resin at 100, 120 and 140 °C for 2 hours was employed. Analysis by ssNMR spectroscopy indicated that in all three cases, ^{31}P signals at a chemical shift of -1.5 ppm were present, additionally the ^{1}H NMR spectrum displayed signals corresponding to elimination product **46** was observed. The amount of elimination product was minor again comparable to performing the reaction at ambient temperature over 24 hours. The broad nature of the polystyrene signal enveloped the signals characteristic of the elimination product, making quantification not possible.

3.2.7. Synthesis of pentabenzylated inositol building block

Phosphatyidylinositol (PI) represents an important subclass of gylcerophospholipids, with both structural and signalling roles *in-vivo*.[227,228] PI lipids represent a synthetically challenging target due to the large number of stereocentres and alcohol moieties. In order to facilitate the synthesis of the correct chemoisomer, a benzyl protected PI was synthesised in solution phase to be later employ as a building block in the solid phase (see Scheme 3.10). The synthesis of protected *myo*-inositol occurred in parallel to optimisation of reactions on the solid support, as these reactions were being optimised and the conditions unknown, a robust protecting group for *myo*-inositol was chosen. Benzyl ethers are tolerant to both acidic and basic conditions so were used as the initial protecting group. Deprotection occurs *via* the use of Pd catalysed hydrogenation, making this building block incompatible with unsaturated lipids. Future syntheses would look to address this issue by replacing benzyl protecting groups for something which requires non-hydrogenating deprotection such as silyl ethers, although a milder acid will likely need to be sought for deprotection of acetal (**68**).

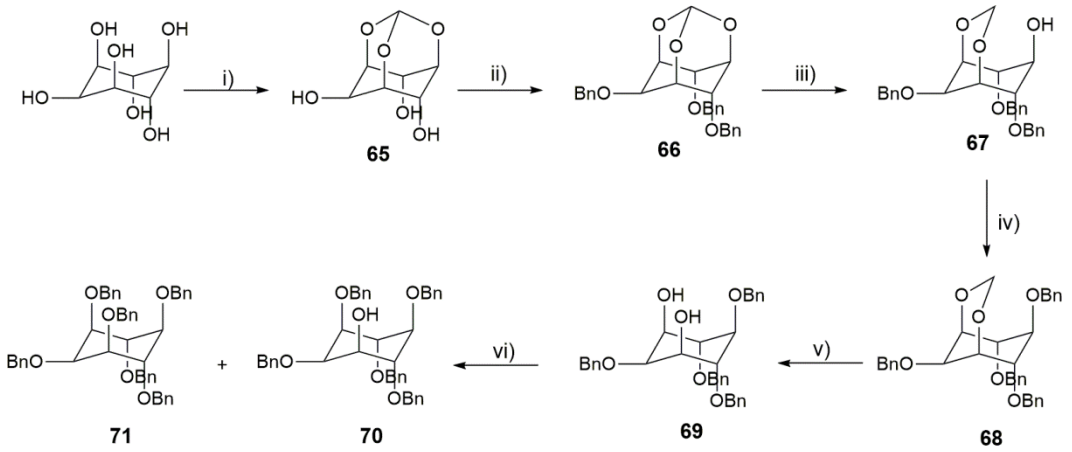

Scheme 3.10. Synthetic route employed in the synthesis of the benzyl protected phosphatidylinositol building block. i) Triethylorthoformate, TsOH, DMF, 62%. ii) NaH, BnBr, DMF, 80%. iii) DIBAL, DCM, 98%. iv) NaH, BnBr, DMF, 77%. v) MeOH, HCl, 78. vi) NaH, BnBr, DMF, 73%.

myo-Inositol was utilised as it possessed the same stereochemistry at each stereocentre as that observed in natural PI lipids, *myo*-inositol was orthoformate protected in 62% as detailed in the literature.[270] Conversion to orthoformate (**65**) was not quantitative progressing to 86% conversion; residual *myo*-inositol was removed by hot filtration using MeOH. The remaining free hydroxyls of **65** were benzylated in 80% yield to produce benzylated orthoformate (**66**). Reduction of the orthoformate functionality afforded the corresponding acetal (**67**) in 97% yield. In agreement with the literature, 2 eq. of Diisobutylaluminium hydride (DIBAL) was found necessary to promote complete reduction to the acetal.[271] The unprotected hydroxyl moiety was benzylated, producing **68** in 71% yield. Addition of aqueous acid led to acetal deprotection producing diol (**69**) in 73% yield. Slow addition of benzyl bromide *via* a syringe pump over 3 hours to a molar excess of **69** (2.5 eq.) afforded the final product (**70**) in 78% yield with hexabenzylated by-product (**71**) also recovered (11%). The pentabenzylated inositol building block (**70**) was successfully synthesised in an overall yield of 21% over six steps.

3.3. Conclusion

A strategy for the production of dialkyl phosphates on the solid phase was devised, based upon a β-hydroxysulfone linker. The optimum methodology devised was to use a

safety catch approach, with oxidation in a penultimate step, activating the resin toward cleavage under basic conditions. Thioether linker was synthesised and bound to the resin quantitatively, with conditions to phosphitylate and oxidise the resultant intermediates determined using a combination of ssNMR spectroscopy and NMR studies of solution phase analogues. The novel methodology was used to synthesise the symmetric didecyl phosphate which was produced in 26-33% yield. The identity of the material was confirmed by a range of methods and compared to authentic material. Whilst a low initial yield, a proof of principle compound has been produced using the linker with scope for optimisation. In parallel, pentabenzylated inositol was synthesised in 21% yield after 6 steps, to use as building block in the solid phase synthesis of PI lipids.

3.4. Future work

3.4.1. Production of asymmetric dialkyl phosphates

If a suitable microwave reactor compatible with solid phase synthesis vessels becomes available then it may become possible to further improve upon the current methodology, shortening reaction times significantly. At present the only microwave reactor available is intended for use with solution phase vessels, so was not compatible with a one pot synthesis. This makes the use of microwave irradiation undesirable with the current methodology due to loss of material during transfer and exposure of sensitive compounds to oxygen and H_2O. Once conditions are further optimised, attention could then be turned toward the synthesis of asymmetric dialkyl phosphates using a phosphoramidite approach with several reagents available as seen in Scheme 3.11. Initially, conditions could be determined using a solution phase analogue in an NMR study in the fashion of that already described (Section 3.2.5). Preliminary studies were conducted; however it was later discovered that the ^{31}P probe of the instrument used (Varian Mercury 400, “M400”) was defective and gave rise to a number of signal artefacts, rendering the data obtained unusable.

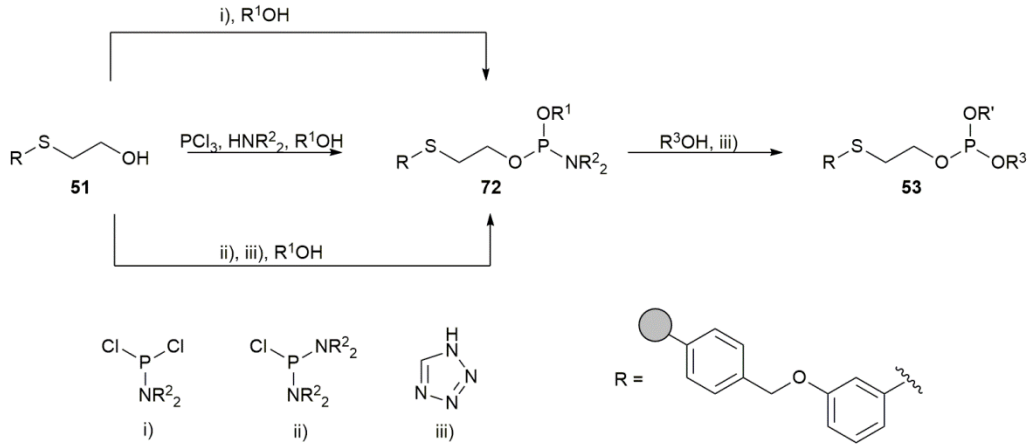

Scheme 3.11. Possible synthetic routes to produce the key dialkyl phosphoramidate (**72**) for the synthesis of asymmetric dialkyl phosphates (**53**). $R^1 \neq R^3$.

3.4.2. Solid phase synthesis of glycerophospholipids

If conditions to produce an asymmetric dialkyl phosphate are deduced, synthesis of a glycerophospholipid could be carried out as described in Scheme 3.12. A small library of natural gylcerophospholipids with various fatty acid chains and head groups should then be synthesised. The synthetic route should be probed as the exact sequence is delicate; the sequence outlined in Scheme 3.12 contains the theoretical ideal point of oxidation. If the oxidation occurs after the addition of a fatty acid, then that fatty acid cannot likely contain any moieties sensitive to oxidation. Therefore the methodology would not be applicable for unsaturated fatty acids, limiting the scope of lipids produced by this methodology. Alternatively post oxidation, the compound should becomes base sensitive and may prematurely cleave from the resin; base cleavage has been observed in the presence of amine bases previously. In the case of premature resin cleavage, oxidation may be moved to after the first addition of the fatty acid which should only inhibit the use of unsaturated fatty acids in the *sn-1* position. This would not be too restricting, considering the bulk of natural fatty acids contain a saturated fatty acid in the *sn*-1 position, whilst the *sn*-2 position contains an unsaturated lipid.[9]

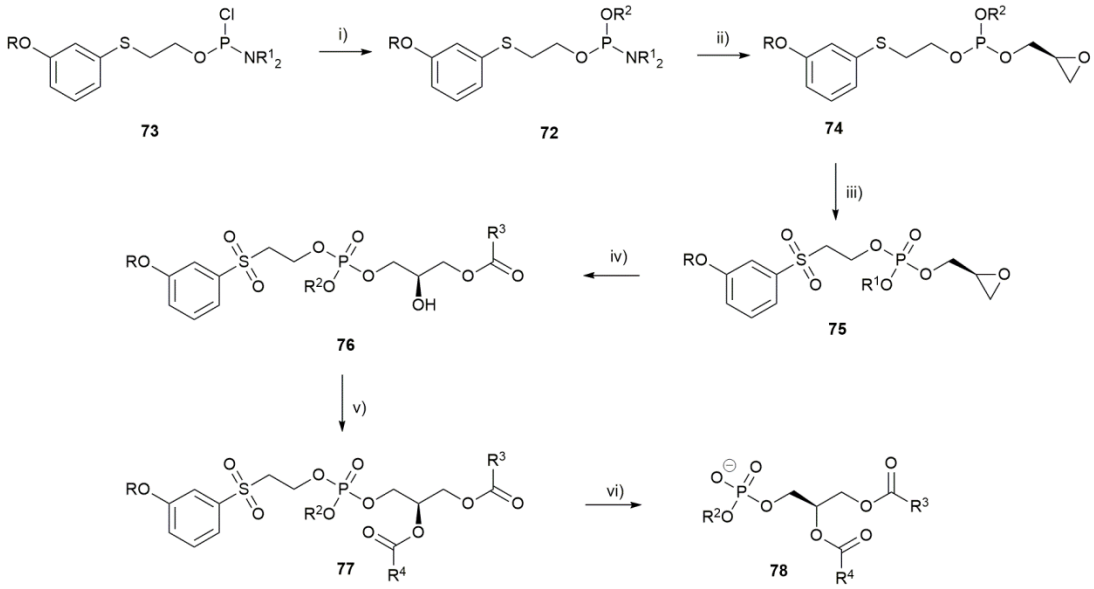

Scheme 3.12. Proposed methodology for the synthesis of gylcerophospholipids. R = Merrified resin. R^2 = serine, ethanolamine, inositol or choline. R^3 and R^4 = alkyl chains. i) R^2OH, DIPEA. ii) (*R*)-(+)-Glycidol, DIPEA. iii) Oxidant (oxone or mCPBA). iv) Fatty carboxylate salt, v) Fatty acid chloride. vi) DIPEA, DCM.

The penta-benzylated inositol building block (**70**) could be utilised, allowing the SPLS methodology to be applicable to forming PI lipids. The benzyl protecting groups should be removed by Pd/C, H_2 after cleavage from the resin; therefore only saturated PI lipids will likely be applicable. An alternative penta-silylated PI building block could also be synthesised, which could be deprotected under acidic conditions, allowing the synthesis of unsaturated PI lipids. Once a library of naturally occurring lipids is obtained, the methodology could be expanded to produce artificial lipids. Reasonable targets include synthesis of fluorescently tagged lipid analogues such as 1,2-dipalmitoyl-sn-glycero-3-phosphoethanolamine-N-(lissamine rhodamine B sulfonyl) (**79**) displayed in Figure 3.10.

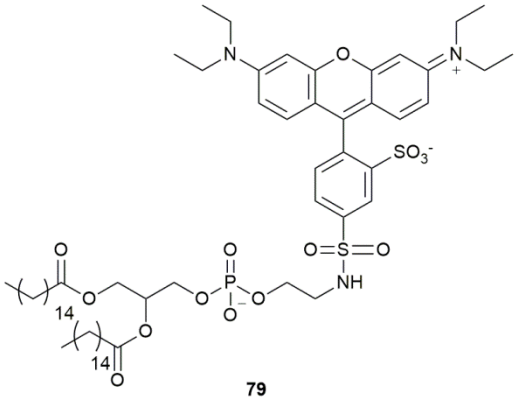

Figure 3.10. Structure of a fluorescently tagged lipid, 1,2-dipalmitoyl-sn-glycero-3-phosphoethanolamine-N-(lissamine rhodamine B sulfonyl).

Chapter 4. The Synthesis of Sterols Enriched in Oxygen Isotopes

4.1. Background and aims

4.1.1. Classic conditions for preparation of ^{17}O and ^{18}O-cholesterol

Cholesterol (**81**) is abundant in many eukaryotic membranes, typically constituting 30-40 mol% of the bilayer.[9] Cholesterol regulates membrane fluidity,[2] improves membrane cold shock resistance[146] and has been shown to drive the phase separation of membranes composed of high T_m and low T_m lipids.[21] As previously described in Section (**1.2.1**), sterols such as cholesterol, cholestanol and 25-hydroxycholesterol (25-HC) have been shown to drive this lateral phase segregation of an ordered (L_o) phase rich in cholesterol and high T_m lipids within a bulk liquid disordered (L_d) phase comprised primarily of low T_m lipid.[21] In model systems, this produces macroscopic phase separation (domains of diameter > 1 μm), whereas in biological membranes, domains (rafts) are more dynamic (diameter ≤ 40 nm). The crucial structural role of cholesterol within eukaryotic bilayers, coupled with its implication in life style diseases,[272] has led to its study using a wide range of analytical techniques.

Classically, electronic paramagnetic resonance and luminescence studies have proved popular,[273-275] and although intrinsically fluorescent cholesterol analogues exist such as dehydroergosterol, it photobleaches rapidly, suffers from a low quantum yield and is not able to condense lipid bilayers as efficiently as cholesterol.[274,276] Usually the sterol structure is modified by inclusion of fluorophores or spin labels, with labelling occurring either in the aliphatic tail, or at the *3-C* hydroxyl group.[26] The use of such bulky tags is undesirable, as large modifications can alter the properties of cholesterol within a bilayer affecting, most notably, the ability of the modified cholesterol to pack within the L_o domains. A striking example is the use of cholesterol bearing a NBD fluorescent label at the *22-C* or *25-C* position. Addition of this bulky group alters the phase behaviour of cholesterol. NBD-cholesterol has shown to favourable partition into the liquid disordered phase whilst cholesterol is known to favour partitioning into liquid ordered phase.[27,277] The NBD

derivative is not representative of natural cholesterol, giving an inaccurate representation of cholesterol function. Typically, labels are incorporated into the aliphatic tail; modification of the chain can drastically alter the partitioning of cholesterol, with shortening the chain length even inhibiting the formation of a L_o phase.[278] Isotopic labelling by ^{17}O or ^{18}O are therefore desirable alternative labels, due to minimal alteration of structure, both sterically and electronically, whilst affording unique markers in NMR spectroscopy and mass spectrometry. ^{17}O is spin active (5/2) allowing direct observation by NMR spectroscopy with a large chemical shift range.[279] The heavier isotope, ^{18}O is known to induce an upfield shift of the associated carbon centre, opening up the possibility of observation by ^{13}C NMR spectroscopy. Due to low isotopic abundance both isotopically enriched sterols must be synthesised.[280] Literature procedures detail one step methods for the acid catalysed reaction of commercially available i-cholesteryl methyl ether (**80**) and H_2O affording labelled cholesterol (**81a-c**) as seen in Scheme 4.1.[281]

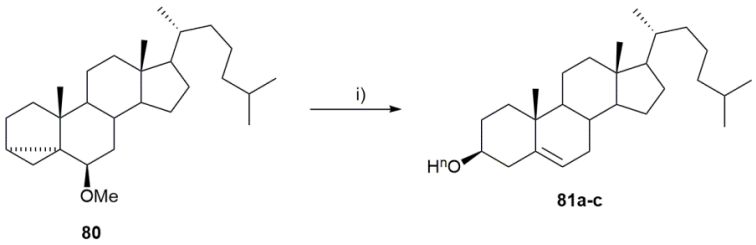

80 **81a-c**

Scheme 4.1. Synthesis of heavy oxygen labelled cholesterol from i-cholesteryl methyl ether. I) H+, $^{n}OH_2$, 1,4-dioxane.a; n = 16, b; n = 17, c; n = 18.

To date, this reaction has been largely exploited for the preparation of unlabelled cholesterol and has employed a massive excess of H_2O (1500 eq.) to drive the reaction to completion.[281] The methodology has been utilised in the production of ^{17}O,[280] and ^{18}O-cholesterol,[282] however both procedures still used an excess (20 and 25 eq. respectively) of labelled H_2O. Use of such an excess to prepare cholesterol bearing heavy oxygen isotopes is undesirable due to the cost of heavy oxygen enriched H_2O. Production of 1 g of ^{17}O-cholesterol (40% enriched) under these conditions would cost in excess of €1100 for the volume of labelled water required. The degree of incorporation was also not accurately

quantified; values obtained were 6.6 and 9.1% higher than the theoretical maximum for ^{17}O and ^{18}O incorporation respectively.[280] Enrichment was determined by spectrometric analysis, by comparison of the $[M]^+$, $[M+1]^+$ and $[M+2]^+$ peaks of the isotopologue envelope. Details were scarce with no further experimental details or calculations presented; therefore the reason for the discrepancy could not be ascertained. In the case of ^{18}O-cholesterol, the target compound was purified by recrystallisation[282] but no indication of purity was given, with the large number of by-products produced (see Figure 4.2); it is unlikely that the target compound would be returned with high purity. Optimisation of this reaction was therefore sought in order to produce a cost effective synthesis of heavy oxygen labelled cholesterol. Our aims were therefore to;

- examine the potential for conducting this reaction using fewer equivalents of H_2O;
- determine optimal conditions for recovery of isotopically enriched cholesterol;
- employ these conditions to prepare labelled cholesterol on a scale of tens of mg to gram scale.

4.1.2. Alternative sterol targets for isotopic labelling

Recently it has been discovered that 6-ketocholestanol (6-KC) (**82**) and 25-HC (**83**) reverse age related nuclear cataracts in mice and human lens cells *ex vivo*.[283] This compliments the work of Zhao who witnessed *in vivo* cataract reduction in dogs by application of lanosterol containing eye drops.[284] Mammalian lenses are composed largely of compacted fiber cells in which protein production is halted, enabling the cells to remain transparent.[285] Due to this low protein turn-over, lens proteins are amongst the oldest found within the human body.[286] In the absence of protein turn-over, regulation is controlled by the thermal shock proteins, αA-Crystallin (cryAA) and αB-crystallins (cryAB) which constitute around 30% of the total lens proteins.[284] These proteins act as molecular chaperones, binding to other misfolded proteins, correcting folding and solubilising the proteins thereby maintaining transparency. Due to genetic or environmental effects, over time cryAA and cryAB can themselves become denatured; this in turn leads to the formation of large masses

of opaque proteins, termed nuclear cataracts, impairing vision. The reversal of cataract formation is hypothesised to be achieved through certain sterols acting as pharmacological chaperones, correcting the misfolding of cryAA and cryAB which can then resume their role as molecular chaperones, solubilising aggregate protein masses restoring cell transparency.[283] A large portion of insoluble crystalline proteins have shown to be membrane bound as well as *in situ*.[287] This work raises the questions of whether the sterols are acting *via* modification of membrane properties to desorb misfolded proteins, or acting *via* refolding of chaperones within the lens. Furthermore, it is unclear how the sterols migrate through the eye to the site of action in the lens, raising the possibility that lipid dynamics in lens membranes are more significant than previously thought.

Therefore, sterols **82**, **83** and **84** shown in Figure 4.1 were identified as isotopically labelled targets that would enable their distributions to be probed by whole cell ssNMR spectroscopy or MALDI imaging methods.

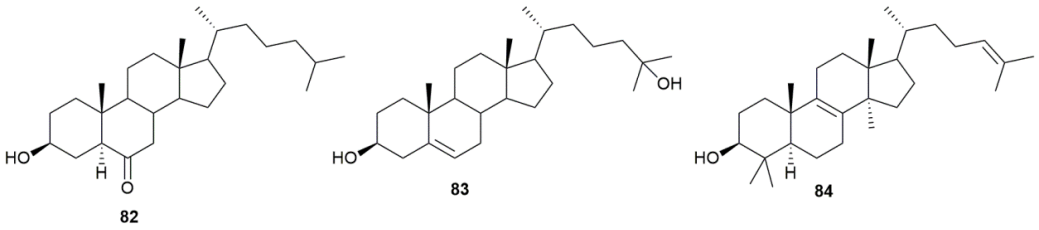

Figure 4.1. Structures of pharmacological chaperones 6-KC (**82)**, 25-HC (**83)** and lanosterol (**84**).

In addition to their action on cataracts the sterols shown in Figure 4.2 are known to partition into different phases. Sterols **82** and **83** occupy the L_o phase like cholesterol whilst sterol **84** occupies the L_d phase.[6] Through the above sterols, total coverage of lipid bilayers can be achieved by spectroscopic means. Whilst the process of enrichment developed for cholesterol (Scheme.4.1) can be extended to producing sterols **82** and **83**, lanosterol (**84**) cannot be prepared by this route. Our aims were therefore to;

- synthesise isotopically enriched analogues of **6-KC** (**82**) and **25-HC** (**83**);
- develop an alternative labelling strategy for lanosterol (**84**);

- prepare each of these sterols in sufficient quantities to enable biological screening.

4.2 Results and discussion

4.2.1. Synthesis of ^{17}O and ^{18}O labelled cholesterol

The initial goal of this work was to optimise the synthesis of cholesterol from i-cholesteryl methyl ether with an emphasis on reducing the volume of heavy oxygen labelled H_2O used. Some parts of this work were carried out by undergraduates and their contributions will be acknowledged as appropriate.

4.2.1.1 Screen of acid catalysts

In order to determine the optimum conditions for the hydration of **80** as shown in Scheme 4.1, a screening of acids was initially performed using inexpensive non-isotopically labelled H_2O in ethereal solvents (carried out in part by C. de la Calle Arregui and C. Haslam) as displayed in Table 4.1. 1,4-dioxane and THF were used due to their H_2O miscibility, lack of exchangeable oxygen and aprotic nature precluding participation in the reaction. A range of acids was chosen, both with and without exchangeable oxygens and with varying pK_a values. Obtaining high enrichment was prioritised over reaction yield, therefore acid catalyst concentrations were kept to a minimum, especially when using acids containing exchangeable oxygen. In addition to cholesterol, several by-products were produced (Figure 4.2) during optimisation of the reaction conditions.

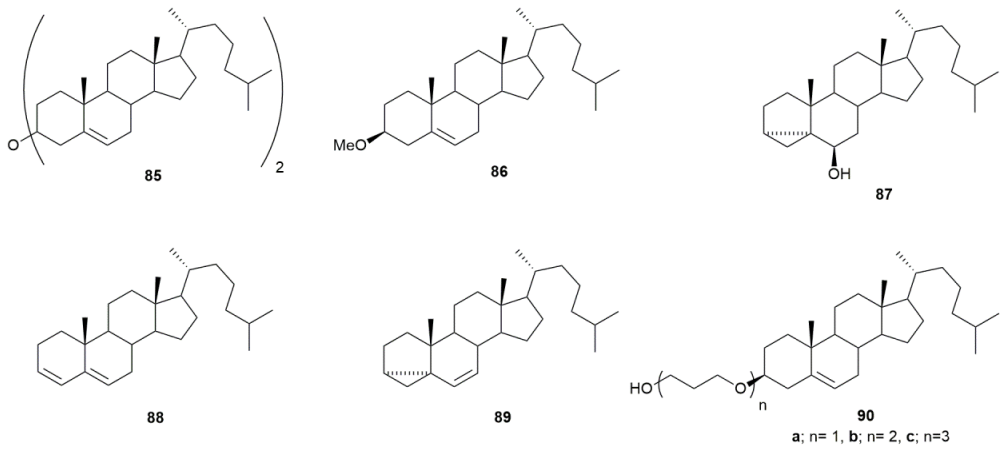

Figure 4.2. Major by-products of cholesterol synthesis shown in Scheme 4.1.

Nucleophilic attack of i-cholesteryl methyl ether (**80**) by cholesterol led to production of dicholesteryl ether (**85**) through the elimination of MeOH. In order to minimise the production of **85**, the reaction mixture was kept dilute, with the concentration of **80** not exceeding 41 mM. MeOH was liberated *in situ* by synthesis of all by-products produced within the reaction mixture, MeOH then acted as a competing nucleophile producing cholesterol methyl ether (**86**). i-Cholesterol by-product (**87**) has two possible mechanisms of formation as displayed in Scheme 4.2.

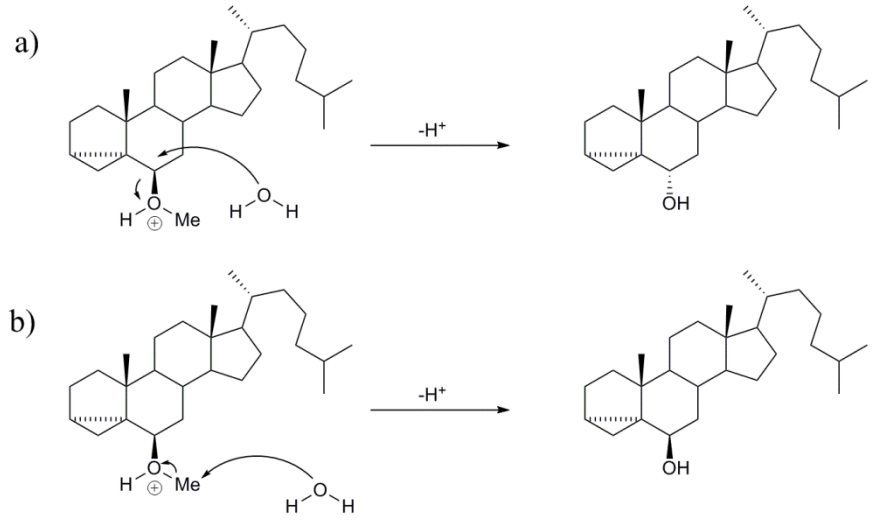

Scheme 4.2. Possible mechanisms for formation of i-cholesterol (**87**).

Mechanism A appears more unlikely due to the sterically crowded α-face preventing nucleophilic attack at the *6-C* position. The coupling constant between the *6β-H* and *7α-H* would be expected to be > 8 Hz due to the Karplus relationship. The obtained coupling of the *6-H* was found to be only 2.9 Hz, suggesting a diaxial arrangement was not present. Mechanism B was further corroborated by synthesis of **87** by an alternative method (see Scheme 4.6) producing identical spectra. Interestingly, mechanism B would expect to produce ^{18}O-MeOH, which in principle could react with i-cholesterol methyl ether to yield a small amount of ^{18}O-labelled **86**. Optimised conditions did not produce **87** as a by-product; therefore confirmation by isotopic labelling is absent. Diene (**88**) and cyclopropyl alkene (**89**) both can be obtained by acid catalysed elimination from i-cholesteryl methyl ether. By-products **85-89** arose regardless of solvent, with butylenegylcol ethers (**90a-c**) only observed

in THF, formed by acid catalysed hydrolysis of THF followed by reaction with i-cholesteryl methyl ether producing **90a-c**. The analogous triethylene glycol functionalised cholesterol was not observed when the reaction was performed in 1,4-dioxane, therefore 1,4-dioxane was found to be the optimum solvent.

Table 4.1. The influence of acid catalyst on the formation of cholesterol from i-cholesteryl methyl ether in the presence of H_2O[a]

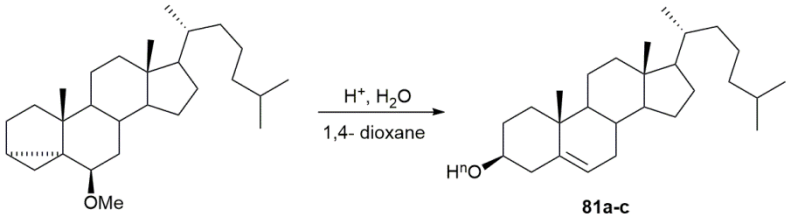

80 **81a-c**

Entry	Acid	Conversion[b] (%)							
		Cholesterol	Reagent	By-products[c]					
		81	**80**	**85**	**86**	**87**	**88**	**89**	Other
1	CF_3SO_3H	73 (61)	trace	9	9	trace	trace	-	9
2	*p*-TsOH	Trace[d]	> 99	trace	trace	trace	-	-	-
3	CH_3SO_3H	1	93	trace	2	2	1	-	Trace
4	HBF_4	18 (16)	55	1	3	12	1	trace	10
5	HCl	7 (6)	79	1	2	9	trace	1	1

[a] Conditions in all cases: 5 eq. H_2O, 0.05 eq. acid, 1,4-dioxane, 80 °C, 5 h. [b]Conversions are calculated from analysis of crude NMR spectra, values in parentheses are isolated yields (%). [c]By-product structures shown in Figure 4.2. [d]Trace products were detectable by TLC but not ^{1}H NMR spectroscopy. The relative conversions of 'other' products were determined on the basis of *3-H* signals or pairs of olefinic signals that could not be attributed to any of **85-89**.

The acid screen presented two candidates for further study, CF_3SO_3H was found to give the largest yield of cholesterol (entry 1), although exchangeable oxygen was expected to result in lower enrichment. HBF_4 was found to be the highest yielding acid catalyst with a non-exchangeable ^{16}OH moiety (entry 4), this reaction was lower yielding than the CF_3SO_3H catalysed reaction, but was expected to give greater enrichment. The yield of the HBF_4 catalysed reaction could be enhanced from 16-40% by increasing the reaction time from 5 to 40 hours.

4.2.1.2 Optimisation of trifluoromethane sulfonic acid catalysed reaction

Further optimisation to improve upon the conversion using CF_3SO_3H was carried out by varying the concentration of acid and H_2O as shown in Table 4.2 (approximately 50% of the work in this paragraph was performed by C. de la Calle Arregui, with the remainder carried out by the author). The optimum conditions employed were 0.05 eq. of acid and 5 eq. of H_2O at 20 °C (entry 6) producing a 76% conversion, employing elevated temperatures yielded no improvement (entry 5), indicating a 73% conversion. Increasing the volume of H_2O (> 5 eq.) was found to give no improvement (entries 6 *vs.* 7), whilst increasing the acid content to above 0.05 eq. was similarly found to afford no benefit in conversion (entries 6 *vs.* 8). Increasing the acid: i-cholesteryl methyl ether ratio increased the number of by-products produced; particularly methylated cholesterol (**86**). Whilst a lower acid content generally favoured formation of cholesterol, the reactions were incomplete and longer reaction times were not pursued due to the maximum obtainable conversion (based on residual starting ether (**80**)). The major expected product from a longer reaction time at lower acid concentration would be the kinetic product, i-cholesterol (**87**).[288] At low acid concentrations the desired thermodynamic product (cholesterol) would be produced sparingly, cholesterol conversion would not exceed that obtained for entry 6.

Table 4.2. Optimisation of the formation of cholesterol from **80** using CF_3SO_3H as a catalyst in 1,4-dioxane as outlined in Scheme 4.1.

				Conversion[b] (%)							
Entry	T (°C)	Eq. CF_3SO_3H[a]	Eq. H_2O[a]	**81**	**80**	**85**	**86**	**87**	**88**	**89**	Other
1	20	0.005	2	9	74	1	2	12	1	-	-
2	20	0.005	5	4	87	-	2	4	-	-	1
3	20	0.01	2	30	36	2	4	7	2	1	18
4	20	0.01	5	21	59	1	2	12	2	1	2
5	80	0.05	5	73	-	9	9	-	-	-	9
6	20	0.05	5	76	-	6	11	-	2	1	4
7	20	0.05	20	7	72	-	2	9	-	-	10
8	20	1	5	59	-	9	23	-	9	-	-
9	20	1	20	57	-	9	27	-	7	-	-

[a]Equivalents relative to **80**. [b]Conversions are calculated from analysis of NMR spectra of the crude reactions.

4.2.1.3 Application of optimised methodology to synthesise heavy oxygen labelled cholesterol

The optimised conditions of the CF_3SO_3H and HBF_4 catalysed reactions were applied using $^{18}OH_2$, affording ^{18}O-cholesterol in 69 and 40% yield respectively. The isotopic enrichments for the CF_3SO_3H and HBF_4 catalysed reactions were found to be 90 ± 1.9 and 91 ± 1.9% respectively, determined by comparison of the integrals of the upfield shifted *3-C* centre in the ^{13}C NMR spectrum shown in Figure 4.3.

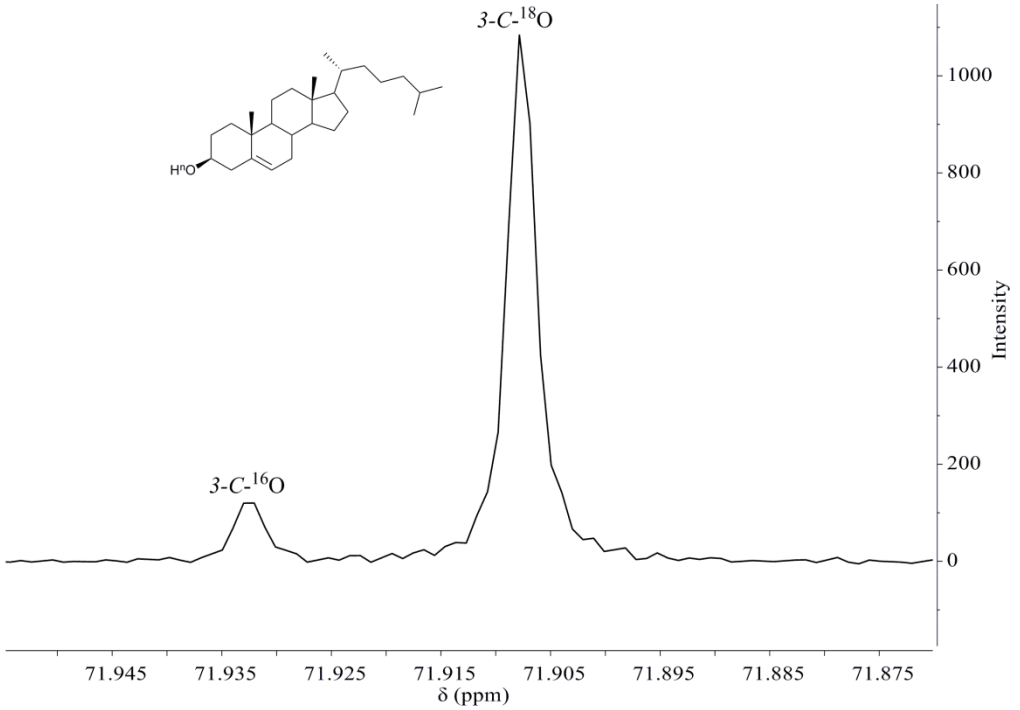

Figure 4.3. ^{13}C NMR spectrum showing the upfield shift of ^{18}O-cholesterol opposed to the residual non-enriched analogue.

This result was found to be lower than anticipated using 98% enriched $^{18}OH_2$ acquired commercially. There are two major sources of $^{16}OH_2$ that will limit the isotopic enrichment for the HBF_4 catalysed procedure, residual H_2O in the solvent (0.007% by Karl Fisher titration) and in the commercial $^{18}OH_2$. Analysis of the commercial $^{18}OH_2$ by laser spectroscopy revealed an enrichment of 95.7%, leading to a maximum theoretical enrichment of 93.5 ± 0.04%. The CF_3SO_3H catalysed route has two additional sources of $^{16}OH_2$ that must be accounted for, the acidic group of the catalyst itself which may exchange with the $^{18}OH_2$ as well as residual H_2O in the acid stock solution. Consideration of these two additional sources of $^{16}OH_2$ establishes the maximum attainable isotopic enrichment to be 92.9 ± 0.04%. Comparison of the modified theoretical and experimental maximum attainable isotopic enrichments of 93.5 ± 0.04 *vs.* 91.0 ± 1.9% and 92.9 ± 0.04 *vs.* 90.0 ± 1.9% for the HBF_4 and CF_3SO_3H routes respectively shows that satisfactory ^{18}O enrichment has been achieved.

For the amount of acid required (0.05 eq.), the dilution in enrichment afforded by exchangeable oxygen in CF_3SO_3H was found to be negligible. CF_3SO_3H and HBF_4 catalysed

enrichments were within error of each other. CF_3SO_3H was found to be the best catalyst due to comparable enrichment and superior yield.[289] Therefore, for use with more expensive $^{17}OH_2$ only CF_3SO_3H was used as a catalyst. The yield was slightly improved (71%) with expected enrichment of 31.7 ± 1.2%. Enrichment could not be determined by ^{13}C NMR isotopic shift in the case of the ^{17}O label. Commercially available $^{17}OH_2$ is a mixture of ^{16}O: ^{17}O: ^{18}O isotopes (15.9:41.1:43.0), this coupled with the quadrapolar nature of ^{17}O leads to the peaks in the ^{13}C spectra being non-resolvable.

It is also of note that these reactions can be performed at gram scale with no diminishment of yield or enrichment. Repetition of the procedure using freshly acquired labelled H_2O and 1,4-dioxane dried over 3Å M.S for 1 week, improved enrichment noticeably, due to no residual H_2O being detected during analysis of the freshly dried 1,4-dioxane. Yields and enrichment are displayed in Table 4.3, in addition to ^{13}C NMR spectroscopy, gas chromatography mass spectrometry (GC-MS) was found to be another effective tool for quantifying label incorporation. X-ray diffraction of ^{18}O-cholesterol revealed no significant difference in the ^{16}O-C and ^{18}O-C bond lengths with average lengths of 1.436 and 1.438 pm respectively. Please note as the isotopically labelled H_2O and 1,4-dioxane are not the same as previously used, the aforementioned maximum theoretical enrichment values quoted no longer apply. The experimental enrichments of ^{18}O-cholesterol shown in Table 4.3 are within >95% of the enrichment content of the $^{18}OH_2$ quoted by the supplier. As the deviation in enrichment was not significant, determination of the exact amount of residual $^{16}OH_2$ was deemed not necessary for this new batch of enriched H_2O.

Table 4.3. Isolated yields and isotope enrichments obtained for ^{17}O & ^{18}O labelled cholesterol as outlined in Scheme 4.1.

Entry	Compound	^{n}O	IY[a] (%)	^{n}O enrichment (%)	
				NMR[b]	GC-MS[c]
1	**81b**	17	71	-[d]	38.0
2	**81c**	18	69	96.1	93.7

[a]IY is isolated yield. [b]Enrichment calculated by integration of ^{13}C NMR signals (error ± 1.9%). [c]Enrichment determined by the intensities of the $[M]^+$, $[M+1]^+$ and $[M+2]^+$ ions in the isotopologue envelope by GC-MS (error ± 1.2%). [d]Peaks were non-resolvable.

4.2.2. Synthesis of ^{17}O and ^{18}O labelled 6-ketocholestanol

Isotopically labelled cholesterol prepared as described in Section 4.2.1, was considered as the starting reagent to produce 6-KC. In order to access the feasibility of the route and optimise the process, the proposed reactions were first attempted on standard ^{16}O-cholesterol. Initially cholesterol was protected to form TBDMS protected cholesterol (**91**) in 77% yield, however hydroboration using borane-THF followed by oxidation, yielded **92** in 45% as shown in Scheme 4.3. The compound contained an estimate of 10 mol% by-products by ^{1}H NMR spectroscopy; a more precise value cannot be presented due to poor resolution of the impurity peaks. A similar literature preparation reports a 30% yield for preparation of **90** from cholesterol.[290] The crude ^{1}H NMR spectrum of the crude borylated mixture shows several peaks at 0.5 ppm corresponding to silyl bound methyl groups. The borylated intermediate would be expected to yield a maximum of two peaks at this chemical shift (diastereomers). Multiple silyl methyl signals imply that either borane or residual BF_3 was promoting deprotection.[291]

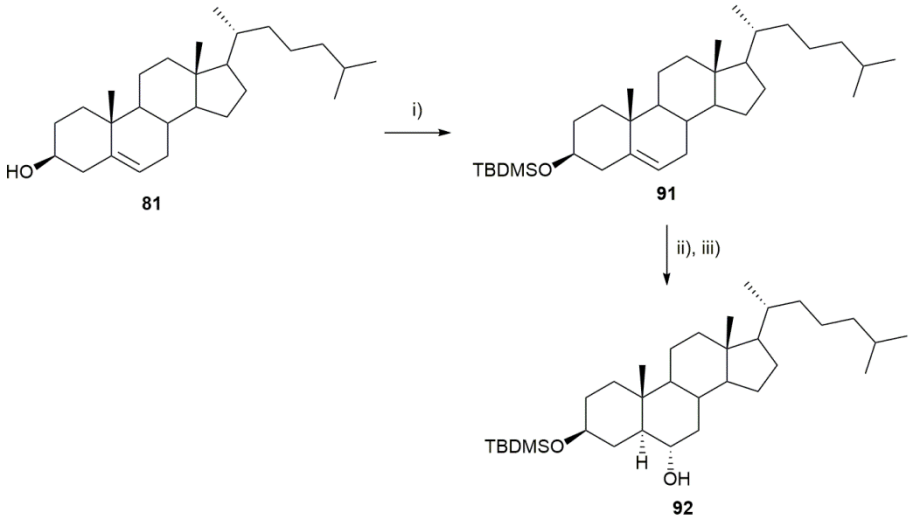

Scheme 4.3. Synthetic route to produce **92**. i) TBDMS-Cl, NMID, I_2, THF, 77%. ii) BF_3.THF, $NaBH_4$, THF. iii) NaOH, H_2O_2, THF, 45%, two steps.

As a consequence of the low yield of **92**; alternative protecting groups were examined. Cholesterol was protected with a tetrahydropyranyl (THP) protecting group, affording compound **93** in higher yield (89%) than the TBDMS analogue (**91**). The THP group presented a small drawback, namely the introduction of a new stereocentre at *2'-C* of the THP ring, complicating analysis by ^{1}H NMR spectroscopy. Hydroboration and oxidation produced alcohol (**94**) in a combined yield of 60% with further oxidation using pyridinum chlorochromate (PCC) producing **95** in 88% yield. Due to the acidic nature of PCC, a small amount of NaOAc was used to prevent premature hydrolysis of the THP-ether.[292] Hydrolysis of the THP-ether was achieved using HCl in 1,4-dioxane to afford 6-KC (**82**) in 82% yield as presented in Scheme 4.4. Deprotection of the THP moiety was initially performed in THF as described in the literature,[293] however butan-1,4-diol was generated as an inseparable by-product on both silica and alumina. Butan-1,4-diol was produced by the acid hydrolysis of THF. Performing the reaction in 1,4-dioxane eliminated by-product formation completely.

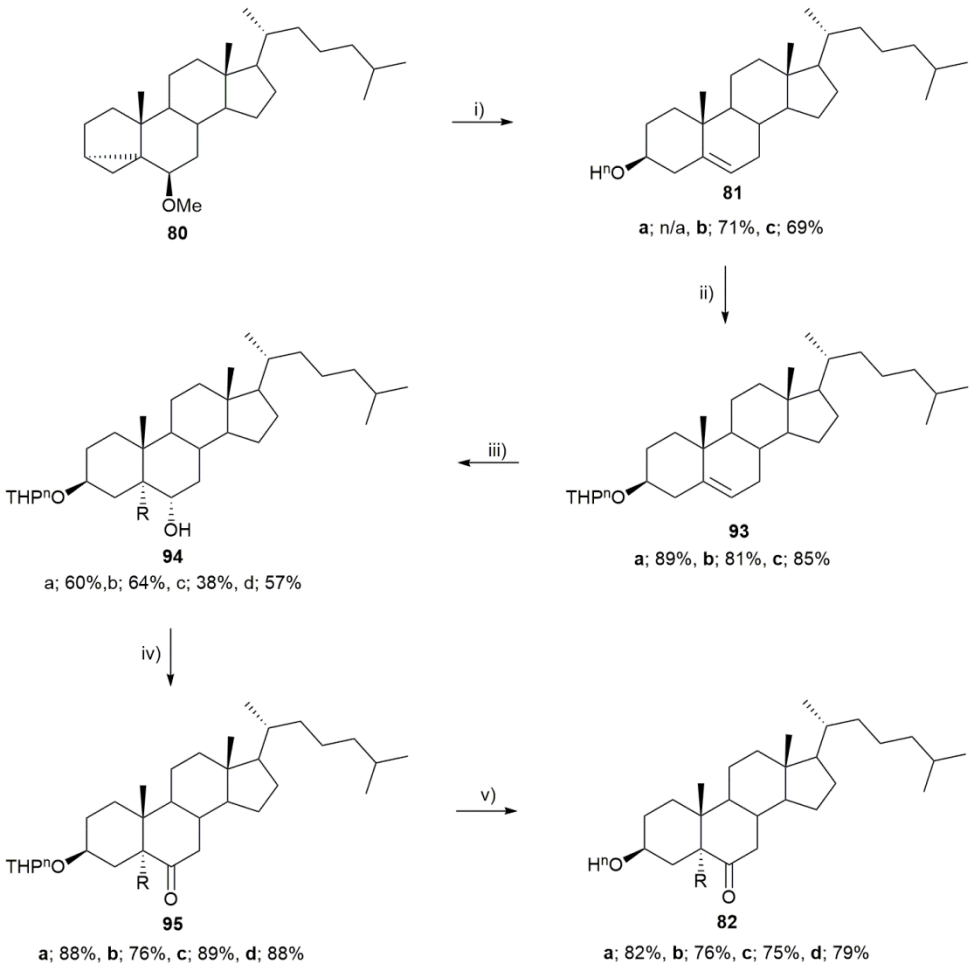

Scheme 4.4. Synthetic route to heavy oxygen atom labelled 6-KC starting from isotopically labelled cholesterol**.** a; n= 16 & R= H, b; n= 17 & R= H, c; n= 18 & R= H, d; n= 18 & R = D. R is only applicable to compounds **94**, **95** and **82**. i) $H_2{}^nO$, CF_3SO_3H, 1,4-dioxane. ii) DHP, PPTS, DCM. iii) $NaBR_4$, $BF_3.OEt_2$, THF, NaOH, H_2O_2. iv) PCC, NaOAc, DCM. v) HCl, 1,4-dioxane.

After sequence optimisation using unlabelled material, the same conditions were employed using ^{17}O and ^{18}O-cholesterol as starting material, yields largely reflected the analogous unlabelled (^{16}O) reactions. For compound **94b** (^{17}O labelled), $NaBD_4$ was used to generate deuterated diborane for hydroboration, producing the deuterated analogue. During subsequent oxidation to produce compound (**95b**), the deuterium label was lost. The loss of deuterium was attributed to the crude mixture being left overnight prior to purification, with the mildly acidic PCC being sufficient to catalyse isotope exchange. In contrast to cholesterol, enrichment values obtained by GC-MS and NMR spectroscopy differed for 6-KC as displayed in Table 4.4 with NMR data indicating lower enrichment than GC-MS. GC-MS indicated no substantial difference in enrichment between cholesterol and 6-KC,

whereas NMR spectroscopy indicated until the final step, isotopic enrichment reflected what was expected with no real deviation from the starting cholesterol. During THP deprotection, partial loss of the label was observed. The ^{18}O label reduced from 96.1 to 53.2 ± 1.9% after stirring for 24 hours in acidic aqueous 1,4-dioxane.

Table 4.4. Isolated yields and isotope enrichments obtained for ^{17}O & ^{18}O labelled cholesterol and 6-KC produced as outlined in Scheme 4.4.

Entry	Compound	^{n}O	R	IY (%)	^{n}O enrichment (%)	
					NMR[a]	GC-MS[b]
1	**82b**	17	H	21	-[c]	33.7
2	**82c**	18	H	15	53.2	93.5
3	**82d**	18	D	23	78.7	90.8

[a]Enrichment calculated by integration of ^{13}C NMR signals (error ± 1.9%). [b]Enrichment determined by the intensities of the $[M]^+$, $[M+1]^+$ and $[M+2]^+$ ions in the isotopologue envelope by GC-MS (error ± 1.2%).[c]Peaks were non-resolvable.

A possible explanation for loss of enrichment was attributed to acid catalysed enol keto tautomerism. The enol form has a configuration analogous to the precursor of i-cholesteryl methyl ether, potentially allowing the formation of the 3,5-cyclopropane ring (Scheme 4.5). This mechanism was corroborated by observation of trace signals consistent with 3,5-cyclocholestan-6-one in the crude ^{1}H NMR spectrum. The signals were compared to authentic synthesised material. In order to probe the proposed mechanism further, a deuterium label was incorporated at the *5-C* position; loss of ^{18}O should correlate to loss of deuterium. Incorporation of D offers an additional spectroscopic marker and due to the kinetic isotope effect a the higher C-D bond strength (*vs* C-H) which should reduce the rate of elimination of $^{18}OH_2$. Incorporation of deuterium was simple, adding little expense by substituting $NaBH_4$ for $NaBD_4$ during hydroboration.

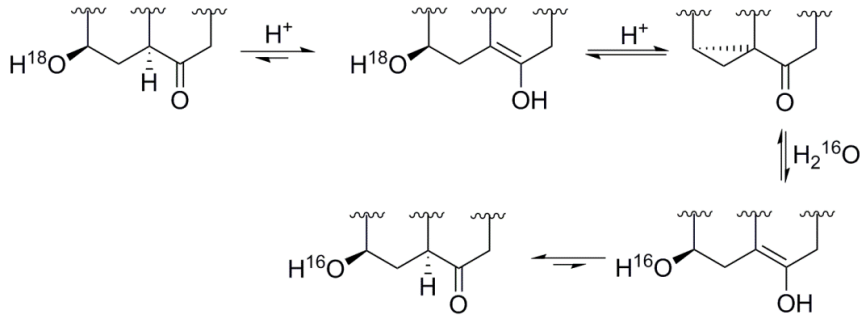

Scheme 4.5. Proposed mechanism for loss of *3-C* ^{18}OH label by conjugated tautomerism of 6-KC.

Compound **82c** was obtained with 77.5% deuterium (^{1}H NMR) and 78.7% ^{18}O enrichment (^{13}C NMR) after 6 hours of stirring in acidic aqueous 1,4-dioxane. The correlation between the loss of D and ^{18}O labels was indicative that they are lost through the same process; this was consistent with the mechanism presented in Scheme 4.5. A possible source of discrepancy between the enrichment values obtained from NMR and GC-MS could be attributed to the more acidic $CDCl_3$ used for NMR spectroscopy *vs.* DCM in GC-MS, this coupled with the compound being in solution longer for the acquisition of the NMR spectrum. In order to validate this theory a sample of unlabelled 6-KC was dissolved in $CDCl_3$ which had been washed by D_2O and the enrichment recorded by GC-MS. Enrichment of the $[M+1]^+$ peak was expected if deuterium exchange occurred, however due to the free alcohol group an exchange of > 100% was necessary to distinguish exchange of the ketone α-H. After a comparable amount of time taken for the ^{13}C NMR spectrum to be recorded (24 hours) the $[M+1]^+$ peak was enriched by 22.5 ± 1.2%. This exchange was attributed to exchange of the more labile ^{1}H of the alcohol. The use of the same D_2O washed $CDCl_3$ for NMR measurement resulted in no exchange over the same period, although it is likely that any acid accumulated in the $CDCl_3$ could have been removed by the D_2O wash. The cause of the difference in enrichment values is still inconclusive at this time. As seen in Figure 4.4, both the ^{13}C and total ion chromatograph (TIC) of the mass spectrum (GC-MS) for D and ^{18}O labelled 6-KC appear to show clean product with no indication of a contaminant which constitutes > 20% of the material.

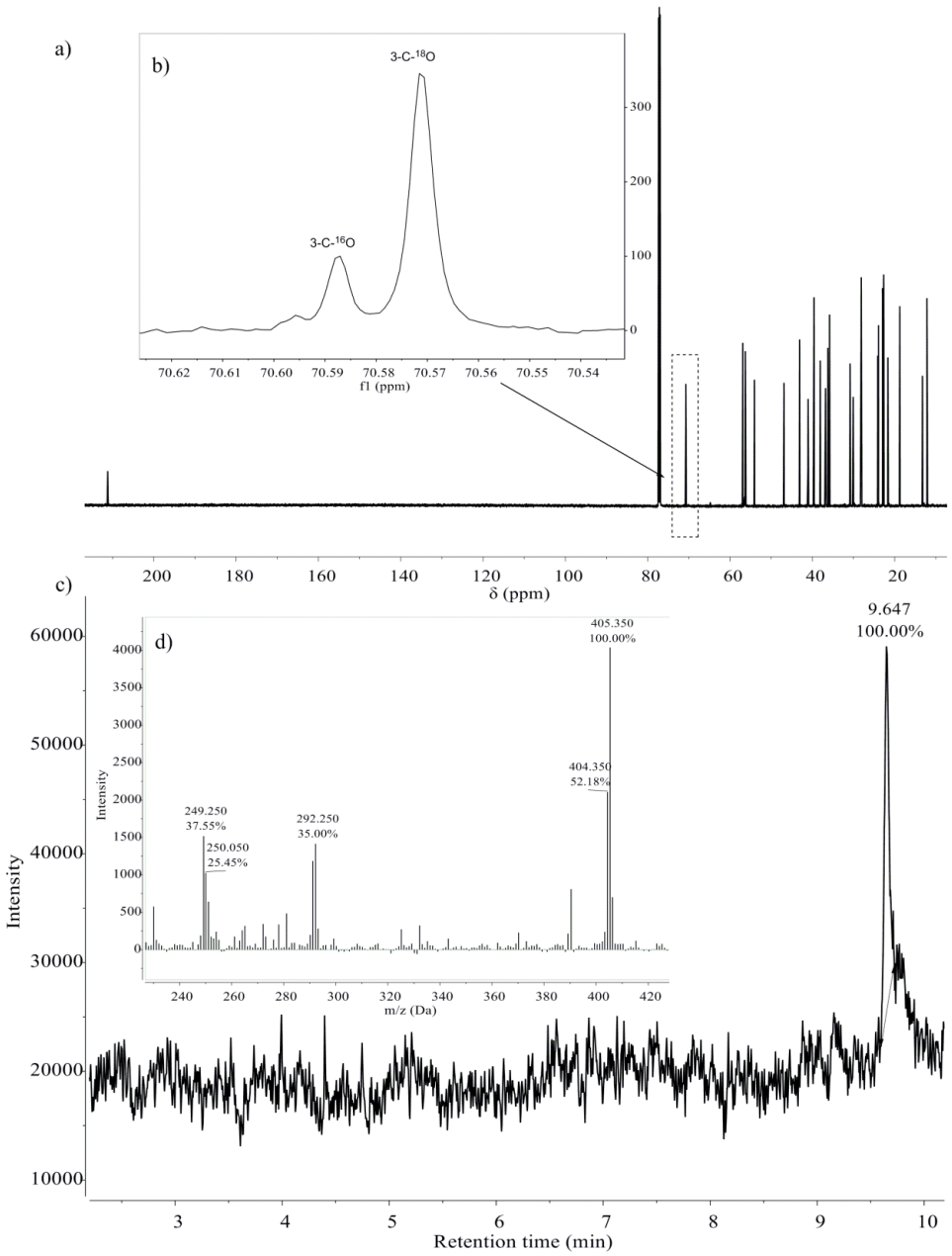

Figure 4.4. a) ^{13}C NMR spectrum of ^{18}O and D labelled 6-KC. b) Enhanced region of the *3-C* peak, showing *3-C*-^{16}O and *3-C*-^{18}O centres. C) GC-MS TIC of ^{18}O and D labelled 6-KC d) Mass spectrum of 6-KC at 9.6 min showing labelled 6-KC (Unlabelled 6-KC; *m*/*z* 402).

It should also be noted the *6-C* exhibits an upfield shift of 75 ppb, which could possibly be indicative of two effects. Firstly, ^{18}O incorporation at *6-C* could occur *via* $^{18}OH_2$ liberated from the *3-C* position forming a hydrate and exchanging at the *6-C* position. Incorporation of 21% does not seem likely as $^{18}OH_2$ would constitute only 0.2% of the total H_2O present within the reaction. Additionally the peak difference was 75 ppb opposed to 16 ppb for the isotopologues of the *3-C* peaks, although ketones are expected to give a larger

chemical shift difference, values of 50 ppb appear more typical.[294] The second more likely possibility was the upfield shift was due to two bond deuterium isotope effect, with a two bond shift of 70 ppb reported for the quaternary carbonyl of benzaldehyde.[295] Additionally repetition of the reaction conditions on substrates bearing ^{17}O and ^{18}O labels without deuterium do not display multiple peaks in the *6-C* region of the ^{13}C NMR spectrum. This further suggests that no enrichment at the *6-C* centre was occurring and the upfield shift was caused by a deuterium isotope effect.

Regardless of the potential loss of isotopic label, the overall yields were 15-23% representing a significant loss when dealing with expensive isotopically labelled intermediates. A more cost effective route with higher enrichment was sought in which ^{16}O-cholesterol was first converted to a 6-KC precursor (**97**), followed by a final step to incorporate the isotopic tag. The best precursor was determined to be the transient 3,5-cyclocholesterol intermediate formed during 6-KC tautomerisation (Scheme 4.5). This alternative synthetic strategy is outlined in Scheme 4.6.

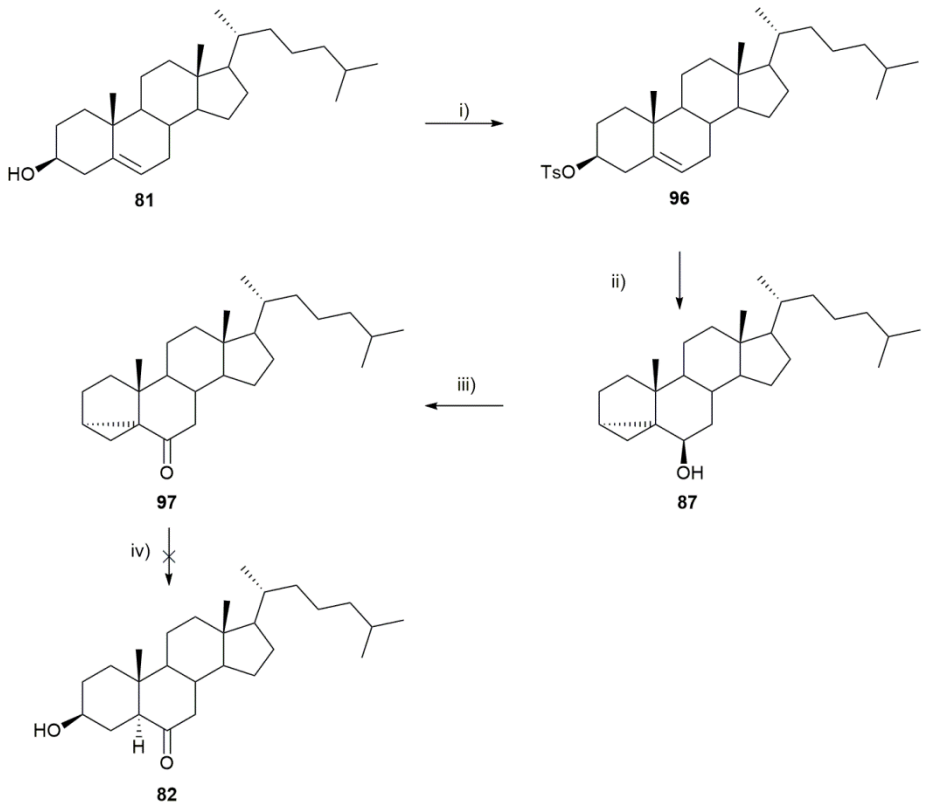

Scheme 4.6. Alternative synthetic route to produce isotopically labelled 6-KC. i) TsCl, Py, DCM, ii) MEK, $NaHCO_3$, 75% (two steps). iii) PCC, NaOAc, DCM, 78%. iv) H_2O, CF_3SO_3H, 1,4-dioxane, no product isolated.

Cholesterol was tosylated and subsequently hydrated with isolation of the desired alcohol (**87**) in 75% yield. Aside from the desired alcohol, cholesterol (**81**) was also obtained as a by-product. The distribution of products was found to be dependent on the reaction conditions; concentrated basic solutions with low H_2O: MEK ratios were found to favour formation of the desired **87** over **81** with a respective ratio of 87:13. Subsequent oxidation by PCC and NaOAc afforded ketone (**97**) in 80% yield**.** In agreement with the literature, a 2:1 ratio of NaOAc: PCC was paramount, lower ratios resulting in olefenic and aldehydic by-products.[296] Refluxing the obtained 3,5-cyclocholestanol with triflic acid and low H_2O concentrations (10 eq.) in 1,4-dioxane formed trace amounts of 6-KC, with sterol functionalised by triethylene glycol in the *3-C* position dominating. Triethylene glycol was produced by acid catalysed ring opening of the solvent, an analogous reaction has been previously observed when using THF under acidic conditions, forming **90a-c**. Similarly, use

of H_2O stable Lewis acid ($CeCl_3$) in refluxing 1,4-dioxane returned only unreacted starting material after several days. Increasing the concentration of H_2O (166 eq.) and HCl (5 eq.) was found to return unreacted starting material and an unknown compound that could not be identified with full confidence. The by-product was suspected to be either a dimer or 3-chloro derivative due to its high R_f value by TLC. GC-MS indicated that the latter was likely as a compound at the same *m*/*z* value with the characteristic chloride isotope distribution was discovered.

An alternative 3-tosyl precursor (**99**) was also explored to incorporate heavy oxygen into 6-KC. The key step was direct substitution of tosyl ether by H_2O; a possible overlooked solution. *3-C* is a secondary centre, with substitution expected to proceed *via* an S_N1 or S_N2 mechanism. An S_N2 mechanism would result in inversion of stereochemistry giving the undesired diastereomer. Direct S_N2 displacement by H_2O cannot occur due to the equatorial position of the tosylate, and cholesterol is conformationally locked; therefore correct angle of attack for the H_2O nucleophile cannot be achieved, eliminating the possibility of a direct S_N2 mechanism. A S_N1 process must occur with gauche 1-3 interactions sterically blocking the α-face, forcing attack from the β-side of the ring and retention of stereochemistry. Tosylation of cholesterol produced the desired tosylated cholesterol (**96**) as a crude mixture also containing TsCl. The crude material could be purified by recrystallisation from MeOH, however excess heating must be avoided to prevent conversion to methylated cholesterol (**86**). Due to the potential to form **86** as a by-product, **96** was used in the subsequent hydroboration reaction producing **98** in 77% yield. Oxidation using PCC generated ketone (**99**) in 78% yield. Although **99** could be produced in good yield, conversion to 6-KC was not possible as shown in Scheme 4.7. Use of CF_3SO_3H as a catalyst with > 10 eq. H_2O afforded no reaction at room temperature and production of 3-triethylene glycol ether by-product at elevated temperatures. Although further optimisation was not pursued, a larger excess of H_2O may produce 6-KC, indicative by formation of methylated cholesterol (**86**) during hot recrytallisation of tosylated cholesterol (**96**) with a large excess of MeOH.

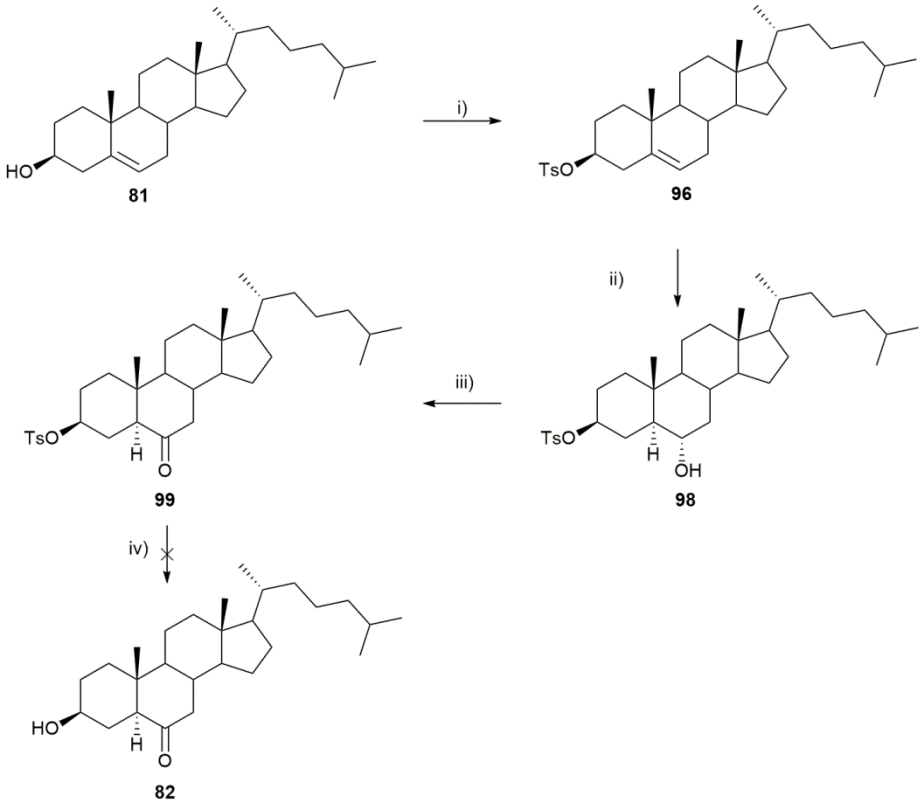

Scheme 4.7. Synthetic route to heavy oxygen atom labelled 6-KC from a non-enriched tosyl intermediate (**99**). i) TsCl, Py, DCM. ii) $NaBH_4$, $BF_3.OEt_2$, THF. iii) NaOH, H_2O_2, 77% (three steps). iv) PCC, NaOAc, DCM, 78%. v) H_2O, CF_3SO_3H, 1,4-dioxane, no product isolated.

Unfortunately addition of an isotopic label in a final step was found to not be viable from both tosyl (**99**) and 3,5-cyclosterol (**97**) precursors; therefore, the best route was determined to be starting with labelled cholesterol as outlined in Scheme 4.4.

4.2.3. Synthesis of ^{17}O and ^{18}O labelled 25-hydroxycholesterol

Heavy oxygen enriched 25-HC was synthesised next; enrichment could in principle be achieved either from isotopically labelled cholesterol or by conversion of unlabelled material to the 3,5-cyclosterol followed by enrichment. The latter route was initially explored due to its less waste of labelled intermediates, lower expense and shorter synthetic pathway. All steps except the final transformation are required to only be performed once, whereas starting from labelled cholesterol requires duplication of every step for the ^{17}O and ^{18}O isotopologues. Although unlabelled 25-HC is commercially available, expense resulted in the need for unlabelled 25-HC to first be synthesised from cholesterol. Although

oxidation of the terminal isopropyl moiety appears challenging, a literature procedure has established a relatively chemoselective oxidation utilising a dioxirane reagent.[297] This procedure can be expanded upon to incorporate isotopically labelled oxygen at the *3-C* position as shown in Scheme 4.8.

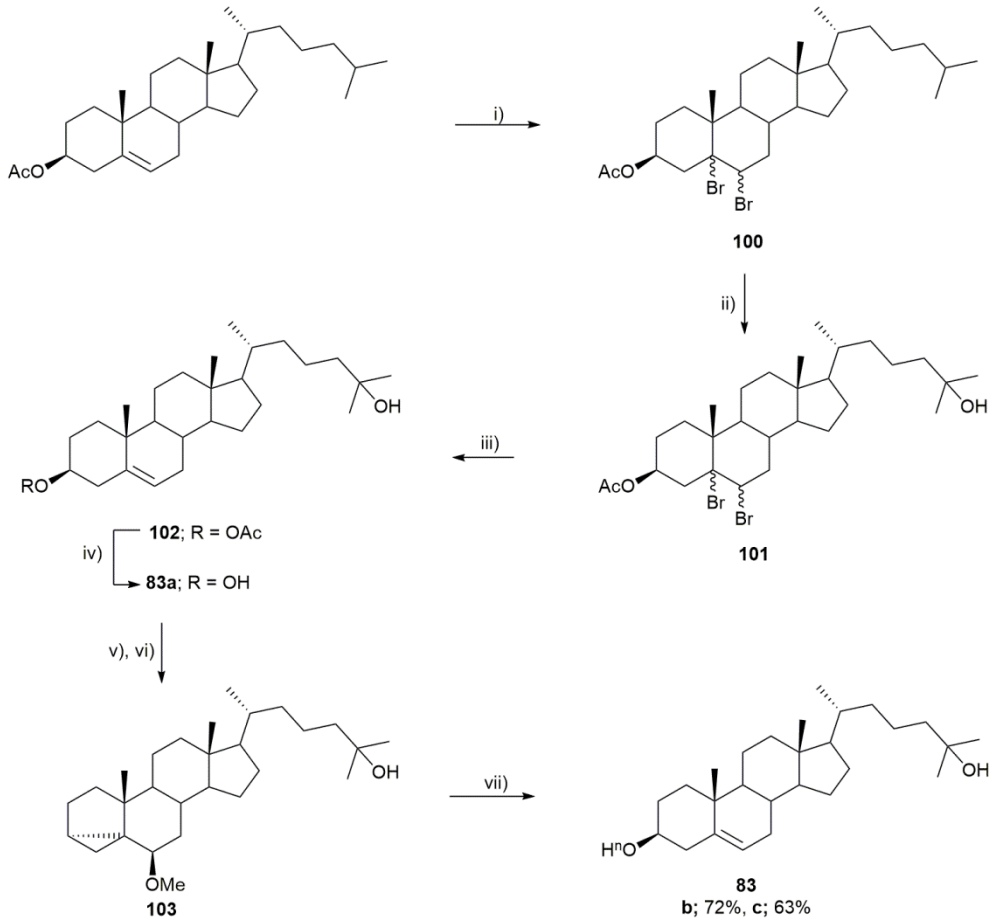

Scheme 4.8. Synthetic route to labelled 25-HC. a; n= 16, b; n= 17, c; n= 18. i) Br_2, DCM, 85%. ii) TFP, oxone, $NaHCO_3$, H_2O: DCM , 39%. iii) Zn, AcOH, Et_2O, 83%. iv) KOH, MeOH, 96%. v) TsCl, Py, vi) $NaHCO_3$, MeOH, 69%. vii) $H_2{}^nO$, CF_3SO_3H, 1,4-dioxane.

Prior to the key oxidation step, the *3-OH* and Δ^5 moieties must be protected, preventing undesired ketone and epoxide formation respectively. Commercially available cholesteryl acetate was brominated (85% yield) producing mixed diastereomers (**100**), the 5α-6β dibromo diastereomer (kinetic product) was predominately obtained. The 5β-6α dibromo diastereomer (thermodynamic product) was also produced; with the kinetic and thermodynamic product interconverting through the α-bromonium ion intermediate as

shown in Figure 4.5. The inter-conversion from kinetic to thermodynamic product was monitored over a period of 9 weeks with no final equilibrium witnessed. After this period of time a ratio of 37:63 kinetic: thermodynamic product was observed. It should be noted that even in the relatively dilute NMR sample, 16% inter-conversion was witnessed after 2 days.

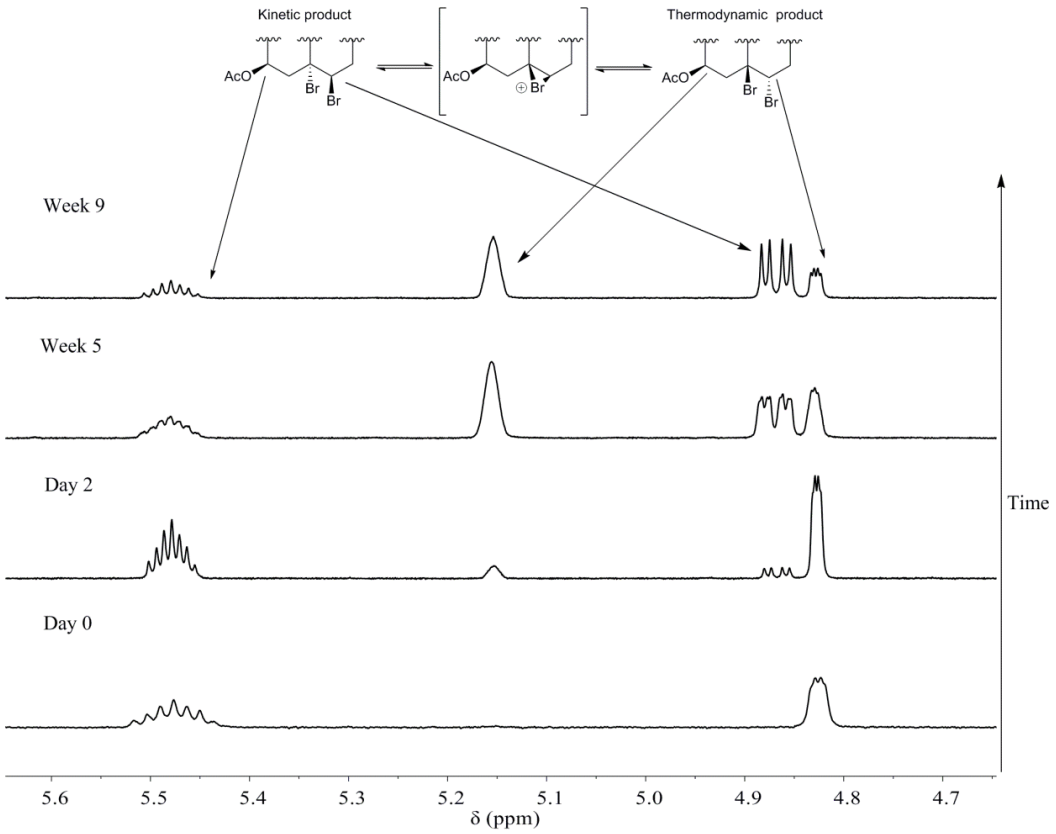

Figure 4.5. ^{1}H NMR spectra showing interconversion of the kinetic and thermodynamic products of bromination of 3β-acetoxycholesterol *via* the α-bromonium ion intermediate.

Higher amounts of thermodynamic product were obtained in concentrated solutions of Br_2 and cholesteryl acetate as displayed in Figure 4.6. The plot broadly follows a bimolecular process, in agreement with nucleophilic attack of the α-bromonium ion by liberated bromide ion, supporting interconversion of the stereogenic centres.[298] Quick reactions with dilute substrate solutions limited thermodynamic product formation; the kinetic product was isolated in 67% yield, allowing full characterisation and elucidation of the crystal structure.

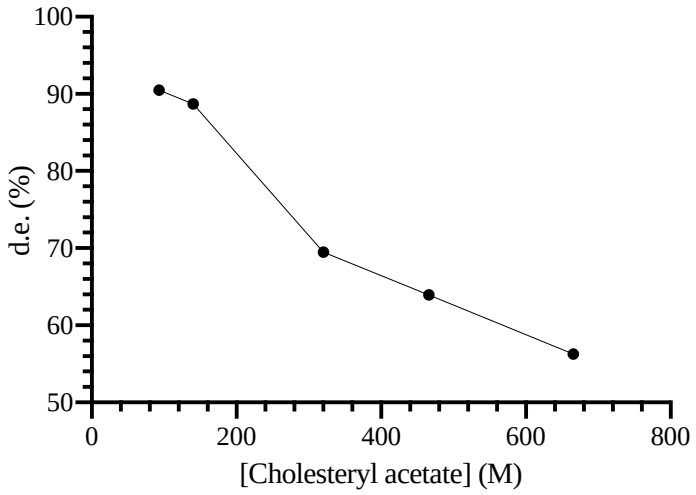

Figure 4.6. The effect of cholesteryl acetate concentration on the d.e. (%) of the kinetic product during bromination. ^{1}H NMR integrations of crude mixtures were used to determine d.e. (%).

Ultimately mixed diastereomers were used in the subsequent oxidation which was performed in DCM. Some interconversion (*ca*. 9%) occurred over the course of the reaction, necessitating recovery of both diastereomers for optimal yield. Resolution of the diastereomers by chromatography was not necessary as treatment of either diastereomer with zinc produces the same desired unsaturated product (**102**).

RuO_4 produced catalytically *in situ* has previously been reported to selectively oxidise tertiary unactivated C-H bonds.[299] Use of similar conditions at room temperature after 3 days returned unmodified starting material. Use of an elevated temperature resulted in the isolation of 3% of cholesterol oxidised at *25-C*, with the remaining material being a mixture of single and multiple oxidation products. Isolation of a trifluoromethyl(methyl)dioxirane (TFDO) was achieved by the reaction of oxone with trifluoropropanone (TFP) in basic aqueous solution. Subsequent oxidation of **100** using TFDO in TFP allowed isolation of the desired oxidised derivative with 22% yield after 3 hours. The starting material (both diastereoisomers) was largely recovered (57%), alongside the oxidised thermodynamic diastereoisomer. The yield of **101** was lower than that previously reported and can be attributed to inaccuracy in measuring the volume of TFDO used.[300] Accurate dispensing of low boiling TFDO (-20 °C) was practically challenging.

TFDO generated *in situ* produced **101** in 39% yield after 10 hours using 60 eq. of TFP. Although such a large excess of ketone appears discouraging, isolation of TFDO proceeded in 1.5-2.3% yield, whilst literature *in situ* oxidation used 300 eq. of ketone obtaining an isolated yield of **101** only 6% greater than reported in this work.[297] The reason for the low literature yield was likely due to Iida only recovering the kinetic product of the bromine exchange, although subsequent reduction of either trans vincial dibromide returns the desired alkene (**102**). Due to handling difficulties, safety concerns of storage and higher yield, *in situ* dioxirane formation was favoured.

Treatment of mixed diastereomers with Zn solely produced the desired product (**102**), which was subsequently deacylated in basic MeOH giving 25-HC in an 80% yield over two steps. 25-HC was toslyated exclusively at the *3β-OH* position upon addition of TsCl and pyridine; steric effects prevented tosylation of the *25-OH* position. The crude tosylated product subsequently underwent methanolysis to form the desired 3,5-cyclosterol (**103**) and 3β-methoxy-25-hydroxycholesterol by-product in a 87:13 ratio in 69% yield over two steps. The structural isomers were inseparable on alumina or silica, resulting in use in the final step being performed on this crude mixture. Use of crude **103** with $^{18}OH_2$ (5 eq.) and CF_3SO_3H (0.05 eq.) generated the heavy oxygen labelled 25-HC isotopologues in a good yields and excellent enrichment as shown in Table 4.5.

As well as the literature method, direct oxidation by TFDO of the commercially available i-cholesteryl methyl ether was examined. The 3,5-cyclosterol motif would simultaneously protect both oxidant sensitive centres, enabling production of labelled 25-HC in two steps. Unfortunately, stirring i-cholesteryl methyl ether with TFDO generated *in situ* for 8 hours did not generate any product (**103**). The mixture contained 35% starting material, with the remaining 65% corresponding to a ketone containing by-product, most likely compound **97**. The basic aqueous conditions resulted in hydration of the 3,5-cyclosterol producing a i-cholesterol (**87**) followed by oxidation by TFDO to form ketone (**97**).

Table 4.5. Isolated yields and isotope enrichments obtained for ^{17}O & ^{18}O 25-HC synthesised as outlined in Scheme 4.7.

Entry	Compound	^{n}O	IY[a] (%)	^{n}O enrichment (%)	
				NMR[b]	GC-MS[c]
1	**83b**	17	72	-[d]	33.4
2	**83c**	18	63	92.6	88.3

[a]Isolated yields are of the heavy oxygen label incorporating step. [b]Enrichment calculated by integration of ^{13}C NMR signals (error ± 1.9%). [c]Enrichment determined by the intensities of the $[M]^+$, $[M+1]^+$ and $[M+2]^+$ ions in the isotopologue envelope by GC-MS (error ± 1.2%). [d]Peaks were non-resolvable.

The overall yields were 13 and 12% for the ^{17}O and ^{18}O derivatives of 25-HC after seven steps; however yields of incorporating the ^{17}O and ^{18}O labels were 71 and 63% respectively. The loss of labelled material was not significant, labelled material could have been obtained by using isotopically labelled cholesterol as starting material; however oxidation of the *25-C* position was low yielding (39%). This is not cost effective due to the loss of large amounts of labelled intermediates. Additionally, starting from labelled material would result in every reaction in the sequence having to be repeated for the ^{17}O and ^{18}O analogues, so was a more time consuming process than splitting material at the final step, and incorporating the label separately.

4.2.4. Alternative route to isotopically labelled sterols

In spite of enrichment *via* the 3,5-cyclosterol intermediate proceeding with good yields, excellent enrichments and low requirements for labelled H_2O, the methodology was limited in substrate scope. This approach requires that substrates have *3-OH* and Δ^5 moieties, to enable formation of 3,5-cyclosterol. Therefore an alternative more widely applicable method was sought, to enable enrichment of compounds of interest without this structural motif, such as lanosterol. Carbonyl moieties can rapidly exchange with labelled H_2O either *via* acid catalysed acetal deprotection or by hydrate formation, the label can then be trapped by reduction, preventing back-exchange.[301] Interestingly, the reductant used may act as a source of deuteride such as a $NaBD_4$, allowing deuterium incorporation in addition to heavy oxygen isotopes. Deuterium labels similarly have applications in NMR spectroscopy and

mass spectrometry. The two routes are displayed in Scheme 4.9. Direct enrichment (Route A) contains fewer steps and, therefore, is quicker, uses fewer reagents and would be expected to produce a higher yield; however the methodology provides some drawbacks. The method can only be tested using labelled H_2O, so has higher initial cost during optimisation. Additionally, the maximum enrichment will be based on the statistical distribution of labelled H_2O: substrate, as the starting ^{16}O of the carbonyl effectively dilutes enrichment. In contrast, the dioxalane method (Route B) has additional steps but optimisation is cheaper, dioxalane deprotection can be monitored by conventional means using $^{16}OH_2$. The theoretical enrichment is larger as there are no sources of $^{16}OH_2$ from the substrate.

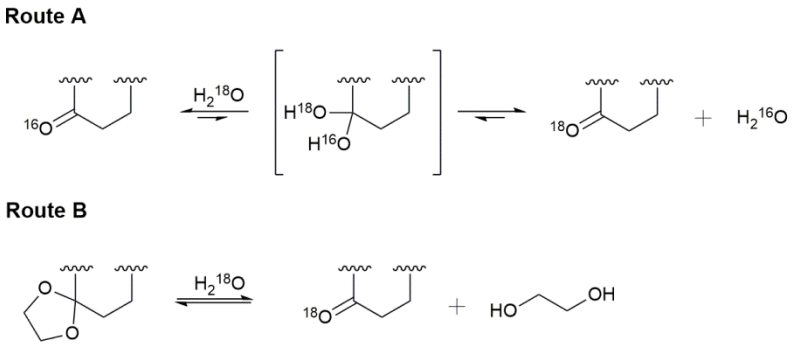

Scheme 4.9. Routes A and B for obtaining isotopically labelled steroidal ketones.

Early efforts focussed on labelling cholesterol, requiring oxidation to form 3-keto-cholest-5-ene. Oxidation with Dess-Martin periodinane produced 3-keto-cholest-5-ene in high conversion (90%) and a small degree of isomerisation producing 3-keto-cholest-4-ene. Purification on silica resulted in the 4-ene isomer being recovered exclusively; 4-ene isomerisation has been reported to proceed under acidic conditions.[302] Subsequent label incorporation proceeds *via* acid catalysed dioxalane hydrolysis, therefore, acid sensitivity prohibits use of 3-keto-cholest-5-ene as a suitable substrate. Focus was shifted to saturated 5α-cholestan-3-one as shown in Scheme 4.10. Methodologies A and B (Scheme 4.9) are complementary to the 3,5-cyclosterol methodology previously discussed (Section 4.2.1). Direct incorporation and dioxalane deprotection procedures are to be utilised in substrates devoid of a Δ^5 moiety which in-turn are unable to produce 3,5-cyclosteroids and hence are

unable to utilise the original methodology. These new approaches simply require a *3-OH* moiety and a sterically crowded α-face, requirements ubiquitous within sterols. The major restrictions are acid and reductant sensitivity of the substrate.

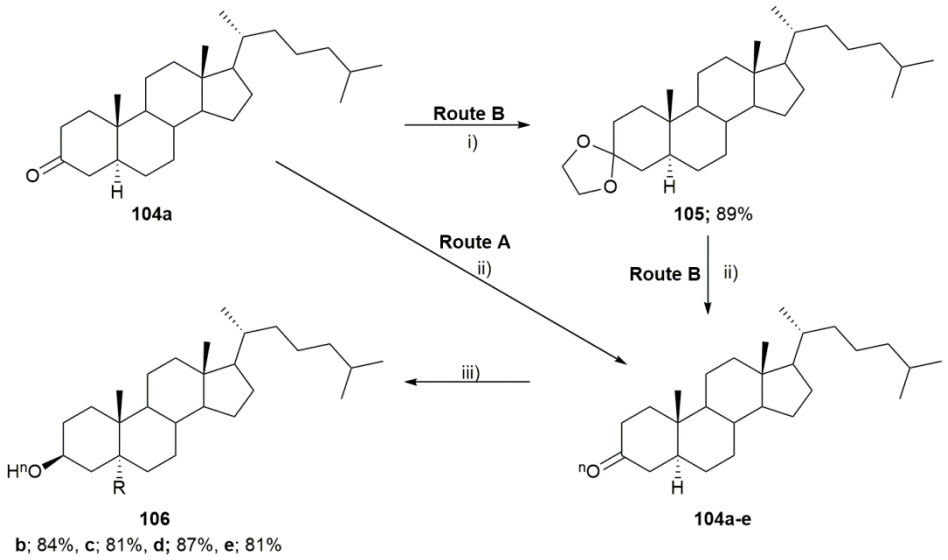

Scheme 4.10. Direct enrichment (Route A) and the 'Dioxalane approach' (Route B) for isotopic enrichment of 5α-cholestan-3β-ol (**106**). IY given for Route A only. a; n = 16, R = H, b; n = 17 & R = H, c; n = 18 & R = H, d; n = 17 & R = D, e; n = 18 & R = D. i) Ethylene glycol, 3Å M.S, TsOH, toluene. ii) $H_2{}^nO$, CF_3SO_3H, 1,4-dioxane. iv) $NaBR_4$, 1,4-dioxane.

Direct incorporation was explored first. 5α-Cholestan-3-one (**104**) was stirred with CF_3SO_3H (0.05 eq.) and $^{18}OH_2$ (5 eq.) in 1,4-dioxane under an argon atmosphere. At 1 hour intervals, an aliquot of solution was removed and added to an air tight mass spectrometry vial containing 3 Å M.S and anhydrous DCM under an argon atmosphere. The beads prevent back-exchange by removing $^{16}OH_2$ as well as quenching the reaction by removing $^{18}OH_2$. The vials were then submitted for GC-MS with 10 repeats per hour. Monitoring of the $[M]^+$ and $[M+2]^+$ peaks allowed determination of the level of enrichment. In order to establish a baseline for the $[M+2]^+$ peak (due to background isotopic enrichment) and determine variation between sample injections, 10 repetitions of **104** were submitted for GC-MS.

Maximum enrichment was obtained in less than 1 hour. A leak in the reaction vessel or introduction of air during sampling was responsible for dropping enrichment (3.9% average) each hour. Consistent values within the repeats of hourly measurements testify to

the mass spectrometry vials remaining air tight over the course of the reaction. The largest standard deviation obtained was 1.2%; therefore subsequent samples were only tested by single injection in order to probe shorter reactions in real time. After less than 10 minutes maximum enrichment was achieved (74. 5 ± 1.2%), which did not change after 1 hour (75.4 ± 1.2%), indicating that a maximum exchange time of 10 minutes was necessary prior to reduction. ^{18}O enriched 5α-cholestanol (**106c**) was produced in 83% yield with an enrichment of 77.5 ± 1.9%, in agreement with the maximum achievable enrichment of 81.6%. Doubling the volume of H_2O (10 eq.) was found to increase enrichment to 84.0 ± 1.9% (maximum enrichment 89.2%). Higher H_2O volumes were not investigated to keep the process economical.

In addition to the desired product, labelled *3α-OH* epimer was also recovered in 7% yield. Efforts were made to limit the production of the 3α-epimer, the use of cyclopentylmagnesium bromide (CpMgBr) has been reported to solely produce the desired 3β-OH epimer,[303] repetition of the procedure produced the 3α-OH epimer in comparable yields as for reduction by $NaBH_4$. A possible source of discrepancy between the findings and literature may be the amount of H_2O present; the epimeric ratio obtained by reduction was shown to be H_2O sensitive.[304] CpMgBr was not pursued further as the reagent was not suitable for a one pot synthesis in 1,4-dioxane due to incomplete conversion.

Improvement of enrichment was next sought using the dioxalane route. Commercially available **104** was protected to afford dioxalane (**105**) in 89% yield. Addition of H_2O (5 eq.) and HCl in anhydrous 1,4-dioxane (0.3 eq.) was shown to produce **104** in 75% conversion after 6 hours with no further improvement after 16 hours, subsequent reduction of **104** yielded the target alcohol (**106**) in 45%. The reactions were non-reproducible with declining yields being obtained each time the reaction was repeated, over a period of five days. Degassing of the stock HCl solution was found to be responsible. Substitution of HCl for less volatile CF_3SO_3H produced **104** reliably for at least 3 weeks. As CF_3SO_3H contains exchangeable oxygen, minimal quantities of acid (0.05 eq.) were used.

Whilst HCl converted dioxalane (**105**) to ketone (**104**) in 75% conversion, CF_3SO_3H only produced a 52% conversion. Doubling the concentration of CF_3SO_3H to 0.1 eq. led to no improvement in conversion. Addition of $NaBH_4$ was shown to increase conversion to **106** to 74%, as the ketone was reduced *in situ*, equilibrium was driven to form more ketone which was subsequently reduced, increasing the overall conversion. Varying the amount of H_2O from 3-8 eq. was also found to give **104**:**105** in an approximate 1:1 ratio, with similar conversion upon addition of $NaBH_4$.

Low conversions led to other acids being assessed. Lewis acids, $InOTf_3$ and $FeOTf_3$ were trialled in the place of Brønsted acids. A one pot mixture in which the acid, hydride and H_2O were all stirred in 1,4-dioxane produced conversions to alcohol (**106**) of 23 and 30% after 16 hours for $FeOTf_3$ and $InOTf_3$ respectively. Staggering the addition of aqueous acid and $NaBH_4$ by 3 hours led to an overall conversion of 74%. A reductive system of $FeOTf_3$ and $NaBH_4$ has previously been described to reduce alkenes in EtOH, although alkene hydrogenation has shown to be limited with competing keto and alcohol groups.[305] In order to test the versatility of the label incorporation, these conditions were applied to crude lanosterone, a sterol bearing two unsaturated moieties at *24-C* and *8-C* (Figure 4.7). Application of the reductive system (in refluxing aqueous 1,4-dioxane) reduced the Δ^{24} content by 21% (determined by GC-MS). The undesired reduction of the alkene moiety stopped further investigation of Lewis acid catalysts.

In contrast to the original hypothesis, Route B (Scheme 4.10) was found to produce lower enrichments (71.9 ± 1.9%) using 5 eq. of labelled H_2O when compared with Route A (77.5 ± 1.9%). The low enrichment may be attributed to further dioxalane deprotection occurring during work-up, producing unlabelled **106**. As Route A produced both higher yields and enrichment in less than 1.5 hours, it was the obvious route for isotopic enrichment; Table 4.6 displays the isotopic enrichment for a combination of labels by Route A.

Table 4.6. Yields and isotopic enrichments obtained for the direct enrichment approach to produce 5α-cholestenol as displayed in Scheme 4.10.

Entry	Compound	^{n}O	R	IY (%)	^{n}O enrichment (%)	
					NMR[a]	GC-MS[b]
1	**106b**	17	H	84	-[c]	29.0
2	**106c**	18	H	81	84.0	86.6
3	**106d**	17	D	87	-[c]	28.3
4	**106e**	18	D	81	-[c]	83.5

[a]Enrichment calculated by integration of ^{13}C NMR signals (error ± 1.9%). [b]Enrichment determined by the intensities of the $[M]^+$, $[M+1]^+$ and $[M+2]^+$ ions in the isotopologue envelope by GC-MS (error ± 1.2%). [c]Peaks were non-resolvable.

4.2.5. Synthesis of heavy oxygen labelled lanosterol

Lanosterol plays a major role *in vivo*, it is biosynthesised from the tri-terpene oxidosqualene and is one of the first sterols produced acting as a precursor in the biosynthetic pathways of cholesterol and ergosterol in animals and fungi.[306,307] Although a different pathway (*via* cycloartenol) to produce phytosterols is thought to be more prevalent in plants, recently lanosterol synthase was isolated from the genus *Arabidopsis*, showing the significance of lanosterol in a wide range of organisms.[308] There is a billion dollar industry dedicated to producing pharmaceuticals which target cholesterol and, hence, low density lipoprotein biosynthesis known as 3-hydroxy-3-methyl-glutaryl-coenzyme A reductase inhibitors or statins.[309] Statins inhibit the production of mevalonate, a precursor to both cholesterol and lanosterol. There is some evidence that prolonged use of statins correlates to an increased incidence of cataract formation.[310] This is somewhat corroborated by lanosterol being amongst a small number of sterols which has been proven to reduce the size of nuclear cataracts in animal models.[284] Chaga mushrooms (*Inonotus obliquus*) have been used as a natural remedy to treat cancer, recently lanosterol isolated from the fungi has been found to be one of the active components. Lanosterol isolated from Chaga mushrooms reduced sarcoma tumour cells within mice, although the underlying mechanism was not investigated.[311] Isotopic labelling of lanosterol will be achieved by applying the direct enrichment methodology optimised using the 5α-cholestanol substrate.

Due to the expense of pure lanosterol, a cheaper technical grade material containing lanosterol, 'isocholesterol' was used to optimise conditions for first oxidising lanosterol to lanosterone, followed by reducing back to lanosterol in the presence of minimal H_2O as seen in Scheme 4.11. This will serve as a trial for direct enrichment by heavy oxygen isotopes using minimal volumes of enriched H_2O. Isocholesterol is composed largely of lanosterol (**84**) and dihydrolanosterol (**107**) typically in a 60:40 ratio depending upon the supplier (other sterols may also be present in smaller quantities).[312] Lanosterol was determined by GC-MS to represent 68% of the technical grade isocholesterol mixture used in the subsequent experiments.

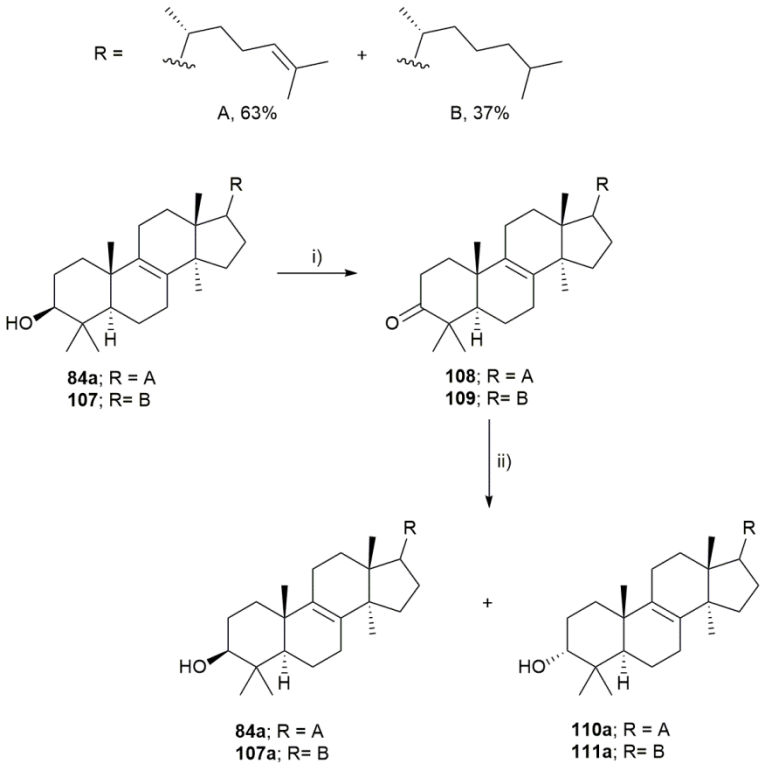

Scheme 4.11. Optimisation of oxidation and reduction steps using technical grade isocholesterol composed primarily of **84** and **107**. i) See Table 4.7. ii) See Table 4.8.

A small range of oxidation conditions were trialled as shown in Table 4.7 Both Jones and Dess-Martin oxidations produced complex mixtures with multiple unidentified signals in the crude ^{1}H NMR spectrum. In contrast, Epp Widlanski oxidation conditions proved completely ineffective at oxidising the mixture with recovery of the starting alcohols (**84** and **107**). Swern oxidation was found to be the best method, producing ketones **108** and

109 in a 72% yield, it was rationalised that the low temperature (-78 °C) and short reaction time (30 minutes) prevented significant by-product formation.

Table 4.7. Isolated yields of mixed lanosterone products (**108**, **109**) obtained under various oxidations of technical grade isocholesterol.[a]

Entry	Common name	Reagents	IY (%)
1	Epp Widlanski[b]	$PhI(OAc)_2$, TEMPO, DCM: H_2O	0
2	Jones	PCC, NaOAc, DCM	35
3	Dess-Martin	Dess-Martin periodinane, DCM	57
4	Swern[c]	$(COCl)_2$, DMSO, NEt_3, DCM	72

[a]All reactions were performed overnight using 1.5 eq. of oxidant at room temperature unless otherwise stated. [b]1.1 eq. of $PhI(OAc)_2$ and 0.3 eq. of TEMPO were used. [c]Reaction was carried out over 30 minutes at -78 °C.

Reduction of the crude mixture of **108** and **109** was performed using $NaBH_4$ to determine the accessibility of the *3-C* position due to the steric bulk afforded by the *4-C* methyl groups. It was also theorised the *3-C* stereoselectivity would be less strictly controlled than in cholesterol derivatives which possess a smooth α-face. The presence of the *4α-H* would restrict nucleophilic attack of the hydride from the α face, thereby decreasing the β-OH: α-OH epimeric ratio. The magnitude of this effect had to be investigated in order to assess the practically of this route. Various conditions were employed as displayed in Table 4.8, After stirring lanosterone with $NaBH_4$ (5 eq.) in 1,4-dioxane overnight, a low conversion of only 27% was obtained, which could be improved by increasing the reaction temperature: performing the reaction at 110 °C was found to give a conversion of 78%. Doubling the amount of $NaBH_4$ used did not improve the conversion. The stereoselectivity of the reduction was found to be slightly reduced, an epimeric ratio of 11:89 was determined for *3α-OH*: *3β-OH*. The reaction was slightly less stereoselective than for the analogous reduction of 5α-cholestan-3-one where a 7:93 epimeric ratio was witnessed. The lower selectivity was due to a more crowded α face, restricting reductant approaching from the α face. Even though a lower selectivity was observed, the majority of the crude mixture was still the desired *3β-OH* epimer which can be isolated on silica.

Table 4.8. Optimised conditions for reduction of technical grade lansoterone.

Entry	$NaBH_4$ (eq.)	Temperature (°C)	Conversion[a] (%)		
			108, **109**	**84**, **107**	**110**, **111**
1	5	25	71	25	4
2	5	70	34	59	7
3[b]	10	70	46	51	5
4	5	100	19	72	9
5	5	110	11	78	11

[a]% given as conversions determined from the crude by ^{1}H NMR spectroscopy. [b]Entry has larger error associated with epimer signal as coincides with the shoulder of the residual 1,4-dioxane peak.

After optimisation using cheap technical grade lanosterol, the conditions were applied to lanosterol purified from the technical grade material. Lanosterol is available commercially in two forms, as cheap technical grade 'isocholesterol' derived from sheep wool and expensive purified lanosterol. Isocholesterol, largely contains the desired lanosterol and 24-dihydrolanosterol, with smaller quantities of agnosterol and 24-dihydroagnosterol sometimes present as shown in Figure 4.7. Isolation of lanosterol from this mixture is difficult, owing to co-elution of components in flash column chromatography and low solubility of lanosterol in solvents typically used for reverse phase HPLC.[313] The difficulty in isolating lanosterol from isocholesterol is reflected by the large cost of high purity lanosterol. The high cost of lanosterol is driving different isolation methods to be sought, with a number of patents on the subject having been filed.[313-315]

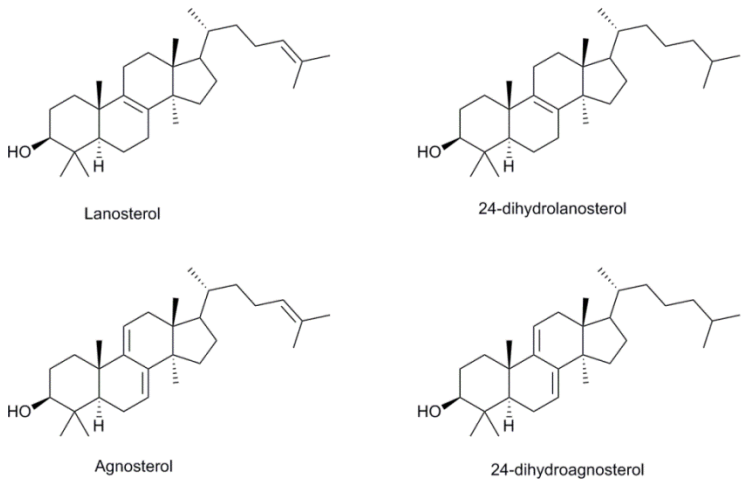

Figure 4.7. Four major components of isocholesterol (commonly employed as technical grade lanosterol).

An alternative to directly trying to separate isocholesterol is selective functionalisation of one moiety, followed by isolation and recovery of the original functionality. This method was chosen due to the potential for higher throughput. As the major by-product in isocholesterol is 24-dihydrolanosterol, techniques typically look at functionalisation of Δ^{24}; however such transformations usually employ toxic reagents such as bromine and mercury.[316,317] Due to lower toxicity and ease of separation, lanosterol was purified utilising a more recent benign route as displayed in scheme 4.12.[318]

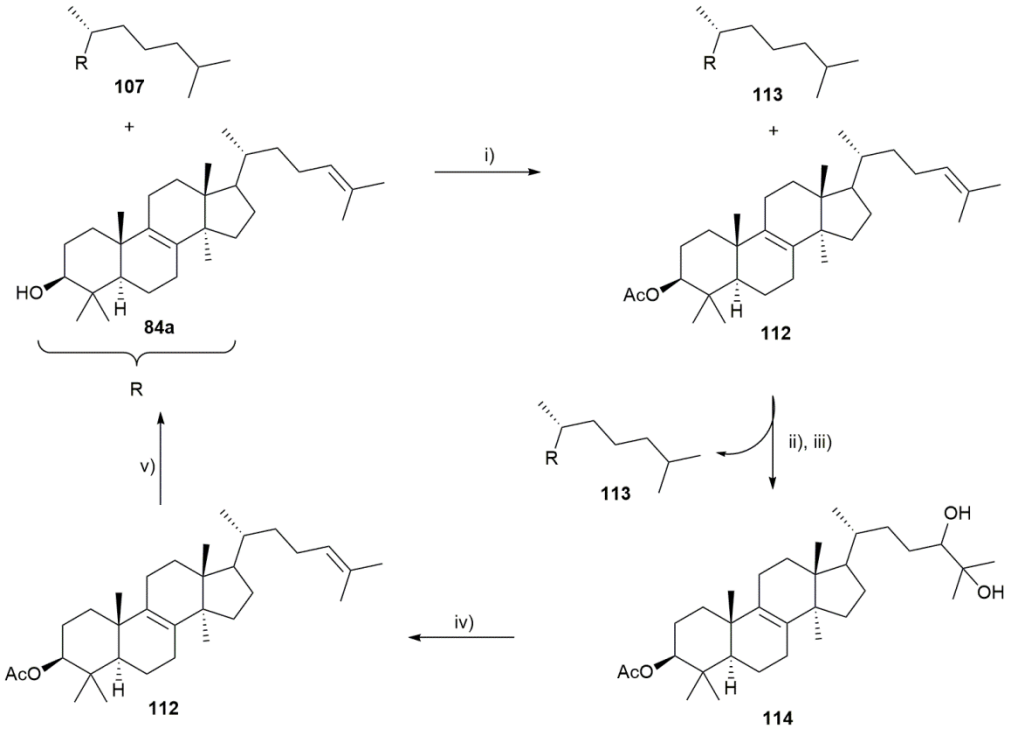

Scheme 4.12. Separation of the two major substituents of isocholesterol *via* conversion of lanosterol to **114** which was separable on silica from contaminant **113**. **114** can then undergo further transformations to reform pure lanosterol. i) Ac_2O, DMAP, Py, DCM, 71%. ii) NBS, H_3PO_2, H_2O: $CO(Me)_2$. iii) H_3PO_2, $NaHCO_3$, IPA: H_2O, 48% (two steps). iv) $NMe_2CH(OMe)_2$, Ac_2O, 73%. v) KOH, EtOH, 93%.

Commercial isocholesterol (68% by GC-MS) was acetylated in 71% yield. Treatment of the mixture containing **112** and **113** with N-bromosuccinimide (NBS) producing a bromohydrin intermediate which was hydrolysed to yield the desired diol (**114**) in a one pot procedure using hypophosphorous acid in a combined yield of 48%. In agreement with the literature, both *24-C* epimers were obtained with an R: S ratio of 1:1.1.[319]

Product **114** and contaminant **113** were easily separated by column chromatography at this stage. Conversion to the dimethylamino dioxalane intermediate followed by reductive elimination utilising Ac_2O produced pure acetylated lanosterol (**112**) in 73% yield. Deacetylation, employing KOH in EtOH afforded lanosterol in 93% yield, GC-MS demonstrated excellent purity of the crude material as shown in Figure 4.8, and therefore the product was not purified further.

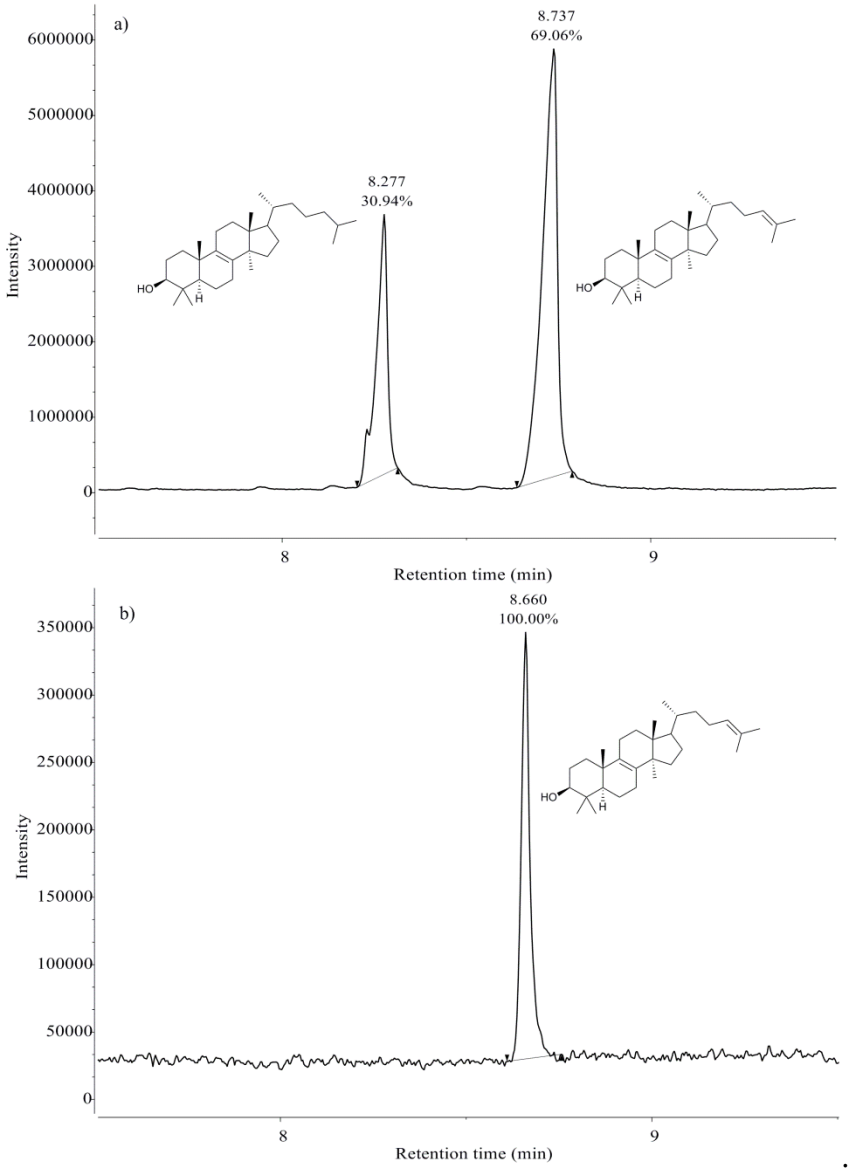

Figure 4.8. a) TIC (GC-MS) of a sample of commercial lanosterol contaminated with dihydrogenlanosterol. b) TIC (GC-MS) of purified lanosterol obtained as outlined in Scheme 4.12. In both chromatographs other peaks were observed at t_R 3.7 and 4.3 minutes, these peaks were present in blank runs so are impurities on the column.

Upon purification, heavy oxygen labelled pure lanosterol was synthesised. Lanosterol was oxidised under Swern conditions in 83% yield, partial migration of the *8-C* unsaturation was observed. 7,9-diene (agnosterone) was produced in 5% yield. Agonsterone and lanosterone were inseparable by column chromatography. Lanosterone was enriched by stirring with labelled H_2O and CF_3SO_3H for 3 hours in 1,4-dioxane. Refluxing with the relevant reductant ($NaBH_4$/ $NaBD_4$) then furnished the desired labelled lanosterone in yields of 61-73%. Up to 10% was recovered as mixed epimers, whilst the corresponding labelled *3α-OH* epimers (**110a-c**) were isolated in 10-17% as displayed in Scheme 4.13.

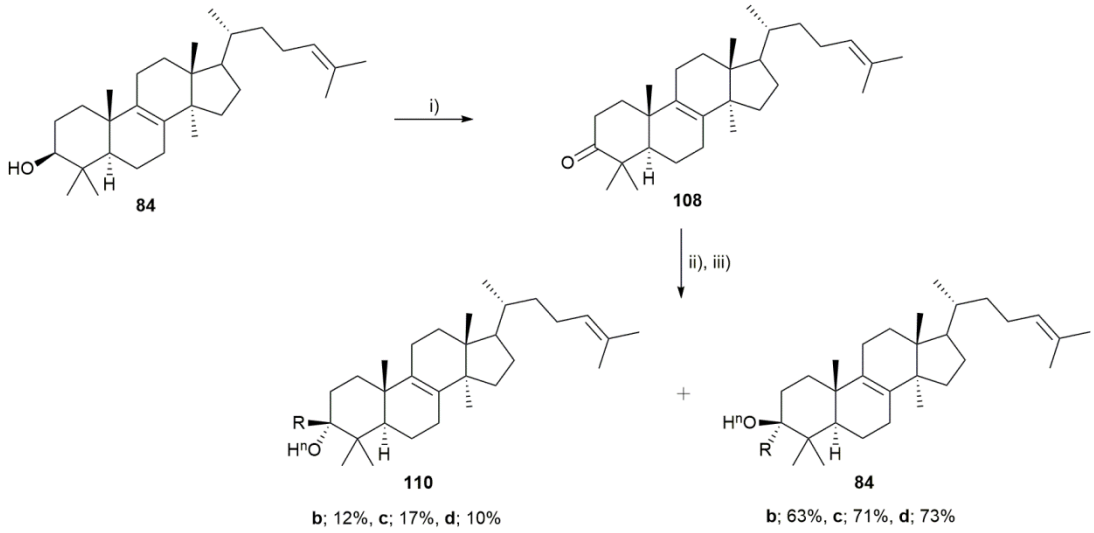

Scheme 4.13. Route to isotopic enrichment of pure lanosterol. i) $(COCl)_2$, DMSO, NEt_3, DCM, 83%. ii) $H_2{}^nO$, CF_3SO_3H, 1,4-dioxane. iv) $NaBR_4$, 1,4-dioxane. b; n = 17 R = H, c; n = 18, R = H, d; n =18, R = D.

Enrichments correlated to what was expected. The enrichments of both the desired *3β-OH* epimer and by-product α-epimer are detailed in Table 4.9. A limited amount of unlabelled lanosterol precursor resulted in choice to not synthesise lanosterol containing both the ^{17}O and D labels. Incorporation of both labels in most cases would be undesirable as splitting by the D label would reduce the peak intensity of the *3-C* position in the ^{13}C NMR spectrum, requiring more concentrated samples to view the label. Use of the doubly labelled sterol would not be necessary in GC-MS; the dominant $[M+2]^+$ peak could be produced cheaper and with greater intensity using an ^{18}O label only.

Table 4.9. Isolated yields and enrichments obtained for ^{17}O and ^{18}O isotopologues of both epimers of lanosterol produced as outlined in Scheme 4.13.

Entry	Compound	^{n}O	R	IY (%)[a]	^{n}O enrichment (%)	
					NMR[b]	GC-MS[c]
1	**84b**	17	H	63	-[d]	35.4
2	**84c**	18	H	71	88.5	80.3
3	**84d**	18	D	73	80.0	82.8
4	**110b**	17	H	12	-[d]	32.4
5	**110c**	18	H	17	90.1	79.0
6	**110d**	18	D	10	-[d]	81.2

[a]Isolated yields are of the heavy oxygen label incorporating step. [b]Enrichment calculated by integration of ^{13}C NMR signals (error ± 1.9%). [c]Enrichment determined by the intensities of the $[M]^+$, $[M+1]^+$ and $[M+2]^+$ ions in the isotopologue envelope by GC-MS (error ± 1.2%). [d]Peaks were non-resolvable.

4.3. Conclusion

A series of sterols have been enriched by ^{17}O and ^{18}O in the *3-C* position using 5-10 eq. of heavy oxygen enriched H_2O dependent upon the method employed. For substrates with a *5-C* unsaturation, enrichment proceeding through a 3,5-cyclosterol intermediate has been refined reducing the volume of H_2O required 5 fold, resulting in a saving of > €750 per 1 g of ^{17}O-sterol synthesised. Enrichments of > 32 and > 88 ± 1.2% for ^{17}O and ^{18}O respectively were obtained, corroborated by ^{13}C NMR spectroscopy and GC-MS. The values were generally in agreement the exception being 6-KC, where lower enrichments were observed by ^{13}C NMR spectroscopy. Diminishment of enrichment was theorised to occur through a transient 3,5-cyclosterol species, the proposed mechanism was support partially by a deuterium study, however the exact cause for loss of the label remains ambiguous. An additional method of direct exchange of a ketone moiety followed by *in situ* reduction was applied to sterols for the first time, producing labelled *5-C* saturated sterols with good yields and enrichments > 28.3 and > 73.5% for ^{17}O and ^{18}O sterols respectively. A summation of heavy oxygen labelled sterols synthesised are presented in Table 4.10.

Table 4.10. Summary of the yields and enrichments for ^{17}O & ^{18}O enriched sterols produced throughout this chapter.

Entry	Structure	Compound	^{n}O	R	IY (%)[a]	^{n}O enrichment (%)		Mass produced (mg)[d]
						NMR[b]	GC-MS[c]	
1	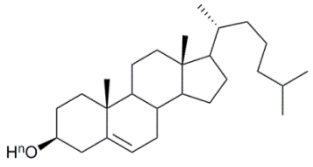	**81b**	17	-	71	-[d]	38.0	640
2		**81c**	18	-	69	96.1	93.7	630
3	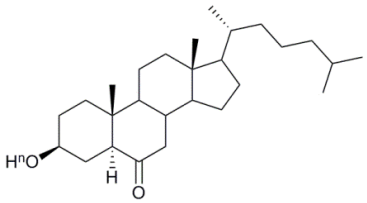	**82b**	17	H	21	-[d]	33.7	103
4		**82c**	18	H	15	53.2	93.5	55
5		**82d**	18	D	23	78.7	90.8	88
6	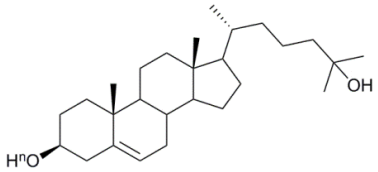	**83b**	17	-	72	-[d]	33.4	26
7		**83c**	18	-	63	92.6	88.3	28
8	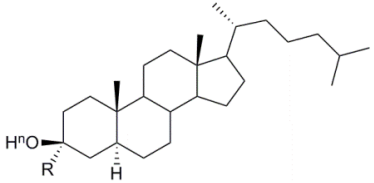	**106b**	17	H	84	-[d]	29.0	26
9		**106c**	18	H	81	84.0	86.6	27
10		**106d**	17	D	87	-[d]	28.3	25
11		**106e**	18	D	81	-[d]	83.5	25

Table 4.10 continues on the next page

Entry	Structure	Compound	^{n}O	R	IY (%)[a]	^{n}O enrichment (%) NMR[b]	^{n}O enrichment (%) GC-MS[c]	Volume produced (mg)[d]
12	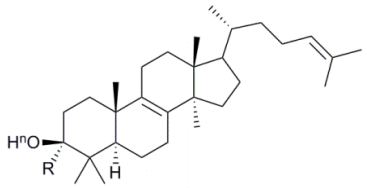	**84b**	17	H	63	-[e]	35.4	87
13		**84c**	18	H	71	88.5	80.3	63
14		**84d**	18	D	73	80.0	82.8	85
15	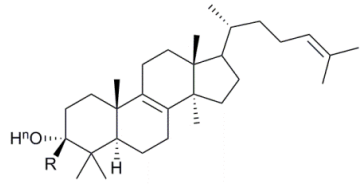	**110b**	17	H	12[f]	-[e]	32.4	11
16		**110c**	18	H	17[f]	90.9	79.0	13
17		**110d**	18	D	10[f]	-[e]	81.2	21

[a]Yields displayed are for the steps in which the isotopically labelled intermediates or products are produced. [b]Enrichment calculated by integration of ^{13}C NMR signals (error ± 1.9%). [c]Enrichment determined by the intensities of the $[M]^+$, $[M+1]^+$ and $[M+2]^+$ ions in the isotopologue envelope by GC-MS (error ± 1.2%). [d]Maximum amount of material produced from a single reaction. [e]Peaks were non-resolvable. [f]Low yields due to compound being a by-product.

4.4. Future Work

4.4.1. Alternative synthesis of 25-HC

A more efficient route to 25-HC could be pursued; one possible route is oxidation of commercially available i-cholesteryl methyl ether by TFDO as shown in Scheme 4.14. This synthesis was attempted briefly by generation of TFDO *in situ*; however hydration in the basic aqueous media followed by oxidation produced a ketone moiety. One avenue of investigation could be to first produce and distil TFDO followed by addition to a solution of i-cholesteryl methyl ether in DCM, however an improved method of handling volatile TFDO (-20 °C boiling point) would need to be devised.

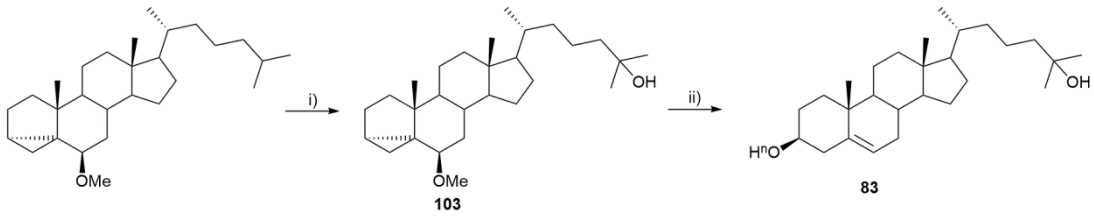

Scheme 4.14. Possible alternative synthesis to 25-HC. i) TFDO, DCM, -40 °C. ii) $H_2{}^{n}O$, CF_3SO_3H, 1,4-dioxane.

4.4.2. Applications of labelled sterols

Potential applications which may be pursued with the ^{18}O labelled sterols could be to track the distribution of sterols within artificial bilayers *in vitro* and in cells *ex vivo* using MALDI imaging or by secondary ion mass spectrometry (SIMS). This would enable examination of the equilibrium positions of sterols and their distribution within different phases (L_o *vs.* L_d) as well as their association with other membrane components, such as proteins. The label would be useful in *ex vivo* systems due to the ability to differentiate native sterol (no label) from doped sterol (labelled). Experiments tracking diffusion of labelled sterols as they progress through the lens membrane would be of particular interest. Elucidating how sterols active in reducing cataract formation reach cryAA and cryAB proteins at the site of action when administered as eye drops would be interesting, especially

as sterol turn-over in the lens nucleus is non-existent. Spin active ^{17}O labelled sterols may be used to determine distributions of sterols within artificial bilayers by ^{1}H NMR spectroscopy.

Chapter 5. Overall conclusion

The overarching aim at the outset of this thesis was to probe asymmetry, *via* the synthesis and development of new methods to produce novel lipids and labelled sterols. The use of molecular recognition lipids was envisaged to produce transversely asymmetric vesicles, whilst the development of non-intrusive heavy oxygen labelled sterols was sought in order to provide new tools for monitoring lateral asymmetry. A new approach to dialkyl phosphate synthesis on the solid phase was also pursued, as a simple mimic of more complex phospholipids. This novel approach to lipid production is hoped to one day progress to a combinatorial approach, allowing the production of a wide range of natural and designer lipids rapidly.

Chapter 2 detailed the synthesis of molecular recognition lipids, BAR and TAP lipid. Separate populations of vesicles doped by these recognition lipids had been shown to hemifuse and were envisaged as a route to produce transversely asymmetric liposomes. TAP lipid was produced by condensation of alkylated malononitrile and guanidinium carbonate in a multi-step synthesis. The analogous Fischer condensation of alkylated malonate ester and urea to produce BAR lipid proved more challenging, with side reactions dominating. The target compound could be produced in 32% conversion but bulk isolation by conventional means proved elusive. Despite a lack of amenities to perform preparative scale HPLC, resolution of the target compound was achieved, as demonstrated by HPLC-MS. These conditions can be utilised once sufficient equipment becomes available to obtain pure BAR lipid. Difficulty in isolating pure BAR lipid by the classic Fischer synthesis, led to alternative methods being explored as displayed in Scheme 2.1, all revolving around the use of barbituric acid as a reagent which would be functionalised at the *5-C* position. Production of 5-decylbarbituric acid was achieved, however translation to produce the desired BAR lipid were frustrated by inability to produce the required precursors, time constraints prevented developing these methodologies further.

Details of implementing a solid phase synthetic methodology using a β-hydroxysulfone linker are presented in Chapter 3. Synthesis of the β-hydroxysulfone linker

in the solution phase and functionalisation of the resin proceeded in good yields; however the linker proved too base liable upon phosphorylation. It was found necessary to attach the β-hydroxythioether linker to the resin, undergo the desired transformations and oxidise in a penultimate step, followed by base mediated cleavage in a 'safety catch approach'. By the use of NMR studies on solution phase analogues and ssNMR analysis of solid phase reactions, conditions to produce didecyl phosphate in 26% yield, using PCl_3 as the source of the phosphate group was determined as a proof of principle. The conditions detailed are preliminary but mark an advancement towards a novel route to produce phospholipids in what is hoped will progress leading to a combinatorial approach for lipid synthesis.

Production of sterols doped enriched with ^{17}O and ^{18}O is detailed in Chapter 4. Synthesis of the sterols was achieved by two routes, *via* a 3,5-cyclocholesterol or ketone precursor for sterols with and without a Δ^5 motif respectively. For both routes conditions were optimised to use < 10 eq. of labelled H_2O, keeping syntheses economical and practical. A range of labelled sterols which have recently garnered interest for their therapeutic effects have been synthesised, with enrichments of > 28 and > 79% for ^{17}O and ^{18}O-sterols respectively (40 and 98% absolute maximum theoretical enrichment). The values were corroborated by both GC-MS and ^{13}C NMR, in the majority of cases the enrichment values correlated well with the noticeable exception being 6-ketocholestanol, which showed lower enrichment by NMR. The cause of the discrepancy was attributed to acid catalysed enol tautomerism (in slightly acidic $CDCl_3$) which led to elimination of the labelled oxygen at the *3-C* position by a transient 3,5-cyclosterol intermediate which was quickly rehydrated by excess $^{16}OH_2$, diluting the enrichment as shown in Scheme 4.5.

Chapter 6. Experimental

6.1. General considerations

Unless indicated otherwise all solutions can be assumed to be aqueous. Various commercial suppliers were used, based at the following locations; Alfa Aesar (Heysham, UK), Carbosynth (Compton, UK), Fisher Scientific (Loughborough, UK), Fluorochem Hadfield, UK), Sigma-Aldrich (Dorset, UK), TCI UK (Oxford, UK) and VWR (Lutterworth, UK). All solvents were received from Fisher Scientific aside from anhydrous DMF, DMSO and 1,4-dioxane which were supplied by Sigma-Aldrich. Solvents were used as supplied unless otherwise stated. Anhydrous DCM was obtained by distillation from calcium hydride under a nitrogen atmosphere. Hexane was distilled before use. Anhydrous MeOH and EtOH were both refluxed for 2 hours under an argon atmosphere in the presence of Mg (5 g) and I_2 (0.5 g) per litre of alcohol prior to distillation and storage over oven activated 3 Å M.S. Anhydrous MeCN was obtained by refluxing MeCN with 1% (w/v) phosphorus pentoxide for 1.5 hours under an argon atmosphere prior to distillation and storage over 3 Å M.S. Anhydrous THF, 1,4-dioxane and pyridine were obtained by storage over oven activated 3 Å M.S for at least 48 hours under an argon atmosphere. Anhydrous MEK was purchased from Fisher Scientific and was used as supplied. Anhydrous DIPEA, dimethylmalonate, N-methylimidazole (NMI), 3,4-Dihydro-2-pyran (DHP) and decan-1-ol were obtained by placing the appropriate compound obtained from Sigma-Aldrich or TCI UK over oven dried 4 Å M.S for at least 48 hours under an argon atmosphere. Molecular sieves (1/ 16 pellets, 4 Å and 3 Å) were obtained respectively from VWR and Alfa Aesar and were activated at 130 °C for at least 24 hours prior to use.

3-hydroxybenzenethiol (98%), decan-1-ol and Merrifield resin were obtained from TCI UK. Merrifield resin refers to chloromethyl polystyrene cross linked by 2% DVB (1.2 mmol g^{-1} loading) (100-200 mesh). Potassium monopersulfate (Oxone) was used from two separate suppliers, as the monopersulfate single salt supplied by Sigma-Aldrich and as the monopersulfate triple salt supplied by Alfa Aesar. 1,1,1-trifluoropropanone was supplied by Fluorochem. Technical grade lanosterol was supplied by Carbosynth. Lanosterol content

was determined to be 68% by GC-MS. Isotopically enriched H_2O was obtained from Cortecnet (Voisins-Le-Bretonneux, France). Isotopic enrichments were 95.7 atom% for $^{18}OH_2$ (our measurement, lot number 139808A-P) and 41.1% for $^{17}OH_2$ (manufacturers specification, lot number 1040171A-P). Standard H_2O samples, IA-R063, IA-R064, IA-R065, were obtained from Iso-Analytical Ltd (Crewe, UK). NaH (60 wt% dispersion in mineral oil), $BF_3.OEt_2$ (46.5% basis), Pd/C (10 wt.% loading, matrix activated carbon support), H_2O_2 (30 wt%) solution, i-cholesteryl methyl ether (95%), 4 M HCl in 1,4-dioxane and benzyl diazoacetate (10% DCM stabiliser) were all supplied by Sigma-Aldrich. All other reagents unless otherwise stated were obtained from Sigma-Aldrich and used without further alteration.

Solutions of NaOMe and NaOEt were produced by transferring sodium sticks stored in mineral oil (Alfa Aesar) into a beaker of petroleum ether. The metal was cut to the appropriate mass which was quickly dried using a paper towel and immediately added to an ice cooled flask under an argon atmosphere containing the appropriate volume of alcohol. The mixture was gently agitated by hand until the metal had fully dissolved, ensuring that the mixture was kept cool to avoid alcohol evaporation.

Purification of crude mixtures was routinely performed by flash column chromatography using a silica support. Silica gel (230-400 mesh, 40-60 μm) was supplied from Sigma-Aldrich. Fractions were analysed using aluminium backed silica gel 60 F_{254} TLC plates supplied by VWR. In cases where alumina was indicated as the stationary phase, activated, neutral Brockmann I, alumina oxide (*ca*. 150 mesh, 58 Å) supplied from Sigma-Aldrich was used. Fractions from alumina solid support columns were analysed using PET supported alumina oxide F_{254} TLC plates supplied by Sigma-Aldrich (Dorset, UK). All TLC plates were visualised using either an ultraviolet (UV) lamp (254 nm), iodine chamber or by use of a dipping stain, followed by heating with a heat gun. Dipping stains used included ninhydrin, phosphomolybdic acid (PMA) and $KMnO_4$. Ninhydrin stain consisted of ninhydrin (3 g) in *n*-butanol (200 mL) and acetic acid (6 mL). PMA stain consisted of PMA

(6 g) and $Ce(SO_4)_2.4H_2O$ (3 g) dissolved in H_2SO_4 (15 mL) and H_2O (230 mL). $KMnO_4$ stain was prepared by dissolving $KMnO_4$ (1.5 g) and K_2CO_3 (10 g) in 10% NaOH solution (1 mL) and H_2O (200 mL).

Routine solution state NMR was performed on samples in $CDCl_3$ supplied by Fluorochem (Hadfield, UK) unless otherwise indicated. All other deuterated solvents used throughout this text were supplied by Goss Scientific (Crewe, UK). Measurements were recorded on a Bruker Avance-400 (at 400 MHz for ^{1}H; 100.6 MHz for ^{13}C; 162 MHz for ^{31}P), Varian VNMRS-600 (at 600 MHz for ^{1}H; 151 MHz for ^{13}C; 92 MHz for D) or a Varian VNMRS-700 (at 700 MHz for ^{1}H; 176 MHz for ^{13}C, 107 MHz for D), operating at ambient probe temperature. Chemical shifts are reported in ppm using residual solvent at 7.26, 77.16 ppm; 2.05, 206.26 ppm and 2.50, 39.52 ppm as internal references for ^{1}H and ^{13}C in $CDCl_3$, acetone-d^6 and DMSO-d^6 respectively. Coupling constants (J) are given in Hz, and the multiplicity of the NMR signals are described as singlet (s), doublet (d), triplet (t), quartet (q) and multiplet (m). As is conventional in the literature, only pertinent signals are reported for the ^{1}H NMR spectra of sterols.

Samples for solid state (ss) NMR were performed by the departmental service at Durham University. In short, for ^{1}H ssNMR, samples were swollen in DCM-d^2; spectra were recorded at 400.17 MHz using a Bruker Avance III HD spectrometer and a 4 mm (rotor o.d.) magic-angle spinning probe. Spectra were obtained using cross-polarisation with a 2 s recycle delay, 3 ms contact time, at ambient probe temperature (~25 °C) and at a sample spin-rate of 8 kHz. Between 1000 and 1600 repetitions were accumulated. Spectral referencing was with respect to an external sample of neat tetramethylsilane (carried out by setting the high-frequency signal from adamantane to 38.5 ppm). ^{31}P ssNMR spectra were recorded at 161.99 MHz using a Varian VNMRS spectrometer and a 4 mm (rotor o.d.) magic-angle spinning probe. Spectra were obtained using cross-polarisation with a 2 s recycle delay, 3 ms contact time, at ambient probe temperature (~25 °C) and at a sample

spin-rate of 12 kHz. Between 1000 and 1600 repetitions were accumulated. Spectral referencing was with respect to an external sample of 85% phosphoric acid.

For liquid chromatography mass spectrometry (LCMS), chromatography was performed using a Acquity UPLC BEH C18 1.7μm (2.1 mm x 50 mm) column (Waters Ltd., Manchester, UK) using a mobile phase of H_2O containing 0.1% formic acid: MeOH. A triple quadrupole detector mass spectrometer (low resolution (LR) electrospray ionisation (ESI) operated in positive or negative ion mode) was used, with samples solubilized in MeOH. High resolution mass spectrometry (HRMS) also known as accurate mass spectrometry was obtained on a Finnigan LTQ-FT in positive or negative electrospray ion mode. Atmospheric solids analysis probe mass spectrometry was performed on a Xevo QToF mass spectrometer (Waters Ltd, Manchester, UK) equipped with an Agilent 7890 GC apparatus (Agilent Technologies UK Ltd, Stockport, UK) at 350 °C. Samples were obtained by removing an aliquot of a 1 mg/ mL solution of analyte in DCM using a capillary tube. The sample was run at 350 °C. Characterisation by GC-MS was performed using a QP2010-Ultra supplied by Shimadzu (Kyoto, Japan), fitted with an Rxi-17Sil MS (0.15 μm × 10 m × 0.15 mm) column. Injection volumes of 0.5 μL using a 25:1 split were used; helium carrier gas was used at a flow rate of 0.41 mL/min. A temperature range of 25-300 °C was used with an increment rate of 25 °C min^{-1}, the final temperature was held for 5 minutes.

The microwave used was an Initiator+ supplied from Biotage (Hengoed, UK). Samples were subject to 30 seconds pre-stir followed by heating at indicated temperature and time under high adsorption settings. Melting points (mp) were obtained by a Griffin melting point apparatus and Infrared (IR) spectra were recorded on a Perkin Elmer Paragon 1000 FT-IR spectrometer with an ATR attachment. The syringe pump utilised was an Al 1000-200 (World Precision Instruments, Herefordshire, UK). Distillations were performed using a Buchi Glass Oven B-585 Kugelrohr operating at a pressure between 0.2-2.0 Torr.

Data from all NMR and mass spectrometry experiments was processed using Mestrenova (Mestralab Research, version 10.0) on a PC running the Windows 7 operating system.

Karl Fischer tests for the H_2O content of 1,4-dioxane were conducted using a Metrohm Karl Fischer 831 KF coulometer with an 832 Thermoprep oven (Metrohm AG, Herisau, Switzerland). The isotopic enrichment of the stock $^{18}OH_2$ was determined by laser spectroscopy using a DLT-100 liquid H_2O isotope analyser supplied by Los Gatos research (Mountain View, CA, USA) in the laboratory of Dr Darren R. Gröcke (Dept. of Earth Sciences, Durham University, UK). An aliquot (20 μL) of the isotopically enriched H_2O was diluted to a total volume of 1 mL using a H_2O standard (IA-R063; ^{18}O composition was calculated to be 2004.4 ± 0.5 ppm). The isotope ratios of the diluted sample were calculated using off-axis integrated cavity output spectroscopy (OA-ICOS). The instrument was calibrated using 10 runs of blanks, IA-R063, IA-R064, IA-R065 and ddH_2O with a 0.75 μL injection volume.

X-ray diffraction experiments were performed by D. Yufit of the departmental service at Durham University. In short, the X-ray single crystal data for compounds **17, 41, 70** and **100** was collected using λMoKα radiation (λ = 0.71073 Å), whilst data for the remaining compounds were collected using λCuKα radiation (λ = 1.54178 Å) on a Bruker D8Venture diffractometer (Photon100 CMOS detector, IμS-microsource, focusing mirrors) equipped with a Cryostream (Oxford Cryosystems) open-flow nitrogen cryostats at the temperature 120.0 (2) K. The crystals of **105** showed some damage during flash-freezing so the crystal of this compound was slowly cooled from 250 K to 150 K and the data was collected at this temperature. All structures were solved by direct method and refined by full-matrix least squares on F^2 for all data using Olex2 and SHELXTL software.[320,321] All non-disordered non-hydrogen atoms were refined anisotropically, hydrogen atoms in **41** and **66** were refined isotropically, the hydrogen atoms in other structures were placed in the calculated positions and refined in riding mode. Disordered atoms were refined isotropically

with fixed SOF; the severely disordered solvent molecules in the structure have been taken into account using MASK procedure of the Olex2 program package. Crystal data and parameters of refinement are listed in Tables A1.1.1-A1.12.7 (Appendicies A1.1-A1.12).

A standard sterol numbering system was employed throughout this document as demonstrated on cholesterol (**81**). Please note that α indicates the moiety is above the planar fused ring system, whilst β indicates that the group lies below this plane. Δ^n indicates that there is an unsaturation starting at the n^{th}-carbon.

6.2. Synthesis of molecular recognition lipids

6.2.1. Synthesis of 14-[(tetrahydro-2H-pyran-2-yl)oxy]-3,6,9,12-tetraoxatetradecan-1-ol, 3

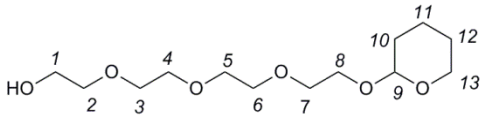

Tetraethylene glycol (45.00 g, 232.00 mmol, 5 eq.), $TsOH.H_2O$ (0.03 g, cat.) and DHP (3.90 g, 46.30 mmol, 1 eq.) were stirred at 100 °C for 3 hours under an argon atmosphere. The solution was allowed to cool to room temperature before being diluted with brine (15 mL) and washed with hexane (3 × 15 mL). The aqueous layer was then extracted into DCM (3 × 15 mL), the combined organic layers were washed with brine (3 × 15 mL). The organic phase was dried by $MgSO_4$, filtered and concentration *in vacuo* to afford a yellow oil (7.36 g, 57%). The crude product was used without further purification. ^{1}H NMR (400 MHz) δ 4.67-4.59 (m, 1H, *9-H*), 3.77-3.57 (m, 14H, *2-8-H*), 3.53-3.46 (*1-H*), 2.57 (s, 1H, *1*-O*H*) 1.89-1.46 (m, 6H, *10-13-H*). ^{13}C NMR (101 MHz) δ 99.1 (*9-C*), 72.8, 70.8, 70.7, 70.5 66.8, 62.4, 61.9, 30.7, 25.6, 19.6. LRMS (ESI) *m*/*z*: 366.220 ($[M+Na]^+$, 99%), 343.598 ($[M]^+$, 67), 342.2 ($[M+H]^+$, 100). HRMS (ESI) *m*/*z*: calculated $[M+H]^+$ 343.1757, found 343.1757. IR (neat) ν_{max} (cm^{-1}); 3451 (s), 2941 (m), 2890 (m), 1725 (m), 1455 (s), 1350 (s), 1201 (s), 1121 (l), 1072 (l), 1032 (l), 986 (m), 931 (m), 872 (m), 814 (m).

6.2.2. Synthesis of 14-[(tetrahydro-2H-pyran-2-yl)oxy]-3,6,9,12-Tetraoxatetradecanoic acid, benzyl ester, 4

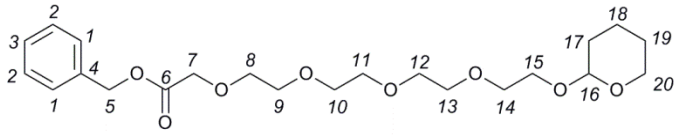

Compound **3** (7.01 g, 25.19 mmol, 1 eq.) was azeotropically distilled with toluene (5 mL), prior to addition to a solution of anhydrous THF (50 mL) and 4 Å M.S (10 g) under an argon atmosphere The solution was stirred for 0.5 hours, followed by transfer by cannula to a stirred suspension of NaH (3.06 g, 75.56 mmol, 3 eq.) in anhydrous THF (80 mL), the suspension was stirred for 1 hour at room temperature under an argon atmosphere. Bromoacetic acid (3.88 g, 27.77 mmol, 1.1 eq.) in anhydrous THF (50 mL) was added dropwise to the mixture which was heated to reflux for a further 16 hours. The solution was left to cool to room temperature, prior to the addition of benzyl bromide (3.30 mL, 27.70 mmol, 1.1 eq.). The mixture was then left to reflux for a further 16 hours, the mixture was filtered and the filtrate concentration *in vacuo*. The brown precipitate was partitioned between DCM (200 mL) and water (100 mL); the aqueous layer was then further extracted with DCM (2 × 50 mL) before the organic layers were combined and washed with H_2O (2 × 50 mL). The mixture was dried in $MgSO_4$, filtered and concentrated *in vacuo* to give a yellow solid (12.35 g). which was purified by column chromatography (50 mm, eluent; hexane: EtOAc 1:1 to EtOAc) to give a colourless oil (4.37 g, 41%) identified as the product (R_f 0.24, EtOAc). ^{1}H NMR (700 MHz) δ 7.37-7.30 (m, 5H, *1-3-H*), 5.17 (s, 2H, *5-H*), 4.61 (dd, *J* = 4.4, 3.0 Hz, 1H, *16-H*), 4.19 (s, 2H, *7-H*), 3.87-3.81 (m, 2H, *15-H* & *20-H*), 3.74-3.71 (m, 2H, *8-H*), 3.69-3.61 (m, 12H, *9-14-H*), 3.60-3.57 (m, 1H, *15-H*), 3.50-3.46 (m, 1H, *20-H*), 1.85-1.78 (m, 1H), 1.72-1.67 (m, 1H), 1.62-1.53 (m, 2H), 1.52-1.46 (m, 2H). ^{13}C NMR (176 MHz) δ 170.3 (*6-C*), 135.4 (*4-C*), 128.6, 128.4, 98.9 (*18-C*), 70.9 (*10-C*), 70.6, 70.5, 68.7, 66.6, 66.5, 62.2, 30.5, 25.4, 19.5. LRMS (ESI) *m*/*z*: 448.915 ([M+Na]$^+$, 100%). HRMS (ESI) *m*/*z*: calculated [M+Na]$^+$ 449.2151, found 449.2139. IR (neat) ν_{max} (cm^{-1});

2943 (s), 2868 (s), 1754 (m), 1456 (s), 1350 (m), 1258 (s), 1199 (m), 1190 (l), 1075 (l), 1032 (l), 987 (m), 872 (s), 814 (s), 752 (s), 698 (m). The data matched literature values.[322]

6.2.3. Synthesis of benzyl 2-(2-(2-hydroxyethoxy)ethoxy)acetate, 5

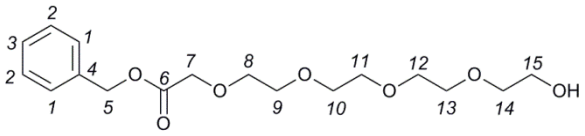

Tetraethylene glycol (18.00 mL, 106.35 mmol, 4 eq.) and benzyl diazoacetate (3.90 mL, 25.92 mmol, 1 eq.) were added to a stirred solution of anhydrous DCM (40 mL) under an argon atmosphere. $BF_3.OEt_2$ (0.10 mL, cat.) was then added at 0 °C, the reaction was allowed to come to room temperature before being stirred for 3 hours. The solution was further diluted with DCM (50 mL) and washed with H_2O (2 × 20 mL). The organic layer was dried over $MgSO_4$, filtered and concentrated *in vacuo* to produce a yellow oil (11.44 g). The oil was subjected to flash column chromatography (50 mm, eluent; EtOAC: hexane 1:1 to EtOAC to EtOAc: MeOH 30:1) to afford a yellow oil (R_f 0.16, DCM: MeOH 16:1) which was identified to be a the desired product (5.53 g, 62%). ^{1}H NMR (400 MHz) δ 7.38-7.33 (m, 5H, *1-3-H*), 5.19 (s, 2H, *5-H*), 4.20 (s, 2H, *7-H*), 3.76-3.59 (m, 16H, *8-15-H*). ^{13}C NMR (101 MHz) δ 170.4 (*6-C*), 135.4 (*4-C*), 128.6 (*1-3-C*), 128.4 (*1-3-C*), 72.5, 71.0, 70.6, 70.5, 70.3, 68.7 (*7-C*), 66.5 (*5-C*), 61.8 (*9-16-C*). LRMS (ESI) *m*/*z*: 366.220 ($[M+Na]^+$, 99%), 343.598 ($[M]^+$, 67), 342.2 ($[M+H]^+$, 100). HRMS (ESI) *m*/*z*: calculated $[M+H]^+$ 343.1757, found 343.1757. IR (neat) ν_{max} (cm^{-1}); 3452, 2866 (m), 1750 (m), 1452 (m), 1196 (m), 1102 (l), 698 (m). The data matched literature values.[195]

6.2.4. Synthesis of benzyl 2-(2-(2-(tosyloxy)ethoxy)ethoxy)acetate, 6

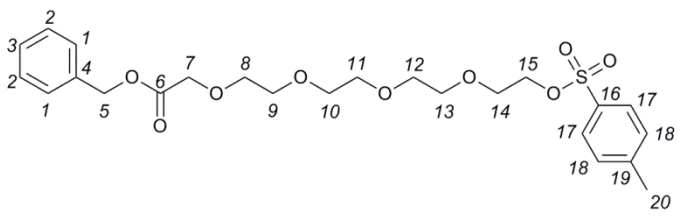

To a stirred solution of compound **5** (5.30 g, 15.47 mmol, 1 eq.) in anhydrous pyridine (23 mL), TsCl (4.42 g, 23.20 mmol, 1.5 eq.) was added to the solution and left to

stir for 4 hours at 0 °C under an argon atmosphere. The mixture was diluted with 5% HCl solution (10 mL) and Et_2O (50 mL), the organic layer was collected and the aqueous layer was extracted with Et_2O (2 × 50 mL). The organic layers were combined and dried using $MgSO_4$, filtrated and concentrated *in vacuo* to afford a yellow oil (7.27 g). The oil was purified by column chromatography (50 mm, eluent; EtOAc) to obtain a pale yellow oil (7.04 g, 92%) identified as the desired product (R_f 0.52, EtOAc). ^{1}H NMR (400 MHz) δ 7.79 (d, *J* = 8 Hz, 2H, *17-H*), 7.37-7.31 (m 7H, *1-3-H & 20-H*), 5.18 (s, 2H, *5-H*), 4.19 (s, 2H, *7-H*), 4.15 (t, *J* = 5 Hz, 2H, *15-H*), 3.75-3.56 (m, 14H, *8-14-H*), 2.44 (s, 3H, *20-H*). ^{13}C NMR (101 MHz) δ 170.5 (*6-C*), 144.9 (*16-C*), 135.6, 133.1, 130.0, 128.8, 128.6, 128.1, 71.1, 70.9, 70.8, 70.7, 69.4, 68.8, 66.7, 21.8 (*22-C*). LRMS (ESI) *m*/*z*: 777.173 (66%), 528.618 (100), 519.770 ($[M+Na]^+$, 74), 497.859 ($[M+H]^+$, 84). HRMS (ESI) *m*/*z*: calculated $[M+H]^+$ 497.1845, found 497.1858. IR (neat) ν_{max} (cm^{-1}); 2870 (m), 1754 (m), 1452 (m), 1352 (m), 1176 (l), 1094 (l), 1010 (m), 920 (l), 816 (m), 752 (m), 662 (l). The data matched literature values.[322]

6.2.5. Synthesis of 2-(2-(2-(tosyloxy)ethoxy)ethoxy)acetic acid, 7

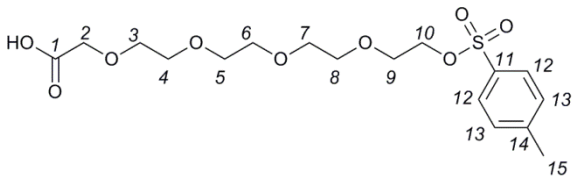

Into a 2 neck flask fitted with a septum and a gas tap, Compound **6** (7.07 g, 14.24 mmol, 1 eq.) and Pd/C (1.42 g, cat.) were added followed by the addition of DCE (25 mL). The suspension was frozen using liquid nitrogen, then degassed by application of high vacuum. The vacuum was stopped and the vessel was back filled by $H_{2(g)}$ using a balloon, the vessel was warmed to room temperature using tepid H_2O. The reaction was stirred for 16 hours, followed by filtration through a celite pad; the pad was washed using DCM (100 mL). Concentration *in vacuo* afforded the desire compound as a pale yellow oil (5.60 g, 97%). The material was used without subsequent purification. ^{1}H NMR (400 MHz) δ 7.79 (d, *J* = 8 Hz, 2H, *12-H*), 7.34 (d, *J* = 8 Hz, 2H, *13-H*), 4.18-4.13 (m, 4H *2-H* & *10-H*), 3.77-3.57 (m,

14H, *3-9-H*), 2.44 (s, 3H, *15-H*).^{13}C NMR (101 MHz) δ 171.7 (*1-C*), 145.0 (*11-C*), 133.1, 130.0, 128.1, 71.7, 70.9, 70.8, 70.5, 70.2, 69.4, 69.2, 68.8, 21.8 (*15-C*). LRMS (ESI) *m*/*z*: 430.737 ([M+Na]$^+$, 100%), 428.119 (58). HRMS (ESI) *m*/*z*: calculated [M+H]$^+$ 407.1376, found 407.1365. IR (neat) ν_{max} (cm^{-1}); 2870 (m), 1738 (m), 1348 (m), 1174 (l), 1094 (l), 914 (l), 816 (m), 774 (m), 662 (l).

6.2.6. Synthesis of 2-(2-(2-(dioctadecylamino)-2-oxoethoxy)ethoxy)ethyl 4-methylbenzenesulfonate, 9

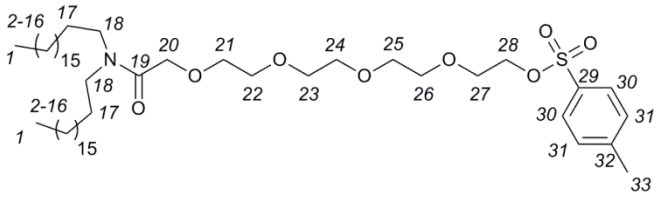

To a stirred solution of compound **7** (3.89 g, 9.57 mmol, 1.1 eq.) in anhydrous DCM (30 mL), oxalyl chloride (2.70 mL, 31.36 mmol, 4 eq.) was added under an argon atmosphere. The solution was allowed to reflux for 2 hours. Once cooled to room temperature the solution was concentrated *in vacuo* to produce a yellow oil, a small aliquot was removed, analysed and confirmed to be the acid chloride intermediate (**8C**). ^{1}H NMR (400 MHz) δ 7.80 (d, *J* = 8 Hz, 2H, *12-H*), 7.34 (d, *J* = 8 Hz, 2H, *13-H*), 4.50 (s, 2H, *2-H*), 4.16 (t, *J* = 4.8 Hz, 2H, *10-H*), 3.82-3.55 (m, 14H, *3-9-H*), 2.45 (s, 3H, *15-H*). ^{13}C NMR (101 MHz) δ 172.1 (*1-C*), 144.8, 133.0, 129.8, 128.0, 71.3, 70.8, 70.7, 70.6, 69.3, 68.7, 21.7 (*15-C*). LRMS (ESI): 443.298 (81%), 442.387 (70), 420.833 (100).

Intermediate **8C** was diluted in anhydrous DCM (5 mL) and added dropwise to a stirred solution of dioctadecylamine (4.62 g, 8.86 mmol, 1 eq.) in DCM (70 mL) at 0 °C under an argon atmosphere. Anhydrous NEt_3 (1.30 mL, 8.86 mmol, 1.3 eq.) was added and the solution was allowed to warm to room temperature and stir for 16 hours. The mixture was then washed with brine (2 × 20 mL), dried with $MgSO_4$, filtered and concentrated *in vacuo* to give a crude solid. The crude mixture was purified by flash column chromatography (50 mm, eluent; EtOAc: hexane 3:1 to EtOAc to EtOAC: MeOH 9:1) to obtain a white waxy solid (R_f 0.35, EtOAc) identified as the product (6.79 g, 84%). ^{1}H NMR

(400 MHz) δ 7.80 (d, *J* = 8 Hz, 2H, *30-H*), 7.34 (d, *J* = 8 Hz, 2H, *31-H*), 4.20-4.13 (m, *20-H* & *28-H*), 3.72-3.56 (m, 14H, *21-27-H*), 3.27 (t, *J* = 7.6 Hz, 2H, *18-H*), 3.17 (t, *J* = 7.6 Hz, 2H, *18-H*), 2.44 (s, 3H, *33-H*), 1.57-1.46 (s, 4H, *17-H*), 1.33-1.19 (m, 30H, *2-16-H*), 0.87 (t, *J* = 6.8 Hz, 6H, *1-H*). ^{13}C NMR (101 MHz) δ 168.8 (*19-C*), 144.9, 133.2, 130.0, 128.1, 70.9, 70.7, 70.1, 69.4, 68.8, 47.1 (*18-C*), 45.9 (*18-C*), 32.1, 29.9, 29.8, 29.7, 29.6, 29.5, 29.1, 27.7, 27.2, 27.0, 22.8, 21.8, 14.3 (*1-C*). LRMS (ASAP): 994.941 (42%), 911.721 ($[M+H_2]^+$, 62), 910.721 ($[M+H]^+$, 100), 774.678 (72), 756.712 (66). HRMS (ASAP) *m*/*z*: calculated $[M+H]^+$ 910.7170, found 910.7172. IR (DCM film) ν_{max} (cm^{-1}); 2918 (l), 2850 (l), 1724 (s), 1643 (m), 1467 (m), 1356 (m), 1242 (m), 1177 (l), 1098 (l), 923 (m), 817 (s), 775 (s), 722 (s), 664 (m), 555 (l).

6.2.7. Synthesis of 2-(2-(2-iodoethoxy)ethoxy)-N,N-dioctadecylacetamide, 10

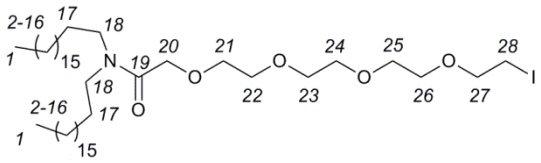

Compound **9** (5.61 g, 6.16 mmol, 1 eq.) and NaI (1.85 g, 12.32 mmol, 2 eq.) in anhydrous MEK (20 mL) were refluxed for 5 hours under an argon atmosphere. The solution was cooled to room temperature, concentrated *in vacuo*, the solid was redissolved in Et_2O (100 mL). The solution was washed with H_2O (2 × 20 mL) and brine (20 mL). The organic layers was dried with $MgSO_4$, filtered and concentrated *in vacuo* to obtain a yellow oil (1.16 g, 96%) which was identified as product (R_f 0.34, EtOAc: DCM 1:1) and was used without further purification. ^{1}H NMR (400 MHz) δ 4.19 (s, 2H, *20-H*), 3.78-3.61 (m, 14H, *21-45-H*), 3.32-3.21 (m, 4H, *18-H* & *28-H*), 3.18 (t, *J* = 7.6 Hz, 2H, *18-H*), 1.58-1.45 (s, 4H, *17-H*), 1.35-1.16 (m, 60H, *2-16-H*), 0.87 (t, *J* = 6.8 Hz, 6H, *1-H*).^{13}C NMR (101 MHz) δ 168.8 (*19-C*), 72.15, 70.8, 70.7, 70.4, 70.2, 47.1 (*18-C*), 46.0 (*18-C*), 32.1, 29.8, 29.5, 29.1, 27.7, 27.2, 27.1, 22.8, 14.3 (*1-C*), 3.1 (*28-C*). LRMS (ESI) *m*/*z*: 889.146 (54%), 888.615 ($[M+Na]^+$, 100), 887.400 (83). HRMS (ESI) *m*/*z*: calculated $[M+H]^+$ 866.6099, found 866.6136. IR

(neat) ν_{max} (cm^{-1}); 2921 (l), 2852 (l), 1647 (m), 1465 (m), 1379 (s), 1350 (s), 1297 (s), 1105 (l), 1190 (l), 1038 (s), 721 (s).

6.2.8. Synthesis 2-(2-(3,3-dicyanopropoxy)ethoxy)-N,N-dioctadecylacetamide, 11

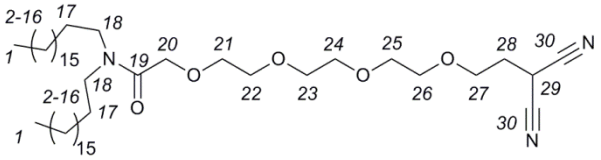

NaH (0.07 g, 1.79 mmol, 3 eq.) was added to a stirred solution of compound **10** (0.52 g, 0.61 mmol, 1 eq.) in anhydrous DMSO (8 mL) under an argon atmosphere. Malononitrile (0.12 g, 1.77 mmol, 3 eq.) was added to the mixture, which was stirred for 16 hours. Crushed ice (5 g) was added and the mixture filtered prior to extraction with Et_2O (2 × 50 mL), washed with 0.2 M HCl solution (10 mL). The organic layers were combined, dried with $MgSO_4$, filtered and concentrated *in vacuo* to produce a green wax. The mixture was subject to flask to flask distillation at 70 °C and 0.8 mmHg to remove excess malononitrile and DMSO. A waxy light brown solid (0.41 g, 84%) was recovered, identified as product. ^{1}H NMR (400 MHz) δ 4.19 (s, 2H, *20-H*), 3.81 (t, *J* = 6.0 Hz, 2H, *27-H*), 3.74-3.62 (m, 13H, *21-26-H* & *47-H*), 3.28 (t, *J* = 7.6 Hz, 2H, *18-H*), 3.17 (t, *J* = 7.6 Hz, 2H, *18-H*), 2.29 (t, *J* = 6.2 Hz, 2H, *28-H*), 1.56-1.47 (s, 4H, *17-H*), 1.33-1.19 (m, 60H, *2-16-H*), 0.88 (t, *J* = 6.8 Hz, 6H, *1-H*). ^{13}C NMR (101 MHz) δ 168.6 (*19-C*), 115.3, 110.1 (*29-C* & *30-C*), 70.7, 70.6, 70.5, 70.0 66.9, 65.9, 47.0 (*18-C*), 45.8 (*18-C*), 37.5, 33.2, 32.0, 29.8, 29.7, 29.6, 29.5, 29.4, 27.6, 27.1, 26.9, 22.7, 14.2 (*1-C & 36-C*). LRMS (ESI) *m*/*z*: 803.605 ($[M]^+$, 29%), 431.091 (100), 412.673 (55). HRMS (ESI) *m*/*z*: calculated $[M+H]^+$ 826.7013, found 826.7011. IR (DCM film) ν_{max} (cm^{-1}); 2917 (l), 2850 (l), 1648 (m), 1467 (m), 1116 (m), 721 (m).

6.2.9. Synthesis dimethyl 2-(15-octadecyl-14-oxo-3,6,9,12-tetraoxa-15-azatritriacontyl)malonate, 12

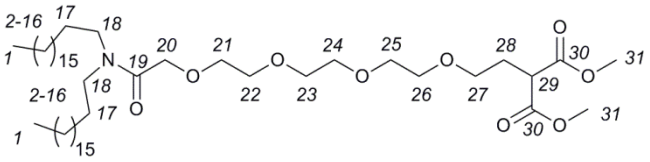

Dimethylmalonate (0.45 mL, 3.92 mmol, 3 eq.), a solution of NaOMe in MeOH (2.15 M; 0.80 mL, 1.70 mmol, 1.3 eq.), and 3 Å M.S (1.00 g) were refluxed in anhydrous MeOH (2 mL) for 30 minutes under an argon atmosphere. Product **10** (1.13 g, 1.31 mmol, 1 eq.) in anhydrous MeOH (2 mL) was added dropwise to the mixture which continued refluxing for an additional 16 hours. Additional NaOMe solution (0.5 mL) was added and refluxed for an additional 3.5 hours. The mixture was cooled to room temperature, filtered and neutralised to pH 7 using acetic acid. The solution was concentrated *in vacuo* and dissolved in Et_2O (50 mL) and H_2O (20 mL), the layers were separated and the aqueous layer was further extracted by Et_2O (3 × 20 mL). The combined organic layers were dried ($MgSO_4$), filtered and concentrated *in vacuo* to afford an off white solid (0.978 g) purified by flash column chromatography (30 mm, eluent; hexane: EtOAc 4:1 to 3:2 to 1:1 to EtOAc) yielding a white solid (0.59 g, 52%) identified as product (R_f 0.31, EtOAc). ^{1}H NMR (700 MHz) δ 4.17 (s, 2H, *19-H*), 3.72 (s, 6H, *31-H*), 3.71-3.52 (m, 15H, *21-27-H* & *29-H*), 3.27 (t, *J* =7.7 Hz, 2H, *18-H*), 3.17 (t, *J* =7.7 Hz, 2H, *18-H*), 2.17 (q, *J* = 6.2 Hz, 2H, *28-H*), 1.54-1.47 (m, 4H, *17-H*), 1.33-1.13 (m, 60H, *2-16-H*), 0.87 (t, *J* =7.1 Hz, 6H *1-H*). ^{13}C NMR (176 MHz) δ 169.9 (*30-C*), 168.7 (*19-C*), 70.7, 70.6, 70.3, 70.1, 68.4, 52.6 (*29-C*) 48.7 (*31-C*), 47.0 (*18-C*), 45.9 (*18-C*), 32.0, 29.8, 29.7, 29.5, 29.4, 27.7, 27.1, 27.0, 22.8, 14.2 (*1-C*). LRMS (ESI) *m*/*z*: 871.587 (51%), 870.600 ($[M+H]^+$, 100), 866.308 (71). HRMS (ESI) *m*/*z*: calculated $[M+H]^+$ 870.7398, found 870.7386. IR ($CDCl_3$ film) ν_{max} (cm^{-1}); 2919 (l), 2851 (l), 1736 (m), 1648 (s), 1467 (s), 1248 (s), 1118 (m).

6.2.10. Synthesis of TAP lipid; N,N-dioctadecyl-2-(2-(2-(2,4,6-triaminopyrimidin-5-yl)ethoxy)ethoxy)acetamide, 1

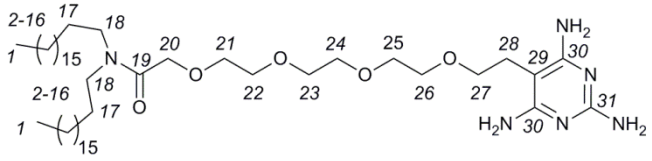

To a stirred solution of compound **11** (0.11 g, 0.14 mmol, 1 eq.) in freshly distilled EtOH (1.3 mL) under an argon atmosphere, a solution of NaOEt in EtOH (1.83 M; 0.12 mL, 0.22 mmol, 1.6 eq.) and guanidine carbonate (0.02 g, 0.18 mmol, 1.3 eq.) were added. The reaction mixture was refluxed for 4 hours. The solution was allowed to cool to room temperature, followed by the addition of EtOH (10 mL), the solution was filtered. The filtrate was concentrated *in vacuo* to afford a crude white solid (0.103 g). The crude product was by recrystallised using MeOH: DCM 95:5 with evaporation of the mother liquor providing the desired product (0.07 g, 58%). ^{1}H NMR (700 MHz) δ 4.20 (s, 2H, *20-H*), 3.73-3.47 (m, 14H, *21-27-H*), 3.29-3.23 (m, 2H, *18-H*), 3.18-3.12 (m, 2H, *18-H*), 2.37 (t, *J* = 6.6 Hz, 2H, *28-H*), 1.56-1.46 (m, 4H, *17-H*), 1.23 (d, *J* = 6.3 Hz, 60H, *2-16-H*), 0.86 (t, *J* = 7.1 Hz, 6H, *1-H*). ^{13}C NMR (176 MHz) δ 168.8 (*19-C*), 129.1 (*30-C* or *31-C*), 128.3 (*30-C* or *31-C*), 70.7, 70.6, 70.5, 70.4, 70.2, 69.9, 67.6 (*27-C*), 47.1 (*18-C*), 46.0 (*18-C*), 43.2, 40.0 (*28-C*), 37.2, 32.9, 32.0, 31.9, 30.1, 29.8, 29.70, 29.6, 29.5, 29.01, 27.7, 27.20, 27.0, 22.8, 14.2 (*1-C*). LRMS (ESI) *m*/*z*: 1600.909 (78%), 863.634 ([M]$^{+}$, 3), 811.920 (100), 734.034 (26). HRMS (ESI) *m*/*z*: calculated [M+H]$^{+}$ 863.7677, found 863.7689.

6.2.11. Synthesis of crude BAR lipid; N,N-dioctadecyl-14-(2,4,6-trioxohexahydropyrimidin-5-yl)-3,6,9,12-tetraoxatetradecanamide 2

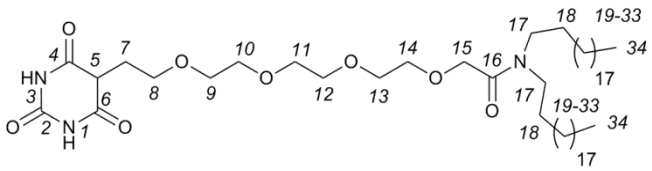

Compound **12** (0.10 g, 0.12 mmol, 1 eq.) was added to a 2 mL microwave vial fitted with a septum under an argon atmosphere. Anhydrous MeOH (0.4 mL) was added to the vial

followed by urea (0.01 g, 0.12 mmol, 1.1 eq.), then freshly prepared NaOMe solution (2.15 M; 0.16 mL, 0.35 mmol, 3 eq.). The septum was removed and quickly replaced with a crimped microwave lid to form an air tight seal. The mixture was heated at 110 °C in a microwave for 1 hour. The mixture was concentrated, and partitioned between $CHCl_3$ (40 mL) and 5% HCl solution (10 mL). The organic layer was separated and washed further with 5% HCl (10 mL) then H_2O (10 mL). The organic layer was collected, dried ($MgSO_4$), filtered and concentrated to return a crude waxy solid. (0.08 g). The mixture was analysed by HPLC-MS as outlined in Section 6.2.29. The target compound was determined to elute at t_R 7.326 minutes. LRMS (ESI) *m*/*z*: 906.267 (23%), 888.694 ($[M+Na]^+$, 17), 867.722 ($[M+H_2]^+$, 52), 866.72 ($[M+H]^+$, 100), 567.991 ($[M_2+Na]^+$, 100), 832.257 (30), 522.590 (15), 391.285 (36). HRMS (ESI) *m*/*z*: calculated $[M+H]^+$ 866.7179, found 866.7187.

6.2.12. Synthesis of dimethyl 2-decylmalonate, 15

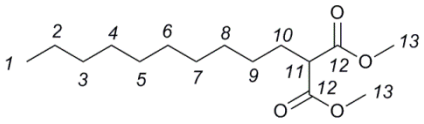

Dimethyl malonate (0.48 mL, 4.22 mmol, 3 eq.) and NaOMe solution in MeOH (2.15 M; 2.00 mL, 4.22 mmol, 3 eq.) were refluxed in anhydrous MeOH (2 mL) for 1 hour. The mixture was cooled and iododecane (0.30 mL, 1.41 mmol, 1 eq.) was added to the solution which was refluxed for 16 hours. The mixture was cooled and neutralised to pH 7 with AcOH. The mixture was concentrated, Et_2O (50 mL) was added and washed with H_2O (3 × 15 mL). The organic phase was collected, dried ($MgSO_4$), filtered and concentrated to produce a crude oil which was purified by flash column chromatography (30 mm, eluent; hexane to EtOAc 10:1) producing a colourless oil (0.33 g, 87%) identified as product (R_f 0.46, hexane: EtOAc 6:1).^{1}H NMR (700 MHz) δ 3.73 (s, 6H, *13-H*), 3.35 (t, *J* = 7.6 Hz, 1H, *11-H*), 1.92-1.86 (m, 2H, *10-H*), 1.31-1.21 (m, 15H, *2-9-H*), 0.88 (t, *J* = 7.1 Hz, 3H, *1-H*). ^{13}C NMR (176 MHz) δ 170.1 (*12-C*), 52.6 (*13-C*), 51.9 (*11-C*), 32.1, 29.7, 29.5, 29.3, 29.0 (*10-C*), 27.5, 22.8, 14.3 (*1-C*). LRMS (ESI) *m*/*z*: 567.991 ($[M_2+Na]^+$, 100%), 295.09 ($[M+Na]^+$, 70), 273.2278 ($[M+H]^+$, 64). HRMS (ESI) *m*/*z*: calculated $[M+H]^+$ 273.2066,

found 273.2054. IR (neat) ν_{max} (cm^{-1}); 2923 (m), 2853 (m), 1756 (m), 1737 (l), 1463 (s), 1435 (m), 1341 (s), 1229 (m), 1197 (m), 1151 (l), 1018 (s), 722 (s).

6.2.13. Synthesis of 5-decanylpyrimidine-(2,4,6) (1*H*,3*H*,5*H*)-trione, 16 by urea condensation.

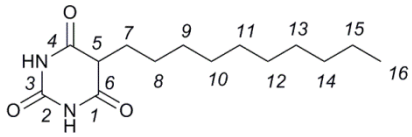

Compound **15** (0.15 g, 0.55 mmol, 1 eq.) was added to a 2 mL microwave vial fitted with a septum under an argon atmosphere. Anhydrous MeOH (1 mL) was added to the vial followed by urea (0.04 g, 0.61 mmol, 1.1 eq.), then freshly prepared NaOMe solution (2.15 M; 0.77 mL, 1.65 mmol, 3 eq.). The septum was removed and quickly replaced with a crimped microwave lid to form an air tight seal. The mixture was heated at 110 °C in a microwave for 1 hour. The mixture was acidified using 5% HCl solution, the mixture was then cooled a 4 °C for 2 hours prior to filtration. The crude material was recrystallised from MeOH to yield a white powder (0.09 g, 64%). CHN analysis; Found: C, 62.40; H, 9.09; N, 10.14. Calc. for $C_{14}H_{24}N_2O_3$: C, 62.66; H, 9.01; N, 10.44%. mp: 199-200 °C. ^{1}H NMR (700 MHz, DMSO-d^6) δ 11.20 (s, 2H, NH), 3.51 (t, *J* = 5.1, 1H, *5-H*), 1.91-1.83 (m, 2H, *7-H*), 1.36-1.17 (m, 16H, *8-15-H*), 0.85 (*J* = 6.8 Hz, 3H, *16-H*). ^{13}C NMR (176 MHz, DMSO-d^6) δ 170.5 (*4-C* & *6-C*), 150.9 (*2-C*), 74.7 (*5-C*), 47.9, 31.3, 28.9, 28.8, 28.7, 27.96, 25.7, 22.1, 14.0 (*16-C*). LRMS (ESI) *m*/*z*: 268.174 (19%), 267.212 ([M-H]$^-$, 100). HRMS (ESI) *m*/*z*: calculated [M-H]$^-$ 267.1709, found 267.1707. IR (neat) ν_{max} (cm^{-1}); 3235 (s), 3091 (s), 2919 (m), 2849 (m) 1756 (m), 1700 (m), 1630 (l), 1538 (l), 1466 (l), 1427 (m), 1404 (m), 1243 (m), 1213 (m), 1120 (s), 967 (s), 770 (l), 755 (l), 707 (s), 539 (s), 524 (l).

6.2.14. Synthesis of tetrabutylammonium 2,4,6-trioxohexahydropyrimidin-5-ide (barbituate), 17

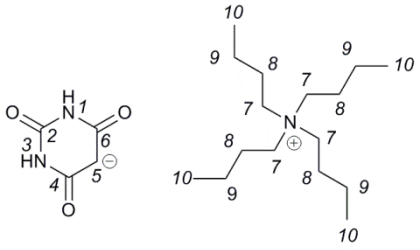

Barbituric acid (0.50 g, 3.90 mmol, 1 eq.) and a solution of tetrabutylammonium hydroxide in MeOH (1M; 3.90 mL, 3.90 mmol, 1 eq.) were stirred for 30 minutes at room temperature, a clear solution was formed. The material was concentrated *in vacuo* and dried over P_2O_5 in-vacuo for 16 hours. The material was not purified further and was produced quantitatively. mp: 180-181 °C. ^{1}H NMR (600 MHz, DMSO-d^6) δ 8.91 (s, 2H, N*H*), 3.70 (d, *J* = 1.5 Hz, 1H, *5-H*), 3.20-3.13 (m, 8H, *7-H*), 1.56 (td, *J* = 11.8, 10.0, 6.1 Hz, 8H, *8-H*), 1.30 (h, *J* = 7.4 Hz, 8H, *9-H*), 0.93 (t, *J* = 7.4 Hz, 12H, *10-H*). ^{13}C NMR (151 MHz, DMSO-d^6) δ 165.6 (*4-C* & *6-C*), 153.0 (*2-C*), 74.6 (*5-C*), 57.5 (*7-C*), 23.1 (*8-C*), 19.2 (*9-C*), 13.5 (*10-C*). LRMS (ESI) *m*/*z*: 496.258 (18%), 332.268 (6), 126.921 ([Barbituate]$^-$, 100). HRMS (ESI) *m*/*z*: calculated [Barbituate]$^-$ 127.0144, found 127.0133.

Single crystals obtained from slow evaporation of EtOAc: EtOH was subject to X-ray diffraction. X-ray diffraction images of the single crystal (obtained as detailed in Section 6.1) allowed elucidation of the unit cell shown in Figure 6.1.

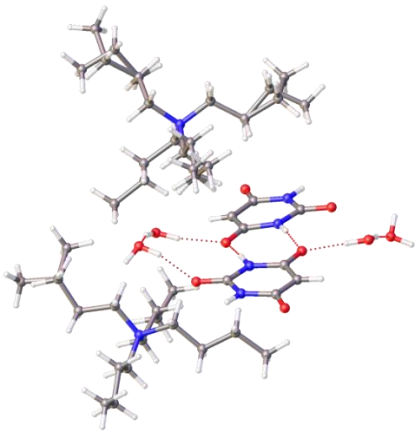

Figure 6.1. Structures from the unit cell of **17**, determined by X-ray diffraction of a single crystal.

6.2.15. Synthesis of , benzyl 2-(2-(2-iodoethoxy)ethoxy)acetate, 18

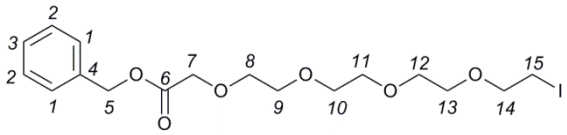

Compound **5** (1.01 g, 2.04 mmol, 1 eq.) and NaI (0.61 g, 4.07 mmol, 2 eq.) were refluxed in anhydrous MEK (7 mL) for 16 hours under an argon atmosphere. The solution was cooled to room temperature concentrated *in vacuo* followed by addition of Et_2O (100 mL). The solution was washed with H_2O (2 × 10 mL), the organic layer was dried ($MgSO_4$), filtered and concentrated *in vacuo* to afford a brown oil (0.77 g, 83%) identified as product. ^{1}H NMR (400 MHz) δ 7.40-7.30 (m, 5H, *1-3-H*), 5.19 (s, 2H, *5-H*), 4.21 (s, 2H, *7-H*), 3.78-3.63 (m, 14H, *8-14-H*), 3.25 (t, *J* = 6.8 Hz, 2H, *15-H*). ^{13}C NMR (101 MHz) δ 170.5 (*6-C*), 128.8, 128.7, 128.6, 127.1, 72.1, 71.1, 70.8, 70.4, 68.8, 66.7, 3.1 (*15-C*). LRMS (ESI) *m*/*z*: 476.09 (15%), 474.838 ($[M+H]^+$, 100). HRMS (ESI) *m*/*z*: calculated $[M+H]^+$ 453.0774, found 453.0766. IR (neat) ν_{max} (cm^{-1}); 3278 (m), 3114 (s), 2955 (s), 2915 (m) 2849 (m), 1755 (m), 1700 (l), 1630 (l), 1568 (m), 1512 (m), 1380 (l), 1283 (m), 1148 (l), 1037 (s), 809 (s), 754 (l), 689 (m), 557 (l), 541 (l).

6.2.16. Synthesis of 5-decanoylpyrimidine-(2,4,6) (1*H*,3*H*,5*H*)-trione, 20

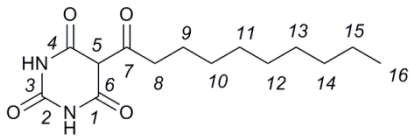

Decanoyl chloride (2.50 mL, 12.05 mmol, 1 eq.) was added to a stirred suspension of barbituric acid (1.68 g, 13.11 mmol, 1.1 eq.) in anhydrous pyridine (30 mL) under an argon atmosphere. The orange solution formed was allowed to stir for a further 16 hours. The solution was poured into a mixture of MeOH (30 mL), H_2O (25 mL) and concentrated HCl solution (75 mL). The solution was left at 4 ° C for an hour until a precipitate formed. The solid was filtered and washed by H_2O: HCl 9:1 to give an off-white solid (3.32 g, 98%), identified as product, which was used without further purification. mp: 193-194 °C. ^{1}H NMR (400 MHz, DMSO-d^6) δ 11.81 (s, 1H, NH), 11.04 (s, 1H, NH), 3.01 (t, *J* = 7.4, 2H, *8-*

H), 1.57 (q, *J* = 7.4 Hz, 2H, *9-H*), 1.35-1.17 (m, 12H, *10-15-H*), 0.85 (t, *J* = 6.8 Hz, 3H, *16-H*). LRMS (ESI) *m*/*z*: 282.231 (28), 281.225 ([M-H]$^-$, 100%). HRMS (ESI) *m*/*z*: calculated [M+H]$^+$ 283.1658, found 283.1654.

6.2.17. Synthesis of 5-decanylpyrimidine-(2,4,6) (1*H*,3*H*,5*H*)-trione, 16 by reduction.

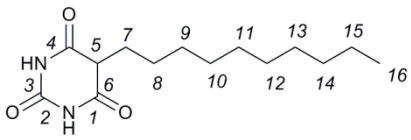

Sodium triacetoxyborohydride (0.01 g, 0.53 mmol, 1 eq.) was added every 10 minutes until four equivalents total were added, to a stirred solution of compound **20** (0.14 g, 0.53 mmol, 1 eq.) in anhydrous THF (2.5 mL) at room temperature under an argon atmosphere. The solution was left stirring overnight prior to concentration and addition of 1 M HCl solution (10 mL), the white foamy precipitate was filtered and washed with 1 M HCl solution to afford a white solid (0.08 g, 57%), identified as product. Data matched that reported in Section 6.2.13.

6.2.18. Synthesis of 2-(2-(2-(benzyloxy)-2-oxoethoxy)ethoxy)acetic acid, 22

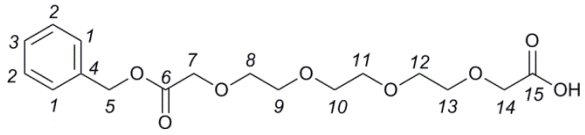

Compound **5** (2.34 g, 6.83 mmol, 1 eq.), diacetoxyiodobenzene (4.84 g, 15.02 mmol, 2.2 eq.) and TEMPO (0.21 g, 1.37 mmol, 0.3 eq.) were stirred vigorously in DCM: H_2O (40 mL) overnight. The layers were separated; the aqueous layer was extracted with DCM (3 × 20 mL). The combined organic layers were dried using $MgSO_4$, filtered and concentrated. The remaining iodobenzene was removed under high-vacuo at 1 mbar and 40 °C leaving a brown oil (2.01 g, 82%) identified as product.^{1}H NMR (400 MHz) δ 7.38-7.26 (m, 5H, *1-3-H*), 5.18 (s, 2H, *5-H*), 4.19 (s, 2H, *7-H*), 4.13 (s, 2H, *14-H*), 3.77-3.61 (m, 12H, *8-13-H*). ^{13}C NMR (101 MHz) δ 170.43 (*6-C*), 135.5, 128.8, 128.6, 71.6, 71.1, 70.8, 70.6, 70.5, 70.3, 69.2, 68.7, 66.8. LRMS (ESI) *m*/*z*: 356.561 ([M]$^-$, 22%), 355.156 ([M-H]$^-$, 100).

HRMS (ESI) *m*/*z*: calculated [M-H]$^-$ 355.1393, found 355.1404. IR (neat) ν_{max} (cm^{-1}); 3460 (s), 2878 (m), 1750 (l), 1194 (l), 1111 (l), 943 (s), 852 (s), 739 (s), 698 (m).

6.2.19. Synthesis of benzyl 2-(2-(2-(2,4,6-trioxohexahydropyrimidin-5-yl)ethoxy)ethoxy)acetate, 23

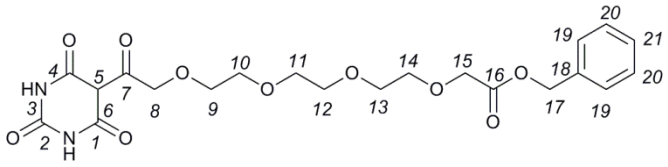

Acid **22** (1.81 g, 5.09 mmol, 1 eq.) and oxalyl chloride (0.87 mL, 10.17 mmol, 2 eq.) were refluxed in anhydrous DCM (2 mL) under an argon atmosphere for 5 hours. The solution was concentrated *in vacuo* and dissolved in anhydrous DCM (2 mL). The solution was added to a stirred suspension of barbituric acid (0.72 g, 5.60 mmol, 1.1 eq.) in anhydrous pyridine (0.46 mL, 5.60 mmol, 1.1 eq.) and anhydrous DCM (3 mL); the suspension was stirred for 2 hours. The DCM was concentrated *in vacuo*, followed by addition of EtOAc (200 mL) and 1 M HCl solution (20 mL), the layers were separated and the aqueous extracted further by EtOAc (2 × 50 mL) the organic layer was dried ($MgSO_4$) filtered and concentrated *in vacuo*. The crude material was dissolved in minimal MeOH and placed in a freezer at -20°C and left for several hours for a precipitate to form. The solid was quickly filtered using a Büchner funnel cooled to -20 °C and washed with MeOH cooled to -20 °C. A brown solid (1.17 g, 49%) identified as product was recovered. ^{1}H NMR (400 MHz) δ 8.61 (s, 1H, N*H*), 8.16 (s, 1H, N*H*), 7.35 (d, *J* = 3.3 Hz, 5H, *19-21-H*), 5.19 (s, 2H, *17-H*), 5.00 (s, 2H, *8-H*), 4.20 (s, 2H, *15-H*), 3.79-3.63 (m, 12H, *9-14-H*). ^{13}C NMR (101 MHz) δ 197.5 (*7-C*), 170.5 (*1-C* & *4-C*), 149.5 (*2-C*), 135.4 (*18-C*), 128.6, 128.5, 128.4, 93.3, 71.3, 70.9, 70.6, 70.5, 68.6. LRMS (ESI) *m*/*z*: 953.632 (21%), 465.227 ([M-H]$^-$, 100). HRMS (ESI) *m*/*z*: calculated [M]$^+$ 467.1666, found 467.1692.

6.2.20. Synthesis of benzyl 15-octadecyl-14-oxo-3,6,9,12-tetraoxa-15-azatritriacontanoate, 24

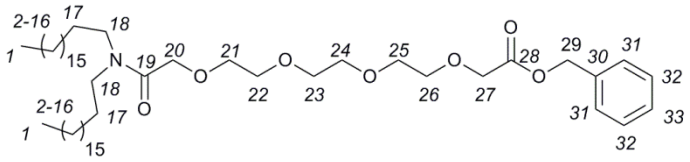

Compound **22** (1.13 g, 3.16 mmol, 1 eq.) was stirred with oxalyl chloride (0.40 mL, 4.74 mmol, 1.5 eq.) and anhydrous DMF (0.05 mL, cat.) in anhydrous DCM (10 mL) under an argon atmosphere for 2 hours. The solution was concentrated and dissolved in fresh anhydrous DCM (2 mL) and transferred to a stirred suspension of dioctadecylamine (1.81 g, 3.47 mmol, 1.1 eq.) and trimethylamine (0.49 mL, 3.47 mmol, 1.1 eq.) in anhydrous DCM (80 mL) at 0 °C under an argon atmosphere. The mixture was allowed to warm to room temperature and was stirred for an additional 16 hours. The mixture was diluted with DCM (50 mL) and washed with 5% HCl solution (2 × 20 mL) and H_2O (2 × 10 mL). The organic layer was collected, dried ($MgSO_4$), filtered and concentrated *in vacuo* to return a yellow solid. The crude solid was purified by flash column chromatography (50 mm, eluent; hexane: EtOAc 3:1 to 1:1) to yield a waxy white solid (1.62 g, 60%) identified as product (R_f 0.18, EtOAc). ^{1}H NMR (400 MHz) δ 7.38-7.30 (m, 5H, *31-33-H*), 5.19 (s, 2H, *29-H*), 4.20 (s, 2H, *20-H*), 4.18 (s, 2H, *27-H*), 3.75-3.62 (m, 12H, *21-26-H*), 3.31-3.25 (m, 2H, *18-H*), 3.21-3.14 (m, 2H, *18-H*), 1.51 (d, *J* = 8.3 Hz, 4H, *17-H*), 1.34-1.18 (m, 60H, *2-16-H*), 0.91-0.82 (m, 6H, *1-H*).^{13}C NMR (101 MHz) δ 170.3 (*28-C*), 168.6 (*19-C*), 135.5 (*30-H*), 128.6, 128.4, 71.0, 70.6, 70.1, 68.7, 66.5, 47.0, 45.8, 31.9, 29.7, 29.6, 29.4, 29.0, 27.6, 27.1, 26.9, 22.7, 14.1 (*1-H*). LRMS (ASAP) *m*/*z*: 862.753 (41%), 861.724 (99), 860.698 ($[M+H]^+$, 100). HRMS (ASAP) *m*/*z*: calculated $[M+H]^+$ 860.7343, found 860.07368.

6.2.21. Synthesis of 15-octadecyl-14-oxo-3,6,9,12-tetraoxa-15-azatritriacontanoic acid, 25

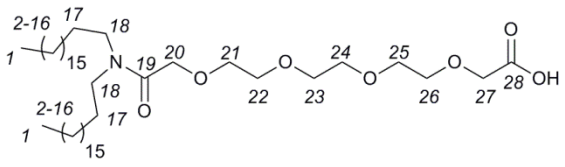

Into a 2 neck flask fitted with a septum and a gas tap, compound **24** (0.43 g, 0.49 mmol, 1 eq.) and Pd/C (0.09 g, cat.) were added followed by the addition of DCE (10 mL). The suspension was frozen using liquid nitrogen, then degassed by application of high vacuum. The vacuum was stopped and the vessel was back filled by $H_{2(g)}$ using a balloon, the vessel was warmed to room temperature using tepid H_2O. The reaction was stirred for 2 days, followed by filtration through a celite pad; the pad was washed using DCM (100 mL). Concentration produced a clear oil (0.36 g, 95%) identified as product. ^{1}H NMR (700 MHz) δ 4.19 (s, 2H, *20-H*), 4.09 (s, 2H, *27-H*), 3.75-3.63 (m, 12H, *21-26-H*), 3.27 (dd, *J* = 9.0, 6.4 Hz, 2H, *18-H*), 3.12 (t, *J* = 7.8 Hz, 2H, *18-H*), 1.55-1.46 (m, 4H, *17-H*), 1.24 (d, *J* = 6.3 Hz, 60H, *2-16-H*), 0.87 (t, *J* = 7.1 Hz, 6H, *1-H*). ^{13}C NMR (176 MHz) δ 173.3 (*28-C*), 169.0 (*19-C*), 70.6, 70.5, 70.4, 70.2, 69.6, 69.3, 47.0, 46.2, 32.1, 29.8, 29.7, 29.6, 29.5, 29.0, 27.7, 27.2, 27.0, 22.8, 14.3 (*1-C*). LRMS (ASAP) *m*/*z*: 712.667 ([M-CH_2CO_2H]$^+$, 100%), 770.696 ([M+H]$^+$, 16), 578.592 (59). HRMS (ASAP) *m*/*z*: calculated [M+H]$^+$ 770.6874, found 770.6842. IR (neat) ν_{max} (cm^{-1}); 2916 (l), 2849 (m) 1737 (s), 1650 (s), 1609 (s), 1467 (m), 1351 (s), 1204 (s), 1117 (l), 855 (s), 720 (m).

6.2.22. Synthesis of 5-decanylpyrimidine-(2,4,6) (1*H*,3*H*,5*H*)-trione, 16 by Knoevenagel condensation.

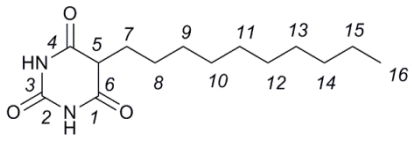

Into a 2 neck flask fitted with a septum and a gas tap, barbituric acid (0.13 g, 1.00 mmol, 1 eq.), decanal (0.44 mL, 2.13 mmol, 2.1 eq.), NEt_3 (0.44 mL, 2.87 mmol, 2.9 eq.) and Pd/C (0.02 g, cat.). The vessel was then charged with DCE (5 mL). The suspension was frozen using liquid nitrogen, then degassed by application of high vacuum. The vacuum was stopped and the vessel was back filled by $H_{2(g)}$ using a balloon, the vessel was warmed to room temperature using tepid H_2O. The suspension was stirred for 16 hours, the mixture was then filtered through celite and concentrated, the material was dissolved in minimum MeOH and 5% HCl solution was added to obtain a white precipitate which was left at 0 °C for at

least 1 hour. The precipitate was filtered, washing with H_2O and Et_2O, upon drying a White powder (0.09 g, 32%) was obtained identified as product. Characterisation matched that reported in Section 6.2.13.

6.2.23. Synthesis of Benzyl 2,2,3,3-tetramethyl-4,7,10,13,16-pentaoxa-3-silaoctadecan-18-oate, 27

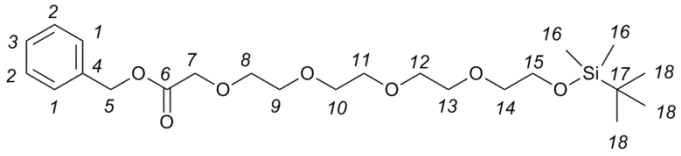

Compound **5** (3.02 g, 8.82 mmol, 1 eq.), I_2 (4.48 g, 17.65 mmol, 2 eq.) and NMI (2.10 mL, 26.47 mmol, 3 eq.) were dissolved in anhydrous THF (30 mL) under an argon atmosphere. *tert*-Butyldimethylsilyl chloride (2.00 g, 13.24 mmol, 1.5 eq.) was added and stirred for 2 hours. The solution was concentrated *in vacuo* and diluted using EtOAc (100 mL), the organic layer was washed with saturated $Na_2S_2O_5$ solution (2 × 10 mL) and H_2O (10 mL). The organic layer was dried ($MgSO_4$), filtered and concentrated. The crude material was purified by flash column chromatography (50 mm, eluent; hexane: EtOAc 10:1 to 5:1 to 2:1) to afford a colourless oil (3.83 g, 95%).^{1}H NMR (700 MHz) δ 7.38-7.30 (m, 5H, *1-3-H*), 5.18 (s, 2H, *5-H*), 4.19 (s, 2H, *7-H*), 3.77-3.61 (m, 14H, *8-14-H*), 3.54 (t, *J* = 5.5 Hz, 2H, *15-H*), 0.88 (s, 9H, *18-H*), 0.05 (s, 6H, *16-H*). ^{13}C NMR (176 MHz) δ 170.5 (*6-C*), 135.6 (*4-C*), 128.7, 128.5, 72.8 (*15-C*), 71.1, 70.8, 70.7, 68.8 (*7-C*), 66.6 (*5-C*), 62.8, 26.1 (*18-C*), 18.5 (*17-C*), -5.1 (*16-C*). LRMS (ESI) *m*/*z*: 480.569 (100%), 458.576 (96), 456.743 ($[M]^+$, 63). HRMS (ESI) *m*/*z*: calculated $[M+H]^+$ 457.2622, found 457.2621. IR (neat) ν_{max} (cm^{-1}); 2930 (m), 2862 (m) 1760 (m), 1460 (s), 1253 (m), 1196 (s), 1148 (l), 941 (s), 835 (m), 777 (s).

6.2.24. Synthesis of 2,2,3,3-tetramethyl-4,7,10,13,16-pentaoxa-3-silaoctadecan-18-oic acid, 28

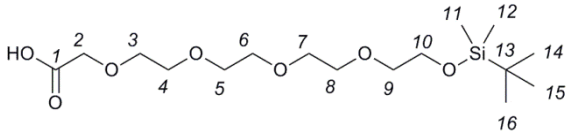

Into a 2 neck flask fitted with a septum and a gas tap, compound **27** (3.20 g, 7.01 mmol, 1 eq.) and Pd/C (0.32 g, cat.) were added followed by the addition of MeCN (28 mL). The suspension was frozen using liquid nitrogen followed by application of high vacuum. The vacuum was stopped and the vessel was back filled by $H_{2(g)}$ using a balloon, the vessel was warmed to room temperature using tepid H_2O. The process of purging and back filling was performed twice more. The mixture was stirred under a hydrogen atmosphere for 16 hours. The suspension was filtered through celite and concentrated *in vacuo* affording a colourless oil, identified as the ethylammonium salt. ^{1}H NMR (400 MHz) δ 4.07 (s, 2H, *2-H*), 3.78-3.60 (m, 14H, *3-9-H*), 3.56 (dd, *J* = 5.7, 5.0 Hz, 2H, *10-H*), 3.09-3.01 (m, 2H, $NH_2CH_2CH_3$), 1.26 (t, *J* = 7.3 Hz, 3H, $NH_2CH_2CH_3$), 0.89 (s, 9H, *13-H*), 0.06 (s, 6H, *11-H*).

The mixture was dissolved in DCM (50 mL) and quickly washed with 5% HCl solution (2 × 10 mL) and H_2O (10 mL). The organic layer was dried ($MgSO_4$), filtered and concentrated *in vacuo* to produce the desired free acid product (2.42 g, 94%).^{1}H NMR (700 MHz) δ 4.02 (s, 2H, *2-H*), 3.77 (dd, *J* = 5.6, 4.7 Hz, 2H, *3-H*), 3.69-3.63 (m, 12H, *4-9-H*), 3.57 (dd, *J* = 5.6, 4.7 Hz, 2H, *10-H*), 0.89 (s, 9H, *13-H*), 0.06 (s, 6H, *11-H*). ^{13}C NMR (176 MHz) δ 174.3 (*1-C*), 72.7 (*10-C*), 70.6, 70.4, 70.3, 70.2 (*4-9-C*), 62.9 (*3-C*), 26.1 (*13-C*), 18.5 (*12-C*), -5.14 (*11-C*). LRMS (ESI) *m*/*z*: 366.156 ($[M]^-$, 41%), 365.259 ($[M-H]^-$, 100). HRMS (ESI) *m*/*z*: calculated $[M+H]^+$ 365.1996, found 365.2010. IR (DCM film) ν_{max} (cm^{-1}); 3478 (s), 2931 (m), 2858 (m), 1739 (m), 1463 (s), 1363 (s), 1252 (m), 1105 (l), 941 (s), 835 (l), 778 (m).

6.2.25. Synthesis of 2,2,3,3-tetramethyl-N,N-dioctadecyl-4,7,10,13,16-pentaoxa-3-silaoctadecan-18-amide, 29

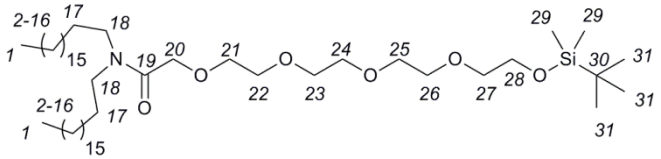

Compound **28** (2.06 g, 5.63 mmol, 1 eq.) in anhydrous DCM (25 mL) was cooled to 0 °C prior to the addition of NHS (0.71 g, 6.19 mmol, 1.1 eq.), DMAP (0.76 g, 6.19 mmol,

1.1 eq.) and diisopropylcarbodimide (0.97 mL, 6.19 mmol, 1.1 eq.). Allow to warm to room temperature and stir for 1.5 hours, dioctadecylamine (3.23 g, 6.19 mmol, 1.1 eq.) was added and stirred for an additional 16 hours. DCM (100 mL) was added and washed with H_2O (2 × 10 mL). The organic layer was dried ($MgSO_4$), filtered and concentrated. The crude waxy solid was purified by flash column chromatography (50 mm, eluent; hexane: EtOAc 10:1 to 5:1 to 2:1 to 1:1) yielding a white waxy solid (3.52 g, 72%) identified as product (R_f 0.22, hexane: EtOAc 2:1). ^{1}H NMR (600 MHz) δ 4.18 (s, 2H, *20-H*), 3.76 (t, *J* = 5.6 Hz, 2H, *27-H*), 3.73-3.62 (m, 12H, *21-26-H*), 3.55 (t, *J* = 5.6 Hz, 2H, *28-H*), 3.28 (t, *J* = 7.7 Hz, 2H, *18-H*), 3.18 (t, *J* = 7.8 Hz, 2H, *18-H*), 1.52 (q, *J* = 8.0 Hz, 4H, *17-H*), 1.33-1.19 (m, 60H, *2-16-H*), 0.92-0.86 (m, 15H, *1-H* & *31-H*), 0.06 (s, 6H, *29-H*). ^{13}C NMR (151 MHz) δ 168.8 (*19-C*), 72.8, 70.9, 70.8, 70.7, 70.3, 62.9, 47.1, 45.9 (*18-C*), 32.1, 29.9, 29.8, 29.7, 29.6, 29.5, 29.1, 27.8, 27.2, 27.1, 26.1 (*31-C*), 22.9, 18.5 (*30-C*), 14.3 (*1-C*), -5.10 (*29-C*). LRMS (ASAP) *m*/*z*: 870.762 ($[M]^+$, 100%), 812.725 ($[M\text{-}C(Me)_3]^+$, 17), 756.715 ($[M\text{-TBDMS}]^+$, 24). HRMS (ASAP) *m*/*z*: calculated $[M+H]^+$ 870.7946, found 870.7953. IR (neat) ν_{max} (cm^{-1}); 2923 (l), 2853 (m) 1650 (m), 1465 (m), 1252 (s), 1107 (s), 836 (s), 778 (s).

6.2.26. Synthesis of 14-hydroxy-N,N-dioctadecyl-3,6,9,12-tetraoxatetradecanamide, 30

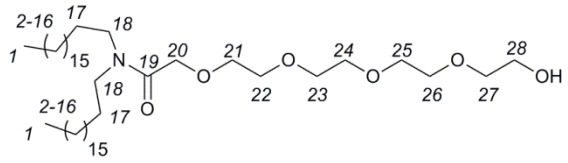

Compound **29** (3.54 g, 4.07 mmol, 1 eq.) and concentrated HCl solution (4.00 mL, 40.07 mmol, 10 eq.) were stirred in 1,4-dioxane (30 mL) for 4 hours. Concentrated *in vacuo* and solvate the solid obtained with DCM (100 mL), wash the organic phase with H_2O (2 × 10 mL). The organic phase was collected, dried ($MgSO_4$), filtered and concentrated to yield a white solid (2.84 g, 93%) which was identified as product (R_f 0.11, EtOAc: MeOH 20:1) and was used without further purification. ^{1}H NMR (700 MHz) δ 4.18 (s, 2H, *21-H*), 3.74-3.63 (m, *21-27-H*), 3.62-3.58 (m, 2H, *28-H*), 3.27 (dd, *J* = 8.9, 6.5 Hz, 2H, *18-H*), 3.17 (t, *J* = 7.7 Hz, 2H, *18-H*), 1.55-1.46 (m, 4H, *17-H*), 1.31-1.20 (m, 60H, *2-16-H*), 0.87 (t, *J* = 7.1

Hz, 6H, *1-H*). ^{13}C NMR (176 MHz) δ 168.6 (*19-C*), 72.5 (*26-C*), 70.6, 70.5, 70.3, 70.0, 67.1, 61.7, 46.9 (*18-C*), 45.8 (*18-H* or *19-H*), 31.9, 29.7, 29.6, 29.4, 29.3, 28.9, 27.6, 27.0, 26.9, 25.6, 22.7, 14.1 (*1-C*). LRMS (ASAP) *m*/*z*: 757.701 ($[M+H^2]^+$, 96%), 756.675 ($[M+H]^+$, 100), 712.685 ($[M-CH_2CH_2OH]^+$, 14). HRMS (ASAP) *m*/*z*: calculated $[M+H]^+$ 756.7081, found 756.7046. IR ($CDCl_3$ film) ν_{max} (cm^{-1}); 3437 (s), 2917 (l), 2850 (l), 1646 (m) 1467 (m), 1379 (s), 1353 (s), 1301 (s), 1251 (s), 1104 (m), 722 (s).

6.2.27. Synthesis of benzyl 1-(1,3-dioxolan-2-yl)-2,5,8,11-tetraoxatridecan-13-oate, 32

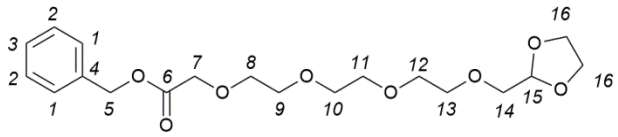

Anhydrous DMSO (1.10 mL, 15.10 mmol, 3 eq.) and anhydrous DCM (15 mL) were cooled to -78 °C and left to stir for 10 minutes under an argon atmosphere. Oxalyl chloride (0.64 mL, 7.55 mmol, 1.5 eq.) was added to the solution and stirred for 10 minutes further. Compound **5** (1.72 g, 5.03 mmol, 1 eq.) was added to the cooled solution, which was stirred for a further hour. Anhydrous DIPEA (4.40 mL, 25.18 mmol, 5 eq.) was added to the solution which was allowed to warm to room temperature and stir for 10 minutes longer. The solution was concentrated *in vacuo*, before addition of EtOAc (100 mL). The solution was washed with H_2O (3 × 10 mL), the organic phase was dried ($MgSO_4$, filtered and concentrated to return a crude oil (1.63 g).

The oil was dissolved in anhydrous toluene under an argon atmosphere, followed by the addition of oven activated 4 Å M.S. Ethylene glycol (2.80 mL, 50.32 mmol, 10 eq.) and $TsOH.H_2O$ (0.29 g, 1.51 mmol, 0.3 eq.) was added to the solution, which was subsequently refluxed for 16 hours. The solution was allowed to cool, followed by the addition of DCM (100 mL). The solution was filtered, with the filtrate being washed with saturated $NaHCO_3$ solution (20 mL) and H_2O (2 × 10 mL). The organic phase was dried ($MgSO_4$), filtered and concentrated *in vacuo* to return a crude oil (1.20 g). The crude oil was purified by flash column chromatography (40 mm, eluent; hexane: EtOAc 5:1 to 2:1 to 1:1 to EtOAc) to yield

a colourless oil (0.59 g, 31%) identified as product (R_f 0.21, EtOAc). ^{1}H NMR (700 MHz) δ 7.38-7.31 (m, 5H, *1-3-H*), 5.18 (s, 2H, *5-H*), 5.05 (t, *J* = 4.1 Hz, 1H, *15-H*), 4.20 (s, 2H, *7-H*), 4.00-3.94 (m, 2H, *16-H*), 3.91-3.85 (m, 2H, *16-H*), 3.76-3.62 (m, 12H, *8-13-H*), 3.57 (d, *J* = 4.1 Hz, 2H, *16-H*). ^{13}C NMR (176 MHz) δ 170.5 (*6-C*), 135.6 (*4-C*), 128.7, 128.6, 128.5, 102.8 (*15-C*), 72.2 (*14-C*), 71.3, 71.1, 70.8, 70.7, 68.8, 66.6 (*5-C*), 65.2 (*16-C*). LRMS (ESI) *m*/*z*: 407.141 (100%), 386.294 ($[M+H_2]^+$, 90), 299.550 (95). HRMS (ESI) *m*/*z*: calculated $[M+Na]^+$ 407.1682, found 407.1693. IR (DCM film) ν_{max} (cm^{-1}); 2884 (m), 1754 (m), 1457 (s), 1197 (s), 1119 (l), 1039 (s), 947 (s), 702 (s).

6.2.28. Synthesis of 1-(1,3-dioxolan-2-yl)-2,5,8,11-tetraoxatridecan-13-oic acid, 33

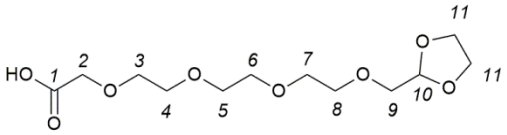

Into a 2 neck flask fitted with a septum and a gas tap, compound **32** (0.59 g, 1.53 mmol, 1 eq.) and Pd/C (0.060 g, cat.) were added followed by the addition of DCE (10 mL). The suspension was frozen using liquid nitrogen followed by application of high vacuum. The vacuum was stopped and the vessel was back filled by $H_{2(g)}$ using a balloon, the vessel was warmed to room temperature using tepid H_2O. The process of purging and back filling was performed twice more. The suspension was stirred under a H_2 atmosphere overnight. The mixture was filtered through a celite plug, washing with DCM (100 mL). The Filtrate was concentrated *in vacuo* to return a colourless oil (0.42 g, 94%) which was identified as product and used without subsequent purification. ^{1}H NMR (700 MHz) δ 5.04 (t, *J* = 4.1 Hz, 1H, *10-H*), 4.11 (s, 2H, *2-H*), 4.01-3.95 (m, 2H, *11-H*), 3.91-3.86 (m, 2H, *11-H*), 3.75-3.63 (m, 12H, *3-8-H*), 3.56 (d, *J* = 4.1 Hz, 2H, *9-H*). ^{13}C NMR (176 MHz) δ 173.0 (*1-C*), 102.4 (10-C), 71.9 (*9-C*), 71.1, 71.0, 70.5, 70.4, 70.3, 70.2, 69.3 (*2-C*) 65.2 (*11-C*). LRMS (ESI) *m*/*z*: 609.244 ($[(M-H)_2+Na]^-$, 12%), 455.807 (5), 239.155 ($[M-H]^-$, 100). HRMS (ESI) *m*/*z*: calculated $[M-H]^-$ 239.1236, found 239.1238. IR ($CDCl_3$ film) ν_{max} (cm^{-1}); 3466 (s), 2879 (m), 1732 (m), 1352 (s) 1246 (s), 1108 (l), 1038 (m), 945 (s), 868 (s).

6.2.29. HPLC-MS of crude BAR lipid

The crude mixture of BAR lipid (**2**) was prepared as a solution in IPA at at 1 µg/mL concentration. For the LC separation a 3.0 µL aliquot was injected onto an Acquity UPLC CSH C18 1.7 µm (2.1 × 150 mm) column supplied by (Waters Ltd, Manchester, UK). Eluents for the mobile phase were A: 60:40 MeCN: H_2O containing 0.1% formic acid and 10 mM ammonium formate. B: 90:10 IPA: MeCN containing 0.1% formic acid and 10 mM ammonium formate. The gradient displayed in Table 6.1 was used; the flow rate was kept constant at 0.1 mL min^{-1}. Mass spectrometric analysis was performed using a Synapt G2S LC ESI TOF detector (Waters Ltd, Manchester, UK) operated in positive ion mode. Data was processed using was processed using Mestrenova (Mestralab Research, version 10.0) on a PC running the Windows 7 operating system.

Table 6.1. HPLC conditions for separation of the crude mixture containing **2**.

Time (min)	% A	%B
0.0	30	70
2.0	20	80
3.5	10	90
5.0	0	90
10.0	0	90

6.3. SPLS Synthetic procedures and characterisation

6.3.1. Synthesis of 3-((2-hydroxyethyl)thio)phenol, 40

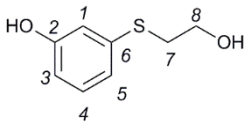

A solution of NaOH (1M; 17.00 mL, 17.26 mmol, 1.1 eq.) was added dropwise over 30 minutes to a stirred solution of 3-hydroxybenzenethiol (1.60 mL, 15.69 mmol, 1 eq.) in MeOH (21 mL) at 0 °C. The mixture was allowed to stir for 1 hour prior to the dropwise addition of bromoethanol (1.45 mL, 20.39 mmol, 1.3 eq.) in MeOH (5 mL) over 15 minutes. The mixture was allowed to heat to room temperature and stir for an additional 16 hours prior to removal of MeOH *in vacuo*. The oil was dissolved in DCM (50 mL) which was subsequently washed with saturated ammonium chloride solution (10 mL), the aqueous layer

was extracted with DCM (3 × 20 mL). The organic layers were combined and washed with brine (20 mL), the organic layer was dried with $MgSO_4$, filtrated and concentrated *in vacuo* to give a brown oil (2.58 g) which was purified by flash column chromatography (50 mm, eluent; EtOAc: hexane 1:1 to EtOAc). A brown oil (2.28 g, 85%) was identified as the product (R_f 0.32, EtOAc: hexane 1:1). ^{1}H NMR (700 MHz, acetone-d^6) δ 7.09 (t, *J* = 7.9 Hz, 1H, *4-H*), 6.82 (t, *J* = 2.1 Hz, 1H, *1-H*), 6.80-6.76 (m, 1H, *3-H*), 6.65-6.61 (m, 1H, *5-H*), 3.66 (t, *J* = 7.1 Hz, 2H, *8-H*), 3.03 (t, *J* = 7.1 Hz, 2H, *7-H*). ^{13}C NMR (176 MHz, acetone-d^6) δ 157.5 (*2-C*), 137.1 (*6-C*), 129.4 (*4-C*), 118.8 (*3-C*), 114.6 (*1-C*), 112.5 (*5-C*), 60.0 (*8-C*), 34.6 (*7-C*). LRMS (ESI) *m*/*z*: 170.623 (7%), 169.094 ([M-H]$^-$, 100). HRMS (ESI) *m*/*z*: calculated [M-H]$^-$ 169.0323, found 169.0327. IR (neat) ν_{max} (cm^{-1}); 3262 (m), 1700 (s), 1580 (l), 1474 (m), 1436 (m), 1214 (m), 1044 (m), 966 (m), 884 (l), 770 (l), 684 (l).

6.3.2. Characterisation of 3,3'-disulfanediyldiphenol, 41

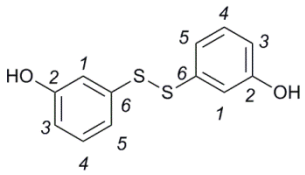

^{1}H NMR (700 MHz, acetone-d^6) δ 8.64 (s, 2H, *2-OH*), 7.19 (t, *J* = 8.0 Hz, 2H, *4-H*), 7.06 (dd, *J* = 2.5, 1.8 Hz, 2H, *1-H*), 6.99 (ddd, *J* = 7.8, 1.8, 0.9 Hz, 2H, *5-H*), 6.76 (ddd, *J* = 8.1, 2.4, 0.9 Hz, 2H, *3-H*). ^{13}C NMR (176 MHz, acetone-d^6) δ 158.4 (*2-C*), 138.0 (*6-C*), 130.5 (*4-C*), 118.2 (*5-C*), 114.8 (*3-C*), 113.6 (*1-C*). LRMS (ESI) *m*/*z*: 498.974 ([$(M-H)_2$]$^-$, 100%), 249.011 ([M-H]$^-$, 96). HRMS (ESI) *m*/*z*: calculated [M+H]$^+$ 251.0200, found 251.0192. IR (neat) ν_{max} (cm^{-1}); 3308 (br,s), 1685 (s), 1579 (l), 1472 (l), 1436 (l), 1300 (m), 1210 (l), 1086 (s), 995 (s), 878 (l), 768 (l), 678 (l), 532 (s), 439 (s).

Crystals suitable for X-ray diffraction was obtained from slow evaporation from EtOAc: EtOH. X-ray diffraction images of the single crystal (obtained as detailed in Section 6.1) allowed elucidation of the unit cell, the structure shown in Figure 6.2 shows one molecule of the unit cell.

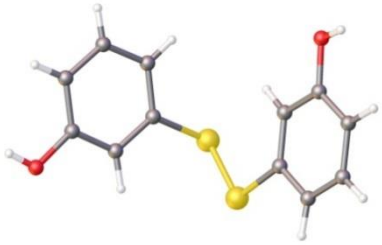

Figure 6.2. One structure from the unit cell of **41**, determined by X-ray diffraction of a single crystal.

6.3.3. Synthesis of 3-((2-hydroxyethyl)sulfinyl)phenol, 42

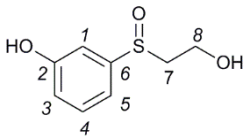

Compound **40** (0.11 g, 0.65 mmol, 1 eq.) in acetic acid (2.5 mL) was added dropwise to a stirred solution of H_2O_2 (0.09 mL, 2.94 mmol, 4.5 eq.) at 0 °C. The reaction was heated to 100 °C and left to stir for 1 hour. The mixture was allowed to cool to room temperature prior to slow addition of the mixture to a solution of saturated $NaHCO_3$ (5 mL) at 0 °C. The solution was extracted with EtOAc (3 × 20 mL), the combined organic layers were dried ($MgSO_4$), filtered and concentrated *in vacuo* to afford a brown oil (0.12 g). The crude oil was purified by flash column chromatography (20 mm, eluent; EtOAc: hexane 4:1 to EtOAc to EtOAc: MeOH 19:1) to yield a colourless oil (0.08 g, 63%) identified as product (R_f 0.0 EtOAc). ^{1}H NMR (400 MHz, acetone-d^6) δ 9.26 (s, 1H, *2-OH*), 7.41 (t, *J* = 7.9 Hz, 1H, *4-H*), 7.29 (dd, *J* = 2.4, 1.6 Hz, 1H, *1-H*), 7.13 (ddd, *J* = 7.7, 1.7, 0.9 Hz, 1H), 7.01 (ddd, *J* = 8.1, 2.5, 0.9 Hz, 1H), 4.49 (s, 1H, *8-OH*), 4.11-3.98 (m, 1H), 3.93-3.81 (m, 1H), 3.17-3.03 (m, 1H), 3.00-2.93 (m, 1H). ^{13}C NMR (101 MHz, acetone-d^6) δ 159.0 (*2-C*), 146.0 (*6-C*), 130.9, 118.6, 115.2, 110.8, 60.7 (*7-C*), 55.8 (*8-C*). LRMS (ESI) *m*/*z*: 371.0399 ($[M_2\text{-H}]^-$, 3), 184.969 ($[M\text{-H}]^-$, 100%). HRMS (ESI) *m*/*z*: calculated $[M\text{-H}]^-$ 185.0272, found 185.0263.

6.3.4. Synthesis of 3-((2-hydroxyethyl)sulfonyl)phenol, 43

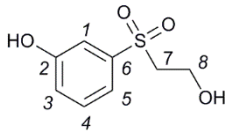

Oxone (Alfa Aesar; 6.92 g, 11.24 mmol, 2 eq.) was added portion wise over 10 minutes to a stirred solution of compound **40** (0.96 g, 5.62 mmol, 1 eq.) in MeOH (5 mL). The solution was then allowed to stir for 3 hours at room temperature. The solution was filtered and 40% sodium hydrogen sulphite (1 mL) was added and the solution adjusted to pH 7 with 1M NaOH. The solution was filtered and concentrated *in vacuo*. The white solid was dissolved in acetone and filtered again to produce a yellow oil (R_f 0.0, EtOAc) identified as the product (1.01 g, 89%). ^{1}H NMR (400 MHz, acetone-d^6) δ 7.46 (t, *J* = 8.1 Hz, 1H, *4-H*), 7.40-7.36 (m, 2H, *1-H*), 7.17 (ddd, *J* = 8.1, 2.4, 1.2 Hz, 1H), 3.86 (t, *J* = 6.4 Hz, 2H, *7-H*), 3.57 (s, 1H, *2-OH*), 3.39 (t, *J* = 6.4 Hz, 2H, *8-H*). 2.09 (s, 1H, *8-OH*). ^{13}C NMR (101 MHz, acetone-d^6) δ 158.9 (*2-C*), 142.1 (*6-C*), 131.2, 121.6, 119.4, 115.3, 113.8, 58.8 (*7-C*), 56.6 (*8-C*). LRMS (ESI) *m*/*z*: 403.059 (11%), 200.968 ([M-H]$^-$, 75), 110.921 (100). HRMS (ESI) *m*/*z*: calculated [M-H]$^-$ 201.0222, found 201.0218. IR (neat) ν_{max} (cm^{-1}); 3376, 2936, 2700, 1590, 1478, 1448, 1390, 1286 & 1129, 1056.

6.3.5. Synthesis of 3-((2-hydroxyethyl)sulfonyl)phenol functionalised resin, 44

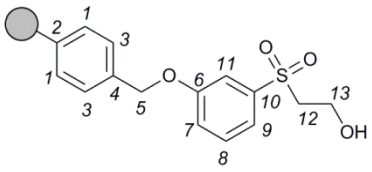

Merrifield resin (1.75 g, 2.10 mmol, 1 eq.), sulfone **43** (2.12 g, 10.50 mmol, 5 eq.), Cs_2CO_3 (3.42 g, 10.50 mmol, 5 eq.) and terabutylammonium iodide (023 g, 0.63 mmol, 0.3 eq.) were shaken at 480 rpm in anhydrous DMF (25 mL) under an argon atmosphere for 71 hours. The resin was then washed with H_2O (3 × 50 mL), MeOH (3 × 50 mL) and DCM (3 × 30 mL). The resin was dried over P_2O_5 overnight to afford a pale yellow solid (2.17 g, 99.7% conversion).^{1}H ssNMR (400 mHz, DCM-d^2) δ 7.75 (s, *8-H*, *9-H* & *11-H*), 7.40-6.27

(m, 30H, resin, *3-H*, *4-H* & *8-H*), 5.09 (s, 2H, *5-H*), 3.98 (s, 2H, *12-H*), 3.39 (s, 2H, *13-H*), 2.93-0.88 (m, 20H, resin).

6.3.6. Synthesis of 3-(vinylsulfonyl)phenol functionalised resin, 46

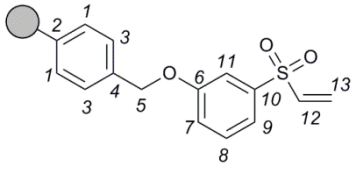

Resin **44** (0.07 g, 0.07 mmol, 1 eq.) was swollen in anhydrous DCM (1 mL) under an argon atmosphere. PCl_3 (0.04 mL, 0.42 mmol, 6 eq.) followed by anhydrous DIPEA (0.07 mL, 0.42 mmol, 6 eq.) was added to the mixture. The mixture was shaken for 2 hours, washed sequentially by MeOH (3 × 5 mL), H_2O (3 × 10 mL), MeOH (3 × 5 mL) then DCM (3 × 10 mL). The white resin was dried *in vacuo*. ^{1}H NMR (400 MHz, DCM-d^2) δ 7.42 (s, 3H, *8-H*, *9-H* & *11-H*), 7.23-6.10 (m, 47H, *3-H*, *4-H*, *8-H*, *12-H*, *13E-H* & *resin*), 5.91 (s, 1H, *13Z-H*), 4.95 (s, 2H, *5-H*), 2.26-0.75 (m, 24H, resin).

6.3.7. Synthesis of 2-((3-(benzylxy)phenyl)thio)ethan-1-ol, 48

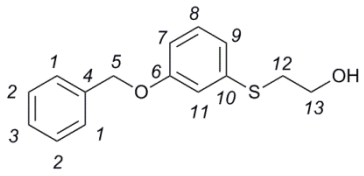

Compound **40** (1.29 g, 7.58 mmol, 1 eq.) and Cs_2CO_3 (2.97 g, 9.10 mmol, 1.2 eq.) were dissolved in anhydrous DMF (10 mL) under an argon atmosphere. Benzyl bromide (1.00 mL, 8.41 mmol, 1.1 eq.) was added and the solution was left to stir for 16 hours at room temperature. H_2O (20 mL) and Et_2O (200 mL) were added to the solution, the layers were separated, followed by washing the organic layer with H_2O (3 × 20 mL). The organic layer was dried ($MgSO_4$), filtered and concentrated *in vacuo* to afford a crude oil (1.94 g). The oil was purified by flash column chromatography (50 mm, eluent; hexane to hexane: EtOAc 2:1 to 1:1) to afford a clear oil (1.45 g, 73%) identified as product (R_f 0.43, EtOAc: hexane 2:1). mp: 43-45 °C. ^{1}H NMR (700 MHz) δ 7.43 (dtt, *J* = 7.8, 1.6, 0.8 Hz, 2H, *1-H*), 7.39 (ddd, *J* = 7.7, 6.7, 1.1 Hz, *2-H*), 7.35-7.32 (m, 1H, *3-H*), 7.21 (t, *J* = 8.0 Hz, 1H, *11-H*),

7.00 (dd, *J* = 2.6, 1.6 Hz, 1H, *9-H*), 6.97 (ddd, *J* = 7.8, 1.7, 0.9 Hz, 1H, *7-H*), 6.83 (ddd, *J* = 8.3, 2.5, 0.9 Hz, 1H, *8-H*), 5.06 (s, 2H, *5-H*), 3.73 (t, *J* = 6.0 Hz, 2H, *13-H*), 3.10 (t, *J* = 6.0 Hz, 2H, *12-H*). ^{13}C NMR (176 MHz) δ 159.3 (*6-C*), 136.8 (*4-C*), 136.3 (*10-C*), 130.1 (*11-C*), 128.8 (*2-C)*, 128.2 (*3-C*), 127.6 (*1-C*), 122.5 (*7-C*), 116.5 (*9-C*), 113.3 (*8-C*), 70.3 (*5-C*), 60.5 (*12-H*), 37.2 (*13-H*). LRMS (ESI) *m*/*z*: 261.195 ([M+H]$^+$, 100%), 243.672 ([M-H_2O]$^+$, 62). HRMS (ESI) *m*/*z*: calculated [M+H]$^+$ 261.0949, found 261.0973. IR (neat) ν_{max} (cm^{-1}); 3370 (s), 2490 (s), 2925 (s), 2875 (s), 1586 (m), 1481 (m), 1463 (m).

6.3.8. Synthesis of 2-((3-(benzyloxy)phenyl)sulfonyl)ethan-1-ol, 49

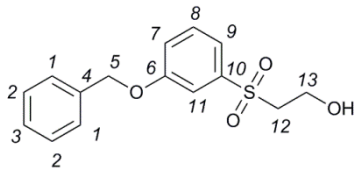

Oxone (Sigma-Aldrich; 2.95 g, 9.60 mmol, 5 eq.) was added portion wise to a stirred solution of compound **48** (0.51 g, 1.95 mmol, 1 eq.) in MeOH (10 mL), the suspension was stirred for 4.5 hours then filtered. A solution of 40% sodium bisulfite (1 mL) was added to the filtrate, followed by neutralisation to pH 7 using 5% NaOH solution. The solution was filtered a second time, the filtrate was recovered and concentrated *in vacuo*. The residue was dissolved in DCM and filtered a final time, concentration of the filtrate *in vacuo* returned a waxy solid (0.51 g, 89%). The material was used without subsequent purification. mp: 67-68 °C ^{1}H NMR (700 MHz) δ 7.51-7.45 (m, 3H), 7.43-7.37 (m, 4H), 7.35-7.32 (m, 1H, *3-H*), 7.26-7.22 (m, 1H), 5.11 (s, 2H, *5-H*), 3.94 (t, *J* = 5.5 Hz, 2H, *12-H*), 3.33-3.30 (m, 2H, *13-H*), 2.81 (s, 1H, *13-OH*).^{13}C NMR (176 MHz) δ 159.3 (6-C), 140.2 (*10-C*), 135.9 (*4-C*), 130.7, 128.8, 128.5 (*3-C*), 127.7, 121.3, 120.4, 113.7, 70.6 (*5-C*), 58.3 (*13-C*), 56.4 (*12-C*). LRMS (ESI) *m*/*z*: 609.127 ([M_2+Na]$^+$, 100%), 315.580 ([M+Na]$^+$, 83), 293.038 ([M+H]$^+$, 8). HRMS (ESI) *m*/*z*: calculated [M+Na]$^+$ 315.0670, found 315.0667. IR (neat) ν_{max} (cm^{-1}); 3500 (s), 2873 (s), 1593 (m), 1580 (m), 1456 (s), 1284 (l), 1235 (l), 1129 (l), 1025 (l), 879 (m), 842 (s), 786 (s), 727 (l), 681 (l), 612 (m).

6.3.9. Synthesis of 1-(benzyloxy)-3-(vinylsulfonyl)benzene, 50

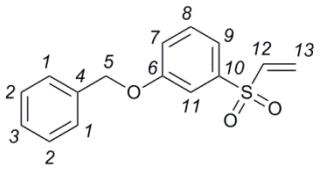

Compound **49** (0.06 g, 0.20 mmol, 1 eq.), $POCl_3$ (0.09 mL, 0.09 mL, 0.94 mmol, 5 eq.) and DIPEA (0.16 mL, 0.94 mmol, 5 eq.) were stirred in anhydrous DCM (5 mL) for 1 hour under an argon atmosphere. The solution was further diluted using DCM (20 mL), the organic layer was washed with saturated $NaHCO_3$ solution (2 × 10 mL), 5% HCl solution (2 × 10 mL) and H_2O (10 mL). The organic layer was dried ($MgSO_4$), filtered and concentrated *in vacuo*, producing a yellow solid. The solid was passed through a silica plug (120 × 15 mm) using EtOAc (50 mL), concentration of the obtained solution yielded a colourless oil (0.05 g, 91%) identified as product (R_f 0.58, hexane: EtOAc 2:1) ^{1}H NMR (700 MHz) δ 7.50-7.38 (m, 7H, *1-H*, *8-H*, *9-H* & *11-H*), 7.36-7.33 (m, 1H, *3-H*), 7.23-7.20 (m, 1H, *7-H*), 6.64 (dd, *J* = 16.5, 9.8 Hz, 1H, *12-H*), 6.44 (d, *J* = 16.5 Hz, 1H, *13E-H*), 6.03 (d, *J* = 9.9 Hz, 1H, *13Z-H*), 5.11 (s, 2H, *5-H*). ^{13}C NMR (176 MHz) δ 159.3 (*6-C*), 140.9 (*10-C*), 138.5 (*12-C*), 136.0 (*4-C*), 130.6, 128.8, 128.5 (*3-C*), 127.9, 127.7 (*13-C*), 120.9 (*7-C*), 120.4, 113.6, 70.6 (*5-C*). LRMS (ESI) *m*/*z*: 571.618 ($[M_2+Na]^+$, 86%), 298.069 ($[M+Na]^+$, 100). HRMS (ESI) *m*/*z*: calculated $[M+Na]^+$ 297.0561, found 297.0566. IR (neat) ν_{max} (cm^{-1}); 3064 (s), 1595 (m), 1480 (m), 1427 (s), 1383 (s), 1308 (l), 1239 (m), 1141 (l), 1095 (s), 1015 (m), 974 (s), 909 (m), 729 (l), 693 (l), 646 (m).

6.3.10. Synthesis of 3-((2-hydroxyethyl)thio)phenol functionalised resin, 51

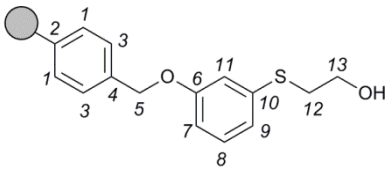

Merrifield resin (1.56 g, 1.88 mmol, 1 eq.), thioether **40** (1.60 g, 9.40 mmol, 5 eq.) and Cs_2CO_3 (3.06 g, 9.40 mmol, 5 eq.) were shaken at 480 rpm in anhydrous DMF (22 mL) under an argon atmosphere for 71 hours. The resin was then washed with H_2O (3 × 50 mL),

MeOH (3 × 50 mL) and DCM (3 × 80 mL). The resin was dried over P_2O_5 overnight to afford a white solid (1.79 g, 95% conversion). ^{1}H ssNMR (400 MHz) δ 7.62-6.17 (m, 21H, resin, *7-10-H* & *11-H*), 5.01 (s, 2H, *5-H*), 3.77 (s, 2H, *13-H*), 3.14 (s, 2H, *12-H*), 2.50-1.09 (m, 15H, resin).

6.3.11. Characterisation of (3-(benzyloxy)phenyl)(2-chloroethyl)sulfane, 59

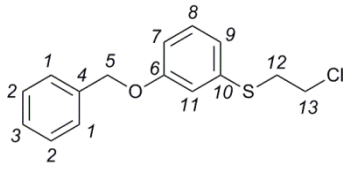

^{1}H NMR (700 MHz) δ 7.45-7.42 (m, 2H, *1-H*), 7.41-7.38 (m, 2H, *2-H*), 7.36-7.32 (m, 1H, *3-H*), 7.23 (t, *J* = 8.0 Hz, 1H, *11-H*), 7.00 (dd, *J* = 2.5, 1.7 Hz, 1H, *9-H*), 6.97 (ddd, *J* = 7.7, 1.8, 0.9 Hz, 1H, *7-H*), 6.86 (ddd, *J* = 8.3, 2.5, 0.9 Hz, 1H, *8-H*), 5.06 (s, 2H, *5-H*), 3.61-3.57 (m, 2H, *13-H*), 3.23-3.18 (m, 2H, *12-H*). ^{13}C NMR (176 MHz) δ 159.1 (*6-C*), 136.6 (*4-C*), 135.5 (*10-C*), 130.0 (*11-C*), 128.6 (*2-C)*, 128.1 (*3-C*), 127.5 (*1-C*), 122.6 (*7-C*), 116.6 (*9-C*), 113.5 (*8-C*), 70.1 (*5-C*), 42.3 (*13-C*), 35.9 (*12-C*). LRMS (ASAP) *m*/*z*: 279.056 ($[M+H]^+$, 100%), 278.055 (M^+, 15). HRMS (ASAP) *m*/*z*: calculated $[M+H]^+$ 279.0610, found 279.0598.

6.3.12. Synthesis of didecyl (2-((3-hydroxyphenyl)sulfonyl)ethyl) phosphate functionalised resin, 63

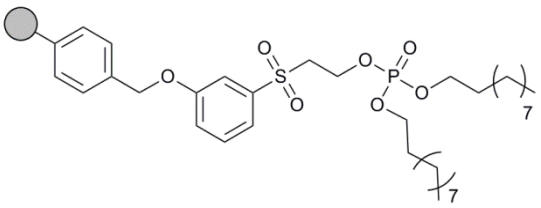

Resin **51** (0.07 g, 0.07 mmol, 1 eq.) was swollen in anhydrous DCM (1 mL) under an argon atmosphere. PCl_3 (0.04 mL, 0.42 mmol, 6 eq.) was added to the slurry, followed by the addition of DIPEA (0.070 mL, 0.42 mmol, 6 eq.), the slurry was shaken for 1 hour at 480 rpm. Maintaining an inert atmosphere, the resin was washed with anhydrous DCM (3 × 2 mL). Anhydrous DCM (2 mL) was added to the resin, followed by the addition of decan-1-

ol (0.08 mL, 0.42 mmol, 6 eq.) then DIPEA (0.07 mL, 0.42 mmol, 6 eq.) to the slurry. The mixture was shaken for 6 hours at 480 rpm under an argon atmosphere. The resin was washed with MeOH (3 × 5 mL), H_2O (3 × 10 mL), MeOH (3 × 5 mL) and DCM (3 × 10 mL). DCM (3 mL) was added to the resin followed by mCPBA (0.07 mg, 0.42 mmol, 6 eq.), the mixture was shaken for 16 hours at 480 rpm. The resin was washed with MeOH (3 × 5 mL), H_2O (3 × 10 mL), MeOH (3 × 5 mL) and DCM (3 × 10 mL). The resin was dried *in vacuo* overnight over P_2O_5 to produce a white solid (0.09 g). ^{1}H ssNMR (400 MHz, DCM-d^2) δ 7.61-6.09 (m, 97H, resin, *8-H*, *9-H* & *11-H*), 4.95 (s, 2H, *5-H*), 4.30 (s, 2H, *13-H*), 3.90 (s, 4H, *14-H*), 3.46 (s, 3H, *12-H*), 2.01-1.02 (m, 96H, resin & *15-22-H*), 0.83 (s, 7H, *23-H*).

6.3.13. Synthesis of didecyl phosphate, 64

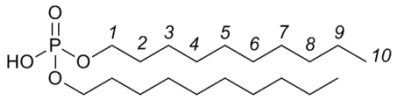

Resin **63** (0.07 g, 0.05 mmol, 1 eq.) was swollen in $CHCl_3$ (2 mL), DIEPA (0.07 mL, 0.42 mmol, 8 eq.) was added and microwaved at 140 °C for 2 hours. The slurry was allowed to cool prior to washing of the resin by $CHCl_3$ (3 × 10 mL) and EtOH (3 × 10 mL). The washing were concentrated *in vacuo* and dissolved in $CHCl_3$ and transferred to a separating funnel. The resin was washed with H_2O (3 × 10 mL), with the washings transferred into the separating funnel containing the organic phase. 5% HCl solution (5 mL) was added to the biphasic mixture, the layers were separated and the organic phase was further washed by 5% HCl solution (2 × 10 mL). The organic phase was collected, dried ($MgSO_4$), filtered and concentrated *in vacuo* to return a white solid (0.005 g, 26%). ^{1}H NMR (400 MHz) δ 4.01 (q, *J* = 6.7 Hz, 4H, *1-H*), 1.67 (t, *J* = 7.3 Hz, 4H, *4-H*), 1.42-1.17 (m, 40H, *3-9-H*), 0.91-0.84 (m, 8H, *10-H*). ^{31}P NMR (162 MHz) δ 1.48. LRMS (ESI) *m*/*z*: 378.206 (M^-, 28%), 377.231 ($[M-H]^-$, 100), 156.906 (10), 154.917 (32). HRMS (ESI) *m*/*z*: calculated $[M-H]^-$ 377.2821, found 377.2819.

6.3.14. Synthesis of (1R,3s,5r,6R,7S,8s,9S)-2,4,10-trioxaadamantane-6,8,9-triol, 65

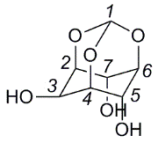

Myo-inositol (5.00 g, 27.75 mmol, 1 eq.), triethyl orthoformate (6.00 mL, 36.10 mmol, 1.3 eq.) and TsOH.H_2O (3.40 g, 17.87 mmol, 0.6 eq.) were stirred in anhydrous DMF (50 mL) for 46 hours under an argon atmosphere at 110 °C. Saturated sodium bicarbonate solution (7 mL) was added to the reaction mixture, which was stirred for an additional 30 minutes. The solution was concentrated *in vacuo* to produce a slurry which underwent a hot filtration using MeOH to remove unreacted *myo*-inositol. The filtrate was concentrated *in vacuo* and recrystallised with MeOH to produce off white crystals (3.26 g, 62%) identified as product. ^{1}H NMR (400 MHz, D_2O) δ 5.51 (d, *J* = 1.3 Hz, 1H, *1-H*), 4.49 (t, *J* = 3.9 Hz, 2H, *2-H*), 4.24 (tt, *J* = 3.5, 1.6 Hz, 1H, *5-H*), 4.17 (q, *J* = 1.9 Hz, 1H, *3-H*), 4.14 (dt, *J* = 4.6, 1.8 Hz, 2H, *5-H*). ^{13}C NMR (D_2O) δ 102.1 (*1-C*), 73.8, 69.3, 66.7, 59.6. LRMS (ESI) *m*/*z*: 304.956 (8%), 213.719 (8), 205.972 (22), 191.198 ($[M+H]^+$, 43), 190.856 (M^+, 100). HRMS (ESI) *m*/*z*: calculated $[M+H]^+$ 190.0556, found 190.0562. IR (neat) ν_{max} (cm^{-1}); 3282 (m), 2920 (s), 1402 (s), 1258 (s), 1158 (m), 1044 (m), 988 (m), 958 (l), 884 (m), 804 (m), 768 (s), 732 (s), 681.

6.3.15. Synthesis of (1R,3s,5r,6R,7S,8s,9S)-6,8,9-tris(benzyloxy)-2,4,10-trioxaadamantane, 66

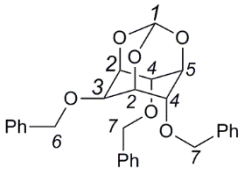

To a solution of product **65** (0.25 g, 1.32 mmol, 1 eq.) in anhydrous DMF (5 mL), NaH (0.21 g, 5.26 mmol, 4 eq.) was added batchwise under an argon atmosphere, the solution was stirred for 30 minutes prior to the addition of benzyl bromide (0.70 mL, 5.92 mmol, 4.5 eq.) in anhydrous DMF (1 mL). The mixture was stirred for 16 hours; excess hydride was quenched with H_2O. The solution was partially concentrated *in vacuo*, followed

by solvation in DCM (50 mL) and H_2O (10 mL), the layers were separated. The aqueous layers were extracted with DCM (4 × 20 mL), the combined organic layers were dried ($MgSO_4$), filtered and concentrated *in vacuo* to afford a solid. The solid was purified by flash column chromatography (30 mm, eluent; hexane: EtOAc 5:1 to 4:1 to 1:1) to afford a white solid (0.49, 80%) identified as product (R_f 016, hexane: EtOAc 4:1). mp: 94-96 °C. ^{1}H NMR (700 MHz) δ 7.39-7.37 (m, 2H, *Ph*), 7.34-7.27 (m, 9H, *Ph*), 7.22-7.19 (m, 4H, *Ph*), 5.53 (d, *J* = 1.4 Hz, 1H, *1-H*), 4.64 (s, 2H, *6-H*), 4.61 (d, *J* = 11.5 Hz, 1H, *7-H*), 4.48 (d, *J* = 11.5 Hz, 1H, *7-H*), 4.45-4.43 (m, 1H, *3-H*), 4.35-4.32 (m, 2H, *2-H*), 4.29 (dt, *J* = 4.4, 1.8 Hz, 2H, *4-H*), 4.05 (q, *J* = 1.7 Hz, 1H, *5-H*). ^{13}C NMR (176 MHz) δ 138, 137.7, 128.6 , 128.3, 128.0, 127.8, 103.4 (*1-C*), 74.2 (*2-C*), 71.8 (*6-C* & *7-C*), 70.7 (*5-C*), 68.3 (*3-C*), 67.4 (*5-C*). LRMS (ESI) *m*/*z*: 943.900 (100%), 942.760 (84), 483.087 ($[M+Na]^+$, 39), 461.138 ($[M+H]^+$, 31). HRMS (ESI) *m*/*z*: calculated $[M+H]^+$ 461.1964, found 461.1967. IR (neat) ν_{max} (cm^{-1}); 2969 (s), 2895 (s), 1494 (s), 1453 (s), 1382 (m), 1165 (l), 1097 (l), 948 (l), 931 (l), 763 (m), 732 (l), 697 (l), 612 (s), 528 (m), 474 (m).

Crystals suitable for X-ray diffraction were obtained by slow evaporation from EtOAc: EtOH. X-ray diffraction images of the single crystal (obtained as detailed in Section 6.1) allowed elucidation of the unit cell, the structure shown in Figure 6.3 shows one molecule of the unit cell.

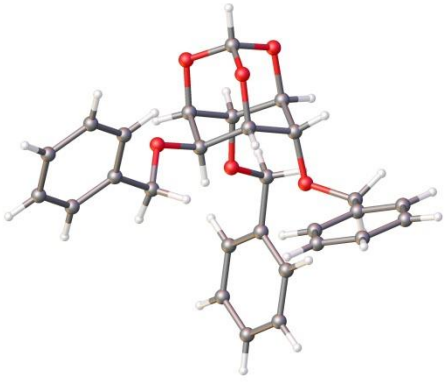

Figure 6.3. One structure from the unit cell of **66**, determined by X-ray diffraction of a single crystal.

6.3.16. Synthesis of (1R,5S,6R,7s,8S,9s)-6,8,9-tris(benzyloxy)-2,4-dioxabicyclo[3.3.1]nonan-7-ol, 67

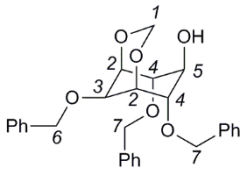

A solution of DIBAL in DCM (1 M; 11.00 mL, 11.00 mmol, 2.4 eq.) was added dropwise to a stirred solution of compound **66** (2.10 g, 4.57 mmol, 1 eq.) in anhydrous DCM (20 mL) under an argon atmosphere at 0 °C. The solution was allowed to warm and stir for an additional 3 hours. The solution was carefully poured onto a vigorously stirred solution of sodium potassium tartrate (1.5 M; 21.00 mL, 31.98 mmol, 7 eq.) and saturated ammonium chloride (20 mL) and EtOAc (220 mL). The layers were separated and the aqueous layer extracted with EtOAc (20 mL). The organic layer was dried ($MgSO_4$), filtered and concentrated *in vacuo* to yield a crude colourless oil (2.23 g). The oil was purified by flash column chromatography (50 mm, eluent; hexane: EtOAc 4:1 to 3:1 to 1:1) to give a colourless oil (2.08 g, 98%), identified as product (R_f 0.18, hexane: EtOAc 3:1). ^{1}H NMR (700 MHz) δ 7.42-7.16 (m, 15H, *Ph*), 5.57 (d, *J* = 4.9 Hz, 1H), 4.69-4.66 (m, 3H, *1-H* & *7-H*), 4.61 (s, 2H, *6-H*), 4.57 (d, *J* = 11.9 Hz, 2H, *7-H*), 4.45-4.44 (m, 2H, *2-H*), 4.31 (t, *J* = 1.5 Hz, 1H, *3-H*), 4.02 (dd, *J* = 3.5, 2.4 Hz, 2H, *4-H*), 3.98 (d, *J* = 9.9 Hz, 1H, *5-H*), 2.98 (d, *J* = 10.4 Hz, 1H, *5-OH*).^{13}C NMR (176 MHz) δ 138.1, 137.8, 128.6, 128.5, 128.0, 127.9, 127.7, 85.8 (*1-C*), 81.3 (*4-C*), 72.8 (*2-C*), 72.2 (*7-C*), 70.9 (*6-C*), 70.3 (*3-C*), 69.6 (*5-C*). LRMS (ESI) *m*/*z*: 947.204 (31%), 486.0 (33), 485.745 ($[M+Na]^+$, 100), 484.682 (59), 271.202 (16). HRMS (ESI) *m*/*z*: calculated $[M+Na]^+$ 485.1940, found 485.1931. IR (neat) ν_{max} (cm^{-1}); 3559 (s), 2919 (s), 1497 (s), 1454 (m), 1178 (m), 1138 (m), 1070 (l), 1027 (l), 883 (s), 844 (s), 734 (l), 695 (l), 608 (s), 585 (s).

6.3.17. Synthesis of (1R,5S,6R,7s,8S,9s)-6,7,8,9-tetrakis(benzyloxy)-2,4-dioxabicyclo[3.3.1]nonane, 68

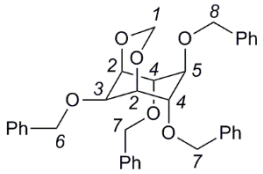

NaH (0.08 g, 1.90 mmol, 1.5 eq.) was added to a stirred solution of product **67** (0.58 g, 1.26 mmol, 1 eq.) in anhydrous DMF (10 mL) under an argon atmosphere. The suspension was stirred for 30 minutes, followed by the addition of benzyl bromide (0.23 mL, 1.90 mmol, 1.5 eq.) in anhydrous DMF (1.5 mL), the suspension was stirred for a further 16 hours. H_2O (20 mL) and Et_2O (150 mL) were added, the layers were separated and the organic layer washed with brine (5 × 10 mL). The organic layer was dried ($MgSO_4$), filtered and concentrated *in vacuo* to afford an oil. The crude oil was purified by flash column chromatography (40 mm, eluent; hexane: EtOAc 5:1 to 3:1) to afford a colourless oil (0.53 g, 77%). ^{1}H NMR (400 MHz) δ 7.40-7.27 (m, 20H, *Ph*), 5.21 (d, *J* = 5.5 Hz, 1H, *1-H*), 4.86 (d, *J* = 5.5 Hz, 1H, *1-H*), 4.66 (s, 4H, *6-H* & *8-H*), 4.62 (d, *J* = 11.8 Hz, 2H, *7-H*), 4.55 (d, *J* = 11.8 Hz, *7-H*), 4.30-4.26 (m, 2H), 3.97 (dd, *J* = 5.6, 1.1 Hz, 2H), 3.86 (t, *J* = 1.9 Hz, 1H), 3.64 (t, *J* = 5.6 Hz, 1H).^{13}C NMR (101 MHz) δ 138.3, 137.7, 137.7, 128.5 128.4, 127.9, 127.8, 85.5, 82.1, 80.1, 73.5, 72.0, 71.7, 71.0, 70.3. LRMS (ESI) *m*/*z*: 1127.045 ($[M_2+Na]^+$, 57%), 575.024 ($[M+Na]^+$, 100). HRMS (ESI) *m*/*z*: calculated $[M+H]^+$ 553.2590, found 553.2611. IR (neat) ν_{max} (cm^{-1}); 2904 (s), 1497 (s), 1454 (m), 1367 (s), 1178 (m), 1069 (l), 889 (s), 733 (l), 695 (l), 606 (s), 463 (s).

6.3.18. Synthesis of (1R,2r,3S,4R,5r,6S)-2,4,5,6-tetrakis(benzyloxy)cyclohexane-1,3-diol, 69

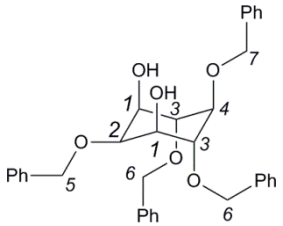

Compound **68** (0.50 g, 0.90 mmol, 1 eq.) and concentrated HCl solution (2 mL) were refluxed in MeOH (20 mL) for 5 hours. The mixture was concentrated *in vacuo* and DCM (50 mL) was added, the solution was washed with saturated $NaHCO_3$ solution (2 × 10 mL), H_2O (2 × 10 mL) and brine (10 mL). The crude oil (0.43 g) was purified by flash column chromatography (25 mm, eluent; hexane EtOAc 5:1 to 2:1 to 1:1) to yield a clear oil (0.35 g, 73%) identified as product (R_f 0.13, hexane: EtOAc 2:1). ^{1}H NMR (700 MHz) δ 7.39-7.28 (m, 20H, *Ph*), 4.92 (d, *J* = 11.1 Hz, 2H, *6-H*), 4.89 (s, 2H, *7-H*), 4.81 (d, *J* = 2.4 Hz, 2H, *5-H*), 4.79 (dd, *J* = 11.2, 2.6 Hz, 2H, *6-H*), 4.01 (t, *J* = 2.8 Hz, 1H, *2-H*), 3.81 (td, *J* = 9.5, 2.6 Hz, 2H, *3-H*), 3.58 (dd, *J* = 9.7, 2.7 Hz, 2H, *1-H*), 3.50 (td, *J* = 9.3, 1.9 Hz, 1H, *4-H*), 2.29 (s, 2H, *1-OH*). ^{13}C NMR (176 MHz) δ 138.7, 138.6, 128.7, 128.6, 128.2, 128.0, 127.9, 127.8, 83.7 (*4-C*), 82.5 (*3-C*), 79.1 (*2-C*), 75.7 (*6-C* & *7-C*), 75.4 (*5-C*), 72.8 (*1-C*). LRMS (ASAP) *m*/*z*: 539.247 (M^+, 100%), 449.200 ($[M\text{-}Bn]^+$, 94), 359.154 ($[M\text{-}(Bn)_2]^+$, 82). HRMS (ASAP) *m*/*z*: calculated $[M+H]^+$ 541.2590, found 541.2572. IR (neat) ν_{max} (cm^{-1}); 3531 (s), 3400 (s), 3032 (s), 2905 (s), 1497 (s), 1454 (m), 1355 (m), 1207 (s), 1122 (m), 1075 (l), 1023 (l), 927 (s), 741 (m), 693 (l), 634 (s), 577 (s).

6.3.19. Synthesis of (1R,2R,3R,4R,5S,6R)-2,3,4,5,6-pentakis(benzyloxy)cyclohexan-1-ol, 70

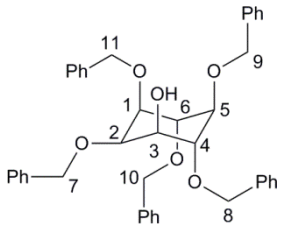

Compound **69** (0.32 g, 0.60 mmol, 2.4 eq.) & NaH (0.01 g, 0.29 mmol, 1.1 eq.) were stirred in anhydrous DMF (10 mL) for 10 minutes at 0 °C under an argon atmosphere. Still at 0 °C, a solution of benzyl bromide in anhydrous DMF (84 mM; 3.00 mL, 0.252 mmol, 1 eq.) was added by syringe pump at a flow rate of 1 mL/ hr, the mixture was allowed to warm to room temperature and stirred for a further 16 hours. The mixture was diluted with Et_2O (100 mL) and washed with brine (5 × 10 mL), the organic layer was collected, dried ($MgSO_4$), filtered and concentrated *in vacuo* to yield a crude oil (0.37 g). The crude material

was purified by flash column chromatography (30 mm, eluent; hexane: EtOAc 10:1 to 5:1 to 4:1 to 3:1 to 1:2). A white solid (0.02 g, 11%) identified as hexabenzylated inositol (**71**) was first isolated (R_f 0.51, hexane: EtOAc 3:1), followed by a waxy white solid (0.12 g, 78%) the desired pentabenzylated inositol (**70**) (R_f 0.28, hexane: EtOAc 3:1). mp: 94-95 °C. Unreacted starting material (**69**) (0.17 g) was also recovered (R_f 0.08, hexane: EtOAc 3:1). ^{1}H NMR (700 MHz) δ 7.36-7.26 (m, 25H, *Ph*), 5.00-4.66 (m, 10H, CH_2Ph), 4.06 (t, *J* = 9.5 Hz, 1H), 4.03 (t, *J* = 2.6 Hz, 1H), 3.81 (t, *J* = 9.5 Hz, 1H), 3.50-3.44 (m, 3H, *3-H*), 2.21 (d, *J* = 6.4 Hz, 1H, *3-OH*).^{13}C NMR (176 MHz) δ 138.9, 138.8, 138.7, 138.4, 128.6, 128.6, 128.5, 128.2, 128.0, 127.9, 127.8, 127.8, 127.7, 83.7, 82.3, 82.0, 81.3, 77.3, 76.0, 75.9, 75.7, 74.9, 73.1, 72.5. LRMS (ASAP) *m/z*: 631.308 ($[M+H]^+$, 100%), 539.242 ($[M-Bn]^+$, 29), 449.196 ($[M-(Bn)_2]^+$, 27). HRMS (ASAP) *m/z*: calculated $[M+H]^+$ 631.3060, found 631.3067. IR (neat) ν_{max} (cm^{-1}); 3582 (s), 3031 (s), 2897 (s), 1496 (m), 1454 (m), 1360 (m), 1208 (s), 1134 (m), 1068 (l), 1024 (l), 935 (s), 738 (m), 695 (l), 641 (s), 592 (s).

Single crystals suitable for X-ray diffraction were obtained by slow evaporation from EtOH: acetone. X-ray diffraction images of the single crystal (obtained as detailed in Section 6.1) allowed elucidation of the unit cell, the structure shown in Figure 6.4 shows one molecule of the unit cell.

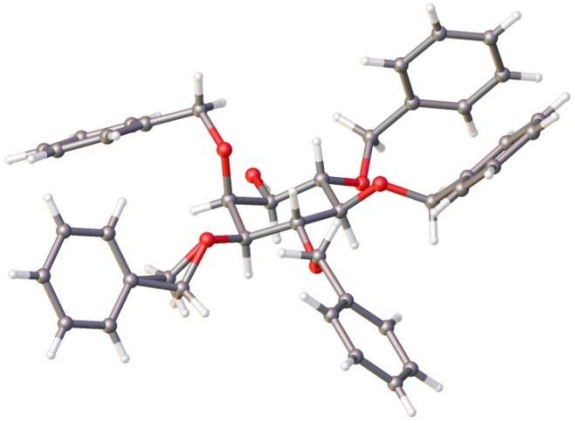

Figure 6.4. One structure from the unit cell of **70**, determined by X-ray diffraction of a single crystal.

6.3.20. Charecterisation of (1R,2r,3S,4R,5s,6S)-1,2,3,4,5,6-hexakis(benzyloxy)cyclohexane, 71

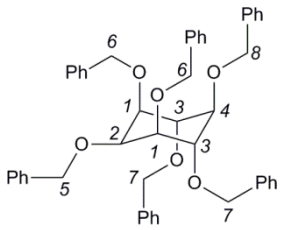

mp: 101-102 °C .^{1}H NMR (700 MHz) δ 7.41 (d, *J* = 7.3 Hz, 2H), 7.34-7.22 (m, 28H), 4.91 (d, *J* = 10.8 Hz, 2H), 4.88 (s, 4H, *5-H* & *8-H*), 4.83 (d, *J* = 10.8 Hz, 2H), 4.65 (d, *J* = 11.8 Hz, 2H), 4.60 (d, *J* = 11.9 Hz, 2H), 4.09 (t, *J* = 9.6 Hz, 2H), 4.03 (d, *J* = 2.9 Hz, 1H), 3.48 (t, *J* = 9.5 Hz, 1H), 3.35 (dd, *J* = 10.0, 2.7 Hz, 2H).^{13}C NMR (176 MHz) δ 139.0, 138.8, 138.4, 128.3, 128.1, 128.0, 127.8, 127.6, 127.5, 127.4, 127.3, 83.7, 81.7, 80.9, 75.9, 75.8, 74.4, 74.1, 72.8. LRMS (ASAP) *m*/*z*: 722.359 (52%), 721.348 ($[M+H]^+$, 100). HRMS (ASAP) *m*/*z*: calculated $[M+H]^+$ 721.3529, found 721.3529. IR (DCM film) ν_{max} (cm^{-1}); 3067 (s), 3030 (s), 2866 (s), 1497 (m), 1454 (m), 1360 (m), 1209 (s), 1131 (m), 1071 (l), 1028 (l), 734 (l), 696 (l).

6.4. Synthesis of labelled sterols

6.4.1. Screening of acids for the synthesis of cholesterol, 81

A solution of the acid (12.5 mM) in anhydrous 1,4-dioxane (1 mL, 12 μmol) was added to a stirred solution of i-cholesteryl methyl ether (0.10 g, 0.25 mmol), and H_2O (22 μL, 1.2 mmol) in 1,4-dioxane (5 mL). The solution was stirred for 5 hours at 20 °C. The solution was concentrated *in vacuo* (~1 mL), DCM (20 mL) was added and the organic solution washed with H_2O (2 × 10 mL). The organic solution was dried ($MgSO_4$), filtered and concentrated *in vacuo*. Purification by flash column chromatography on silica using a gradient of DCM/hexane, 1:1 to DCM.

The procedure when using HBF_4 as acid catalyst followed the same procedure, except that the solution was heated at 80 °C for 40 hours.

6.4.2. Optimised acid catalysed hydration of i-cholesteryl methyl ether to produce cholesterol, 81

An aliquot of 11.3 mM CF_3SO_3H (0.05 eq.) in anhydrous 1,4-dioxane was added to a stirred solution of i-cholesteryl methyl ether (1 eq.), and H_2O (5 eq.) in 1,4-dioxane (1 mL). The solution was stirred for 5 hours at 20 °C. The solution was concentrated *in vacuo*, DCM (20 mL) was added and the organic solution washed with H_2O (2 × 10 mL). The organic solution was dried ($MgSO_4$), filtered and concentrated *in vacuo*. The crude mixture was purified by flash column chromatography (eluent; hexane to hexane: DCM 4:1 to 2:1 to 1:1 to 3:2 to DCM) to obtain the desired product as a white solid (R_f 0.11, DCM). Data matched authentic material.

6.4.3. Synthesis of ^{17}O-cholesterol, 81b

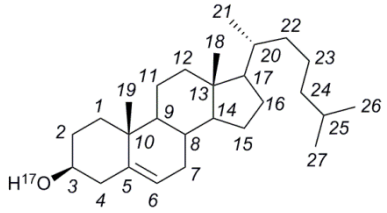

A solution of CF_3SO_3H in anhydrous 1,4-dioxane (111.89 mM; 1.10 mL, 0.12 mmol, 0.05 eq.) was added to a stirred solution of i-cholesteryl methyl ether (0.98 g, 2.32 mmol, 1 eq.) and $^{17}OH_2$ (0.22 mL, 11.57 mmol, 5 eq.) in anhydrous 1,4-dioxane (60 mL). Other conditions were the same as those described in Section 6.4.2. A white solid was obtained (0.64 g, 71%), identified as product. ^{1}H NMR (700 MHz) δ 5.37-5.32 (m, 1H, *6-H*), 3.55-3.48 (m, 1H, *3α-H*), 2.31-2.20 (m, 2H), 2.03-1.94 (m, 2H), 1.87-1.79 (m, 2H), 1.00 (s, 3H, *19-H*), 0.91 (d, *J* = 6.5, 3H, *21-H*), 0.86 (dd, *J* = 6.6, 1.8, 6H, *26-H* & *27-H*), 0.67 (s, 3H, *18-H*).^{13}C NMR (176 MHz) δ 140. 9 (*6-C)*, 121.8 (*5-C*), 71.92 (3-*C*-^{16}OH) , 71.91(3-*C*-^{17}OH), 71.89 (3-*C*-^{18}OH), 56.9, 56.3, 50.3, 42.5, 42.4, 39.9, 39.7, 37.4, 36.6, 36.3, 35.9, 32.1, 32.0, 31.8, 28.4, 28.2, 24.4, 24.0, 23.0, 22.7 (*26-C* or *27-C)*, 21.2 (*26-C* or *27-C)*, 19.5 (*19-C*), 18.9 (*21-C*), 12.0 (*18-C*). LRMS (ASAP) m/z: 388.4 ([^{17}O–M+H]$^+$, 8%), 387.4 ([^{17}O-M$^+$] and [^{16}O-M+H]$^+$, 9), 386.4 ([^{16}O-M]$^+$, 6), 385.4 (2), 369.4 (100). IR (neat) ν_{max} (cm^{-1}); 3301 (s), 2934 (l), 1461 (m), 1383 (s), 1035 (l), 955 (m), 838 (s), 801 (s), 738 (s).

6.4.4. Synthesis of ^{18}O-cholesterol, 81c

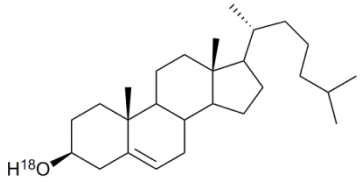

A solution of CF_3SO_3H in anhydrous 1,4-dioxane (111.89 mM; 1.10 mL, 0.13 mmol, 0.05 eq.) was added to a stirred solution of i-cholesteryl methyl ether (0.99 g, 2.35 mmol, 1 eq.) and $^{18}OH_2$ (0.24 mL, 11.99 mmol, 5 eq.) in 1,4-dioxane (60 mL). Other conditions were the same as those detailed in Section 6.4.2. A white solid was isolated (0.63 g, 69%), identified as product. ^{1}H NMR (400 MHz) δ 5.36-5.34 (m, 1H, *6-H*), 3.52 (m, 1H, *3α-H*), 2.25 (m, 2H), 2.06-1.93 (m, 2H), 1.83 (m, 2H), 1.01 (s, 3H, *19-H*), 0.91 (d, *J* = 6.5, 3H, *21-H*), 0.86 (dd, *J* = 6.6, 1.8, 6H, *26-H* & *27-H*), 0.68 (s, 3H, *18-H*).^{13}C NMR (700 MHz) δ 140.9 (*6-C*), 121.9 (*5-C*), 71.93 (3-*C*-^{16}OH), 71.90 (*3-C*-^{18}OH), 56.9, 56.3, 50.3, 42.5, 39.9, 39.7, 37.4, 36.7, 36.3, 35.9, 32.1, 31.8, 28.4, 28.2, 24.4, 24.0, 23.0, 22.8 (*26-C* or *27-C)*, 22.6 (*26-C* or *27-C)*, 21.2, 19.5 (*19-C*), 18.9 (*21-C*), 12.0 (*18-C*). LRMS (ASAP) *m/z*: 388.369 ([^{18}O -M]$^+$, 13%), 387.378 ([^{16}O-M+H]$^+$, 2), 369.352 ([M-(OH)$_2$]$^+$, 100). HRMS (ASAP) *m/z*: calculated [M+H]$^+$ 388.3591, found 388.3596. IR (neat) ν_{max} (cm^{-1}); 3307 (s), 2934 (l), 1463 (m), 1381 (s), 1035 (l), 952 (m), 801 (s).

Single crystals suitable for X-ray diffraction were obtained by slow evaporation from EtOAc. X-ray diffraction images of the single crystal (obtained as detailed in Section 6.1) allowed elucidation of the unit cell, the structure shown in Figure 6.5 shows one structure of the unit cell.

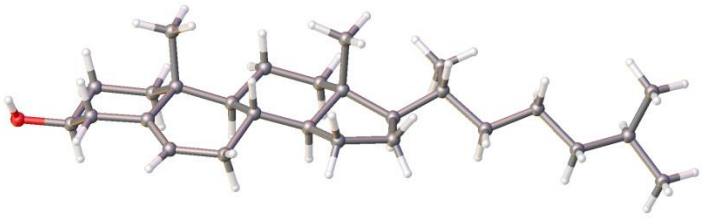

Figure 6.5. One structure from the unit cell of **81c**, determined by X-ray diffraction of a single crystal.

6.4.5. Characterisation of 3β-dicholesterylether, 85

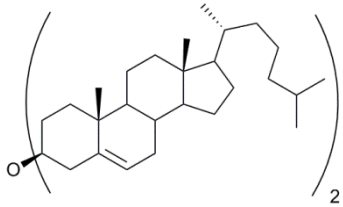

mp: 185-187 °C. ^{1}H NMR (400 MHz) δ 5.42-5.34 (m, 1H, *6-H*), 4.79-4.68 (m, 1H, *3α-H*), 2.39-2.29 (m, 2H), 2.06-1.76 (m, 5H), 1.02 (s, 3H, *19-H*), 0.91 (d, *J* = 6.5, 3H, *21-H*), 0.86 (dd, *J* = 6.6, 1.9, 6H, *26-H* & *27-H*), 0.68 (s, 3H, *18-H*).^{13}C NMR (101 MHz) δ 141.5 (*5-C*), 121.5 (*6-C*), 76.5 (*3-C*), 56.9, 56.3, 50.4, 42.5, 40.2, 40.0, 39.7, 37.6, 37.0, 36.4, 35.9, 32.1, 32.1, 29.6, 28.4, 28.2, 24.5, 24.0, 23.0, 22.7 (*26-C* or *27-C)*, 21.2 (*26-C* or *27-C)*, 19.6 (*19-C*), 18.9 (*21-C*), 12.0 (*18-C*). LRMS (ASAP) *m*/*z*: 754 ([M]$^{+}$, 1%), 386 (2), 385 (6), 370 (34), 369 (100). HRMS (ASAP) *m*/*z*: calculated [M]$^{+}$ 754.6992, found 754.6967. IR (neat) ν_{max} (cm^{-1}); 2914 (l), 2900 (l), 2851 (l), 1464 (m), 1373 (m), 1367 (s), 1059 (l), 1022 (s), 945 (s), 837 (s), 598 (s). Data obtained reflected literature values.[323]

6.4.6. Characterisation of 3β-methoxy-5-cholestene, 86

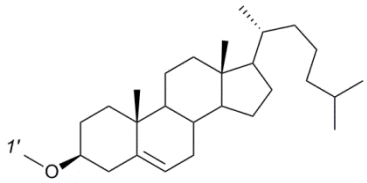

mp: 83-84 °C. ^{1}H NMR (400 MHz) δ 5.37-5.32 (m, 1H, *6-H*), 3.34 (s, 3H, *1'-H*), 3.11-3.00 (m, 1H, *3α-H*), 2.38 (m, 1H), 2.15 (m, 1H), 2.06-1.73 (m, 4H), 0.99 (s, 3H, *19-H*), 0.91 (d, *J* = 6.5, 3H, *21-H*), 0.86 (dd, *J* = 6.6, 1.8, 6H, *26-H* & *27-H*), 0.67 (s, 3H, *18-H*). ^{13}C NMR (101 MHz) δ 141.0 (*5-C*), 121.7 (*6-C*), 80.5 (*3-C*), 56.9, 56.3, 55.7, 53.5, 50.4 (*1'-C*), 42.5, 39.9, 39.7, 38.8, 37.3, 37.0, 36.3, 35.9, 32.1, 32.0, 29.9, 28.4, 28.2, 28.0, 24.4, 24.0, 23.0, 22.7 (*26-C* or *27-C)*, 21.2 (*26-C* or *27-C)*, 19.5 (*19-C*), 18.9 (*21-C*), 12.0 (*18-C*). LRMS (ASAP) *m*/*z*: 401 ([M+H]$^{+}$, 14%), 400 ([M]$^{+}$, 10), 386 (2), 370 (78), 369 (100), 287 (4), 161 (1). HRMS (ASAP) *m*/*z*: calculated [M]$^{+}$ 401.3783, found 401.3776. IR (neat) ν_{max}

(cm^{-1}); 2934 (l), 2865 (l), 2849 (l), 1468 (m), 1379 (m), 1191 (m), 1104 (l), 944 (m), 801 (s), 739 (s), 626 (s), 492 (s). Data obtained reflected literature values.[324]

Single crystals suitable for X-ray diffraction were obtained by slow evaporation EtOAc. X-ray diffraction images of the single crystal (obtained as detailed in Section 6.1) revealed the structure shown in Figure 6.6 to constitute the unit cell.

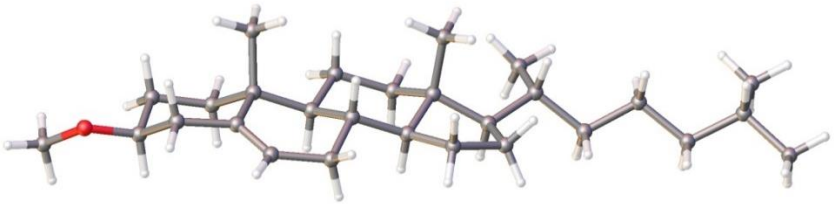

Figure 6.6. One structure from the unit cell of **86**, determined by X-ray diffraction of a single crystal.

6.4.7. Characterisation of i-cholesterol, 87

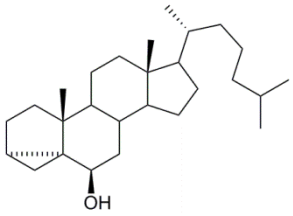

^{1}H NMR (400 MHz) δ 3.26 (t, *J* = 2.8, 1H, *6α-H*), 2.00 (dt, *J* = 3.5 and 12.5, 1H), 1.91-1.69 (4H, m), 1.66-0.94 (m, 26H), 0.91 (d, *J* = 6.6, 3H, *21-H*), 0.86 (dd, *J* = 6.6 and 1.8, 6H, *26-H & 27-H*), 0.72 (s, 3H, *18-H*), 0.52 (t, *J* = 4.2, 1H, *4β-H*), 0.29 (dd, *J* = 4.9, 8.1, 1H, *4α-H*). ^{13}C NMR (101 MHz) δ 73.8 (*6-C*), 56.5, 56.4, 47.7, 42.9, 42.7, 40.2, 39.5, 38.9, 37.2, 36.2, 35.8, 33.21, 29.9, 28.3, 28.0, 25.0, 24.3, 24.2, 23.9, 22.8, 22.7, 22.6, 20.2, 18.7, 12.2, 11.6.MS (ASAP) *m*/*z*: 386 ($[M]^+$, 6%), 385 (10), 370 (78), 369 (100), 287 (3), 243 (3), 161 (1). IR (neat) ν_{max} (cm^{-1}); 3611 (s), 2932 (l), 2861 (l), 2845 (l), 1473 (l), 1383 (m), 1036 (m), 1014 (l), 928 (m), 607 (m). Data obtained matched literature values.[325]

6.4.8. Characterisation of cholesta-3, 5-diene, 88 and 3,5-cyclocholest-6-ene, 89

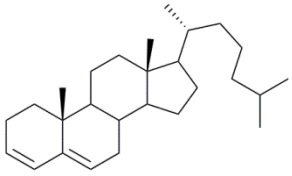

88

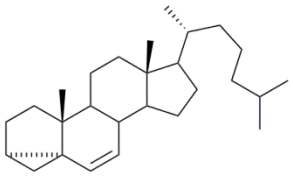

89

86:[1]H NMR (400 MHz) δ 5.92 (d, *J* = 9.7, 1H, *4-H*), 5.62–5.56 (m, 1H, *3-H*), 5.35-5.32 (m, 1H, *6-H*).

87: [1]H NMR (400 MHz) δ 5.51 (t, *J* = 9.0, 1H, *6-H*), 5.18 (dd, *J* = 9.7 and 2.6, 1H, *7-H*), 0.80 (t, *J* = 4.9, 1H, *4β-H*), 0.43 (dd, *J* = 5.0 and 8.0, 1H, *4α-H*).

The remaining signals could not be identified unambiguously due to overlap.

LRMS (ASAP) *m*/*z*: 369 ([M+H]$^+$, 100%), 368 ([M]$^+$, 48), 367 (39), 145 (1). (Note: the compounds are isobaric). Data obtained matched literature values.[326,327]

6.4.9. Characterisation of Cholest-5-en-3β-oxybutan-4-ol (butan-1,4-diol monocholesteryl ether), 90a

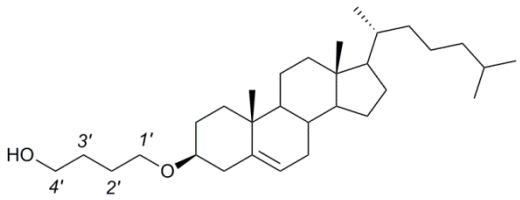

[1]H NMR (400 MHz) δ 5.36-5.33 (m, 1H, *6-H*), 3.67-3.62 (m, 2H, *4'-H*), 3.55-3.47 (m, 2H, *1'-H*), 3.22-3.12 (m, 1H, *3α-H*), 2.37 (ddd, *J* = 13.2, 4.7, 2.3 Hz, 1H), 2.24-2.13 (m, 1H), 1.71-1.65 (m, 4H, *2'-H* & *3'-H*), 0.99 (s, 3H, *19-H*), 0.91 (d, *J* = 6.6 Hz, 3H, *21-H*), 0.86 (dd, *J* = 6.6, 1.8 Hz, 6H, *26-H* & *27-H*), 0.67 (s, 3H, *18-H*). LRMS (ASAP) *m*/*z*: 369 ([M-butanediol]$^+$, 100%), 368 (1), 370 (55), 287(2), 243 (2), 161(1). Data matched literature values.[328]

6.4.10. Characterisation of 5-(Cholest-5-en-3β-yloxy)-5-oxanonan-9-ol (dibutylene glycol monocholesteryl ether), 90b

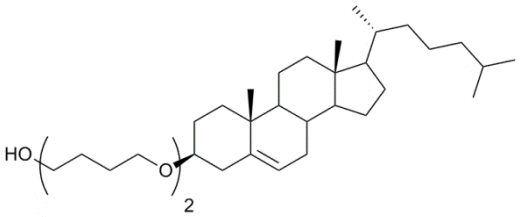

^{1}H NMR (400 MHz) δ 5.37-5.30 (m, 1H, *6-H*), 3.69 (brs, 2H,), 3.51-3.38 (m, 6H, *1'-H* & *4'-H*), 3.16-3.07 (m, 1H, *3α-H*), 2.38-2.31 (m, 1H), 2.23-2.13 (m, 1H), 2.04-1.93 (m, 2H), 1.75-1.58 (m, 12H, *2'-H* & *3-H*), 0.99 (s, 3H, *19-H*), 0.91 (d, *J* = 6.6 Hz, 3H, *21-H*), 0.86 (dd, *J* = 6.6, 1.8 Hz, 6H, *26-H* & *27-H*), 0.67 (s, 3H, *18-H*). LRMS (ASAP) *m*/*z*: 531 ([M+H]$^+$, 1%), 386 (1), 370 (79), 369 ([M-dibutyleneglycol]$^+$, 100), 287 (3), 243 (3), 219 (1). Data matched literature values.[328]

6.4.11. Characterisation of 5-(Cholest-5-en-3β-yloxy)-5,10-oxatetradecan-14-ol (tributylene glycol monocholesteryl ether), 90c

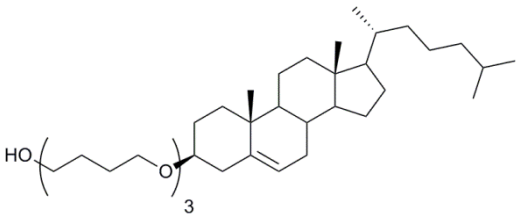

^{1}H NMR (400 MHz) δ: 5.35-5.32 (m, 1H, 6-H), 3.64 (t, *J* = 5.9 Hz, 2H, *4'-H*), 3.49-3.38 (m, 10H, *1'-H & 4'-H*), 3.17-3.07 (m, 1H, *3α-H*), 2.38-2.31 (m, 1H), 2.21-2.13 (m, 1H), 2.06-1.76 (m, 5H), 1.76-1.42 (m, 40H, CH2CH2/H2O), 0.99 (s, 3H, *19-H*), 0.91 (d, *J* = 6.5 Hz, 3H, *21-H*), 0.86 (dd, *J* = 6.6 and 1.8 Hz, 6H, *26-H/27-H*), 0.67 (s, 3H, *18-H*). LRMS (ASAP) *m*/*z*: 383 (17%), 369 ([M-tributyleneglycol]$^+$, 100), 368 (31), 367 (47), 161 (1). Data matched literature values.[328]

6.4.12. Synthesis of 3β-tert-butyldimethylsilyl cholesterol, 91

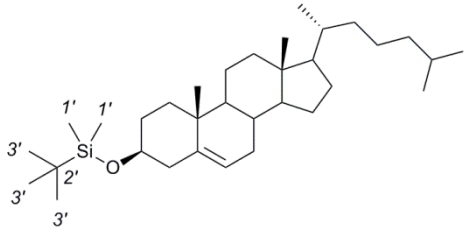

Cholesterol (1.50 g, 3.88 mmol, 1 eq.), iodine (1.97 g, 7.76 mmol, 2 eq.) and NMI (1.00 mL, 11.64 mmol, 3 eq.) were dissolved in anhydrous THF (15 mL) under an argon atmosphere. tert-Butyldimethylsilyl chloride (0.87 g, 5.77 mmol, 1.5 eq.) was added and the solution stirred for 1 hour at ambient temperature. The solution was concentrated *in vacuo* prior to addition of EtOAc (100 mL) and saturated aq. sodium thiosulfate solution (20 mL). The layers were separated, the organic layer was dried ($MgSO_4$), filtered and concentrated *in vacuo* to afford a crude yellow solid (1.80 g). The crude mixture was purified by flash column chromatography (50 mm, eluent; hexane to hexane: EtOAc 1:1) to afford a white solid (1.49 g, 77%) identified as product (R_f 0.60, hexane: EtOAc 6:1). mp: 136-138 °C. ^{1}H NMR (400 MHz) δ 5.35-5.28 (m, 1H, *6-H*), 3.53-3.43 (m, 1H, *3α-H*), 2.26 (m, 1H), 2.16 (m, 1H), 2.05-1.92 (m, 2H), 1.88-1.77 (m, 2H), 1.76-1.67 (m, 1H), 1.00 (s, 3H, *19-H*), 0.92 (d, *J* = 6.5, 3H, *21-H*), 0.89 (s, 9H, *3'-H*), 0.87 (dd, *J* = 6.6, 1.8, 6H, *26-H & 27-H*), 0.67 (s, 3H, *18-H*), 0.06 (s, 6H, *1'-H*). ^{13}C NMR (101 MHz) δ 141.6 (*6-C*), 121.2 (*5-C*), 72.7 (*3-C*), 56.8, 56.2, 50.2, 42.9, 42.4, 39.8, 39.6, 37.4, 36.6, 36.2, 35.8, 32.1, 32.0, 31.9, 28.3, 28.0, 26.0 (*3'-C*), 24.3, 23.9, 22.8, 22.6, 21.1, 19.5, 18.7, 18.3 (*2'-C*), 11.9, -4.8 (*1'-C*). LRMS (ASAP) *m*/*z*: 501.456 ($[M+H]^+$, 12%), 443.380 (29), 370.351 (49), 369.364 ($[M-TBDMSO]^+$, 100%). HRMS (ASAP) *m*/*z*: calculated $[M+H]^+$ 501.4492, found 501.4499. IR (neat) ν_{max} (cm^{-1}); 1716 (s), 1525 (s), 1440 (s), 1352 (m), 1269 (m), 1196 (s), 1137 (s), 1102 (s), 978 (s), 926 (s), 825 (s), 780 (s), 719 (l), 487 (s). The data matched literature values.[329]

Single crystals suitable for X-ray diffraction were obtained by slow evaporation from EtOAc. X-ray diffraction images of the single crystal (obtained as detailed in Section

6.1) allowed elucidation of the unit cell, the structure shown in Figure 6.7 depicts one structure of the unit cell.

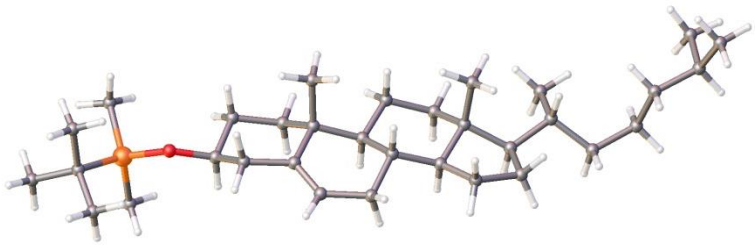

Figure 6.7. One structure from the unit cell of **91**, determined by X-ray diffraction of a single crystal.

6.4.13. Synthesis of 3β-tert-butyldimethylsilyl-5α-cholestan-6α-ol, 92

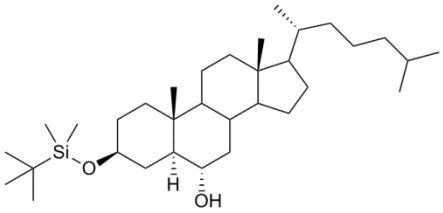

Compound **91** (0.06 g, 0.12 mmol, 1 eq.) and a solution of BH_3.THF in THF (1M; 0.20 mL, 0.19 mmol, 1.5 eq.) were added to a round bottom flask containing anhydrous THF (2 mL), under an argon atmosphere at 0 °C. The solution was allowed to warm to room temperature and stirred for 4 hours, solutions of NaOH (2 M; 0.30 mL, 0.60 mmol, 5 eq.) and 30 wt% H_2O_2 (0.10 mL, 0.88 mmol, 7 eq.) were added to the mixture. The reaction was refluxed for a further 2 hours. The sample was concentrated *in vacuo*, the solid was dissolved in EtOAc (50 mL), which was then washed with a solution of saturated NH_4Cl (10 mL) then brine (10 mL). The organic phase was collected, dried ($MgSO_4$), filtered and concentrated *in vacuo* to return a white solid. The crude material was purified by flash column chromatography (hexane: EtOAc 8:1 to 6:1 to 4:1) to yield a white solid (0.03 g, 45%), identified as product. ^{1}H NMR (400 MHz) δ 3.57-3.47 (m, 1H, *3β-OH*), 3.40 (td, *J* = 10.7, 4.5 Hz, 1H, *6α-OH*), 2.08-1.93 (m, 3H), 1.88-1.76 (m, 1H), 0.87-0.85 (s, 12H, *21-H* & *3'-H*), 0.86 (dd, *J* = 6.6, 1.9 Hz, 6H, *26-H* & *27-H*), 0.80 (s, 3H, *19-H*), 0.64 (s, 3H, *18-H*), 0.05 (s, 6H, *2'-H*). LRMS (ASAP) *m*/*z*: 519.439 ($[M+H]^+$, 2%), 518.451 ($[M+H]^+$, 4),

501.458 ([M-OH]$^+$, 31), 369.356 ([M-OTBDMS-OH]$^+$, 100). Data matched literature values.[290]

6.4.14. Synthesis of 3β-tetrahydro-2H-pyran-2-ylcholesterol, 93a

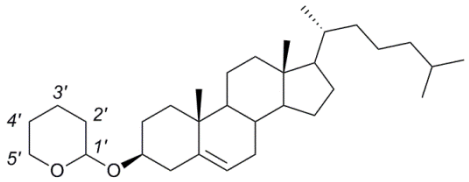

Cholesterol (3.00 g, 7.76 mmol, 1 eq.), PCC (0.36 g, 1.55 mmol, 0.2 eq.) and DHP (1.10 mL, 3.88 mmol, 1.5 eq.) were stirred in anhydrous DCM (30 mL) for 2 hours under an argon atmosphere. Further DCM (50 mL) and H_2O (2 × 20 mL) was added, the layers were separated and the organic layer was dried using $MgSO_4$, filtered and concentrated *in vacuo* to yield a crude white solid. The crude material was purified using flash column chromatography (50 mm, eluent; hexane to hexane: EtOAc 10:1 to 6:1) to afford a white solid (3.23 g, 88%) identified as product (R_f 0.47, hexane: EtOAc 6:1). mp: 147-149 °C. ^{1}H NMR (400 MHz) δ 5.38-5.29 (m, 1H, *6-H*), 4.71 (t, *J* = 3.6, 1H, *1'-H*), 3.96-3.97 (m, *3α-H*), 3.58-3.40 (m, 2H, *5'-H*), 2.40-2.27 (m, 2H), 2.20 (td, *J* = 12.8, 12.1, 2.8, 1H), 1.00 (s, 3H, *19-H*), 0.91 (d, *J* = 6.5, 3H, *21-H*), 0.86 (dd, *J* = 6.6, 1.8, 6H, *26-H* & *27-H*), 0.67 (s, 3H, *18-H*). ^{13}C NMR (101 MHz) δ 141.2, 141.0 (*5-C*), 121.7, 121.6 (*6-C*), 97.1, 97.0 (*1'-C*), 76.1 (*3-C*), 63.0, 62.9 (*5'-C*), 56.9, 56.3, 50.3, 42.4, 40.4, 39.9, 39.6, 38.9, 37.6, 37.3, 36.9, 36.3, 35.9, 32.1, 32.0, 31.4, 29.8, 28.4, 28.1, 25.6, 24.4, 23.9, 22.9, 22.7 (*26-C* or *27-C)*, 21.2 (*26-C* or *27-C)*, 20.2, 19.5 (*19-C*), 18.8 (*21-C*), 12.0 (*18-C*). LRMS (ASAP) *m*/*z*: 471.424 ([M+H]$^+$, 1%), 369.364 ([M-OTHP]$^+$, 100). IR (neat) ν_{max} (cm^{-1}); 2933 (s), 1669 (s), 1510 (s), 1465 (s), 1255 (s), 1183 (s), 1112 (m), 1032 (l), 975 (m), 823 (s). Data matched literature values.[330]

6.4.15. Synthesis of 3β-^{17}O-tetrahydro-2H-pyran-2-yl-5α-cholesterol, 93b

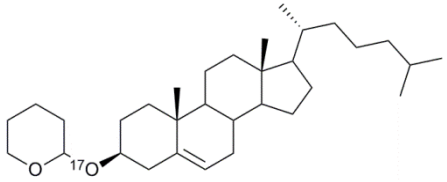

81b (0.49 g, 1.27 mmol, 1 eq.), PPC (0.06 g, 0.26 mmol, 0.2 eq.) and DHP (0.18 mL, 1.91 mmol, 1.5 eq.) were stirred in anhydrous DCM (8 mL) for 2 hours under an argon atmosphere. Other conditions were identical to those described in Section 6.4.14. A white solid (0.49 g, 81%) identified as product (R_f 0.47, hexane: EtOAc 6:1) was obtained. ^{1}H NMR (700 MHz) δ 5.37-5.31 (m, 1H, *6-H*), 4.73-4.70 (m, 1H, *1'-H*), 3.95-3.88 (m, 1H, *3α-H*), 3.55-3.46 (m, 2H, *5'-H*), 2.38-2.32 (m, 1H), 2.23-2.18 (m, 1H), 2.03-1.93 (m, 2H), 1.01 (s, 3H, *19-H*), 0.91 (d, *J* = 6.5, 3H, *21-H*), 0.86 (dd, *J* = 6.6, 3.1, 6H, *26-H* & *27-H*), 0.67 (s, 3H, *18-H*). ^{13}C NMR (176 MHz) δ 141.2, 141.1 (*5-C*), 121.7, 121.6 (6-C), 97.1, 97.0 (*1'-C*), 76.19, 76.18, 76.17, 76.15 (*3-C*), 63.1, 63.0 (*5'-C*), 56.9, 56.3, 50.4, 50.3, 42.5, 40.4, 40.0, 39.7, 38.9, 37.6, 37.4, 37.0, 36.9, 36.4, 35.9, 32.1, 31.5, 31.4, 29.9, 28.4, 28.2, 25.7, 24.5, 24.0, 23.0, 22.7 (*26-C* or *27-C)*, 21.2 (*26-C* or *27-C)*, 20.3, 20.2, 19.5 (*19-C*), 18.9 (*21-C*), 12.0 (*18-C*). LRMS (ASAP) *m*/*z*: 471.429 ([M]$^+$, 0.14%), 369.352 ([M-OTHP]$^+$, 100). IR (neat) ν_{max} (cm^{-1}); 2934 (l), 2867 (m), 1466 (m), 1372 (m), 1364 (m), 1200 (m), 1108 (l), 1021 (l), 970 (l), 910 (s), 817 (s), 799 (s), 427 (s).

6.4.16. Synthesis of 3β-^{18}O-tetrahydro-2H-pyran-2-yl-5α-cholesterol, 93c

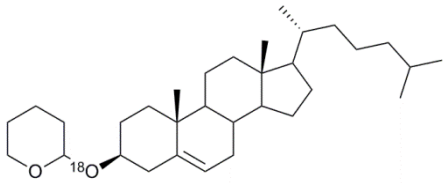

81c (0.51 g, 1.30 mmol, 1 eq.), PPC (0.07 g, 0.26 mmol, 0.2 eq.) and DHP (0.18 mL, 1.91 mmol, 1.5 eq.) were stirred in anhydrous DCM (8 mL) for 2 hours under an argon atmosphere. Other conditions were identical to those described in Section 6.4.14. A white solid (0.52 g, 85%) identified as product (R_f 0.47, hexane: EtOAc 6:1) was obtained. ^{1}H

NMR (700 MHz) δ 5.37-5.32 (m, 1H, *6-H*), 4.73-4.69 (m, 1H, *1'-H*), 3.94-3.88 (m, 1H, *3α-H*), 3.56-3.46 (m, 2H, *5'-H*), 2.38-2.30 (m, 1H), 2.23-2.17 (m, 1H), 1.00 (s, 3H, *19-H*), 0.91 (d, *J* = 6.5, 3H, *21-H*), 0.86 (dd, *J* = 6.6, 3.1, 6H, *26-H* & *27-H*), 0.67 (s, 3H, *18-H*). ^{13}C NMR (176 MHz) δ 141.2, 141.1 (*5-C*), 121.7, 121.6 (*6-C*), 97.1, 97.0 (1'-C), 76.19 (3-*C*-^{16}OTHP), 76.16, 76.14 (3-*C*-^{18}OTHP), 63.1, 63.0, 56.9, 56.3, 50.4, 50.3, 42.5, 40.4, 40.0, 39.9, 39.7, 38.9, 37.6, 37.4, 37.0, 36.9, 36.4, 35.9, 32.1, 31.5, 31.4, 29.9, 28.4, 28.2, 25.7, 24.5, 24.0, 23.0, 22.7 (*26-C* or *27-C)*, 21.2 (*26-C* or *27-C)*, 20.3, 20.2, 19.5 (*19-C*), 18.9 (*21-C*), 12.0 (*18-C*). LRMS (ASAP) *m*/*z*: 473.426 ([M+H]$^+$, 0.3%), 369.327 ([M-OTHP]$^+$, 100). HRMS (ASAP) *m*/*z*: calculated [M]$^+$ 473.4245, found 473.4265. IR (neat) ν_{max} (cm^{-1}); 2935 (l), 1465 (m), 1364 (s), 1260 (m), 1060 (l), 1021 (l), 800 (l), 598 (s).

6.4.17. Synthesis of 3β-tetrahydro-2H-pyran-2-yl-5α-cholestan-6α-ol, 94a

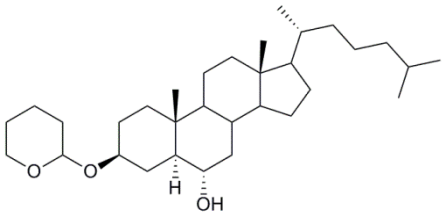

$BF_3.OEt_2$, (0.45 mL, 1.70 mmol, 2 eq.) was added to a suspension of $NaBH_4$ (0.10 g, 2.55 mmol, 3 eq.) in anhydrous THF (2 mL) at 0 °C under an argon atmosphere. The mixture was stirred for 30 minutes, prior to the addition of **93a** (0.40 g, 0.85 mmol, 1 eq.) in anhydrous THF (5 mL), the suspension continued stirring at 0 °C for a further 2 hours. Solutions of 20% NaOH (1.50 mL, 7.65 mmol, 9 eq.) and 30% H_2O_2 (0.87 mL, 7.65 mmol, 9 eq.) were added and stirred at 0 °C for 2 hours. The suspension was concentrated *in vacuo*, followed by the addition of DCM (70 mL) and H_2O (10 mL). The layers were separated and the aqueous layer extracted with DCM (30 mL). The combined organic layers were dried ($MgSO_4$), filtered and concentrated *in vacuo* to afford a white solid (0.42 g). The crude material was purified by flash column chromatography (20 mm, alumina, eluent; hexane to hexane: EtOAc 4:1) to afford a white solid (0.25 g, 60%) identified as product (R_f 0.64 and 0.59, hexane: EtOAc 6:1). ^{1}H NMR (700 MHz) δ 4.76-4.71 (m, 1H, *1'-H*), 3.95-3.88 (m, *5'-H*), 3.61-3.53 (m, 1H, *3α-H*), 3.52-3.45 (m, 1H, *5'-H*), 3.50-3.45 (m, 1H, *6β-H*), 2.27-2.19

(m, 1H), 0.90 (d, *J* = 6.5, 3H, *21-H*), 0.86 (dd, *J* = 6.6, 1.9, 6H, *26-H* & *27-H*), 0.81 (s, 3H, *19-H*), 0.64 (s, 3H, *18-H*). ^{13}C NMR (176 MHz) δ 97.1 (*1'-C*), 96.6 (*1'-C*), 75.5, 75.2 (*3-C*), 69.9 (*6-C*), 69.8 (*6-C*), 63.3 (*5'-C*), 62.7 (*5'-C*), 56.4, 56.3, 56.3, 54.0, 54.0, 52.1, 51.8, 42.7, 42.0, 41.6, 40.0, 39.6, 37.6, 37.4, 36.6, 36.6, 36.3, 35.9, 34.5, 34.4, 31.5, 31.4, 30.4, 29.3, 28.6, 28.3, 28. 2, 27.6, 25.7, 25.6, 24.3, 24.0, 23.0, 22.7 (*26-C* & *27-C*), 21.3, 21.3, 20.4, 19.9, 18.8*(21-C)*, 13.6 *(19-C)*, 12.2 (*18-C*). LRMS (ASAP, 200 °C) *m/z*: 489.429 ([M+H]$^+$, 52%), 387.362 (40), 369.350 ([M-OTHP]$^+$, 100). HRMS (ASAP, 200 °C) *m/z*: calculated [M+H]$^+$ 489.4308, found 489.4286. IR (neat) ν_{max} (cm^{-1}); 3400 (s), 2930 (l), 1470 (s), 1382 (s), 1201 (s), 1134 (m), 1112 (m), 1020 (l), 869 (s), 737 (s). Data matched literature values.[331]

6.4.18. Synthesis of 3β-^{17}O-tetrahydro-2H-pyran-2-yl-5α-cholestan-6α-ol, 94b

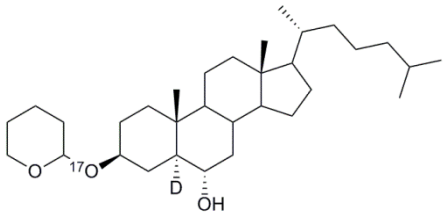

$BF_3.OEt_2$, (0.27 mL, 1.04 mmol, 2 eq.) was added to a suspension of $NaBD_4$ (0.07 g, 1.59 mmol, 3 eq.) in anhydrous THF (2 mL) at 0 °C under an argon atmosphere. The mixture was stirred for 30 minutes, prior to the addition of **93b** (0.25 g, 0.52 mmol, 1 eq.) in anhydrous THF (8 mL), the suspension was warmed to room temperature and stirred for a further 2 hours. Solutions of 20% NaOH (1.00 mL, 5.00 mmol, 9.6 eq.) and 30% H_2O_2 (0.67 mL, 5.90 mmol, 11 eq.) were added and stirred at 0 °C for 2 hours. The other conditions were identical to those described in Section 6.4.17. A white solid (0.16 g, 64%) identified as product (R_f 0.64 and 0.59, hexane: EtOAc 6:1) was obtained. ^{1}H NMR (700 MHz) δ 4.73 (p, *J* = 2.4, 1H, *1'-H*), 3.90 (td, *J* = 7.6, 3.7, 1H, *5'-H*), 3.60-3.53 (m, 1H, *3α-H*), 3.49-3.43 (m, 1H, *5'-H*), 3.42-3.36 (m, 1H, *6-H*), 2.23-217 (m, 1H), 1.97 (tt, *J* = 9.2, 4.5, 2H), 0.89 (d, *J* = 6.5, 4H, *21-H*), 0.85 (dd, *J* = 6.6, 3.2, 8H, *26-H* & *27-H*), 0.80 (s, 3H, *19-H*), 0.63 (s, 4H, *18-H*). ^{13}C NMR (176 MHz) δ 97.0 (*1'-C*), 96.5 (*1'-C*), 75.45 (*3-C-^{16}OTHP*), 75.43 (*3-C-^{17}OTHP)*, 75.42 (*3-C-^{18}OTHP)*, 75.24 (*3-C-^{16}OTHP)*, 75.23 (*3-C-^{17}OTHP)*, 75.21 (*3-C-*

^{18}OTHP), 69.8 (*6-C*), 69.7 (*6-C*), 63.2 (*5'-C*), 62.6 (*5'-C*), 56.4, 56.3, 42.7, 40.0, 39.6, 36.5, 36.3, 35.9, 34.4, 31.3, 28.3, 25.7, 24.3, 23.9, 22.9, 22.7 (*26-C* & *27-C*), 18.8 (*21-C*), 13.5 (*19-C*), 12.2 (*18-C*). D NMR (92 MHz) δ 0.99 (*5α-D*). LRMS (ASAP, 200 °C) *m*/*z*: 490.434 ($[M]^+$, 48%), 388.368 ($[M\text{-}OTHP]^+$, 31), 370.357 ($[M\text{-}OTHP\text{-}OH]^+$, 100). HRMS (ASAP, 200 °C) *m*/*z*: calculated $[M]^+$ 490.4334, found 490.4340. IR (neat) ν_{max} (cm^{-1}); 3424 (s), 2933 (l), 2866 (l), 1471 (s), 1452 (s), 1373 (s), 1100 (m), 1021 (l), 973 (m), 869 (s).

6.4.19. Synthesis of 3β-18O-tetrahydro-2H-pyran-2-yl-5α-cholestan-6α-ol, 94c

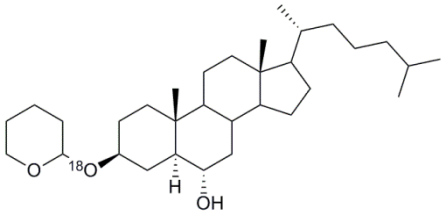

$BF_3.OEt_2$, (0.28 mL, 1.03 mmol, 2 eq.) was added to a suspension of $NaBH_4$ (0.06 g, 1.61 mmol, 3 eq.) in anhydrous THF (2 mL) at 0 °C under an argon atmosphere. The mixture was stirred for 30 minutes, prior to the addition of **93c** (0.25 g, 0.54 mmol, 1 eq.) in anhydrous THF (8 mL), the suspension was warmed to room temperature and stirred for a further 2 hours. Solutions of 20% NaOH (1.00 mL, 4.83 mmol, 9.6 eq.) and aqueous 30% H_2O_2 (0.67 mL, 4.83 mmol, 11 eq.) were added and stirred at 0 °C for 2 hours. The other conditions were identical to those described in Section 6.4.17. A white solid (0.10 g, 38%) identified as product (R_f 0.64 and 0.59, hexane: EtOAc 6:1) was obtained. ^{1}H NMR (700 MHz) δ 4.76-4.72 (m, 1H, *1'-H*), 3.94-3.90 (m, *6'-H*), 3.62-3.54 (m, 1H, *3α-H*), 3.51-3.45 (m, 1H, *5'-H*), 3.44-3.37 (m, 1H, *6β-H*), 2.28-2.20 (m, 1H), 1.97 (tt, *J* = 10.3, 3.9, 2H), 1.87-1.79 (m, 3H), 1.74-1.66 (m, 2H), 0.90 (d, *J* = 6.5, 3H, *21-H*), 0.86 (dd, *J* = 6.6, 3.2, 7H, *26-H* & *27-H*), 0.81 (s, 3H, *19-H*), 0.64 (s, 3H, *18-H*). ^{13}C NMR (176 MHz,) δ 97.1 (*1'-C*), 96.6 (*1'-C*), 75.47 (*3-C-^{16}OTHP*), 75.45 (*3-C-^{18}OTHP*), 75.24 (*3-C-^{16}OTHP*), 75.21 (*3-C-^{18}OTHP*), 69.9 (*6-C*), 69.8 (*6-C*), 63.3 (*5'-C*), 62.7 (*5'-C*), 56.4, 56.3, 54.0, 52.1, 51.8, 42.7, 42.0, 41.7, 40.0, 39.7, 37.6, 37.4, 36.6, 36.3, 35.9, 34.5, 31.5, 31.4, 30.4, 29.4, 28.6, 28.3, 28.2, 27.6, 25.7, 24.4, 24.3, 24.0, 23.0, 22.7 (*26-C* & *27-C*), 21.3, 20.4, 20.0, 18.8 (*21-C*), 13.6 (*19-C*), 12.2 (*18-C*). LRMS (ASAP, 200 °C) *m*/*z*: 491.432 ($[M+H]^+$, 48%), 387.360

([M-OTHP]$^+$, 28), 369.346 ([M-OTHP-OH]$^+$, 100). HRMS (ASAP, 200 °C) *m/z*: calculated [M+H]$^+$ 491.4350, found 491.4328. IR (neat) ν_{max} (cm^{-1}); 3400 (s), 2930 (l), 1470 (s), 1382 (s), 1201 (s), 1134 (m), 1112 (m), 1020 (l), 869 (s), 737 (s).

6.4.20. Synthesis of 3β-^{18}O-tetrahydro-2H-pyran-2-yl-5α-cholestan-6α-ol, 94d

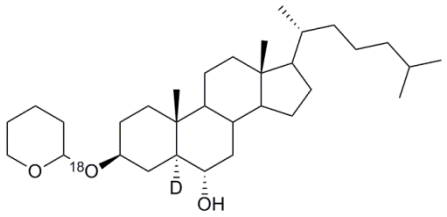

$BF_3.OEt_2$, (0.32 mL, 1.20 mmol, 2 eq.) was added to a suspension of $NaBD_4$ (0.08 g, 1.80 mmol, 3 eq.) in anhydrous THF (5 mL) at 0 °C under an argon atmosphere. The mixture was stirred for 30 minutes, prior to the addition of **93c** (0.28 g, 0.60 mmol, 1 eq.) in anhydrous THF (8 mL), the suspension was warmed to room temperature and stirred for a further 2 hours. Solutions of 20% NaOH (1.00 mL, 5.39 mmol, 9 eq.) and 30% H_2O_2 (0.73 mL, 5.39 mmol, 9 eq.) were added and stirred at 0 °C for 2 hours. The other conditions were identical to those described in Section 6.4.17. A white solid (0.17 g, 57%) identified as product (R_f 0.64 and 0.59, hexane: EtOAc 6:1) was obtained. ^{1}H NMR (700 MHz) δ 4.75-4.71 (m, 1H, *1'-H*), 3.93-3.88 (m, 1H, *5'-H*), 3.60-3.52 (m, 1H, *3α'-H*), 3.49-3.43 (m, 1H, *6'-H*), 3.41-3.37 (m, 1H, *6β-H*), 2.25-2.18 (m, 1H), 2.00-1.92 (m, 2H), 1.88-1.78 (m, 4H), 1.74-1.64 (m, 2H), 0.89 (d, *J* = 6.5, 3H, *21-H*), 0.85 (dd, *J* = 6.6, 3.2, 8H, *26-H* & *27-H*), 0.80 (s, 3H, *19-H*), 0.64 (s, 3H, *18-H*).^{13}C NMR (176 MHz) δ 97.0 (*1'-C*), 96.6 (*1'-C*), 75.45 (*3-C-^{16}OTHP*), 75.42 (*3-C-^{18}OTHP*), 75.24 (*3-C-^{16}OTHP*), 75.21 (*3-C-^{18}OTHP*), 69.8 (*6-C*), 69.7 (*6-C*), 63.2 (*5'-C*), 62.9 (*5'-C*), 56.4, 56.3, 54.0, 51.6, 51.5 (t, 18.6, 5-C), 51.2 (t, 17.4, 5-C) , 42.7, 41.9, 41.6, 40.0, 39.6, 37.6, 37.3, 36.5, 36.3, 35.9, 34.5, 34.4, 31.5, 31.3, 30.3, 29.3, 28.3, 28.1, 27.6, 25.7, 25.6, 24.3, 24.0, 23.0, 22.7 (*26-C* & *27-C*), 21.3, 19.9, 18.8 (*21-C*), 13.5 (*19-C)*, 12.2 (*18-C*). D NMR (92 MHz) δ 1.00 (s, 1H, *5α-D*). LRMS (ASAP, 200 °C) *m/z*: 492.442 ([M]$^+$, 40%), 388.370 ([M-OTHP]$^+$, 25), 370.359 ([M-OTHP-OH]$^+$, 100). HRMS (ASAP, 200 °C) *m/z*: calculated [M+H]$^+$ 492.4413, found 492.4416. IR (neat) ν_{max}

(cm^{-1}); 3400 (s), 2930 (l), 2860 (l), 1467 (s), 1374 (s), 1200 (s), 1106 (m), 1020 (l), 966 (m), 867 (s).

6.4.21. Synthesis of 3β-tetrahydro-2H-pyran-2-yl-5α-cholestan-6-one, 95a

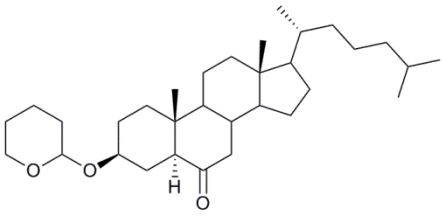

94a (0.25 g, 0.51 mmol, 1 eq.), PCC (0.16 g, 0.76 mmol, 1.5 eq.) and sodium acetate (0.01 g, 0.15 mmol, 0.3 eq.) were stirred in anhydrous DCM (4 mL) for 2 hours under an argon atmosphere. Et_2O (50 mL) was added and filtered through celite, the mixture was then concentrated *in vacuo* and purified by flash column chromatography (20 mm, alumina, eluent; hexane to hexane: EtOAc 5:1). A white solid (0.22 g, 88%) identified as product (R_f 0.32, hexane: EtOAc 5:1). ^{1}H NMR (400 MHz) δ 4.78-4.71 (m, 1H, *1'-H*), 3.93-3.84 (m, 1H, *5'-H*), 3.66-3.50 (m, 1H, *3α-H*), 3.50-3.42 (m, 1H, *5'-H*), 2.30 (dt, *J* = 13.1, 4.7, 1H, *4α-H*), 2.24-2.10 (m, 1H, *5-H*), 2.06-1.89 (m, 3H), 0.90 (d, *J* = 6.5, 3H, *19-H*), 0.85 (dd, *J* = 6.6, 3.1, 6H, *26-H* & *27-H*), 0.75 (s, 3H, *19-H*), 0.65 (s, 3H, *18-H*).^{13}C NMR (101 MHz) δ 211.4 (*6-C*), 211.1 (*6-C*), 96.4 (*1'-C*), 74.6 (*3-C*), 74.1 (*3-C*), 63.1 (*5'-C*), 62.1 (*5'-C*), 57.2, 57.1, 56.9, 56.8 (*5-C*), 56.3, 55.4, 54.1, 54.1, 46.9 (*4-C*), 43.2, 43.1, 41.3, 41.3, 39.7, 39.6, 39.6, 38.2, 38.1, 38.0, 37.0, 36.9, 36.2, 35.8, 31.3, 31.2, 28.9, 28.3, 28.2, 28.1, 28.1, 27.4, 26.0, 25.7, 25.7, 25.6, 24.1, 23.9, 23.0, 22.7 (*26-C* & *27-C*), 21.7, 21.6, 21.3, 20.2, 20.0, 19.4, 18.8 (*21-C*), 13.3 (*19-C*), 12.2 (*18-C*), 12.1 (*18-C*). LRMS (ASAP, 200 °C) *m*/*z*: 487.415 ($[M+H]^+$, 1%), 444.385 (14), 403.040 (100), 385.350 ($[M\text{-}OTHP]^+$, 16). HRMS (ASAP, 200 °C) *m*/*z*: calculated $[M+H]^+$ 487.4151, found 487.4126. IR (neat) ν_{max} (cm^{-1}); 2937 (l), 1707 (l), 1465 (s), 1353 (s), 1118 (m), 1063 (m), 1032 (l), 981 (m), 910 (m), 870 (m), 819 (s).

6.4.22. Synthesis of 3β-^{17}O-tetrahydro-2H-pyran-2-yl-5α-cholestan-6-one, 95b

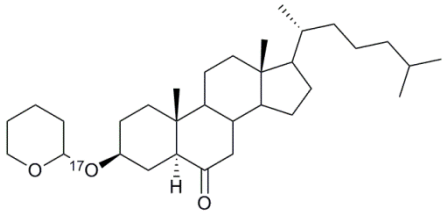

94b (0.23 g, 0.47 mmol, 1 eq.), PCC (0.15 g, 0.71 mmol, 1.5 eq.) and sodium acetate (0.01 g, 0.14 mmol, 0.3 eq.) were stirred in anhydrous DCM (4 mL) for 2 hours under an argon atmosphere. The other conditions were the same as described in Section 6.4.21. A white solid (0.18 g, 76%) identified as product (R_f 0.32, hexane: EtOAc 5:1) was isolated. ^{1}H NMR (700 MHz) δ 4.76-4.70 (m, 1H, *1'-H*), 3.91-3.85 (m, 1H, *5'-H*), 3.60-3.51 (m, 1H, *3α-H*), 3.47-3.42 (m, 1H, *6'-H*), 2.32-2.26 (m, 1H, *4-H*), 2.21-2.11 (m, 1H, *5-H*), 0.90-0.88 (m, 3H, *21-H*), 0.84 (dd, *J* = 6.7, 3.1, 6H, *26-H* & *27-H*), 0.73 (s, 3H, *19-H*), 0.64 (d, *J* = 1.2, 3H, *18-H*). ^{13}C NMR (176 MHz) δ 211.3 (*6-C*), 210.9 (*6-C*), 96.3 (*1'-C*), 96.2 (*1'-C*), 74.53 (*3-C*-^{16}OTHP), 74.52 (*3-C*-^{17}OTHP), 74.51 (*3-C*-^{18}OTHP), 74.04 (*3-C*-^{16}OTHP), 74.03 (*3-C*-^{17}OTHP), 74.01 (*3-C*-^{18}OTHP), 63.0 (*5'-C*), 62.0 (*5'-C*), 57.2, 56.9, 56.8 (*5-C*), 56.3, 56.2, 54.1, 46.9 (*7-C*), 46.8 (*7-C*), 43.1, 41.3, 41.2, 39.6, 38.0, 37.0, 36.8, 36.2, 35.8, 31.3, 31.1, 28.9, 28.2, 28.1, 27.3, 26.0, 25.7, 25.6, 24.1, 23.9, 22.9, 22.7 (*26-C* & *27-C*), 21.6, 20.1, 19.4, 18.8 (*21-C*), 13.2 (*19-C*), 12.1 (*18-C*). LRMS (ASAP, 200 °C) *m*/*z*: 488.422 ([M+H]$^+$, 1%), 405.365 (100), 385.348 ([M-OTHP]$^+$, 37). HRMS (ASAP, 200 °C) *m*/*z*: calculated [M+H]$^+$ 488.4193, found 488.4166. IR (neat) ν_{max} (cm^{-1}); 2936 (l), 2868 (l), 1707 (m), 1466 (s), 1380 (s), 1201 (s), 1114 (s), 1023 (l), 979 (m), 906 (s), 869 (s), 816 (s).

6.4.23. Synthesis of 3β-^{18}O-tetrahydro-2H-pyran-2-yl-5α-cholestan-6-one, 95c

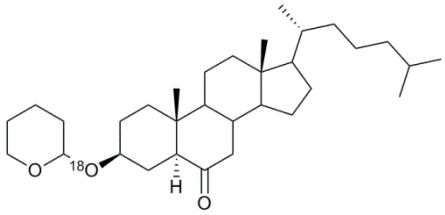

94c (0.10 g, 0.21 mmol, 1 eq.), PCC (0.07 g, 0.31 mmol, 1.5 eq.) and sodium acetate (0.01 g, 0.06 mmol, 0.3 eq.) were stirred in anhydrous DCM (5 mL) for 2 hours under an

argon atmosphere. The other conditions were the same as described in Section 6.4.21. A white solid (0.09 g, 89%) identified as product (R_f 0.32, hexane: EtOAc 5:1). ^{1}H NMR (700 MHz) δ 4.77-4.72 (m, 1H, *1'-H*), 3.92-3.86 (m, 1H, *5'-C*), 3.63-3.52 (m, 1H, *3α-H*), 3.49-3.44 (m, 1H, *5'-C*), 2.33-2.27 (m, 1H, *7-H*), 2.22-2.13 (m, 1H, *5-H*), 0.91 (d, *J* = 6.5, 3H, *21-H*), 0.86 (dd, *J* = 6.6, 3.1, 6H, *26-H* & *27-H*), 0.75 (s, 3H, 19-H), 0.65 (s, 3H, *18-H*). ^{13}C NMR (176 MHz) δ 211.4 (*1'-C*), 211.0 (*1'-C*), 96.4 (*5'-C*), 96.3 (*5'-C*), 74.57 (*3-C*-^{16}OTHP), 74.55 (*3-C*-^{18}OTHP), 74.09 (*3-C*-^{16}OTHP), 74.06 (*3-C*-^{18}OTHP), 63.1 (*5'-C*), 62.1 (*5'-C*), 57.2, 56.9, 56.8 (*5-C*), 56.3, 54.2, 46.9 (*7-C*), 43.1, 41.3, 41.3, 39.7, 39.7, 39.6, 38.1, 38.0, 37.0, 36.9, 36.3, 35.8, 31.3, 31.2, 28.9, 28.2, 28.1, 27.4, 26.1, 25.7, 24.1, 24.0, 23.0, 22.7 (*26-C* & *27-C*), 21.7, 21.6, 20.2, 19.4, 18.8 (*21-C*), 13.3 (*19-C*), 12.2 (*18-C*). LRMS (ASAP, 200 °C) *m*/*z*: 489.421 ($[M+H]^+$, 0.7%), 405.365 (100), 385.346 ($[M-OTHP]^+$, 16). HRMS (ASAP, 200 °C) *m*/*z*: calculated $[M+H]^+$ 489.4194, found 489.4214. IR (neat) ν_{max} (cm^{-1}); 3400 (s), 2930 (l), 2860 (l), 1467 (s), 1374 (s), 1200 (s), 1106 (m), 1020 (l), 966 (m), 867 (s). IR (neat) ν_{max} (cm^{-1}); 2931 (l), 2867 (l), 1704 (l), 1467 (s), 1381 (s), 1201 (s), 1115 (m), 1020 (l), 977 (m), 904 (m), 869 (s), 812 (s).

6.4.24. Synthesis of 3β-^{18}O-tetrahydro-2H-pyran-2-yl-5α-cholestan-6-one, 95d

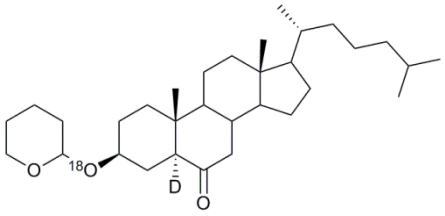

94d (0.15 g, 0.31 mmol, 1 eq.), PCC (0.10 g, 0.47 mmol, 1.5 eq.) and sodium acetate (0.01 g, 0.09 mmol, 0.3 eq.) were stirred in anhydrous DCM (5 mL) for 2 hours under an argon atmosphere. The other conditions were the same as described in Section 6.4.21. A white solid (0.13 g, 88%) identified as product (R_f 0.32, hexane: EtOAc 5:1). ^{1}H NMR (700 MHz) δ 4.76-4.70 (m, 1H, *2'-H*), 3.91-3.85 (m, 1H, *6-H*), 3.60-3.50 (m, 1H, *3α-H*), 3.48-3.42 (m, 1H, *6'-H*), 2.31-2.25 (m, 1H, *7-H*), 0.89 (d, *J* = 6.5, 3H, *21-H*), 0.84 (dd, *J* = 6.7, 3.1, 6H, *26-He & 27-H*), 0.73 (s, 3H, *19-H*), 0.63 (s, 3H, *18-H*). ^{13}C NMR (176 MHz) δ 211.3 (*6-C*), 211.0 (*6-C*), 96.3 (*1'-C*), 96.2 (*1'-C*), 74.52 (*3-C*-^{16}OTHP), 74.49 (*3-C*-

^{18}OTHP), 74.01 (*3-C*-^{16}OTHP), 73.99 (*3-C*-^{18}OTHP), 63.1 (*5'-C*), 62.0 (*5'-C*), 56.9 (*5-C*), 56.3, 54.1, 46.9 (*7-C*), 43.1, 41.2, 39.6, 38.1, 38.0, 37.0, 36.8, 36.2, 35.8, 31.3, 31.1, 28.9, 28.2, 28.1, 28.0, 27.3, 25.9, 25.7, 25.6, 24.1, 23.9, 22.9, 22.7 (*26-C & 27-C*), 21.6, 20.1, 19.4, 18.7 (*21-C*), 13.2 (*19-C*), 12.1 (*18-C*). D NMR (92 MHz) δ 2.17 (s, 1H, *5α-D*). LRMS (ASAP, 200 °C) *m*/*z*: 489.425 ([M]$^+$, 0.6%), 406.363 (100), 386.355 ([M-OTHP]$^+$, 15). HRMS (ASAP, 200 °C) *m*/*z*: calculated [M]$^+$ 489.4178, found 489.4263. IR (neat) ν_{max} (cm^{-1}); 2933 (l), 2868 (l), 1704 (m), 1467 (s), 1379 (s), 1259 (s), 1112 (m), 1074 (m), 1030 (l), 988 (l), 904 (s), 870 (s), 816 (s), 738 (m).

6.4.25. Synthesis of 3β-hydroxy-5α-cholestan-6-one, 82a

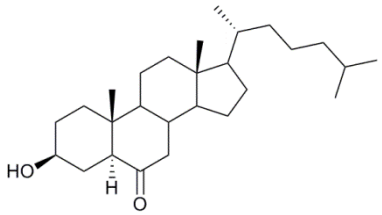

95a (0.07 g, 0.14 mmol, 1 eq.) was dissolved in THF (2 mL) prior to the addition of concentrated HCl solution (0.05 mL, 0.61 mmol, 2 eq.). The solution was stirred at 50 °C for 2 days. The solution was cooled and concentrated. The crude material was dissolved in Et_2O (50 mL) which was then washed with H_2O (10 mL). The organic layer was dried using $MgSO_4$, filtered and concentrated. The crude white powder was purified by flash column chromatography (10 mm, eluent; hexane to hexane: EtOAc 1:1) to afford a white solid (0.05 g, 83%), identified as product (R_f 0.32, hexane: EtOAc 1:1). mp: 137-139 °C . ^{1}H NMR (400 MHz) δ 3.65-3.54 (m, 1H, *3α-H*), 2.34 (dd, *J* = 13.2, 4.5, 1H, *7β-H*), 2.23 (dd, *J* = 12.6, 3.0, 1H, *5-H*), 0.94 (d, *J* = 6.5, 3H, *19-H*), 0.89 (dd, *J* = 6.6, 1.9, 6H, *26-H* & *27-H*), 0.78 (s, 3H, *21-H*), 0.68 (s, 3H, *18-H*). ^{13}C NMR (101 MHz) δ 211.1 (*6-C*), 70.7 (*3-C*), 56. 9, 56.8, 56.2, 54.0, 46.8, 43.1, 41.1, 39.6, 39.6, 38.0, 36.8, 36.2, 35.8, 30.8, 30.1, 28.2, 28.1, 24.1, 23.9, 22.9, 22.7, 21.6, 18.8, 13.3, 12.1 (*18-C*). LRMS (ASAP) *m*/*z*: 402.365 ([M+]$^+$, 13%), 385.353 ([M-OH]$^+$, 100). HRMS (ASAP) *m*/*z*: calculated [M-H]$^+$ 402.3507, found 402.3498. IR (neat) ν_{max} (cm^{-1}); 3478 (s), 2935 (l), 2866 (l), 1707 (l), 1691 (l), 1467 (m), 1364 (m), 1064 (l), 964 (m), 639 (s). Data matched literature values.[293]

6.4.26. Synthesis of 3β-^{17}O-hydroxy-5α-cholestan-6-one, 82b

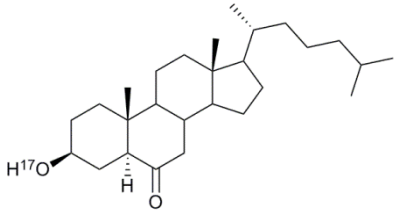

95b (0.16 g, 0.34 mmol, 1 eq.) was dissolved in 1,4-dioxane (5 mL) prior to the addition of HCl solution (1.67 M; 1.00 mL, 1.68 mmol, 5 eq.). The solution was stirred at room temperature for 5.5 hours. The solution was concentrated and dissolved in Et_2O (60 mL), which was then washed with H_2O (20 mL). The organic layer was dried using $MgSO_4$, filtered and concentrated. The crude white powder was purified by flash column chromatography (10 mm, eluent; hexane to hexane: EtOAc 1:1) to afford a white solid (0.10 g, 76%), identified as product (R_f 0.32, hexane: EtOAc 1:1). ^{1}H NMR (700 MHz) δ 3.59-3.53 (m, 1H, *3α-H*), 2.30 (dd, *J* = 13.3, 4.6, 1H, *7β-H*), 2.22-2.16 (m, 1H, *5-H*), 2.02 (dt, *J* = 12.7, 3.4 Hz, 1H), 1.97-1.90 (m, 1H, *7α-H*), 0.90 (d, *J* = 6.5, 3H, *21-H*), 0.85 (dd, *J* = 6.6, 3.2, 6H, *26-H* & *27-H*), 0.74 (s, 3H, *19-H*), 0.65 (s, 3H, *18-H*). ^{13}C NMR (176 MHz) δ 211.1 (*6-C*), 70.78 (*3-C*-^{16}OH), 70.77 (*3-C*-^{17}*OH*), 70.76 (*3-C*-^{18}*OH*), 56.9 (*5-C*), 56.3, 54.1, 46.9 (*7-C*), 43.1, 41.1, 39.6, 39.6, 38.1, 36.8, 36.2, 35.8, 30.8, 30.2, 28.2, 28.1, 24.1, 23.9, 22.9, 22.7 (*26-C* & *27-C*), 21.7, 18.8 (*21-C*), 13.3 (*19-C*), 12.2 (*18-C*). LRMS (ASAP) *m*/*z*: 405.363 ([^{18}O-M+H]$^+$, 100%), 404.361 ([^{17}O-M+H]$^+$, 91), 385.345 ([M-OH]$^+$, 29). HRMS (ASAP) *m*/*z*: calculated [M+H]$^+$ 404.3615, found 404.3618. IR (neat) ν_{max} (cm^{-1}); 3459 (s), 2935 (l), 2866 (l), 1691 (l), 1468 (m), 1368 (m), 1247 (s), 1219 (s), 1060 (l), 964 (m), 640 (s), 598 (m).

6.4.27. Synthesis of 3β-^{18}O-hydroxy-5α-cholestan-6-one, 82c

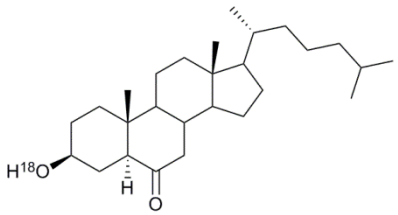

95c (0.09 g, 0.18 mmol, 1 eq.) was dissolved in 1,4-dioxane (5 mL) prior to the addition of HCl solution (1.67 M; 0.54 mL, 0.90 mmol, 5 eq.). The solution was stirred at room temperature for 16 hours. Other conditions were identical to those outlined in Section 6.4.26. A white solid (0.06 g, 75%), identified as product (R_f 0.32, hexane: EtOAc 1:1) was recovered. ^{1}H NMR (700 MHz) δ 3.60-3.51 (m, 1H, *3α-H*), 2.31 (dd, *J* = 13.3, 4.6, 1H, *7β-H*), 2.19 (dd, *J* = 12.5, 3.0, 1H, *5-H*), 2.03 (dt, *J* = 13.1, 3.5, 1H), 1.97-1.91 (m, 1H, *7α-H*), 0.90 (d, *J* = 6.5, 3H, *21-H*), 0.86 (dd, *J* = 6.6, 3.2, 6H, *26-H* & *27-H*), 0.74 (s, 3H, *19-H*), 0.65 (s, 3H, *18-H*). ^{13}C NMR (176 MHz) δ 211.1 (*6-C*), 70.80 (*3-C-^{16}OH)*, 70.79 (*3-C-^{16}OH)*, 56.9, 56.9 (*5-C*), 56.3, 54.1, 46.9 (*7-C*), 43.1, 41.1, 39.7, 39.6, 38.1, 36.8, 36.2, 35.8, 30.9, 30.8, 30.2, 28.2, 28.1, 24.1, 24.0, 22.9, 22.7 (*26-C* & *27-C*), 21.7, 18.8 (*21-C*), 13.3 (*19-C*), 12.2 (*18-C*). LRMS (ASAP) *m*/*z*: 405.356 ($[M+H]^+$, 100%), 404.359 ($[M]^+$, 10%), 385.341 ($[M-OH]^+$, 75). HRMS (ASAP) *m*/*z*: calculated $[M+H]^+$ 405.3619, found 405.3605. IR (DCM film) ν_{max} (cm^{-1}); 3473 (s), 2937 (l), 2866 (l), 1736 (m), 1708 (l), 1692 (l), 1471 (s), 1364 (m), 1215 (s), 1057 (m), 964 (s).

6.4.28. Synthesis of 3β-^{18}O-Hydroxy-5α-D-cholestan-6-one, 82d

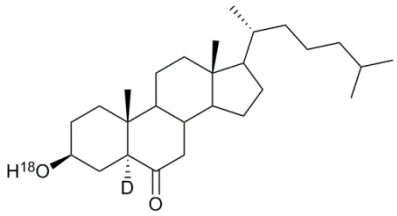

95d (0.13 g, 0.27 mmol, 1 eq.) was dissolved in 1,4-dioxane (5 mL) prior to the addition of HCl solution (1.67 M; 0.82 mL, 1.37 mmol, 5 eq.). The solution was stirred at room temperature for 5.5 hours. Other conditions were identical to those outlined in Section 6.4.26. A white solid (0.09 g, 79%), identified as product (R_f 0.32, hexane: EtOAc 1:1) was recovered. ^{1}H NMR (700 MHz) δ 3.59-3.50 (m, 1H, *3α-H*), 2.30 (dd, *J* = 13.2, 4.6, 1H, *7β-H*), 2.02 (dt, *J* = 12.8, 3.5, 1H), 1.93 (t, *J* = 12.8, 1H, 7α-H), 0.90 (d, *J* = 6.6, 3H, *21-H*), 0.85 (dd, *J* = 6.6, 3.2, 6H, *26-H* & *27-H*), 0.74 (s, 3H, *19-H*), 0.65 (s, 3H, *18-H*). ^{13}C NMR (176 MHz) δ 211.19 (*6-C-5-H*), 211.11 (*6-C-5-D)*, 70.74 (*3-C-^{16}OH*), 70.73 (*3-C-^{18}OH*), 56.9 (*5-C-H*), 56.4 (t, *J* = 18.1, 1H, *5-C-D*), 56.3, 54.1, 46.9 (*7-C*), 43.1, 41.0, 39.6, 38.1, 36.8, 36.2,

35.8, 30.8, 30.1, 28.2, 28.1, 24.1, 23.9, 22.9, 22.7 (*26-C* & *27-C*), 21.7, 18.8 (*21-C*), 13.3 (*19-C*), 12.1 (*18-C*). ^{2}H NMR (107 MHz) δ 2.19 (s, 1H, *5α-D*). LRMS (ASAP, 200 °C) *m*/*z*: 406.362 ($[M]^+$, 100%), 405.358 ($[M+H]^+$, 73), 386.352 ($[M-OH]^+$, 22). HRMS (ASAP, 200 °C) *m*/*z*: calculated $[M-H]^+$ 406.3681, found 406.3658. IR (DCM film) ν_{max} (cm^{-1}); 3464 (s), 2935 (l), 2871 (l), 1706 (m), 1692 (l), 1467 (M), 1374 (m), 1242 (s), 1054 (s), 1013 (s), 983 (m), 907 (s), 735 (l), 640 (s).

6.4.29. Synthesis of 3β-tosyl cholesterol, 96

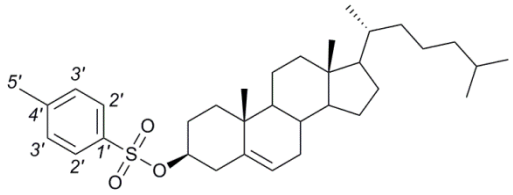

Cholesterol (1.50 g, 3.88 mmol, 1 eq.), TsCl (1.98 g, 10.37 mmol, 2.7 eq.) and anhydrous pyridine (2.00 mL, 23.27 mmol, 6 eq.) were stirred in anhydrous DCM (20 mL) under an argon atmosphere overnight. The solution was diluted with DCM (50 mL) and the organic phase was washed with 5% HCl solution (3 × 10 mL) followed by H_2O (2 × 10 mL). The organic layer was collected, dried ($MgSO_4$), filtered and concentrated *in vacuo* producing a crude white solid (2.77 g). A mixture containing TsCl and product (60.4% by mass, determined by the crude ^{1}H NMR) was obtained. The mixture was used in subsequent reactions as crude, although the material can be purified by careful recrystallisation from MeOH to produce a white powder (1.08, 49%). mp: 122-123 °C. ^{1}H NMR (700 MHz) δ 7.81-7.78 (m, 2H, *3'-H*), 7.34-7.31 (m, 2H, *2'-H*), 5.31-5.28 (m, 1H, *6-H*), 4.35-4.29 (m, 1H, *3α-H*), 2.44 (s, 3H, *5'-H*), 2.29-2.24 (m, 1H), 2.01-1.91 (m, 2H), 1.85-1.77 (m, 3H), 1.74-1.66 (m, 1H), 0.96 (s, 3H, *19-H*), 0.90 (d, *J* = 6.6 Hz, 3H, *21-H*), 0.86 (dd, *J* = 6.6, 3.3 Hz, 6H, *26-H* & *27-H*), 0.65 (s, 3H, *18-H*). ^{13}C NMR (176 MHz) δ 144.5 (*4'-C*), 139.0 (*5-C*), 134.9 (*1'-C*), 129.9 (*2'-C*), 127.8 (*3'-C*), 123.7 (*6-C*), 82.6 (*3-C*), 56.8, 56.3, 50.1, 42.5, 39.8, 39.7, 39.0, 37.1, 36.5, 36.3, 35.9, 32.0, 31.9, 28.8, 28.4, 28.2, 24.4, 24.0, 23.0, 22.7 (*26-C* & *27-C*), 21.8 (*7'-C*), 21.2, 19.3 (*19-C*), 18.9 (*21-C*), 12.0 (*18-C*). LRMS (ASAP) *m*/*z*: 737.696 (18%), 540.366 ($[M+H]^+$, 0.8), 369.334 ($[M-OTs]^+$, 100).

6.4.30. Synthesis of i-cholesterol *via* 3β-tosyl cholesterol, 87

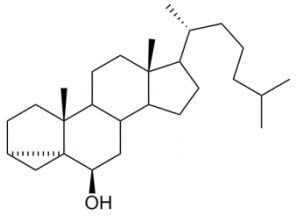

96 (0.61 g, 1.12 mmol, 1 eq.) and sodium bicarbonate (0.28 g, 3.36 mmol, 3 eq.) were refluxed in anhydrous MEK (15 mL) and H_2O (0.5 mL) for 16 hours. EtOAc (20 mL) and H_2O (10 mL) were added and the layers separated, the organic layer was washed with H_2O (10 mL). The organic layer was collected, dried ($MgSO_4$) and filtered to obtain a crude white powder (0.42 g) which was purified by flash column chromatography (30 mm, alumina, eluent; hexane to hexane :EtOAc 3:1 to 2:1) to obtain a white powder (0.30 g, 69%) identified as product (R_f 0.42, hexane: EtOAc 5:1). Characterisation data was identical to that displayed in Section 6.4.7.

6.4.31. Synthesis of 3,5-Cyclo-5*α*-cholestan-6-one, 97

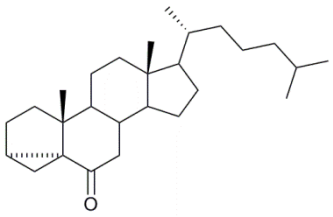

87 (0.65 g, 1.69 mmol, 1 eq.), PCC (0.55 g, 2.53 mmol, 1.5 eq.) and sodium acetate (0.42 g, 5.06 mmol, 3 eq.) were stirred in anhydrous DCM (10 mL) for 4.5 hours under an argon atmosphere. The crude mixture was passed through a short alumina plug (15 mm × 80 mm) using Et_2O (200 mL), the solution was concentrated followed by flash column chromatography (30 mm, alumina, eluent; hexane: EtOAc 10:1) to afford a white solid (0.52 g, 80%) identified as product (R_f 0.47, hexane: EtOAc 6:1). mp: 74-76 °C. ^{1}H NMR (700 MHz) δ 2.46-2.41 (m, 1H), 2.05 (dt, *J* = 12.7, 3.5, 1H), 1.96-1.82 (m, 4H), 1.79 (dd, *J* = 13.8, 8.1, 1H), 1.72-1.66 (m, 2H), 1.00 (s, 3H, *19-H*), 0.92 (d, *J* = 6.5, 3H, *21-H*), 0.87 (dd, *J* = 6.6, 3.1, 6H, *26-H* & *27-H*), 0.71 (d, *J* = 2.1, 4H, 18-H & *4α-H*).^{13}C NMR (176 MHz) δ 209.9 (*5-C*), 57.2, 56.3, 46.9, 46.5, 46.2, 45.0, 42.9, 39.9, 39.6, 36.3, 35.9, 35.4, 35.0, 33.6,

28.3, 28.2, 26.1, 24.2, 24.0, 23.0, 22.7 (*26-C* & *27-C*), 19.8 (*19-C*), 18.8 (*21-C*), 12.2 (*18-C*), 11.8 (*4-C*). LRMS (ASAP) *m*/*z*: 385.339 ($[M+H]^+$, 100%). HRMS (ASAP) *m*/*z*: calculated $[M-H]^+$ 385.3470, found 385.3473. IR (neat) ν_{max} (cm^{-1}); 2938 (m), 2864 (m), 1678 (l), 1467 (s), 1375 (m), 1297 (m), 1168 (s), 871 (s). Data matched literature values.[332]

6.4.32. Synthesis of 3β-tosyl-5α-cholestan-6α-ol, 98

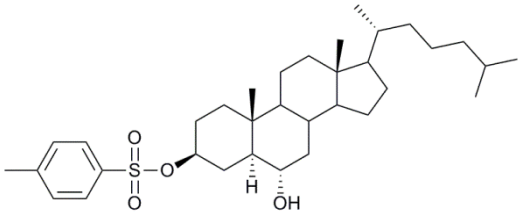

$BF_3.OEt_2$ (0.53 mL, 2.01 mmol, 2 eq.) was added to a suspension of $NaBH_4$ (0.11 g, 3.02 mmol, 3 eq.) in anhydrous THF (6 mL) at 0 °C under an argon atmosphere. The suspension was stirred for 30 minutes at 0 °C prior to the addition of 60.4% pure (by mass) **96** (0.90 g, 1.01 mmol, 1 eq.) in anhydrous THF (6.5 mL), the mixture was warmed to room temperature and stirred for a further 2 hours. The solution was cooled to 0 °C followed by the slow addition of 20% NaOH solution (1.50 mL, 7.50 mmol, 7.5 eq.) and 30% H_2O_2 solution (1.50 mL, 14.55 mmol, 14.5 eq.), the mixture was warmed to room temperature and stirred for a further 2 hours. The mixture was concentrated, followed by the addition of DCM (60 mL). The organic phase as washed with saturated NH_4Cl solution (2 × 20 mL), H_2O (2 × 20 mL) and brine (2 × 20 mL). The organic layer was collected, dried ($MgSO_4$), filtered and concentrated to afford a crude white solid (0.91 g). The crude material was purified using flash column chromatography (50 mm, eluent; hexane: EtOAc 9:1 to 5:1 to 4:1 to afford a white solid (0.43 g, 77%) identified as product (R_f 0.16, hexane: EtOAc 4:1). mp: 130-132 °C. ^{1}H NMR (400 MHz) δ 7.84-7.79 (m, 2H, *3'-H*), 7.39-7.31 (m, 2H, *2'-H*), 4.47-4.36 (m, 1H, *3α-H*), 3.42-3.34 (m, 1H, *6β-H*), 2.46 (s, 3H), 2.27-2.16 (m, 1H), 1.98 (dt, *J* = 12.3, 4.0, 2H), 0.91 (d, *J* = 6.5, 3H, *21-H*), 0.88 (dd, *J* = 6.6, 1.9, 6H, *26-H & 27-H*), 0.80 (s, 3H), 0.65 (s, 3H, *18-H*).^{13}C NMR (151 MHz) δ 144.5 (*4'-C*), 134.8 (*1'-C*), 129.9 (*3'-C*), 127.75.8 (*2'-C*), 82.6 (*3-C*), 69.3 (*6-C*), 56.3, 56.2, 53.7, 51.7, 42.7, 41.8, 39.8, 39.6, 37.2, 36.3, 36.2, 35.9, 34.4, 29.3, 28.4, 28.3, 28.2, 24.3, 23.9, 23.0, 22.7, 21.8, 21.2, 18.8,

13.4 (*19-C*), 12.2. LRMS (ASAP) *m*/*z*: 387.366 ([M-OTs]$^+$,13.6%), 369.351 ([M-OH-OTs]$^+$, 100). HRMS (ASAP) *m*/*z*: calculated [M]$^+$ 558.3743, found 588.3724. IR (neat) ν_{max} (cm^{-1}); 3555 (s), 2927 (m), 1599 (s), 1319 (m), 1188 (m), 1172 (l), 1096 (s), 918 (l), 900 (l), 869 (l), 813 (m), 697 (l), 575 (m), 551 (m). Data matched literature values.[293]

6.4.33. Synthesis of 3β-tosyl-5α-cholestan-6-one, 99

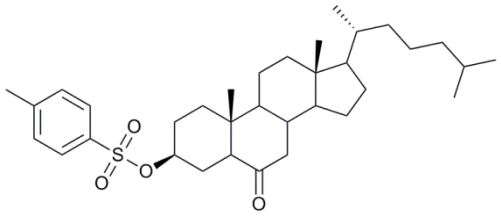

98 (0.33 g, 0.58 mmol, 1 eq.), sodium acetate (0.10 g, 1.20 mmol, 2 eq.) and PCC (0.19 g, 0.87 mmol, 1.5 eq.) were stirred for 5 hours in DCM (4 mL) at room temperature. The solution was concentrated to *ca*. 1 mL of DCM and purified directly by flash column chromatography (20 mm, eluent; hexane: EtOAc 9:1 to 4:1) yielding a white powder (0.25 g, 78%) identified as product (R_f 0.44, hexane: EtOAc 3:1). mp: 169-170 °C. ^{1}H NMR (400 MHz) δ 7.77 (d, *J* = 8.3, 2H, *2'-H*), 7.34-7.29 (d, *J* = 8.3, 2H, *3'-H*), 4.45-4.35 (m, 1H, *3α-H*), 2.43 (s, 3H, *5'-H*), 2.28 (dd, *J* = 13.2, 4.4, 1H), 2.13 (dd, *J* = 2.9, 12.4, 1H), 2.02 (dt, *J* = 12.9, 3.3, 1H), 0.90 (d, *J* = 6.5, 3H, *21-H*), 0.86 (dd, *J* = 6.6, 1.9, 6H, *26-H* & *27-H*), 0.72 (s, 3H, *19-H*), 0.64 (s, 3H, *18-H*).^{13}C NMR (101 MHz) δ 209.6 (*6-C*), 144.6 (*4'-C*), 134.7 (1'-C), 129.9 (*3'-C*), 127.7 (2'-C), 81.6 (*3-C*), 56.8, 56.5, 56.2, 53.8, 46.7, 43.1, 40.8, 39.6, 39.5, 38.0, 36.6, 36.2, 35.8, 28.2, 28.1, 27.0, 24.1, 23.9, 22.9, 22.7, 21.8, 21.6, 18.8, 13.1 (*19-C*), 12.1. LRMS (ASAP, 200 °C) *m*/*z*: 557.365 ([M+H]$^+$, 3%), 385.347 ([M-OTs]$^+$, 100%). HRMS (ASAP, 200 °C) *m*/*z*: calculated [M]$^+$ 557.3665, found 557.3655. IR (neat) ν_{max} (cm^{-1}); 2943 (m), 2868 (m), 1709 (l), 1597 (s), 1469 (s), 1350 (l), 1187 (l), 1170 (l), 1097 (m), 993 (s), 932 (l), 816 (l), 667 (l), 573 (l), 560 (l), 547 (l). Data matched literature values.[293]

Single crystals suitable for X-ray diffraction were obtained by slow evaporation from EtOAc. X-ray diffraction images of the single crystal (obtained as detailed in Section 6.1) revealed the structure shown in Figure 6.8 to constitute the unit cell.

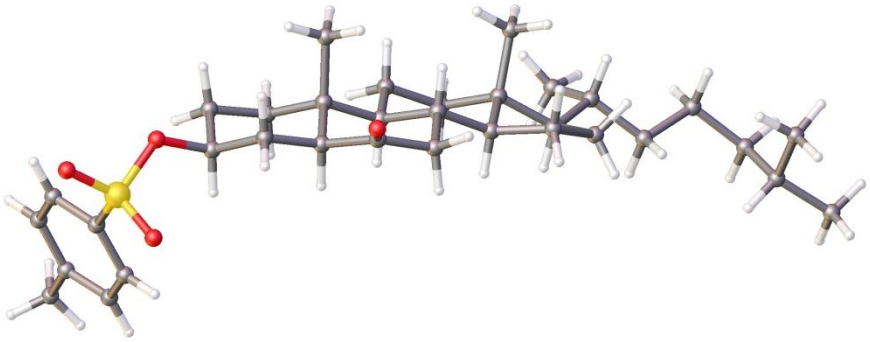

Figure 6.8. One structure from the unit cell of **99**, determined by X-ray diffraction of a single crystal.

6.4.34. Synthesis of 3β-Acetoxy-5,6-dibromo-5α-cholestane, 100

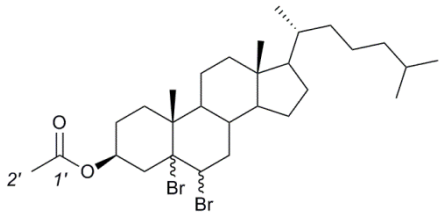

Bromine (0.11 mL, 2.06 mmol, 1.1 eq.) was added to a solution of cholesteryl acetate (0.80 g, 1.87 mmol, 1 eq.) in $CHCl_3$ (20 mL), and hand-shaken for 2 minutes. The reaction was quenched with saturated $Na_2S_2O_5$ solution (10 mL) and the layers were separated, the organic phase was washed further with saturated $Na_2S_2O_5$ solution (2 × 10 mL and H_2O (3 × 10 mL). The organic layer was collected, dried ($MgSO_4$), filtered and concentrated *in vacuo* to yield a crude yellow solid. The mixture was purified by flash column chromatography (50 mm, eluent; hexane to hexane: EtOAc 20:1 to 10:1) yielding a white solid (0.93 g, 85%) identified as mixed diastereomers (R_f 0.26 & 0.22, hexane: EtOAc 6:1)

The 5α, 6β-dibromo (kinetic) product can be isolated by recrystallisation from MeOH; EtOAc (R_f 0.26, 6:1 hexane: EtOAc)

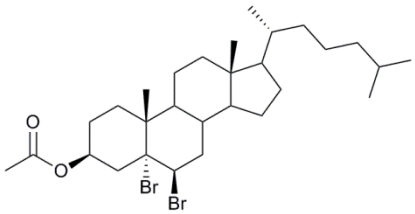

mp: 105-107 °C. ^{1}H NMR (400 MHz) δ 5.54-5.41 (m, 1H, *3α-H*), 4.85-4.81 (m, 1H, *6α-H*), 2.73-2.53 (m, 2H), 2.30-2.24 (m, 1H), 2.05 (s, 3H, *2'-H*), 1.55 (s, 1H), 1.46 (s, 3H, *19-H*), 0.91 (d, *J* = 6.5, 3H, *21-H*), 0.86 (dd, *J* = 6.7, 1.9, 6H, *26-H* & *27-H*), 0.70 (s, 3H, *18-H*).^{13}C NMR (101 MHz) δ 170.5(*1'-C*), 88.3 (*5-C*), 72.2 (*3-C*), 56.2 (*6-C*), 55.3, 47.4, 42.8, 42.1 (*4-C*), 42.0, 39.8, 39.7, 39.7, 37.4 (*7-C*), 36.6, 36.3, 35.9, 31.0, 28.3, 28.2, 26.3, 24.2, 24.0, 23.0 (*26-C* or *27-C*), 22.7 (*26-C* or *27-C*), 21.5, 21.4, 20.3 (*19-C*), 18.8 (*21-C*), 12.3 (*18-C*). LRMS (ASAP) m/z (%): 385.358 ([M-COMe-Br_2]$^+$, 36%), 367.341 ([M-OAc-Br_2]$^+$, 100). IR (neat) ν_{max} (cm^{-1}); 2946 (m), 2868 (m), 1734 (l), 1467 (s), 1433 (s), 1377 (m), 1366 (m), 1257 (l), 1237 (l), 1210 (s), 1162 (s), 1031 (m), 912 (s), 605 (s). Data matched literature values.[297]

Single crystals suitable for X-ray diffraction were obtained by slow vapour diffusion of MeOH and toluene. X-ray diffraction images of the single crystal (obtained as detailed in Section 6.1) revealed the structure shown in Figure 6.9 to constitute the unit cell.

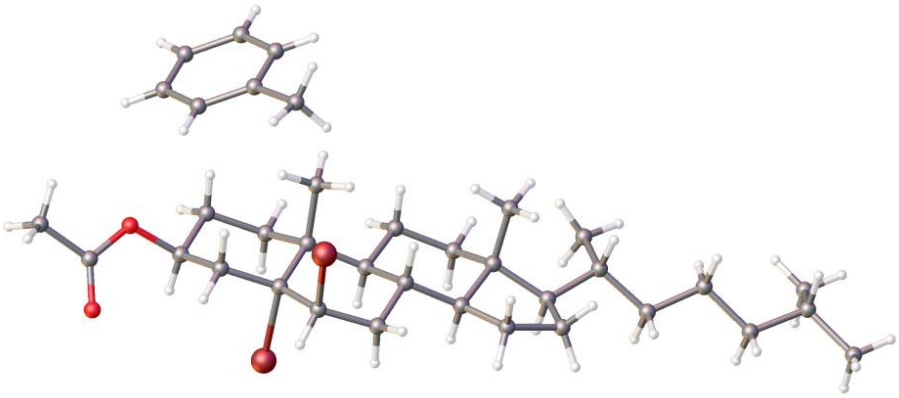

Figure 6.9. Structure from the unit cell of **100**, determined by X-ray diffraction of a single crystal.

6.4.35. Synthesis of 25-hydroxy-3β-acetoxy-5,6β-dibromo-5α-cholestane, 101

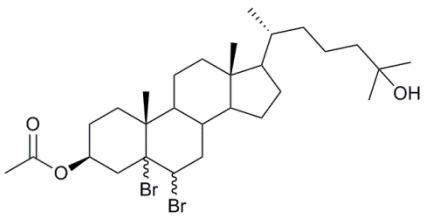

A 2 neck flask fitted with a dry ice/ acetone condenser was cooled to 0 °C. The flask was charged with $NaHCO_3$ (3.00 g) and H_2O (70 mL), followed by the addition of Oxone (Sigma-Aldrich; 4.86 g, 15.82 mmol, 10 eq.) portion-wise (a neutral pH solution was obtained). **100** (0.93 g, 1.58 mmol, 1 eq.) in DCM (20 mL) was added, followed by TFP (4.30 mL, 47.46 mmol, 30 eq.). The solution was then brought to pH 7.5-8.5 by adding $NaHCO_3$ (*ca*. 40 g) portion-wise using a solid addition funnel cooled to -20 °C. The mixture was vigorously stirred for 7 hours. Additional DCM (100 mL) and H_2O (50 mL) was added and the layers separated, the aqueous layer was extracted with DCM (3 × 30 mL). The combined organic layers were dried ($MgSO_4$), filtered and concentrated to obtain a white solid (1.36 g). The procedure was repeated with the same amounts, although the mixture was only stirred for an additional 3 hours. After work-up a crude white solid was obtained which was purified by flash column chromatography (50 mm, eluent; hexane to hexane: EtOAc 9:1 to 4:1 to 1:1) yielding a white solid (0.37 g, 39%) identified as the kinetic (R_f 0.27, hexane: EtOAc 3:1) and thermodynamic product (R_f 0.23, hexane: EtOAc 3:1).

A small amount of 5α-6β diastereomer (kinetic bromination product) was isolated.

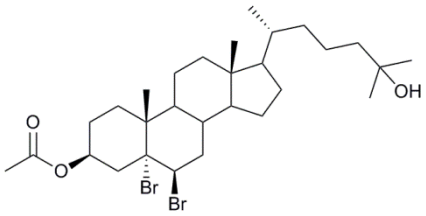

^{1}H NMR (400 MHz) δ 5.55-5.45 (m, 1H, *3α-H*), 4.85 (dd, *J* = 4.3, 2.0, 1H, *6α-H*), 2.74-2.57 (m, 2H), 2.35-2.23 (m, 1H), 2.07 (s, 3H, *2'-H*), 1.48 (s, 3H, *19-H*), 1.23 (s, 6H, *25-H* & *26-H*), 0.95 (d, *J* = 6.5, 3H, *21-H*), 0.92-0.84 (m, 1H, *24-H*), 0.73 (s, 3H, *18-H*).^{13}C NMR (101 MHz) δ 170.5 (*1'-C*), 88.2 (*5-C*), 72.2 (*3-C*), 71.2 (*25-C*), 56.2, 56.2, 55.3, 47.4, 44.5, 42.8, 42.1(*4-C*), 42.0, 39.7, 37.3, 36.6, 36.5, 35.9, 31.0, 29.5 (*26-C* or *27-C*), 29.4 (*26-C* or *27-C*), 28.3, 26.3, 24.2, 21.5, 21.4, 20.9, 20.3 (*19-C*), 18.8 (*21-C*), 12.3 (*18-C*). LRMS (ASAP) m/z (%): 527.170 ($[M-Br]^+$, 100%), 445.248 ($[M-Br_2]^+$, 21), 383.331 ($[M-OAc]^+$, 34), 365.322 (100). IR (neat) ν_{max} (cm^{-1}); 3276 (s), 2942 (m), 2868 (m), 1733 (l), 1470 (s),

1433 (s), 1366 (m), 1258 (l), 1162 (m), 1031 (m), 911 (m), 558 (m), 560 (m). Data matched literature values.[297]

6.4.36. Synthesis of 25-hydroxy-3β-acetoxycholesterol, 102

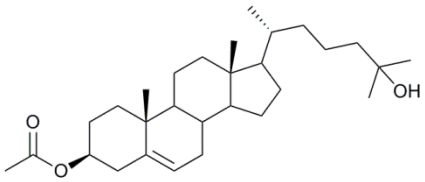

101 (0.33 g, 0.55 mmol, 1 eq.), Zn dust (0.33 g) and AcOH (0.16 mL) were stirred in Et_2O (8 mL) for 1 hour at room temperature. The suspension was filtered using Et_2O (30 mL), the organic phase was washed with saturated $NaHCO_3$ solution (2 × 10 mL), H_2O (2 × 10 mL) and brine (10 mL). The organic layer was dried ($MgSO_4$), filtered and concentrated to yield a white solid (0.20 g, 83%) which was used without subsequent purification. ^{1}H NMR (400 MHz) δ 5.39-5.31 (m, *6-H*), 4.68-4.50 (m, 1H, *3α-H*), 2.36-2.26 (m, 2H), 2.02 (s, 3H, *2'-H*), 1.89-1.76 (m, 3H), 1.20 (s, 6H, *26-H* & *27-H*), 1.01 (s, 3H, *19-H*), 0.92 (d, *J* = 6.5, 3H, *21-H*), 0.67 (s, 3H, *18-H*). ^{13}C NMR (101 MHz) δ 170.6 (*1'-C*), 139.8 (*5-C*), 122.7 (*6-C*), 74.1 (*3-C*), 71.2 (*25-C*), 56.8, 56.2, 50.1, 44.6, 42.5, 39.8, 38.2, 37.1, 36.7, 36.6, 35.9, 32.0, 29.5 (*26-C* or *27-C*), 29.3 (*26-C* or *27-C*), 28.4, 27.9, 24.4, 21.6, 21.1, 20.9, 19.4 (*19-C*), 18.8 (*21-C*), 12.0 (*18-C*). LRMS (ASAP) m/z (%): 427.371 ($[M\text{-}OH]^+$, 8%), 385.350 ($[M\text{-}OAc]^+$, 9), 367.366 ($[M\text{-}OH\text{-}OAc]^+$, 100). IR (neat) ν_{max} (cm^{-1}); 3478 (s), 3317 (s), 2941 (m), 1729 (l), 1465 (s), 1375 (m), 1239 (l), 1153 (s), 1035 (l), 940 (s), 912 (s), 801 (s), 615 (s). Data matched literature values.[297]

Single crystals suitable for X-ray diffraction were obtained by slow evaporation from EtOAc. X-ray diffraction images of the single crystal (obtained as detailed in Section 6.1) revealed the structure shown in Figure 6.10 to constitute the unit cell.

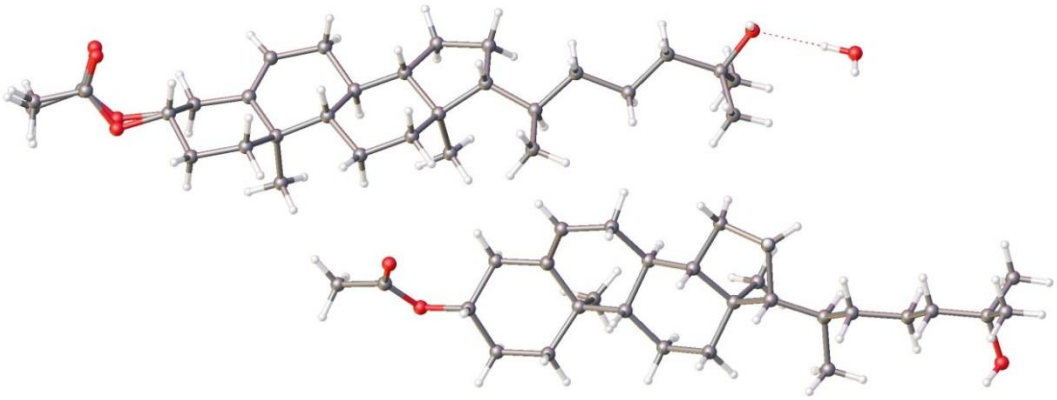

Figure 6.10. Structures from the unit cell of **102**, determined by X-ray diffraction of a single crystal.

6.4.37. Synthesis of 25-hydroxycholesterol, 83a

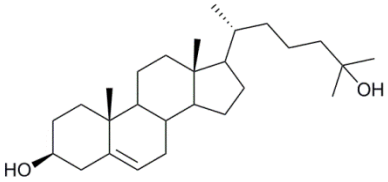

102 (0.20 g, 0.46 mmol, 1 eq.) was refluxed in 5% KOH in MeOH solution (20 mL) for 1 hour. The solution was concentrated *in vacuo* and the residue was dissolved in $CHCl_3$ (50 mL). The solution was washed with H_2O (2 × 10 mL). The organic layer was dried ($MgSO_4$), filtered and concentrated *in vacuo* to yield a white powder (0.18 g, 96%) which was used in subsequent steps without purification. ^{1}H NMR (400 MHz) δ 5.38-5.32 (m, 1H, *6-H*), 3.59-3.46 (m, 1H, *3α-H*), 2.33-2.18 (m, 2H), 2.05-1.92 (m, 2H), 1.89-1.76 (m, 3H), 1.21 (s, 6H, *26-H* & *27-H*), 1.00 (s, 3H, *19-H*), 0.93 (d, *J* = 6.6, 3H, *21-H*), 0.68 (s, 3H, *18-H*).^{13}C NMR (101 MHz) δ 140.9 (*5-C*), 121.8 (*6-C*), 71.9 (*3-C*), 71.3 (*25-C*), 56.9, 56.2, 50.3, 44.6, 42.5, 42.4, 39.9, 37.4, 36.6, 35.9, 32.0, 31.8, 29.5, 29.3 (*26-C* & *27-C*), 28.4, 24.4, 21.2, 20.9, 19.5 (*19-C)*, 18.8 (*21-C*), 12.0 (*18-C*). LRMS (ASAP) m/z: 402.351 ($[M]^+$, 0.6%), 385.348 ($[M\text{-}OH]^+$, 51), 367.344 ($[M\text{-}(OH)_2]^+$, 100). IR (neat) ν_{max} (cm^{-1}); 3276 (s), 2933 (l), 1472 (l), 1377 (s), 1153 (m), 1054 (m), 955 (m), 914 (m). Data matched literature values.[297]

6.4.38. Synthesis of 3,5-Cyclo-6β-methoxycholestan-6β, 25-diol, 103

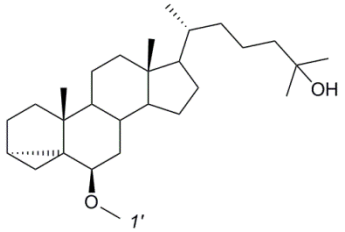

83a (0.18 g, 0.44 mmol, 1 eq.) and TsCl (0.42 g, 2.20 mmol, 5 eq.) were dissolved in anhydrous DCM (10 mL), anhydrous pyridine (0.71 mL, 8.80 mmol, 20 eq.) was then added the mixture which was stirred for 16 hours under an argon atmosphere. The solution was diluted with DCM (50 mL) which was then washed with 1 M HCl solution (2 × 10 mL), H_2O (2 × 10 mL) and brine (10 mL). The organic layer was dried ($MgSO_4$), filtered and concentrated *in vacuo* to yield a white solid (0.31 g). The solid was determined to be 72% pure (by mass from ^{1}H NMR) with the remaining 28% being TsCl. The crude material was used without subsequent purification. mp: 141-145 °C. ^{1}H NMR (400 MHz) δ 5.35-5.27 (m, 1H, *5-H*), 4.39-4.26 (m, 1H, *3α-H*), 2.46 (s, 3H, *4'-H*), 2.28 (m, 1H), 2.04-1.91 (m, 2H), 1.23 (s, 6H, *26-H* & *27-H*), 0.98 (s, 3H, *19-H*), 0.93 (d, *J* = 6.5, 3H, *21-H*), 0.67 (s, 3H, *18-H*).

The crude material (0.44 mmol, 1 eq.) and $NaHCO_3$ (0.19 g, 2.20 mmol, 5 eq.) were refluxed in MeOH (20 mL) for 5 hours. The mixture was concentrated *in vacuo*, $CHCl_3$ (50 mL) and H_2O (20 mL) were added, the aqueous layer was extracted with $CHCl_3$ (20 mL). The combined organic layers were dried ($MgSO_4$), filtered and concentrated *in vacuo* yielding a solid which was unable to be resolved by column chromatography (0.13 g). The fractions were determined to be 65% pure by mass (^{1}H NMR, the remainder was determined to be 3β-methoxy-25-hydroxycholesterol). ^{1}H NMR (400 MHz) δ 3.34 (s, 3H, *1'-H*), 2.79 (t, *J* = 2.9, 1H, 6α-H), 1.23 (s, 6H, *25-H* & *26-H*), 0.73 (s, 3H, *18-H*), 0.67 (dd, *J* = 5.0, 3.8, 1H, *4β-H*), 0.45 (dd, *J* = 8.0, 5.0, 1H, *4α-H*). The remaining signals could not be resolved and reported with confidence. LRMS (ASAP) m/z: 417.379 ($[M+H]^+$, 9%), 399.379 ($[M-OH]^+$, 9),

385.348 ([M-OMe]$^+$, 7), 367.327 ([M-OH-OMe]$^+$, 100). HRMS (ASAP) *m/z*: calculated [M]$^+$ 416.3654, found 416.3669.

6.4.39. Synthesis of 25-hydroxycholestan-3β-^{17}O-ol, 83b

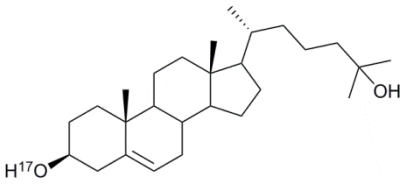

65% pure (by mass) **103** (0.057 g, 0.090 mmol, 1 eq.) was dissolved in anhydrous 1,4-dioxane (3 mL). A solution of triflic acid in anhydrous 1,4-dioxane (11.30 mM; 0.40 mL, 4.5 × 10^{-3} mmol, 0.05 eq.) and $^{17}OH_2$ (0.009 mL, 0.450 mmol, 5 eq.) were added to the solution which was stirred for 5 hours at room temperature under an argon atmosphere. The mixture was concentrated *in vacuo*, $CHCl_3$ (50 mL) was added to the mixture which was subsequently washed with H_2O (2 × 10 mL) and brine (10 mL). The organic layer was collected, dried with $MgSO_4$, filtered and concentrated *in vacuo* to yield a crude solid (0.073 g) which was purified by flash column chromatography (10 mm, alumina, eluent; hexane: EtOAc 10:1 to 5:1 to 3:1 to 2:1) yielding a white powder (0.026 g, 72%) identified as product (R_f 0.10, hexane: EtOAc 3:1).^{1}H NMR (700 MHz) δ 5.37-5.31 (m, 1H, *6-H*), 3.54-3.47 (m, 1H, *3α-H*), 2.32-2.20 (m, 2H), 2.03-1.94 (m, 2H), 1.85-1.78 (m, 3H), 1.21 (s, 6H, *26-H* & *27-H*), 1.00 (s, 3H, *19-H*), 0.93 (d, *J* = 6.6, 4H, *21-H*), 0.68 (s, 3H, *18-H*).^{13}C NMR (176 MHz) δ 140.92 (*5-C)*, 121.83 (*6-C*), 71.95 (*3-C-*^{16}*OH*), 71.94 (*3-C-*^{17}*OH*), 71.92 (*3-C-*^{18}*OH*), 71.3 (*25-C*), 56.9, 56.2, 50.3, 44.6, 42.5, 39.9, 37.4, 36.7, 36.6, 35.9, 32.1, 31.8, 29.5, 29.4 (*26-C* & *27-C*), 28.4, 24.4, 21.2, 20.9, 19.6 (19-C), 18.8 (*21-C*), 12.0 (*18-C*). LRMS (ASAP) m/z: 403.351 ([M]$^+$, 0.7%), 386.350 ([M-^{16}OH]$^+$, 21), 367.337 ([M-OH-OH_2]$^+$, 100%). HRMS (ASAP) *m/z*: calculated [M]$^+$ 403.3500, found 403.3540.

6.4.40. Synthesis of 25-hydroxycholestan-3β-^{18}O-ol, 83c

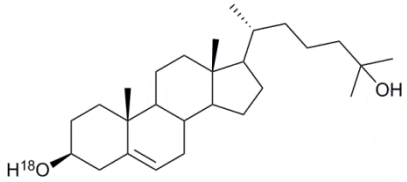

65% pure (by mass) **103** (0.070 g, 0.109 mmol, 1 eq.) was dissolved in anhydrous 1,4-dioxane (3 mL). A solution of triflic acid in anhydrous 1,4-dioxane (11.30 mM; 0.49 mL, 5.46×10^{-3} mmol, 0.05 eq.) and $^{18}OH_2$ (0.011 mL, 0.545 mmol, 5 eq.) were added to the mixture which was stirred for 5 hours at room temperature under an argon atmosphere. The remaining conditions are identical to those outlined in Section 6.4.39. A white powder (0.028 g, 63%) identified as product (R_f 0.10, 3:1 hexane: EtOAc). ^{1}H NMR (700 MHz) δ 5.36-5.32 (m, 1H, *6-H*), 3.54-3.47 (m, 1H, *3α-H*), 2.33-2.18 (m, 2H), 2.04-1.91 (m, 1H), 1.87-1.76 (m, 3H), 1.21 (s, 6H, *26-H* & *27-H*), 1.00 (s, 3H, *19-H*), 0.93 (d, *J* = 6.6, 3H, *21-H*), 0.68 (s, 3H, *18-H*).^{13}C NMR (176 MHz) δ 140.9 (*5-C*), 121.8 (*6-C*), 71.93 (3-*C*-^{16}OH*)*, 71.90 (3-*C*-^{18}OH*)*, 71.3 (*25-C*), 56.9, 56.2, 50.3, 44.6, 42.5, 42.4, 39.9, 37.4, 36.6, 36.6, 35.9, 32.0, 31.8, 29.5, 29.3 (*26-C* & *27-C*), 28.4, 24.4, 21.2, 20.9, 19.5 (19-C), 18.8 (*21-C*), 12.0 (*18-C*). LRMS (ASAP) m/z: 404.355 ($[M]^+$, 1%), 387.351 ($[M-^{16}OH]^+$, 33), 367.336 ($[M-(OH)_2]^+$, 100). HRMS (ASAP) *m/z*: calculated $[M]^+$ 404.3540, found 404.3546. IR (neat) ν_{max} (cm^{-1}); 3288 (m), 2936 (l), 1467 (s), 1442 (s), 1363 (m), 1205 (s), 1191 (s), 1037 (m), 950 (m), 800 (m), 738 (s).

6.4.41. Synthesis of 5α-cholestan-3-one ethylene ketal, 105

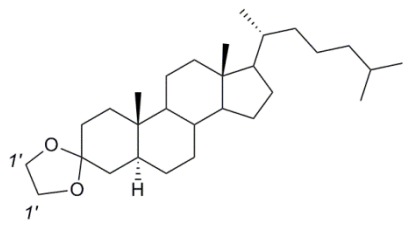

5α-Cholestan-3-one (0.50 g, 1.29 mmol, 1 eq.) and 3 Å M.S (0.20 g) were added to a round bottom flask fitted with a reflux condenser under an argon atmosphere. The flask was charged with anhydrous toluene (15 mL) followed by the addition of ethylene glycol (0.72

mL, 12.93 mmol, 10 eq.) and TsOH (0.07 g, 0.39 mmol, 0.3 eq.). The mixture was refluxed for 16 hours. The mixture was allowed to cool to room temperature and diluted with DCM (50 mL) which was subsequently filtered to remove the molecular sieves. The organic layer was washed with H_2O (2 × 10 mL) and brine (10 mL). The organic layer was then dried ($MgSO_4$), filtered and concentrated *in vacuo* to yield a white solid (0.49 g, 89%). The crude product was used without subsequent purification. mp: 98-100 °C. ^{1}H NMR (700 MHz) δ 3.95-3.88 (m, 4H, *1'-H*), 1.94 (dt, *J* = 12.7, 3.5, 1H), 1.79 (m, 1H), 1.68-1.45 (m, 8H), 0.88 (d, *J* = 6.6, 4H, *19-H*), 0.85 (dd, *J* = 6.6, 3.3, 6H, *26-H* & *27-H*), 0.79 (s, 3H, *21-H*), 0.70 (m, 1H), 0.63 (s, 3H, *18-H*). ^{13}C NMR (176 MHz) δ 109.4 (*3-C*), 64.1 (*1'-C)*, 56.5, 56.2, 54.0, 43.7, 42.6, 40.0, 39.5, 38.0, 36.2, 36.0, 35.8, 35.5, 35.4, 31.9, 31.1, 28.6, 28.2, 28.0, 24.2, 23.8, 22.8 (*26-C* or *27-C*), 22.5 (*26-C* or *27-C*), 21.2, 18.6(*19-C*), 12.1 (*18-C*), 11.4 (*21-C*). LRMS (ASAP) *m*/*z*: 432.390 (58%), 431.406 ($[M+H]^+$, 100%), 387.387 ($[M-(CH_2)_2O]^+$, 6). HRMS (ASAP) *m*/*z*: calculated $[M+H]^+$ 431.3889, found 431.3906. IR (neat) ν_{max} (cm^{-1}); 2930 (l), 2868 (l), 1470 (m), 1443 (m), 1375 (m), 1138 (m), 1093 (l), 1071 (l), 931 (m), 685 (s).

Single crystals suitable for X-ray diffraction were obtained by slow evaporation from EtOAc. X-ray diffraction images of the single crystal (obtained as detailed in Section 6.1) allowed elucidation of the unit cell, the structure shown in Figure 6.11 shows one molecule of the unit cell.

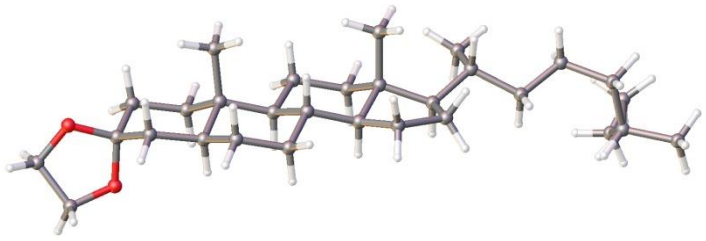

Figure 6.11. One structure from the unit cell of **105**, determined by X-ray diffraction of a single crystal.

6.4.42. Synthesis of 5α-cholestan-3β-^{17}O-ol, 106b by Route A (Scheme 4.10)

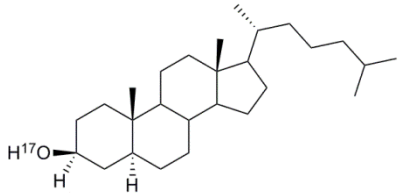

5α-cholestan-3-one (0.030 g, 0.078 mmol, 1 eq.) was dissolved in anhydrous 1,4-dioxane (1 mL) a in Schlenk round bottom flask under an argon atmosphere. A solution of triflic acid in anhydrous 1,4-dioxane (111.89 mM; 0.035 mL, 3.92×10^{-3} mmol, 0.05 eq.) and $^{17}OH_2$ (0.015 mL, 0.780 mmol, 10 eq.) were added sequentially to the flask, the solution was stirred for 10 minutes. Under positive argon flow, $NaBH_4$ (0.015 g, 0.390 mmol, 5 eq.) was added and the suspension was stirred for 1 hour. The solution was concentrated in *vacuo* followed by the addition of Et_2O (40 mL). The organic layer was washed with H_2O (2 × 10 mL) and brine (10 mL). The organic layer was dried ($MgSO_4$), filtered and concentrated *in vacuo*, the crude material was purified by flash column chromatography (10 mm, eluent; hexane to hexane: EtOAc 10:1 to 6:1) producing a white solid (0.026 g, 84%) identified as product (R_f 0.26, hexane: EtOAc 3:1). ^{1}H NMR (700 MHz) δ 3.61-3.55 (m, 1H, *3α-H*), 1.96 (m, 1H), 1.80 (m, 2H), 1.70 (dt, *J* = 13.3, 3.6, 1H), 1.67-1.63 (m, 1H), 0.89 (d, *J* = 6.6, 3H, *21-H*), 0.86 (dd, *J* = 6.6, 3.2, 7H, *26-H* & *27-H*), 0.80 (d, *J* = 0.7, 3H, *19-H*), 0.67-0.58 (m, 4H, *18-H*, & *5-H*). ^{13}C NMR (176 MHz) δ 71.53 (3-*C*-^{16}OH), 71.52 (3-*C*-^{17}OH), 71.51 (3-*C*-^{18}OH), 56.7, 56.5, 45.0, 42.8, 40.2, 39.7, 38.4, 37.2, 36.3, 34.0, 35.7, 35.6, 32.3, 31.7, 28.9, 28.4, 28.2, 24.4, 24.0, 23.0 (*26-C* & *27-C*), 22.7 (*26-C* & *27-C*), 21.4, 18.8 (*21-C*), 12.5 (*19-C*), 12.2 (*18-C*). LRMS (ASAP) *m*/*z*: 389.372 ($[M+H]^+$, 13%), 371.357 ($[M-OH]^+$, 100%). HRMS (ASAP) *m*/*z*: calculated $[M+H]^+$ 389.3747, found 389.3723. IR (neat) ν_{max} (cm^{-1}); 3350 (s), 2929 (l), 2852 (l), 1467 (m), 1374 (m), 1137 (s), 1077 (s), 1033 (l), 1071 (l), 932 (s).

6.4.43. Synthesis of 5α-cholestan-3β-^{17}O-D-ol, 106c by Route A (Scheme 4.10)

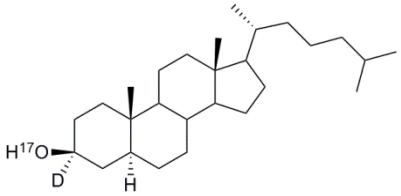

5α-cholestan-3-one (0.031 g, 0.080 mmol, 1 eq.) was dissolved in anhydrous 1,4-dioxane (1 mL) a in Schlenk round bottom flask under an argon atmosphere. A solution of triflic acid in anhydrous 1,4-dioxane (111.89 mM; 0.035 mL, 3.92×10^{-3} mmol, 0.04 eq.) and $^{17}OH_2$ (0.015 mL, 0.780 mmol, 10 eq.) were added sequentially to the flask, the solution was stirred for 10 minutes. Under positive argon flow, $NaBD_4$ (0.016 g, 0.390 mmol, 5 eq.) was added and the suspension was stirred for 1 hour. The other conditions were the same as detailed in Section 6.4.42. A white solid was obtained (0.027 g, 84%) identified as product (R_f 0.26, hexane: EtOAc 3:1). ^{1}H NMR (700 MHz) δ 1.98-1.94 (m, 1H), 1.80 (m, 2H), 1.73-1.69 (m, 1H), 1.65 (dq, *J* = 12.9, 3.1, 1H), 0.89 (d, *J* = 6.6, 3H, *21-H*), 0.86 (dd, *J* = 6.6, 3.2, 6H, *26-H* & *27-H*), 0.80 (d, *J* = 0.7, 3H, *19-H*), 0.64 (s, 3H, *18-H*), 0.61 (m, 1H). ^{13}C NMR (176 MHz) δ 71.19-70.87 (m, *3-C-D*), 56.7, 56.5, 54.5, 45.0, 42.8, 40.2, 39.7, 38.3, 37.2, 36.3, 36.0, 35.7, 35.6, 32.3, 31.6, 28.9, 28.4, 28.2, 24.4, 24.0, 23.0 (*26-C* & *27-C*), 22.7 (*26-C* & *27-C*), 21.4, 18.8 (*21-C*), 12.5 (*19-C*), 12.2 (*18-C*). D NMR (92 MHz) δ 3.58 (s, 1H, *3α-D*). LRMS (ASAP) *m*/*z*: 390.379 ([M]$^+$, 5%), 372.364 ([M-OH]$^+$, 100). HRMS (ASAP) *m*/*z*: calculated [M]$^+$ 390.3810, found 390.3796. IR (neat) ν_{max} (cm^{-1}); 3345 (s), 2929 (l), 2851 (l), 1467 (m), 1366 (s), 1135 (m), 1088 (m), 1058 (m), 932 (m), 635 (s).

6.4.44. Synthesis of 5α-cholestan-3β-^{18}O-ol, 106d by Route A (Scheme 4.10)

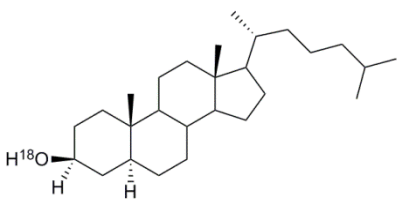

5α-cholestan-3-one (0.030 g, 0.078 mmol, 1 eq.) was dissolved in anhydrous 1,4-dioxane (1 mL) a in Schlenk round bottom flask under an argon atmosphere. A solution of

triflic acid in anhydrous 1,4-dioxane (111.89 mM; 0.035 mL, 3.92×10^{-3} mmol, 0.04 eq.) and $^{18}OH_2$ (0.016 mL, 0.780 mmol, 10 eq.) were added sequentially to the flask, the solution was stirred for 10 minutes. Under positive argon flow, $NaBH_4$ (0.015 g, 0.390 mmol, 5 eq.) was added and the suspension was stirred for 1 hour. The other conditions were the same as detailed in Section 6.4.42. A white solid (0.025 g, 81%) was obtained identified as product (R_f 0.26, hexane: EtOAc 3:1).^{1}H NMR (700 MHz) δ 3.62-3.54 (m, 1H, *3α-H*), 1.98-1.93 (m, 1H), 1.80 (m, 2H), 1.70 (m, 1H), 1.65 (dq, *J* = 12.9, 3.5, 1H), 0.89 (d, *J* = 6.6, 3H, *19-H*), 0.86 (dd, *J* = 6.6, 3.2, 7H, *26-H* & *27-H*), 0.80 (s, 3H, *21-H*), 0.64 (s, 3H, *18-H*), 0.63-0.59 (m, 1H). ^{13}C NMR (176 MHz) δ 71.54 (3-*C*-^{16}OH), 71.51 (3-*C*-^{18}OH), 56.7, 56.5, 54.5, 45.0, 42.8, 40.2, 39.7, 38.4, 37.2, 36.3, 36.0, 35.7, 35.6, 32.3, 31.7, 28.9, 28.4, 28.2, 24.4, 24.0, 23.0, 22.7(*26-C & 27-C)*, 21.4, 18.8 (*21-C)*, 12.5(*19-C)*, 12.2(*18-C*). LRMS (ASAP) *m*/*z*: 390.375 ($[M]^+$, 6%), 371.357 ($[M\text{-}OH]^+$, 100). HRMS (ASAP) *m*/*z*: calculated $[M]^+$ 390.3748, found 390.3750. IR (neat) ν_{max} (cm^{-1}); 3313 (s), 2929 (l), 2865 (l), 1467 (m), 1374 (m), 1138 (m), 1093 (l), 1071 (l), 931 (m), 685 (s).

6.4.45. Synthesis of 5α-cholestan-3β-^{18}O-D-ol, 106e by Route A (Scheme 4.10)

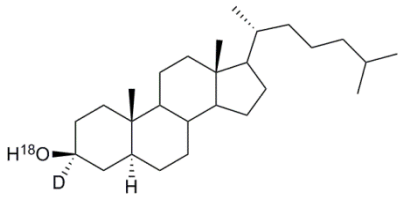

5α-cholestan-3-one (0.030 g, 0.078 mmol, 1 eq.) was dissolved in anhydrous 1,4-dioxane (1 mL) a in Schlenk round bottom flask under an argon atmosphere. A solution of triflic acid in anhydrous 1,4-dioxane (111.89 mM; 0.035 mL, 3.92×10^{-3} mmol, 0.04 eq.) and $^{18}OH_2$ (0.016 mL, 0.780 mmol, 10 eq.) were added sequentially to the flask, the solution was stirred for 10 minutes. Under positive argon flow, $NaBD_4$ (0.016 g, 0.39 mmol, 5 eq.) was added and the suspension was stirred for 1 hour. The other conditions were the same as detailed in Section 6.4.42. A white solid (0.025 g, 81%) was obtained identified as product (R_f 0.26, hexane: EtOAc 3:1). ^{1}H NMR (700 MHz) δ 1.98-1.93 (m, 1H), 1.80 (m, 2H), 1.72-1.68 (m, 1H), 1.65 (dq, *J* = 12.9, 3.1, 1H), 0.89 (d, *J* = 6.6, 3H, *21-H*), 0.86 (dd, *J* = 6.6, 3.2,

6H, *26-H* & *27-H*), 0.80 (s, 3H, *19-H*), 0.64 (s, 3H, *18-H*), 0.61 (m, 1H). ^{13}C NMR (176 MHz) δ 71.17 (3-*C*-^{16}OH), 71.16 (3-*C*-^{17}OH), 71.14 (3-*C*-^{18}OH), 71.04 (3-*C*-^{16}OH), 71.03 (3-*C*-^{17}OH), 71.02 (3-*C*-^{18}OH), 70.93 (3-*C*-^{16}OH), 70.91 (3-*C*-^{17}OH), 70.90 (3-*C*-^{18}OH), 56.7, 56.5, 45.0, 42.8, 40.2, 39.7, 38.3, 37.2, 36.3, 36.0, 35.7, 35.6, 32.3, 31.6, 28.9, 28.4, 28.2, 24.4, 24.0, 23.0, 22.7 (*26-C* & *27-C*), 21.4, 18.8 (*21-C*), 12.5 (*19-C*), 12.2 (*18-C*). D NMR (92 MHz) δ 3.58 (s, 1H, *3α-D*). LRMS (ASAP) *m*/*z*: 391.383 ([M]$^+$, 3%), 372.364 ([M-OH]$^+$, 100). HRMS (ASAP) *m*/*z*: calculated [M]$^+$ 391.3810, found 390.3805. IR (neat) ν_{max} (cm^{-1}); 3290 (s), 2928 (l), 2851 (l), 1467 (m), 1384 (s), 1135 (m), 1087 (m), 1056 (m), 931 (m), 685 (s).

6.4.46. Synthesis of 5α-cholestan-3β-ol, 106a by Route B (Scheme 4.10)

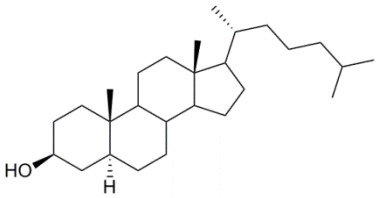

Compound **105** (0.070 g, 0.163 mmol, 1 eq.) was dissolved in anhydrous 1,4-dioxane (1.3 mL) under an argon atmosphere. To the solution, H_2O (0.015 mL, 0.833 mmol, 5 eq.) and a solution of HCl in anhydrous 1,4-dioxane (78.40 mM; 0.63 mL, 0.05 mmol, 0.3 eq.) were added sequentially and the solution was stirred for 6 hours. $NaBH_4$ (0.052 g, 1.370 mmol, 8.4 eq.) was added to the solution which was stirred for a further 16 hours. The mixture was concentrated *in vacuo*, followed by the addition of Et_2O (40 mL). The organic phase was washed twice with H_2O (2 × 10 mL) and brine (10 mL). The organic phase was dried ($MgSO_4$), filtered and concentrated *in vacuo* to yield a white solid which was purified by flash column chromatography (20 mm, eluent; hexane to hexane: EtOAc 10:1 to 6:1 to 3:1) producing 5α-cholestan-3α-ol (0.005 g, 7%) and the desired 5α-cholestan-3β-ol (0.028 g, 44%).

3α-OH epimer: ^{1}H NMR (400 MHz) δ 4.06-4.02 (m, 1H, *3β-H*), 2.01-1.93 (m, 2H), 1.87-1.76 (m, 1H), 0.90 (d, *J* = 6.5, 3H, *19-H*), 0.86 (dd, *J* = 6.6, 1.9, 6H, *26-H* & *27-H*),

0.77 (s, 3H, *21-H*), 0.65 (s, 3H, *18-H*). LRMS (ASAP) *m*/*z*: 388.372 ([M+H]$^+$, 6%), 387.387 (([M]$^+$, 6), 371.369 ([M-OH]$^+$, 100). HRMS (ASAP) *m*/*z*: calculated [M+H]$^+$ 388.3705, found 388.3702.

3β-OH epimer: ^{1}H NMR (700 MHz) δ 3.67-3.52 (m, 1H, *3α-H*), 1.95 (dt, *J* = 12.7, 3.5, 1H), 1.84-1.78 (m, 1H), 1.67 (ddt, *J* = 37.8, 12.9, 3.6, 2H), 0.88 (d, *J* = 6.5, 3H, *19-H*), 0.85 (dd, *J* = 6.6, 3.2, 7H, *26-H* & *27-H*), 0.79 (s, 3H, *21-H*), 0.63 (s, 3H, *18-H*), 0.61 (m, 1H). ^{13}C NMR (176 MHz) δ 71.53 (3-*C*-^{16}OH), 71.50 (3-*C*-^{18}OH), 56.7, 56.4, 54.5, 45.0, 42.8, 40.2, 39.7, 38.4, 37.2, 36.3, 35.9, 35.7, 35.6, 32.2, 31.7, 28.9, 28.4, 28.2, 24.4, 24.0, 23.0, 22.7 (*26-C & 27-C)*, 21.4, 18.8 (*21-C)*, 12.5 (*21-C*), 12.2 (*18-C)*. LRMS (ASAP) *m*/*z*: 388.373 ([M+H]$^+$, 9%), 371.358 ([M-OH]$^+$, 100). HRMS (ASAP) *m*/*z*: calculated [M+H]$^+$ 388.3705, found 388.3702. The analytical data matched an authentic standard.

6.4.47. Synthesis of lanosterol acetate, 112 and dihydrolanosterol acetate, 113

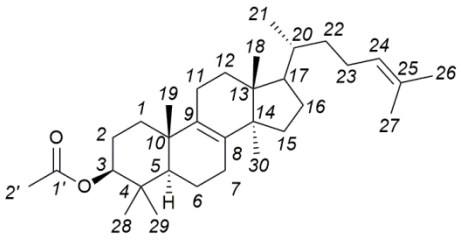

112

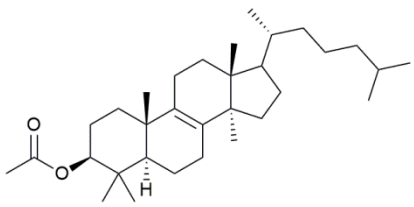

113

Technical grade lanosterol (2.13 g, 5.00 mmol, 1 eq.), DMAP (0.04 g, 0.35 mmol, 0.1 eq.) and Ac_2O (0.71 mL, 7.50 mmol, 1.5 eq.) were stirred in anhydrous pyridine (3.20 mL, 40.00 mmol, 8 eq.) and anhydrous DCM (18 mL) for 3 hours. $CHCl_3$ (110 mL) was added and washed with 5% HCl solution (2 × 20 mL), saturated $NaHCO_3$ solution (2 × 20 mL) and H_2O (20 mL). The organic layer was dried ($MgSO_4$), filtered and concentrated *in vacuo* to yield a yellow solid (2.17 g) which was purified by flash column chromatography (50 mm, eluent; 12:1 hexane: EtOAc) yielding a white solid (1.67 g, 71%) identified as a mixture of **110**:**111** 64:36 determined by ^{1}H NMR (R_f 0.21, 12:1 hexane: EtOAc). ^{1}H NMR (400 MHz) δ 5.12 (t, *J* = 7.2, 0.6 H, *24-H*), 4.52 (dd, *J* = 11.6, 4.6, 1H, *3α-H*), 2.07 (s, 3H, *2'-C*), 1.71 (d, *J* = 1.4, 4H), 1.63 (d, *J* = 1.1, 3H), 1.03 (s, 4H), 0.96-0.83 (m, 20H), 0.71 (s,

4H). LRMS (ASAP) m/z: 470.413 ([By-product-M]$^+$, 12%), 468.417 ([M]$^+$, 18), 411.393 ([By-product-OAc]$^+$, 61), 409.399 ([M-OAc]$^+$, 100).

6.4.48. Synthesis of 3β-acetoxy-5α-lanostan-24, 25-diol, 114

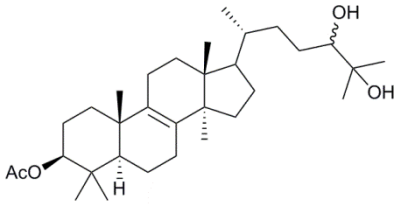

The mixture of **112** and **113** (1.67 g, 3.56 mmol, 1 eq.) was dissolved in acetone (100 mL) and H_2O (1.70 mL), 50% hypophosphorous acid solution (0.78 mL, 7.13 mmol, 2 eq.) and NBS (0.83 g, 4.63 mmol, 1.3 eq.) were added. The mixture was sonicated to aid solvation and stirred for 15 minutes at room temperature. $NaHCO_3$ (0.82 g, 9.77 mmol, 2.7 eq.) was added and concentrated *in vacuo*. Isopropyl alcohol (45 mL), H_2O (15 mL), 50% hypophosphorous acid solution (1.90 mL, 17.36 mmol, 4.9 eq.) and $NaHCO_3$ (1.28 g, 15.25 mmol, 4.3 eq.) were added and refluxed for 4 hours. The solution was cooled and concentrated *in vacuo* to remove isopropyl alcohol, $CHCl_3$ (100 mL) and H_2O (30 mL). The aqueous layer was extracted with $CHCl_3$ (3 × 30 mL). The combined organic layers were dried ($MgSO_4$), filtered and concentrated *in vacuo* to yield a crude white solid (1.84 g). The crude was purified by flash column chromatography (50 mm, eluent: hexane: EtOAc 10:1 to 7:1 to 5:1 to 1:1) to yield a white solid (0.58 g, 48%) identified as product (R_f 0.36, hexane: EtOAc 1:1). The R: S ratio was determined to 1:1.06. ^{1}H NMR (400 MHz) δ 4.48 (dd, *J* = 11.5, 4.6, 1H, *3α-H*), 3.37-3.30 (m, 0.48 H, *R*-24-H), 3.27 (dd, *J* = 10.1, 2.0, 0.51 H, *S-24-H*), 2.04 (s, 3H, *2'-H*), 1.20 (s, 3H), 1.15 (d, *J* = 0.9, 4H), 0.99 (s, 3H), 0.90 (dd, *J* = 6.3, 3.5, 3H), 0.86 (d, *J* = 2.5, 8H), 0.68 (d, *J* = 2.1, 3H). ^{13}C NMR (101 MHz) δ 171.2, 134.6, 134.4, 81.1, 79.7, 78.9, 73.33, 73.28, 50.7, 50.6, 50.5, 49.9, 49.9, 44.6, 44.6, 37.9, 37.0, 36.9, 36.4, 35.4, 33.7, 33.2, 31.1, 30.9, 28.8, 28.5, 28.4, 28.3, 28.0, 26.7, 26.6, 26.5, 24.4, 24.3, 23.4, 23.3, 21.5, 21.1, 19.3, 19.0, 18.7, 18.2, 16.7, 15.9. LRMS (ASAP) m/z: 502.415 ([M]$^+$, 28%), 485.410 ([M-OH]$^+$, 87), 433.401 ([M-OAc]$^+$, 100). HRMS (ASAP) *m/z*: calculated [M]$^+$ 502.4022, found 502.4004. IR (neat) ν_{max} (cm^{-1}); 3585 (s), 2950 (s), 1720 (m), 1496 (s),

1453 (m), 1366 (m), 1258 (m), 1208 (s), 1134 (m), 1070 (l), 1026 (l), 914 (m), 740 (m), 695 (l), 641 (s), 592 (s), 476 (s). Data matched literature values.[319]

6.4.49. Synthesis of pure lanosterol acetate, 112

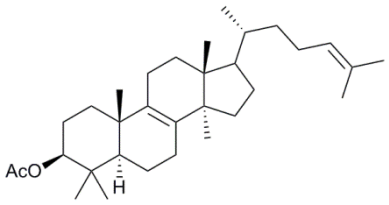

114 (0.58 g, 1.15 mmol, 1 eq.) and dimethylformamide dimethyl acetate (0.76 mL, 5.74 mmol, 5 eq.) were refluxed in DCM (5 mL) for 2.5 hours. The solution was cooled to room temperature and Ac_2O (1.00 mL) was added, the mixture was concentrated *in vacuo.* Additional Ac_2O (5 mL) was added to the solution which was refluxed for an additional 3 hours at 130 °C. Upon cooling $CHCl_3$ (100 mL) and H_2O (50 mL) was added to the solution, the layers were separated and the aqueous layer was extracted with $CHCl_3$ (2 × 20 mL), the combined organic layers were combined and washed by saturated $NaHCO_3$ solution (20 mL) then H_2O (10 mL). The organic layers were dried ($MgSO_4$), filtered and concentrated *in vacuo* to yield a brown solid (0.48 g). The solid was purified by flash column chromatography (20 mm, eluent; hexane: DCM 2:1) to yield a white solid (0.39 g, 73%) identified as product (R_f 0.66, hexane: DCM 2:1). ^{1}H NMR (700 MHz) δ 5.12-5.07 (m, *J* = 8.5, 5.6, 1.4, 1H, *24-H*), 4.50 (dd, *J* = 11.8, 4.5, 1H, *3α-H*), 2.04 (s, 3H, *2'-H*), 1.70-1.64 (m, 3H, *27-H*), 1.62-1.59 (m, 3H, *26-H*), 1.19-1.11 (m, 2H), 1.00 (s, 3H, *19-H*), 0.91 (d, *J* = 6.5, 3H, *21-H*), 0.87 (dd, *J* = 7.3, 1.5, 9H, *28-H*, *29-H* & *30-H*), 0.71-0.67 (m, 3H, *18-H*). ^{13}C NMR (176 MHz) δ 171.1 (*1'-C*), 134.6 (*8-C*), 134.3 (*9-C*), 131.0 (*25-C*), 125.4 (*24-C*), 81.1 (*3-C*), 50.7, 50.5, 49.9, 44.6, 37.9 (*4-C*), 37.0, 36.5, 36.4, 35.4, 31.1, 31.0, 28.3, 28.1 (*28-C*), 26.5, 25.9 (*C-27*), 25.1, 24.4, 24.3 (*30-C*), 21.5, 21.1 (*2'-C*), 19.3 (*19-C*), 18.8 (*21-C*), 18.3, 17.8 (*26-C*), 16.7 (*29-C*), 15.9 (*18-C*). LRMS (ASAP) m/z: 468.413 ($[M]^+$, 29%), 409.389 ($[M\text{-}OAc]^+$, 100). HRMS (ASAP) *m/z*: calculated $[M]^+$ 468.3967, found 468.3943. IR (neat) ν_{max} (cm^{-1}); 2953 (m), 1733 (l), 1454 (s), 1366 (m), 1244 (l), 1027 (m), 982 (m). Data was consistent with literature values.[319]

Single crystals suitable for X-ray diffraction were obtained by slow evaporation from EtOAc: EtOH. X-ray diffraction images of the single crystal (obtained as detailed in Section 6.1) revealed the structure shown in Figure 6.12 to constitute the unit cell.

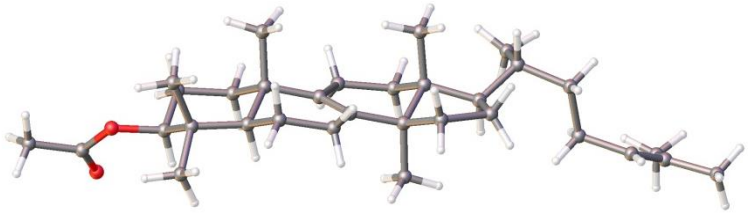

Figure 6.12. One structure from the unit cell of **112**, determined by X-ray diffraction of a single crystal.

6.4.50. Synthesis of lanosterol, 84a

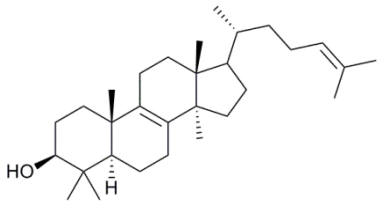

Compound **112** (0.39 g, 0.85 mmol, 1 eq.) and KOH (0.39 g) were stirred at 65 °C in EtOH (20 mL) for 2 hours. The mixture was concentrated *in vacuo*. $CHCl_3$ (100 mL) and H_2O (30 mL) were added to the solid and the layers separated, the aqueous layer was further extracted with $CHCl_3$ (3 × 30 mL). The combined organic layers were dried ($MgSO_4$) filtered and concentrated *in vacuo* to yield a white solid (0.34 g, 93%). The recovered crude was determined to have high purity and was used in subsequent reactions without further purification. ^{1}H NMR (700 MHz) δ 5.12-5.07 (m, 1H, *24-H*), 3.23 (dd, *J* = 11.8, 4.4, 1H, *3α-H*), 2.08-1.97 (m, 5H), 1.95-1.90 (m, 1H), 1.89-1.83 (m, 1H), 1.76-1.70 (m, 2H), 1.71-1.64 (m, 5H, *27-H*), 1.60 (s, 4H, *26-H*), 1.07-1.03 (m, 2H), 1.00 (s, 3H, *19-H*), 0.98 (s, 3H, *30-H*), 0.91 (d, *J* = 6.4, 3H, *21-H*), 0.87 (s, 3H, *28-H* or *29-H*), 0.81 (s, 3H, *28-H* or *29-H*), 0.69 (s, 3H, *18-H*). ^{13}C NMR (176 MHz) δ 134.6 (*8-C*), 134.5 (*9-C*), 131.0 (*25-C*), 125.4 (*24-C*), 79.1 (*3-C*), 50.6, 50.0, 44.6, 39.0 (*4-C*), 37.2, 36.5, 36.4, 35.8, 31.2, 31.0, 28.4, 28.1, 28.0 (*19-C*), 27.1, 26.7, 25.9 (*27-C*), 25.2, 25.1, 24.4 (*28-C* or *29-C)*, 21.2, 19.3 (*30-C*), 18.8 (*21-*

C), 18.4, 17.8 (*26-C*), 15.9 (18-C), 15.6 (*28-C* or *29-C)*. LRMS (ASAP) m/z: 427.394 ($[M+H]^+$, 63%), 409.374 ($[M-OH]^+$, 100). HRMS (ASAP) *m/z*: calculated $[M+H]^+$ 427.3940, found 427.3951. IR (neat) ν_{max} (cm^{-1}); 3290 (s), 2943 (l), 1448 (m), 1371 (l), 1099 (s), 1028 (l), 825 (s). Data matched literature values.[319]

6.4.51. Synthesis of Lanosterone, 108

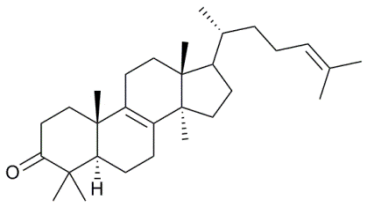

Anhydrous DCM (10 mL), and anhydrous DMSO (0.22 mL, 3.04 mmol, 3 eq.) were cooled to -78 °C under an argon atmosphere for 10 minutes. Oxalyl chloride (0.13 mL, 1.52 mmol, 1.5 eq.) was added to the solution which was stirred for 10 minutes. Still at -78 °C, **84a** (0.43 g, 1.02 mmol, 1 eq.) in anhydrous DCM (5 mL) was added to the solution and stirred for 30 minutes. Anhydrous trimethylamine (0. 71 mL, 5.08 mmol, 5 eq.) was added to the mixture and stirred for 10 minutes further. The solution was allowed to warm followed by concentration *in vacuo*. The solid was dissolved in Et_2O (50 mL) which was washed with sat. NH_4Cl solution (10 mL) and H_2O (3 × 10 mL), the organic layer was dried ($MgSO_4$), filtered and concentrated *in vacuo* to produce a crude waxy solid (0.50 g) which was purified by flash column chromatography (20 mm, eluent; hexane: EtOAc 14:1) producing a white solid (0.36 g, 83%) identified as product (R_f 0.53, hexane: EtOAc 6: 1). ^{1}H NMR (700 MHz) δ 5.12-5.07 (m, 1H, *24-H*), 2.61-2.54 (m, 1H), 2.43-2.37 (m, 1H), 1.68 (d, *J* = 1.5, 3H, 27-H), 1.64-1.58 (m, 9H, *26-H*), 1.11 (s, 3H, *19-H*), 1.09 (s, 3H, *29-H*), 1.06 (s, 3H, *28-H*), 0.91 (d, *J* = 6.5, 3H, *21-H*), 0.88 (d, *J* = 1.0, 3H, *30-H*), 0.71 (s, 3H, (*18-H*). ^{13}C NMR (176 MHz) δ 218.0 (*3-C*), 135.5 (*9-C*), 133.3 (*8-C*), 131.1 (*25-C*), 125.3 (*24-C*), 51.4, 50.5, 50.1, 47.5, 44.6, 37.1, 36.5, 36.4, 36.2, 34.8, 31.1, 28.3, 26.5, 26.3 (*28-C*), 25.9 (*27-C*), 25.1, 24.4 (*30-C*), 21.4, 21.2 (*29-C*), 19.6, 18.8 (*19-C*), 18.7 (*21-C)*, 17.8 (*26-C*), 16.0 (*18-C*). LRMS (ASAP) m/z: 425.375 ($[M+H]^+$, 100%). HRMS (ASAP) *m/z*: calculated $[M+H]^+$ 425.3783,

found 425.3778. IR (neat) ν_{max} (cm^{-1}); 2944 (l), 2875 (l), 1709 (l), 1452 (m), 1372 (l), 1113 (s), 1028 (m), 826 (s). Data matched literature values.[333]

6.4.52. Synthesis of ^{17}O-lanosterol, 84b and ^{17}O-epi lanosterol, 110b

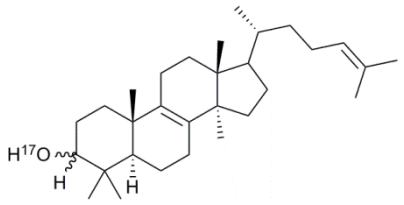

106 (0.119 g, 0.280 mmol, 1 eq.) and a solution of triflic acid in anhydrous 1,4-dioxane (111.89 mM; 0.13 mL, 0.01 mmol, 0.05 eq.) were diluted in anhydrous 1,4-dioxane (3.60 mL). $^{17}OH_2$ (0.054 mL, 2.80 mmol, 10 eq.) was added to the solution and stirred under an argon atmosphere for 2 hours. The solution was transferred to a flask fitted with a reflux condenser containing $NaBH_4$ (0.053 g, 1.401 mmol, 5 eq.), the suspension was refluxed for 17 hours at 120 °C. The solution was allowed to cool, concentrated *in vacuo* and partitioned with DCM (50 mL) and H_2O (10 mL). The layers were separated and washed further by H_2O (2 × 10 mL) and brine (10 mL). The organic layer was collected, dried ($MgSO_4$), filtered and concentrated *in vacuo*. The crude solid was purified by flash column chromatography (20 mm, hexane to hexane: EtOAc 20:1 to 15:1 to 10:1). A white solid was first isolated (0.011 g, 10%) identified as **110b** by-product (R_f 0.30, hexane: EtOAc 6:1). Further elution with the solvent gradient returned a white solid (0.087 g, 73%) identified as the desired **84b** (R_f 0.27, hexane: EtOAc 6:1).

3α-OH epimer, **110b**; ^{1}H NMR (700 MHz) δ 5.13-5.05 (m, 1H, *24-H*), 3.44-3.41 (m, 1H, *3β-H*), 2.09-1.97 (m, 5H), 1.68 (d, *J* = 1.4, 3H, *27-H*), 1.60 (d, *J* = 1.3, 3H, *26-H*), 0.99 (s, 3H, *19-H*), 0.97 (s, 3H, *28-H* or *29-H*), 0.91 (d, *J* = 6.5, 3H, *21-H*), 0.88-0.87 (m, 6H, *28-H* or *29-H & 30-H*), 0.69 (s, 3H, *18-H*). ^{13}C NMR (176 MHz) δ 134.8 (*8-C*), 134.3 (*9-C*), 131.0 (*25-C*), 125.43 (*24-C*), 76.22 (3-*C*-^{16}OH), 76.21 (3-*C*-^{17}OH), 76.19 (3-*C*-^{18}OH), 50.5, 50.0, 44.6, 44.4, 37.8 (*4-C*), 37.1, 36.5, 36.4, 31.2, 31.0, 30.3, 28.4, 28.2 (*28-C* or *29-C*), 26.2, 25.9 (*27-C*), 25.1, 22.4 (*28-C* or *29-C*), 21.1 (*30-C)*, 19.1, 18.8 (*21-C*), 18.3 (*21-C*),

17.8 (*26-C*), 15.9 (*18-C*). LRMS (ASAP) *m*/*z*: 427.394 ([^{17}O-M]$^+$, 27%), 409.380 ([M-H_2O]$^+$, 100), 393.354 ([M-H_2O-Me]$^+$, 14). HRMS (ASAP) *m*/*z*: calculated [M]$^+$ 427.3904, found 427.3936. IR (neat) ν_{max} (cm^{-1}); 3379 (s), 2942 (l), 2876 (l), 1454 (m), 1371 (l), 1063 (m), 976 (m), 959 (m), 817 (s).

3β-OH epimer, **84b**; ^{1}H NMR (700 MHz) δ 5.12-5.07 (m, 1H, *24-H*), 3.23 (dd, *J* = 11.8, 4.4, 1H, *3α-H*), 2.06-1.98 (m, 5H), 1.96-1.83 (m, 2H), 1.68 (s, 3H, *27-H*), 1.60 (s, 3H, *26-H*), 1.00 (s, 3H, *28-H* or *29-H*), 0.98 (s, 3H, *19-H*), 0.91 (d, *J* = 6.4, 3H, 21-H), 0.87 (s, 3H, *30-H*), 0.81 (s, 3H, *28-H* or *29-H*), 0.68 (s, 3H, *18-H*). ^{13}C NMR (176 MHz) δ 134.6 (*8-C*), 134.5 (*9-C*), 131.0 (*25-C*), 125.4 (*24-C*), 79.13 (3-*C*-^{16}OH), 79.11 (3-*C*-^{17}OH), 79.10 (3-*C*-^{18}OH), 50.6 (*5-C*), 50.0, 44.6, 39.0 (*4-C*), 37.2, 36.5, 36.4, 35.8, 31.2, 31.0, 28.4, 28.1, 28.0 (*28-C* or *29-C*), 26.7, 25.9 (*27-C*), 25.1, 24.4 (*30-C)*, 21.2, 19.3 (*19-C*), 18.8 (*21-C*), 18.4, 17.8 (*26-C*), 15.9 (*18-C*), 15.6 (*28-C* or *29-C)*. LRMS (ASAP) *m*/*z*: 427.392 ([^{17}O-M]$^+$, 33%), 409.374 ([M-H_2O]$^+$, 100), 393.353 ([M-H_2O-Me]$^+$, 16). HRMS (ASAP) *m*/*z*: calculated [M]$^+$ 427.3904, found 427.3924. IR (neat) ν_{max} (cm^{-1}); 3236 (s), 2943 (l), 2874 (l), 1450 (m), 1372 (l), 1021 (l), 1001 (m), 931 (s).

6.4.53. Synthesis of ^{18}O-lanosterol, 84c and ^{18}O-epi lanosterol, 110c

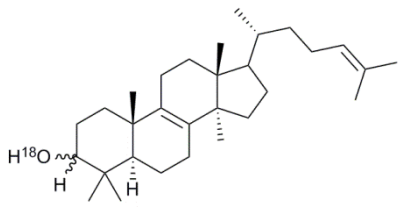

108 (0.107 g, 0.251 mmol, 1 eq.) and a solution of triflic acid in anhydrous 1,4-dioxane (111.89 mM; 0.11 mL, 0.01 mmol, 0.05 eq.) were diluted in anhydrous 1,4-dioxane (3.60 mL). $^{18}OH_2$ (0.051 mL, 2.52 mmol, 10 eq.) was added to the solution and stirred under an argon atmosphere for 2 hours. The solution was transferred to a flask fitted with a reflux condenser containing $NaBH_4$ (0.048 g, 1.26 mmol, 5 eq.), the suspension was refluxed for 17 hours at 120 °C. The reminder of the procedure was the same as that described in Section 6.4.52. A white solid was first isolated (0.013 g, 12%) identified as **110c** by-product (R_f

0.30, hexane: EtOAc 6:1). Further elution with the solvent gradient returned a white solid (0.068 g, 63%) identified as the desired **84c** (R_f 0.27, hexane: EtOAc 6:1).

3α-OH epimer, **110c**; ^{1}H NMR (700 MHz) δ 5.13-5.06 (m, 1H, *24-H*), 3.42 (t, *J* = 2.9, 1H, *3β-H*), 2.10-1.96 (m, 5H), 1.68 (s, 3H, *27-H*), 1.60 (s, 3H, *26-H*), 0.99 (s, 3H, *19-H*), 0.97 (s, 3H, *28-H* or *29-H*), 0.91 (d, *J* = 6.5, 3H, *21-H*), 0.88-0.87 (m, 6H, *28-H* or *29-H* & *30-H*), 0.69 (s, 3H, 18-H). ^{13}C NMR (176 MHz) δ 134.8 (*8-C*), 134.3 (*9-C*), 131.0 (*25-C*), 125.4 (*24-C*), 76.22 (3-*C*-^{16}OH), 76.19 (3-*C*-^{18}OH), 50.5, 50.0, 44.6, 44.4, 37.8 (*4-C*), 37.1, 36.5, 36.4, 31.2, 31.0, 30.3, 28.4, 28.2 (*28-C or 29-C*), 26.2, 25.9 (*27-C*), 25.1, 24.4 (*28-C or 29-C*), 21.1 (*30-C*), 19.1, 18.8 (*19-C*), 18.3 (*21-C*), 17.8 (*26-C*), 15.9 (*18-C*). LRMS (ASAP) m/z: 428.397 ($[M]^+$, 19%), 409.372 ($[M-H_2O]^+$, 100), 393.354 ($[M-H_2O-Me]^+$, 18). HRMS (ASAP) *m*/*z*: calculated $[M+H]^+$ 429.3982, found 429.3989. IR (neat) ν_{max} (cm^{-1}); 3391 (s), 2943 (l), 2873 (l), 1454 (m), 1371 (l), 1042 (s), 975 (m), 960 (m).

3β-OH epimer, **84c**; ^{1}H NMR (700 MHz) δ 5.13-5.07 (m, 1H, *24-H*), 3.23 (dd, *J* = 11.8, 4.4, 1H, *3α-H*), 2.08-1.97 (m, 5H), 1.68 (d, *J* = 1.4, 3H, *27-H*), 1.60 (d, *J* = 1.3, 3H, *26-H*), 1.08-1.04 (m, 2H), 1.00 (s, 3H, *28-H* or *29-H*), 0.98 (s, 3H, *19-H*), 0.91 (d, *J* = 6.5, 3H, *21-H*), 0.87 (d, *J* = 1.1, 3H, *30-H*), 0.81 (s, 3H, *28-H* or *29-H*), 0.69 (s, 3H, *18-H*). ^{13}C NMR (176 MHz) δ 134.6 (*8-C*), 134.5 (*9-C*), 131.0 (*25-C*), 125.4 (*24-C*), 79.13 (3-*C*-^{16}OH), 79.10 (3-*C*-^{18}OH), 50.6 (*5-C*), 50.0, 44.6, 39.0 (*4-C*), 37.2, 36.5, 36.4, 35.8, 31.2, 31.0, 28.4, 28.1, 28.0 (*28-C* or *29-C*), 26.7, 25.9 (*27-C*), 25.1, 24.4 (*30-C)*, 21.2, 19.3 (*19-C)*, 18.8 (*21-C*), 18.4, 17.8 (*26-C*), 15.9 (*18-C*), 15.6 (*28-C* or *29-C)*. LRMS (ASAP) m/z: 428.394 ($[M]^+$, 22%), 409.363 ($[M-H_2O]^+$, 100), 393.352 ($[M-H_2O-Me]^+$, 17). HRMS (ASAP) *m*/*z*: calculated $[M+H]^+$ 429.3982, found 429.3994. IR (neat) ν_{max} (cm^{-1}); 3239 (s), 2944 (l), 2873 (l), 1450 (m), 1372 (l), 1018 (l), 1001 (m), 933 (s).

6.4.54. Synthesis of ^{18}O-D-lanosterol, 84d and ^{18}O-D-epi lanosterol, 110d

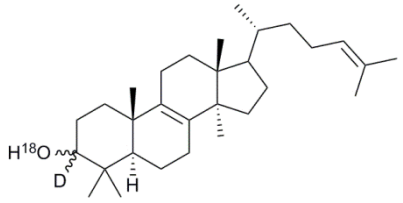

108 (0.118 g, 0.278 mmol, 1 eq.) and a solution of triflic acid in anhydrous 1,4-dioxane (111.89 mM; 0.13 mL, 0.01 mmol, 0.05 eq.) were diluted in anhydrous 1,4-dioxane (3.60 mL). $^{18}OH_2$ (0.055 mL, 2.780 mmol, 10 eq.) was added to the solution and stirred under an argon atmosphere for 2 hours. The solution was transferred to a flask fitted with a reflux condenser containing $NaBD_4$ (0.058 g, 1.390 mmol, 5 eq.), the suspension was refluxed for 17 hours at 120 °C. The reminder of the procedure was the same as that described in Section 6.4.52. A white solid was first isolated (0.021 g, 17%) identified as the *3α-OH* epimer by-product (**110d**) (R_f 0.30, hexane: EtOAc 6:1). Further elution with the solvent gradient returned a white solid (0.085 g, 71%) identified as the desired *3β-OH* epimer product (**84d**) (R_f 0.27, hexane: EtOAc 6:1).

3α-OH epimer, **110d**; ^{1}H NMR (700 MHz) δ 5.12-5.07 (m, 1H, *24-H*), 2.09-1.97 (m, 5H), 1.96-1.88 (m, 2H), 1.68 (s, 3H, *27-H*), 1.60 (s, 3H, *26-H*), 0.99 (s, 3H, *19-H*), 0.97 (s, 3H, *28-H* or *29-H*), 0.91 (d, *J* = 6.5, 3H, *21-H*), 0.90-0.86 (m, 6H, *28-H* or *29-H & 30-H*), 0.69 (s, 3H, *18-H*). ^{13}C NMR (176 MHz) δ 134.8 (*8-C*), 134.3 (*9-C*), 131.0 (*25-C*), 125.4 (*24-C*), 50.5, 50.0, 44.6, 44.4, 37.7 (*4-C*), 37.1, 36.5, 36.4, 31.2, 31.0, 30.2, 28.4, 28.2 (*28-C* or *29-C*), 26.2, 25.9 (*27-C*), 25.8, 25.1, 24.4 (*28-C* or *29-C*), 22.3, 21.1 (*30-C*), 19.1, 18.8 (*19-C*), 18.3 (*21-C*), 17.8 (*26-C*), 15.90 (*18-C*). D NMR (107 MHz, *3β-D*) δ 3.44 (s, 1H). LRMS (ASAP) m/z: 430.397 ($[M+H]^+$, 60%), 429.397 ($[M]^+$, 21), 410.379 ($[M-H_2O]^+$, 100), 394.358 ($[M-H_2O-Me]^+$, 16). HRMS (ASAP) *m/z*: calculated $[M+H]^+$ 430.4045, found 430.4047. IR (neat) ν_{max} (cm^{-1}); 3379 (s), 2943 (l), 2880 (l), 1454 (m), 1371 (l), 1069 (s), 976 (m), 937 (m), 818 (s).

3β-OH epimer, **84d**; ^{1}H NMR (700 MHz) δ 5.11-5.07 (m,1H, *24-H*), 2.09-1.97 (m, 5H), 1.94-1.88 (m, 1H), 1.88-1.81 (m, 1H), 1.68 (t, *J* = 1.4, 4H, *27-H*), 1.60 (d, *J* = 1.4, 3H, *26-H*), 0.99 (s, 3H, *28-H* or *29-H*), 0.98 (s, 3H, *19-H*), 0.91 (d, *J* = 6.5, 3H, *21-H*), 0.87 (s, 3H, *30-H*), 0.80 (s, 3H, *28-H* or *29-H*), 0.69 (s, 3H, *18-H*).^{13}C NMR (176 MHz) δ 134.6 (*8-C*), 134.5 (*9-C*), 131.1 (*25-C*), 125.4 (*24-C*), 78.7 - 78.4 (t, *J* = 21.3, 1H, *3-C*), 50.6 (5-C), 50.0, 44.6, 39.0 (*4-C*), 37.2, 36.5, 36.4, 35.8, 31.2, 31.0, 28.4, 28.1, 27.9 (*28-C* or *29-C*), 26.7, 25.9 (*27-C*), 25.1, 24.4 (*30-C*), 21.2, 19.3 (*19-C*), 18.8 (21-C), 18.4, 17.8 (*26-C*), 15.9 (*18-C*), 15.6 (*28-C* or *29-C*). D NMR (107 MHz) δ 3.23 (s, 1H, 3*α-D*). LRMS (ASAP) m/z: 430.403 ($[M+H]^+$, 68%), 429.401 ($[M]^+$, 22), 410.375 ($[M-H_2O]^+$, 100), 394.359 ($[M-H_2O-Me]^+$, 12). HRMS (ASAP) *m*/*z*: calculated $[M+H]^+$ 430.4045, found 430.4043. IR (neat) ν_{max} (cm^{-1}); 3244 (s), 2943 (l), 2873 (l), 1450 (m), 1372 (l), 1037 (m), 928 (m), 822 (s).

6.4.55. Calculation of heavy oxygen enrichment enrichments by GC-MS

The desired unlabelled sterol (*ca*. 1 mg) was dissolved in DCM (1 mL) and submitted for GC-MS under conditions specified in general considerations. The intensity ratios (R_n) of the intenstites of the $[M+1]^+$ and $[M+2]^+$ peaks relative to the $[M]^+$ peak were calculated as shown in Eqn 1. This indicates the expected values of the $[M+n]^+$ peaks in enriched samples due to natural isotopes (mainly ^{13}C) as well as $[M+H]^+$ adducts. I_n = original intensities obtained for $[M+n]^+$ peaks. (n = 0, 1, 2, 3). Corrected intensities of the $[M+n]^+$ peaks (C_n) of samples enriched in ^{17}O and ^{18}O were then calculated according to Eqn 2, Eqn 3 and Eqn 4 respectively.

$$R_n = \frac{I_n}{I_0} \tag{1.1}$$

$$C_1 = I_1 - (I_0 \times R_1) \tag{1.2}$$

$$C_2 = I_2 - ((I_0 \times R_2) + (C_1 \times R_1)) \tag{1.3}$$

$$C_3 = I_3 - ((I_0 \times R_3) + (C_1 \times R_2) + (C_2 \times R_3)) \tag{1.4}$$

After correcting the intensities obtained by removing contributions to the intensity from natural heavier isotopes, the percentages (E_n) of the $[M+n]^+$, peaks were calculated by

Eqn 1.5. In the case of only heavy oxygen enrichment, $[M+1]^+$ was indicative of ^{17}O enrichment whilst an $[M+2]^+$ percentage represents ^{18}O enrichment. In cases where a deuterium label was also present, the percentages of $[M+2]^+$ and $[M+3]^+$ peak intensities represent the level ^{17}O and ^{18}O enrichment respectively. The C_3 term was discounted in cases without deuterium enrichment.

$$E_n\ \% = \frac{C_n}{C_0 + C_1 + C_2 + C_3} \tag{1.5}$$

In the case of deuterium enriched compounds, the level of deuterium incorporation must also be determined, lower deuterium enrichment decreases the intensity of the $[M+2]^+$ and $[M+3]^+$ peaks giving the impression of lower ^{17}O and ^{18}O enrichment respectively. As $[M+1]^+$ peak was representative of only deuterium incorporation, Eqn 1.6 was applied to determine deuterium enrichment (D). As complete deuterium incorporation was not achieved Eqn 1.7 must be applied to correct the intensity of the $[M+3]^+$ peak and hence determine the percentage of heavy oxygen (O_n) enrichment . Where O_n = peak intensity of $[M+n]^+$ peaks containing deuterium.

$$D_n\% = \frac{C_n}{C_n + C_0} \times 100 \tag{1.6}$$

$$O_n\% = \frac{E_n}{D_n} \times 100 \tag{1.7}$$

6.4.56. Determination of 5*α*-cholestan-3-one enrichment by GC-MS

5α-cholestan-3-one (10.00 mg, 2.59×10^{-2} mmol, 1 eq.), $^{18}OH_2$ (2.60 µL, 0.13 mmol, 5 eq.) and a solution of triflic acid in anhydrous 1,4-dioxane (111.89 mM; 11.00 µL, 1.23×10^{-3} mmol, 0.05 eq.) were stirred in anhydrous 1,4-dioxane (1 mL) under an argon atmosphere. At indicated intervals an aliquot was removed and injected into an air tight mass spectrometry vial under an argon atmosphere containing anhydrous DCM (1 mL) and 3 Å M.S (3 beads). Samples were submitted for GC-MS, with 10 repetitions of each time point. Determination of the standard deviation of the data set provided the error associated with determining enrichment by GC-MS (± 1.2%).

Chapter 7. References

1. S. J. Singer and G. L. Nicholson, *Science*, 1972, **175**, 720-731.

2. J. M. Sanderson, *Mol. Membr. Biol.*, 2012, **29**, 118-143.

3. G. van Meer, D. R. Voelker and G. W. Feigenson, *Nat. Rev. Mol. Cell Bio*., 2008, **9**, 112-124.

4. N. Sapay, W. F. D. Bennett and D. P Tieleman, *Soft Matter*, 2009, **5**, 3295-3302.

5. P. J. Quinn and C. Wolf, *Biochim. Biophys. Acta*, 2009, **1788**, 33-46.

6. O. G. Mouritsen, *Biochim. Biophys. Acta*, 2010, **1798**, 1286-1288.

7. A. Filippov, G. Oradd and G. Lindblom, *Biophys. J*., 2004, **86**, 891-896.

8. J. B. German, *Matern. Child Nutr.*, 2011, **7**, 2-16.

9. T. P. W. McMullen, R. N. A. H. Lewis and R. N. McElhaney, *Curr. Opin. Colloid In.*, 2004, **8**, 459-468.

10. M. E. Beattie, S. L. Veatch, B. L. Stottrup, and S. L. Keller, *Biophys. J*., 2005, **89**, 1760-1768.

11. Y. Barenholz, *Prog. Lipid Res*., 2002, **4**, 1-5.

12. J. A. Clarke, A. J. Heron, J. M. Seddon and R. V. Law, *Biophys. J*., 2006, **90**, 2383-2393.

13. L. J. Pike, *J. Lipid Res.*, 2009, **50**, S323-S328.

14. A. S. Shaw, *Nat. Immunol.*, 2006, **7**, 1139-1142.

15. M. -P. Mingeot-Leclercq, M. Deleu, R. Brasseur and Y. F. Dufrêne, *Nat. Protoc*., 2008, **3**, 1654-1659.

16. *NMR In Physiology and Biomedicine*, R. J. Gillies, Academic Press, Ltd., London, UK, 1994.

17. D. A. Brown and J. K. Rose, *Cell*, 1992, **68**, 533-*544.*

18. S. N. Ahmed, D. A. Brown and E. London, *Biochemistry*, 1997, **36**, 10944-10953.

19. D. Lingwood and K. Simons, *Nat. Protoc.*, 2007, **2**, 2159-2165.

20. H. Heerklotz, *Biophys. J*., 2002, **83**, 2693-2701.

21. D. Lichtenberg, F. M. Goñi and H. Heerklotz, *Trends. Biochem. Sci.*, 2005, **30**, 430-436.

22. H. M. Kim, H. -J. Choo, S. -Y. Jung, Y. -G. Ko, W. -H. Park, S. -J. Jeon, C. H. Kim, T. Joo and B. R. Cho, *ChembioChem*., 2007, **8**, 553-559.

23. C. Yuan, J. Furlong, P. Burgos and L. J. Johnston, *Biophys. J.*, 2002, **82**, 2526-2535.

24. S. P. Soni, D. S. LoCascio, Y. Liu, J. A. Williams, R. Bittman, W. Stillwell and S. R. Wassall, *Biophys. J.*, 2008, **95**, 203-214.

25. M. M. Lozano, Z. Liu, E. Sunnick, A. Janshoff, K. Kumar and S.G. Boxer, *J. Am. Chem. Soc*., 2013, **135**, 5620-5630.

26. A. S. Klymchenko and R. Kreder, *Chem. Biol.*, 2014, **21**, 97-113.

27. P. Sengupta, A. Hammond, D. Holowka, B. Baird, *Biochim. Biophsy. Acta*, 2008, **1778**, 20-32.

28. M. Ikeda, A. Kihara and Y. Igarashi, *Biol. Pharm. Bull*., 2006, **29**, 1542-1546.

29. V. A. Fadok, D. R. Voelker, P. A. Campbell, J. J. Cohen, D. L. Bratton and P. M. Henson, *J. Immunol.*, 1992, **148**, 2207-2216.

30. C. Janko, I. Jeremic, M. Biermann, R. Chaurio, C. Schorn, L. E. Muñoz and M. Herrman, *Phys. Biol*., 2013, **10**, 1-6.

31. P. K. Tarafdar, H. Chakraborty, S. M. Dennison, B. R. Lentz, *Biophys. J*., 2012, **103**, 1880-1889

32. D. L. Daleke, *J. Lipid Res.*, 2003, **44**, 233-242.

33. K. de Jong, S. K. Larkin, L. A. Styles, R. M. Bookchin and F. A. Kuypers, *Blood*, 2001, **98**, 859-867.

34. M. Melina Soares, S. W. King and P. E. Thorpe, *Nat. Med.*, 2008, **14**, 1357-1362.

35. M. R. Clark, *Nat. Immunol.*, 2011, **12**, 373-375.

36. B. Fadeel and D. Xue, *Crit. Rev. Biochem. Mol. Biol*., 2009, **44**, 264-277.

37. R. Homan and H. J. Pownall, *Biochim. Biophys. Acta*, 1988, **938**, 155-166.

38. *Biochemistry*, J. M. Berg, J. L. Tymoczko, and L.Stryer, W. H. Freeman, New York, USA, 2002.

39. A. Choubey, R. K. Kalia, N. Malmstadt, A. Nakano and P. Vashishta, *Biophys. J*., 2013, **104**, 2429- 2436

40. G. Parisio, M. M. Sperotto and A. Ferrarini, *J. Am. Chem. Soc*., 2012, **134**, 12198-12208.

41. K. John, S. Schreiber, J. Kubelt, A. Herrmann, and P. Müller, *Biophys. J*., 2002, **83**, 3315-3323.

42. G. Parisio, A. Ferrarini and M. M. Sperotto, *Int. J. Adv. Eng. Sci. Appl. Math*, 2016, **8**, 134-146.

43. S. Matosevic and B. M. Paegel, *Nat. Chem*., 2013, **5**, 958-963.

44. R. D. Kornberg and H. M. McConnell, *Biochemistry*, 1971, **10**, 1111-1120.

45. L. I. Barsukov, A.V. Victorov, I.A. Vasilenko, R.P. Evstigneeva, and L.D. Bergelson, *Biochim. Biophys. Acta*, 1980, **598**, 153-168.

46. J. Liu and J. C. Conboy, *Biophys. J.*, 2005, **89**, 2522-2532.

47. P. F. Devaux, P. Fellmann and P. Hervé, *Chem. Phys. Lipids*, 2002, **116**, 115-134.

48. O. G. Mouritsen, *Eur. J. Lipid Sci. Technol*., 2011, **113**, 1174-1187.

49. V. T. Armstrong, M. R. Brzustowicz, S. R. Wassall, Laura J. Jenski and W. Stillwell, *Arch. Biochem. Biophys.*, 2003, **414**, 74-82.

50. Q. Lin and E. London, PLoS One, 2014, **9**, e87903.

51. S. Pautot, B. J. Frisken and D. A. Weitz, *Langmuir*, 2003, **19**, 2870-2879.

52. S. S. Chrai, R. Murari and I. Ahmed, *Biopharm*, 2001, **14**, 10-14.

53. A. D. Bangham, M. M. Standish and J. C. Watkins, *J. Mol. Biol*., 1965, **13**, 238-252.

54. D. van Swaay and A. deMello, *Lab Chip*, 2013, **13**, 752-767.

55. R. M. Levine, T. R. Pearce, M. Adil and E. Kokkoli, *Langmuir*, 2013, **29**, 9208-9215.

56. K. Buyens, S. C. de Smedt, K. Braeckmans, J. Demeester, L. Peeters, L. A. van Grunsven, X. de Mollerat du Jeu, R. Sawant, V. Torchilin, K. Farkasova, M. Ogris and N. N. Sanders, *J. Control. Release*, 2012, **158**, 362-370.

57. V. S. Trubetskoy, J. A. Cannillo, A. Milschtein, G. L. Wolf and V. P. Torchilin, *Magn. Reson. Imaging*, 1995, **13**, 31-37.

58. D. T. Schühle, P. van Rijn, S. Laurent, L. V. Elst, R. N. Muller, M. C. A. Stuart, J. Schartz, and J. A. Peters, *Chem. Commun*., 2010, **46**, 4399-4401.

59. H. Anwekar, S. Patel, A. K. Singhai, *Int. J. Pharm. Life Sci*., 2011, **2**, 945-951.

60. T. M. Allen and P. R. Cullis, *Adv. Drug Deliver. Rev.*, 2013, **65**, 36-48.

61. A. Fischer, A. Franco, and T. Oberholzer, *ChemBioChem*, 2002, **3**, 409-417.

62. P. M. Gardner, K. Winzer and B. G. Davis, *Nat. Chem.*, 2009, **1**, 377-383.

63. K. Hosoda, T. Sunami, Y. Kazuta, T. Matsuura, H. Suzuki, and T. Yomo, *Langmuir*, 2008, **24**, 13540-13548.

64. R. Genc, G. Clergeaud, M. Ortiz and C. K. O'Sullivan, *Langmuir*, 2011, **27**, 10894-10900.

65. R. Genc, G. Clergeaud, M. Ortiz and C. K. O'Sullivan, *Langmuir*, 2013, **29**, 15405-15413.

66. A. Akbarzadeh, R. Rezaei-Sadabady, S. Davaran, S. W. Joo, N. Zarghami, Y. Hanifehpour, M. Samiei, M. Kouhi and K. Nejati-Koshki, *Nanoscale Res. Lett.*, 2013, **8**, 102.

67. H. I. Ingólfsson and O. S. Anderson, *Biophys. J*., 2011, **101**, 847-855.

68. Y. P. Patil and S. Jadhav, *Chem. Phys. Lipids*, 2014, **177**, 8-18.

69. *Liposomes: A Practical Approach*, R. R. C. New, Oxford University Press, USA, New York, 1990.

70. C. -H. Huang, *Biochemistry*, 1969, **8**, 344-352.

71. E. S. Richardson, W. G. Pitt and D. J. Woodbury, *Biophys. J*., 2007, **93**, 4100-4107.

72. Y. Yang, Y. Yang, X. Xie, X. Cai, H. Zhang, W. Gong, Z. Wang and X. Mei, *Biomaterials*, 2014, **35**, 4368-4381.

73. E. Naderkhani, A. Erber, N. Škalko-Basnet and G. E. Flaten, *J. Pharma. Sci*., 2014, **103**, 661-668.

74. T. Yamaguchi, M. Nomura, T. Matsuoka, S. Koda, *Chem. Phys. Lipids*, 2009, **160**, 58-62.

75. G. Maulucci, M. de Spirito, G. Arcovito, F. Boffi, A. Congiu-Castellano and G. Brigant, *Biophys.*

J., 2005, **88**, 3545-3550.

76. J. S. Dua, A. C. Rana and A. K. Bhandari, *Int J Pharm Pharm Sci*, 2012, **3**, 14-20.

77. H. M. S Santos and J. L. Capelo, *Talanta*, 2007, **73**, 795-802.

78. *Sample Preparation of pharmaceutical dosage forms. Challenges and Strategies for Sample Preparation and Extraction*, B. Nickerson, Springer, New York, USA, 2011.

79. M. J. Hope, M. B. Bally, G. Webb and P. R. Curtis, *Biochim Phys. Acta*, 1985, **812**, 55-65.

80. *Water- Insoluble Drug Formulation*, R. Liu, CRC Press, Florida, USA, 2008.

81. O. A. Ogunsola, M. E. Kraeling, S. Zhong, D. J. Pochan, R. L. Bronaugh and S. R. Raghavan, *Soft Matter*, 2012, **8**, 10226-10232.

82. F. Olson, C. A. Hunt, F. C. Szoka, W. J. Vail and D. Papahadjopoulos, *Biochim. Phys. Acta*, 1979, **557**, 9-23.

83. M. F. Poyton and P. S. Cremer, *Anal. Chem*., 2013, **85**, 10803-10811.

84. M. Przybylo, J. Procek, M. Hof and M. Langner, *Chem. Phys. Lipids*, 2014, **178**, 38-44.

85. M. M. Lapinski, A. Castro-Forero, A. J. Greiner, R. Y. Ofoli, and G. J. Blanchard, *Langmuir*, 2007, **23**, 11677-11683.

86. S. F. Aliño, M. Garcia-Sanz, A. Irruarrizaga, J. Alfaro, J. Hernandez, *J. Microencapsul.*, 1990, **7**, 497-503.

87. A. A. Mokhtarieh, S. J. Davarpanah and M. K. Lee, *DARU*, 2013, **21**, 32-35.

88. J. T. Buboltz and G. W. Feigenson, *Biochim. Biophys. Acta*, 1999, **1417**, 232-245.

89. J. Huang, J T. Buboltz and G. W. Feigenson, *Biochim. Biophys. Acta*, 1999, **1417**, 89-100.

90. M. D. Rejwan, K. H. Cheng, and J. Huang, *P. Natl. Acad. Sci. USA.*, 2007, **13**, 5372-5377.

91. D. J. McGillivray, G. Valincius, D. J. Vanderah, W. Febo-Ayala, J. T. Woodward, F. Heinrich, J. J. Kasianowicz, and M. Lösche, *Biointerphases*, 2007, **2**, 21-33.

92. R. Ali, K. H. Cheng and J. Huang, *Proc. Natl. Acad. Sci. USA*., 2007, **104**, 5372-5377.

93. J. T. Buboltz, *Rev. Sci. Instrum*., 2009, **80**, 124301.

94. S. Batzri and E. D. Korn, *Biochim. Biophys. Acta*, 1973, **298**, 1015-1019.

95. M. Patra, E. Salonen, E. Terama, I. Vattulainen, R. Faller, B. W. Lee, J. Holopainen and M. Karttunen, *Biophys. J.*, 2006, **90**, 1121-1135.

96. I. Setiawan and G. J. Blanchard, *J. Phys. Chem. B*, 2014, **118**, 537-546.

97. C. Charcosset, A. Juban, J. -P. Valour, S. Urbaniak, H. Fessi, *Chem. Eng. Res. Des.*, 2015, **94**, 508-515.

98. A. Laouini, C. Charcosset, H. Fessi, R.G. Holdich and G.T. Vladisavljević, *RSC Adv*., 2013, **3**,

4985-4994.

99. O. Rodriguez Justo and A. Maria Moraes, *J. Pharm. Pharmacol.*, **57**, 23-30.

100. J. C. Mathai and V. Sitaramam, *Biochem. Educ.*, 1987, **15**, 147-149.

101. M. J. Hope, T. E. Redelmeier, K. F. Wong, W. Rodrigueza and P. R. Cullis, *Biochemistry*, 1989, **28**, 4181-4187.

102. F. Szoka Jr. and D. Papahadjopoulos, *Proc. Natl, Acad, Sci. USA*., 1978, **75**, 4194-4198.

103. I. -Y. Kim, Y. -S. Kang, D. S. Lee, H. -J. Park, E. -K. Choi, Y. -K. Oh, H. -J. Son, J. -S. Kim, *J. Control. Release*, 2009, **140**, 55-60.

104. D. C. Drummond, O. Meyer, K. Hong, D. B. Kirpotin, and D. Papahadjopoulos, *Pharmacol. Rev.*, 1999, **51**, 691-743.

105. H. Xu, J. Paxton, J. Lim, Y. Li, W. Zhang, L. Duxfield and Z. Wu, *Pharma. Res*., 2014, **31**, 2583-2592.

106. A. A. Mokhtarieh, S. Cheong, S. Kim, B. H. Chung and M. K. Lee, *Biochim. Biophys. Acta*, 2012, **1818**, 1633-1641.

107. L. -R. Montes, A. Alonso, F. M. Goñi and Luis A. Bagatolli, *Biophys. J.*, 2007, **93**, 3548-3554.

108. N. F. Morales-Penningston, J. Wu, E. R. Farkas, S. L. Goh, T. M. Konyakhina, J. Y. Zheng, W. W. Webb and G. W. Feigenson, *Biochim. Biophys. Acta*, 2010, **1798**, 1324-1332.

109. Y. M. Serafini Micheletto, C. M. Marques, N. Pesce da Silveira and A. P. Schroder, *Langmuir*, 2016, **32**, 8123-8130.

110. M. I. Angelova, D.S. Dimitrov, *Faraday Discuss. Chem. Soc.*, 1986, **81**, 303-311.

111. Y. P. Patil and S. Jadhav, *Chem. Phys. Lipids*, 2014, **177**, 8-18.

112. T. Pott, H. Bouvrais, P. Méléard, *Chem. Phys. Lipids*, 2008, **154**, 115-119.

113. M. I. Angelova, S. Soléau, P. Méléard, J. F. Faucon and P. Bothorel, *Prog. Coll. Pol. Sci*., 1992, **89**, 127-131.

114. E. Baykal-Caglar, E. Hassan-Zadeh, B. Saremi, J. Huang, *Biochim. Biophys. Acta*, 2012, **1818**, 2598-2604.

115. N. Rodriguez, F. Pincet and S. Cribier, *Colloid. Surface. B.*, 2005, **42**, 125-130.

116. P. Taylor, C. Xu, P. D. I. Fletcher and V. N. Paunov, *Chem Commun*., 2003, **14**, 1732-1733.

117. H. Bi, B. Yang, L. Wang, W. Cao and X. Han, *J. Mater. Chem. A*., 2013, **1**, 7125-7130.

118. P. M. Shaklee, S. Semrau, M. Malkus, S. Kubick, M. Dogterom and T. Schmidt, *ChemBioChem*, 2010, **11**, 175-179.

119. D. J. Estes and M. Meyer, *BBA-Biomembranes*, 2005, **1712**, 152-160.

120. P. Mueller, D. O. Rudin, H. T. Tien and W. C. Wescott, *Proc. Nature*., 1962, **194**, 979-980.

121. M. Montal and P. Mueller, *P. Natl. Acad. Sci. USA*., 1972, **69**, 3561-3566.

122. H. Schindler, FEBS. Lett., 1980, **122**, 77-79.

123. K. B. Blodgett, *J. Am. Chem. Soc*., 1935, **57**, 1007-1022.

124. L. K. Tamm and H. M. McConnell, *Biophys. J.*, 1985, **47**, 105-113.

125. A. Coutable, C. Thibault, J. Chalmeau, J. M. François, C. Vieu, V. Noireaux and E. Trévisiol,, *Langmuir*, 2014, **30**, 3132-3141.

126. R. P. Richter and A. R. Brisson, *Biophys. J.*, 2005, **88**, 3422-3433.

127. L. Becucci, R. Guidelli, C. B. Karim, D. D. Thomas and G. Veglia, *Biophys. J.*, 2007, **93**, 2678-2687.

128. A. A. Brian and H. M. McConnell, *P. Natl. Acad. Sci. USA*., 1984, **81**, 6159-6163.

129. S. Stanglmaier, S. Hertrich, K. Fritz, J. F. Moulin, M. Haese-Seiller, J. O. Rädler and B. Nickel, *Langmuir*, 2012, **28**, 10818-10821.

130. R. P. Richter, N. Maury and A. R. Brisson, *Langmuir*, 2005, **21**, 299-304.

131. E. Kalb, S. Frey and L. K. Tamm, *Biochim. Biophys. Acta*, 1992, **1103**, 307-316.

132. M. L. Wagner and L. K. Tamm, *Biophys, J.*, 2000, **79**, 1400-1414.

133. R. Budvytyte, G. Valincius, G. Niaura, V. Voiciuk, M. Mickevicius, H. Chapman, H. Goh, P. Shekhar, F. Heinrich, S. Shenoy, M. Lösche, and D. J. Vanderah, *Langmuir*, 2013, **29**, 8645-8656.

134. K. Ataka, F. Giess, W. Knoll, R. Naumann, S. Haber-Pohlmeier, B. Richter and J. Heberle, *J. Am. Chem. Soc*., 2004, **126**, 16199-16206.

135. A. A. Yildiz, U. H. Yildiz, B. Liedberg and E. -K. Sinner, *Colloid. Surface. B.*, 2013, **103**, 510-516.

136. M. T. L. Casford, A. Ge, P. J. N. Kett, S. Ye and P. B. Davis, *J. Phys. Chem. B*., 2014, **118**, 3335-3345.

137. S. Sam, L. Touahir, J. S. Andresa, P. Allongue, J. N. Chazalviel, A. C. Gouget-Laemmel, C. H. de Villeneuve, A. Moraillon, F. Ozanamm, N. Gabouze and S.Djebbar, *Langmuir*, 2010, **26**, 809-814.

138. J. Chalmeau, C. le Grimelle, J. Sternick, C. Vieu, *Colloids and Surfaces B*, 2012, **89**, 188-195.

139. S. Pautot, B. J. Frisken and D. A. Weitz, *P. Natl. Acad. Sci. USA*, 2003, **19**, 10718-10721.

140. J. Whittenton, S. Harendra, R. Pitchumani, K. Mohanty, C. Vipulanandan and S. Thevananther, *Langmuir*, 2008, **24**, 8533-8540.

141. T. Hamada, Y. Miura, Y. Komatsu, Y. Kishimoto, M. Vestergaard and M.Takagi, *J. Phys. Chem. B*., 2008, **112**, 14678-14681.

142. D. L. Richmond, E. M. Schmid, S. Martens, J. C. Stachowiak, N. Liska, and D. A. Fletcher, *P. Natl. Acad. Sci*. USA, 2011, **108**, 9431-9436.

143. Y. Elani, S. Purushothaman, P. J. Booth, J. M. Seddon, N. J. Brooks, R. V. Law and O. Ces., *Chem. Commun*, 2015, **51**, 6976-6979.

144. R. Watanabe, N. Soga, T. Yamanaka and H. Noji, *Sci. Rep*., 2014, **4**, 7076-7081.

145. S. Deshpande, Y. Caspi, A. E.C. Meijering, C. Dekker, *Nat. Chem*., 2016, **7**, 1-9.

146. C. Konyali, C. Thomás, E. Blanch, E.A. Gómez, J. K. Graham and E. Mocé, *Cryobiology*, 2013, **67**, 124-131.

147. T. G. Anderson, A. Tan, P. Ganz and J. Seelig, *Biochemistry*, 2004, **43**, 2251-2261.

148. H. -T. Cheng, Megha and E. London, *J. Biol. Chem.*, 2009, **284**, 6079-6092.

149. H. -T. Cheng and E. London, *Biophys. J.*, 2011, **100,** 2671-2678.

150. S. Chiantia, P. Schwille, A.S. Klymchenko and E. London, *Biophy. J*., 2011, **100**, L1-L3.

151. I. Visco, S, Chiantia and P, Schwille, *Langmuir*, 2014, **30**, 7475-7484

152. M. Son and E. London, *J. Lipid Res.*, 2013, **54**, 223-231.

153. V. Kainu, M. Hermansson and P. Somerharju, *J. Lipid Res.*, 2010, **51**, 3533-3541.

154. G. Li, J. Kim, Z. Huang, J .R. St. Clair, D. A. Brown and E. London, *P. Natl. Acad. Sci. USA*., 2016, **113**, 14025-14030.

155. Y. Akae, T. Arai, Y. Koyama, H. Okamura, K. Johmoto, H. Uekusa, S. Kuwata and T. Takata, *Chem. Lett*., 2012, **41**, 806-808.

156. Z. Huang and E. London, *Langmuir*, 2013, **29**, 14631-14638.

157. M. A. Holden, D. Needham and H. Bayley, *J. Am. Chem. Soc*., 2007, **129**, 8651-8655.

158. K. Funakoshi, H. Suzuki and S. Takeuchi, *Anal. Chem*. 2006, **78**, 8169-8174.

159. W. L. Hwang, M. Chen, B. Cornin, M. A. Holden, and H. Bayley, *J. Am. Chem. Soc*., 2008, **130**, 5878-5879.

160. W. Shinoda, M. Mikami, T. Baba, M. Hato, *J. Phys. Chem. B*, 2003, **107**, 14030-14035.

161. C. E. Stanley, K. S. Elvira, X. Z. Niu, A.D. Gee, O. Ces, J. B. Edel and A. J. deMello, *Chem. Commun*., 2010, **46**, 1620-1622.

162. Y. Elani, A. J. de Mello, X. Niu and O. Ces, *Lab Chip*, 2012, **12**, 3514-3520.

163. Y. Elani, R. V. Law and O. Ces, *Nat. Commun*., 2014, **5**, 5305-5309.

164. S. Punnamaraju, H. You, and A. J. Steckl, *Langmuir*, 2012, **28**, 7657-7664.

165. Y. Elani, A. Gee, R. V. Law and O. Ces, *Chem. Sci*., 2013, **4**, 3332-3338.

166. R. D. Snook, T. J. Harvey, E. Correia Faria and P. Gardner, *Integr. Biol*., 2009, **1**, 43-52.

167. K. Funakoshi, H. Suzuki and S. Takeuchi, *J. Am. Chem. Soc*., 2007, **129**, 12608-12609.

168. J. C. Stachowiak, D. L. Richmond, T. H. Li, A. P. Liu, S. H. Parekh, and D. A. Fletcher, *P. Natl. Acad. Sci. USA*., 2008, **105**, 4697-4702.

169. J. Østergaard, C. Vergnolle, F. Schoentgen and J. C. Kader, *Biochim Biophys. Acta*, 1993, **1170**, 109-117.

170. K. W. A. Wirtz, *FEBS Letters*, 2006, **580**, 5436-5441.

171. B. Bloj and D B. Zilversmit, *J. Biol. Chem*. 1977, **252**, 1613-1619.

172. M. Abdul-Hammed, B. Breiden, M. A. Adebayo, J. O. Babalola, G. Schwarzmann and K. Sandhoff, *J. Lipid. Res*., 2010, **51**, 1747-1760.

173. M. Holzer, J. Momm and R. Schubert, *Langmuir*, 2010, **26**, 4142-4150.

174. L. V. Chernomordik and M. M. Kozlov, *Cell*, 2005, **123**, 375-382.

175. F. Pincet, L. Lebeau and S. Cribier, *Eur. Biophys. J*., 2001, **30**, 91-97.

176. Y. Xu, A. B. Seven, L. Su, Q. X. Jiang, J. Rizo, *PLoS One*, 2011, **6**, e22012.

177. D. P. Pantazatos, R. C. MacDonald, *J. Membr. Biol*., 1999, **170**, 27-38.

178. K. Hayashi, T. Tatsui, T. Shimanouchi and H. Umakoshi, *Colloid. Surface, B.*, 2013, **106**, 258-264.

179. V. Marchi-Artzner, T. Gulik-Krzywicki, M. A. Guedeau-Boudeville, C. Gosse, J. M. Sanderson, J. C. Dedieu and J. M. Lehn, *ChemPhysChem*, 2001, **2**, 367-376.

180. M. Mascal, P. S. Fallon, A. S. Batsanov, A. Brigid, B. R. Heywood, S. Champ and M. Colclough, *J. Chem. Soc., Chem Commun*., 1995. **8**, 805-806.

181. T. M. Bohanon, P. L. Caruso, S. Denzinger, R. Fink, D. Möbius, W. Paulus, J. A. Preece, H. Ringsdorf and D. Schollmeyer, *Langmuir*, 1999, **15**, 174-184.

182. V. Marchi-Artzner, J. M. Lehn, and T. Kunitake, *Langmuir*, 1998, **14**, 6470-6478.

183. V. Marchi-Artzner, PhD Thesis, University of Paris VI, 1997.

184. A. von Baeyer, *Liebigs. Ann. Chem*., 1864, **131**, 291-302.

185. E. Grimaux, *Bull. Soc. Chim.*, 1879, **31**, 146-149.

186. E. von Fischer and A. Dilthey, *Liebigs. Ann. Chem*., 1904, **335**, 334-368.

187. F. López-Muñoz, R. Ucha Udabe and C. Alamo, *Neuropsychiatr. Dis. Treat*., 2005, **1**, 329-343.

188. D. J. Gunnell, *International Review of Psychiatry*, 2000, **12**, 21-26.

189. M. K. Carter, *J. Chem. Educ*., 1951, **28**, 524-526.

190. A. Kohlmeier, L. Vogel and D. Janietz, *Soft Matter*, 2013, **9**, 9476-9486.

191. G. Majetich and R. Hicks, *Res. Chem. Intermed*., 1994, **20**, 61-77.

192. H. Koroniak, A. Jankowski and M. Krasnowski, *Org. Prep. Proced. Int*., 1993, **25**, 563-568.

193. B. S. Jursic and D. M. Neumann, *Tetrahedron Lett.*, 2001, **42**, 4103-4107.

194. A. Haworth, MSc thesis, Durham University, 2013.

195. V. Marchi-Artzner, B. Lorz, U. Hellerer, M. Kantlehner, H. Kessler and E. Sackmann, *Chem. Eur. J.*, 2001, **7**, 1095-1101.

196. J. Coste, D. Le-Nguyen and B. Castro, *Tetrahedron Lett.*, 1990, **31**, 205-208.

197. *Malononitrile. e-EROS Encyclopaedia of Reagents for Organic Synthesis*, F. Freeman, John Wiley & Sons., New York, USA, 2001

198. A. Abbaspour and M. Ali Kamyabi, *J. Chem. Eng. Data*, 2001, **46**, 623-625.

199. D. M. Neumann, A. Cammarata, G. Backes, G. E. Palmer, B. S. Jursic, *Bioorgan. Med. Chem*., 2014, **22**, 813-826.

200. E. D. Stevens and B. S. Jursic, *Tetrahedron Lett*., 2003, **44**, 2203-2210.

201. A. S. Kende, K. Koch and C. A. Smith, *J. Am. Chem. Soc*., 1988, **110**, 2210-2218.

202. J. B. Epp, T. S. Widlanski, *J. Org. Chem*., 1999, **64**, 293-295.

203. *Oxidation of Primary Alcohols to Carboxylic Acids: A Guide to Current Common Practice*, G. Tojo and M. I. Fernandez, Springer, New York, USA, 2007.

204. S. J. Kalita, H. Mecadon and D. C. Deka, *RSC Adv*., 2014, **4**, 32207-32213.

205. B. S. Jursic, *J. Heterocyclic Chem*., 2001, **38**, 655-657.

206. K. Hattori, H. Sajiki, K. Hirota, *Tetrahedron*, 2001, **57**, 2109-2114.

207. H. Sajiki, T. Ikawa, K. Hattori and K. Hirota, *Chem. Commun*, 2003, **5**, 654-655.

208. T. Ikawa, K. Hattori, H. Sajiki, K. Hirota, *Tetrahedron*, 2004, **60**, 6901-6911.

209. K. C. Nicolaou and C. J. N. Mathison, Angew. *Chem. Int. Ed*. 2005, **44**, 5992-5997.

210. J. M. Palomo, *RSC. Adv*. 2014, **4**, 32658-32672.

211. B. Yan, *Acc. Chem. Res*., 1998, **31**, 621-630.

212. D. D. Laws, H. -M. L. Bitter and A. Jerschow, *Agnew. Chem. Int. Ed. Engl*., 2002, **17**, 3096-3129.

213. *Combinatorial Chemistry and Technologies: Methods and Applications*, G. Fassina and S. Miertus, Taylor and Francis Group, Florida, USA, 2005.

214. *Solid phase synthesis and combinatorial technologies*, P. Seneci, John Wiley & Sons, Inc, New York, USA, 2000.

215. G. S. W. Whiteley, B. J. Fuller and K. E. F. Hobbs, *Cryobiology*, 1992, **29**, 668-673.

216. E. G. Bligh and W. J. Dyer, *Can. J. Biochem. Phys.*, 1959, **37**, 911-917.

217. J. Folch, M. Lees and G. H. Sloane Stanley, *J. Biol. Chem*., 1957, **226**, 497-509.

218. A. Reis, A. Rudnitskaya, G. J. Blackburn, N. Mohd Fauzi, A. R. Pitt and C. M. Spickett, *J. Lipid. Res.*, 2013, **54**, 1812-1824.

219. Z. Zhao and Y. Xu, *J. Lipid. Res*., 2010, **51**, 652-659.

220. S. Bergheim, K. E. Malterud and T. Anthonsen, *J. Lipid. Res*., 1991, **32**, 877-879.

221. J. S. Ellingson and R. L. Zimmerman, *J. Lipid. Res*., 1987, **28**, 1016-1018.

222. H . -Y. Kim and N. Salem Jr., *J. Lipid. Res*., 1990, **31**, 2285-2289.

223. F. Sahena, I. S. M. Zaidul, S. Jinap, K. A. Abbas, N. A. N. Norulaini, A. K. M. Omar, *J. Food Eng*., 2009, **95**, 240-253.

224. A. Pietsch and R. L. Lorenz, *Lipids*, 1993, **28**, 945-947.

225. G. Gunati, L. Banfi, L. Bondanza, G. Guglieri, K. Powles and R. Riva, *Amino Acids*, 2010, **39**, 367-373.

226. A. Blokland, W. Honig, F. Brouns and J. Jolles, 1999, *Nutrition*, **15**, 778-783.

227. S. S. le Corre, M. Berchel, N. Belmadi, C. Denis, J. -P. Haelters, T. le Gall, P. Lehn, T. Montier and P. -A. Jaffrès, *Org. and Biomol. Chem*., 2014, **12**, 1463 -1474.

228. I. Lindh and J. Stawiński, *J. Org. Chem*., 1989, **54**, 1338-1342.

229. K. S. Bruzik, G. Salamończyk and W. J. Stec, *J. Org. Chem*., 1986, **51**, 2370-2374.

230. S. L. Beaucage and M. H. Caruthers, *Tetrahedron Lett*., 1981, **22**, 1859-1862.

231. P. Shakya, D.K. Dubey, D. Pardasani, M. Palit, and A.K. Gupta, *Catal. Commun.*, 2005, **6**, 669-673.

232. J. M. Collins, K. A. Porter, S. K. Singh, and G. S. Vanier, *Org. Lett.*, 2014, **16**, 940-943.

233. R. A. Houghten, *P. Natl. Acad. Sci. USA*, 1985, **82**, 5131-5135.

234. R. B. Merrifield, J. Am. Chem. Soc., 1963, **85**, 2149-2154.

235. A. Katolik, R. Johnsson, E. Montemayor, J. G. Lackey, P. J. Hart and M. J. Damha, *J. Org. Chem*., 2014, **79**, 963-975.

236. Y. Nukaga, N. Oka and T. Wada, *J. Org. Chem*., 2016, **81**, 2753-2762.

237. J. Kandasamy, F. Schuhmacher, H.S Hahm, J. C. Klein and P. H. Seeberger, *Chem. Commun.*, 2014, **50**, 1875-1877.

238. C. S. Bennett, *Org. Biomol. Chem*., 2014, **12**, 1686-1698.

239. M. Lumbierres, J. M. Palomo, G. Kragol, S, Roehrs, O. Müller and H. Waldmann, *Chem. Eur. J*., 2005, **11**, 7405-7415.

240. M. Oliver, M. R. Jorgensen and A. Miller, *Tetrahedron Lett.*, 2004, **45**, 3105-3107.

241. B. E. Yingyongnarongkul, M. Howarth, T. Elliott and M. Bradley, *Chem. Eur. J*., 2004, **10**, 463-473.

242. K. Parang, *Bioorg. Med. Chem. Lett.*, 2002, **12**, 1863-1866.

243. G. M. Tenner, *J. Am. Chem. Soc*., 1961, **83**, 159-168.

244. X. Wei, *Tetrahedron*, 2013, **69**, 3615-3637.

245. *Advanced Organic Chemistry: Reaction Mechansims*, R. Bruckner, Academic Press, San Diego, USA, 2001.

246. J. T. W. A. R. M. Buis, G. I. Tesser and R. J. F. Nivard, *Tetrahedron*, 1976, **32**, 2321-2325.

247. W. Cheng and M. J. Kurth, *J. Org. Chem*., 2002, **67**, 4387-4391.

248. Y. Chen, Y. Lam, Y. Lai, *Org. Lett*. 2002, **4**, 3935-3937.

249. L. A. McAllister, R. A. McCormick and D. J. Procter, *Tetrahedron*, 2005, **61**, 11527-11576.

250. C. -H. Tai, H. -C. Wu and W. -R. Li, *Org. Lett*., 2004, **6**, 2905-2908.

251. *Combinatorial Chemistry: Synthesis and Application*. S. R. Wilson and A. W. Czarnik, John Wiley & sons, New York, USA, 1997.

252. K. Bahrami, M. M. Khodaei, S. Sohrabnezhad, *Tetrahedron Lett.*, 2011, **52**, 6420-6423.

253. B. Rangarajan, A. Havey, E. A. Grulke, and P. D. Culnan, *J. Am. Chem. Soc*., 1995, **72**, 1161-1169.

254. G. Dijkstra, W. H. Kruizinga, *J. Org. Chem*, 1987, **52**, 4230-4234.

255. J. W. Lee, C. W. Lee, J. H. Jung and D. Y. Oh, *Synthetic Commun.*, 2000, **30**, 2897-2902.

256. J. W. Perich, P. F. Alewood and R. B. Johns, *Phosphorus, Sulfur Silicon Relat. Elem.*, 1995, **105**, 1-10.

257. J. Nilsson, A. Kraszewski and J. Stawinski, *J. Chem. Soc*., *Perkin Trans.*, 2001, **2**, 2263-2266.

258. J. Dhineshkumar and K. R. Prabhu, *Org. Lett*., 2003, **15**, 6062-6065.

259. S. M. Gryasnov and R. L. Letsinger, 1992, *Nucleic Acids Res.*, **20**, 1879-1882.

260. S. Paul and M. H. Caruthers, *J. Am. Chem. Soc*., 2016, **138**, 15663-15672.

261. R. J. Cvetovich, *Org. Process Res. Dev*., 2010, **14**, 295-297.

262. S. Pérez-Rentero, A. V. Garibotti and R. Eritja, *Molecules*, 2010, **15**, 5692-5707.

263. M. C. Uzagare, K. J. Padiya, M. M. Salunkhe and Y. S. Sanghvi, *Bioorg Med. Chem. Lett.*, 2003, **13**, 3537-3540.

264. M. A. Maier, Y. Choi, H. Gaus, J. J. Barchi Jr, V. E. Marquez and M. Manoharan, *Nucleic Acids Res.*, 2004, **32**, 3642-3650.

265. *Integrated Drug Discovery Technologies*, H. -Y. Mei and A. W. Czarnik, Marcel Dekker AG,

Basel, Switzerland, 2002.

266. C. M. Temperley and M. J. Waters, *J. Fluorine Chem.*, 2001, **109**, 103-111.

267. F. H. Ebetino and J. D. Berk, *J. Organomet. Chem.*, 1997, **529**, 135-141.

268. J. M. Carrick, B. A. Kashemirov and C. E. McKenna, *Tetrahedron*, 2000, **56**, 2391-2396.

269. J. Dhineshkumar and K. Ramaiah Prabhu, *Org. Lett*., 2013, **15**, 6062-6065.

270. F. Song, J. Zhang, Y. Zhao, W. Chen, L. Lib and Z. Xi, *Org. Biomol. Chem*., 2012, **10**, 3642-3654.

271. S. J. Conway, J. Gardiner, S. J. A. Grove, M. K. Johns, Z. -Y. Lim, G. F. Painter, D. E. J. E. Robinson, C. Schieber, J. W. Thuring, L. S. M. Wong, M. -X. Yin, A.W. Burgess, B. Catimel, P. T. Hawkins, N. T. Ktistakis, L. R. Stephens and A. B. Holmes, *Org. Biomol. Chem*., 2010, **8**, 66-76.

272. D. Kromhout, A. Menotti, H. Kesteloot and S. Sans, *Circulation*, 2002, **105**, 893-898.

273. I. A. Boldyrev, X. Zhai, M. M. Momsen, H. L. Brockman, R. E. Brown and J. G. Molotkovsky, *J. Lipid. Res*., 2007, **48**, 1518-1532.

274. H. A. Scheidt, P. Müller, A. Herrmann and D. Huster, *J. Biol. Chem*., 2003, **278**, 45563-45569.

275. S. Milles, T. Meyer, H. A. Scheidt, R. Schwarzer, L. Thomas, M. Marek, L. Szente, R. Bittman, A. Herrmann, T. G. Pomorski, D. Huster and P. Müller, *BBA-Biomembranes*, 2013, **1828**, 1822-1828.

276. D. Wüstner, N. J. Faergeman, *Cytom. Part A*, 2008, **73A**, 727-744.

277. L. M. Loura, A. Fedorov and M. Prieto, *Biochim. Biophys. Acta*, 2001, ***1511***, 236-243.

278. X. Xu, R. Bittman, G. Duportail, D. Heissler, C. Vilcheze and E. London, *J. Biol. Chem*., 2001, **276**, 33540-33546.

279. W. G. Klemperer, *Ange. Chem. Int. Ed.*, 1978, **17**, 246-254.

280. L. L Smith, J. E. Herz and E. L. Ezell, Steroids, 1993, **58**, 260-267.

281. N. R. Schmuff and B. M. Trost, *J. Org. Chem*., 1983, **48**, 1404-1412.

282. W. W. Wong, D. L. Hachey, L. L. Clarke and S. Zhang, *J. Nutr*. 1995, **125**, S612-S618

283. L. N. Makley, K. A. McMenimen, B. T. de Vree, J. W. Goldman, B. N. McGlasson, P. Rajagopal, B. M. Dunyak, T. J. McQuade, A. D. Thompson, R. Sunahara, R. E. Klevit, U. P. Andley and J. E. Gestwicki, *Science*, 2015, **350**, 674-677.

284. L. Zhao, X. -J. Chen, J. Zhu *et al*., *Nature*, 2015, **523**, 607-614.

285. M. A. Wride, *Philos. Trans. R. Soc. Lond. B. Biol. Sci*. 2011, **366**, 1219-1233.

286. J. F. Hejtmancik, *Nature*, 2015, **523**, 540-541.

287. H. C. Tjondro, Y. -B. Xi, X. -J. Chen, J. -T. Su, Y. -B. Yan, *Biochem. Bioph. Res. Co.*, 2016,

473, 1-7.

288. A. M. Tomkiel, A. Biedrzycki, J. Płoszyńska, D. Naróg, A. Sobkowiak and J. W. Morzycki, *Beilstein J. Org. Chem.* 2015**, 11**, 162-168.

289. C. de la Calle Aregui, J. A. Purdie, C. Haslam, R. V. Law and J. M. Sanderson, *Chem. Phys. Lipids*, 2016, **195**. 58-62.

290. F. Karaki, K. Ohgane, K. Dodo and Y. Hashimoto, *Bioorg. Med. Chem.*, 2013, **21**, 5297-5309.

291. E. J. Corey, M. C. Kang, M. C. Desai, A. K. Ghosh, I. N. Houpis, *J. Am. Chem. Soc.* 1988, **110**, 649-651.

292. E. J. Corey and J. W. Suggs, *Tetrahedron Lett.*, 1975, **31**, 2647-2650.

293. S. Takatsuto and N. Ikekawa, *Chem. Pharm. Bull*., 1987, **35**, 986-995.

294. T. Daikur, T. T. Nakashima, J. C. Vederas, *Can. J. Chem.*, 1980, **58**, 1311-1315.

295. P. Vujanić, E. Gacs-Baitz, Z. Meić, T. Ŝuste, V. Smrečki, *Magn. Res. Chem.*, 1995, **33**, 426-430.

296. P. Yates and S. Stiver, *Can. J. Chem*., 1987, **65**, 2203-2216.

297. S. Ogawa, G. Kakiyama, A. Muto, A. Hosoda, K. Mitamura, S. Ikegawa, A. F. Hofmann, T. Iida, *Steroids*, 2009, **74**, 81-87.

298. D. H. R. Barton and J. F. King, *J. Chem. Soc*., 1958, **0**, 4398-4402.

299. E. McNeill and J. Du Bois, *J. Am. Chem. Soc*., 2010, **132**, 10202-10204.

300. P. Bovicelli, P. Lupattelli, E. Mincione, T. Prencipe and R. Curci, J. Org. Chem., 1992, **57**, 5052-5054.

301. V. Theodorou, K. Skobridis, D. Alvertis and I. P. Gerothanassis, *J. Labelled Compd. Rad.*, 2014, **57**, 481-508.

302. J. -G. Cuia, L. Fana, L. -L. Huanga, H. -L. Liub and A. -M. Zhoub, *Steroids*, 2009, **74**, 62-72.

303. S. Roy, A. Sharma, S. Mula, and S. Chattopadhyay, *Chem. Eur. J*., 2009, **15**, 1713-1722.

304. E. St'astná, I. Ćerný, V. Pouzar, and H. Chodounská, *Steroids*, 2010, **75**, 721-725.

305. A. J. MacNair, M. -M. Tran, J. E. Nelson, G. Usherwood Sloan, A. Ironmonger and S. P. Thomas, *Org. Biomol. Chem*., 2014, **12**, 5082-5088.

306. R.B. Clayton and K. Bloch, *J. Biol. Chem*., 1956, **218**, 305-318.

307. R.B. Clayton and K. Bloch, *J. Biol. Chem*., 1956, **218**, 319-325.

308. M. D. Kolesnikova, Q. Xiong, S. Lodeiro, L. Hua, S. P. T. Matsuda, *Arch. Biochem. Biophys.*, 2006, **447**, 87-95.

309. B. D. Roth, D. F. Ortwine. M. L. Hoefle. C. D. Stratton, D. R. Sliskovic, M. W. Wilson and R. S. Newton, *J. Med. Chem*., 1990, **33**, 21-31.

310. S. J. Wise, N. A. Nathoo, M. Etminan, F. S. Mikelberg and G. B. Mancini, *Can. J. Cardiol*., 2014, **12**, 1613-1619.

311. M. J. Chung, C. -K. Chung, Y. Jeong and S. -S. Ham, *Nut. Res. Pract*., 2010, **4**, 177-182.

312. R. B. Boar, D. A. Lewis, J. F. McGhie, *Chem. Soc., Perkin Trans*., 1973, **1**, 1583-1588.

313. *China Pat*., CN 105017367 A, 2015.

314. *Rus Pat*., RU2283318, 2006.

315. *US pat*, US 20050038301 A1, 2005.

316. J. D. Johnston, F. Gautschi and K. Bloch, *J. Biol. Chem*., 1957, **224**, 185-190.

317. W. J. Rodewald and J. J. Jagodzinski, *Polish. J. Chem*., 1978, **52**, 2473-2477.

318. L. V. Kavtaradze, M. Manley-Harris and B. K. Nicholson, *Steroids*, 2004, **69**, 227-233.

319. L. V. Kavtaradze, M. Manley-Harris and B. K. Nicholson, *Steroids*, 2004, **69**, 697-700.

320. O. V. Dolomanov, L. J. Bourhis, R. J. Gildea, J. A. K. Howard and H. Puschmann, *J. Appl. Cryst.*, 2009, **42**, 339-341.

321. G. M. Sheldrick, *Acta Cryst*., 2008, **A64**, 112-122.

322. C. Boutin, A. Stopin, F. Lenda, T. Brotin, J. -P. Dutasta, N. Jamin, A. Sanson, Y. Boulard, F. Leteurtre, G. Huber, A. Bogaert-Buchmann, N. Tassali, H. Desvaux, M. Carrière and P. Berthault, *Bioorg. Med. Chem*., 2011, **19**, 4135-4143.

323. J. Kowalski, Z. Lotowski, J. W. Morzycki, J. Płoszyńska, A. Sobkowiak, A. Z. Wilczewska, *Steroids*, 2008, **73**, 543-548.

324. P. Kocovsky, J. Srogl, M. Pour and A. Gogoll, *J. Am. Chem. Soc*. 1994, **116**, 186-197.

325. N. V. Kovganko and V. L. Survilo, *Chem. Nat. Compd*., 1999, **35**, 324–327.

326. A. L. J. Beckwith and G. Phillipou, *Aust. J. Chem*., 1976, **29**, 123-131.

327. P. M. Fischer and M. E. H. Howden, *J. Chem. Soc., Perkin Trans*, 1987, **1**, 475-489.

328. *GB Pat*., GB2458080A, 2010.

329. A. Bartoszewicz, M. Kalek and J. Stanwinski, *Tetrahedron*, 2008, **64**, 8843-8850.

330. B. Choucair, M. Dherbomez, C. Roussakis and L. El Kihel, *Tetrahedron*, 2004, **60**, 11477-11486.

331. L. M. Arnoštová, V. Pouzar and P. Drašar, *Steroids*, 1992, **57**, 233-235.

332. A. Kasal and M. Budesinsky, *Tetrahedron*, 2013, **69**, 9663-9674.

333. C. C. Mendes, L. Q. Sandes, F. G. Cruz and N. F. Roque, *Chem. Biodivers*., 2009, **6**, 1463-1470.

Appendix 1. X-ray diffraction data

All diffraction experiments were carried out D. Yufit of the Durham University crystallographic service.

A1.1. Crystal structure data of tetrabutylammonium 2,4,6-trioxohexahydropyrimidin-5-ide (barbituate), 17

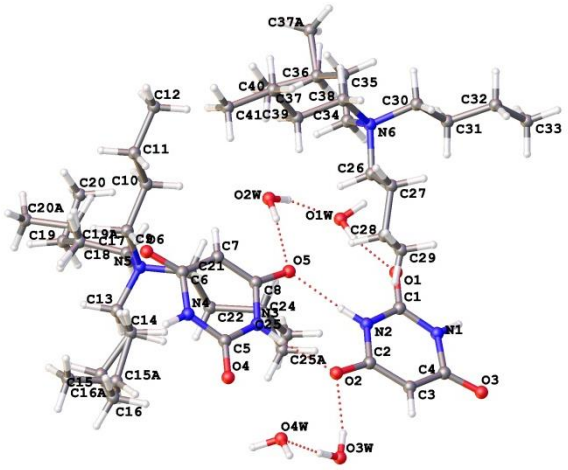

A1.1. Structures from the unit cell of **17**, determined by X-ray diffraction of a single crystal.

Table A1.1.1. Crystal data and structure refinement for **17**

Empirical formula	$C_{20}H_{43}N_3O_5$
Formula weight	405.57
Temperature (K)	120
Crystal system	triclinic
Space group	P-1
a (Å)	8.5757(4)
b (Å)	18.2984(8)
c (Å)	19.0841(8)
α (°)	111.2415(16)
β (°)	92.4738(18)
γ (°)	94.3069(18)
Volume (Å^3)	2775.4(2)
Z	4
ρ_{calc}g (cm^3)	0.971
μ (mm^{-1})	0.069
F(000)	896
Crystal size (mm^3)	0.26 × 0.18 × 0.06
Radiation	MoKα (λ = 0.71073)
2Θ range for data collection (°)	4.594 to 51.998
Index ranges	$-12 \le h \le 12$, $-26 \le k \le 26$, $-28 \le l \le 28$
Reflections collected	67331
Independent reflections	10896 [R_{int} = 0.1014, R_{sigma} = 0.1556]
Data/ restraints/ parameters	10896/34/522
Goodness-of-fit on F^2	1.016
Final R indexes [I > = 2σ (I)]	R_1 = 0.0868, wR_2 = 0.2373
Final R indexes [all data]	R_1 = 0.1457, wR_2 = 0.2744
Largest diff. peak/ hole (e Å^{-3})	0.79/-0.37

Table A1.1.2. Fractional atomic coordinates ($\times 10^4$) and equivalent isotropic displacement parameters ($Å^2 \times 10^3$) for **17**. U_{eq} is defined as 1/3 of the trace of the orthogonalised U_{IJ} tensor.

Atom	*x*	*y*	*z*	U(eq)
O1	4378(3)	936.5(12)	474.4(12)	30.5(5)
O2	2218(3)	2155.8(13)	-963.4(13)	39.2(6)
O3	3925(3)	-380.1(13)	-2057.0(12)	34.9(6)
N1	4176(3)	307.9(14)	-795.5(14)	25.2(6)
N2	3339(3)	1541.2(14)	-264.1(14)	25.3(6)
C1	3989(3)	931.0(17)	-161.1(18)	24.7(7)
C2	2826(4)	1551.5(18)	-957.9(18)	27.1(7)
C3	3015(4)	881.8(18)	-1592.0(19)	28.8(7)
C4	3696(3)	244.9(18)	-1525.4(17)	26.1(7)
O1W	5880(3)	1815.1(13)	1892.5(14)	43.6(6)
O2W	3905(4)	3061.1(15)	2456.3(14)	47.9(7)
O3W	1766(5)	2227(2)	-2368.6(17)	71.1(10)
O4	703(3)	4079.5(13)	-471.7(13)	36.8(6)
O5	2602(3)	2831.4(12)	1005.4(12)	31.1(5)
O6	705(3)	5321.7(13)	2064.4(12)	33.2(5)
N3	1691(3)	3478.2(15)	284.5(15)	27.7(6)
N4	736(3)	4689.1(15)	803.0(14)	28.3(6)
C5	1031(4)	4079.5(18)	167.5(18)	27.8(7)
C6	1033(4)	4723.6(18)	1538.1(18)	27.7(7)
C7	1678(4)	4074.7(19)	1610(2)	28.9(7)
C8	2016(4)	3438.8(18)	989.6(18)	26.4(7)
O4W	-527(4)	3255.2(16)	-1963.6(17)	66.9(9)
N5	6009(4)	5410(2)	2569(2)	58.4(10)
C9	4591(4)	5597(3)	3037(3)	56.7(12)
C10	4391(5)	5189(3)	3604(3)	61.5(12)
C11	2847(5)	5370(3)	3974(3)	65.2(13)
C12	2597(6)	4954(4)	4519(3)	87.4(18)
C13	6106(5)	5882(2)	2068(3)	71.0(15)
C14	4789(6)	5679(3)	1447(3)	72.8(15)
C15	5185(10)	6268(5)	1061(5)	75(2)
C15A	4917(19)	6013(7)	811(6)	75(2)
C16	3898(10)	6098(6)	440(5)	82(3)
C16A	4530(20)	6857(8)	1133(10)	118(6)
C17	7516(5)	5607(3)	3079(3)	75.0(16)
C18	7794(5)	6417(3)	3626(4)	99(2)
C19	9494(8)	6684(7)	3969(5)	69(4)
C19A	9336(10)	6478(5)	4104(6)	60(3)
C20	9421(15)	6329(7)	4569(7)	97(4)
C20A	9893(14)	7310(5)	4619(6)	91(3)
C21	5837(5)	4540(2)	2119(3)	53.5(11)
C22	7085(5)	4229(2)	1586(3)	61.5(13)
C24	6652(5)	3342(3)	1133(3)	76.3(16)
C25	7992(9)	2908(6)	747(6)	61(3)
C25A	7736(9)	3014(5)	504(4)	41(2)
N6	1105(3)	1200(2)	2531.4(19)	48.8(8)
C26	1183(4)	1244(2)	1760(2)	45(1)
C27	-301(4)	934(2)	1241(2)	43.6(9)
C28	-124(4)	1125(2)	535(2)	43.3(9)
C29	-1584(5)	873(2)	1(2)	49(1)
C30	807(5)	353(3)	2484(3)	56.0(11)
C31	2094(5)	-175(3)	2170(3)	59.4(12)
C32	1543(6)	-1038(3)	2014(3)	78.5(16)
C33	2806(7)	-1579(3)	1709(4)	96(2)
C34	2692(4)	1577(3)	2956(2)	56.9(11)

C35	2922(5)	1583(3)	3738(3)	71.8(14)
C36	4498(6)	2025(3)	4106(3)	81.2(16)
C37	4643(9)	2899(3)	4272(4)	61.4(19)
C37A	4800(20)	2075(12)	4911(6)	130(7)
C38	-227(5)	1647(3)	2931(2)	58.9(12)
C39	-223(5)	2487(3)	2975(3)	68.7(14)
C40	-1563(6)	2875(3)	3401(3)	78.8(17)
C41	-1666(7)	3706(4)	3436(4)	108(2)

Table A1.1.3. Anisotropic displacement parameters ($Å^2 \times 10^3$) for **17**. The anisotropic displacement factor exponent takes the form: $-2\pi^2[h^2a^{*2}U_{11}+2hka^*b^*U_{12}+\ldots]$.

Atom	U_{11}	U_{22}	U_{33}	U_{23}	U_{13}	U_{12}
O1	37.9(13)	22.5(11)	29.1(12)	5.7(9)	0.1(10)	10.6(10)
O2	58.0(16)	24.5(12)	39.8(14)	14.5(11)	3.9(12)	18.6(11)
O3	46.6(14)	24.9(12)	30.1(12)	4.7(10)	1.2(11)	13(1)
N1	27.0(14)	18.7(13)	30.2(14)	7.9(11)	0.9(11)	9.5(11)
N2	28.3(14)	17.9(13)	29.6(14)	7.1(11)	5.3(11)	8.0(11)
C1	21.1(15)	20.1(16)	30.8(18)	6.5(14)	2.5(13)	3.2(12)
C2	27.2(17)	22.0(17)	35.2(18)	13.7(14)	3.5(14)	3.8(13)
C3	32.4(18)	23.9(17)	32.0(18)	12.6(15)	-0.3(15)	2.8(14)
C4	23.0(16)	24.4(17)	30.5(17)	9.2(14)	2.9(13)	3.2(13)
O1W	56.3(16)	24.5(12)	44.2(14)	6.7(11)	-13.8(12)	8.4(11)
O2W	67.0(19)	34.0(14)	42.4(15)	11.0(12)	-2.0(13)	22.8(13)
O3W	105(3)	61(2)	60.4(19)	33.9(17)	11.5(19)	28.1(19)
O4	55.8(16)	27.6(12)	30.9(13)	11.9(10)	6.8(11)	21.0(11)
O5	36.7(13)	21.1(11)	38.2(13)	12.9(10)	2.1(10)	9.9(10)
O6	39.6(13)	25.6(12)	33.5(12)	7.7(10)	7.6(10)	12.1(10)
N3	31.5(15)	21.8(14)	32.3(15)	11.1(12)	5.7(12)	10.3(11)
N4	34.7(15)	18.8(13)	32.6(15)	8.8(12)	7.8(12)	10.6(11)
C5	27.8(17)	22.6(17)	35.1(19)	11.8(14)	5.0(14)	7.8(13)
C6	23.2(16)	26.9(17)	32.1(18)	10.0(15)	0.8(14)	0.7(13)
C7	30.1(18)	28.6(18)	30.4(19)	13.1(15)	2.2(15)	6.2(14)
C8	24.8(16)	23.1(17)	35.3(18)	15.2(14)	2.7(14)	4.3(13)
O4W	101(3)	32.9(15)	58.7(18)	9.2(13)	-16.1(17)	7.6(16)
N5	29.2(17)	56(2)	74(2)	4.3(19)	10.7(17)	4.3(15)
C9	30(2)	56(3)	70(3)	4(2)	8.7(19)	11.5(18)
C10	41(2)	77(3)	58(3)	11(2)	4(2)	20(2)
C11	42(2)	83(3)	57(3)	8(3)	4(2)	15(2)
C12	64(3)	137(5)	67(3)	41(4)	16(3)	26(3)
C13	52(3)	29(2)	114(4)	5(2)	17(3)	-4.3(19)
C14	66(3)	55(3)	110(4)	44(3)	25(3)	-1(2)
C17	31(2)	71(3)	89(4)	-11(3)	4(2)	3(2)
C18	40(3)	85(4)	118(5)	-22(3)	-10(3)	-2(3)
C21	36(2)	44(2)	74(3)	13(2)	15(2)	2.1(18)
C22	38(2)	46(2)	88(3)	9(2)	27(2)	1.2(19)
C24	47(3)	45(3)	114(4)	2(3)	23(3)	-6(2)
N6	25.2(16)	55(2)	56(2)	11.3(17)	0.4(14)	-7.2(14)
C26	28.9(19)	44(2)	54(2)	9.6(19)	10.0(17)	-4.1(16)
C27	29.1(19)	39(2)	55(2)	9.8(18)	6.7(17)	-4.4(16)
C28	35(2)	34(2)	59(2)	13.8(18)	16.9(18)	4.7(16)
C29	47(2)	37(2)	57(2)	10.5(19)	9(2)	5.0(18)
C30	39(2)	74(3)	56(3)	29(2)	0.1(19)	-14(2)
C31	45(2)	61(3)	73(3)	29(2)	3(2)	-11(2)
C32	71(3)	65(3)	108(4)	46(3)	3(3)	-15(3)
C33	85(4)	58(3)	159(6)	59(4)	-2(4)	-6(3)
C34	28(2)	65(3)	66(3)	14(2)	-6.0(19)	-7.2(19)
C35	50(3)	83(4)	68(3)	14(3)	-5(2)	-2(2)
C36	60(3)	77(4)	94(4)	21(3)	-30(3)	4(3)

C38	30(2)	81(3)	54(3)	11(2)	3.4(18)	0(2)
C39	44(3)	78(4)	65(3)	2(3)	3(2)	12(2)
C40	49(3)	101(4)	56(3)	-8(3)	-8(2)	25(3)
C41	85(4)	109(5)	102(5)	-3(4)	-1(4)	51(4)

Table A1.1.4. Bond lengths for **17**.

Atom	Atom	Length (Å)	Atom	Atom	Length (Å)
O1	C1	1.240(4)	C15	C16	1.512(5)
O2	C2	1.261(4)	C15A	C16A	1.509(5)
O3	C4	1.259(4)	C17	C18	1.465(7)
N1	C1	1.355(4)	C18	C19	1.540(6)
N1	C4	1.396(4)	C18	C19A	1.546(6)
N2	C1	1.356(4)	C19	C20	1.510(5)
N2	C2	1.384(4)	C19A	C20A	1.509(5)
C2	C3	1.402(5)	C21	C22	1.507(5)
C3	C4	1.385(4)	C22	C24	1.546(6)
O4	C5	1.240(4)	C24	C25	1.509(5)
O5	C8	1.263(4)	C24	C25A	1.523(5)
O6	C6	1.249(4)	N6	C26	1.507(5)
N3	C5	1.357(4)	N6	C30	1.521(6)
N3	C8	1.391(4)	N6	C34	1.531(5)
N4	C5	1.367(4)	N6	C38	1.522(5)
N4	C6	1.393(4)	C26	C27	1.516(5)
C6	C7	1.395(4)	C27	C28	1.520(5)
C7	C8	1.387(5)	C28	C29	1.510(6)
N5	C9	1.526(5)	C30	C31	1.520(6)
N5	C13	1.503(6)	C31	C32	1.529(6)
N5	C17	1.522(6)	C32	C33	1.513(8)
N5	C21	1.502(5)	C34	C35	1.493(7)
C9	C10	1.530(7)	C35	C36	1.522(6)
C10	C11	1.529(6)	C36	C37	1.507(5)
C11	C12	1.509(7)	C36	C37A	1.516(5)
C13	C14	1.523(7)	C38	C39	1.508(7)
C14	C15	1.535(6)	C39	C40	1.507(6)
C14	C15A	1.548(6)	C40	C41	1.509(9)

Table A1.1.5. Bond angles for **17**.

Atom	Atom	Atom	Angle (°)	Atom	Atom	Atom	Angle (°)
C1	N1	C4	124.8(3)	N5	C13	C14	115.7(3)
C1	N2	C2	124.6(3)	C13	C14	C15	103.2(4)
O1	C1	N1	121.7(3)	C13	C14	C15A	120.2(7)
O1	C1	N2	122.3(3)	C16	C15	C14	105.5(6)
N1	C1	N2	116.0(3)	C16A	C15A	C14	107.0(10)
O2	C2	N2	117.3(3)	C18	C17	N5	116.1(4)
O2	C2	C3	125.9(3)	C17	C18	C19	115.6(6)
N2	C2	C3	116.8(3)	C17	C18	C19A	107.5(5)
C4	C3	C2	121.4(3)	C20	C19	C18	97.3(8)
O3	C4	N1	117.2(3)	C20A	C19A	C18	113.4(7)
O3	C4	C3	126.4(3)	N5	C21	C22	116.5(3)
C3	C4	N1	116.4(3)	C21	C22	C24	109.2(3)
C5	N3	C8	124.6(3)	C25	C24	C22	114.5(5)
C5	N4	C6	125.1(3)	C25A	C24	C22	112.1(4)
O4	C5	N3	122.7(3)	C26	N6	C30	111.5(3)
O4	C5	N4	121.7(3)	C26	N6	C34	105.8(3)
N3	C5	N4	115.6(3)	C26	N6	C38	110.2(3)
O6	C6	N4	117.9(3)	C30	N6	C34	110.8(3)
O6	C6	C7	126.3(3)	C30	N6	C38	107.7(3)
N4	C6	C7	115.8(3)	C38	N6	C34	110.9(3)

C8	C7	C6	122.1(3)	N6	C26	C27	115.6(3)
O5	C8	N3	117.1(3)	C26	C27	C28	109.4(3)
O5	C8	C7	126.1(3)	C29	C28	C27	113.1(3)
C7	C8	N3	116.8(3)	C31	C30	N6	116.0(3)
C13	N5	C9	110.3(3)	C30	C31	C32	111.1(4)
C13	N5	C17	108.6(4)	C33	C32	C31	112.4(4)
C17	N5	C9	110.5(3)	C35	C34	N6	116.1(4)
C21	N5	C9	107.5(3)	C34	C35	C36	110.0(4)
C21	N5	C13	111.6(3)	C37	C36	C35	115.6(5)
C21	N5	C17	108.2(3)	C37A	C36	C35	113.2(9)
N5	C9	C10	116.1(4)	C39	C38	N6	115.9(4)
C11	C10	C9	110.1(4)	C40	C39	C38	111.1(4)
C12	C11	C10	111.2(4)	C39	C40	C41	113.6(5)

Table A1.1.6. Hydrogen bonds for **17**.

D	H	A	d(D-H) (Å)	d(H-A) (Å)	d(D-A) (Å)	D-H-A (°)
N2	H2	O5	0.88	1.97	2.838(3)	169.8
O1W	H1WA	O3[1]	0.85	1.92	2.771(3)	173.8
O1W	H1WB	O1	0.86	1.95	2.794(3)	166.2
O2W	H2WA	O5	0.87	1.95	2.813(3)	169.4
O2W	H2WB	O1W	0.87	2.03	2.861(3)	160.3
O3W	H3WA	O2	0.87	1.91	2.744(4)	160.2
O3W	H3WB	O4W	0.87	1.9	2.763(5)	172.3
N3	H3A	O2	0.88	1.92	2.795(3)	172.8
N4	H4	O4[2]	0.88	2.02	2.895(3)	172.8
O4W	H4WA	O6[2]	0.88	1.91	2.695(4)	147.8

Table A1.1.7. Torsion angles for **17**.

A	B	C	D	Angle (°)	A	B	C	D	Angle (°)
C9	C10	C11	C12	178.3(4)	C22	C21	N5	C17	-63.2(5)
C10	C9	N5	C13	-177.0(4)	C24	C22	C21	N5	-175.9(4)
C10	C9	N5	C17	-56.9(5)	C26	C27	C28	C29	-177.1(3)
C10	C9	N5	C21	61.0(5)	C27	C26	N6	C30	62.1(4)
C11	C10	C9	N5	-174.6(4)	C27	C26	N6	C34	-177.4(3)
C13	C14	C15	C16	-179.4(6)	C27	C26	N6	C38	-57.4(4)
C13	C14	C15A	C16A	-78.2(13)	C28	C27	C26	N6	171.8(3)
C14	C13	N5	C9	-66.6(5)	C30	C31	C32	C33	-179.3(5)
C14	C13	N5	C17	172.2(4)	C31	C30	N6	C26	64.7(4)
C14	C13	N5	C21	53.0(5)	C31	C30	N6	C34	-52.8(5)
C15	C14	C13	N5	178.2(5)	C31	C30	N6	C38	-174.3(4)
C15A	C14	C13	N5	-168.8(6)	C32	C31	C30	N6	-169.5(4)
C17	C18	C19	C20	-82.4(9)	C34	C35	C36	C37	67.8(7)
C17	C18	C19A	C20A	171.8(9)	C34	C35	C36	C37A	178.5(9)
C18	C17	N5	C9	-55.7(6)	C35	C34	N6	C26	-178.2(4)
C18	C17	N5	C13	65.4(6)	C35	C34	N6	C30	-57.3(5)
C18	C17	N5	C21	-173.2(5)	C35	C34	N6	C38	62.3(5)
C19	C18	C17	N5	-162.4(6)	C36	C35	C34	N6	-176.1(4)
C19A	C18	C17	N5	177.6(7)	C38	C39	C40	C41	-177.4(4)
C21	C22	C24	C25	-163.4(6)	C39	C38	N6	C26	-53.2(4)
C21	C22	C24	C25A	171.8(5)	C39	C38	N6	C30	-175.0(4)
C22	C21	N5	C9	177.4(4)	C39	C38	N6	C34	63.7(5)
C22	C21	N5	C13	56.3(5)	C40	C39	C38	N6	-178.3(4)

Table A1.1.8. Hydrogen atom coordinates ($Å \times 10^4$) and isotropic displacement parameters ($Å^2 \times 10^3$) for **17**.

Atom	*x*	*y*	*z*	U(eq)
H1	4634	-86	-744	30
H2	3236	1960	138	30
H3	2670(40)	885(19)	-2068(19)	29(9)
H1WA	5930	1390	1978	50
H1WB	5433	1617	1442	50
H2WA	3390	2971	2026	72
H2WB	4604	2727	2396	72
H3WA	2079	2132	-1973	107
H3WB	1107	2584	-2243	107
H3A	1929	3086	-113	33
H4	326	5091	743	34
H7	1820(40)	4076(19)	2050(19)	25(9)
H4WA	-278	3759	-1867	50
H4WB	-1158	3140	-2363	50
H9A	3635	5452	2687	68
H9B	4664	6174	3315	68
H10A	4396	4613	3343	74
H10B	5278	5376	3995	74
H11A	2859	5945	4245	78
H11B	1967	5199	3579	78
H12A	2592	4385	4252	131
H12B	1590	5070	4739	131
H12C	3445	5138	4922	131
H13A	7116	5810	1831	85
H13B	6119	6446	2387	85
H14C	3816	5848	1694	87
H14D	4640	5098	1203	87
H14A	3754	5752	1660	87
H14B	4785	5130	1089	87
H15A	5206	6816	1425	90
H15B	6220	6191	849	90
H15C	5992	5989	640	90
H15D	4172	5704	375	90
H16A	3841	5542	108	123
H16B	4127	6431	147	123
H16C	2893	6210	662	123
H16D	3493	6875	1330	176
H16E	4536	7080	737	176
H16F	5318	7164	1543	176
H17A	7508	5245	3359	90
H17B	8411	5500	2758	90
H18C	6912	6544	3954	118
H18D	7886	6792	3361	118
H18A	7105	6473	4042	118
H18B	7478	6778	3376	118
H19A	10271	6456	3601	82
H19B	9708	7265	4185	82
H19C	9176	6148	4412	71
H19D	10163	6264	3761	71
H20A	9136	5759	4344	145
H20B	8652	6574	4925	145
H20C	10464	6434	4836	145
H20D	10644	7542	4368	136
H20E	10394	7318	5094	136
H20F	8981	7615	4725	136

H21A	4810	4404	1822	64
H21B	5812	4260	2476	64
H22A	8112	4310	1874	74
H22B	7169	4518	1237	74
H24C	6712	3050	1478	92
H24D	5558	3259	911	92
H24A	6248	3091	1478	92
H24B	5795	3282	746	92
H25A	7635	2348	491	91
H25B	8855	2968	1124	91
H25C	8355	3126	377	91
H25D	7700	3310	168	61
H25E	7394	2457	218	61
H25F	8811	3064	724	61
H26A	2048	943	1512	54
H26B	1452	1801	1822	54
H27A	-1207	1181	1503	52
H27B	-494	357	1103	52
H28A	137	1700	684	52
H28B	760	859	269	52
H29A	-1416	1027	-433	74
H29B	-2469	1129	263	74
H29C	-1814	300	-173	74
H30A	640	360	2997	67
H30B	-177	116	2166	67
H31A	3025	-9	2536	71
H31B	2403	-119	1697	71
H32A	1217	-1090	2486	94
H32B	617	-1202	1644	94
H33A	2397	-2124	1613	144
H33B	3713	-1429	2080	144
H33C	3124	-1535	1238	144
H34A	3527	1295	2659	68
H34B	2834	2128	2981	68
H35A	2883	1036	3722	86
H35B	2069	1841	4039	86
H36A	4704	1942	4585	97
H36B	5325	1790	3772	97
H36C	5342	1758	3804	97
H36D	4540	2566	4101	97
H37A	4452	2991	3803	92
H37B	5701	3127	4496	92
H37C	3870	3146	4625	92
H37D	4730	2616	5258	196
H37E	5853	1923	4978	196
H37F	4020	1719	5018	196
H38A	-1233	1355	2668	71
H38B	-191	1648	3450	71
H39A	782	2787	3231	82
H39B	-310	2496	2459	82
H40A	-1445	2881	3922	95
H40B	-2558	2555	3158	95
H41A	-1805	3705	2923	162
H41B	-698	4032	3690	162
H41C	-2561	3922	3717	162

Table A1.1.9. Atomic occupancy for **17**

Atom	Occupancy	Atom	Occupancy	Atom	Occupancy
H14C	0.4	H14D	0.4	H14A	0.6
H14B	0.6	C15	0.6	H15A	0.6
H15B	0.6	C15A	0.4	H15C	0.4
H15D	0.4	C16	0.6	H16A	0.6
H16B	0.6	H16C	0.6	C16A	0.4
H16D	0.4	H16E	0.4	H16F	0.4
H18C	0.5	H18D	0.5	H18A	0.5
H18B	0.5	C19	0.5	H19A	0.5
H19B	0.5	C19A	0.5	H19C	0.5
H19D	0.5	C20	0.5	H20A	0.5
H20B	0.5	H20C	0.5	C20A	0.5
H20D	0.5	H20E	0.5	H20F	0.5
H24C	0.5	H24D	0.5	H24A	0.5
H24B	0.5	C25	0.5	H25A	0.5
H25B	0.5	H25C	0.5	C25A	0.5
H25D	0.5	H25E	0.5	H25F	0.5
H36A	0.6	H36B	0.6	H36C	0.4
H36D	0.4	C37	0.6	H37A	0.6
H37B	0.6	H37C	0.6	C37A	0.4
H37D	0.4	H37E	0.4	H37F	0.4

Table A1.1.10. Solvent masks information for **17**.

Number	X	Y	Z	Volume	Electron count	Content
1	-0.761	0	0.5	454.2	119.3	?

A1.2. Crystal structure data of 3,3'-disulfanediyldiphenol, 41

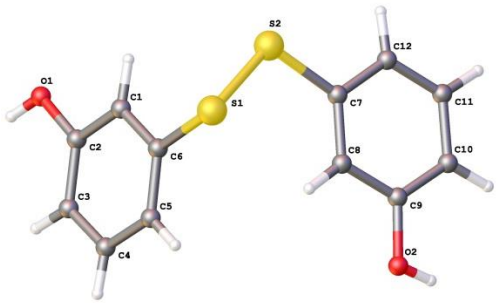

Figure A1.2. One Structure from the unit cell of **41**, determined by X-ray diffraction of a single crystal.

Table A1.2.1. Crystal data and structure refinement for **41**

Empirical formula	$C_{12}H_{10}O_2S_2$
Formula weight	250.32
Temperature (K)	120
Crystal system	monoclinic
Space group	C2/c
a (Å)	19.4475(10)
b (Å)	6.4379(4)
c (Å)	18.9028(10)
α (°)	90
β (°)	102.838(2)

γ (°)	90
Volume (Å^3)	2307.5(2)
Z	8
ρ_{calc}g (cm^3)	1.441
μ (mm^{-1})	0.441
F(000)	1040
Crystal size (mm^3)	0.51 × 0.12 × 0.11
Radiation	MoKα (λ = 0.71073)
2Θ range for data collection (°)	5.438 to 57.99
Index ranges	-26 ≤ h ≤ 26, -8 ≤ k ≤ 8, -25 ≤ l ≤ 25
Reflections collected	16628
Independent reflections	3064 [R_{int} = 0.0950, R_{sigma} = 0.0740]
Data/ restraints/ parameters	3064/0/185
Goodness-of-fit on F^2	1.031
Final R indexes [I > = 2σ (I)]	R_1 = 0.0478, wR_2 = 0.1065
Final R indexes [all data]	R_1 = 0.0781, wR_2 = 0.1191
Largest diff. peak/ hole (e Å^{-3})	0.38/-0.34

Table A1.2.2. Fractional atomic coordinates (×10^4) and equivalent isotropic displacement parameters (Å^2×10^3) for **41**. U_{eq} is defined as 1/3 of the trace of the orthogonalised U_{IJ} tensor.

Atom	*x*	*y*	*z*	U(eq)
S1	3004.3(3)	4243.4(10)	4733.0(3)	30.15(18)
S2	3480.5(3)	7046(1)	4718.3(3)	29.72(17)
O1	1058.3(8)	7045(3)	2692.4(9)	28.8(4)
O2	5038.0(8)	2541(2)	3469.3(9)	25.5(4)
C4	1503.7(11)	3600(4)	2520.6(11)	24.0(5)
C5	1966.0(12)	2019(4)	2793.6(12)	26.8(5)
C6	2437.5(12)	2222(4)	3462.1(12)	25.3(5)
C7	4222.5(10)	6554(3)	4332.6(10)	20.5(4)
C8	4351.2(10)	4659(3)	4047.2(10)	18.8(4)
C9	4946.1(10)	4445(3)	3756(1)	18.8(4)
C10	5405.9(11)	6077(3)	3758.6(11)	24.0(5)
C11	5264.0(12)	7962(4)	4050.6(13)	29.2(5)
C12	4670.5(12)	8222(3)	4325.0(12)	26.9(5)

Table A1.2.3. Anisotropic displacement parameters (Å^2×10^3) for **41**. The anisotropic displacement factor exponent takes the form: $-2\pi^2[h^2a^{*2}U_{11}+2hka^*b^*U_{12}+\ldots]$.

Atom	U_{11}	U_{22}	U_{33}	U_{23}	U_{13}	U_{12}
S1	20.9(3)	55.1(4)	14.9(3)	7.0(2)	4.8(2)	-0.1(2)
S2	24.9(3)	42.9(4)	20.7(3)	-10.0(2)	3.6(2)	6.7(2)
O1	23.0(8)	36.6(10)	25.4(8)	-0.2(7)	2.0(7)	6.8(7)
O2	20.8(8)	25.8(9)	31.1(9)	-5.3(6)	8.7(7)	2.3(6)
C1	15.8(9)	37.4(13)	14.1(9)	3.7(9)	6.2(7)	-1.1(9)
C2	17.9(10)	35.2(13)	17.7(10)	-2.0(9)	8.8(8)	-0.1(9)
C3	14.2(9)	32.0(12)	17.8(10)	4.6(8)	7.8(7)	3.4(8)
C4	18.1(10)	38.6(13)	15.8(10)	-2.7(9)	4.8(8)	-4.0(9)
C5	25.8(11)	30.5(13)	26.9(12)	-5.2(10)	11.7(9)	-3.4(9)
C6	20.8(10)	32.1(13)	25.4(11)	5.6(10)	10.3(9)	5.4(9)
C7	18.2(10)	28.4(12)	12.7(9)	0.4(8)	-1.3(7)	1.9(8)
C8	19.1(10)	20.5(11)	15.9(10)	1.7(8)	1.9(8)	-1.8(8)
C9	18.7(9)	20.6(11)	16.0(9)	2.2(8)	1.7(7)	2.0(8)
C10	18.6(10)	29.3(12)	23.8(10)	6.3(9)	4.0(8)	-2.7(9)
C11	26.4(12)	25.1(12)	32.6(13)	2.2(10)	-0.8(9)	-6.7(10)
C12	29.4(12)	20.2(12)	26.3(11)	-4.7(9)	-4.0(9)	0.3(9)

Table A1.2.4. Bond lengths for **41**.

Atom	Atom	Length (Å)	Atom	Atom	Length (Å)
S1	S2	2.0311(9)	C4	C5	1.380(3)
S1	C1	1.786(2)	C5	C6	1.393(3)
S2	C7	1.784(2)	C7	C8	1.379(3)
O1	C3	1.382(3)	C7	C12	1.385(3)
O2	C9	1.368(2)	C8	C9	1.394(3)
C1	C2	1.390(3)	C9	C10	1.379(3)
C1	C6	1.389(3)	C10	C11	1.386(3)
C2	C3	1.382(3)	C11	C12	1.377(3

Table A1.2.5. Bond angles for **41**.

Atom	Atom	Atom	Angle (°)	Atom	Atom	Atom	Angle (°)
C1	S1	S2	103.92(8)	C1	C6	C5	118.8(2)
C7	S2	S1	105.10(8)	C8	C7	S2	123.40(16)
C2	C1	S1	120.43(17)	C8	C7	C12	120.8(2)
C6	C1	S1	118.70(16)	C12	C7	S2	115.75(17)
C6	C1	C2	120.78(19)	C7	C8	C9	118.72(19)
C3	C2	C1	119.0(2)	O2	C9	C8	115.97(18)
O1	C3	C2	115.59(19)	O2	C9	C10	122.86(19)
C4	C3	O1	123.14(19)	C10	C9	C8	121.2(2)
C4	C3	C2	121.3(2)	C9	C10	C11	118.8(2)
C3	C4	C5	119.3(2)	C12	C11	C10	121.0(2)
C4	C5	C6	120.9(2)	C11	C12	C7	119.4(2)

Table A1.2.6. Hydrogen bonds for **41**.

D	H	A	d(D-H) (Å)	d(H-A) (Å)	d(D-A) (Å)	D-H-A (°)
O1	H1	O2[a]	0.81(3)	1.98(3)	2.718(2)	151(3)
O2	H2	O1[b]	0.79(3)	1.98(3)	2.737(2)	162(3)

[a]1/2-X,1/2+Y,1/2-Z; [b]1/2+X,-1/2+Y,+Z

Table A1.2.7. Torsion angles for **41**.

A	B	C	D	Angle (°)
C2	C1	S1	S2	-51.10(17)
C6	C1	S1	S2	132.28(15)
C8	C7	S2	S1	6.35(18)
C12	C7	S2	S1	-174.49(14)

Table A1.2.8. Hydrogen atom coordinates ($Å \times 10^4$) and isotropic displacement parameters ($Å^2 \times 10^3$) for **41**.

Atom	*x*	*y*	*z*	U(eq)
H1	758(17)	6740(50)	2334(17)	59(10)
H2	5377(17)	2570(50)	3309(16)	52(10)
H2A	1994(13)	6960(40)	3858(13)	31(7)
H4	1167(14)	3410(40)	2084(13)	35(7)
H5	1935(12)	750(40)	2543(13)	29(6)
H6	2743(13)	1180(40)	3612(13)	36(7)
H8	4061(11)	3480(30)	4061(11)	17(5)
H10	5833(13)	5910(40)	3575(13)	34(7)
H11	5588(13)	9100(40)	4036(13)	33(7)
H12	4545(12)	9570(40)	4497(12)	32(7)

A1.3. Crystal structure data of (1R,3s,5r,6R,7S,8s,9S)-6,8,9-tris(benzyloxy)-2,4,10-trioxaadamantane, 66

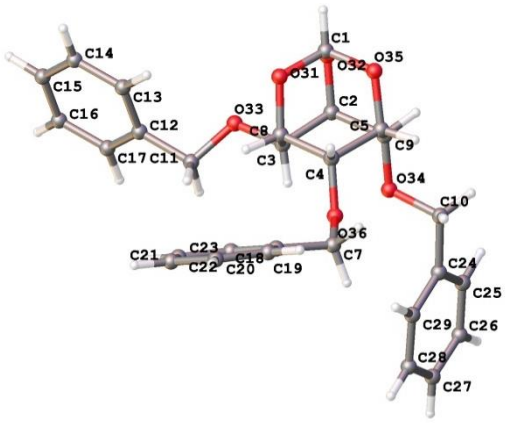

Figure A1.3. One Structure from the unit cell of **66**, determined by X-ray diffraction of a single crystal.

Table A1.3.1. Crystal data and structure refinement for **66**.

Empirical formula	$C_{28}H_{28}O_6$
Formula weight	460.5
Temperature (K)	120
Crystal system	monoclinic
Space group	$P2_1/c$
a (Å)	18.2169(10)
b (Å)	6.0144(3)
c (Å)	20.5746(12)
α (°)	90
β (°)	94.120(2)
γ (°)	90
Volume ($Å^3$)	2248.4(2)
Z	4
ρ_{calc}g (cm^3)	1.36
μ (mm^{-1})	0.776
F(000)	976
Crystal size (mm^3)	0.32 × 0.1 × 0.06
Radiation	CuKα (λ = 1.54178)
2Θ range for data collection (°)	9.59 to 144.974
Index ranges	$-21 \leq h \leq 22$, $-7 \leq k \leq 7$, $-24 \leq l \leq 25$
Reflections collected	24822
Independent reflections	4434 [R_{int} = 0.0373, R_{sigma} = 0.0259]
Data/ restraints/ parameters	4434/0/419
Goodness-of-fit on F^2	1.065
Final R indexes [I > = 2σ (I)]	R_1 = 0.0356, wR_2 = 0.0830
Final R indexes [all data]	R_1 = 0.0447, wR_2 = 0.0881
Largest diff. peak/ hole (e $Å^{-3}$)	0.24/-0.25

Table A1.3.2. Fractional atomic coordinates ($\times 10^4$) and equivalent isotropic displacement parameters ($Å^2 \times 10^3$) for **66**. U_{eq} is defined as 1/3 of the trace of the orthogonalised U_{IJ} tensor.

Atom	*x*	*y*	*z*	U(eq)
O1	9262.4(5)	4596.6(14)	5395.1(4)	18.1(2)
O2	8133.7(5)	5093.4(15)	5832.8(4)	18.7(2)

O3	9027.4(5)	7831.0(14)	5958.7(4)	17.6(2)
O4	8927.6(5)	9275.1(14)	4245.8(4)	16.03(19)
O5	7577.0(5)	9589.7(16)	5761.1(4)	20.1(2)
O6	7869.8(5)	5725.0(14)	4058.5(4)	17.2(2)
C1	8889.3(7)	5541(2)	5907.1(6)	17.8(3)
C2	8996.7(7)	5508(2)	4766.2(6)	15.1(3)
C3	8175.9(7)	4961(2)	4674.8(6)	15.6(3)
C4	7807.1(7)	6054(2)	5237.6(6)	16.0(3)
C5	7933.2(7)	8563(2)	5246.7(6)	15.3(3)
C6	8759.3(7)	8957(2)	5368.4(6)	15.1(3)
C7	9165.4(7)	8017(2)	4805.2(6)	14.2(3)
C8	9314.2(8)	8758(2)	3679.0(6)	21.4(3)
C9	9006.0(7)	10226(2)	3135.2(6)	17.2(3)
C10	9346.0(7)	12229(2)	2998.0(6)	20.4(3)
C11	9043.3(8)	13618(2)	2509.6(7)	23.5(3)
C12	8394.8(8)	13035(3)	2158.0(6)	24.7(3)
C13	8051.6(8)	11043(3)	2293.1(6)	24.8(3)
C14	8358.8(7)	9640(2)	2774.2(6)	21.5(3)
C15	6833.9(7)	10183(3)	5584.8(6)	22.1(3)
C16	6464.3(7)	10683(2)	6199.5(6)	18.9(3)
C17	6470.2(8)	9111(3)	6694.4(7)	26.1(3)
C18	6116.2(9)	9540(3)	7257.8(7)	32.0(4)
C19	5757.1(8)	11547(3)	7329.1(7)	32.3(4)
C20	5752.1(8)	13115(3)	6842.3(8)	32.0(4)
C21	6104.5(8)	12687(2)	6276.5(7)	25.3(3)
C22	7531.5(7)	3987(2)	3666.6(6)	20.2(3)
C23	6788.1(7)	3310(2)	3879.0(6)	17.9(3)
C24	6525.0(8)	1156(2)	3775.5(7)	25.5(3)
C25	5818.0(9)	595(3)	3933.5(8)	32.9(4)
C26	5375.7(8)	2149(3)	4208.8(8)	35.2(4)
C27	5634.7(8)	4288(3)	4319.1(7)	29.7(3)
C28	6334.0(7)	4867(2)	4150.2(6)	21.3(3)

Table A1.3.3. Anisotropic displacement parameters ($Å^2 \times 10^3$) for **66**. The anisotropic displacement factor exponent takes the form: $-2\pi^2[h^2a^{*2}U_{11}+2hka^*b^*U_{12}+\ldots]$.

Atom	U_{11}	U_{22}	U_{33}	U_{23}	U_{13}	U_{12}
O1	17.7(5)	15.8(4)	20.4(4)	4.0(4)	-0.7(3)	2.6(4)
O2	17.1(4)	22.3(5)	16.6(4)	4.9(4)	-0.2(3)	-3.5(4)
O3	19.4(5)	17.6(4)	15.2(4)	1.7(4)	-3.8(3)	-1.4(4)
O4	17.7(4)	15.9(4)	14.8(4)	2.8(3)	3.6(3)	2.5(3)
O5	15.3(5)	28.7(5)	16.1(4)	-5.8(4)	0.3(3)	5.3(4)
O6	18.6(5)	17.8(4)	14.8(4)	-1.3(4)	-1.7(3)	-2.9(4)
C1	16.9(6)	18.0(6)	18.2(6)	3.6(5)	-1.3(5)	-2.2(5)
C2	15.1(6)	13.5(6)	16.5(6)	1.7(5)	1.0(5)	1.7(5)
C3	17.1(6)	12.9(6)	16.6(6)	0.2(5)	0.0(5)	-1.5(5)
C4	14.0(6)	19.7(6)	14.0(6)	1.5(5)	-0.2(4)	-2.4(5)
C5	15.2(6)	18.5(6)	12.3(6)	-1.8(5)	1.4(4)	1.9(5)
C6	16.6(6)	13.0(6)	15.2(6)	1.1(5)	-1.4(5)	-0.6(5)
C7	12.6(6)	13.6(6)	16.0(6)	2.4(5)	-0.8(4)	-0.6(5)
C8	22.9(7)	23.2(7)	18.9(6)	2.3(6)	7.4(5)	6.3(6)
C9	18.4(6)	19.3(6)	14.5(6)	-1.3(5)	5.1(5)	3.4(5)
C10	19.1(7)	22.5(7)	19.7(6)	-1.0(5)	2.5(5)	-0.3(5)
C11	28.6(7)	20.1(7)	22.7(7)	2.9(6)	8.9(5)	1.1(6)
C12	29.5(8)	31.6(8)	13.2(6)	2.1(6)	3.5(5)	10.7(6)
C13	23.2(7)	34.4(8)	16.5(6)	-7.3(6)	-1.4(5)	1.5(6)
C14	23.2(7)	22.0(7)	19.6(6)	-5.1(5)	4.6(5)	-2.5(6)
C15	17.8(6)	30.1(8)	18.4(6)	-0.6(6)	0.7(5)	7.7(6)
C16	14.4(6)	24.0(7)	18.2(6)	-3.2(5)	0.8(5)	-0.1(5)
C17	27.8(8)	27.1(8)	23.4(7)	0.5(6)	1.9(6)	1.0(6)

C18	31.0(8)	44.1(9)	21.1(7)	2.6(7)	2.5(6)	-9.4(7)
C19	21.0(7)	53.4(10)	23.3(7)	-14.7(7)	7.5(6)	-8.6(7)
C20	24.5(8)	34.8(9)	37.2(8)	-14.7(7)	6.7(6)	3.3(7)
C21	21.0(7)	26.7(7)	28.5(7)	-1.9(6)	4.1(5)	2.2(6)
C22	19.2(7)	23.4(7)	18.1(6)	-7.5(5)	1.5(5)	-3.3(5)
C23	17.4(6)	21.1(7)	14.4(6)	1.4(5)	-3.4(5)	-1.6(5)
C24	26.7(7)	21.7(7)	26.5(7)	0.8(6)	-8.2(6)	-2.1(6)
C25	28.6(8)	27.6(8)	40.3(9)	10.6(7)	-12.9(7)	-12.6(7)
C26	17.6(7)	46.7(10)	40.5(9)	18.3(8)	-4.5(6)	-8.0(7)
C27	18.3(7)	40.7(9)	30.1(8)	7.4(7)	2.1(6)	2.7(6)
C28	18.3(7)	24.2(7)	21.0(6)	1.4(6)	-1.1(5)	-0.5(5)

Table A1.3.4. Bond lengths for **66**.

Atom	Atom	Length (Å)	Atom	Atom	Length (Å)
O1	C1	1.4134(16)	C9	C14	1.3928(18)
O1	C2	1.4557(14)	C10	C11	1.3899(19)
O2	C1	1.4002(15)	C11	C12	1.385(2)
O2	C4	1.4431(14)	C12	C13	1.389(2)
O3	C1	1.4026(15)	C13	C14	1.388(2)
O3	C6	1.4446(14)	C15	C16	1.5053(18)
O4	C7	1.4190(14)	C16	C17	1.389(2)
O4	C8	1.4391(15)	C16	C21	1.3863(19)
O5	C5	1.4219(14)	C17	C18	1.391(2)
O5	C15	1.4216(15)	C18	C19	1.386(2)
O6	C3	1.4242(14)	C19	C20	1.375(2)
O6	C22	1.4322(15)	C20	C21	1.393(2)
C2	C3	1.5294(17)	C22	C23	1.5084(18)
C2	C7	1.5407(17)	C23	C24	1.3929(19)
C3	C4	1.5283(17)	C23	C28	1.3924(19)
C4	C5	1.5262(18)	C24	C25	1.392(2)
C5	C6	1.5262(17)	C25	C26	1.382(2)
C6	C7	1.5275(17)	C26	C27	1.384(2)
C8	C9	1.5022(18)	C27	C28	1.389(2)
C9	C10	1.3927(18)			

Table A1.3.5. Bond angles of **63**.

Atom	Atom	Atom	Angle (°)
C1	O1	C2	111.35(9)
C1	O2	C4	110.96(9)
C1	O3	C6	110.42(9)
C7	O4	C8	113.79(9)
C15	O5	C5	113.35(9)
C3	O6	C22	113.02(10)
O2	C1	O1	111.28(10)
O2	C1	O3	111.51(10)
O3	C1	O1	110.96(10)
O1	C2	C3	106.74(10)
O1	C2	C7	105.68(9)
C3	C2	C7	114.00(10)
O6	C3	C2	110.91(10)
O6	C3	C4	111.75(10)
C4	C3	C2	107.06(10)
O2	C4	C3	107.09(10)
O2	C4	C5	109.44(10)
C5	C4	C3	111.13(10)
O5	C5	C4	111.24(10)
O5	C5	C6	107.92(10)
C4	C5	C6	107.55(10)

O3	C6	C5	109.57(10)
O3	C6	C7	108.13(10)
C5	C6	C7	110.09(10)
O4	C7	C2	115.59(10)
O4	C7	C6	106.36(9)
O4	C8	C9	107.34(10)
C10	C9	C8	120.77(12)
C14	C9	C8	120.34(12)
C14	C9	C10	118.84(12)
C11	C10	C9	120.48(13)
C12	C11	C10	120.30(13)
C11	C12	C13	119.55(13)
C14	C13	C12	120.19(13)
C13	C14	C9	120.62(13)
O5	C15	C16	108.12(10)
C17	C16	C15	119.96(12)
C21	C16	C15	120.88(12)
C21	C16	C17	119.14(13)
C16	C17	C18	120.34(14)
C19	C18	C17	120.03(15)
C20	C19	C18	119.91(14)
C19	C20	C21	120.18(15)
C16	C21	C20	120.39(14)
O6	C22	C23	113.12(10)
C24	C23	C22	120.86(12)
C28	C23	C22	120.41(12)
C28	C23	C24	118.63(13)
C25	C24	C23	120.24(14)
C26	C25	C24	120.55(14)
C25	C26	C27	119.62(14)
C26	C27	C28	120.02(15)

Table A1.3.6. Torsion angles for **66.**

A	B	C	D	Angle (°)	A	B	C	D	Angle (°)
O1	C2	C3	O6	-177.98(9)	C4	C5	C6	O3	-55.19(12)
O1	C2	C7	O4	-177.90(9)	C4	C5	C6	C7	63.59(13)
O2	C4	C3	O6	177.46(9)	C5	C4	O2	C1	-58.77(13)
O2	C4	C5	O5	-63.22(13)	C5	C4	C3	O6	-63.05(13)
O3	C6	C5	O5	64.91(12)	C5	C6	O3	C1	59.26(13)
O3	C6	C7	O4	-175.76(9)	C5	C6	C7	O4	64.58(12)
C2	O1	C1	O2	61.18(13)	C6	O3	C1	O1	61.97(12)
C2	O1	C1	O3	-63.61(12)	C6	O3	C1	O2	-62.69(13)
C2	C3	O6	C22	122.67(11)	C6	C5	O5	C15	154.80(11)
C2	C3	C4	O2	-60.91(12)	C6	C5	C4	O2	54.75(13)
C2	C3	C4	C5	58.57(13)	C6	C7	O4	C8	173.98(10)
C2	C7	O4	C8	-67.13(14)	C6	C7	C2	O1	-59.51(12)
C2	C7	C6	O3	60.02(12)	C7	C2	O1	C1	61.64(12)
C2	C7	C6	C5	-59.64(12)	C7	C2	C3	O6	65.73(13)
C3	C2	O1	C1	-60.07(12)	C7	C6	O3	C1	-60.73(12)
C3	C2	C7	O4	-61.00(14)	C7	C6	C5	O5	-176.31(10)
C3	C2	C7	C6	57.39(13)	C9	C8	O4	C7	-179.57(10)
C3	C4	O2	C1	61.79(12)	C10	C9	C8	O4	95.28(14)
C3	C4	C5	O5	178.71(9)	C14	C9	C8	O4	-82.42(15)
C3	C4	C5	C6	-63.32(13)	C16	C15	O5	C5	165.46(11)
C4	O2	C1	O1	-61.85(13)	C17	C16	C15	O5	-55.14(17)
C4	O2	C1	O3	62.63(13)	C21	C16	C15	O5	125.95(13)
C4	C3	O6	C22	-117.95(11)	C23	C22	O6	C3	76.58(14)
C4	C3	C2	O1	59.86(12)	C24	C23	C22	O6	-151.41(12)

C4	C3	C2	C7	-56.43(13)	C28	C23	C22	O6	32.20(17)
C4	C5	O5	C15	-87.45(13)					

Table A1.3.7. Hydrogen atom coordinates (Å×10^4) and isotropic displacement parameters (Å^2×10^3) for **66**.

Atom	*x*	*y*	*z*	U(eq)
H1	9090(8)	4810(20)	6329(7)	16(3)
H2	9274(7)	4750(20)	4445(7)	11(3)
H3	8124(8)	3320(20)	4708(7)	15(3)
H4	7274(9)	5670(20)	5229(7)	20(4)
H5	7769(7)	9210(20)	4827(7)	12(3)
H6	8863(8)	10520(20)	5431(6)	12(3)
H7	9700(8)	8180(20)	4904(7)	18(4)
H8A	9234(9)	7170(30)	3551(8)	29(4)
H8B	9855(9)	9030(30)	3785(8)	28(4)
H10	9796(9)	12630(30)	3259(8)	28(4)
H11	9293(9)	15010(30)	2421(8)	31(4)
H12	8176(9)	13970(30)	1814(8)	33(4)
H13	7608(10)	10610(30)	2039(8)	34(4)
H14	8122(9)	8240(30)	2872(8)	34(4)
H15A	6810(9)	11510(30)	5281(8)	32(4)
H15B	6575(9)	8910(30)	5338(8)	30(4)
H17	6741(9)	7690(30)	6638(8)	33(4)
H18	6124(10)	8420(30)	7601(9)	48(5)
H20	5515(10)	14540(30)	6888(8)	37(5)
H19	5522(9)	11840(30)	7728(8)	37(5)
H21	6106(9)	13850(30)	5924(8)	33(4)
H22A	7869(9)	2670(30)	3665(7)	29(4)
H22B	7474(8)	4620(30)	3214(8)	24(4)
H24	6841(9)	80(30)	3589(8)	26(4)
H25	5644(10)	-890(30)	3830(8)	37(5)
H26	4893(11)	1750(30)	4330(9)	46(5)
H27	5318(11)	5390(30)	4508(9)	43(5)
H28	6508(9)	6390(30)	4216(8)	28(4)

A1.4. Crystal structure data of Synthesis of (1R,2R,3R,4R,5S,6R)-2,3,4,5,6-pentakis(benzyloxy)cyclohexan-1-ol, 70

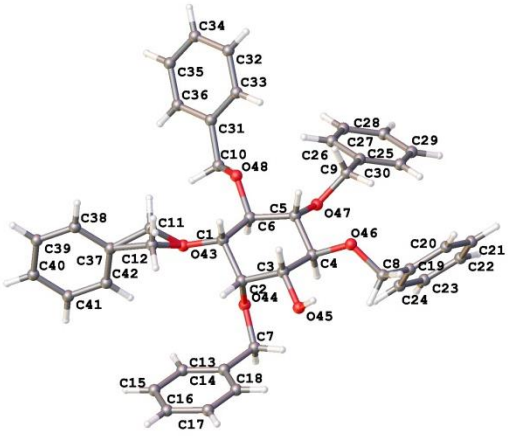

Figure A1.4. One Structure from the unit cell of **70**, determined by X-ray diffraction of a single crystal.

Table A1.4.1. Crystal data and structure refinement for **70**.

Empirical formula	$C_{41}H_{42}O_6$
Formula weight	630.74
Temperature (K)	120
Crystal system	monoclinic
Space group	$P2_1/c$
a (Å)	5.9094(4)
b (Å)	19.6749(12)
c (Å)	28.4930(17)
α (°)	90
β (°)	92.498(3)
γ (°)	90
Volume (Å^3)	3309.6(4)
Z	4
ρ_{calc}g (cm^3)	1.266
μ (mm^{-1})	0.084
F(000)	1344
Crystal size (mm^3)	0.3 × 0.05 × 0.03
Radiation	MoKα (λ = 0.71073)
2Θ range for data collection (°)	4.766 to 52.998
Index ranges	$-7 \le h \le 7$, $-24 \le k \le 24$, $-35 \le l \le 35$
Reflections collected	41702
Independent reflections	6874 [R_{int} = 0.1152, R_{sigma} = 0.0936]
Data/ restraints/ parameters	6874/2/424
Goodness-of-fit on F^2	1.018
Final R indexes [I > = 2σ (I)]	R_1 = 0.0588, wR_2 = 0.1007
Final R indexes [all data]	R_1 = 0.1244, wR_2 = 0.1193
Largest diff. peak/ hole (e Å^{-3})	0.23/-0.25

Table A1.4.2. Fractional atomic coordinates (×10^4) and equivalent isotropic displacement parameters (Å^2×10^3) for **70**. U_{eq} is defined as 1/3 of the trace of the orthogonalised U_{IJ} tensor.

Atom	*x*	*y*	*z*	U(eq)
O1	-528(2)	2751.1(8)	4481.9(5)	23.3(4)
O2	-785(2)	3913.7(7)	3866.3(5)	20.1(4)
O3	3491(2)	4222.2(7)	3422.4(5)	20.8(4)
O4	4887(2)	3004.6(7)	2965.7(5)	20.3(4)
O5	6000(2)	1976.4(7)	3665.5(5)	21.8(4)
O6	4627(2)	2731.9(7)	4428.2(5)	17.5(4)
C1	747(4)	2805.4(11)	4070.1(7)	17.1(5)
C2	1268(3)	3540.7(11)	3945.4(7)	16.3(5)
C3	2524(4)	3567.0(11)	3490.6(7)	17.1(5)
C4	4464(4)	3064.5(10)	3456.2(7)	16.3(5)
C5	3957(3)	2359.9(10)	3645.0(7)	16.3(5)
C6	2947(3)	2406.4(11)	4125.4(7)	16.2(5)
C21	-1537(4)	4294.8(11)	4263.2(8)	25.0(6)
C22	-695(4)	5016.0(11)	4262.2(8)	22.1(5)
C23	-2007(4)	5532.4(12)	4059.4(8)	31.0(6)
C24	-1235(5)	6197.1(13)	4062.9(9)	40.4(7)
C25	863(5)	6354.6(13)	4261.0(9)	39.3(7)
C26	2186(5)	5848.9(13)	4458.4(9)	34.4(6)
C27	1407(4)	5186.7(12)	4462.2(8)	27.5(6)
C31	2244(4)	4655.9(12)	3102.3(8)	28.2(6)
C32	3721(4)	5247.9(11)	2999.1(7)	19.5(5)
C33	3110(4)	5900.1(12)	3126.6(8)	28.9(6)
C34	4493(5)	6444.3(13)	3031.6(9)	39.8(7)
C35	6482(5)	6346.6(14)	2808.4(9)	41.0(7)
C36	7108(4)	5698.0(14)	2679.6(8)	35.3(7)

C37	5730(4)	5154.5(12)	2774.7(8)	25.9(6)
C41	7159(4)	3141.5(11)	2853.6(7)	18.1(5)
C42	7327(4)	3163(1)	2329.6(7)	15.8(5)
C43	5549(4)	3391.5(11)	2040.0(8)	22.4(5)
C44	5736(4)	3394.9(12)	1556.3(8)	29.1(6)
C45	7687(5)	3174.5(12)	1360.1(8)	32.0(6)
C46	9480(4)	2956.9(12)	1645.3(8)	31.0(6)
C47	9301(4)	2952.2(11)	2128.7(8)	22.8(5)
C51A	5569(8)	1275(2)	3588(3)	24.1(19)
C51B	5923(6)	1369.6(16)	3405.8(14)	24.5(10)
C52	7817(4)	899.0(11)	3585.2(8)	25.0(6)
C53	8322(5)	370.2(12)	3285.0(9)	35.9(7)
C54	10112(4)	-59.4(12)	3388.3(8)	33.1(6)
C55	11441(4)	35.5(12)	3790.3(9)	33.9(6)
C56	10946(5)	557.3(12)	4091.5(9)	34.9(7)
C57	9148(4)	986.4(11)	3986.5(8)	25.0(6)
C61	4200(4)	2711.1(11)	4922.4(7)	19.9(5)
C62	3984(4)	2001.0(11)	5108.9(7)	17.4(5)
C63	5736(4)	1535.9(11)	5062.3(7)	21.4(5)
C64	5530(4)	879.3(12)	5228.6(8)	26.4(6)
C65	3598(4)	678.9(12)	5448.5(7)	26.5(6)
C66	1857(4)	1136.7(12)	5497.0(8)	27.0(6)
C67	2057(4)	1793.0(12)	5326.2(7)	22.8(5)

Table A1.4.3. Anisotropic displacement parameters ($Å^2 \times 10^3$) for **70**. The anisotropic displacement factor exponent takes the form: $-2\pi^2[h^2a^{*2}U_{11}+2hka^*b^*U_{12}+\ldots]$.

Atom	**U_{11}**	**U_{22}**	**U_{33}**	**U_{23}**	**U_{13}**	**U_{12}**
O1	14.7(9)	34.5(10)	20.9(9)	6.7(7)	2.1(7)	-2.0(8)
O2	16.6(9)	19.8(9)	23.8(9)	-4.3(7)	-2.1(7)	3.6(7)
O3	19.5(9)	16.1(8)	26.2(9)	7.9(7)	-6.5(7)	-3.2(7)
O4	15.0(9)	32.4(9)	13.3(8)	-1.3(7)	0.3(6)	-4.3(7)
O5	13.9(9)	15.7(8)	35.3(10)	-4.7(7)	-3.8(7)	2.1(7)
O6	15.9(8)	20.8(8)	15.5(8)	0.8(6)	-2.4(6)	-4.1(7)
C1	16.2(12)	21.2(13)	14.0(12)	0.1(9)	2.6(9)	-3.9(10)
C2	10.6(12)	20.6(12)	17.4(12)	-1.1(9)	-2.9(9)	-0.7(10)
C3	14.7(12)	18.0(12)	18.1(12)	1.0(9)	-5.1(9)	-4.7(10)
C4	15.0(12)	21.2(12)	12.5(11)	0.5(9)	-2.1(9)	-1.4(10)
C5	12.0(12)	18.4(12)	18.0(12)	-0.8(9)	-3.2(9)	-2.2(10)
C6	13.3(12)	15.6(12)	19.2(12)	3.6(9)	-4.5(9)	-3.4(9)
C21	22.1(14)	26.4(14)	26.9(13)	-8.4(11)	6.7(11)	2.1(11)
C22	23.7(14)	25.2(13)	17.7(12)	-7(1)	4.3(10)	1.8(11)
C23	31.4(16)	34.2(16)	26.8(14)	-8.2(11)	-4.6(12)	7.4(12)
C24	64(2)	25.8(15)	31.3(16)	-1.5(12)	-3.4(14)	11.5(15)
C25	60(2)	26.6(15)	32.0(15)	-10.7(12)	7.5(14)	-5.7(14)
C26	34.8(16)	32.5(16)	36.2(15)	-13.9(12)	3.8(12)	-6.1(13)
C27	28.7(15)	27.3(15)	26.2(14)	-8.0(11)	-0.2(11)	4.4(12)
C31	21.6(14)	26.2(14)	35.8(15)	13.4(11)	-9.5(11)	0.1(11)
C32	18.1(13)	19.9(13)	20.1(12)	7.1(10)	-4.7(10)	1.3(10)
C33	29.0(15)	26.8(15)	30.6(14)	3.2(11)	-2.8(11)	6.3(12)
C34	53(2)	18.2(14)	46.5(17)	-0.2(12)	-13.9(15)	4.4(14)
C35	44.5(19)	29.4(16)	47.6(18)	17.5(13)	-14.1(15)	-18.0(14)
C36	27.0(15)	47.1(18)	31.9(15)	7.8(13)	2.6(12)	-7.0(13)
C37	27.3(15)	22.2(14)	28.0(14)	-0.7(11)	-3.6(11)	2.7(11)
C41	12.8(12)	22.4(13)	18.7(12)	2.3(10)	-2.4(9)	-1.3(10)
C42	18.3(13)	11.8(11)	17.2(12)	0.6(9)	-1.2(10)	-3.3(10)
C43	19.4(13)	24.4(13)	23.3(13)	4.7(10)	0.3(10)	-2.5(11)
C44	31.1(15)	32.2(15)	23.1(14)	8.0(11)	-7.5(12)	-9.2(12)
C45	45.5(18)	36.6(16)	14.3(13)	-0.5(11)	5.6(12)	-18.2(13)
C46	34.8(16)	32.3(15)	26.7(14)	-4.4(11)	9.8(12)	-6.2(12)

C47	22.4(14)	22.4(13)	23.4(13)	0.8(10)	0.4(10)	-0.9(11)
C52	21.7(14)	19.1(13)	34.0(14)	-1.8(11)	-2.1(11)	3.4(11)
C53	45.8(18)	32.4(15)	28.3(15)	-8.5(12)	-13.9(13)	11.4(13)
C54	46.2(18)	25.2(14)	27.9(15)	-5.7(11)	1.2(13)	12.9(13)
C55	38.0(16)	24.8(14)	38.3(16)	2.8(12)	-6.4(13)	12.1(13)
C56	50.0(18)	22.2(14)	30.9(15)	1.5(11)	-14.4(13)	3.3(13)
C57	33.3(15)	16.6(13)	25.4(13)	-1.6(10)	5.1(11)	-1.4(11)
C61	19.0(13)	23.6(13)	16.9(12)	-1.5(10)	-0.3(10)	-1.8(10)
C62	19.8(13)	21.7(13)	10.5(11)	-0.2(9)	-2.8(9)	-1.9(10)
C63	20.4(13)	26.6(14)	17.1(12)	-0.7(10)	-0.4(10)	-0.6(11)
C64	29.2(15)	25.4(14)	24.1(13)	-0.1(11)	-4.8(11)	5.9(11)
C65	39.1(16)	21.3(13)	18.8(13)	4.7(10)	-4.7(11)	-5.5(12)
C66	24.7(14)	34.2(15)	22.1(13)	2.9(11)	0.7(11)	-10.5(12)
C67	21.9(14)	27.8(14)	18.5(12)	-1.8(10)	0(1)	0.1(11)

Table A1.4.4. Bond lengths of **70**.

Atom	Atom	Length (Å)	Atom	Atom	Length (Å)
O1	C1	1.426(2)	C32	C37	1.385(3)
O2	C2	1.427(2)	C33	C34	1.381(3)
O2	C21	1.443(2)	C34	C35	1.374(4)
O3	C3	1.427(2)	C35	C36	1.383(4)
O3	C31	1.430(2)	C36	C37	1.378(3)
O4	C4	1.435(2)	C41	C42	1.501(3)
O4	C41	1.420(2)	C42	C43	1.383(3)
O5	C5	1.423(2)	C42	C47	1.385(3)
O5	C51A	1.419(4)	C43	C44	1.387(3)
O5	C51B	1.404(3)	C44	C45	1.374(3)
O6	C6	1.437(2)	C45	C46	1.375(3)
O6	C61	1.442(2)	C46	C47	1.386(3)
C1	C2	1.524(3)	C51A	C52	1.521(5)
C1	C6	1.521(3)	C51B	C52	1.524(4)
C2	C3	1.522(3)	C52	C53	1.388(3)
C3	C4	1.521(3)	C52	C57	1.370(3)
C4	C5	1.521(3)	C53	C54	1.376(3)
C5	C6	1.520(3)	C54	C55	1.373(3)
C21	C22	1.504(3)	C55	C56	1.377(3)
C22	C23	1.389(3)	C56	C57	1.380(3)
C22	C27	1.385(3)	C61	C62	1.502(3)
C23	C24	1.385(3)	C62	C63	1.392(3)
C24	C25	1.375(4)	C62	C67	1.382(3)
C25	C26	1.371(4)	C63	C64	1.383(3)
C26	C27	1.382(3)	C64	C65	1.383(3)
C31	C32	1.492(3)	C65	C66	1.379(3)
C32	C33	1.386(3)	C66	C67	1.387(3)

Table A1.4.5. Bond angles for **70**.

Atom	Atom	Atom	Angle (°)	Atom	Atom	Atom	Angle (°)
C2	O2	C21	115.59(16)	C37	C32	C33	118.8(2)
C3	O3	C31	115.33(16)	C34	C33	C32	120.2(2)
C41	O4	C4	114.19(15)	C35	C34	C33	120.5(2)
C51A	O5	C5	111.3(2)	C34	C35	C36	119.7(2)
C51B	O5	C5	114.93(18)	C37	C36	C35	119.8(3)
C6	O6	C61	115.35(15)	C36	C37	C32	120.9(2)
O1	C1	C2	112.48(17)	O4	C41	C42	109.49(17)
O1	C1	C6	110.85(16)	C43	C42	C41	121.4(2)
C6	C1	C2	109.47(17)	C43	C42	C47	118.9(2)
O2	C2	C1	110.22(17)	C47	C42	C41	119.75(19)
O2	C2	C3	106.90(16)	C42	C43	C44	120.2(2)

C3	C2	C1	109.98(17)	C45	C44	C43	120.5(2)
O3	C3	C2	111.08(17)	C44	C45	C46	119.8(2)
O3	C3	C4	105.72(17)	C45	C46	C47	120.0(2)
C4	C3	C2	115.46(17)	C42	C47	C46	120.7(2)
O4	C4	C3	106.24(16)	O5	C51A	C52	108.9(3)
O4	C4	C5	108.35(16)	O5	C51B	C52	109.5(2)
C3	C4	C5	114.12(18)	C53	C52	C51A	125.4(3)
O5	C5	C4	108.52(17)	C53	C52	C51B	115.0(2)
O5	C5	C6	111.13(16)	C57	C52	C51A	113.8(3)
C6	C5	C4	110.79(17)	C57	C52	C51B	126.2(2)
O6	C6	C1	113.40(17)	C57	C52	C53	118.5(2)
O6	C6	C5	106.24(16)	C54	C53	C52	120.8(2)
C5	C6	C1	107.75(16)	C55	C54	C53	120.1(2)
O2	C21	C22	112.07(18)	C54	C55	C56	119.5(2)
C23	C22	C21	120.8(2)	C55	C56	C57	120.2(2)
C27	C22	C21	121.3(2)	C52	C57	C56	120.8(2)
C27	C22	C23	117.9(2)	O6	C61	C62	113.14(17)
C24	C23	C22	120.7(2)	C63	C62	C61	120.2(2)
C25	C24	C23	120.4(2)	C67	C62	C61	121.2(2)
C26	C25	C24	119.5(2)	C67	C62	C63	118.6(2)
C25	C26	C27	120.2(2)	C64	C63	C62	120.3(2)
C26	C27	C22	121.2(2)	C63	C64	C65	120.5(2)
O3	C31	C32	107.58(17)	C66	C65	C64	119.6(2)
C33	C32	C31	120.6(2)	C65	C66	C67	119.9(2)
C37	C32	C31	120.5(2)	C62	C67	C66	121.1(2)

Table A1.4.6. Hydrogen bonds for **70**.

D	H	A	d(D-H) (Å)	d(H-A) (Å)	d(D-A) (Å)	D-H-A (°)
O1	H1	O6[a]	0.84	2.05	2.861(2)	163

[a]-1+X,+Y,+Z

Table A1.4.7. Torsion angles for **70**.

A	B	C	D	Angle (°)	A	B	C	D	Angle (°)
O1	C1	C2	O2	-59.5(2)	C4	C5	C6	O6	-61.0(2)
O1	C1	C6	O6	-74.7(2)	C5	C4	O4	C41	-112.16(19)
O2	C2	C3	O3	73.9(2)	C5	C4	C3	O3	164.57(16)
O3	C3	C4	O4	-76.11(19)	C5	C6	O6	C61	-168.59(16)
O4	C4	C5	O5	71.4(2)	C5	C6	C1	O1	167.99(16)
O5	C5	C6	O6	59.7(2)	C6	C1	C2	O2	176.76(16)
C1	C2	O2	C21	96.0(2)	C6	C5	O5	C51A	89.5(4)
C1	C2	C3	O3	-166.45(16)	C6	C5	O5	C51B	115.9(3)
C1	C2	C3	C4	-46.1(2)	C6	C5	C4	O4	-166.31(16)
C1	C6	O6	C61	73.2(2)	C22	C21	O2	C2	93.0(2)
C1	C6	C5	O5	-178.45(16)	C23	C22	C21	O2	93.4(3)
C1	C6	C5	C4	60.8(2)	C27	C22	C21	O2	-86.5(3)
C2	C1	C6	O6	49.9(2)	C32	C31	O3	C3	-168.35(18)
C2	C1	C6	C5	-67.3(2)	C33	C32	C31	O3	-116.4(2)
C2	C3	O3	C31	-100.4(2)	C37	C32	C31	O3	63.5(3)
C2	C3	C4	O4	160.67(16)	C42	C41	O4	C4	-171.89(16)
C2	C3	C4	C5	41.3(2)	C43	C42	C41	O4	32.4(3)
C3	C2	O2	C21	-144.46(17)	C47	C42	C41	O4	-147.79(19)
C3	C2	C1	O1	-177.15(16)	C52	C51A	O5	C5	176.6(3)
C3	C2	C1	C6	59.1(2)	C52	C51B	O5	C5	-160.4(2)
C3	C4	O4	C41	124.81(18)	C53	C52	C51A	O5	-140.6(4)
C3	C4	C5	O5	-170.45(16)	C53	C52	C51B	O5	-163.4(3)
C3	C4	C5	C6	-48.2(2)	C57	C52	C51A	O5	56.8(6)
C4	C3	O3	C31	133.61(18)	C57	C52	C51B	O5	10.8(5)
C4	C3	C2	O2	-165.77(17)	C62	C61	O6	C6	58.2(2)

C4	C5	O5	C51A	-148.4(4)	C63	C62	C61	O6	56.9(3)
C4	C5	O5	C51B	-122.1(3)	C67	C62	C61	O6	-122.7(2)

Table A1.4.8. Hydrogen atom coordinates (Å×10^4) and isotropic displacement parameters (Å^2×10^3) for **70**.

Atom	*x*	*y*	*z*	U(eq)
H1	-1918	2767	4407	35
H1A	-175	2603	3802	20
H2	2208	3756	4205	20
H3	1407	3477	3224	20
H4	5843	3251	3627	20
H5	2841	2131	3423	20
H6	2632	1940	4245	19
H21A	-988	4069	4557	30
H21B	-3213	4296	4257	30
H23	-3449	5429	3917	37
H24	-2161	6547	3928	48
H25	1392	6811	4261	47
H26	3644	5954	4593	41
H27	2330	4842	4605	33
H31A	837	4813	3244	34
H31B	1829	4407	2809	34
H33	1735	5973	3280	35
H34	4066	6890	3121	48
H35	7423	6723	2743	49
H36	8484	5627	2526	42
H37	6164	4710	2685	31
H41A	8169	2783	2988	22
H41B	7645	3583	2991	22
H43	4195	3547	2173	27
H44	4505	3551	1359	35
H45	7798	3172	1028	38
H46	10840	2810	1511	37
H47	10546	2803	2324	27
H51A	4723	1211	3284	29
H51B	4640	1093	3840	29
H51C	6103	1470	3069	29
H51D	4439	1145	3438	29
H53	7420	304	3005	43
H54	10429	-422	3181	40
H55	12691	-256	3860	41
H56	11846	622	4372	42
H57	8829	1347	4195	30
H61A	2786	2963	4977	24
H61B	5453	2945	5099	24
H63	7078	1670	4916	26
H64	6725	563	5192	32
H65	3472	229	5565	32
H66	524	1003	5647	32
H67	847	2105	5359	27

Table A1.4.9. Atomic occupancy of **70**.

Atom	Occupancy	Atom	Occupancy	Atom	Occupancy
C51A	0.35	H51A	0.35	H51B	0.35
C51B	0.65	H51C	0.65	H51D	0.65

A1.5. Crystal structure data of ^{18}O-cholesterol, 81c

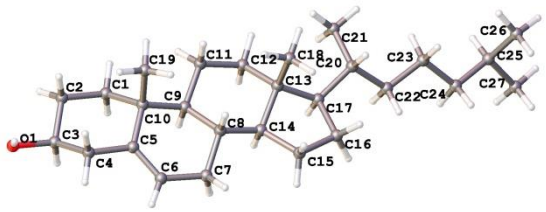

Figure A1.5. One Structure from the unit cell of **81c**, determined by X-ray diffraction of a single crystal.

Table A1.5.1. Crystal data and structure refinement for **81c**

Empirical formula	$C_{27}H_{46}O$
Formula weight	386.64
Temperature (K)	120
Crystal system	triclinic
Space group	P1
a (Å)	10.2708(5)
b (Å)	14.0681(7)
c (Å)	33.9790(17)
α (°)	95.976(3)
β (°)	94.431(3)
γ (°)	90.458(3)
Volume (Å^3)	4867.7(4)
Z	8
ρ_{calc}g (cm^3)	1.055
μ (mm^{-1})	0.454
F(000)	1728
Crystal size (mm^3)	0.23 × 0.1 × 0.06
Radiation	CuKα (λ = 1.54178)
2Θ range for data collection (°)	5.246 to 139.996
Index ranges	-12 ≤ h ≤ 12, -16 ≤ k ≤ 14, -41 ≤ l ≤ 41
Reflections collected	62860
Independent reflections	29489 [R_{int} = 0.0735, R_{sigma} = 0.1036]
Data/ restraints/ parameters	29489/3/2059
Goodness-of-fit on F^2	1.013
Final R indexes [I > = 2σ (I)]	R_1 = 0.0604, wR_2 = 0.1145
Final R indexes [all data]	R_1 = 0.0993, wR_2 = 0.1312
Largest diff. peak/ hole (e Å^{-3})	0.22/-0.21
Flack parameter	-0.2(2)

Table A1.5.2. Fractional atomic coordinates (×10^4) and equivalent isotropic displacement parameters (Å^2×10^3) for **81c**. U_{eq} is defined as 1/3 of the trace of the orthogonalised U_{IJ} tensor.

Atom	*x*	*y*	*z*	U(eq)
O1	6223(3)	9566(3)	1235.8(10)	35(1)
C1	7111(5)	9855(4)	2342.9(14)	23.1(11)
C2	6697(5)	10151(4)	1931.2(14)	25.9(12)
C3	6654(5)	9300(4)	1618.9(14)	25.2(12)
C4	5764(5)	8515(4)	1723.2(14)	26.5(12)
C5	6118(4)	8237(3)	2138.4(14)	18.8(10)
C6	6325(4)	7335(4)	2197.4(14)	22.3(11)
C7	6643(4)	6976(3)	2591.5(13)	20.0(11)

C8	6344(4)	7730(3)	2935.9(14)	17.4(10)
C9	6867(5)	8715(3)	2857.7(14)	19.0(11)
C10	6225(4)	9063(3)	2468.7(14)	18.7(11)
C11	6800(5)	9464(3)	3220.2(13)	21.6(11)
C12	7371(5)	9132(3)	3613.5(14)	21.3(11)
C13	6741(4)	8185(3)	3693.5(14)	17.3(10)
C14	6960(4)	7460(3)	3327.9(13)	17.2(10)
C15	6610(5)	6490(3)	3463.7(14)	23.9(11)
C16	7137(5)	6592(3)	3907.6(14)	21.6(11)
C17	7438(5)	7676(3)	4034.1(14)	19.9(11)
C18	5282(5)	8303(4)	3756.8(15)	25.1(12)
C19	4863(5)	9471(4)	2529.8(15)	24.7(12)
C20	7149(5)	7962(3)	4468.0(14)	20.8(11)
C21	8040(5)	7370(4)	4736.8(15)	25.9(12)
C22	7803(5)	7488(4)	5179.9(14)	27.6(12)
C23	8696(6)	6823(4)	5404.8(15)	32.7(13)
C24	8756(6)	7020(4)	5858.4(16)	36.4(14)
C25	7479(7)	6765(5)	6020.6(18)	50.1(18)
C26	9890(7)	6481(5)	6054.5(17)	54.0(19)
C27	7342(5)	9032(3)	4599.6(15)	26.6(12)
O1A	1318(3)	9858(2)	1190.5(9)	25.8(8)
C1A	974(4)	9204(3)	2221.4(13)	17.7(10)
C2A	683(5)	9691(4)	1839.6(14)	22.2(11)
C3A	1680(5)	9420(3)	1546.9(14)	22.6(11)
C4A	1751(5)	8338(3)	1459.2(14)	21.9(11)
C5A	1947(4)	7826(3)	1830.5(13)	17.8(10)
C6A	2857(5)	7164(3)	1862.4(14)	19.8(11)
C7A	3091(5)	6598(4)	2209.0(14)	20.3(11)
C8A	1991(5)	6685(3)	2492.6(13)	17.3(10)
C9A	1570(4)	7728(3)	2551.9(13)	16.9(10)
C10A	1024(4)	8102(3)	2153.8(14)	17.1(10)
C11A	646(5)	7894(3)	2884.8(13)	19.6(11)
C12A	1165(5)	7517(3)	3274.5(14)	19.6(11)
C13A	1482(4)	6454(3)	3211.2(14)	18.1(10)
C14A	2472(4)	6348(3)	2892.0(13)	17.3(10)
C15A	2966(5)	5324(4)	2900.8(14)	24.4(11)
C16A	2935(5)	5149(4)	3345.4(14)	25.9(12)
C17A	2294(4)	6035(3)	3555.3(14)	19.9(11)
C18A	237(5)	5844(4)	3093.0(15)	25.6(12)
C19A	-340(5)	7672(3)	2017.0(14)	21.6(11)
C20A	1624(5)	5788(4)	3920.9(15)	25.9(12)
C21A	2543(5)	5310(4)	4216.4(15)	26.9(12)
C22A	3763(5)	5891(4)	4375.3(15)	33.0(13)
C23A	4533(5)	5478(4)	4722.2(16)	34.7(14)
C24A	3850(5)	5507(5)	5106.0(16)	38.5(15)
C25A	3547(8)	6515(6)	5270(2)	75(2)
C26A	4703(6)	5011(5)	5411.5(18)	54.1(19)
C27A	992(6)	6655(4)	4137.2(16)	39.2(15)
O1B	1432(3)	2588(3)	2485.2(10)	31.8(9)
C1B	704(4)	1099(4)	3310.8(13)	20.2(11)
C2B	777(5)	1364(4)	2882.2(14)	24.4(12)
C3B	1404(5)	2337(4)	2882.1(14)	20.9(11)
C4B	2761(5)	2352(4)	3090.0(14)	22.3(11)
C5B	2742(4)	2067(3)	3506.9(14)	17.4(10)
C6B	3332(4)	2609(4)	3812.0(14)	21.3(11)
C7B	3426(5)	2385(3)	4232.5(14)	23.2(11)
C8B	3052(5)	1345(3)	4271.3(14)	20.9(11)
C9B	1843(5)	1039(3)	3993.7(14)	17.9(10)
C10B	2049(4)	1121(3)	3548.7(14)	17.7(10)
C11B	1309(5)	57(4)	4069.5(14)	25.6(12)

C12B	1111(5)	-40(4)	4506.5(14)	22.7(11)
C13B	2359(5)	212(4)	4776.4(14)	20.3(11)
C14B	2781(5)	1217(3)	4696.4(14)	20.7(11)
C15B	3858(5)	1514(4)	5027.8(14)	28.2(12)
C16B	3396(5)	1047(4)	5386.5(15)	28.4(12)
C17B	2201(5)	388(4)	5228.7(14)	22.6(11)
C18B	3413(5)	-541(4)	4694.9(15)	28.2(12)
C19B	2879(5)	283(4)	3379.3(14)	26.0(12)
C20B	2053(5)	-461(4)	5477.1(15)	27.0(12)
C21B	1817(5)	-51(4)	5906.0(15)	29.5(12)
C22B	1644(6)	-799(4)	6194.3(15)	33.6(13)
C23B	1421(6)	-325(4)	6611.5(15)	35.5(14)
C24B	952(6)	-1007(4)	6896.6(16)	37.0(14)
C25B	1950(7)	-1766(5)	6980.0(19)	56.2(19)
C26B	602(7)	-439(5)	7279.7(17)	50.0(17)
C27B	946(6)	-1144(4)	5303.1(16)	36.1(14)
O1C	6636(3)	2609(3)	2527.5(9)	28.6(8)
C1C	8444(5)	3644(4)	3497.6(14)	24.3(12)
C2C	7821(5)	3623(4)	3068.0(14)	25.7(12)
C3C	7238(5)	2648(4)	2923.8(14)	24.4(12)
C4C	6208(5)	2394(3)	3194.0(14)	21.2(11)
C5C	6782(4)	2413(3)	3620.9(14)	19.0(11)
C6C	6583(5)	1679(3)	3821.9(14)	19.8(11)
C7C	7104(5)	1600(3)	4244.1(14)	24.5(12)
C8C	7616(5)	2559(3)	4458.4(13)	17.8(10)
C9C	8381(5)	3102(3)	4180.0(14)	18.7(10)
C10C	7536(4)	3314(3)	3799.8(14)	18.7(10)
C11C	9087(5)	3987(4)	4400.3(14)	25.3(12)
C12C	9919(5)	3784(4)	4780.8(14)	25.5(12)
C13C	9122(5)	3285(3)	5064.3(14)	20.6(11)
C14C	8494(5)	2384(3)	4822.4(14)	21.3(11)
C15C	7939(5)	1815(4)	5133.6(14)	25.8(12)
C16C	8925(5)	2032(4)	5502.0(15)	25.2(12)
C17C	9889(5)	2819(3)	5404.3(14)	22.4(11)
C18C	8088(5)	3961(4)	5238.5(15)	25.3(12)
C19C	6533(5)	4092(4)	3893.6(15)	25.4(12)
C20C	10454(5)	3437(4)	5777.1(14)	24.5(11)
C21C	11055(6)	2802(4)	6083.1(15)	33.4(13)
C22C	11375(6)	3302(4)	6500.0(15)	34.3(14)
C23C	11878(6)	2590(4)	6789.7(16)	38.3(15)
C24C	12174(6)	3010(4)	7215.1(17)	38.9(15)
C25C	10965(7)	3358(5)	7404.8(18)	54.9(19)
C26C	12889(8)	2271(5)	7454.4(19)	62(2)
C27C	11463(6)	4167(4)	5682.9(16)	36.5(14)
O1D	8949(3)	2448(3)	2132.3(10)	28.2(9)
C1D	8064(5)	3198(4)	1123.3(14)	23.3(11)
C2D	7939(5)	2696(4)	1497.6(15)	25.5(12)
C3D	9126(5)	2916(3)	1784.3(14)	19.6(11)
C4D	9308(5)	3986(4)	1889.3(14)	24.5(12)
C5D	9356(4)	4531(3)	1525.0(13)	18.1(10)
C6D	10297(5)	5161(3)	1495.4(14)	20.6(11)
C7D	10391(5)	5742(4)	1152.6(14)	22.0(11)
C8D	9138(4)	5710(3)	872.1(13)	16.6(10)
C9D	8601(4)	4676(3)	809.7(13)	16.7(10)
C10D	8245(5)	4298(4)	1201.8(14)	20.5(11)
C11D	7495(5)	4533(4)	478.2(14)	23.5(11)
C12D	7822(5)	4914(3)	88.6(14)	22.4(11)
C13D	8259(4)	5965(3)	155.4(14)	18(1)
C14D	9419(4)	6036(3)	473.2(14)	18.4(10)
C15D	9972(5)	7045(3)	466.6(14)	24.8(12)

C16D	9737(5)	7230(4)	23.2(14)	26.7(12)
C17D	8903(5)	6375(4)	-188.5(14)	20.7(11)
C18D	7112(5)	6596(4)	282.9(15)	28.8(13)
C19D	6993(5)	4749(4)	1347.4(15)	27.9(12)
C20D	8052(5)	6655(4)	-548.1(14)	23.3(11)
C21D	8848(5)	7111(4)	-845.7(15)	26.6(12)
C22D	9909(5)	6482(4)	-1018.1(16)	31.3(13)
C23D	10481(5)	6879(4)	-1373.3(15)	32.5(13)
C24D	9580(6)	6831(5)	-1751.8(16)	39.5(15)
C25D	10224(6)	7355(5)	-2061.0(18)	56(2)
C26D	9223(8)	5810(6)	-1917(2)	77(3)
C27D	7214(5)	5830(4)	-761.4(15)	34.7(14)
O1E	3734(3)	9560(3)	10842.6(9)	27.0(8)
C1E	5038(5)	8617(4)	9865.0(13)	22.1(11)
C2E	4631(5)	8598(4)	10289.8(14)	23.5(11)
C3E	4129(5)	9559(3)	10447.8(13)	20.9(11)
C4E	2961(4)	9818(4)	10179.9(14)	20.8(11)
C5E	3318(4)	9847(3)	9757.7(13)	16(1)
C6E	3013(5)	10601(3)	9564.7(14)	21.8(11)
C7E	3315(5)	10708(3)	9148.8(14)	21.7(11)
C8E	3707(5)	9772(3)	8921.1(14)	19(1)
C9E	4626(4)	9222(3)	9193.1(14)	17.9(10)
C10E	3968(4)	8968(3)	9568.3(14)	18.3(10)
C11E	5234(5)	8359(4)	8962.0(14)	25.6(12)
C12E	5865(5)	8598(4)	8588.1(14)	25.3(12)
C13E	4902(5)	9097(3)	8311.7(14)	21.1(11)
C14E	4403(5)	9978(3)	8559.4(14)	19.1(10)
C15E	3663(5)	10557(4)	8255.9(14)	26.1(12)
C16E	4461(5)	10371(4)	7886.4(14)	24.1(11)
C17E	5493(5)	9596(3)	7974.6(14)	22.2(11)
C18E	3790(5)	8417(3)	8133.0(15)	25.1(12)
C19E	2921(5)	8180(3)	9462.4(14)	22.8(11)
C20E	5872(5)	8997(3)	7597.3(14)	22.2(11)
C21E	6273(5)	9649(4)	7293.0(15)	29.9(13)
C22E	6440(6)	9155(4)	6878.5(15)	32.3(13)
C23E	6787(6)	9876(4)	6593.1(16)	39.6(15)
C24E	6913(6)	9437(4)	6168.0(16)	34.9(14)
C25E	5614(6)	9059(5)	5966.7(18)	51.0(17)
C26E	7499(8)	10174(5)	5927.6(19)	60(2)
C27E	6971(5)	8308(4)	7690.1(15)	32.1(13)
O1F	3954(3)	2516(3)	12199.4(10)	32.4(9)
C1F	4174(5)	2288(4)	11088.2(14)	22.4(11)
C2F	3969(5)	1963(4)	11497.0(15)	29.3(13)
C3F	4184(5)	2800(4)	11814.3(14)	24.4(12)
C4F	3268(5)	3607(4)	11723.2(14)	23.7(11)
C5F	3398(4)	3909(4)	11309.7(14)	19.4(11)
C6F	3621(4)	4816(4)	11261.8(14)	21.0(11)
C7F	3720(4)	5205(3)	10869.3(14)	19.1(10)
C8F	3225(4)	4486(3)	10522.1(13)	16.6(10)
C9F	3752(4)	3481(3)	10588.1(13)	16.8(10)
C10F	3289(4)	3111(3)	10971.4(14)	17.1(10)
C11F	3476(5)	2763(3)	10214.5(14)	20.7(11)
C12F	3875(5)	3135(3)	9830.6(13)	18.9(10)
C13F	3218(4)	4084(3)	9760.7(13)	16.9(10)
C14F	3630(4)	4780(3)	10129.6(13)	16.7(10)
C15F	3237(5)	5763(3)	10011.5(14)	20.4(11)
C16F	3496(5)	5697(3)	9568.0(14)	21.5(11)
C17F	3744(5)	4629(3)	9428.8(13)	17.9(10)
C18F	1728(5)	3973(4)	9695.4(14)	23.3(11)
C19F	1865(5)	2748(4)	10906.3(15)	24.2(11)

C20F	3239(5)	4365(3)	8990.5(13)	19.3(10)
C21F	3989(5)	4975(4)	8729.7(14)	24.9(12)
C22F	3558(5)	4876(4)	8286.5(14)	25.6(12)
C23F	4366(5)	5547(4)	8068.6(14)	28.7(12)
C24F	4211(6)	5363(4)	7613.3(15)	31.2(13)
C25F	2869(6)	5652(4)	7446.1(17)	43.8(16)
C26F	5274(7)	5873(4)	7425.7(17)	46.1(17)
C27F	3349(5)	3301(4)	8850.9(15)	28.6(12)
O1G	8574(3)	-214(3)	10919.7(10)	38.1(10)
C1G	7327(5)	1212(4)	10083.7(13)	21.0(11)
C2G	7625(5)	965(4)	10509.3(15)	27.5(12)
C3G	8312(5)	14(4)	10516.6(14)	25.0(12)
C4G	9563(5)	42(4)	10310.7(14)	24.1(12)
C5G	9314(4)	324(3)	9890.6(14)	19.5(11)
C6G	9761(5)	-218(3)	9587.8(14)	21.1(11)
C7G	9632(5)	21(4)	9165.1(14)	23.7(11)
C8G	9231(5)	1045(3)	9127.9(14)	20.6(11)
C9G	8126(4)	1315(3)	9402.0(14)	19.3(11)
C10G	8558(5)	1239(4)	9847.5(14)	20.6(11)
C11G	7541(5)	2289(4)	9327.3(14)	26.1(12)
C12G	7141(5)	2394(4)	8888.4(14)	25.0(12)
C13G	8279(4)	2186(3)	8628.9(14)	18.1(10)
C14G	8759(5)	1175(3)	8703.1(14)	20.4(11)
C15G	9686(5)	915(4)	8378.7(14)	26.9(12)
C16G	9047(5)	1393(4)	8019.4(15)	30.3(13)
C17G	7908(5)	2012(3)	8174.3(14)	22.4(11)
C18G	9351(5)	2955(4)	8719.4(15)	27.9(12)
C19G	9434(5)	2101(4)	10024.2(15)	27.7(12)
C20G	7636(5)	2865(4)	7929.2(14)	24.3(12)
C21G	7206(5)	2475(4)	7496.4(14)	26.8(12)
C22G	6886(5)	3218(4)	7210.2(14)	30.0(13)
C23G	6492(6)	2747(4)	6791.3(15)	33.6(13)
C24G	5891(6)	3419(4)	6502.9(16)	39.3(15)
C25G	6839(7)	4191(5)	6425.1(19)	61(2)
C26G	5369(7)	2860(5)	6114.6(17)	51.0(18)
C27G	6605(6)	3524(4)	8100.6(15)	35.7(14)

Table A1.5.3. Anisotropic displacement parameters ($Å^2 \times 10^3$) for **81c**. The anisotropic displacement factor exponent takes the form: $-2\pi^2[h^2a^{*2}U_{11}+2hka^*b^*U_{12}+\ldots]$.

Atom	U_{11}	U_{22}	U_{33}	U_{23}	U_{13}	U_{12}
O1	24(2)	60(3)	24(2)	20.4(19)	4.8(17)	2.1(18)
C1	20(3)	24(3)	26(3)	6(2)	1(2)	1(2)
C2	22(3)	31(3)	27(3)	13(2)	2(2)	0(2)
C3	19(3)	40(3)	19(3)	12(2)	2(2)	3(2)
C4	25(3)	35(3)	20(3)	5(2)	2(2)	2(2)
C5	14(2)	21(3)	21(3)	2(2)	4(2)	-3.7(19)
C6	19(3)	27(3)	21(3)	-1(2)	3(2)	-2(2)
C7	17(2)	20(3)	23(3)	3(2)	2(2)	-3(2)
C8	15(2)	18(3)	20(3)	5(2)	4(2)	1.7(19)
C9	17(2)	20(3)	21(3)	4(2)	5(2)	1.5(19)
C10	16(2)	20(3)	21(3)	8(2)	1(2)	2.7(19)
C11	32(3)	16(3)	17(3)	0(2)	4(2)	0(2)
C12	29(3)	15(3)	21(3)	5(2)	0(2)	0(2)
C13	20(2)	14(3)	19(3)	2.2(19)	2(2)	3.1(19)
C14	15(2)	17(3)	20(3)	4(2)	4(2)	-0.3(19)
C15	27(3)	19(3)	25(3)	1(2)	-1(2)	-3(2)
C16	24(3)	15(3)	27(3)	5(2)	4(2)	0(2)
C17	21(3)	13(3)	25(3)	4(2)	2(2)	3(2)
C18	21(3)	26(3)	29(3)	6(2)	3(2)	4(2)

C19	18(3)	34(3)	23(3)	8(2)	0(2)	6(2)
C20	28(3)	18(3)	18(3)	6(2)	1(2)	0(2)
C21	35(3)	16(3)	26(3)	1(2)	1(2)	6(2)
C22	38(3)	25(3)	20(3)	4(2)	4(2)	1(2)
C23	52(4)	17(3)	29(3)	7(2)	-1(3)	0(2)
C24	57(4)	23(3)	29(3)	5(2)	-6(3)	0(3)
C25	78(5)	44(4)	29(3)	12(3)	1(3)	-12(3)
C26	83(5)	43(4)	32(3)	6(3)	-21(4)	16(4)
C27	36(3)	21(3)	22(3)	3(2)	0(2)	3(2)
O1A	26.6(19)	34(2)	18.6(18)	12.9(15)	0.6(15)	2.7(16)
C1A	18(2)	20(3)	16(2)	2(2)	3(2)	2.7(19)
C2A	25(3)	20(3)	23(3)	7(2)	1(2)	7(2)
C3A	23(3)	23(3)	23(3)	7(2)	-1(2)	1(2)
C4A	21(3)	27(3)	19(3)	6(2)	4(2)	1(2)
C5A	15(2)	18(3)	19(3)	-1(2)	-1(2)	-4.3(19)
C6A	20(3)	21(3)	18(3)	-1(2)	5(2)	-1(2)
C7A	23(3)	21(3)	18(3)	2(2)	6(2)	5(2)
C8A	23(3)	15(3)	14(2)	0.4(19)	3(2)	-1.2(19)
C9A	16(2)	18(3)	17(2)	0.7(19)	2(2)	1.3(19)
C10A	15(2)	18(3)	19(2)	2.8(19)	2(2)	0.8(19)
C11A	24(3)	18(3)	16(2)	3(2)	3(2)	4(2)
C12A	20(3)	21(3)	19(3)	3(2)	6(2)	5(2)
C13A	14(2)	21(3)	20(3)	6(2)	0(2)	-0.4(19)
C14A	14(2)	19(3)	19(3)	2(2)	2(2)	0.0(19)
C15A	27(3)	24(3)	23(3)	6(2)	2(2)	7(2)
C16A	27(3)	29(3)	23(3)	8(2)	0(2)	2(2)
C17A	17(2)	20(3)	24(3)	6(2)	3(2)	1(2)
C18A	21(3)	33(3)	24(3)	7(2)	0(2)	-2(2)
C19A	21(3)	22(3)	23(3)	7(2)	-1(2)	3(2)
C20A	23(3)	35(3)	21(3)	9(2)	7(2)	0(2)
C21A	30(3)	32(3)	20(3)	10(2)	3(2)	-1(2)
C22A	30(3)	47(4)	25(3)	18(3)	1(3)	-1(3)
C23A	24(3)	50(4)	32(3)	13(3)	-1(3)	1(3)
C24A	26(3)	65(4)	26(3)	14(3)	0(3)	3(3)
C25A	81(6)	96(7)	46(5)	-4(4)	12(4)	29(5)
C26A	38(4)	92(6)	36(4)	29(4)	-5(3)	-3(4)
C27A	35(3)	60(4)	28(3)	18(3)	10(3)	26(3)
O1B	24(2)	56(3)	19.5(19)	19.2(18)	4.2(16)	6.7(18)
C1B	16(2)	25(3)	20(3)	4(2)	3(2)	2(2)
C2B	20(3)	31(3)	21(3)	3(2)	-2(2)	2(2)
C3B	18(2)	26(3)	21(3)	9(2)	3(2)	7(2)
C4B	22(3)	27(3)	20(3)	5(2)	6(2)	4(2)
C5B	14(2)	19(3)	20(3)	6(2)	5(2)	6.5(19)
C6B	18(3)	25(3)	22(3)	6(2)	3(2)	-2(2)
C7B	25(3)	23(3)	22(3)	3(2)	2(2)	-2(2)
C8B	24(3)	22(3)	18(3)	5(2)	2(2)	4(2)
C9B	20(3)	16(3)	18(2)	1.8(19)	2(2)	4.1(19)
C10B	19(2)	17(3)	16(2)	1.6(19)	-2(2)	2.7(19)
C11B	29(3)	22(3)	26(3)	9(2)	-1(2)	-6(2)
C12B	26(3)	21(3)	22(3)	6(2)	3(2)	-3(2)
C13B	20(3)	25(3)	17(3)	5(2)	0(2)	1(2)
C14B	22(3)	21(3)	19(3)	2(2)	1(2)	-1(2)
C15B	31(3)	37(3)	16(3)	5(2)	-2(2)	-9(2)
C16B	32(3)	32(3)	21(3)	5(2)	1(2)	-5(2)
C17B	28(3)	22(3)	18(3)	4(2)	1(2)	1(2)
C18B	30(3)	30(3)	27(3)	8(2)	9(2)	6(2)
C19B	32(3)	24(3)	21(3)	-1(2)	5(2)	6(2)
C20B	31(3)	26(3)	25(3)	8(2)	2(2)	1(2)
C21B	36(3)	29(3)	25(3)	8(2)	6(3)	5(2)
C22B	42(3)	34(3)	26(3)	10(2)	4(3)	-1(3)

C23B	53(4)	29(3)	25(3)	7(2)	7(3)	1(3)
C24B	47(4)	40(4)	27(3)	12(3)	8(3)	-6(3)
C25B	81(5)	57(5)	36(4)	23(3)	10(4)	15(4)
C26B	65(5)	58(5)	31(3)	12(3)	19(3)	0(4)
C27B	48(4)	34(3)	29(3)	12(3)	7(3)	-9(3)
O1C	25(2)	46(2)	14.2(17)	3.8(16)	1.2(15)	-2.3(17)
C1C	23(3)	26(3)	25(3)	8(2)	0(2)	-3(2)
C2C	27(3)	32(3)	19(3)	8(2)	2(2)	-2(2)
C3C	23(3)	30(3)	20(3)	1(2)	-2(2)	3(2)
C4C	21(3)	18(3)	24(3)	3(2)	0(2)	1(2)
C5C	14(2)	18(3)	25(3)	0(2)	5(2)	5.3(19)
C6C	22(3)	17(3)	20(3)	0(2)	0(2)	-2(2)
C7C	28(3)	19(3)	26(3)	3(2)	2(2)	-3(2)
C8C	23(3)	15(3)	15(2)	1.6(19)	4(2)	2(2)
C9C	19(2)	17(3)	20(3)	1(2)	2(2)	0.7(19)
C10C	21(3)	16(3)	20(3)	3(2)	2(2)	3(2)
C11C	34(3)	21(3)	21(3)	4(2)	3(2)	-8(2)
C12C	30(3)	27(3)	20(3)	7(2)	0(2)	-8(2)
C13C	25(3)	15(3)	22(3)	1(2)	3(2)	0(2)
C14C	27(3)	15(3)	23(3)	3(2)	3(2)	2(2)
C15C	34(3)	22(3)	21(3)	2(2)	1(2)	-5(2)
C16C	28(3)	24(3)	26(3)	5(2)	5(2)	3(2)
C17C	25(3)	22(3)	20(3)	1(2)	2(2)	6(2)
C18C	32(3)	19(3)	24(3)	2(2)	-3(2)	2(2)
C19C	28(3)	21(3)	28(3)	5(2)	2(2)	1(2)
C20C	28(3)	24(3)	21(3)	3(2)	-2(2)	1(2)
C21C	42(3)	29(3)	28(3)	4(2)	-8(3)	2(3)
C22C	42(3)	35(4)	25(3)	4(2)	-7(3)	2(3)
C23C	46(4)	34(4)	33(3)	2(3)	-12(3)	4(3)
C24C	48(4)	32(4)	35(3)	9(3)	-11(3)	-2(3)
C25C	61(5)	68(5)	38(4)	17(3)	0(4)	-5(4)
C26C	91(6)	53(5)	41(4)	17(3)	-26(4)	2(4)
C27C	41(3)	42(4)	25(3)	1(3)	-3(3)	-13(3)
O1D	24.8(19)	42(2)	20.7(19)	18.0(16)	-3.1(16)	-1.9(16)
C1D	23(3)	28(3)	20(3)	6(2)	-3(2)	-6(2)
C2D	22(3)	28(3)	28(3)	10(2)	1(2)	-5(2)
C3D	18(2)	25(3)	17(2)	8(2)	2(2)	1(2)
C4D	20(3)	39(3)	15(3)	5(2)	-1(2)	2(2)
C5D	18(2)	20(3)	16(2)	2(2)	1(2)	4(2)
C6D	20(3)	23(3)	17(2)	-1(2)	-5(2)	7(2)
C7D	17(2)	22(3)	25(3)	-1(2)	-1(2)	-1(2)
C8D	15(2)	15(3)	20(3)	1.1(19)	1(2)	3.3(18)
C9D	17(2)	19(3)	14(2)	6.0(19)	-1(2)	4.8(19)
C10D	18(3)	27(3)	17(3)	4(2)	-1(2)	3(2)
C11D	20(3)	31(3)	21(3)	9(2)	-1(2)	-6(2)
C12D	22(3)	27(3)	18(3)	4(2)	-3(2)	-4(2)
C13D	17(2)	19(3)	19(3)	5(2)	0(2)	4.8(19)
C14D	15(2)	19(3)	21(3)	3(2)	2(2)	2.4(19)
C15D	32(3)	22(3)	20(3)	2(2)	-1(2)	-4(2)
C16D	30(3)	27(3)	25(3)	10(2)	-2(2)	-3(2)
C17D	19(3)	25(3)	20(3)	9(2)	3(2)	3(2)
C18D	22(3)	39(3)	28(3)	15(2)	7(2)	12(2)
C19D	19(3)	41(3)	26(3)	11(2)	4(2)	7(2)
C20D	21(3)	27(3)	25(3)	12(2)	4(2)	9(2)
C21D	29(3)	27(3)	25(3)	10(2)	-1(2)	4(2)
C22D	26(3)	43(4)	28(3)	17(3)	5(2)	8(2)
C23D	28(3)	46(4)	25(3)	9(3)	6(3)	1(3)
C24D	28(3)	65(5)	28(3)	13(3)	8(3)	5(3)
C25D	49(4)	89(6)	36(4)	29(4)	12(3)	22(4)
C26D	74(6)	101(7)	53(5)	-5(5)	-3(4)	-26(5)

C27D	30(3)	49(4)	26(3)	16(3)	-8(3)	-10(3)
O1E	26(2)	41(2)	15.8(18)	8.6(16)	2.1(15)	7.8(16)
C1E	23(3)	25(3)	18(3)	4(2)	-1(2)	10(2)
C2E	25(3)	30(3)	17(3)	10(2)	-2(2)	6(2)
C3E	24(3)	24(3)	15(2)	6(2)	0(2)	0(2)
C4E	19(3)	23(3)	21(3)	5(2)	2(2)	3(2)
C5E	17(2)	15(3)	16(2)	1.5(19)	1(2)	1.1(19)
C6E	27(3)	17(3)	21(3)	1(2)	2(2)	1(2)
C7E	28(3)	14(3)	24(3)	5(2)	0(2)	7(2)
C8E	20(3)	16(3)	22(3)	5(2)	0(2)	4.1(19)
C9E	18(2)	16(3)	19(2)	1.7(19)	1(2)	-2.0(19)
C10E	19(3)	17(3)	18(2)	2(2)	1(2)	0(2)
C11E	32(3)	26(3)	19(3)	4(2)	3(2)	10(2)
C12E	30(3)	25(3)	21(3)	2(2)	5(2)	10(2)
C13E	26(3)	18(3)	19(3)	-1(2)	4(2)	5(2)
C14E	21(3)	17(3)	20(3)	6(2)	0(2)	0(2)
C15E	37(3)	20(3)	23(3)	4(2)	6(2)	11(2)
C16E	29(3)	20(3)	24(3)	8(2)	1(2)	5(2)
C17E	25(3)	23(3)	19(3)	6(2)	0(2)	1(2)
C18E	37(3)	16(3)	23(3)	-1(2)	6(2)	1(2)
C19E	28(3)	18(3)	23(3)	0(2)	4(2)	-2(2)
C20E	28(3)	20(3)	19(3)	2(2)	5(2)	5(2)
C21E	38(3)	25(3)	28(3)	5(2)	10(3)	3(2)
C22E	44(3)	28(3)	26(3)	4(2)	8(3)	3(3)
C23E	54(4)	33(4)	34(3)	5(3)	15(3)	1(3)
C24E	49(4)	31(3)	27(3)	6(2)	11(3)	7(3)
C25E	57(4)	60(5)	36(4)	7(3)	6(3)	10(3)
C26E	100(6)	48(4)	39(4)	17(3)	35(4)	3(4)
C27E	39(3)	33(3)	26(3)	4(2)	9(3)	10(3)
O1F	24(2)	57(3)	18.7(19)	13.0(18)	4.0(16)	6.6(18)
C1F	24(3)	24(3)	20(3)	5(2)	0(2)	8(2)
C2F	33(3)	30(3)	27(3)	10(2)	4(3)	9(2)
C3F	22(3)	40(3)	13(2)	11(2)	4(2)	2(2)
C4F	24(3)	33(3)	15(3)	2(2)	5(2)	-2(2)
C5F	12(2)	28(3)	18(3)	1(2)	2(2)	4(2)
C6F	20(3)	22(3)	19(3)	-5(2)	2(2)	3(2)
C7F	16(2)	18(3)	22(3)	-3(2)	0(2)	2.8(19)
C8F	15(2)	17(3)	17(2)	1.3(19)	0(2)	2.0(19)
C9F	12(2)	19(3)	20(3)	1(2)	0(2)	2.9(18)
C10F	13(2)	17(3)	21(3)	3(2)	0(2)	1.7(19)
C11F	23(3)	15(3)	24(3)	0(2)	2(2)	5(2)
C12F	25(3)	13(3)	19(3)	2.1(19)	4(2)	2(2)
C13F	18(2)	18(3)	15(2)	1.1(19)	2(2)	0.9(19)
C14F	14(2)	15(3)	21(3)	-0.6(19)	3(2)	0.7(18)
C15F	22(3)	15(3)	23(3)	0(2)	1(2)	5(2)
C16F	24(3)	14(3)	27(3)	5(2)	1(2)	-1(2)
C17F	18(2)	16(3)	20(3)	4(2)	1(2)	2.5(19)
C18F	27(3)	23(3)	20(3)	4(2)	-2(2)	-4(2)
C19F	24(3)	24(3)	24(3)	4(2)	1(2)	-2(2)
C20F	25(3)	16(3)	16(2)	2.7(19)	0(2)	0(2)
C21F	33(3)	20(3)	21(3)	3(2)	0(2)	0(2)
C22F	35(3)	22(3)	21(3)	4(2)	3(2)	1(2)
C23F	43(3)	22(3)	22(3)	4(2)	5(3)	2(2)
C24F	53(4)	20(3)	22(3)	6(2)	8(3)	0(2)
C25F	61(4)	43(4)	29(3)	8(3)	2(3)	18(3)
C26F	72(5)	41(4)	29(3)	9(3)	20(3)	-1(3)
C27F	42(3)	21(3)	23(3)	4(2)	3(3)	1(2)
O1G	24(2)	72(3)	22(2)	22(2)	0.7(17)	-1.5(19)
C1G	22(3)	24(3)	18(3)	4(2)	5(2)	2(2)
C2G	26(3)	33(3)	25(3)	4(2)	8(2)	-7(2)

C3G	21(3)	39(3)	17(3)	13(2)	-3(2)	-5(2)
C4G	19(3)	30(3)	23(3)	7(2)	-1(2)	-2(2)
C5G	18(2)	18(3)	22(3)	4(2)	-3(2)	-3(2)
C6G	22(3)	20(3)	22(3)	6(2)	-3(2)	4(2)
C7G	23(3)	27(3)	21(3)	4(2)	2(2)	6(2)
C8G	19(3)	21(3)	23(3)	6(2)	5(2)	0(2)
C9G	18(2)	21(3)	19(3)	1(2)	2(2)	-1(2)
C10G	20(3)	27(3)	15(2)	3(2)	2(2)	-3(2)
C11G	29(3)	31(3)	19(3)	5(2)	5(2)	8(2)
C12G	25(3)	30(3)	22(3)	10(2)	0(2)	9(2)
C13G	17(2)	19(3)	19(3)	6(2)	0(2)	2.6(19)
C14G	20(3)	23(3)	18(3)	3(2)	-2(2)	2(2)
C15G	33(3)	33(3)	16(3)	6(2)	3(2)	9(2)
C16G	38(3)	37(3)	17(3)	9(2)	2(2)	14(3)
C17G	23(3)	21(3)	23(3)	1(2)	1(2)	2(2)
C18G	27(3)	31(3)	25(3)	6(2)	-2(2)	-4(2)
C19G	36(3)	24(3)	22(3)	4(2)	-1(2)	-8(2)
C20G	31(3)	23(3)	20(3)	6(2)	0(2)	1(2)
C21G	35(3)	25(3)	21(3)	5(2)	-2(2)	-2(2)
C22G	38(3)	29(3)	22(3)	7(2)	-7(3)	1(2)
C23G	44(4)	32(3)	25(3)	7(2)	-3(3)	1(3)
C24G	53(4)	40(4)	27(3)	14(3)	-2(3)	9(3)
C25G	95(6)	54(5)	36(4)	20(3)	-12(4)	-16(4)
C26G	70(5)	50(4)	31(3)	8(3)	-12(3)	3(4)
C27G	53(4)	30(3)	25(3)	7(2)	-1(3)	16(3)

Table A1.5.4. Bond lengths of **81c.**

Atom	Atom	Length (Å)	Atom	Atom	Length (Å)
O1	C3	1.430(6)	O1D	C3D	1.435(5)
C1	C2	1.531(6)	C1D	C2D	1.531(6)
C1	C10	1.547(6)	C1D	C10D	1.550(7)
C2	C3	1.513(7)	C2D	C3D	1.509(6)
C3	C4	1.515(7)	C3D	C4D	1.517(7)
C4	C5	1.521(6)	C4D	C5D	1.526(6)
C5	C6	1.322(7)	C5D	C6D	1.322(7)
C5	C10	1.526(7)	C5D	C10D	1.530(6)
C6	C7	1.493(6)	C6D	C7D	1.500(7)
C7	C8	1.546(6)	C7D	C8D	1.539(6)
C8	C9	1.539(6)	C8D	C9D	1.540(6)
C8	C14	1.516(6)	C8D	C14D	1.523(6)
C9	C10	1.557(6)	C9D	C10D	1.553(6)
C9	C11	1.541(6)	C9D	C11D	1.533(6)
C10	C19	1.537(6)	C10D	C19D	1.532(7)
C11	C12	1.537(6)	C11D	C12D	1.538(6)
C12	C13	1.534(6)	C12D	C13D	1.530(7)
C13	C14	1.554(6)	C13D	C14D	1.541(6)
C13	C17	1.554(6)	C13D	C17D	1.546(6)
C13	C18	1.538(6)	C13D	C18D	1.542(6)
C14	C15	1.534(6)	C14D	C15D	1.527(6)
C15	C16	1.554(7)	C15D	C16D	1.556(6)
C16	C17	1.563(6)	C16D	C17D	1.551(7)
C17	C20	1.539(6)	C17D	C20D	1.534(6)
C20	C21	1.551(6)	C20D	C21D	1.535(7)
C20	C27	1.532(7)	C20D	C27D	1.525(7)
C21	C22	1.536(7)	C21D	C22D	1.523(7)
C22	C23	1.535(7)	C22D	C23D	1.536(7)
C23	C24	1.534(7)	C23D	C24D	1.521(7)
C24	C25	1.517(8)	C24D	C25D	1.531(8)
C24	C26	1.540(8)	C24D	C26D	1.518(10)

O1A	C3A	1.440(5)	O1E	C3E	1.431(5)
C1A	C2A	1.540(6)	C1E	C2E	1.536(6)
C1A	C10A	1.546(6)	C1E	C10E	1.553(6)
C2A	C3A	1.506(7)	C2E	C3E	1.511(7)
C3A	C4A	1.524(7)	C3E	C4E	1.519(6)
C4A	C5A	1.518(6)	C4E	C5E	1.512(6)
C5A	C6A	1.331(6)	C5E	C6E	1.331(6)
C5A	C10A	1.528(6)	C5E	C10E	1.517(6)
C6A	C7A	1.494(6)	C6E	C7E	1.492(6)
C7A	C8A	1.538(6)	C7E	C8E	1.530(6)
C8A	C9A	1.530(6)	C8E	C9E	1.540(6)
C8A	C14A	1.531(6)	C8E	C14E	1.521(6)
C9A	C10A	1.568(6)	C9E	C10E	1.560(6)
C9A	C11A	1.533(6)	C9E	C11E	1.539(7)
C10A	C19A	1.540(6)	C10E	C19E	1.534(6)
C11A	C12A	1.537(6)	C11E	C12E	1.536(7)
C12A	C13A	1.530(6)	C12E	C13E	1.536(7)
C13A	C14A	1.540(6)	C13E	C14E	1.539(7)
C13A	C17A	1.552(6)	C13E	C17E	1.563(7)
C13A	C18A	1.538(6)	C13E	C18E	1.531(7)
C14A	C15A	1.533(7)	C14E	C15E	1.539(6)
C15A	C16A	1.558(6)	C15E	C16E	1.553(7)
C16A	C17A	1.548(7)	C16E	C17E	1.562(6)
C17A	C20A	1.535(6)	C17E	C20E	1.537(6)
C20A	C21A	1.535(7)	C20E	C21E	1.529(7)
C20A	C27A	1.532(7)	C20E	C27E	1.529(7)
C21A	C22A	1.522(7)	C21E	C22E	1.527(7)
C22A	C23A	1.536(7)	C22E	C23E	1.532(7)
C23A	C24A	1.524(7)	C23E	C24E	1.526(7)
C24A	C25A	1.512(10)	C24E	C25E	1.517(8)
C24A	C26A	1.533(7)	C24E	C26E	1.531(8)
O1B	C3B	1.431(5)	O1F	C3F	1.444(5)
C1B	C2B	1.547(6)	C1F	C2F	1.536(6)
C1B	C10B	1.544(6)	C1F	C10F	1.544(6)
C2B	C3B	1.509(7)	C2F	C3F	1.515(7)
C3B	C4B	1.513(6)	C3F	C4F	1.521(7)
C4B	C5B	1.513(6)	C4F	C5F	1.525(6)
C5B	C6B	1.325(7)	C5F	C6F	1.323(7)
C5B	C10B	1.529(6)	C5F	C10F	1.518(7)
C6B	C7B	1.491(6)	C6F	C7F	1.504(7)
C7B	C8B	1.530(7)	C7F	C8F	1.525(6)
C8B	C9B	1.531(6)	C8F	C9F	1.550(6)
C8B	C14B	1.521(6)	C8F	C14F	1.524(6)
C9B	C10B	1.559(6)	C9F	C10F	1.557(6)
C9B	C11B	1.535(6)	C9F	C11F	1.544(6)
C10B	C19B	1.548(7)	C10F	C19F	1.538(6)
C11B	C12B	1.534(6)	C11F	C12F	1.538(6)
C12B	C13B	1.535(7)	C12F	C13F	1.533(6)
C13B	C14B	1.533(7)	C13F	C14F	1.538(6)
C13B	C17B	1.552(6)	C13F	C17F	1.555(6)
C13B	C18B	1.540(7)	C13F	C18F	1.534(6)
C14B	C15B	1.539(6)	C14F	C15F	1.528(6)
C15B	C16B	1.547(7)	C15F	C16F	1.544(6)
C16B	C17B	1.559(7)	C16F	C17F	1.556(6)
C17B	C20B	1.546(7)	C17F	C20F	1.545(6)
C20B	C21B	1.548(7)	C20F	C21F	1.539(6)
C20B	C27B	1.525(7)	C20F	C27F	1.530(7)
C21B	C22B	1.529(7)	C21F	C22F	1.528(6)
C22B	C23B	1.537(7)	C22F	C23F	1.535(7)
C23B	C24B	1.533(7)	C23F	C24F	1.537(7)

C24B	C25B	1.518(8)	C24F	C25F	1.525(8)
C24B	C26B	1.524(8)	C24F	C26F	1.518(8)
O1C	C3C	1.434(5)	O1G	C3G	1.445(5)
C1C	C2C	1.545(6)	C1G	C2G	1.531(6)
C1C	C10C	1.542(6)	C1G	C10G	1.551(6)
C2C	C3C	1.510(7)	C2G	C3G	1.519(7)
C3C	C4C	1.518(7)	C3G	C4G	1.512(7)
C4C	C5C	1.521(7)	C4G	C5G	1.524(6)
C5C	C6C	1.319(6)	C5G	C6G	1.329(7)
C5C	C10C	1.525(7)	C5G	C10G	1.522(7)
C6C	C7C	1.508(6)	C6G	C7G	1.505(6)
C7C	C8C	1.533(6)	C7G	C8G	1.517(7)
C8C	C9C	1.533(6)	C8G	C9G	1.548(6)
C8C	C14C	1.516(6)	C8G	C14G	1.517(6)
C9C	C10C	1.556(6)	C9G	C10G	1.559(6)
C9C	C11C	1.532(6)	C9G	C11G	1.538(7)
C10C	C19C	1.536(6)	C10G	C19G	1.545(7)
C11C	C12C	1.547(6)	C11G	C12G	1.538(6)
C12C	C13C	1.532(6)	C12G	C13G	1.530(7)
C13C	C14C	1.545(6)	C13G	C14G	1.547(6)
C13C	C17C	1.552(6)	C13G	C17G	1.556(6)
C13C	C18C	1.542(7)	C13G	C18G	1.529(7)
C14C	C15C	1.531(6)	C14G	C15G	1.530(7)
C15C	C16C	1.551(7)	C15G	C16G	1.558(6)
C16C	C17C	1.557(7)	C16G	C17G	1.555(7)
C17C	C20C	1.532(7)	C17G	C20G	1.546(6)
C20C	C21C	1.537(7)	C20G	C21G	1.545(7)
C20C	C27C	1.527(7)	C20G	C27G	1.522(7)
C21C	C22C	1.525(7)	C21G	C22G	1.521(7)
C22C	C23C	1.541(7)	C22G	C23G	1.529(7)
C23C	C24C	1.511(7)	C23G	C24G	1.531(7)
C24C	C25C	1.505(9)	C24G	C25G	1.511(8)
C24C	C26C	1.542(8)	C24G	C26G	1.521(8)

Table A1.5.5. Bond angles of **81c**.

Atom	Atom	Atom	Angle (°)	Atom	Atom	Atom	Angle (°)
C2	C1	C10	113.4(4)	C2D	C1D	C10D	114.3(4)
C3	C2	C1	111.0(4)	C3D	C2D	C1D	110.0(4)
O1	C3	C2	111.3(4)	O1D	C3D	C2D	107.9(4)
O1	C3	C4	109.3(4)	O1D	C3D	C4D	110.8(4)
C2	C3	C4	111.1(4)	C2D	C3D	C4D	110.8(4)
C3	C4	C5	112.1(4)	C3D	C4D	C5D	112.9(4)
C4	C5	C10	115.4(4)	C4D	C5D	C10D	115.4(4)
C6	C5	C4	120.7(4)	C6D	C5D	C4D	121.7(4)
C6	C5	C10	123.8(4)	C6D	C5D	C10D	122.9(4)
C5	C6	C7	125.4(5)	C5D	C6D	C7D	124.8(4)
C6	C7	C8	111.5(4)	C6D	C7D	C8D	113.6(4)
C9	C8	C7	109.6(4)	C7D	C8D	C9D	108.6(4)
C14	C8	C7	110.8(4)	C14D	C8D	C7D	110.7(4)
C14	C8	C9	109.8(4)	C14D	C8D	C9D	109.5(4)
C8	C9	C10	112.7(4)	C8D	C9D	C10D	112.8(4)
C8	C9	C11	112.1(4)	C11D	C9D	C8D	112.5(4)
C11	C9	C10	112.6(4)	C11D	C9D	C10D	113.1(4)
C1	C10	C9	108.4(4)	C1D	C10D	C9D	107.9(4)
C5	C10	C1	108.6(4)	C5D	C10D	C1D	109.0(4)
C5	C10	C9	110.0(4)	C5D	C10D	C9D	109.9(4)
C5	C10	C19	109.5(4)	C5D	C10D	C19D	108.5(4)
C19	C10	C1	109.0(4)	C19D	C10D	C1D	110.0(4)
C19	C10	C9	111.4(4)	C19D	C10D	C9D	111.6(4)

C12	C11	C9	114.3(4)	C9D	C11D	C12D	113.9(4)
C13	C12	C11	111.5(4)	C13D	C12D	C11D	111.6(4)
C12	C13	C14	106.1(4)	C12D	C13D	C14D	107.0(4)
C12	C13	C17	115.7(4)	C12D	C13D	C17D	116.9(4)
C12	C13	C18	111.3(4)	C12D	C13D	C18D	110.1(4)
C14	C13	C17	101.0(4)	C14D	C13D	C17D	100.2(4)
C18	C13	C14	111.8(4)	C14D	C13D	C18D	112.3(4)
C18	C13	C17	110.4(4)	C18D	C13D	C17D	110.1(4)
C8	C14	C13	114.9(4)	C8D	C14D	C13D	115.6(4)
C8	C14	C15	119.1(4)	C8D	C14D	C15D	118.3(4)
C15	C14	C13	103.8(4)	C15D	C14D	C13D	104.2(4)
C14	C15	C16	103.2(4)	C14D	C15D	C16D	103.5(4)
C15	C16	C17	107.4(4)	C17D	C16D	C15D	106.7(4)
C13	C17	C16	103.9(4)	C13D	C17D	C16D	103.3(4)
C20	C17	C13	120.4(4)	C20D	C17D	C13D	119.9(4)
C20	C17	C16	111.4(4)	C20D	C17D	C16D	112.1(4)
C17	C20	C21	108.1(4)	C17D	C20D	C21D	112.6(4)
C27	C20	C17	113.7(4)	C27D	C20D	C17D	113.4(4)
C27	C20	C21	110.2(4)	C27D	C20D	C21D	109.9(4)
C22	C21	C20	115.8(4)	C22D	C21D	C20D	114.9(4)
C23	C22	C21	110.1(4)	C21D	C22D	C23D	112.7(4)
C24	C23	C22	114.8(5)	C24D	C23D	C22D	115.7(5)
C23	C24	C26	111.0(5)	C23D	C24D	C25D	109.5(5)
C25	C24	C23	111.9(5)	C26D	C24D	C23D	112.3(5)
C25	C24	C26	110.2(5)	C26D	C24D	C25D	110.5(6)
C2A	C1A	C10A	114.2(4)	C2E	C1E	C10E	114.6(4)
C3A	C2A	C1A	110.6(4)	C3E	C2E	C1E	111.0(4)
O1A	C3A	C2A	107.9(4)	O1E	C3E	C2E	112.2(4)
O1A	C3A	C4A	110.9(4)	O1E	C3E	C4E	108.4(4)
C2A	C3A	C4A	111.0(4)	C2E	C3E	C4E	109.3(4)
C5A	C4A	C3A	113.3(4)	C5E	C4E	C3E	111.2(4)
C4A	C5A	C10A	116.0(4)	C4E	C5E	C10E	116.7(4)
C6A	C5A	C4A	121.0(4)	C6E	C5E	C4E	120.1(4)
C6A	C5A	C10A	123.0(4)	C6E	C5E	C10E	123.1(4)
C5A	C6A	C7A	124.9(4)	C5E	C6E	C7E	124.9(4)
C6A	C7A	C8A	113.3(4)	C6E	C7E	C8E	113.3(4)
C9A	C8A	C7A	109.3(4)	C7E	C8E	C9E	109.6(4)
C9A	C8A	C14A	110.0(4)	C14E	C8E	C7E	110.1(4)
C14A	C8A	C7A	109.8(4)	C14E	C8E	C9E	109.2(4)
C8A	C9A	C10A	112.3(4)	C8E	C9E	C10E	112.2(4)
C8A	C9A	C11A	111.8(4)	C11E	C9E	C8E	111.9(4)
C11A	C9A	C10A	113.2(4)	C11E	C9E	C10E	113.7(4)
C1A	C10A	C9A	108.1(4)	C1E	C10E	C9E	108.5(4)
C5A	C10A	C1A	108.5(4)	C5E	C10E	C1E	110.1(4)
C5A	C10A	C9A	109.5(4)	C5E	C10E	C9E	109.6(4)
C5A	C10A	C19A	108.7(4)	C5E	C10E	C19E	108.1(4)
C19A	C10A	C1A	110.8(4)	C19E	C10E	C1E	109.1(4)
C19A	C10A	C9A	111.2(4)	C19E	C10E	C9E	111.5(4)
C9A	C11A	C12A	113.6(4)	C12E	C11E	C9E	114.2(4)
C13A	C12A	C11A	111.5(4)	C13E	C12E	C11E	111.5(4)
C12A	C13A	C14A	106.6(4)	C12E	C13E	C14E	106.9(4)
C12A	C13A	C17A	116.6(4)	C12E	C13E	C17E	116.7(4)
C12A	C13A	C18A	111.1(4)	C14E	C13E	C17E	99.7(4)
C14A	C13A	C17A	99.6(4)	C18E	C13E	C12E	111.1(4)
C18A	C13A	C14A	112.6(4)	C18E	C13E	C14E	112.3(4)
C18A	C13A	C17A	109.8(4)	C18E	C13E	C17E	109.6(4)
C8A	C14A	C13A	114.9(4)	C8E	C14E	C13E	115.6(4)
C8A	C14A	C15A	118.8(4)	C8E	C14E	C15E	117.4(4)
C15A	C14A	C13A	104.4(4)	C15E	C14E	C13E	105.0(4)
C14A	C15A	C16A	103.4(4)	C14E	C15E	C16E	102.6(4)

C17A	C16A	C15A	106.6(4)	C15E	C16E	C17E	107.7(4)
C16A	C17A	C13A	103.3(4)	C16E	C17E	C13E	102.7(4)
C20A	C17A	C13A	119.8(4)	C20E	C17E	C13E	120.0(4)
C20A	C17A	C16A	111.6(4)	C20E	C17E	C16E	112.9(4)
C21A	C20A	C17A	112.9(4)	C21E	C20E	C17E	110.3(4)
C27A	C20A	C17A	112.8(4)	C21E	C20E	C27E	110.3(4)
C27A	C20A	C21A	109.5(4)	C27E	C20E	C17E	111.6(4)
C22A	C21A	C20A	115.1(4)	C22E	C21E	C20E	115.6(4)
C21A	C22A	C23A	113.6(4)	C21E	C22E	C23E	111.4(5)
C24A	C23A	C22A	115.7(5)	C24E	C23E	C22E	114.3(5)
C23A	C24A	C26A	109.1(5)	C23E	C24E	C26E	110.0(5)
C25A	C24A	C23A	112.4(5)	C25E	C24E	C23E	112.1(5)
C25A	C24A	C26A	110.7(5)	C25E	C24E	C26E	110.3(5)
C10B	C1B	C2B	113.2(4)	C2F	C1F	C10F	114.6(4)
C3B	C2B	C1B	111.0(4)	C3F	C2F	C1F	109.8(4)
O1B	C3B	C2B	110.6(4)	O1F	C3F	C2F	110.6(4)
O1B	C3B	C4B	111.4(4)	O1F	C3F	C4F	109.1(4)
C2B	C3B	C4B	109.8(4)	C2F	C3F	C4F	110.2(4)
C3B	C4B	C5B	111.6(4)	C3F	C4F	C5F	112.1(4)
C4B	C5B	C10B	116.3(4)	C6F	C5F	C4F	120.3(4)
C6B	C5B	C4B	120.5(4)	C6F	C5F	C10F	123.7(4)
C6B	C5B	C10B	123.1(4)	C10F	C5F	C4F	115.9(4)
C5B	C6B	C7B	125.4(5)	C5F	C6F	C7F	125.2(4)
C6B	C7B	C8B	112.6(4)	C6F	C7F	C8F	111.9(4)
C7B	C8B	C9B	110.3(4)	C7F	C8F	C9F	109.7(4)
C14B	C8B	C7B	110.8(4)	C14F	C8F	C7F	111.3(4)
C14B	C8B	C9B	109.4(4)	C14F	C8F	C9F	110.2(4)
C8B	C9B	C10B	112.9(4)	C8F	C9F	C10F	112.5(4)
C8B	C9B	C11B	112.0(4)	C11F	C9F	C8F	111.7(4)
C11B	C9B	C10B	113.4(4)	C11F	C9F	C10F	113.3(4)
C1B	C10B	C9B	109.0(4)	C1F	C10F	C9F	109.1(4)
C1B	C10B	C19B	109.5(4)	C5F	C10F	C1F	108.4(4)
C5B	C10B	C1B	108.6(4)	C5F	C10F	C9F	109.9(4)
C5B	C10B	C9B	109.9(4)	C5F	C10F	C19F	109.0(4)
C5B	C10B	C19B	109.2(4)	C19F	C10F	C1F	109.2(4)
C19B	C10B	C9B	110.5(4)	C19F	C10F	C9F	111.1(4)
C12B	C11B	C9B	114.2(4)	C12F	C11F	C9F	113.8(4)
C11B	C12B	C13B	111.9(4)	C13F	C12F	C11F	111.5(4)
C12B	C13B	C17B	116.6(4)	C12F	C13F	C14F	106.0(4)
C12B	C13B	C18B	110.5(4)	C12F	C13F	C17F	116.2(4)
C14B	C13B	C12B	106.4(4)	C12F	C13F	C18F	111.9(4)
C14B	C13B	C17B	99.9(4)	C14F	C13F	C17F	100.6(4)
C14B	C13B	C18B	112.9(4)	C18F	C13F	C14F	111.6(4)
C18B	C13B	C17B	110.1(4)	C18F	C13F	C17F	109.9(4)
C8B	C14B	C13B	116.4(4)	C8F	C14F	C13F	115.5(4)
C8B	C14B	C15B	118.2(4)	C8F	C14F	C15F	118.7(4)
C13B	C14B	C15B	104.2(4)	C15F	C14F	C13F	104.6(4)
C14B	C15B	C16B	103.2(4)	C14F	C15F	C16F	103.2(4)
C15B	C16B	C17B	107.0(4)	C15F	C16F	C17F	107.5(4)
C13B	C17B	C16B	103.2(4)	C13F	C17F	C16F	103.7(4)
C20B	C17B	C13B	120.6(4)	C20F	C17F	C13F	120.3(4)
C20B	C17B	C16B	112.3(4)	C20F	C17F	C16F	111.6(4)
C17B	C20B	C21B	108.0(4)	C21F	C20F	C17F	108.6(4)
C27B	C20B	C17B	112.1(4)	C27F	C20F	C17F	113.5(4)
C27B	C20B	C21B	110.8(4)	C27F	C20F	C21F	110.6(4)
C22B	C21B	C20B	115.0(4)	C22F	C21F	C20F	116.8(4)
C21B	C22B	C23B	111.3(5)	C21F	C22F	C23F	110.7(4)
C24B	C23B	C22B	114.9(5)	C22F	C23F	C24F	114.9(4)
C25B	C24B	C23B	112.2(5)	C25F	C24F	C23F	111.8(5)
C25B	C24B	C26B	111.2(5)	C26F	C24F	C23F	111.4(5)

C26B	C24B	C23B	109.8(5)	C26F	C24F	C25F	110.1(5)
C10C	C1C	C2C	115.2(4)	C2G	C1G	C10G	113.3(4)
C3C	C2C	C1C	110.8(4)	C3G	C2G	C1G	111.3(4)
O1C	C3C	C2C	112.2(4)	O1G	C3G	C2G	110.7(4)
O1C	C3C	C4C	108.1(4)	O1G	C3G	C4G	110.7(4)
C2C	C3C	C4C	109.8(4)	C4G	C3G	C2G	110.1(4)
C3C	C4C	C5C	111.0(4)	C3G	C4G	C5G	111.5(4)
C4C	C5C	C10C	117.2(4)	C6G	C5G	C4G	119.7(4)
C6C	C5C	C4C	119.7(4)	C6G	C5G	C10G	123.9(4)
C6C	C5C	C10C	123.1(4)	C10G	C5G	C4G	116.4(4)
C5C	C6C	C7C	125.2(4)	C5G	C6G	C7G	124.1(4)
C6C	C7C	C8C	112.6(4)	C6G	C7G	C8G	113.1(4)
C9C	C8C	C7C	110.2(4)	C7G	C8G	C9G	109.8(4)
C14C	C8C	C7C	109.5(4)	C14G	C8G	C7G	110.9(4)
C14C	C8C	C9C	109.8(4)	C14G	C8G	C9G	109.2(4)
C8C	C9C	C10C	112.7(4)	C8G	C9G	C10G	112.2(4)
C11C	C9C	C8C	111.8(4)	C11G	C9G	C8G	111.7(4)
C11C	C9C	C10C	113.5(4)	C11G	C9G	C10G	113.1(4)
C1C	C10C	C9C	108.9(4)	C1G	C10G	C9G	109.1(4)
C5C	C10C	C1C	109.8(4)	C5G	C10G	C1G	108.6(4)
C5C	C10C	C9C	109.8(4)	C5G	C10G	C9G	110.2(4)
C5C	C10C	C19C	107.5(4)	C5G	C10G	C19G	108.8(4)
C19C	C10C	C1C	109.4(4)	C19G	C10G	C1G	109.1(4)
C19C	C10C	C9C	111.5(4)	C19G	C10G	C9G	111.0(4)
C9C	C11C	C12C	113.8(4)	C9G	C11G	C12G	114.2(4)
C13C	C12C	C11C	112.1(4)	C13G	C12G	C11G	111.5(4)
C12C	C13C	C14C	106.7(4)	C12G	C13G	C14G	106.5(4)
C12C	C13C	C17C	117.4(4)	C12G	C13G	C17G	115.7(4)
C12C	C13C	C18C	110.7(4)	C14G	C13G	C17G	99.3(4)
C14C	C13C	C17C	100.1(4)	C18G	C13G	C12G	111.2(4)
C18C	C13C	C14C	112.0(4)	C18G	C13G	C14G	113.1(4)
C18C	C13C	C17C	109.6(4)	C18G	C13G	C17G	110.5(4)
C8C	C14C	C13C	115.7(4)	C8G	C14G	C13G	115.8(4)
C8C	C14C	C15C	118.5(4)	C8G	C14G	C15G	118.0(4)
C15C	C14C	C13C	104.4(4)	C15G	C14G	C13G	104.5(4)
C14C	C15C	C16C	103.5(4)	C14G	C15G	C16G	102.9(4)
C15C	C16C	C17C	107.1(4)	C17G	C16G	C15G	107.1(4)
C13C	C17C	C16C	103.3(4)	C16G	C17G	C13G	103.1(4)
C20C	C17C	C13C	120.3(4)	C20G	C17G	C13G	120.4(4)
C20C	C17C	C16C	112.3(4)	C20G	C17G	C16G	111.7(4)
C17C	C20C	C21C	110.2(4)	C21G	C20G	C17G	108.8(4)
C27C	C20C	C17C	112.2(4)	C27G	C20G	C17G	112.1(4)
C27C	C20C	C21C	110.4(4)	C27G	C20G	C21G	110.5(4)
C22C	C21C	C20C	115.4(4)	C22G	C21G	C20G	116.3(4)
C21C	C22C	C23C	111.3(5)	C21G	C22G	C23G	111.4(4)
C24C	C23C	C22C	115.4(5)	C22G	C23G	C24G	115.1(5)
C23C	C24C	C26C	109.8(5)	C25G	C24G	C23G	112.4(5)
C25C	C24C	C23C	112.1(5)	C25G	C24G	C26G	110.4(5)
C25C	C24C	C26C	111.2(5)	C26G	C24G	C23G	110.8(5)

Table A1.5.6. Hydrogen bonds for **81c**.

D	H	A	d(D-H) (Å)	d(H-A) (Å)	d(D-A) (Å)	D-H-A (°)
O1	H1	O1G[a]	0.84	1.92	2.745(5)	167.2
O1A	H1AA	O1E[b]	0.84	2.04	2.845(5)	159.5
O1B	H1BA	O1F[b]	0.84	2.02	2.835(5)	163.3
O1C	H1C	O1D	0.84	2	2.817(5)	162.4
O1D	H1D	O1B[c]	0.84	1.91	2.729(5)	165.9
O1E	H1E	O1[d]	0.84	2.04	2.791(5)	149
O1F	H1F	O1C[d]	0.84	2.07	2.887(5)	162.7

O1G	H1G	O1A[e]	0.84	2.09	2.895(5)	159.3

[a]+X,1+Y,-1+Z; [b]+X,+Y,-1+Z; [c]1+X,+Y,+Z; [d]+X,+Y,1+Z; [e]1+X,-1+Y,1+Z

Table A1.5.7. Torsion angles for **81c**.

A	B	C	D	Angle (°)	A	B	C	D	Angle (°)
O1	C3	C4	C5	-176.6(4)	O1D	C3D	C4D	C5D	-173.9(4)
C1	C2	C3	O1	177.9(4)	C1D	C2D	C3D	O1D	178.8(4)
C1	C2	C3	C4	55.9(5)	C1D	C2D	C3D	C4D	57.3(5)
C2	C1	C10	C5	51.8(5)	C2D	C1D	C10D	C5D	50.8(5)
C2	C1	C10	C9	171.2(4)	C2D	C1D	C10D	C9D	170.1(4)
C2	C1	C10	C19	-67.4(5)	C2D	C1D	C10D	C19D	-68.0(5)
C2	C3	C4	C5	-53.4(6)	C2D	C3D	C4D	C5D	-54.2(5)
C3	C4	C5	C6	-127.2(5)	C3D	C4D	C5D	C6D	-130.1(5)
C3	C4	C5	C10	52.1(6)	C3D	C4D	C5D	C10D	50.1(6)
C4	C5	C6	C7	-178.4(4)	C4D	C5D	C6D	C7D	-178.3(4)
C4	C5	C10	C1	-49.8(5)	C4D	C5D	C10D	C1D	-46.6(5)
C4	C5	C10	C9	-168.2(4)	C4D	C5D	C10D	C9D	-164.7(4)
C4	C5	C10	C19	69.1(5)	C4D	C5D	C10D	C19D	73.1(5)
C5	C6	C7	C8	15.3(7)	C5D	C6D	C7D	C8D	12.5(7)
C6	C5	C10	C1	129.4(5)	C6D	C5D	C10D	C1D	133.6(5)
C6	C5	C10	C9	11.1(6)	C6D	C5D	C10D	C9D	15.5(6)
C6	C5	C10	C19	-111.7(5)	C6D	C5D	C10D	C19D	-106.7(5)
C6	C7	C8	C9	-45.2(5)	C6D	C7D	C8D	C9D	-41.9(5)
C6	C7	C8	C14	-166.5(4)	C6D	C7D	C8D	C14D	-162.2(4)
C7	C8	C9	C10	60.9(5)	C7D	C8D	C9D	C10D	60.8(5)
C7	C8	C9	C11	-170.7(4)	C7D	C8D	C9D	C11D	-169.8(4)
C7	C8	C14	C13	178.8(4)	C7D	C8D	C14D	C13D	175.7(4)
C7	C8	C14	C15	-57.3(5)	C7D	C8D	C14D	C15D	-59.8(5)
C8	C9	C10	C1	-161.0(4)	C8D	C9D	C10D	C1D	-165.7(4)
C8	C9	C10	C5	-42.5(5)	C8D	C9D	C10D	C5D	-46.9(5)
C8	C9	C10	C19	79.1(5)	C8D	C9D	C10D	C19D	73.4(5)
C8	C9	C11	C12	49.1(5)	C8D	C9D	C11D	C12D	50.0(6)
C8	C14	C15	C16	-166.4(4)	C8D	C14D	C15D	C16D	-163.6(4)
C9	C8	C14	C13	57.6(5)	C9D	C8D	C14D	C13D	55.9(5)
C9	C8	C14	C15	-178.5(4)	C9D	C8D	C14D	C15D	-179.6(4)
C9	C11	C12	C13	-54.3(5)	C9D	C11D	C12D	C13D	-54.3(6)
C10	C1	C2	C3	-56.6(5)	C10D	C1D	C2D	C3D	-57.5(6)
C10	C5	C6	C7	2.4(8)	C10D	C5D	C6D	C7D	1.5(8)
C10	C9	C11	C12	177.5(4)	C10D	C9D	C11D	C12D	179.3(4)
C11	C9	C10	C1	70.9(5)	C11D	C9D	C10D	C1D	65.3(5)
C11	C9	C10	C5	-170.5(4)	C11D	C9D	C10D	C5D	-176.0(4)
C11	C9	C10	C19	-48.9(5)	C11D	C9D	C10D	C19D	-55.7(5)
C11	C12	C13	C14	56.6(5)	C11D	C12D	C13D	C14D	55.7(5)
C11	C12	C13	C17	167.7(4)	C11D	C12D	C13D	C17D	166.9(4)
C11	C12	C13	C18	-65.3(5)	C11D	C12D	C13D	C18D	-66.6(5)
C12	C13	C14	C8	-61.0(5)	C12D	C13D	C14D	C8D	-59.2(5)
C12	C13	C14	C15	167.2(4)	C12D	C13D	C14D	C15D	169.3(4)
C12	C13	C17	C16	-150.3(4)	C12D	C13D	C17D	C16D	-156.2(4)
C12	C13	C17	C20	84.1(5)	C12D	C13D	C17D	C20D	78.2(6)
C13	C14	C15	C16	-37.2(5)	C13D	C14D	C15D	C16D	-33.6(5)
C13	C17	C20	C21	-177.0(4)	C13D	C17D	C20D	C21D	176.1(4)
C13	C17	C20	C27	-54.3(6)	C13D	C17D	C20D	C27D	-58.3(6)
C14	C8	C9	C10	-177.2(4)	C14D	C8D	C9D	C10D	-178.1(4)
C14	C8	C9	C11	-48.9(5)	C14D	C8D	C9D	C11D	-48.7(5)
C14	C13	C17	C16	-36.3(4)	C14D	C13D	C17D	C16D	-41.1(4)
C14	C13	C17	C20	-161.8(4)	C14D	C13D	C17D	C20D	-166.8(4)
C14	C15	C16	C17	14.0(5)	C14D	C15D	C16D	C17D	7.3(5)
C15	C16	C17	C13	14.2(5)	C15D	C16D	C17D	C13D	21.4(5)

C15	C16	C17	C20	145.2(4)	C15D	C16D	C17D	C20D	151.9(4)
C16	C17	C20	C21	61.0(5)	C16D	C17D	C20D	C21D	54.7(6)
C16	C17	C20	C27	-176.2(4)	C16D	C17D	C20D	C27D	-179.7(4)
C17	C13	C14	C8	178.0(4)	C17D	C13D	C14D	C8D	178.5(4)
C17	C13	C14	C15	46.2(4)	C17D	C13D	C14D	C15D	46.9(4)
C17	C20	C21	C22	-174.6(4)	C17D	C20D	C21D	C22D	59.3(6)
C18	C13	C14	C8	60.6(5)	C18D	C13D	C14D	C8D	61.7(5)
C18	C13	C14	C15	-71.2(5)	C18D	C13D	C14D	C15D	-69.9(5)
C18	C13	C17	C16	82.2(5)	C18D	C13D	C17D	C16D	77.3(5)
C18	C13	C17	C20	-43.4(6)	C18D	C13D	C17D	C20D	-48.4(6)
C20	C21	C22	C23	176.8(4)	C20D	C21D	C22D	C23D	168.2(4)
C21	C22	C23	C24	168.0(5)	C21D	C22D	C23D	C24D	-70.4(7)
C22	C23	C24	C25	69.2(6)	C22D	C23D	C24D	C25D	173.5(5)
C22	C23	C24	C26	-167.3(5)	C22D	C23D	C24D	C26D	-63.3(7)
C27	C20	C21	C22	60.7(6)	C27D	C20D	C21D	C22D	-68.2(6)
O1A	C3A	C4A	C5A	-172.2(4)	O1E	C3E	C4E	C5E	179.0(4)
C1A	C2A	C3A	O1A	177.2(4)	C1E	C2E	C3E	O1E	179.6(4)
C1A	C2A	C3A	C4A	55.5(5)	C1E	C2E	C3E	C4E	59.3(5)
C2A	C1A	C10A	C5A	51.3(5)	C2E	C1E	C10E	C5E	44.3(6)
C2A	C1A	C10A	C9A	170.0(4)	C2E	C1E	C10E	C9E	164.2(4)
C2A	C1A	C10A	C19A	-67.9(5)	C2E	C1E	C10E	C19E	-74.2(5)
C2A	C3A	C4A	C5A	-52.2(5)	C2E	C3E	C4E	C5E	-58.4(5)
C3A	C4A	C5A	C6A	-131.6(5)	C3E	C4E	C5E	C6E	-129.9(5)
C3A	C4A	C5A	C10A	49.7(5)	C3E	C4E	C5E	C10E	52.8(5)
C4A	C5A	C6A	C7A	-177.7(4)	C4E	C5E	C6E	C7E	180.0(4)
C4A	C5A	C10A	C1A	-47.5(5)	C4E	C5E	C10E	C1E	-44.3(5)
C4A	C5A	C10A	C9A	-165.2(4)	C4E	C5E	C10E	C9E	-163.5(4)
C4A	C5A	C10A	C19A	73.1(5)	C4E	C5E	C10E	C19E	74.8(5)
C5A	C6A	C7A	C8A	12.5(7)	C5E	C6E	C7E	C8E	14.5(7)
C6A	C5A	C10A	C1A	133.9(5)	C6E	C5E	C10E	C1E	138.5(5)
C6A	C5A	C10A	C9A	16.1(6)	C6E	C5E	C10E	C9E	19.3(6)
C6A	C5A	C10A	C19A	-105.6(5)	C6E	C5E	C10E	C19E	-102.4(5)
C6A	C7A	C8A	C9A	-42.3(5)	C6E	C7E	C8E	C9E	-41.8(5)
C6A	C7A	C8A	C14A	-163.1(4)	C6E	C7E	C8E	C14E	-162.0(4)
C7A	C8A	C9A	C10A	61.2(5)	C7E	C8E	C9E	C10E	60.3(5)
C7A	C8A	C9A	C11A	-170.3(4)	C7E	C8E	C9E	C11E	-170.5(4)
C7A	C8A	C14A	C13A	176.7(4)	C7E	C8E	C14E	C13E	177.6(4)
C7A	C8A	C14A	C15A	-58.7(5)	C7E	C8E	C14E	C15E	-57.6(6)
C8A	C9A	C10A	C1A	-165.2(4)	C8E	C9E	C10E	C1E	-168.0(4)
C8A	C9A	C10A	C5A	-47.2(5)	C8E	C9E	C10E	C5E	-47.8(5)
C8A	C9A	C10A	C19A	73.0(5)	C8E	C9E	C10E	C19E	71.8(5)
C8A	C9A	C11A	C12A	51.2(5)	C8E	C9E	C11E	C12E	50.7(6)
C8A	C14A	C15A	C16A	-162.6(4)	C8E	C14E	C15E	C16E	-164.1(4)
C9A	C8A	C14A	C13A	56.4(5)	C9E	C8E	C14E	C13E	57.3(5)
C9A	C8A	C14A	C15A	-179.0(4)	C9E	C8E	C14E	C15E	-177.9(4)
C9A	C11A	C12A	C13A	-55.9(5)	C9E	C11E	C12E	C13E	-54.2(6)
C10A	C1A	C2A	C3A	-57.3(5)	C10E	C1E	C2E	C3E	-53.7(6)
C10A	C5A	C6A	C7A	0.9(7)	C10E	C5E	C6E	C7E	-3.0(8)
C10A	C9A	C11A	C12A	179.2(4)	C10E	C9E	C11E	C12E	179.0(4)
C11A	C9A	C10A	C1A	67.1(5)	C11E	C9E	C10E	C1E	63.8(5)
C11A	C9A	C10A	C5A	-174.9(4)	C11E	C9E	C10E	C5E	-176.0(4)
C11A	C9A	C10A	C19A	-54.7(5)	C11E	C9E	C10E	C19E	-56.3(5)
C11A	C12A	C13A	C14A	56.8(5)	C11E	C12E	C13E	C14E	55.2(5)
C11A	C12A	C13A	C17A	166.9(4)	C11E	C12E	C13E	C17E	165.8(4)
C11A	C12A	C13A	C18A	-66.2(5)	C11E	C12E	C13E	C18E	-67.6(5)
C12A	C13A	C14A	C8A	-59.3(5)	C12E	C13E	C14E	C8E	-59.7(5)
C12A	C13A	C14A	C15A	168.8(4)	C12E	C13E	C14E	C15E	169.3(4)
C12A	C13A	C17A	C16A	-156.4(4)	C12E	C13E	C17E	C16E	-155.5(4)
C12A	C13A	C17A	C20A	78.7(6)	C12E	C13E	C17E	C20E	78.3(6)
C13A	C14A	C15A	C16A	-33.0(5)	C13E	C14E	C15E	C16E	-34.2(5)

C13A	C17A	C20A	C21A	175.5(4)	C13E	C17E	C20E	C21E	173.3(4)
C13A	C17A	C20A	C27A	-59.7(6)	C13E	C17E	C20E	C27E	-63.7(6)
C14A	C8A	C9A	C10A	-178.1(4)	C14E	C8E	C9E	C10E	-179.0(4)
C14A	C8A	C9A	C11A	-49.6(5)	C14E	C8E	C9E	C11E	-49.8(5)
C14A	C13A	C17A	C16A	-42.4(4)	C14E	C13E	C17E	C16E	-40.9(4)
C14A	C13A	C17A	C20A	-167.3(4)	C14E	C13E	C17E	C20E	-167.1(4)
C14A	C15A	C16A	C17A	5.8(5)	C14E	C15E	C16E	C17E	7.4(5)
C15A	C16A	C17A	C13A	23.1(5)	C15E	C16E	C17E	C13E	21.2(5)
C15A	C16A	C17A	C20A	153.1(4)	C15E	C16E	C17E	C20E	151.9(4)
C16A	C17A	C20A	C21A	54.6(6)	C16E	C17E	C20E	C21E	52.0(6)
C16A	C17A	C20A	C27A	179.4(4)	C16E	C17E	C20E	C27E	174.9(4)
C17A	C13A	C14A	C8A	179.1(4)	C17E	C13E	C14E	C8E	178.4(4)
C17A	C13A	C14A	C15A	47.2(4)	C17E	C13E	C14E	C15E	47.4(5)
C17A	C20A	C21A	C22A	58.0(6)	C17E	C20E	C21E	C22E	-169.6(4)
C18A	C13A	C14A	C8A	62.8(5)	C18E	C13E	C14E	C8E	62.4(5)
C18A	C13A	C14A	C15A	-69.1(5)	C18E	C13E	C14E	C15E	-68.5(5)
C18A	C13A	C17A	C16A	76.0(5)	C18E	C13E	C17E	C16E	77.0(5)
C18A	C13A	C17A	C20A	-48.9(6)	C18E	C13E	C17E	C20E	-49.2(6)
C20A	C21A	C22A	C23A	169.8(5)	C20E	C21E	C22E	C23E	177.7(5)
C21A	C22A	C23A	C24A	-67.0(7)	C21E	C22E	C23E	C24E	-177.6(5)
C22A	C23A	C24A	C25A	-60.5(7)	C22E	C23E	C24E	C25E	67.2(7)
C22A	C23A	C24A	C26A	176.3(5)	C22E	C23E	C24E	C26E	-169.8(5)
C27A	C20A	C21A	C22A	-68.5(6)	C27E	C20E	C21E	C22E	66.8(6)
O1B	C3B	C4B	C5B	-178.8(4)	O1F	C3F	C4F	C5F	-176.7(4)
C1B	C2B	C3B	O1B	-178.3(4)	C1F	C2F	C3F	O1F	178.2(4)
C1B	C2B	C3B	C4B	58.4(5)	C1F	C2F	C3F	C4F	57.5(5)
C2B	C1B	C10B	C5B	49.5(5)	C2F	C1F	C10F	C5F	51.0(5)
C2B	C1B	C10B	C9B	169.3(4)	C2F	C1F	C10F	C9F	170.7(4)
C2B	C1B	C10B	C19B	-69.7(5)	C2F	C1F	C10F	C19F	-67.7(5)
C2B	C3B	C4B	C5B	-55.9(5)	C2F	C3F	C4F	C5F	-55.0(5)
C3B	C4B	C5B	C6B	-128.9(5)	C3F	C4F	C5F	C6F	-126.7(5)
C3B	C4B	C5B	C10B	52.9(5)	C3F	C4F	C5F	C10F	51.9(6)
C4B	C5B	C6B	C7B	-177.4(4)	C4F	C5F	C6F	C7F	-177.7(4)
C4B	C5B	C10B	C1B	-48.4(5)	C4F	C5F	C10F	C1F	-47.9(5)
C4B	C5B	C10B	C9B	-167.5(4)	C4F	C5F	C10F	C9F	-167.1(4)
C4B	C5B	C10B	C19B	71.0(5)	C4F	C5F	C10F	C19F	70.9(5)
C5B	C6B	C7B	C8B	13.7(7)	C5F	C6F	C7F	C8F	13.3(7)
C6B	C5B	C10B	C1B	133.5(5)	C6F	C5F	C10F	C1F	130.6(5)
C6B	C5B	C10B	C9B	14.3(6)	C6F	C5F	C10F	C9F	11.4(6)
C6B	C5B	C10B	C19B	-107.1(5)	C6F	C5F	C10F	C19F	-110.6(5)
C6B	C7B	C8B	C9B	-42.3(5)	C6F	C7F	C8F	C9F	-43.8(5)
C6B	C7B	C8B	C14B	-163.7(4)	C6F	C7F	C8F	C14F	-166.1(4)
C7B	C8B	C9B	C10B	59.4(5)	C7F	C8F	C9F	C10F	61.0(5)
C7B	C8B	C9B	C11B	-171.1(4)	C7F	C8F	C9F	C11F	-170.3(4)
C7B	C8B	C14B	C13B	178.5(4)	C7F	C8F	C14F	C13F	178.1(4)
C7B	C8B	C14B	C15B	-56.3(6)	C7F	C8F	C14F	C15F	-56.6(5)
C8B	C9B	C10B	C1B	-163.0(4)	C8F	C9F	C10F	C1F	-162.1(4)
C8B	C9B	C10B	C5B	-44.1(5)	C8F	C9F	C10F	C5F	-43.3(5)
C8B	C9B	C10B	C19B	76.6(5)	C8F	C9F	C10F	C19F	77.5(5)
C8B	C9B	C11B	C12B	50.3(6)	C8F	C9F	C11F	C12F	49.2(5)
C8B	C14B	C15B	C16B	-165.7(4)	C8F	C14F	C15F	C16F	-166.2(4)
C9B	C8B	C14B	C13B	56.6(5)	C9F	C8F	C14F	C13F	56.1(5)
C9B	C8B	C14B	C15B	-178.2(4)	C9F	C8F	C14F	C15F	-178.6(4)
C9B	C11B	C12B	C13B	-54.2(6)	C9F	C11F	C12F	C13F	-55.9(5)
C10B	C1B	C2B	C3B	-57.0(5)	C10F	C1F	C2F	C3F	-57.6(6)
C10B	C5B	C6B	C7B	0.7(8)	C10F	C5F	C6F	C7F	3.9(7)
C10B	C9B	C11B	C12B	179.5(4)	C10F	C9F	C11F	C12F	177.5(4)
C11B	C9B	C10B	C1B	68.3(5)	C11F	C9F	C10F	C1F	70.0(5)
C11B	C9B	C10B	C5B	-172.8(4)	C11F	C9F	C10F	C5F	-171.2(4)
C11B	C9B	C10B	C19B	-52.1(5)	C11F	C9F	C10F	C19F	-50.4(5)

C11B	C12B	C13B	C14B	54.8(5)	C11F	C12F	C13F	C14F	57.9(5)
C11B	C12B	C13B	C17B	165.1(4)	C11F	C12F	C13F	C17F	168.6(4)
C11B	C12B	C13B	C18B	-68.1(5)	C11F	C12F	C13F	C18F	-64.0(5)
C12B	C13B	C14B	C8B	-58.8(5)	C12F	C13F	C14F	C8F	-60.5(5)
C12B	C13B	C14B	C15B	169.2(4)	C12F	C13F	C14F	C15F	167.2(4)
C12B	C13B	C17B	C16B	-155.1(4)	C12F	C13F	C17F	C16F	-150.9(4)
C12B	C13B	C17B	C20B	78.5(6)	C12F	C13F	C17F	C20F	83.6(5)
C13B	C14B	C15B	C16B	-34.7(5)	C13F	C14F	C15F	C16F	-35.8(5)
C13B	C17B	C20B	C21B	-176.0(4)	C13F	C17F	C20F	C21F	-176.5(4)
C13B	C17B	C20B	C27B	-53.6(6)	C13F	C17F	C20F	C27F	-53.1(6)
C14B	C8B	C9B	C10B	-178.4(4)	C14F	C8F	C9F	C10F	-176.1(4)
C14B	C8B	C9B	C11B	-49.0(5)	C14F	C8F	C9F	C11F	-47.4(5)
C14B	C13B	C17B	C16B	-41.1(5)	C14F	C13F	C17F	C16F	-37.1(4)
C14B	C13B	C17B	C20B	-167.4(4)	C14F	C13F	C17F	C20F	-162.6(4)
C14B	C15B	C16B	C17B	8.2(5)	C14F	C15F	C16F	C17F	11.6(5)
C15B	C16B	C17B	C13B	20.6(5)	C15F	C16F	C17F	C13F	16.1(5)
C15B	C16B	C17B	C20B	152.1(4)	C15F	C16F	C17F	C20F	147.0(4)
C16B	C17B	C20B	C21B	62.0(6)	C16F	C17F	C20F	C21F	61.7(5)
C16B	C17B	C20B	C27B	-175.7(5)	C16F	C17F	C20F	C27F	-174.8(4)
C17B	C13B	C14B	C8B	179.5(4)	C17F	C13F	C14F	C8F	178.1(4)
C17B	C13B	C14B	C15B	47.5(5)	C17F	C13F	C14F	C15F	45.8(4)
C17B	C20B	C21B	C22B	179.8(4)	C17F	C20F	C21F	C22F	-175.4(4)
C18B	C13B	C14B	C8B	62.6(5)	C18F	C13F	C14F	C8F	61.6(5)
C18B	C13B	C14B	C15B	-69.4(5)	C18F	C13F	C14F	C15F	-70.7(5)
C18B	C13B	C17B	C16B	78.0(5)	C18F	C13F	C17F	C16F	80.7(4)
C18B	C13B	C17B	C20B	-48.4(6)	C18F	C13F	C17F	C20F	-44.8(6)
C20B	C21B	C22B	C23B	179.8(5)	C20F	C21F	C22F	C23F	178.3(4)
C21B	C22B	C23B	C24B	167.7(5)	C21F	C22F	C23F	C24F	168.1(4)
C22B	C23B	C24B	C25B	63.0(7)	C22F	C23F	C24F	C25F	70.7(6)
C22B	C23B	C24B	C26B	-172.8(5)	C22F	C23F	C24F	C26F	-165.6(5)
C27B	C20B	C21B	C22B	56.6(6)	C27F	C20F	C21F	C22F	59.5(6)
O1C	C3C	C4C	C5C	179.6(4)	O1G	C3G	C4G	C5G	-177.5(4)
C1C	C2C	C3C	O1C	179.2(4)	C1G	C2G	C3G	O1G	-179.4(4)
C1C	C2C	C3C	C4C	59.0(5)	C1G	C2G	C3G	C4G	57.9(5)
C2C	C1C	C10C	C5C	44.0(6)	C2G	C1G	C10G	C5G	49.9(5)
C2C	C1C	C10C	C9C	164.3(4)	C2G	C1G	C10G	C9G	170.0(4)
C2C	C1C	C10C	C19C	-73.7(5)	C2G	C1G	C10G	C19G	-68.5(5)
C2C	C3C	C4C	C5C	-57.8(5)	C2G	C3G	C4G	C5G	-54.8(6)
C3C	C4C	C5C	C6C	-129.9(5)	C3G	C4G	C5G	C6G	-128.0(5)
C3C	C4C	C5C	C10C	52.0(5)	C3G	C4G	C5G	C10G	52.6(6)
C4C	C5C	C6C	C7C	179.4(4)	C4G	C5G	C6G	C7G	-176.7(4)
C4C	C5C	C10C	C1C	-43.8(5)	C4G	C5G	C10G	C1G	-48.5(5)
C4C	C5C	C10C	C9C	-163.4(4)	C4G	C5G	C10G	C9G	-167.9(4)
C4C	C5C	C10C	C19C	75.1(5)	C4G	C5G	C10G	C19G	70.2(5)
C5C	C6C	C7C	C8C	14.3(7)	C5G	C6G	C7G	C8G	13.6(7)
C6C	C5C	C10C	C1C	138.2(5)	C6G	C5G	C10G	C1G	132.1(5)
C6C	C5C	C10C	C9C	18.5(6)	C6G	C5G	C10G	C9G	12.7(6)
C6C	C5C	C10C	C19C	-102.9(5)	C6G	C5G	C10G	C19G	-109.2(5)
C6C	C7C	C8C	C9C	-41.3(5)	C6G	C7G	C8G	C9G	-43.7(5)
C6C	C7C	C8C	C14C	-162.2(4)	C6G	C7G	C8G	C14G	-164.5(4)
C7C	C8C	C9C	C10C	59.7(5)	C7G	C8G	C9G	C10G	60.5(5)
C7C	C8C	C9C	C11C	-171.1(4)	C7G	C8G	C9G	C11G	-171.2(4)
C7C	C8C	C14C	C13C	178.2(4)	C7G	C8G	C14G	C13G	178.2(4)
C7C	C8C	C14C	C15C	-56.6(6)	C7G	C8G	C14G	C15G	-56.9(6)
C8C	C9C	C10C	C1C	-167.1(4)	C8G	C9G	C10G	C1G	-162.9(4)
C8C	C9C	C10C	C5C	-46.8(5)	C8G	C9G	C10G	C5G	-43.8(5)
C8C	C9C	C10C	C19C	72.2(5)	C8G	C9G	C10G	C19G	76.8(5)
C8C	C9C	C11C	C12C	50.7(6)	C8G	C9G	C11G	C12G	50.6(6)
C8C	C14C	C15C	C16C	-164.1(4)	C8G	C14G	C15G	C16G	-165.0(4)
C9C	C8C	C14C	C13C	57.1(5)	C9G	C8G	C14G	C13G	57.0(5)

C9C	C8C	C14C	C15C	-177.7(4)	C9G	C8G	C14G	C15G	-178.0(4)
C9C	C11C	C12C	C13C	-54.0(6)	C9G	C11G	C12G	C13G	-54.9(6)
C10C	C1C	C2C	C3C	-53.7(6)	C10G	C1G	C2G	C3G	-56.8(6)
C10C	C5C	C6C	C7C	-2.7(8)	C10G	C5G	C6G	C7G	2.7(8)
C10C	C9C	C11C	C12C	179.5(4)	C10G	C9G	C11G	C12G	178.4(4)
C11C	C9C	C10C	C1C	64.6(5)	C11G	C9G	C10G	C1G	69.6(5)
C11C	C9C	C10C	C5C	-175.2(4)	C11G	C9G	C10G	C5G	-171.3(4)
C11C	C9C	C10C	C19C	-56.2(5)	C11G	C9G	C10G	C19G	-50.7(5)
C11C	C12C	C13C	C14C	54.3(5)	C11G	C12G	C13G	C14G	55.6(5)
C11C	C12C	C13C	C17C	165.4(4)	C11G	C12G	C13G	C17G	164.8(4)
C11C	C12C	C13C	C18C	-67.7(5)	C11G	C12G	C13G	C18G	-68.0(5)
C12C	C13C	C14C	C8C	-58.6(5)	C12G	C13G	C14G	C8G	-59.8(5)
C12C	C13C	C14C	C15C	169.3(4)	C12G	C13G	C14G	C15G	168.5(4)
C12C	C13C	C17C	C16C	-155.4(4)	C12G	C13G	C17G	C16G	-155.1(4)
C12C	C13C	C17C	C20C	78.5(6)	C12G	C13G	C17G	C20G	79.6(6)
C13C	C14C	C15C	C16C	-33.6(5)	C13G	C14G	C15G	C16G	-34.7(5)
C13C	C17C	C20C	C21C	174.8(4)	C13G	C17G	C20G	C21G	-176.3(4)
C13C	C17C	C20C	C27C	-61.7(6)	C13G	C17G	C20G	C27G	-53.8(6)
C14C	C8C	C9C	C10C	-179.6(4)	C14G	C8G	C9G	C10G	-177.7(4)
C14C	C8C	C9C	C11C	-50.4(5)	C14G	C8G	C9G	C11G	-49.4(5)
C14C	C13C	C17C	C16C	-40.6(4)	C14G	C13G	C17G	C16G	-41.7(5)
C14C	C13C	C17C	C20C	-166.7(4)	C14G	C13G	C17G	C20G	-167.0(4)
C14C	C15C	C16C	C17C	7.5(5)	C14G	C15G	C16G	C17G	7.6(6)
C15C	C16C	C17C	C13C	21.0(5)	C15G	C16G	C17G	C13G	21.7(5)
C15C	C16C	C17C	C20C	152.1(4)	C15G	C16G	C17G	C20G	152.4(4)
C16C	C17C	C20C	C21C	53.0(6)	C16G	C17G	C20G	C21G	62.5(5)
C16C	C17C	C20C	C27C	176.5(4)	C16G	C17G	C20G	C27G	-175.0(4)
C17C	C13C	C14C	C8C	178.7(4)	C17G	C13G	C14G	C8G	179.7(4)
C17C	C13C	C14C	C15C	46.6(5)	C17G	C13G	C14G	C15G	48.1(4)
C17C	C20C	C21C	C22C	-166.8(5)	C17G	C20G	C21G	C22G	179.6(4)
C18C	C13C	C14C	C8C	62.7(5)	C18G	C13G	C14G	C8G	62.6(5)
C18C	C13C	C14C	C15C	-69.4(5)	C18G	C13G	C14G	C15G	-69.0(5)
C18C	C13C	C17C	C16C	77.2(5)	C18G	C13G	C17G	C16G	77.4(5)
C18C	C13C	C17C	C20C	-48.9(6)	C18G	C13G	C17G	C20G	-47.9(6)
C20C	C21C	C22C	C23C	175.9(5)	C20G	C21G	C22G	C23G	179.2(5)
C21C	C22C	C23C	C24C	-177.8(5)	C21G	C22G	C23G	C24G	168.2(5)
C22C	C23C	C24C	C25C	65.8(7)	C22G	C23G	C24G	C25G	63.6(7)
C22C	C23C	C24C	C26C	-170.1(5)	C22G	C23G	C24G	C26G	-172.4(5)
C27C	C20C	C21C	C22C	68.7(6)	C27G	C20G	C21G	C22G	56.1(6)

Table A1.5.8. Hydrogen atom coordinates ($Å \times 10^4$) and isotropic displacement parameters ($Å^2 \times 10^3$) for **81c**.

Atom	*x*	*y*	*z*	U(eq)
H1	6873	9636	1105	52
H1A	7098	10423	2541	28
H1B	8019	9625	2345	28
H2A	5823	10443	1934	31
H2B	7323	10637	1864	31
H3	7556	9043	1606	30
H4A	5824	7946	1528	32
H4B	4850	8734	1705	32
H6	6267	6876	1970	27
H7A	7580	6815	2618	24
H7B	6127	6386	2607	24
H8	5377	7763	2950	21
H9	7815	8633	2817	23
H11A	7278	10049	3171	26
H11B	5876	9636	3247	26
H12A	8325	9050	3604	26

H12B	7225	9628	3834	26
H14	7924	7456	3303	21
H15A	7043	5962	3310	29
H15B	5654	6373	3435	29
H16A	7941	6215	3943	26
H16B	6476	6354	4072	26
H17	8398	7774	4020	24
H18A	5178	8815	3970	38
H18B	4926	7703	3830	38
H18C	4814	8465	3511	38
H19A	4951	10092	2690	37
H19B	4361	9030	2667	37
H19C	4407	9549	2271	37
H20	6220	7785	4498	25
H21A	7924	6686	4637	31
H21B	8960	7550	4709	31
H22A	7982	8160	5291	33
H22B	6879	7334	5213	33
H23A	8391	6155	5328	39
H23B	9591	6880	5319	39
H24	8924	7720	5930	44
H25A	6766	7116	5896	75
H25B	7537	6937	6308	75
H25C	7307	6076	5962	75
H26A	9752	5791	5987	81
H26B	9922	6632	6343	81
H26C	10715	6677	5958	81
H27A	8234	9227	4557	40
H27B	7198	9158	4882	40
H27C	6717	9394	4444	40
H1AA	1911	9774	1034	39
H1AB	294	9385	2405	21
H1AC	1823	9451	2352	21
H2AA	-200	9495	1719	27
H2AB	696	10394	1905	27
H3A	2556	9676	1661	27
H4AA	933	8097	1307	26
H4AB	2481	8183	1291	26
H6A	3399	7043	1649	24
H7AA	3923	6817	2358	24
H7AB	3183	5916	2110	24
H8A	1229	6278	2374	21
H9A	2380	8114	2643	20
H11C	-205	7578	2794	24
H11D	493	8589	2936	24
H12C	1964	7883	3383	24
H12D	503	7615	3471	24
H14A	3230	6776	2997	21
H15C	3863	5269	2815	29
H15D	2385	4864	2728	29
H16C	2419	4563	3370	31
H16D	3831	5072	3466	31
H17A	3011	6507	3652	24
H18D	-388	5974	3295	38
H18E	458	5165	3072	38
H18F	-154	6004	2836	38
H19D	-979	7947	2195	32
H19E	-324	6977	2024	32
H19F	-587	7817	1746	32
H20A	907	5317	3824	31

H21C	2049	5174	4444	32
H21D	2815	4690	4085	32
H22C	3506	6551	4464	40
H22D	4341	5926	4157	40
H23C	4736	4805	4637	42
H23D	5373	5834	4779	42
H24A	3008	5140	5048	46
H25D	4361	6890	5326	112
H25E	3111	6498	5516	112
H25F	2972	6810	5075	112
H26D	4820	4342	5310	81
H26E	4277	5039	5661	81
H26F	5557	5336	5459	81
H27D	1632	7182	4191	59
H27E	697	6483	4388	59
H27F	243	6854	3971	59
H1BA	2158	2444	2400	48
H1BB	122	1552	3452	24
H1BC	313	451	3300	24
H2BA	1290	879	2731	29
H2BB	-115	1361	2749	29
H3B	868	2817	3033	25
H4BA	3147	3002	3101	27
H4BB	3320	1906	2936	27
H6B	3729	3190	3758	26
H7BA	2842	2813	4385	28
H7BB	4331	2512	4349	28
H8B	3796	928	4195	25
H9B	1151	1507	4065	22
H11E	463	-65	3911	31
H11F	1921	-440	3974	31
H12E	838	-705	4534	27
H12F	403	387	4593	27
H14B	2025	1637	4756	25
H15E	3923	2218	5085	34
H15F	4717	1266	4955	34
H16E	3141	1544	5593	34
H16F	4106	667	5503	34
H17B	1405	785	5260	27
H18G	3078	-1172	4739	42
H18H	4194	-379	4875	42
H18I	3637	-549	4419	42
H19G	2368	-313	3358	39
H19H	3668	230	3557	39
H19I	3128	403	3116	39
H20B	2889	-821	5484	32
H21E	2565	373	6012	35
H21F	1027	347	5897	35
H22E	2432	-1198	6208	40
H22F	888	-1221	6095	40
H23E	2248	-15	6730	43
H23F	767	183	6586	43
H24B	140	-1340	6768	44
H25G	2122	-2142	6731	84
H25H	1608	-2188	7161	84
H25I	2762	-1458	7102	84
H26G	1384	-108	7413	75
H26H	257	-875	7455	75
H26I	-62	32	7218	75

H27G	132	-789	5276	54
H27H	843	-1643	5480	54
H27I	1152	-1439	5042	54
H1C	7215	2559	2365	43
H1CA	9220	3232	3496	29
H1CB	8749	4305	3589	29
H2CA	7130	4108	3058	31
H2CB	8494	3785	2891	31
H3C	7946	2164	2931	29
H4CA	5844	1748	3102	25
H4CB	5486	2855	3181	25
H6C	6070	1159	3690	24
H7CA	7821	1133	4244	29
H7CB	6401	1354	4391	29
H8C	6859	2951	4543	21
H9C	9080	2661	4087	22
H11G	8431	4473	4473	30
H11H	9662	4261	4219	30
H12G	10661	3377	4706	31
H12H	10281	4395	4919	31
H14C	9237	2001	4721	26
H15G	7899	1123	5043	31
H15H	7054	2033	5192	31
H16G	9406	1448	5559	30
H16H	8461	2261	5738	30
H17C	10640	2480	5285	27
H18J	8524	4522	5389	38
H18K	7580	3625	5415	38
H18L	7504	4164	5022	38
H19J	6991	4690	3999	38
H19K	5972	3892	4091	38
H19L	5997	4192	3651	38
H20C	9720	3795	5897	29
H21G	10441	2265	6100	40
H21H	11868	2527	5985	40
H22G	10582	3614	6597	41
H22H	12049	3806	6491	41
H23G	11215	2073	6784	46
H23H	12682	2297	6693	46
H24C	12777	3572	7215	47
H25J	10585	3876	7264	82
H25K	11194	3593	7683	82
H25L	10329	2830	7390	82
H26J	12327	1704	7452	94
H26K	13094	2551	7729	94
H26L	13699	2088	7334	94
H27J	12151	3837	5541	55
H27K	11847	4512	5931	55
H27L	11037	4622	5517	55
H1D	9654	2466	2276	42
H1DA	7270	3053	942	28
H1DB	8819	2932	987	28
H2DA	7144	2916	1625	31
H2DB	7854	1997	1425	31
H3D	9917	2656	1659	24
H4DA	10130	4111	2060	29
H4DB	8579	4229	2044	29
H6D	10961	5251	1707	25
H7DA	11125	5505	999	26
H7DB	10593	6415	1257	26

H8D	8475	6137	996	20
H9D	9335	4272	715	20
H11I	6708	4858	572	28
H11J	7283	3841	424	28
H12I	8526	4528	-28	27
H12J	7041	4846	-103	27
H14D	10093	5593	366	22
H15I	10915	7079	554	30
H15J	9505	7515	640	30
H16I	9269	7836	0	32
H16J	10580	7272	-97	32
H17D	9527	5885	-292	25
H18M	6369	6483	84	43
H18N	7382	7270	305	43
H18O	6857	6435	540	43
H19M	6240	4490	1173	42
H19N	7045	5444	1343	42
H19O	6894	4602	1619	42
H20D	7438	7152	-445	28
H21I	8242	7284	-1067	32
H21J	9261	7709	-712	32
H22I	9539	5834	-1103	38
H22J	10619	6422	-809	38
H23I	10742	7555	-1295	39
H23J	11283	6523	-1432	39
H24D	8757	7168	-1689	47
H25M	10391	8024	-1957	84
H25N	9641	7326	-2304	84
H25O	11051	7049	-2120	84
H26M	10021	5454	-1966	116
H26N	8678	5812	-2167	116
H26O	8740	5504	-1726	116
H27M	7763	5273	-817	52
H27N	6810	6020	-1012	52
H27O	6530	5667	-593	52
H1E	4354	9376	10990	40
H1EA	5291	7964	9764	26
H1EB	5819	9037	9873	26
H2EA	3940	8104	10292	28
H2EB	5390	8427	10464	28
H3E	4835	10053	10447	25
H4EA	2250	9341	10185	25
H4EB	2638	10451	10281	25
H6E	2569	11108	9702	26
H7EA	4034	11183	9154	26
H7EB	2537	10960	9005	26
H8E	2906	9374	8833	23
H9E	5367	9671	9292	21
H11K	5905	8085	9140	31
H11L	4546	7864	8884	31
H12K	6639	9019	8667	30
H12L	6164	8001	8444	30
H14E	5196	10370	8664	23
H15K	3662	11245	8352	31
H15L	2749	10323	8197	31
H16K	4902	10968	7834	29
H16L	3875	10142	7650	29
H17E	6302	9946	8096	27
H18P	4152	7866	7980	38
H18Q	3191	8752	7958	38

H18R	3316	8196	8347	38
H19P	3325	7599	9346	34
H19Q	2253	8392	9270	34
H19R	2516	8046	9703	34
H20E	5089	8612	7479	27
H21K	5607	10149	7270	36
H21L	7109	9974	7396	36
H22K	5618	8813	6774	39
H22L	7139	8678	6895	39
H23K	6106	10370	6590	48
H23L	7624	10199	6695	48
H24E	7525	8889	6177	42
H25P	5294	8541	6107	76
H25Q	5729	8817	5691	76
H25R	4980	9577	5972	76
H26P	6879	10692	5896	90
H26Q	7677	9865	5666	90
H26R	8314	10436	6067	90
H27P	7705	8664	7840	48
H27Q	7261	7995	7441	48
H27R	6650	7824	7848	48
H1F	4671	2482	12334	49
H1FA	4017	1734	10885	27
H1FB	5097	2494	11086	27
H2FA	3070	1703	11497	35
H2FB	4588	1450	11554	35
H3F	5107	3036	11820	29
H4FA	3463	4165	11923	28
H4FB	2356	3398	11744	28
H6F	3728	5256	11494	25
H7FA	4643	5374	10840	23
H7FB	3204	5795	10864	23
H8F	2250	4458	10511	20
H9F	4723	3553	10631	20
H11M	3953	2167	10254	25
H11N	2531	2602	10183	25
H12M	4835	3226	9847	23
H12N	3626	2654	9603	23
H14F	4607	4787	10153	20
H15M	3776	6277	10168	24
H15N	2304	5884	10049	24
H16M	4268	6095	9531	26
H16N	2733	5929	9411	26
H17F	4712	4547	9444	22
H18S	1502	3448	9487	35
H18T	1355	4568	9614	35
H18U	1373	3830	9943	35
H19S	1824	2135	10739	36
H19T	1331	3215	10775	36
H19U	1532	2662	11163	36
H20F	2296	4536	8961	23
H21M	3915	5654	8834	30
H21N	4925	4811	8761	30
H22M	2622	5032	8249	31
H22N	3669	4207	8173	31
H23M	5300	5487	8158	34
H23N	4115	6214	8147	34
H24F	4299	4661	7540	37
H25S	2190	5335	7575	66
H25T	2770	5461	7160	66

H25U	2784	6347	7496	66
H26S	5212	6565	7494	69
H26T	5166	5726	7137	69
H26U	6132	5658	7525	69
H27S	4259	3106	8894	43
H27T	3065	3187	8568	43
H27U	2794	2928	9002	43
H1G	9339	-40	11002	57
H1GA	6907	1844	10092	25
H1GB	6698	733	9942	25
H2GA	8186	1475	10660	33
H2GB	6800	934	10640	33
H3G	7725	-496	10369	30
H4GA	9967	-596	10300	29
H4GB	10182	507	10466	29
H6G	10189	-792	9642	25
H7GA	8975	-416	9011	28
H7GB	10479	-89	9048	28
H8G	10002	1479	9211	25
H9G	7411	829	9326	23
H11O	8189	2798	9429	31
H11P	6763	2389	9481	31
H12O	6407	1946	8794	30
H12P	6836	3052	8863	30
H14G	7981	739	8637	25
H15O	9733	214	8316	32
H15P	10576	1178	8458	32
H16O	9696	1799	7911	36
H16P	8711	899	7806	36
H17G	7105	1595	8137	27
H18V	8987	3580	8674	42
H18W	10056	2812	8545	42
H18X	9696	2967	8997	42
H19V	8912	2682	10041	42
H19W	10146	2178	9853	42
H19X	9800	1991	10290	42
H20G	8466	3242	7930	29
H21O	7911	2070	7392	32
H21P	6425	2059	7499	32
H22O	7658	3640	7203	36
H22P	6162	3618	7306	36
H23O	5856	2224	6810	40
H23P	7275	2455	6679	40
H24G	5135	3738	6627	47
H25V	7086	4593	6673	92
H25W	6426	4585	6231	92
H25X	7621	3896	6321	92
H26V	6092	2540	5985	76
H26W	4952	3299	5939	76
H26X	4727	2381	6169	76
H27V	5800	3156	8117	54
H27W	6427	4032	7929	54
H27X	6924	3806	8367	54

A1.6. Crystal structure data of 3β-methoxy-5-cholestene, 86

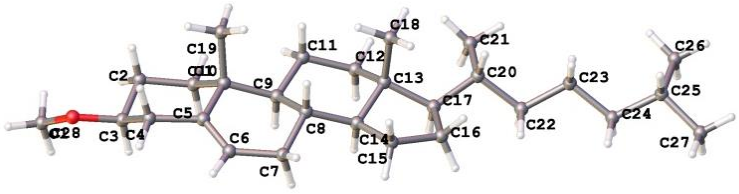

Figure A1.6. One Structure from the unit cell of **86**, determined by X-ray diffraction of a single crystal.

Table A1.6.1. Crystal data and structure refinement for **86**.

Empirical formula	$C_{28}H_{48}O$
Formula weight	400.66
Temperature (K)	120
Crystal system	monoclinic
Space group	$P2_1$
a (Å)	11.7356(6)
b (Å)	7.5183(4)
c (Å)	15.0889(8)
α (°)	90
β (°)	112.177(3)
γ (°)	90
Volume (Å^3)	1232.83(11)
Z	2
ρ_{calc}g (cm^3)	1.079
μ (mm^{-1})	0.463
F(000)	448
Crystal size (mm^3)	0.49 × 0.04 × 0.01
Radiation	CuKα (λ = 1.54178)
2Θ range for data collection (°)	6.32 to 143.96
Index ranges	-14 ≤ h ≤ 14, -9 ≤ k ≤ 8, -18 ≤ l ≤ 18
Reflections collected	14466
Independent reflections	4276 [R_{int} = 0.0661, R_{sigma} = 0.0706]
Data/ restraints/ parameters	4276/1/268
Goodness-of-fit on F^2	1.066
Final R indexes [I > = 2σ (I)]	R_1 = 0.0673, wR_2 = 0.1540
Final R indexes [all data]	R_1 = 0.0926, wR_2 = 0.1722
Largest diff. peak/ hole (e Å^{-3})	0.20/-0.20
Flack parameter	0.1(6)

Table A1.6.2. Fractional atomic coordinates (×10^4) and equivalent isotropic displacement parameters (Å^2×10^3) for **86**. U_{eq} is defined as 1/3 of the trace of the orthogonalised U_{IJ} tensor.

Atom	*x*	*y*	*z*	U(eq)
O1	15961(2)	6026(4)	4641.3(17)	33.7(6)
C1	13119(3)	4089(5)	2707(2)	25.5(7)
C2	14360(3)	4044(5)	3560(2)	27.1(8)
C3	14837(3)	5920(5)	3816(3)	29.1(8)
C4	13913(3)	7029(6)	4050(3)	32.3(8)
C5	12648(3)	7005(5)	3254(2)	26.7(7)
C6	12075(3)	8534(5)	2913(3)	28.5(8)
C7	10816(3)	8667(5)	2145(3)	27.3(8)
C8	10126(3)	6904(5)	1932(2)	23.2(7)
C9	10987(3)	5378(5)	1919(2)	21.4(7)

C10	12113(3)	5192(5)	2883(2)	23.0(7)
C11	10274(3)	3635(5)	1575(3)	28.2(8)
C12	9146(3)	3809(5)	635(2)	26.6(8)
C13	8265(3)	5277(5)	689(2)	21.8(7)
C14	9047(3)	6974(5)	975(2)	22.4(7)
C15	8111(3)	8475(5)	812(3)	28.9(8)
C16	7001(3)	7844(5)	-70(3)	27.1(8)
C17	7265(3)	5890(4)	-278(2)	22.5(7)
C18	7666(3)	4793(5)	1404(3)	30.6(8)
C19	11746(3)	4256(5)	3649(2)	31.7(8)
C20	16974(3)	5199(6)	4511(3)	35.5(9)
C21	6073(3)	4809(5)	-730(2)	25.3(8)
C22	6296(3)	2843(5)	-868(3)	35.8(9)
C23	5262(3)	5650(5)	-1695(3)	28.3(8)
C24	3910(3)	5096(5)	-2058(3)	30.2(8)
C25	3109(3)	6086(5)	-2961(2)	27.8(8)
C26	1720(3)	5710(5)	-3292(3)	30.0(8)
C27	991(3)	7002(6)	-4083(3)	37.5(9)
C28	1400(4)	3799(6)	-3629(3)	37.4(9)

Table A1.6.3. Anisotropic displacement parameters ($Å^2 \times 10^3$) for **86**. The anisotropic displacement factor exponent takes the form: $-2\pi^2[h^2a^{*2}U_{11}+2hka^*b^*U_{12}+\ldots]$.

Atom	U_{11}	U_{22}	U_{33}	U_{23}	U_{13}	U_{12}
O1	21.6(12)	40.0(14)	32.4(14)	-7.2(12)	2.2(10)	1.7(11)
C1	21.2(17)	25.5(17)	26.2(19)	-4.3(15)	5.0(14)	2.4(15)
C2	19.4(17)	32.1(19)	26.8(19)	-2.3(15)	5.2(14)	2.9(15)
C3	20.3(17)	36(2)	24.3(18)	0.6(16)	0.8(14)	1.6(16)
C4	25.4(18)	35(2)	30(2)	-10.6(18)	3.6(15)	-0.2(17)
C5	20.8(17)	32.9(18)	23.8(18)	-5.8(16)	5.5(13)	1.2(16)
C6	24.4(18)	28.7(18)	27.3(19)	-5.1(15)	4.0(15)	-0.5(15)
C7	24.4(18)	23.1(17)	30.0(19)	-2.8(15)	5.3(15)	1.5(14)
C8	18.0(15)	25.4(16)	24.3(17)	0.4(15)	5.6(13)	2.0(15)
C9	17.6(16)	25.6(17)	19.4(17)	0.5(13)	5.4(13)	1.3(13)
C10	19.8(17)	28.1(18)	18.8(18)	-0.2(14)	4.6(13)	4.5(14)
C11	21.2(17)	24.4(18)	33(2)	-0.5(15)	3.4(15)	0.8(15)
C12	21.2(17)	23.1(18)	29.2(19)	-4.0(15)	2.4(14)	2.1(14)
C13	15.8(15)	26.5(17)	21.6(18)	2.8(14)	5.4(13)	2.2(14)
C14	19.6(16)	24.7(17)	21.8(17)	0.3(15)	6.6(13)	2.8(15)
C15	23.9(18)	24.3(18)	32(2)	-1.5(15)	2.5(15)	4.6(15)
C16	23.6(18)	25.9(17)	28(2)	2.3(15)	5.3(15)	2.7(15)
C17	20.6(16)	25.4(17)	21.2(17)	1.2(15)	7.5(13)	0.4(14)
C18	26.2(18)	34(2)	31(2)	4.4(16)	9.7(15)	-2.4(15)
C19	27.5(18)	40(2)	26.2(19)	1.2(16)	9.1(15)	1.0(16)
C20	18.6(18)	45(2)	40(2)	-3.8(19)	7.1(16)	-1.4(17)
C21	17.3(16)	31.6(19)	24.7(18)	2.4(15)	5.3(14)	0.9(14)
C22	28(2)	31(2)	41(2)	-1.5(18)	3.7(17)	-1.6(17)
C23	20.1(17)	32(2)	29(2)	4.4(15)	5.2(14)	-1.1(14)
C24	20.7(17)	37(2)	29(2)	0.3(17)	4.7(14)	-5.8(15)
C25	18.1(16)	36.0(19)	26.8(19)	3.4(16)	5.8(14)	-4.1(15)
C26	19.9(18)	43(2)	25.3(19)	-0.5(16)	6.1(14)	-4.2(16)
C27	20.0(18)	54(2)	32(2)	6(2)	2.2(15)	2.6(18)
C28	32(2)	45(2)	30(2)	-1.3(18)	6.1(16)	-7.5(19)

Table A1.6.4. Bond lengths of **86**.

Atom	Atom	Length (Å)	Atom	Atom	Length (Å)
O1	C3	1.434(4)	C11	C12	1.538(4)
O1	C20	1.420(4)	C12	C13	1.535(4)
C1	C2	1.537(4)	C13	C14	1.535(5)

C1	C10	1.545(4)	C13	C17	1.558(4)
C2	C3	1.512(5)	C13	C18	1.539(4)
C3	C4	1.511(5)	C14	C15	1.529(5)
C4	C5	1.517(4)	C15	C16	1.544(5)
C5	C6	1.333(5)	C16	C17	1.557(5)
C5	C10	1.517(5)	C17	C21	1.536(5)
C6	C7	1.497(5)	C21	C22	1.529(5)
C7	C8	1.523(5)	C21	C23	1.542(5)
C8	C9	1.533(5)	C23	C24	1.528(5)
C8	C14	1.520(4)	C24	C25	1.525(5)
C9	C10	1.559(4)	C25	C26	1.540(4)
C9	C11	1.536(5)	C26	C27	1.526(5)
C10	C19	1.547(5)	C26	C28	1.523(5)

Table A1.6.5. Bond angles of **86**.

Atom	Atom	Atom	Angle (°)	Atom	Atom	Atom	Angle (°)
C20	O1	C3	113.5(3)	C13	C12	C11	112.0(3)
C2	C1	C10	114.3(3)	C12	C13	C14	105.6(2)
C3	C2	C1	109.6(3)	C12	C13	C17	116.6(3)
O1	C3	C2	113.8(3)	C12	C13	C18	111.3(3)
O1	C3	C4	105.8(3)	C14	C13	C17	100.2(3)
C4	C3	C2	110.2(3)	C14	C13	C18	112.5(3)
C3	C4	C5	112.5(3)	C18	C13	C17	110.1(3)
C6	C5	C4	119.7(3)	C8	C14	C13	115.7(3)
C6	C5	C10	123.7(3)	C8	C14	C15	117.9(3)
C10	C5	C4	116.6(3)	C15	C14	C13	104.6(2)
C5	C6	C7	124.2(3)	C14	C15	C16	103.4(3)
C6	C7	C8	113.3(3)	C15	C16	C17	107.3(3)
C7	C8	C9	110.7(3)	C16	C17	C13	103.1(3)
C14	C8	C7	110.8(3)	C21	C17	C13	119.8(3)
C14	C8	C9	109.3(3)	C21	C17	C16	111.8(3)
C8	C9	C10	112.7(3)	C17	C21	C23	109.6(3)
C8	C9	C11	111.4(3)	C22	C21	C17	113.5(3)
C11	C9	C10	113.6(3)	C22	C21	C23	110.2(3)
C1	C10	C9	108.8(3)	C24	C23	C21	114.5(3)
C1	C10	C19	109.3(3)	C25	C24	C23	113.2(3)
C5	C10	C1	108.0(3)	C24	C25	C26	114.9(3)
C5	C10	C9	110.5(3)	C27	C26	C25	110.5(3)
C5	C10	C19	109.0(3)	C28	C26	C25	112.3(3)
C19	C10	C9	111.2(3)	C28	C26	C27	110.2(3)
C9	C11	C12	114.1(3)				

Table A1.6.6. Tosion angles for **86**.

A	B	C	D	Angle (°)	A	B	C	D	Angle (°)
O1	C3	C4	C5	-178.1(3)	C11	C9	C10	C5	-171.1(3)
C1	C2	C3	O1	176.7(3)	C11	C9	C10	C19	-49.9(4)
C1	C2	C3	C4	58.1(4)	C11	C12	C13	C14	55.6(4)
C2	C1	C10	C5	51.0(4)	C11	C12	C13	C17	165.8(3)
C2	C1	C10	C9	171.0(3)	C11	C12	C13	C18	-66.7(4)
C2	C1	C10	C19	-67.5(4)	C12	C13	C14	C8	-60.5(3)
C2	C3	C4	C5	-54.7(4)	C12	C13	C14	C15	168.0(3)
C3	C4	C5	C6	-128.3(4)	C12	C13	C17	C16	-153.0(3)
C3	C4	C5	C10	51.0(4)	C12	C13	C17	C21	82.0(4)
C4	C5	C6	C7	-178.6(3)	C13	C14	C15	C16	-34.4(3)
C4	C5	C10	C1	-47.1(4)	C13	C17	C21	C22	-54.3(4)
C4	C5	C10	C9	-166.0(3)	C13	C17	C21	C23	-178.0(3)
C4	C5	C10	C19	71.6(4)	C14	C8	C9	C10	-179.1(3)
C5	C6	C7	C8	12.4(5)	C14	C8	C9	C11	-50.1(4)

C6	C5	C10	C1	132.3(4)	C14	C13	C17	C16	-39.7(3)
C6	C5	C10	C9	13.4(5)	C14	C13	C17	C21	-164.7(3)
C6	C5	C10	C19	-109.1(4)	C14	C15	C16	C17	8.6(4)
C6	C7	C8	C9	-41.6(4)	C15	C16	C17	C13	19.6(3)
C6	C7	C8	C14	-163.1(3)	C15	C16	C17	C21	149.7(3)
C7	C8	C9	C10	58.5(4)	C16	C17	C21	C22	-175.1(3)
C7	C8	C9	C11	-172.5(3)	C16	C17	C21	C23	61.3(4)
C7	C8	C14	C13	-179.0(3)	C17	C13	C14	C8	178.0(3)
C7	C8	C14	C15	-54.2(4)	C17	C13	C14	C15	46.5(3)
C8	C9	C10	C1	-161.7(3)	C17	C21	C23	C24	-161.3(3)
C8	C9	C10	C5	-43.2(4)	C18	C13	C14	C8	61.1(4)
C8	C9	C10	C19	78.0(4)	C18	C13	C14	C15	-70.4(3)
C8	C9	C11	C12	50.4(4)	C18	C13	C17	C16	78.9(3)
C8	C14	C15	C16	-164.5(3)	C18	C13	C17	C21	-46.1(4)
C9	C8	C14	C13	58.7(4)	C20	O1	C3	C2	64.9(4)
C9	C8	C14	C15	-176.5(3)	C20	O1	C3	C4	-174.1(3)
C9	C11	C12	C13	-54.5(4)	C21	C23	C24	C25	174.4(3)
C10	C1	C2	C3	-58.5(4)	C22	C21	C23	C24	73.2(4)
C10	C5	C6	C7	2.1(6)	C23	C24	C25	C26	-174.0(3)
C10	C9	C11	C12	178.9(3)	C24	C25	C26	C27	169.8(3)
C11	C9	C10	C1	70.5(4)	C24	C25	C26	C28	-66.8(4)

Table A1.6.7. Hydrogen atom coordinates ($Å \times 10^4$) and isotropic displacement parameters ($Å^2 \times 10^3$) for **86**.

Atom	*x*	*y*	*z*	U(eq)
H1A	12819	2854	2548	31
H1B	13251	4587	2146	31
H2A	14254	3478	4117	33
H2B	14960	3333	3393	33
H3	14968	6462	3257	35
H4A	14211	8272	4168	39
H4B	13849	6572	4645	39
H6	12492	9609	3174	34
H7A	10890	9112	1552	33
H7B	10329	9546	2343	33
H8	9803	6664	2446	28
H9	11329	5704	1426	26
H11A	9998	3194	2080	34
H11B	10839	2736	1488	34
H12A	9426	4080	107	32
H12B	8701	2661	488	32
H14	9414	7140	481	27
H15A	8441	9615	681	35
H15B	7880	8627	1375	35
H16A	6899	8610	-628	33
H16B	6237	7902	62	33
H17	7664	5939	-758	27
H18A	7071	5716	1395	46
H18B	8302	4707	2049	46
H18C	7241	3648	1225	46
H19A	12433	4319	4270	48
H19B	11548	3008	3470	48
H19C	11026	4850	3692	48
H20A	17023	5612	3911	53
H20B	16863	3905	4487	53
H20C	17736	5509	5046	53
H21	5613	4882	-293	30
H22A	6725	2288	-242	54
H22B	6800	2736	-1256	54

H22C	5505	2246	-1194	54
H23A	5310	6961	-1627	34
H23B	5601	5321	-2182	34
H24A	3850	3803	-2192	36
H24B	3588	5317	-1548	36
H25A	3383	5764	-3485	33
H25B	3245	7379	-2845	33
H26	1472	5908	-2735	36
H27A	109	6766	-4274	56
H27B	1226	6845	-4636	56
H27C	1168	8225	-3846	56
H28A	1624	3577	-4183	56
H28B	514	3609	-3811	56
H28C	1855	2982	-3110	56

A1.7. Crystal structure data for cholesterol tertbutyldimethylsilyl ether, 91

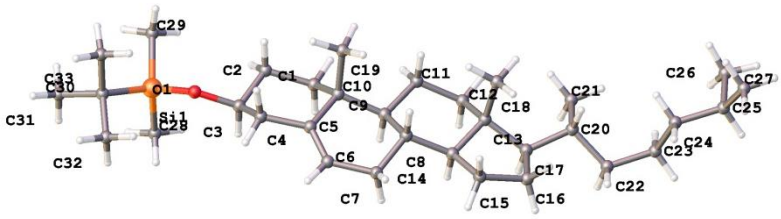

Figure A1.7. One Structure from the unit cell of **91**, determined by X-ray diffraction of a single crystal.

Table A1.7.1. Crystal data and structure refinement for **91**.

Empirical formula	$C_{33}H_{60}OSi$
Formula weight	500.9
Temperature (K)	120
Crystal system	monoclinic
Space group	$P2_1$
a (Å)	7.4276(3)
b (Å)	9.4843(4)
c (Å)	45.7777(17)
α (°)	90
β (°)	91.508(2)
γ (°)	90
Volume ($Å^3$)	3223.7(2)
Z	4
$\rho_{calc}g$ (cm^3)	1.032
μ (mm^{-1})	0.779
F(000)	1120
Crystal size (mm^3)	0.33 × 0.14 × 0.02
Radiation	CuKα (λ = 1.54178)
2Θ range for data collection (°)	5.8 to 144.9
Index ranges	$-9 \le h \le 8$, $-11 \le k \le 11$, $-53 \le l \le 52$
Reflections collected	42069
Independent reflections	11889 [R_{int} = 0.0743, R_{sigma} = 0.0723]
Data/ restraints/ parameters	11889/61/651
Goodness-of-fit on F^2	1.042
Final R indexes [I > = 2σ (I)]	R_1 = 0.0600, wR_2 = 0.1258
Final R indexes [all data]	R_1 = 0.0821, wR_2 = 0.1357
Largest diff. peak/ hole (e $Å^{-3}$)	0.28/-0.30

Flack parameter	-0.02(3)

Table A1.7.2. Fractional atomic coordinates ($\times 10^4$) and equivalent isotropic displacement parameters ($Å^2 \times 10^3$) for **91**. U_{eq} is defined as 1/3 of the trace of the orthogonalised U_{IJ} tensor.

Atom	*x*	*y*	*z*	U(eq)
Si1	1000.9(13)	3624.9(11)	-1606.57(19)	33.1(2)
O1	1630(3)	2605(2)	-1333.4(5)	32.4(6)
C1	832(4)	3223(3)	-535.3(6)	21.1(7)
C2	375(4)	2903(3)	-854.5(6)	24.6(7)
C3	2044(4)	2977(3)	-1037.1(6)	24.8(7)
C4	3468(4)	1953(3)	-918.6(6)	25.0(7)
C5	3875(4)	2139(3)	-595.0(6)	19.9(6)
C6	5568(4)	2181(3)	-492.0(6)	22.8(7)
C7	6113(4)	2292(3)	-176.5(6)	21.5(7)
C8	4566(4)	2042(3)	30.2(6)	17.9(6)
C9	2856(4)	2789(3)	-91.8(6)	17.1(6)
C10	2253(4)	2215(3)	-396.4(6)	19.6(6)
C11	1346(4)	2780(3)	130.7(6)	22.6(7)
C12	1922(4)	3299(3)	436.1(6)	20.3(7)
C13	3526(4)	2449(3)	560.3(6)	19.9(7)
C14	5030(4)	2586(3)	334.2(6)	17.9(6)
C15	6694(4)	1976(3)	496.3(6)	24.6(7)
C16	6444(4)	2428(4)	815.2(7)	25.2(7)
C17	4514(4)	3067(3)	833.8(6)	19.6(6)
C18	2976(4)	908(3)	614.3(6)	25.0(7)
C19	1426(4)	729(3)	-373.7(6)	21.8(7)
C20	3680(4)	2858(3)	1136.1(7)	24.8(7)
C21	1795(4)	3489(4)	1150.5(7)	32.9(8)
C22	4907(4)	3479(4)	1380.2(7)	29.9(7)
C23	4446(5)	2998(4)	1686.8(7)	35.8(9)
C24	5680(5)	3602(4)	1923.8(7)	43.5(9)
C25	5426(4)	3000(4)	2229.3(7)	47.5(10)
C26B	3467(7)	2958(10)	2328(2)	39(2)
C26C	3608(9)	3470(14)	2343(3)	68(4)
C27B	6553(12)	3757(12)	2465.7(19)	45(3)
C27C	6989(13)	3578(16)	2421(2)	72(4)
C28B	-250(13)	5186(8)	-1471(2)	57(3)
C28C	472(11)	5448(5)	-1487.8(16)	32.9(18)
C29B	2940(9)	3697(12)	-1857.1(18)	53(3)
C29C	3007(10)	4236(11)	-1806(2)	59(3)
C30B	-938(8)	2701(7)	-1790.6(14)	44(2)
C30C	-520(9)	2518(7)	-1841.4(14)	45(2)
C31B	-365(15)	1204(8)	-1876(2)	66(3)
C31C	445(16)	1201(10)	-1949(3)	78(3)
C32B	-1700(14)	3596(11)	-2044.2(19)	57(3)
C32C	-1195(14)	3255(10)	-2119.9(18)	54(3)
C33B	-2138(13)	2023(11)	-1668(2)	67(3)
C33C	-2433(12)	2505(11)	-1570(2)	55(2)
Si1A	311.3(12)	5940(1)	3488.01(18)	26.0(2)
O1A	1395(3)	5064(2)	3748.5(4)	27.7(5)
C1A	739(4)	5800(3)	4548.7(6)	18.6(6)
C2A	210(4)	5456(3)	4232.2(6)	21.7(7)
C3A	1841(4)	5489(3)	4039.5(6)	21.3(7)
C4A	3289(4)	4497(3)	4156.4(6)	22.6(7)
C5A	3755(4)	4705(3)	4476.9(6)	19.2(6)
C6A	5463(4)	4758(3)	4572.4(6)	19.6(6)
C7A	6049(4)	4872(3)	4887.1(6)	19.7(6)
C8A	4538(4)	4627(3)	5100.1(6)	18.7(6)

C9A	2802(4)	5346(3)	4985.2(6)	16.2(6)
C10A	2164(4)	4788(3)	4681.4(6)	16.4(6)
C11A	1336(4)	5282(3)	5214.6(6)	18.3(6)
C12A	1921(4)	5860(3)	5513.4(6)	20.0(6)
C13A	3585(4)	5080(3)	5634.4(6)	17.7(6)
C14A	5043(4)	5214(3)	5403.1(6)	18.0(6)
C15A	6740(4)	4654(4)	5558.2(6)	24.5(7)
C16A	6542(4)	5161(3)	5876.6(6)	24.0(7)
C17A	4601(4)	5771(3)	5899.6(6)	21.1(6)
C18A	3125(4)	3533(3)	5704.7(6)	23.6(7)
C19A	1339(4)	3307(3)	4707.7(6)	21.2(7)
C20A	3858(4)	5610(3)	6210.4(6)	25.2(7)
C21A	1934(4)	6161(4)	6231.8(7)	31.9(8)
C22A	5120(5)	6361(4)	6431.5(7)	29.7(8)
C23A	4582(5)	6276(4)	6753.4(7)	32.9(8)
C24A	4539(5)	4792(4)	6874.2(7)	35.6(9)
C25A	4064(5)	4683(4)	7196.4(8)	38.7(9)
C26A	2053(6)	5040(5)	7235.7(9)	54.4(11)
C27A	4441(6)	3225(5)	7314.7(8)	57.2(12)
C28A	-2172(4)	5718(5)	3517.0(8)	42.1(10)
C29A	868(6)	7851(4)	3514.4(8)	43.9(10)
C30A	1150(4)	5133(4)	3143.8(7)	30.1(8)
C31A	3214(5)	5217(4)	3144.2(8)	37.3(9)
C32A	371(5)	5906(5)	2872.1(7)	48(1)
C33A	596(5)	3573(4)	3128.6(8)	41.3(9)

Table A1.7.3. Anisotropic displacement parameters (Å2×103) for **91**. The anisotropic displacement factor exponent takes the form: -2π2[h2a*2U11+2hka*b*U12+…].

Atom	U_{11}	U_{22}	U_{33}	U_{23}	U_{13}	U_{12}
Si1	37.9(6)	38.3(6)	22.8(5)	2.5(4)	-5.6(4)	-0.3(5)
O1	42.8(14)	35.0(14)	19.0(12)	-1.7(10)	-4.5(10)	5.8(11)
C1	17.7(16)	20.8(17)	24.6(17)	-1.5(12)	-2.6(12)	1.3(12)
C2	23.2(17)	27.0(18)	23.2(17)	1.1(13)	-5.6(13)	2.8(14)
C3	31.4(19)	28.6(18)	14.3(16)	-1.0(12)	-3.6(12)	-0.2(15)
C4	24.1(18)	28.9(18)	22.3(17)	-4.9(13)	3.8(13)	3.7(14)
C5	19.7(17)	17.7(16)	22.2(17)	-1.1(12)	0.4(12)	-0.7(12)
C6	22.0(18)	26.6(17)	20.1(17)	-2.4(13)	5.1(12)	-2.1(13)
C7	12.5(16)	29.2(18)	22.7(17)	-1.2(13)	0.8(12)	-0.7(13)
C8	11.6(15)	19.6(16)	22.4(16)	1.3(12)	1.4(11)	0.8(12)
C9	16.0(15)	15.9(15)	19.1(16)	-0.7(12)	-2.0(11)	-2.4(12)
C10	18.0(16)	21.0(16)	19.9(16)	-0.3(12)	0.6(12)	-1.3(13)
C11	16.1(16)	27.5(18)	24.1(17)	-1.5(13)	-0.8(12)	3.1(13)
C12	13.7(15)	27.9(17)	19.2(16)	-4.0(12)	-0.5(11)	3.4(13)
C13	16.9(16)	22.9(16)	20.1(16)	-0.6(12)	-0.7(12)	-1.1(13)
C14	13.3(15)	17.9(15)	22.3(16)	1.1(12)	-0.4(11)	-3.5(12)
C15	19.2(17)	29.3(18)	25.2(18)	-0.3(14)	-3.4(13)	6.2(14)
C16	22.4(17)	29.5(18)	23.5(18)	0.1(13)	-2.0(13)	4.2(14)
C17	17.2(16)	23.6(16)	18.0(16)	1.7(12)	-1.9(11)	-1.1(12)
C18	26.8(17)	23.4(16)	24.8(17)	2.2(14)	-0.5(12)	-5.4(15)
C19	21.8(16)	19.6(16)	23.9(16)	-1.8(13)	-1.6(12)	-2.5(13)
C20	26.2(18)	25.6(18)	22.5(17)	-0.1(13)	-0.6(13)	-1.6(14)
C21	26.8(18)	49(2)	22.8(18)	-0.9(16)	4.7(13)	4.1(17)
C22	30.4(19)	31.9(19)	27.4(18)	-1.7(15)	-1.6(14)	1.7(16)
C23	40(2)	43(2)	24.4(19)	1.2(15)	-2.6(15)	0.0(17)
C24	59(3)	46(2)	25.0(19)	1.9(17)	-8.9(17)	1(2)
C25	61(3)	56(3)	25(2)	-1.8(17)	-11.5(18)	9(2)
Si1A	24.5(5)	32.4(5)	20.8(5)	-1.1(4)	-4.7(3)	1.2(4)
O1A	30.6(13)	34.4(13)	17.7(12)	-0.7(9)	-5.0(9)	7.6(10)

C1A	16.9(15)	16.2(15)	22.7(16)	-0.1(13)	-0.4(11)	2.9(13)
C2A	20.6(16)	23.4(17)	20.9(16)	-1.4(12)	-4.9(12)	5.2(13)
C3A	21.9(17)	24.5(17)	17.4(16)	-2.1(12)	-2.5(12)	-0.3(13)
C4A	19.0(17)	27.8(17)	21.0(17)	-2.9(13)	0.1(12)	1.8(13)
C5A	20.9(17)	16.9(15)	19.8(16)	-1.2(12)	1.1(12)	-0.3(12)
C6A	15.3(16)	23.8(16)	19.9(16)	-1.0(12)	3.8(12)	0.6(13)
C7A	12.7(15)	23.8(16)	22.7(17)	-2.3(12)	0.4(12)	-0.7(13)
C8A	13.3(15)	22.9(16)	19.8(16)	-1.1(12)	0.0(11)	4.5(12)
C9A	13.1(15)	15.5(15)	20.0(16)	-1.2(11)	-0.1(11)	-1.3(12)
C10A	12.2(15)	16.8(15)	20.1(16)	-0.3(11)	-1.6(11)	0.1(12)
C11A	10.9(15)	23.2(16)	20.6(16)	-0.4(12)	0.0(11)	0.9(12)
C12A	14.8(15)	22.8(16)	22.3(16)	-0.3(13)	1.1(11)	2.6(13)
C13A	15.9(15)	19.3(16)	17.8(16)	2.8(12)	1.7(11)	0.4(12)
C14A	12.1(15)	20.4(15)	21.4(16)	0.1(12)	0.2(11)	-0.5(12)
C15A	18.2(17)	35.1(18)	20.2(17)	-0.3(13)	1.1(12)	2.8(14)
C16A	20.8(17)	30.3(18)	20.7(17)	2.1(13)	-2.4(12)	0.3(14)
C17A	17.3(15)	23.8(16)	22.3(16)	0.6(13)	1.4(12)	-0.2(13)
C18A	27.9(17)	21.1(16)	21.8(16)	-0.4(13)	2.4(12)	-4.3(14)
C19A	19.3(16)	22.7(16)	21.5(16)	-1.1(12)	-2.1(12)	-3.0(13)
C20A	30.9(18)	27.6(19)	16.9(16)	-0.8(12)	-1.9(13)	-1.7(14)
C21A	28.4(18)	44(2)	23.5(18)	-4.9(15)	5.5(13)	0.8(17)
C22A	33(2)	34(2)	21.5(18)	-2.9(13)	0.6(14)	-7.5(15)
C23A	39(2)	40(2)	20.1(18)	-4.9(14)	-1.5(14)	-4.7(16)
C24A	44(2)	42(2)	20.9(19)	-4.1(15)	-0.9(15)	2.2(18)
C25A	50(2)	40(2)	25(2)	-1.8(16)	0.6(16)	-1.4(19)
C26A	59(3)	65(3)	40(3)	6(2)	16(2)	3(2)
C27A	87(3)	57(3)	28(2)	6.9(19)	7(2)	8(2)
C28A	25.4(19)	60(3)	41(2)	-0.9(19)	-0.8(15)	2.5(19)
C29A	61(3)	36(2)	33(2)	-0.1(16)	-11.6(18)	1.2(19)
C30A	30.1(19)	39(2)	21.6(18)	-2.8(14)	-2.9(13)	4.6(16)
C31A	34(2)	46(2)	32(2)	-1.2(17)	3.9(15)	-2.5(17)
C32A	57(2)	64(3)	22.4(19)	-3.3(19)	-8.8(16)	9(2)
C33A	46(2)	42(2)	35(2)	-10.5(18)	0.5(16)	-4(2)

Table A1.7.4. Bond lengths for **91**.

Atom	Atom	Length (Å)	Atom	Atom	Length (Å)
Si1	O1	1.639(2)	C30B	C33C	1.531(4)
Si1	C28B	1.863(4)	C30C	C31C	1.528(4)
Si1	C28C	1.858(4)	C30C	C32C	1.527(4)
Si1	C29B	1.866(4)	C30C	C33B	1.530(4)
Si1	C29C	1.860(4)	Si1A	O1A	1.646(2)
Si1	C30B	1.868(4)	Si1A	C28A	1.865(3)
Si1	C30C	1.863(4)	Si1A	C29A	1.862(4)
O1	C3	1.427(4)	Si1A	C30A	1.873(3)
C1	C2	1.522(4)	O1A	C3A	1.422(3)
C1	C10	1.548(4)	C1A	C2A	1.526(4)
C2	C3	1.515(4)	C1A	C10A	1.542(4)
C3	C4	1.525(4)	C2A	C3A	1.517(4)
C4	C5	1.515(4)	C3A	C4A	1.516(4)
C5	C6	1.332(4)	C4A	C5A	1.512(4)
C5	C10	1.530(4)	C5A	C6A	1.332(4)
C6	C7	1.494(4)	C5A	C10A	1.528(4)
C7	C8	1.526(4)	C6A	C7A	1.498(4)
C8	C9	1.546(4)	C7A	C8A	1.524(4)
C8	C14	1.516(4)	C8A	C9A	1.539(4)
C9	C10	1.552(4)	C8A	C14A	1.532(4)
C9	C11	1.535(4)	C9A	C10A	1.551(4)
C10	C19	1.542(4)	C9A	C11A	1.534(4)
C11	C12	1.532(4)	C10A	C19A	1.538(4)

C12	C13	1.535(4)	C11A	C12A	1.526(4)
C13	C14	1.548(4)	C12A	C13A	1.531(4)
C13	C17	1.550(4)	C13A	C14A	1.540(4)
C13	C18	1.540(4)	C13A	C17A	1.557(4)
C14	C15	1.538(4)	C13A	C18A	1.543(4)
C15	C16	1.538(4)	C14A	C15A	1.525(4)
C16	C17	1.560(4)	C15A	C16A	1.545(4)
C17	C20	1.544(4)	C16A	C17A	1.560(4)
C20	C21	1.526(4)	C17A	C20A	1.547(4)
C20	C22	1.540(4)	C20A	C21A	1.527(4)
C22	C23	1.523(5)	C20A	C22A	1.536(4)
C23	C24	1.514(5)	C22A	C23A	1.539(4)
C24	C25	1.527(5)	C23A	C24A	1.513(5)
C25	C26B	1.535(4)	C24A	C25A	1.529(5)
C25	C26C	1.526(4)	C25A	C26A	1.547(5)
C25	C27B	1.529(4)	C25A	C27A	1.509(5)
C25	C27C	1.537(4)	C30A	C31A	1.535(5)
C30B	C31B	1.536(4)	C30A	C32A	1.543(5)
C30B	C32B	1.534(4)	C30A	C33A	1.537(5)

Table A1.7.5. Bond angles for **91**.

Atom	Atom	Atom	Angle (°)	Atom	Atom	Atom	Angle (°)
O1	Si1	C28B	110.4(3)	C27B	C25	C26B	108.1(6)
O1	Si1	C28C	112.6(3)	C27B	C25	C27C	15.9(7)
O1	Si1	C29B	106.3(3)	C31B	C30B	Si1	109.4(6)
O1	Si1	C29C	110.0(4)	C32B	C30B	Si1	110.3(5)
O1	Si1	C30B	105.6(2)	C32B	C30B	C31B	114.7(7)
O1	Si1	C30C	105.3(2)	C33C	C30B	Si1	108.9(5)
C28B	Si1	C29B	125.1(5)	C33C	C30B	C31B	105.5(7)
C28B	Si1	C30B	97.9(4)	C33C	C30B	C32B	107.9(7)
C28C	Si1	C28B	18.5(4)	C31C	C30C	Si1	111.3(6)
C28C	Si1	C29B	108.6(4)	C31C	C30C	C33B	107.3(7)
C28C	Si1	C29C	91.8(4)	C32C	C30C	Si1	113.9(5)
C28C	Si1	C30B	113.7(3)	C32C	C30C	C31C	104.6(7)
C28C	Si1	C30C	124.3(4)	C32C	C30C	C33B	109.1(7)
C29B	Si1	C30B	109.8(4)	C33B	C30C	Si1	110.3(5)
C29C	Si1	C28B	109.2(5)	O1A	Si1A	C28A	110.94(15)
C29C	Si1	C29B	17.4(4)	O1A	Si1A	C29A	109.91(15)
C29C	Si1	C30B	122.9(4)	O1A	Si1A	C30A	103.67(13)
C29C	Si1	C30C	111.9(4)	C28A	Si1A	C30A	111.42(16)
C30C	Si1	C28B	109.9(4)	C29A	Si1A	C28A	108.89(19)
C30C	Si1	C29B	97.6(4)	C29A	Si1A	C30A	111.95(17)
C30C	Si1	C30B	13.2(3)	C3A	O1A	Si1A	129.3(2)
C3	O1	Si1	129.0(2)	C2A	C1A	C10A	113.4(2)
C2	C1	C10	113.8(2)	C3A	C2A	C1A	111.0(2)
C3	C2	C1	110.8(2)	O1A	C3A	C2A	111.7(2)
O1	C3	C2	110.7(2)	O1A	C3A	C4A	107.5(2)
O1	C3	C4	108.1(2)	C4A	C3A	C2A	110.6(2)
C2	C3	C4	110.1(3)	C5A	C4A	C3A	113.8(2)
C5	C4	C3	113.1(2)	C4A	C5A	C10A	116.1(2)
C4	C5	C10	116.5(2)	C6A	C5A	C4A	121.0(3)
C6	C5	C4	120.8(3)	C6A	C5A	C10A	122.8(3)
C6	C5	C10	122.6(3)	C5A	C6A	C7A	124.6(3)
C5	C6	C7	125.0(3)	C6A	C7A	C8A	113.8(2)
C6	C7	C8	113.5(2)	C7A	C8A	C9A	109.8(2)
C7	C8	C9	109.2(2)	C7A	C8A	C14A	110.9(2)
C14	C8	C7	111.1(2)	C14A	C8A	C9A	109.4(2)
C14	C8	C9	109.9(2)	C8A	C9A	C10A	112.9(2)
C8	C9	C10	112.3(2)	C11A	C9A	C8A	110.6(2)

C11	C9	C8	111.4(2)	C11A	C9A	C10A	113.3(2)
C11	C9	C10	113.3(2)	C1A	C10A	C9A	109.3(2)
C1	C10	C9	109.3(2)	C5A	C10A	C1A	108.9(2)
C5	C10	C1	108.9(2)	C5A	C10A	C9A	110.1(2)
C5	C10	C9	109.7(2)	C5A	C10A	C19A	108.5(2)
C5	C10	C19	108.6(2)	C19A	C10A	C1A	109.1(2)
C19	C10	C1	108.9(2)	C19A	C10A	C9A	110.7(2)
C19	C10	C9	111.5(2)	C12A	C11A	C9A	114.1(2)
C12	C11	C9	114.4(2)	C11A	C12A	C13A	111.0(2)
C11	C12	C13	111.4(2)	C12A	C13A	C14A	106.7(2)
C12	C13	C14	106.0(2)	C12A	C13A	C17A	116.7(2)
C12	C13	C17	116.6(2)	C12A	C13A	C18A	110.7(2)
C12	C13	C18	110.6(2)	C14A	C13A	C17A	99.6(2)
C14	C13	C17	100.0(2)	C14A	C13A	C18A	112.7(2)
C18	C13	C14	112.7(2)	C18A	C13A	C17A	110.1(2)
C18	C13	C17	110.6(2)	C8A	C14A	C13A	115.6(2)
C8	C14	C13	115.8(2)	C15A	C14A	C8A	118.3(2)
C8	C14	C15	118.4(2)	C15A	C14A	C13A	103.8(2)
C15	C14	C13	103.3(2)	C14A	C15A	C16A	103.5(2)
C16	C15	C14	103.7(2)	C15A	C16A	C17A	106.9(2)
C15	C16	C17	107.1(2)	C13A	C17A	C16A	102.8(2)
C13	C17	C16	103.0(2)	C20A	C17A	C13A	119.9(2)
C20	C17	C13	118.9(2)	C20A	C17A	C16A	112.2(2)
C20	C17	C16	112.9(2)	C21A	C20A	C17A	112.5(2)
C21	C20	C17	112.3(2)	C21A	C20A	C22A	110.8(3)
C21	C20	C22	110.2(3)	C22A	C20A	C17A	109.5(3)
C22	C20	C17	111.0(2)	C20A	C22A	C23A	115.9(3)
C23	C22	C20	114.3(3)	C24A	C23A	C22A	114.0(3)
C24	C23	C22	113.6(3)	C23A	C24A	C25A	115.0(3)
C23	C24	C25	115.3(3)	C24A	C25A	C26A	110.2(3)
C24	C25	C26B	114.8(4)	C27A	C25A	C24A	111.3(3)
C24	C25	C27B	113.2(5)	C27A	C25A	C26A	109.3(3)
C24	C25	C27C	106.2(6)	C31A	C30A	Si1A	109.4(2)
C26B	C25	C27C	123.4(7)	C31A	C30A	C32A	109.2(3)
C26C	C25	C24	109.5(6)	C31A	C30A	C33A	108.4(3)
C26C	C25	C26B	18.8(6)	C32A	C30A	Si1A	111.0(2)
C26C	C25	C27B	95.5(7)	C33A	C30A	Si1A	109.7(2)
C26C	C25	C27C	111.3(7)	C33A	C30A	C32A	109.1(3)

Table A1.7.6. Torsion angles for **91.**

A	B	C	D	Angle (°)	A	B	C	D	Angle (°)
Si1	O1	C3	C2	90.4(3)	C29B	Si1	C30C	C33B	169.1(7)
Si1	O1	C3	C4	-148.9(2)	C29C	Si1	O1	C3	91.5(4)
O1	Si1	C30B	C31B	-55.4(6)	C29C	Si1	C30B	C31B	71.6(7)
O1	Si1	C30B	C32B	177.5(5)	C29C	Si1	C30B	C32B	-55.4(8)
O1	Si1	C30B	C33C	59.4(6)	C29C	Si1	C30B	C33C	-173.5(6)
O1	Si1	C30C	C31C	-59.2(6)	C29C	Si1	C30C	C31C	60.3(7)
O1	Si1	C30C	C32C	-177.2(6)	C29C	Si1	C30C	C32C	-57.7(8)
O1	Si1	C30C	C33B	59.8(6)	C29C	Si1	C30C	C33B	179.3(6)
O1	C3	C4	C5	-173.7(3)	C30B	Si1	O1	C3	-134.0(3)
C1	C2	C3	O1	177.0(2)	C30B	Si1	C30C	C31C	-152.2(19)
C1	C2	C3	C4	57.4(3)	C30B	Si1	C30C	C32C	89.9(17)
C2	C1	C10	C5	50.4(3)	C30B	Si1	C30C	C33B	-33.2(14)
C2	C1	C10	C9	170.2(2)	C30C	Si1	O1	C3	-147.7(3)
C2	C1	C10	C19	-67.8(3)	C30C	Si1	C30B	C31B	35.3(15)
C2	C3	C4	C5	-52.6(4)	C30C	Si1	C30B	C32B	-91.8(17)
C3	C4	C5	C6	-133.7(3)	C30C	Si1	C30B	C33C	150.1(19)
C3	C4	C5	C10	48.7(4)	Si1A	O1A	C3A	C2A	75.1(3)
C4	C5	C6	C7	-177.0(3)	Si1A	O1A	C3A	C4A	-163.4(2)

C4	C5	C10	C1	-45.7(3)	O1A	Si1A	C30A	C31A	-55.3(3)
C4	C5	C10	C9	-165.3(3)	O1A	Si1A	C30A	C32A	-175.8(3)
C4	C5	C10	C19	72.7(3)	O1A	Si1A	C30A	C33A	63.6(3)
C5	C6	C7	C8	12.4(5)	O1A	C3A	C4A	C5A	-173.2(2)
C6	C5	C10	C1	136.7(3)	C1A	C2A	C3A	O1A	175.5(2)
C6	C5	C10	C9	17.1(4)	C1A	C2A	C3A	C4A	55.8(3)
C6	C5	C10	C19	-104.9(3)	C2A	C1A	C10A	C5A	51.7(3)
C6	C7	C8	C9	-41.6(3)	C2A	C1A	C10A	C9A	172.1(2)
C6	C7	C8	C14	-163.0(3)	C2A	C1A	C10A	C19A	-66.6(3)
C7	C8	C9	C10	61.1(3)	C2A	C3A	C4A	C5A	-51.1(3)
C7	C8	C9	C11	-170.6(2)	C3A	C4A	C5A	C6A	-134.1(3)
C7	C8	C14	C13	177.4(2)	C3A	C4A	C5A	C10A	48.3(4)
C7	C8	C14	C15	-59.1(3)	C4A	C5A	C6A	C7A	-176.1(3)
C8	C9	C10	C1	-167.0(2)	C4A	C5A	C10A	C1A	-46.8(3)
C8	C9	C10	C5	-47.6(3)	C4A	C5A	C10A	C9A	-166.7(2)
C8	C9	C10	C19	72.6(3)	C4A	C5A	C10A	C19A	71.9(3)
C8	C9	C11	C12	50.4(3)	C5A	C6A	C7A	C8A	11.7(4)
C8	C14	C15	C16	-164.6(3)	C6A	C5A	C10A	C1A	135.7(3)
C9	C8	C14	C13	56.4(3)	C6A	C5A	C10A	C9A	15.8(4)
C9	C8	C14	C15	179.9(2)	C6A	C5A	C10A	C19A	-105.6(3)
C9	C11	C12	C13	-55.9(3)	C6A	C7A	C8A	C9A	-40.6(3)
C10	C1	C2	C3	-58.4(3)	C6A	C7A	C8A	C14A	-161.6(2)
C10	C5	C6	C7	0.5(5)	C7A	C8A	C9A	C10A	59.4(3)
C10	C9	C11	C12	178.2(2)	C7A	C8A	C9A	C11A	-172.5(2)
C11	C9	C10	C1	65.7(3)	C7A	C8A	C14A	C13A	177.7(2)
C11	C9	C10	C5	-175.0(2)	C7A	C8A	C14A	C15A	-58.3(4)
C11	C9	C10	C19	-54.7(3)	C8A	C9A	C10A	C1A	-165.6(2)
C11	C12	C13	C14	56.5(3)	C8A	C9A	C10A	C5A	-46.0(3)
C11	C12	C13	C17	166.6(2)	C8A	C9A	C10A	C19A	74.1(3)
C11	C12	C13	C18	-66.0(3)	C8A	C9A	C11A	C12A	53.5(3)
C12	C13	C14	C8	-59.7(3)	C8A	C14A	C15A	C16A	-165.6(3)
C12	C13	C14	C15	169.2(2)	C9A	C8A	C14A	C13A	56.4(3)
C12	C13	C17	C16	-154.7(3)	C9A	C8A	C14A	C15A	-179.5(3)
C12	C13	C17	C20	79.5(3)	C9A	C11A	C12A	C13A	-57.2(3)
C13	C14	C15	C16	-35.1(3)	C10A	C1A	C2A	C3A	-58.2(3)
C13	C17	C20	C21	-59.1(4)	C10A	C5A	C6A	C7A	1.3(5)
C13	C17	C20	C22	177.1(3)	C10A	C9A	C11A	C12A	-178.6(2)
C14	C8	C9	C10	-176.8(2)	C11A	C9A	C10A	C1A	67.7(3)
C14	C8	C9	C11	-48.5(3)	C11A	C9A	C10A	C5A	-172.7(2)
C14	C13	C17	C16	-41.1(3)	C11A	C9A	C10A	C19A	-52.6(3)
C14	C13	C17	C20	-166.9(3)	C11A	C12A	C13A	C14A	55.9(3)
C14	C15	C16	C17	8.9(3)	C11A	C12A	C13A	C17A	166.1(2)
C15	C16	C17	C13	20.4(3)	C11A	C12A	C13A	C18A	-67.0(3)
C15	C16	C17	C20	150.0(3)	C12A	C13A	C14A	C8A	-58.4(3)
C16	C17	C20	C21	180.0(3)	C12A	C13A	C14A	C15A	170.3(2)
C16	C17	C20	C22	56.2(3)	C12A	C13A	C17A	C16A	-155.7(2)
C17	C13	C14	C8	178.7(2)	C12A	C13A	C17A	C20A	79.0(3)
C17	C13	C14	C15	47.7(3)	C13A	C14A	C15A	C16A	-35.9(3)
C17	C20	C22	C23	-165.0(3)	C13A	C17A	C20A	C21A	-57.4(4)
C18	C13	C14	C8	61.3(3)	C13A	C17A	C20A	C22A	179.0(3)
C18	C13	C14	C15	-69.7(3)	C14A	C8A	C9A	C10A	-178.7(2)
C18	C13	C17	C16	77.9(3)	C14A	C8A	C9A	C11A	-50.6(3)
C18	C13	C17	C20	-47.9(3)	C14A	C13A	C17A	C16A	-41.4(3)
C20	C22	C23	C24	179.2(3)	C14A	C13A	C17A	C20A	-166.7(3)
C21	C20	C22	C23	70.0(4)	C14A	C15A	C16A	C17A	9.1(3)
C22	C23	C24	C25	-172.3(3)	C15A	C16A	C17A	C13A	20.5(3)
C23	C24	C25	C26B	-48.9(6)	C15A	C16A	C17A	C20A	150.6(3)
C23	C24	C25	C26C	-68.4(7)	C16A	C17A	C20A	C21A	-178.1(3)
C23	C24	C25	C27B	-173.6(6)	C16A	C17A	C20A	C22A	58.3(4)
C23	C24	C25	C27C	171.2(6)	C17A	C13A	C14A	C8A	179.9(2)

C28B	Si1	O1	C3	-29.1(4)	C17A	C13A	C14A	C15A	48.6(3)
C28B	Si1	C30B	C31B	-169.3(6)	C17A	C20A	C22A	C23A	-179.0(3)
C28B	Si1	C30B	C32B	63.7(7)	C18A	C13A	C14A	C8A	63.3(3)
C28B	Si1	C30B	C33C	-54.5(6)	C18A	C13A	C14A	C15A	-68.0(3)
C28B	Si1	C30C	C31C	-178.2(7)	C18A	C13A	C17A	C16A	77.1(3)
C28B	Si1	C30C	C32C	63.9(7)	C18A	C13A	C17A	C20A	-48.2(4)
C28B	Si1	C30C	C33B	-59.2(7)	C20A	C22A	C23A	C24A	61.9(4)
C28C	Si1	O1	C3	-9.4(4)	C21A	C20A	C22A	C23A	56.3(4)
C28C	Si1	C30B	C31B	-179.4(6)	C22A	C23A	C24A	C25A	178.2(3)
C28C	Si1	C30B	C32B	53.6(7)	C23A	C24A	C25A	C26A	70.9(4)
C28C	Si1	C30B	C33C	-64.5(6)	C23A	C24A	C25A	C27A	-167.7(3)
C28C	Si1	C30C	C31C	168.8(6)	C28A	Si1A	O1A	C3A	-85.7(3)
C28C	Si1	C30C	C32C	50.8(8)	C28A	Si1A	C30A	C31A	-174.6(3)
C28C	Si1	C30C	C33B	-72.2(7)	C28A	Si1A	C30A	C32A	64.8(3)
C29B	Si1	O1	C3	109.4(4)	C28A	Si1A	C30A	C33A	-55.8(3)
C29B	Si1	C30B	C31B	58.8(7)	C29A	Si1A	O1A	C3A	34.8(3)
C29B	Si1	C30B	C32B	-68.2(7)	C29A	Si1A	C30A	C31A	63.2(3)
C29B	Si1	C30B	C33C	173.6(6)	C29A	Si1A	C30A	C32A	-57.4(3)
C29B	Si1	C30C	C31C	50.1(7)	C29A	Si1A	C30A	C33A	-178.0(2)
C29B	Si1	C30C	C32C	-67.9(7)	C30A	Si1A	O1A	C3A	154.6(3)

Table A1.7.7. Hydrogen atom coordinates ($Å \times 10^4$) and isotropic displacement parameters ($Å^2 \times 10^3$) for **91**.

Atom	*x*	*y*	*z*	U(eq)
H1A	-284	3165	-422	25
H1B	1287	4202	-520	25
H2A	-160	1950	-871	29
H2B	-526	3592	-930	29
H3	2538	3957	-1030	30
H4A	3048	976	-954	30
H4B	4591	2089	-1027	30
H6	6500	2136	-630	27
H7A	6619	3243	-139	26
H7B	7076	1596	-133	26
H8	4327	1006	42	21
H9	3191	3800	-121	20
H11A	348	3382	56	27
H11B	878	1807	147	27
H12A	896	3210	569	24
H12B	2256	4307	426	24
H14	5263	3619	313	21
H15A	6728	936	479	30
H15B	7818	2372	419	30
H16A	7360	3140	874	30
H16B	6572	1606	947	30
H17	4627	4106	802	24
H18A	1960	883	747	38
H18B	3997	393	703	38
H18C	2621	465	428	38
H19A	249	793	-283	33
H19B	2226	127	-254	33
H19C	1276	323	-570	33
H20	3578	1821	1171	30
H21A	1825	4476	1087	49
H21B	1379	3439	1352	49
H21C	968	2957	1022	49
H22A	6168	3213	1343	36
H22B	4829	4521	1372	36
H23A	3191	3278	1726	43

H23B	4509	1956	1695	43
H24A	5492	4635	1931	52
H24B	6942	3438	1868	52
H25A	5858	2002	2225	57
H25	5484	1948	2223	57
H26A	2982	3919	2331	59
H26B	3423	2546	2523	59
H26C	2746	2384	2190	59
H26D	3456	4485	2310	102
H26E	3558	3270	2552	102
H26F	2641	2957	2239	102
H27A	7833	3678	2421	67
H27B	6338	3323	2656	67
H27C	6210	4754	2471	67
H27D	8137	3296	2338	107
H27E	6910	3196	2619	107
H27F	6917	4609	2428	107
H28A	-1364	4873	-1381	85
H28B	-544	5817	-1635	85
H28C	500	5689	-1326	85
H28D	-466	5418	-1341	49
H28E	43	6000	-1657	49
H28F	1559	5887	-1403	49
H29A	3990	4101	-1753	79
H29B	2622	4287	-2027	79
H29C	3228	2743	-1923	79
H29D	3757	4831	-1677	88
H29E	2614	4780	-1978	88
H29F	3706	3418	-1868	88
H31A	616	1258	-2015	99
H31B	-1392	709	-1967	99
H31C	49	691	-1701	99
H31D	1557	1477	-2044	117
H31E	-340	696	-2089	117
H31F	738	585	-1782	117
H32A	-2253	4452	-1967	86
H32B	-2611	3051	-2154	86
H32C	-725	3857	-2174	86
H32D	-1762	4152	-2069	82
H32E	-2078	2652	-2222	82
H32F	-178	3433	-2247	82
H33A	-1735	1348	-1518	100
H33B	-3017	1569	-1801	100
H33C	-2698	2836	-1575	100
H33D	-1987	1918	-1408	83
H33E	-3471	2045	-1666	83
H33F	-2797	3428	-1495	83
H1AA	-352	5763	4668	22
H1AB	1214	6774	4558	22
H2AA	-349	4509	4223	26
H2AB	-690	6151	4159	26
H3A	2334	6470	4036	26
H4AA	2880	3514	4126	27
H4AB	4391	4634	4043	27
H6A	6375	4720	4431	24
H7AA	6562	5822	4922	24
H7AB	7016	4174	4927	24
H8A	4317	3591	5117	22
H9A	3099	6365	4959	19
H11C	277	5823	5142	22

H11D	955	4289	5238	22
H12C	922	5754	5651	24
H12D	2197	6877	5496	24
H14A	5243	6248	5376	22
H15C	7837	5051	5471	29
H15D	6793	3612	5548	29
H16C	7448	5896	5925	29
H16D	6719	4364	6014	29
H17A	4678	6804	5858	25
H18D	2131	3505	5841	35
H18E	4184	3070	5794	35
H18F	2768	3041	5524	35
H19D	163	3377	4799	32
H19E	2139	2712	4828	32
H19F	1189	2890	4513	32
H20A	3852	4583	6260	30
H21D	1893	7153	6172	48
H21E	1544	6077	6434	48
H21F	1131	5607	6103	48
H22C	5193	7367	6376	36
H22D	6341	5955	6415	36
H23C	5443	6842	6873	40
H23D	3374	6704	6772	40
H24C	5736	4356	6848	43
H24D	3651	4236	6757	43
H25B	4813	5377	7311	46
H26G	1792	5970	7151	82
H26H	1790	5049	7444	82
H26I	1304	4327	7136	82
H27G	3757	2530	7199	86
H27H	4081	3175	7519	86
H27I	5732	3022	7303	86
H28G	-2459	4714	3534	63
H28H	-2778	6105	3342	63
H28I	-2584	6219	3690	63
H29G	430	8229	3699	66
H29H	292	8355	3350	66
H29I	2177	7975	3508	66
H31G	3591	6206	3158	56
H31H	3653	4807	2963	56
H31I	3715	4693	3312	56
H32G	-947	5880	2874	72
H32H	787	5441	2695	72
H32I	780	6889	2875	72
H33G	1055	3082	3304	62
H33H	1101	3140	2954	62
H33I	-721	3503	3118	62

Table A1.7.8. Atomic occupancy for **91**.

Atom	Occupancy	Atom	Occupancy	Atom	Occupancy
H25A	0.5	H25	0.5	C26B	0.5
H26A	0.5	H26B	0.5	H26C	0.5
C26C	0.5	H26D	0.5	H26E	0.5
H26F	0.5	C27B	0.5	H27A	0.5
H27B	0.5	H27C	0.5	C27C	0.5
H27D	0.5	H27E	0.5	H27F	0.5
C28B	0.5	H28A	0.5	H28B	0.5
H28C	0.5	C28C	0.5	H28D	0.5
H28E	0.5	H28F	0.5	C29B	0.5

H29A	0.5	H29B	0.5	H29C	0.5
C29C	0.5	H29D	0.5	H29E	0.5
H29F	0.5	C30B	0.5	C30C	0.5
C31B	0.5	H31A	0.5	H31B	0.5
H31C	0.5	C31C	0.5	H31D	0.5
H31E	0.5	H31F	0.5	C32B	0.5
H32A	0.5	H32B	0.5	H32C	0.5
C32C	0.5	H32D	0.5	H32E	0.5
H32F	0.5	C33B	0.5	H33A	0.5
H33B	0.5	H33C	0.5	C33C	0.5
H33D	0.5	H33E	0.5	H33F	0.5

A1.8. Crystal structure data for 3-(4-methylbenzenesulfonate)-5α-cholestan-6-one, 99

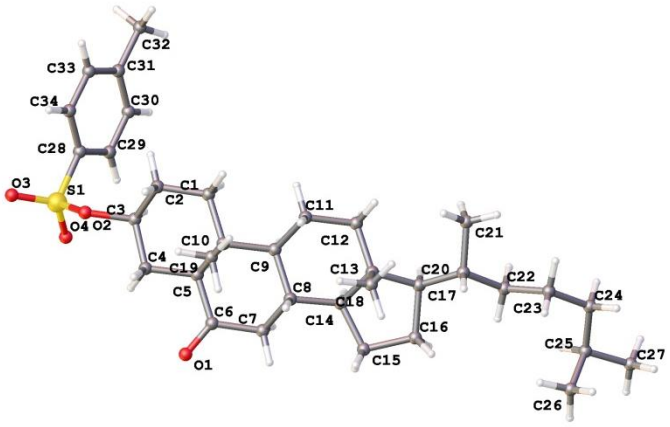

Figure A1.8. One Structure from the unit cell of **99**, determined by X-ray diffraction of a single crystal.

Table A1.8.1. Crystal data and structure refinement for **99**.

Empirical formula	$C_{34}H_{52}O_4S$
Formula weight	556.81
Temperature (K)	120
Crystal system	monoclinic
Space group	$P2_1$
a (Å)	7.1094(6)
b (Å)	10.9745(10)
c (Å)	20.2341(19)
α (°)	90
β (°)	91.355(6)
γ (°)	90
Volume ($Å^3$)	1578.3(2)
Z	2
$\rho_{calc}g$ (cm^3)	1.172
μ (mm^{-1})	1.176
F(000)	608
Crystal size (mm^3)	0.21 × 0.14 × 0.09
Radiation	CuKα (λ = 1.54178)
2Θ range for data collection (°)	8.742 to 139.984
Index ranges	$-8 \le h \le 8$, $-11 \le k \le 13$, $-24 \le l \le 24$
Reflections collected	16321
Independent reflections	5137 [R_{int} = 0.0684, R_{sigma} = 0.0719]
Data/ restraints/ parameters	5137/1/358
Goodness-of-fit on F^2	1.083
Final R indexes [I > = 2σ (I)]	R_1 = 0.0670, wR_2 = 0.1457

Final R indexes [all data]	R_1 = 0.0828, wR_2 = 0.1542
Largest diff. peak/ hole (e Å^{-3})	0.24/-0.45
Flack parameter	0.02(3)

Table A1.8.2. Fractional atomic coordinates (×10^4) and equivalent isotropic displacement parameters (Å^2×10^3) for **99**. U_{eq} is defined as 1/3 of the trace of the orthogonalised U_{IJ} tensor.

Atom	*x*	*y*	*z*	U(eq)
S1	4098(2)	8726.4(15)	10046.0(7)	33.4(4)
O1	8385(6)	6912(4)	7661(2)	34.6(10)
O2	3365(7)	9922(4)	10141(2)	42.7(12)
O3	6067(7)	8504(5)	10143(2)	41.5(12)
O4	3515(6)	8400(4)	9315(2)	32.7(11)
C1	2571(8)	5390(5)	8482(3)	25.7(13)
C2	2164(9)	6620(6)	8793(3)	29.1(14)
C3	3983(9)	7173(6)	9069(3)	28.2(14)
C4	5498(9)	7291(6)	8561(3)	28.4(14)
C5	5883(8)	6027(6)	8272(3)	22.7(12)
C6	7513(8)	6006(6)	7807(3)	26.9(13)
C7	7977(8)	4765(6)	7535(3)	26.7(14)
C8	6268(8)	4071(5)	7263(3)	22.3(13)
C9	4661(8)	4094(5)	7759(3)	21.3(13)
C10	4099(8)	5410(5)	7954(3)	22.5(13)
C11	3007(8)	3301(5)	7510(3)	26.1(13)
C12	3600(8)	1994(6)	7337(3)	26.7(13)
C13	5157(8)	1970(5)	6826(3)	24.0(13)
C14	6806(7)	2758(5)	7110(3)	21.2(12)
C15	8402(9)	2504(6)	6641(3)	30.2(14)
C16	8160(9)	1134(6)	6471(3)	34.0(15)
C17	6192(8)	737(5)	6735(3)	24.9(13)
C18	4420(9)	2434(6)	6151(3)	30.8(14)
C19	3410(9)	6145(6)	7346(3)	27.0(13)
C20	5313(9)	-279(6)	6310(3)	28.7(14)
C21	6608(9)	-1402(6)	6314(3)	30.2(14)
C22	6208(10)	-2304(6)	5750(3)	37.8(16)
C23	7475(10)	-3428(6)	5764(3)	36.5(16)
C24	9584(9)	-3194(6)	5766(3)	30.4(14)
C25	10678(11)	-4403(6)	5717(4)	41.9(18)
C26	10145(11)	-2355(7)	5208(4)	47.4(19)
C27	3354(10)	-627(6)	6535(4)	41.1(17)
C28	2870(9)	7680(6)	10525(3)	30.3(14)
C29	946(10)	7818(7)	10613(3)	38.0(16)
C30	-7(10)	6959(7)	10974(4)	41.8(18)
C31	891(10)	5961(7)	11255(3)	36.1(16)
C32	2806(10)	5835(7)	11159(3)	38.2(17)
C33	3801(9)	6682(6)	10797(3)	33.3(15)
C34	-154(12)	5017(7)	11652(4)	52(2)

Table A1.8.3. Anisotropic displacement parameters (Å2×103) for **99**. The anisotropic displacement factor exponent takes the form: -2π2[h2a*2U11+2hka*b*U12+…].

Atom	U_{11}	U_{22}	U_{33}	U_{23}	U_{13}	U_{12}
S1	38.7(9)	28.6(9)	33.2(7)	-9.1(7)	3.6(7)	-2.8(8)
O1	34(2)	26(3)	43(3)	-1(2)	3(2)	-4(2)
O2	52(3)	31(3)	46(3)	-13(2)	5(2)	0(2)
O3	39(3)	47(3)	38(2)	-7(2)	6(2)	-7(2)
O4	43(3)	23(2)	32(2)	-6.1(17)	2(2)	8(2)
C1	22(3)	23(3)	31(3)	1(2)	3(3)	5(3)
C2	30(3)	24(3)	33(3)	-6(3)	8(3)	-2(3)

C3	30(3)	25(4)	30(3)	-7(3)	-1(3)	5(3)
C4	29(3)	23(3)	33(3)	-6(3)	-1(3)	-3(3)
C5	19(3)	22(3)	27(3)	-2(2)	-4(2)	4(3)
C6	24(3)	26(4)	30(3)	-1(3)	-3(3)	-2(3)
C7	16(3)	27(3)	38(3)	-4(3)	3(3)	-7(3)
C8	15(3)	20(3)	31(3)	-2(2)	5(2)	-3(2)
C9	18(3)	20(3)	26(3)	0(2)	4(2)	0(2)
C10	25(3)	17(3)	25(3)	1(2)	2(2)	-2(2)
C11	20(3)	22(3)	37(3)	-4(2)	6(3)	-1(2)
C12	19(3)	25(3)	36(3)	1(3)	4(3)	-4(3)
C13	29(3)	15(3)	28(3)	0(2)	2(3)	-3(3)
C14	13(3)	19(3)	31(3)	-2(2)	4(2)	2(2)
C15	25(3)	24(3)	42(4)	-7(3)	5(3)	-1(3)
C16	40(4)	23(3)	38(3)	-3(3)	1(3)	-2(3)
C17	30(3)	16(3)	29(3)	0(2)	1(3)	0(3)
C18	38(4)	22(3)	32(3)	-1(3)	-5(3)	-1(3)
C19	29(3)	22(3)	30(3)	-1(3)	-3(3)	-1(3)
C20	30(4)	22(3)	34(3)	-3(3)	2(3)	4(3)
C21	35(3)	21(3)	34(3)	-3(3)	3(3)	2(3)
C22	44(4)	28(4)	41(4)	-9(3)	-1(3)	1(3)
C23	45(4)	23(4)	42(4)	-8(3)	2(3)	-3(3)
C24	38(4)	22(3)	31(3)	-2(3)	5(3)	5(3)
C25	51(5)	33(4)	42(4)	-4(3)	4(3)	9(3)
C26	50(5)	48(5)	45(4)	12(4)	7(4)	3(4)
C27	34(4)	24(4)	66(5)	-10(3)	6(4)	-2(3)
C28	29(3)	30(4)	32(3)	-13(3)	0(3)	2(3)
C29	34(4)	36(4)	44(4)	-12(3)	2(3)	1(3)
C30	26(4)	46(5)	53(4)	-15(4)	6(3)	-2(3)
C31	36(4)	31(4)	41(4)	-13(3)	6(3)	-7(3)
C32	44(4)	36(4)	35(4)	-9(3)	1(3)	6(3)
C33	30(3)	35(4)	35(3)	-8(3)	0(3)	-3(3)
C34	48(5)	48(5)	62(5)	-14(4)	13(4)	-10(4)

Table A1.8.4. Bond lengths for **99**.

Atom	Atom	Length (Å)	Atom	Atom	Length (Å)
S1	O2	1.427(5)	C13	C14	1.555(8)
S1	O3	1.430(5)	C13	C17	1.554(8)
S1	O4	1.569(4)	C13	C18	1.538(8)
S1	C28	1.749(7)	C14	C15	1.523(8)
O1	C6	1.212(8)	C15	C16	1.551(9)
O4	C3	1.476(7)	C16	C17	1.571(9)
C1	C2	1.520(8)	C17	C20	1.531(8)
C1	C10	1.542(8)	C20	C21	1.539(8)
C2	C3	1.523(9)	C20	C27	1.524(9)
C3	C4	1.512(8)	C21	C22	1.531(8)
C4	C5	1.532(8)	C22	C23	1.528(9)
C5	C6	1.510(8)	C23	C24	1.521(9)
C5	C10	1.563(8)	C24	C25	1.543(9)
C6	C7	1.508(9)	C24	C26	1.517(9)
C7	C8	1.526(8)	C28	C29	1.392(9)
C8	C9	1.540(8)	C28	C33	1.387(9)
C8	C14	1.524(8)	C29	C30	1.380(10)
C9	C10	1.551(8)	C30	C31	1.383(10)
C9	C11	1.539(8)	C31	C32	1.387(9)
C10	C19	1.540(8)	C31	C34	1.516(10)
C11	C12	1.538(8)	C32	C33	1.388(10)
C12	C13	1.533(8)			

Table A1.8.5. Bond angles for **99**.

Atom	Atom	Atom	Angle (°)	Atom	Atom	Atom	Angle (°)
O2	S1	O3	119.9(3)	C12	C13	C14	106.9(5)
O2	S1	O4	104.4(3)	C12	C13	C17	116.5(5)
O2	S1	C28	109.9(3)	C12	C13	C18	110.9(5)
O3	S1	O4	109.1(2)	C17	C13	C14	100.0(4)
O3	S1	C28	108.1(3)	C18	C13	C14	112.5(5)
O4	S1	C28	104.4(3)	C18	C13	C17	109.5(5)
C3	O4	S1	118.0(4)	C8	C14	C13	114.2(5)
C2	C1	C10	114.7(5)	C15	C14	C8	119.5(5)
C1	C2	C3	109.7(5)	C15	C14	C13	103.5(5)
O4	C3	C2	106.9(5)	C14	C15	C16	103.6(5)
O4	C3	C4	108.7(5)	C15	C16	C17	106.8(5)
C4	C3	C2	113.3(5)	C13	C17	C16	103.1(5)
C3	C4	C5	108.6(5)	C20	C17	C13	120.9(5)
C4	C5	C10	113.5(5)	C20	C17	C16	111.5(5)
C6	C5	C4	113.4(5)	C17	C20	C21	110.2(5)
C6	C5	C10	111.3(5)	C27	C20	C17	112.3(5)
O1	C6	C5	123.0(6)	C27	C20	C21	110.4(5)
O1	C6	C7	122.3(5)	C22	C21	C20	114.5(5)
C7	C6	C5	114.7(5)	C23	C22	C21	114.1(5)
C6	C7	C8	113.8(5)	C24	C23	C22	116.4(6)
C7	C8	C9	110.7(5)	C23	C24	C25	110.7(6)
C14	C8	C7	110.1(5)	C26	C24	C23	112.1(6)
C14	C8	C9	109.9(4)	C26	C24	C25	109.4(6)
C8	C9	C10	112.3(4)	C29	C28	S1	120.3(5)
C11	C9	C8	110.4(4)	C33	C28	S1	119.9(5)
C11	C9	C10	114.3(5)	C33	C28	C29	119.7(6)
C1	C10	C5	107.4(5)	C30	C29	C28	119.3(7)
C1	C10	C9	110.6(5)	C29	C30	C31	122.1(6)
C9	C10	C5	107.2(5)	C30	C31	C32	117.8(7)
C19	C10	C1	110.2(5)	C30	C31	C34	122.2(7)
C19	C10	C5	110.0(5)	C32	C31	C34	120.0(7)
C19	C10	C9	111.3(5)	C31	C32	C33	121.5(7)
C12	C11	C9	113.0(5)	C28	C33	C32	119.6(6)
C13	C12	C11	112.0(5)				

Table A1.8.6. Torsion angles for **99**.

A	B	C	D	Angle (°)	A	B	C	D	Angle (°)
S1	O4	C3	C2	126.6(5)	C10	C5	C6	O1	127.1(6)
S1	O4	C3	C4	-110.7(5)	C10	C5	C6	C7	-52.8(7)
S1	C28	C29	C30	177.8(5)	C10	C9	C11	C12	-178.6(5)
S1	C28	C33	C32	-178.0(5)	C11	C9	C10	C1	56.5(6)
O1	C6	C7	C8	-131.6(6)	C11	C9	C10	C5	173.3(5)
O2	S1	O4	C3	-176.8(4)	C11	C9	C10	C19	-66.3(6)
O2	S1	C28	C29	36.5(6)	C11	C12	C13	C14	55.4(6)
O2	S1	C28	C33	-145.9(5)	C11	C12	C13	C17	166.2(5)
O3	S1	O4	C3	54.0(5)	C11	C12	C13	C18	-67.6(7)
O3	S1	C28	C29	169.1(5)	C12	C13	C14	C8	-58.2(6)
O3	S1	C28	C33	-13.4(6)	C12	C13	C14	C15	170.2(5)
O4	S1	C28	C29	-74.9(5)	C12	C13	C17	C16	-154.5(5)
O4	S1	C28	C33	102.6(5)	C12	C13	C17	C20	80.2(7)
O4	C3	C4	C5	-176.1(5)	C13	C14	C15	C16	-37.1(6)
C1	C2	C3	O4	175.6(5)	C13	C17	C20	C21	-179.0(5)
C1	C2	C3	C4	55.9(7)	C13	C17	C20	C27	-55.5(8)
C2	C1	C10	C5	53.2(7)	C14	C8	C9	C10	177.9(5)
C2	C1	C10	C9	169.9(5)	C14	C8	C9	C11	-53.3(6)
C2	C1	C10	C19	-66.6(7)	C14	C13	C17	C16	-39.7(5)

C2	C3	C4	C5	-57.4(7)	C14	C13	C17	C20	-165.1(5)
C3	C4	C5	C6	-174.1(5)	C14	C15	C16	C17	11.6(6)
C3	C4	C5	C10	57.5(6)	C15	C16	C17	C13	18.1(6)
C4	C5	C6	O1	-2.4(8)	C15	C16	C17	C20	149.2(5)
C4	C5	C6	C7	177.7(5)	C16	C17	C20	C21	59.7(6)
C4	C5	C10	C1	-54.7(6)	C16	C17	C20	C27	-176.8(5)
C4	C5	C10	C9	-173.6(5)	C17	C13	C14	C8	180.0(5)
C4	C5	C10	C19	65.2(6)	C17	C13	C14	C15	48.4(5)
C5	C6	C7	C8	48.3(7)	C17	C20	C21	C22	-161.7(5)
C6	C5	C10	C1	175.8(5)	C18	C13	C14	C8	63.8(6)
C6	C5	C10	C9	56.9(6)	C18	C13	C14	C15	-67.8(6)
C6	C5	C10	C19	-64.3(6)	C18	C13	C17	C16	78.6(6)
C6	C7	C8	C9	-48.5(7)	C18	C13	C17	C20	-46.7(7)
C6	C7	C8	C14	-170.2(5)	C20	C21	C22	C23	-178.9(6)
C7	C8	C9	C10	56.1(6)	C21	C22	C23	C24	-55.9(8)
C7	C8	C9	C11	-175.0(5)	C22	C23	C24	C25	-174.9(6)
C7	C8	C14	C13	-179.7(5)	C22	C23	C24	C26	-52.4(8)
C7	C8	C14	C15	-56.5(7)	C27	C20	C21	C22	73.7(7)
C8	C9	C10	C1	-176.6(5)	C28	S1	O4	C3	-61.4(5)
C8	C9	C10	C5	-59.9(6)	C28	C29	C30	C31	0.3(10)
C8	C9	C10	C19	60.5(6)	C29	C28	C33	C32	-0.4(9)
C8	C9	C11	C12	53.6(6)	C29	C30	C31	C32	-0.6(10)
C8	C14	C15	C16	-165.4(5)	C29	C30	C31	C34	179.9(7)
C9	C8	C14	C13	58.1(6)	C30	C31	C32	C33	0.4(10)
C9	C8	C14	C15	-178.6(5)	C31	C32	C33	C28	0.1(9)
C9	C11	C12	C13	-56.2(7)	C33	C28	C29	C30	0.3(9)
C10	C1	C2	C3	-54.4(7)	C34	C31	C32	C33	179.9(6)

Table A1.8.7. Hydrogen atom coordinates ($Å \times 10^4$) and isotropic displacement parameters ($Å^2 \times 10^3$) for **99**.

Atom	*x*	*y*	*z*	U(eq)
H1A	1392	5071	8277	31
H1B	2967	4816	8836	31
H2A	1256	6518	9152	35
H2B	1596	7172	8456	35
H3	4466	6662	9446	34
H4A	6661	7623	8770	34
H4B	5079	7854	8205	34
H5	6268	5501	8655	27
H7A	8587	4274	7890	32
H7B	8893	4862	7178	32
H8	5821	4472	6844	27
H9	5163	3698	8172	26
H11A	2043	3269	7855	31
H11B	2427	3686	7112	31
H12A	4051	1575	7744	32
H12B	2493	1542	7160	32
H14	7187	2380	7543	25
H15A	9641	2661	6858	36
H15B	8282	3014	6238	36
H16A	9176	649	6687	41
H16B	8208	1007	5988	41
H17	6418	389	7186	30
H18A	3958	3270	6197	46
H18B	3392	1908	5992	46
H18C	5441	2418	5834	46
H19A	4432	6216	7032	41
H19B	3020	6959	7486	41
H19C	2340	5725	7133	41

H20	5196	26	5845	34
H21A	7928	-1123	6288	36
H21B	6479	-1834	6740	36
H22A	4881	-2572	5771	45
H22B	6361	-1877	5324	45
H23A	7186	-3909	6163	44
H23B	7146	-3936	5374	44
H24	9949	-2795	6195	36
H25A	10308	-4949	6075	63
H25B	12032	-4240	5756	63
H25C	10390	-4789	5290	63
H26A	9718	-2702	4785	71
H26B	11517	-2266	5212	71
H26C	9563	-1554	5268	71
H27A	3396	-797	7010	62
H27B	2924	-1354	6294	62
H27C	2482	48	6444	62
H29	295	8496	10427	46
H30	-1321	7056	11031	50
H32	3450	5154	11345	46
H33	5113	6579	10737	40
H34A	-471	5362	12082	78
H34B	646	4298	11719	78
H34C	-1311	4781	11412	78

A1.9. Crystal structure data for 3β-Acetoxy-5,6-dibromo-5α-cholestane, 100

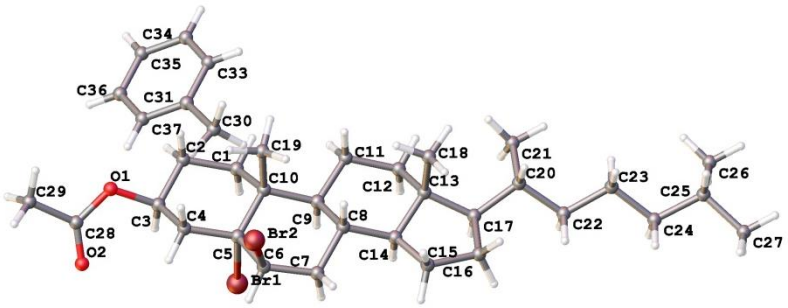

Figure A1.9. One Structure from the unit cell of **100**, determined by X-ray diffraction of a single crystal.

Table A1.9.1. Crystal data and structure refinement for **100**.

Empirical formula	$C_{32.5}H_{52}Br_2O_2$
Formula weight	634.56
Temperature (K)	120
Crystal system	monoclinic
Space group	$P2_1$
a (Å)	10.2061(5)
b (Å)	7.6759(4)
c (Å)	19.3256(10)
α (°)	90
β (°)	94.7795(18)
γ (°)	90
Volume ($Å^3$)	1508.72(13)
Z	2
ρ_{calc}g (cm^3)	1.397

μ (mm^{-1})	2.714
F(000)	666
Crystal size (mm^3)	0.22 × 0.09 × 0.02
Radiation	MoKα (λ = 0.71073)
2Θ range for data collection (°)	4.38 to 59.98
Index ranges	-14 ≤ h ≤ 14, -10 ≤ k ≤ 10, -27 ≤ l ≤ 27
Reflections collected	33495
Independent reflections	8786 [R_{int} = 0.0467, R_{sigma} = 0.0526]
Data/ restraints/ parameters	8786/1/321
Goodness-of-fit on F^2	1.028
Final R indexes [I > = 2σ (I)]	R_1 = 0.0337, wR_2 = 0.0613
Final R indexes [all data]	R_1 = 0.0473, wR_2 = 0.0646
Largest diff. peak/ hole (e $Å^{-3}$)	0.53/-0.37
Flack parameter	-0.006(5)

Table A1.9.2. Fractional atomic coordinates ($\times 10^4$) and equivalent isotropic displacement parameters ($Å^2 \times 10^3$) for **100**. U_{eq} is defined as 1/3 of the trace of the orthogonalised U_{IJ} tensor.

Atom	*x*	*y*	*z*	U(eq)
Br1	6397.5(2)	9986.0(3)	7953.26(11)	16.70(6)
Br2	9445.7(2)	12690.0(3)	6678.24(12)	21.62(6)
O1	5880.7(18)	7912(2)	5748.8(8)	25.4(4)
O2	4131.1(18)	9598(3)	5898.5(10)	33.7(5)
C1	7999(2)	6813(3)	7370.6(12)	14.6(5)
C2	7248(2)	6599(3)	6654.6(12)	17.8(5)
C3	6351(2)	8134(3)	6481.6(12)	19.6(5)
C4	7059(2)	9885(3)	6565.2(11)	16.3(4)
C5	7829.1(19)	10060(3)	7273.2(10)	13.3(4)
C6	8385(2)	11873(3)	7429.5(12)	13.8(5)
C7	9184(2)	12023(3)	8125.0(12)	14.6(5)
C8	10160(2)	10541(3)	8280.0(11)	12.7(5)
C9	9472(2)	8745(3)	8191.5(12)	11.2(4)
C10	8793(2)	8524(3)	7442.9(12)	12.1(5)
C11	10407(2)	7252(3)	8411.3(12)	16.5(5)
C12	11110(2)	7491(3)	9140.3(12)	16.3(5)
C13	11825(2)	9240(3)	9215.8(11)	13.1(4)
C14	10797(2)	10660(3)	9022.4(12)	12.5(4)
C15	11483(2)	12370(3)	9253.7(12)	17.1(5)
C16	12373(2)	11832(3)	9906.6(13)	16.4(5)
C17	12303(2)	9813(3)	9965.8(11)	13.1(4)
C18	9844(2)	8432(3)	6909.9(12)	17.3(5)
C19	12977(2)	9285(3)	8753.6(12)	17.0(5)
C20	13580(2)	9026(3)	10316.0(12)	16.3(5)
C21	13842(2)	9739(3)	11055.9(11)	14.8(5)
C22	15171(2)	9264(3)	11425.2(12)	16.9(5)
C23	15381(2)	10068(4)	12149.0(11)	18.7(5)
C24	16672(2)	9572(3)	12560.6(13)	19.0(5)
C25	16921(3)	10763(4)	13191.3(14)	28.8(6)
C26	16675(2)	7671(4)	12797.7(13)	26.5(5)
C27	13549(2)	7029(3)	10319.1(13)	18.2(5)
C28	4758(3)	8716(3)	5534.5(15)	28.3(6)
C29	4388(4)	8376(4)	4779.6(15)	50.1(10)
C1S	9237(4)	5835(5)	4906(3)	38(2)
C6S	8497(3)	7312(6)	4727(2)	45.9(17)
C5S	9058(4)	8956(5)	4817(2)	45.1(17)
C4S	10358(4)	9121(5)	5086(2)	38.8(15)
C3S	11098(3)	7643(6)	5264(2)	34.7(13)
C2S	10538(4)	6000(5)	5174(2)	38.3(16)
C1SA	11083(9)	10988(9)	5175(5)	46(2)

Table A1.9.3. Anisotropic displacement parameters ($Å^2×10^3$) for **100**. The anisotropic displacement factor exponent takes the form: $-2\pi^2[h^2a^{*2}U_{11}+2hka^*b^*U_{12}+\ldots]$.

Atom	U_{11}	U_{22}	U_{33}	U_{23}	U_{13}	U_{12}
Br1	15.36(10)	19.81(12)	14.96(11)	-3.37(10)	1.39(8)	0.88(10)
Br2	29.45(13)	15.26(12)	20.89(12)	4.25(11)	6.46(10)	-0.04(11)
O1	39.5(10)	20.3(10)	14.1(8)	-4.2(7)	-10.9(7)	6.2(8)
O2	32.4(10)	36.5(13)	30.1(11)	-0.3(9)	-9.9(9)	5.7(9)
C1	18.9(12)	11.2(12)	12.8(11)	0.5(9)	-3.0(9)	-0.1(10)
C2	25.8(13)	14.4(12)	12.5(12)	0.0(9)	-2.2(10)	-0.2(10)
C3	27.4(13)	19.2(13)	10.9(11)	-2.2(9)	-5.6(10)	-1.5(10)
C4	22.9(11)	14.5(11)	11(1)	0.2(10)	-1.8(8)	5.1(11)
C5	15.3(10)	14(1)	10.9(10)	-1(1)	2.9(8)	2.1(10)
C6	16.1(12)	12.7(12)	12.8(11)	1.3(9)	2.8(9)	2.8(9)
C7	18.6(12)	9.7(10)	15.0(12)	0.0(9)	-0.7(9)	1.4(9)
C8	13.8(11)	10.6(11)	13.6(11)	0.4(8)	0.9(9)	0.7(8)
C9	13.4(11)	7.2(10)	12.7(11)	-0.1(8)	-1.6(9)	-0.1(8)
C10	15.5(11)	9.6(11)	11.0(11)	-1.3(9)	-1.0(9)	1.2(9)
C11	23.4(12)	7.1(11)	17.9(12)	-1.0(9)	-4.8(10)	0.9(9)
C12	20.5(11)	11.6(12)	15.7(11)	3(1)	-5.1(9)	-1.8(10)
C13	16.4(11)	10.7(10)	11.7(11)	-0.1(8)	-2.3(9)	-0.8(8)
C14	14.8(11)	8.4(10)	14.0(11)	-0.7(8)	-0.3(9)	-0.2(8)
C15	20.3(12)	12.1(13)	18.0(12)	0.5(9)	-2.9(9)	1.5(9)
C16	15.6(11)	12.7(12)	20.1(12)	-1.9(9)	-3.8(9)	0.5(9)
C17	11.9(9)	13.7(11)	13.7(10)	-2(1)	1.6(8)	1.0(9)
C18	19.7(12)	15.1(12)	17.1(12)	-0.4(10)	2.2(10)	4.1(10)
C19	18.3(12)	17.4(11)	15.6(12)	3.5(9)	2.8(9)	3.6(9)
C20	14.7(12)	19.3(13)	15.0(12)	0.7(10)	1.7(9)	2.5(9)
C21	16.3(10)	12.7(12)	15.1(11)	-1.7(9)	-0.2(8)	0.2(9)
C22	13.6(11)	19.7(12)	16.7(12)	-1.1(10)	-2.7(9)	-0.6(9)
C23	17.8(11)	19.9(12)	18.0(11)	-2.0(12)	-1.4(9)	1.1(11)
C24	14.6(11)	24.6(15)	17.2(12)	0.5(10)	-2.1(9)	-2.7(9)
C25	25.8(14)	32.4(15)	26.6(15)	-5.4(12)	-8.0(12)	-2.1(12)
C26	25.9(13)	27.8(14)	24.3(13)	0.3(13)	-6.8(10)	3.0(12)
C27	18.7(12)	18.2(12)	16.9(12)	-2.2(10)	-2.8(10)	2(1)
C28	40.5(17)	15.8(13)	25.7(15)	0.8(11)	-15.4(13)	-1.0(11)

Table A1.9.4. Bond lengths for **100**.

Atom	Atom	Length (Å)	Atom	Atom	Length (Å)
Br1	C5	2.046(2)	C13	C17	1.554(3)
Br2	C6	1.984(2)	C13	C19	1.534(3)
O1	C3	1.467(3)	C14	C15	1.536(3)
O1	C28	1.336(3)	C15	C16	1.548(3)
O2	C28	1.199(3)	C16	C17	1.556(3)
C1	C2	1.533(3)	C17	C20	1.541(3)
C1	C10	1.543(3)	C20	C21	1.534(3)
C2	C3	1.513(3)	C20	C27	1.533(4)
C3	C4	1.528(3)	C21	C22	1.523(3)
C4	C5	1.526(3)	C22	C23	1.527(3)
C5	C6	1.523(3)	C23	C24	1.530(3)
C5	C10	1.553(3)	C24	C25	1.527(3)
C6	C7	1.518(3)	C24	C26	1.530(4)
C7	C8	1.524(3)	C28	C29	1.499(4)
C8	C9	1.550(3)	C1S	C6S	1.39
C8	C14	1.528(3)	C1S	C2S	1.39
C9	C10	1.561(3)	C6S	C5S	1.39
C9	C11	1.529(3)	C5S	C4S	1.39
C10	C18	1.550(3)	C4S	C3S	1.39
C11	C12	1.538(3)	C4S	C1SA	1.615(9)

C12	C13	1.529(3)	C3S	C2S	1.39
C13	C14	1.538(3)			

Table A1.9.5. Bond angles for **100**.

Atom	Atom	Atom	Angle (°)	Atom	Atom	Atom	Angle (°)
C28	O1	C3	116.6(2)	C12	C13	C19	110.32(19)
C2	C1	C10	113.07(19)	C14	C13	C17	100.39(17)
C3	C2	C1	111.34(19)	C19	C13	C14	112.50(18)
O1	C3	C2	105.44(18)	C19	C13	C17	109.90(18)
O1	C3	C4	108.55(18)	C8	C14	C13	114.47(18)
C2	C3	C4	112.9(2)	C8	C14	C15	118.18(19)
C5	C4	C3	112.09(19)	C15	C14	C13	104.44(17)
C4	C5	Br1	103.39(13)	C14	C15	C16	103.40(18)
C4	C5	C10	113.10(19)	C15	C16	C17	107.33(18)
C6	C5	Br1	99.92(14)	C13	C17	C16	103.10(18)
C6	C5	C4	114.4(2)	C20	C17	C13	119.12(18)
C6	C5	C10	115.64(18)	C20	C17	C16	112.36(19)
C10	C5	Br1	108.47(15)	C21	C20	C17	110.18(18)
C5	C6	Br2	111.15(15)	C27	C20	C17	112.1(2)
C7	C6	Br2	109.78(16)	C27	C20	C21	110.8(2)
C7	C6	C5	114.14(19)	C22	C21	C20	115.52(19)
C6	C7	C8	114.29(19)	C21	C22	C23	112.55(19)
C7	C8	C9	111.09(18)	C22	C23	C24	115.1(2)
C7	C8	C14	111.09(18)	C25	C24	C23	110.2(2)
C14	C8	C9	108.06(18)	C25	C24	C26	109.6(2)
C8	C9	C10	111.17(18)	C26	C24	C23	111.9(2)
C11	C9	C8	111.72(18)	O1	C28	C29	111.2(3)
C11	C9	C10	113.26(18)	O2	C28	O1	124.4(2)
C1	C10	C5	107.97(18)	O2	C28	C29	124.5(3)
C1	C10	C9	111.47(18)	C6S	C1S	C2S	120
C1	C10	C18	106.77(18)	C5S	C6S	C1S	120
C5	C10	C9	109.76(17)	C6S	C5S	C4S	120
C18	C10	C5	110.84(18)	C5S	C4S	C3S	120
C18	C10	C9	109.99(18)	C5S	C4S	C1SA	122.4(4)
C9	C11	C12	113.44(19)	C3S	C4S	C1SA	117.6(4)
C13	C12	C11	112.00(19)	C2S	C3S	C4S	120
C12	C13	C14	106.75(18)	C3S	C2S	C1S	120
C12	C13	C17	116.62(19)				

Table A1.9.6. Torsion angles for **100**.

A	B	C	D	Angle (°)	A	B	C	D	Angle (°)
Br1	C5	C6	Br2	-163.16(10)	C11	C9	C10	C1	58.5(2)
Br1	C5	C6	C7	72.0(2)	C11	C9	C10	C5	178.08(19)
Br1	C5	C10	C1	59.28(19)	C11	C9	C10	C18	-59.7(2)
Br1	C5	C10	C9	-62.4(2)	C11	C12	C13	C14	55.5(2)
Br1	C5	C10	C18	175.89(15)	C11	C12	C13	C17	166.70(19)
Br2	C6	C7	C8	-80.2(2)	C11	C12	C13	C19	-67.0(2)
O1	C3	C4	C5	-167.88(18)	C12	C13	C14	C8	-60.9(2)
C1	C2	C3	O1	170.41(19)	C12	C13	C14	C15	168.34(18)
C1	C2	C3	C4	52.1(3)	C12	C13	C17	C16	-155.2(2)
C2	C1	C10	C5	55.9(2)	C12	C13	C17	C20	79.6(3)
C2	C1	C10	C9	176.56(19)	C13	C14	C15	C16	-33.3(2)
C2	C1	C10	C18	-63.3(2)	C13	C17	C20	C21	-178.6(2)
C2	C3	C4	C5	-51.4(3)	C13	C17	C20	C27	-54.7(3)
C3	O1	C28	O2	0.5(4)	C14	C8	C9	C10	179.91(18)
C3	O1	C28	C29	-179.7(2)	C14	C8	C9	C11	-52.5(2)
C3	C4	C5	Br1	-63.6(2)	C14	C13	C17	C16	-40.3(2)
C3	C4	C5	C6	-171.23(19)	C14	C13	C17	C20	-165.6(2)

C3	C4	C5	C10	53.5(2)	C14	C15	C16	C17	7.3(2)
C4	C5	C6	Br2	-53.4(2)	C15	C16	C17	C13	20.8(2)
C4	C5	C6	C7	-178.23(18)	C15	C16	C17	C20	150.26(19)
C4	C5	C10	C1	-54.8(2)	C16	C17	C20	C21	60.8(3)
C4	C5	C10	C9	-176.48(18)	C16	C17	C20	C27	-175.3(2)
C4	C5	C10	C18	61.8(2)	C17	C13	C14	C8	177.04(18)
C5	C6	C7	C8	45.4(3)	C17	C13	C14	C15	46.3(2)
C6	C5	C10	C1	170.49(19)	C17	C20	C21	C22	-171.8(2)
C6	C5	C10	C9	48.8(2)	C19	C13	C14	C8	60.3(2)
C6	C5	C10	C18	-72.9(2)	C19	C13	C14	C15	-70.5(2)
C6	C7	C8	C9	-52.5(3)	C19	C13	C17	C16	78.4(2)
C6	C7	C8	C14	-172.77(19)	C19	C13	C17	C20	-46.9(3)
C7	C8	C9	C10	57.8(2)	C20	C21	C22	C23	178.1(2)
C7	C8	C9	C11	-174.59(19)	C21	C22	C23	C24	177.4(2)
C7	C8	C14	C13	-178.37(19)	C22	C23	C24	C25	166.7(2)
C7	C8	C14	C15	-54.7(3)	C22	C23	C24	C26	-71.1(3)
C8	C9	C10	C1	-174.73(18)	C27	C20	C21	C22	63.5(3)
C8	C9	C10	C5	-55.2(2)	C28	O1	C3	C2	157.6(2)
C8	C9	C10	C18	67.0(2)	C28	O1	C3	C4	-81.2(3)
C8	C9	C11	C12	51.8(3)	C1S	C6S	C5S	C4S	0
C8	C14	C15	C16	-161.9(2)	C6S	C1S	C2S	C3S	0
C9	C8	C14	C13	59.5(2)	C6S	C5S	C4S	C3S	0
C9	C8	C14	C15	-176.78(19)	C6S	C5S	C4S	C1SA	177.6(6)
C9	C11	C12	C13	-54.1(3)	C5S	C4S	C3S	C2S	0
C10	C1	C2	C3	-55.8(3)	C4S	C3S	C2S	C1S	0
C10	C5	C6	Br2	80.70(19)	C2S	C1S	C6S	C5S	0
C10	C5	C6	C7	-44.1(3)	C1SA	C4S	C3S	C2S	-177.7(6)
C10	C9	C11	C12	178.31(19)					

Table A1.9.7. Hydrogen atom coordinates (Å×10^4) and isotropic displacement parameters (Å^2×10^3) for **100**.

Atom	*x*	*y*	*z*	U(eq)
H1A	8607	5817	7455	17
H1B	7364	6784	7731	17
H2A	7884	6490	6297	21
H2B	6719	5517	6648	21
H3	5591	8106	6776	23
H4A	7671	10008	6196	20
H4B	6405	10837	6507	20
H6	7621	12684	7442	17
H7A	8574	12062	8497	17
H7B	9673	13138	8138	17
H8	10862	10616	7950	15
H9	8758	8730	8516	13
H11A	11076	7150	8071	20
H11B	9903	6149	8400	20
H12A	10456	7417	9490	20
H12B	11752	6536	9233	20
H14	10074	10485	9335	15
H15A	10836	13263	9368	20
H15B	12012	12830	8888	20
H16A	12062	12384	10326	20
H16B	13291	12207	9862	20
H17	11583	9536	10268	16
H18A	10270	7287	6937	26
H18B	10506	9341	7015	26
H18C	9423	8611	6441	26
H19A	13411	10423	8797	26
H19B	12646	9093	8269	26

H19C	13608	8368	8900	26
H20	14323	9401	10044	20
H21A	13771	11025	11037	18
H21B	13144	9306	11338	18
H22A	15877	9667	11142	20
H22B	15237	7981	11465	20
H23A	14643	9711	12419	22
H23B	15346	11352	12102	22
H24	17405	9736	12254	23
H25A	16932	11979	13038	43
H25B	17771	10471	13438	43
H25C	16221	10602	13503	43
H26A	15973	7492	13107	40
H26B	17525	7393	13046	40
H26C	16528	6909	12392	40
H27A	12734	6629	10502	27
H27B	14305	6587	10613	27
H27C	13587	6596	9844	27
H29A	5157	7944	4561	75
H29B	4079	9460	4553	75
H29C	3686	7503	4732	75
H1S	8854	4712	4844	46
H6S	7608	7199	4544	55
H5S	8552	9966	4696	54
H3S	11987	7757	5447	42
H2S	11043	4990	5295	46
H1SA	10514	11894	4956	69
H1SB	11912	10953	4954	69
H1SC	11263	11249	5671	69

Table A1.9.8. Atomic occupancy for **100**.

Atom	Occupancy	Atom	Occupancy	Atom	Occupancy
C1S	0.5	H1S	0.5	C6S	0.5
H6S	0.5	C5S	0.5	H5S	0.5
C4S	0.5	C3S	0.5	H3S	0.5
C2S	0.5	H2S	0.5	C1SA	0.5
H1SA	0.5	H1SB	0.5	H1SC	0.5

A1.10. Crystal structure data for 25-hydroxy-3β-acetoxycholesterol, 102

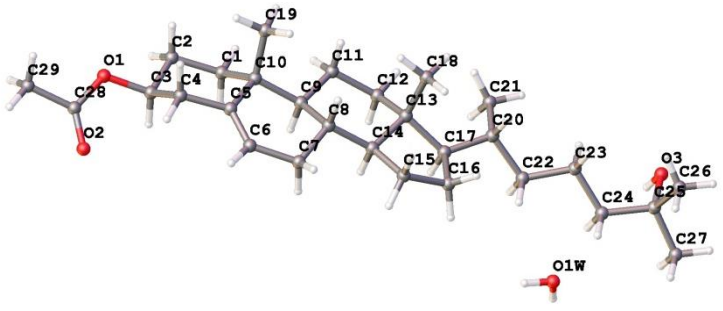

Figure A1.10. One Structure from the unit cell of **102**, determined by X-ray diffraction of a single crystal.

Table A1.10.1. Crystal data and structure refinement for **102**.

Empirical formula	$C_{58}H_{98}O_7$
Formula weight	907.36
Temperature (K)	120
Crystal system	monoclinic
Space group	$P2_1$
a (Å)	12.7390(3)
b (Å)	6.1143(2)
c (Å)	35.9230(9)
α (°)	90
β (°)	100.1178(13)
γ (°)	90
Volume (Å^3)	2754.53(13)
Z	2
ρ_{calc}g (cm^3)	1.094
μ (mm^{-1})	0.538
F(000)	1004
Crystal size (mm^3)	0.5 × 0.09 × 0.05
Radiation	CuKα (λ = 1.54178)
2Θ range for data collection (°)	4.998 to 144.988
Index ranges	$-15 \le h \le 15$, $-7 \le k \le 7$, $-44 \le l \le 43$
Reflections collected	32626
Independent reflections	10187 [R_{int} = 0.0567, R_{sigma} = 0.0550]
Data/restraints/ parameters	10187/6/605
Goodness-of-fit on F^2	1.046
Final R indexes [I > = 2σ (I)]	R_1 = 0.0547, wR_2 = 0.1326
Final R indexes [all data]	R_1 = 0.0642, wR_2 = 0.1397
Largest diff. peak/ hole (e Å^{-3})	0.47/-0.39
Flack parameter	-0.2(2)

Table A1.10.2. Fractional atomic coordinates (×10^4) and equivalent isotropic displacement parameters (Å^2×10^3) for **102**. U_{eq} is defined as 1/3 of the trace of the orthogonalised U_{IJ} tensor.

Atom	*x*	*y*	*z*	U(eq)
O1	6334.5(19)	7964(5)	4036.7(6)	35.9(6)
O2	7225(3)	4965(7)	3907.1(9)	68.9(11)
O3	-2915.0(17)	9020(4)	114.2(7)	28.9(5)
C1	3787(3)	8782(6)	3345.7(9)	28.4(7)
C2	4582(3)	8941(6)	3717.9(9)	31.0(7)
C3	5593(3)	7712(6)	3679.7(9)	29.8(7)
C4	6083(2)	8652(6)	3358.8(9)	26.5(7)
C5	5294(2)	8575(5)	2990.5(8)	22.0(6)
C6	5555(3)	7593(6)	2692.3(9)	27.0(7)
C7	4852(3)	7432(6)	2313.1(9)	28.5(7)
C8	3902(2)	8981(5)	2271.9(8)	20.0(6)
C9	3406(2)	8957(5)	2631.7(8)	20.5(6)
C10	4206(2)	9626(5)	2992.8(8)	21.4(6)
C11	2355(3)	10232(7)	2576.3(9)	34.1(8)
C12	1555(2)	9557(7)	2220.7(9)	30.6(8)
C13	2043(2)	9696(5)	1860.7(8)	20.9(6)
C14	3065(2)	8307(5)	1938.4(8)	21.2(6)
C15	3396(3)	8073(8)	1554.6(9)	40.9(10)
C16	2323(3)	7870(7)	1279.1(9)	35.1(9)
C17	1431(2)	8479(5)	1507.1(8)	23.0(6)
C18	2266(3)	12067(6)	1761.6(12)	41.0(9)
C19	4364(3)	12123(5)	3016.4(10)	29.9(7)
C20	7110(3)	6474(8)	4109.5(11)	46.2(11)
C21	7822(4)	6962(10)	4483.0(12)	59.3(13)
C22	474(3)	9552(6)	1255.9(9)	29.0(7)

C23	-387(3)	10291(9)	1475.4(12)	53.7(13)
C24	-9(3)	7970(6)	940.7(9)	32.1(8)
C25	-794(3)	8973(6)	614.7(10)	32.4(8)
C26	-1201(3)	7288(6)	310.8(9)	30.0(7)
C27	-2016(2)	8087(6)	-23.0(9)	26.5(7)
C28	-1581(3)	9912(7)	-236.9(10)	39.2(9)
C29	-2394(3)	6191(7)	-288.5(10)	36.0(8)
O1AA	12960(4)	-1599(8)	4900.3(15)	28.0(7)
O1AB	12743(4)	-2169(8)	4905.6(15)	28.0(7)
O2AA	14348(5)	-2838(12)	4711.5(19)	53.8(11)
O2AB	14105(5)	-3744(11)	4677.3(19)	53.8(11)
O3A	5961.3(17)	6196(4)	463.0(6)	23.0(5)
C1A	10621(3)	-1694(6)	4071.3(10)	33.8(8)
C1B	13746(8)	-3049(15)	4927(3)	34.1(12)
C1C	14288(7)	-3326(14)	5324(2)	34.4(12)
C1D	13846(8)	-2597(15)	4977(3)	34.1(12)
C1E	14253(7)	-2758(14)	5396(2)	34.4(12)
C2A	11197(3)	-2232(6)	4472.1(10)	37.7(9)
C3A	12320(3)	-1419(7)	4519.4(10)	39.9(9)
C4A	12335(3)	1047(7)	4456.8(10)	34.7(8)
C5A	11729(3)	1673(5)	4071.9(9)	25.8(7)
C6A	12181(3)	2942(6)	3845.4(9)	28.9(7)
C7A	11650(2)	3692(6)	3462.5(9)	25.0(7)
C8A	10455(2)	3242(5)	3381.3(8)	19.4(6)
C9A	10202(2)	980(5)	3532.1(8)	22.2(6)
C10A	10594(2)	766(5)	3966.8(9)	23.0(6)
C11A	9020(2)	373(5)	3406.6(9)	24.6(7)
C12A	8611(2)	640(5)	2979.5(9)	22.4(6)
C13A	8817(2)	2948(5)	2844.9(8)	17.8(6)
C14A	10027(2)	3336(5)	2956.9(8)	20.1(6)
C15A	10243(2)	5373(5)	2743.5(9)	24.9(7)
C16A	9442(3)	5216(6)	2366.0(9)	26.1(7)
C17A	8675(2)	3282(5)	2407.2(8)	21.4(6)
C18A	8155(2)	4616(5)	3019.8(8)	21.5(6)
C19A	9862(3)	2013(6)	4192.5(9)	27.3(7)
C22A	7549(2)	3679(5)	2180.4(8)	23.0(6)
C23A	6760(3)	1873(7)	2233(1)	35.5(8)
C24A	7598(2)	3933(6)	1757.2(9)	26.5(7)
C25A	6611(3)	4972(6)	1521.2(9)	28.4(7)
C26A	6694(2)	5116(5)	1101.5(8)	22.4(6)
C27A	5749(2)	6191(5)	847.8(8)	20.2(6)
C28A	5640(3)	8599(5)	942.2(10)	30.8(7)
C29A	4713(2)	4950(6)	847.3(9)	26.9(7)
O1W	4216(2)	7451(4)	-111.6(8)	38.5(6)

Table A1.10.3. Anisotropic displacement parameters ($Å^2 \times 10^3$) for **102**. The anisotropic displacement factor exponent takes the form: $-2\pi^2[h^2a^{*2}U_{11}+2hka^*b^*U_{12}+\ldots]$.

Atom	U_{11}	U_{22}	U_{33}	U_{23}	U_{13}	U_{12}
O1	30.5(12)	52.3(16)	23.0(11)	0.0(12)	-1.1(9)	6.1(12)
O2	80(2)	85(2)	39.7(17)	5.4(18)	3.9(16)	51(2)
O3	21.1(11)	25.4(11)	42.2(14)	8.5(11)	11.1(10)	5.5(9)
C1	24.1(16)	35.8(18)	26.6(16)	-5.3(15)	8.1(13)	-2.3(14)
C2	29.2(17)	40.2(19)	24.0(16)	-4.7(15)	6.3(13)	1.4(15)
C3	27.7(17)	37.9(19)	22.4(15)	-1.3(15)	0.2(13)	3.9(15)
C4	21.9(15)	28.4(16)	28.1(16)	1.8(14)	1.6(12)	1.7(13)
C5	19.5(14)	23.7(15)	22.4(15)	3.2(13)	2.8(12)	3.4(12)
C6	23.0(15)	32.8(17)	25.1(16)	0.4(14)	4.0(12)	10.6(14)
C7	25.2(16)	37.5(18)	23.3(16)	-0.5(15)	5.4(13)	12.6(14)
C8	17.6(14)	20.2(14)	22.4(14)	1.8(12)	4.0(11)	2.7(12)

C9	17.3(14)	20.5(14)	23.8(15)	-4.4(13)	3.6(11)	-0.8(12)
C10	20.2(15)	21.6(15)	22.5(15)	-3.9(13)	4.1(12)	0.5(12)
C11	23.3(16)	52(2)	25.9(16)	-14.4(17)	1.2(13)	9.8(16)
C12	18.0(15)	49(2)	24.1(16)	-9.3(16)	2.9(12)	3.5(14)
C13	18.6(14)	19.7(14)	24.2(15)	-0.4(13)	3.0(12)	4.6(12)
C14	22.2(15)	18.7(14)	23.3(15)	0.5(13)	5.8(12)	4.4(12)
C15	27.4(17)	72(3)	23.7(16)	-4.2(19)	5.5(14)	18.4(19)
C16	28.8(17)	55(2)	20.8(15)	-3.3(16)	2.4(13)	18.1(17)
C17	23.0(15)	23.2(15)	22.9(15)	-0.8(13)	4.4(12)	6.0(13)
C18	43(2)	20.2(16)	53(2)	4.2(17)	-10.8(18)	2.8(15)
C19	28.6(17)	21.6(15)	36.3(18)	-6.1(15)	-3.7(14)	2.1(13)
C20	44(2)	70(3)	24.9(19)	13(2)	6.0(16)	17(2)
C21	43(2)	97(4)	34(2)	18(2)	-3.6(18)	4(3)
C22	26.8(17)	31.3(17)	27.1(16)	-5.0(15)	-0.6(13)	8.7(14)
C23	31(2)	85(3)	41(2)	-30(2)	-5.7(16)	24(2)
C24	30.0(17)	38.5(19)	25.9(16)	-5.0(16)	-0.8(13)	9.3(15)
C25	27.8(17)	39.0(19)	27.7(17)	-0.2(16)	-2.3(13)	7.2(15)
C26	25.1(16)	38.2(19)	25.5(16)	-2.2(15)	1.3(13)	9.9(15)
C27	16.9(14)	35.3(18)	27.9(16)	2.6(15)	5.2(12)	2.4(13)
C28	26.2(18)	57(2)	33.4(18)	11.1(19)	2.4(14)	-7.6(18)
C29	28.5(18)	47(2)	30.6(18)	-3.5(17)	-0.3(14)	2.8(16)
O3A	27.6(12)	22.7(11)	18.8(11)	-1.0(9)	5.0(9)	0.2(9)
C1A	45(2)	22.3(16)	27.9(17)	0.6(14)	-9.3(15)	4.0(15)
C2A	55(2)	27.0(18)	25.7(17)	0.7(15)	-8.5(16)	7.3(17)
C3A	44(2)	51(2)	21.3(16)	-0.1(17)	-4.7(15)	23.3(19)
C4A	27.5(17)	48(2)	25.9(17)	-4.2(17)	-3.1(14)	2.1(16)
C5A	24.1(16)	30.7(17)	20.5(15)	-4.8(14)	-1.8(12)	4.6(13)
C6A	19.7(15)	37.1(18)	27.3(16)	-5.3(15)	-3.2(12)	2.7(14)
C7A	19.2(14)	29.6(16)	25.5(15)	-3.4(14)	1.9(12)	1.0(13)
C8A	16.9(13)	17.1(13)	22.6(14)	-4.4(12)	-0.5(11)	2.3(11)
C9A	24.0(15)	19.4(14)	21.7(15)	-3.5(13)	0.1(12)	1.9(12)
C10A	25.3(16)	19.1(14)	22.3(15)	-1.4(13)	-1.9(12)	4.2(12)
C11A	24.8(16)	18.9(14)	27.6(16)	1.9(13)	-2.6(13)	-2.9(12)
C12A	22.2(15)	16.4(14)	25.9(16)	0.3(12)	-3.2(12)	-0.7(12)
C13A	17.5(14)	14.9(13)	19.3(14)	-1.2(12)	-1.7(11)	3.2(11)
C14A	16.2(14)	21.0(14)	21.8(14)	-1.6(12)	-0.2(11)	4.9(12)
C15A	22.7(15)	26.6(16)	24.0(15)	2.8(13)	0.5(12)	-1.3(13)
C16A	25.4(16)	28.6(16)	23.8(15)	4.8(14)	2.8(12)	1.1(13)
C17A	18.8(14)	23.0(15)	20.9(14)	-1.4(13)	-0.6(12)	5.3(12)
C18A	20.5(15)	19.9(14)	23.8(15)	1.2(13)	3.1(12)	5.6(12)
C19A	29.8(17)	27.5(16)	24.0(16)	-1.6(14)	3.4(13)	3.0(14)
C22A	18.6(14)	25.9(16)	22.7(15)	1.2(13)	-1.4(12)	2.6(12)
C23A	27.0(17)	43(2)	32.1(18)	7.0(16)	-7.8(14)	-5.6(16)
C24A	20.8(15)	34.6(17)	22.9(15)	0.5(14)	0.8(12)	4.6(14)
C25A	24.9(16)	36.1(18)	23.9(15)	3.5(15)	3.4(13)	8.9(14)
C26A	19.7(14)	26.7(15)	20.8(15)	-2.1(13)	3.1(11)	2.3(13)
C27A	22.0(15)	21.0(14)	18.4(14)	-1.0(12)	5.7(11)	0.0(12)
C28A	40.2(19)	24.7(17)	27.7(17)	-2.4(14)	6.3(14)	3.7(15)
C29A	21.6(15)	33.8(17)	25.4(16)	-1.5(15)	4.5(12)	-2.9(14)
O1W	33.0(14)	29.0(13)	46.0(15)	16.5(12)	-13.3(12)	-10.1(11)

Table A1.10.4. Bond lengths for **102**.

Atom	Atom	Length (Å)	Atom	Atom	Length (Å)
O1	C3	1.461(4)	O1AB	C1B	1.376(12)
O1	C20	1.336(5)	O1AB	C3A	1.471(6)
O2	C20	1.200(6)	O2AA	C1D	1.247(12)
O3	C27	1.441(4)	O2AB	C1B	1.157(11)
C1	C2	1.532(5)	O3A	C27A	1.454(3)
C1	C10	1.548(4)	C1A	C2A	1.532(5)

C2	C3	1.518(5)	C1A	C10A	1.549(4)
C3	C4	1.518(4)	C1B	C1C	1.481(13)
C4	C5	1.515(4)	C1D	C1E	1.507(13)
C5	C6	1.321(4)	C2A	C3A	1.495(6)
C5	C10	1.529(4)	C3A	C4A	1.525(6)
C6	C7	1.496(4)	C4A	C5A	1.510(4)
C7	C8	1.523(4)	C5A	C6A	1.326(5)
C8	C9	1.535(4)	C5A	C10A	1.533(5)
C8	C14	1.515(4)	C6A	C7A	1.494(4)
C9	C10	1.556(4)	C7A	C8A	1.524(4)
C9	C11	1.532(4)	C8A	C9A	1.540(4)
C10	C19	1.540(4)	C8A	C14A	1.527(4)
C11	C12	1.544(4)	C9A	C10A	1.559(4)
C12	C13	1.532(4)	C9A	C11A	1.540(4)
C13	C14	1.538(4)	C10A	C19A	1.541(4)
C13	C17	1.558(4)	C11A	C12A	1.540(4)
C13	C18	1.531(5)	C12A	C13A	1.529(4)
C14	C15	1.517(4)	C13A	C14A	1.542(4)
C15	C16	1.545(5)	C13A	C17A	1.564(4)
C16	C17	1.558(4)	C13A	C18A	1.527(4)
C17	C22	1.531(4)	C14A	C15A	1.513(4)
C20	C21	1.511(6)	C15A	C16A	1.550(4)
C22	C23	1.527(5)	C16A	C17A	1.558(4)
C22	C24	1.533(5)	C17A	C22A	1.539(4)
C24	C25	1.529(4)	C22A	C23A	1.527(5)
C25	C26	1.524(5)	C22A	C24A	1.540(4)
C26	C27	1.522(4)	C24A	C25A	1.526(4)
C27	C28	1.514(5)	C25A	C26A	1.532(4)
C27	C29	1.524(5)	C26A	C27A	1.525(4)
O1AA	C1D	1.271(11)	C27A	C28A	1.523(4)
O1AA	C3A	1.469(6)	C27A	C29A	1.523(4)

Table A1.10.5. Bond angles for **102**.

Atom	Atom	Atom	Angle (°)	Atom	Atom	Atom	Angle (°)
C20	O1	C3	116.2(3)	O1AB	C1B	C1C	111.7(8)
C2	C1	C10	115.1(3)	O2AB	C1B	O1AB	126.2(9)
C3	C2	C1	109.3(3)	O2AB	C1B	C1C	121.6(9)
O1	C3	C2	107.2(3)	O1AA	C1D	C1E	112.6(8)
O1	C3	C4	109.8(3)	O2AA	C1D	O1AA	116.5(9)
C2	C3	C4	110.5(3)	O2AA	C1D	C1E	128.7(9)
C5	C4	C3	110.7(3)	C3A	C2A	C1A	109.0(3)
C4	C5	C10	116.5(3)	O1AA	C3A	C2A	116.4(3)
C6	C5	C4	119.9(3)	O1AA	C3A	C4A	101.1(3)
C6	C5	C10	123.6(3)	O1AB	C3A	C2A	100.9(3)
C5	C6	C7	124.9(3)	O1AB	C3A	C4A	115.8(4)
C6	C7	C8	112.7(3)	C2A	C3A	C4A	110.4(3)
C7	C8	C9	110.5(2)	C5A	C4A	C3A	111.6(3)
C14	C8	C7	110.2(2)	C4A	C5A	C10A	116.2(3)
C14	C8	C9	109.1(2)	C6A	C5A	C4A	120.2(3)
C8	C9	C10	113.2(2)	C6A	C5A	C10A	123.5(3)
C11	C9	C8	111.4(3)	C5A	C6A	C7A	124.7(3)
C11	C9	C10	113.8(2)	C6A	C7A	C8A	113.3(3)
C1	C10	C9	109.0(2)	C7A	C8A	C9A	111.0(3)
C5	C10	C1	107.9(2)	C7A	C8A	C14A	110.7(2)
C5	C10	C9	110.2(2)	C14A	C8A	C9A	109.0(2)
C5	C10	C19	107.9(3)	C8A	C9A	C10A	112.2(2)
C19	C10	C1	110.2(3)	C11A	C9A	C8A	111.6(2)
C19	C10	C9	111.5(3)	C11A	C9A	C10A	113.4(3)
C9	C11	C12	114.0(3)	C1A	C10A	C9A	108.3(2)

C13	C12	C11	112.1(3)	C5A	C10A	C1A	108.2(3)
C12	C13	C14	105.8(2)	C5A	C10A	C9A	109.8(3)
C12	C13	C17	116.3(3)	C5A	C10A	C19A	108.9(3)
C14	C13	C17	99.8(2)	C19A	C10A	C1A	110.0(3)
C18	C13	C12	111.6(3)	C19A	C10A	C9A	111.6(2)
C18	C13	C14	112.3(3)	C12A	C11A	C9A	114.1(3)
C18	C13	C17	110.4(3)	C13A	C12A	C11A	111.5(2)
C8	C14	C13	116.7(2)	C12A	C13A	C14A	106.2(2)
C8	C14	C15	118.4(3)	C12A	C13A	C17A	116.3(2)
C15	C14	C13	104.4(2)	C14A	C13A	C17A	100.1(2)
C14	C15	C16	103.5(3)	C18A	C13A	C12A	110.4(2)
C15	C16	C17	106.8(3)	C18A	C13A	C14A	112.9(2)
C16	C17	C13	103.6(2)	C18A	C13A	C17A	110.6(2)
C22	C17	C13	120.6(3)	C8A	C14A	C13A	114.8(2)
C22	C17	C16	111.8(3)	C15A	C14A	C8A	118.2(3)
O1	C20	C21	110.3(4)	C15A	C14A	C13A	104.9(2)
O2	C20	O1	124.8(4)	C14A	C15A	C16A	104.0(2)
O2	C20	C21	124.9(4)	C15A	C16A	C17A	106.9(2)
C17	C22	C24	109.8(3)	C16A	C17A	C13A	103.4(2)
C23	C22	C17	113.1(3)	C22A	C17A	C13A	119.0(2)
C23	C22	C24	109.7(3)	C22A	C17A	C16A	111.8(2)
C25	C24	C22	115.9(3)	C17A	C22A	C24A	110.1(2)
C26	C25	C24	111.8(3)	C23A	C22A	C17A	113.1(3)
C27	C26	C25	116.5(3)	C23A	C22A	C24A	109.6(3)
O3	C27	C26	109.3(3)	C25A	C24A	C22A	114.7(3)
O3	C27	C28	105.4(3)	C24A	C25A	C26A	112.2(2)
O3	C27	C29	109.4(3)	C27A	C26A	C25A	115.4(2)
C26	C27	C29	110.2(3)	O3A	C27A	C26A	108.1(2)
C28	C27	C26	112.1(3)	O3A	C27A	C28A	104.4(2)
C28	C27	C29	110.3(3)	O3A	C27A	C29A	107.8(2)
C1D	O1AA	C3A	124.4(6)	C28A	C27A	C26A	112.2(3)
C1B	O1AB	C3A	111.0(6)	C29A	C27A	C26A	112.3(3)
C2A	C1A	C10A	115.0(3)	C29A	C27A	C28A	111.6(3)

Table A1.10.6. Hydrogen bonds for **102**.

D	H	A	d(D-H) (Å)	d(H-A) (Å)	d(D-A) (Å)	D-H-A (°)
O3	H3	O3A[a]	0.850(7)	1.877(15)	2.689(3)	159(4)
O3A	H3A	O1W[b]	0.850(7)	1.770(12)	2.606(3)	167(4)
O1W	H1WA	O3A	0.851(7)	2.010(8)	2.860(3)	176(4)
O1W	H1WB	O3[c]	0.851(7)	1.822(8)	2.672(3)	178(5)

[a]-1+X,+Y,+Z; [b]1-X,-1/2+Y,-Z; [c]-X,-1/2+Y,-Z

Table A1.10.7. Torsion angles for **102**.

A	B	C	D	Angle (°)	A	B	C	D	Angle (°)
O1	C3	C4	C5	-175.4(3)	C1A	C2A	C3A	O1AB	-177.4(3)
C1	C2	C3	O1	178.4(3)	C1A	C2A	C3A	C4A	59.7(4)
C1	C2	C3	C4	58.8(4)	C1B	O1AB	C3A	C2A	136.8(5)
C2	C1	C10	C5	49.5(4)	C1B	O1AB	C3A	C4A	-104.0(6)
C2	C1	C10	C9	169.2(3)	C1D	O1AA	C3A	C2A	123.7(7)
C2	C1	C10	C19	-68.1(4)	C1D	O1AA	C3A	C4A	-116.8(7)
C2	C3	C4	C5	-57.4(4)	C2A	C1A	C10A	C5A	49.3(4)
C3	O1	C20	O2	-0.9(6)	C2A	C1A	C10A	C9A	168.3(3)
C3	O1	C20	C21	179.1(3)	C2A	C1A	C10A	C19A	-69.5(4)
C3	C4	C5	C6	-124.9(3)	C2A	C3A	C4A	C5A	-57.1(4)
C3	C4	C5	C10	53.6(4)	C3A	O1AA	C1D	O2AA	22.8(12)
C4	C5	C6	C7	-179.3(3)	C3A	O1AA	C1D	C1E	-172.7(6)
C4	C5	C10	C1	-48.0(3)	C3A	O1AB	C1B	O2AB	-22.1(12)
C4	C5	C10	C9	-166.9(3)	C3A	O1AB	C1B	C1C	166.5(6)

C4	C5	C10	C19	71.1(3)	C3A	C4A	C5A	C6A	-128.6(4)
C5	C6	C7	C8	14.0(5)	C3A	C4A	C5A	C10A	51.4(4)
C6	C5	C10	C1	130.5(3)	C4A	C5A	C6A	C7A	-178.9(3)
C6	C5	C10	C9	11.5(4)	C4A	C5A	C10A	C1A	-46.0(4)
C6	C5	C10	C19	-110.4(4)	C4A	C5A	C10A	C9A	-164.0(3)
C6	C7	C8	C9	-43.0(4)	C4A	C5A	C10A	C19A	73.6(4)
C6	C7	C8	C14	-163.6(3)	C5A	C6A	C7A	C8A	11.4(5)
C7	C8	C9	C10	58.7(3)	C6A	C5A	C10A	C1A	134.1(3)
C7	C8	C9	C11	-171.5(3)	C6A	C5A	C10A	C9A	16.1(4)
C7	C8	C14	C13	179.3(3)	C6A	C5A	C10A	C19A	-106.4(4)
C7	C8	C14	C15	-54.7(4)	C6A	C7A	C8A	C9A	-40.4(4)
C8	C9	C10	C1	-159.9(3)	C6A	C7A	C8A	C14A	-161.6(3)
C8	C9	C10	C5	-41.7(3)	C7A	C8A	C9A	C10A	59.0(3)
C8	C9	C10	C19	78.1(3)	C7A	C8A	C9A	C11A	-172.5(2)
C8	C9	C11	C12	51.2(4)	C7A	C8A	C14A	C13A	-178.8(2)
C8	C14	C15	C16	-168.4(3)	C7A	C8A	C14A	C15A	-54.1(3)
C9	C8	C14	C13	57.9(3)	C8A	C9A	C10A	C1A	-163.2(3)
C9	C8	C14	C15	-176.2(3)	C8A	C9A	C10A	C5A	-45.3(3)
C9	C11	C12	C13	-54.6(4)	C8A	C9A	C10A	C19A	75.5(3)
C10	C1	C2	C3	-56.7(4)	C8A	C9A	C11A	C12A	50.4(3)
C10	C5	C6	C7	2.3(5)	C8A	C14A	C15A	C16A	-163.8(2)
C10	C9	C11	C12	-179.4(3)	C9A	C8A	C14A	C13A	58.8(3)
C11	C9	C10	C1	71.5(3)	C9A	C8A	C14A	C15A	-176.5(2)
C11	C9	C10	C5	-170.2(3)	C9A	C11A	C12A	C13A	-54.6(3)
C11	C9	C10	C19	-50.4(4)	C10A	C1A	C2A	C3A	-58.1(4)
C11	C12	C13	C14	54.3(4)	C10A	C5A	C6A	C7A	1.0(5)
C11	C12	C13	C17	164.1(3)	C10A	C9A	C11A	C12A	178.3(2)
C11	C12	C13	C18	-68.1(4)	C11A	C9A	C10A	C1A	69.2(3)
C12	C13	C14	C8	-59.1(3)	C11A	C9A	C10A	C5A	-172.8(3)
C12	C13	C14	C15	168.2(3)	C11A	C9A	C10A	C19A	-52.0(3)
C12	C13	C17	C16	-151.7(3)	C11A	C12A	C13A	C14A	56.5(3)
C12	C13	C17	C22	82.3(4)	C11A	C12A	C13A	C17A	166.8(2)
C13	C14	C15	C16	-36.7(4)	C11A	C12A	C13A	C18A	-66.2(3)
C13	C17	C22	C23	-54.5(4)	C12A	C13A	C14A	C8A	-61.5(3)
C13	C17	C22	C24	-177.4(3)	C12A	C13A	C14A	C15A	167.1(2)
C14	C8	C9	C10	179.9(2)	C12A	C13A	C17A	C16A	-152.5(3)
C14	C8	C9	C11	-50.3(3)	C12A	C13A	C17A	C22A	82.9(3)
C14	C13	C17	C16	-38.5(3)	C13A	C14A	C15A	C16A	-34.3(3)
C14	C13	C17	C22	-164.5(3)	C13A	C17A	C22A	C23A	-56.3(4)
C14	C15	C16	C17	11.5(4)	C13A	C17A	C22A	C24A	-179.3(3)
C15	C16	C17	C13	17.3(4)	C14A	C8A	C9A	C10A	-178.8(2)
C15	C16	C17	C22	148.6(3)	C14A	C8A	C9A	C11A	-50.3(3)
C16	C17	C22	C23	-176.6(3)	C14A	C13A	C17A	C16A	-38.6(3)
C16	C17	C22	C24	60.5(4)	C14A	C13A	C17A	C22A	-163.3(3)
C17	C13	C14	C8	179.8(2)	C14A	C15A	C16A	C17A	9.0(3)
C17	C13	C14	C15	47.2(3)	C15A	C16A	C17A	C13A	18.9(3)
C17	C22	C24	C25	-166.0(3)	C15A	C16A	C17A	C22A	148.1(3)
C18	C13	C14	C8	62.8(4)	C16A	C17A	C22A	C23A	-176.7(3)
C18	C13	C14	C15	-69.9(4)	C16A	C17A	C22A	C24A	60.3(3)
C18	C13	C17	C16	79.9(3)	C17A	C13A	C14A	C8A	177.2(2)
C18	C13	C17	C22	-46.1(4)	C17A	C13A	C14A	C15A	45.8(3)
C20	O1	C3	C2	158.9(3)	C17A	C22A	C24A	C25A	-163.1(3)
C20	O1	C3	C4	-81.0(4)	C18A	C13A	C14A	C8A	59.6(3)
C22	C24	C25	C26	178.2(3)	C18A	C13A	C14A	C15A	-71.8(3)
C23	C22	C24	C25	69.0(4)	C18A	C13A	C17A	C16A	80.6(3)
C24	C25	C26	C27	178.2(3)	C18A	C13A	C17A	C22A	-44.0(4)
C25	C26	C27	O3	-56.2(4)	C22A	C24A	C25A	C26A	-178.3(3)
C25	C26	C27	C28	60.3(4)	C23A	C22A	C24A	C25A	71.8(4)
C25	C26	C27	C29	-176.5(3)	C24A	C25A	C26A	C27A	-178.5(3)
O1AA	C3A	C4A	C5A	179.1(3)	C25A	C26A	C27A	O3A	179.8(3)

O1AB	C3A	C4A	C5A	-170.9(3)	C25A	C26A	C27A	C28A	65.2(4)
C1A	C2A	C3A	O1AA	174.0(3)	C25A	C26A	C27A	C29A	-61.4(4)

Table A1.10.8. Hydrogen atom coordinates (Å×10^4) and isotropic displacement parameters (Å^2×10^3) for **102**.

Atom	*x*	*y*	*z*	U(eq)
H1A	3141	9623	3372	34
H1B	3574	7233	3303	34
H2A	4752	10495	3779	37
H2B	4265	8305	3926	37
H3B	5427	6128	3632	36
H4A	6302	10185	3418	32
H4B	6728	7803	3332	32
H6	6241	6939	2721	32
H7A	4588	5912	2273	34
H7B	5277	7769	2115	34
H8	4149	10498	2229	24
H9	3215	7398	2671	25
H11C	2513	11811	2559	41
H11D	2017	10016	2801	41
H12C	1314	8040	2252	37
H12D	923	10524	2194	37
H14	2828	6815	2002	25
H15C	3840	6752	1545	49
H15D	3799	9372	1495	49
H16C	2221	6357	1181	42
H16D	2306	8877	1062	42
H17	1169	7074	1600	28
H18D	1597	12896	1721	61
H18E	2577	12096	1531	61
H18F	2766	12725	1970	61
H19D	3706	12820	3063	45
H19E	4535	12664	2777	45
H19F	4949	12474	3223	45
H21A	7978	8532	4500	89
H21B	8490	6142	4500	89
H21C	7461	6528	4691	89
H22	735	10870	1135	35
H23D	-600	9055	1619	81
H23E	-1007	10826	1298	81
H23F	-106	11468	1650	81
H24C	581	7291	835	39
H24D	-379	6787	1054	39
H25C	-1406	9599	714	39
H25D	-438	10177	501	39
H26C	-581	6696	212	36
H26D	-1522	6062	432	36
H28D	-2131	10389	-447	59
H28E	-959	9382	-336	59
H28F	-1370	11145	-66	59
H29D	-2732	5079	-152	54
H29E	-1782	5546	-380	54
H29F	-2911	6727	-504	54
H3	-3130(30)	7940(40)	230(9)	29(10)
H1AA	9878	-2233	4043	41
H1AB	10973	-2503	3889	41
H1CA	13760	-3262	5492	52
H1CB	14651	-4745	5353	52
H1CC	14812	-2154	5390	52

H1EA	14669	-4105	5451	52
H1EB	13648	-2782	5531	52
H1EC	14706	-1493	5479	52
H2AA	10825	-1525	4660	45
H2AB	11194	-3832	4514	45
H3AB	12702	-2174	4335	48
H3AA	12697	-2168	4333	48
H4AA	12013	1791	4654	42
H4AB	13083	1549	4481	42
H6A	12893	3408	3933	35
H7AA	11987	2948	3269	30
H7AB	11769	5283	3441	30
H8A	10085	4385	3510	23
H9A	10621	-106	3410	27
H11A	8916	-1165	3478	30
H11B	8583	1303	3546	30
H12A	8972	-436	2839	27
H12B	7836	334	2924	27
H14A	10378	2106	2842	24
H15A	10987	5390	2698	30
H15B	10116	6708	2885	30
H16A	9825	4943	2153	31
H16B	9036	6597	2317	31
H17A	8966	1952	2299	26
H18A	7402	4189	2966	32
H18B	8238	6063	2911	32
H18C	8400	4667	3294	32
H19A	9165	1290	4160	41
H19B	9771	3521	4100	41
H19C	10183	2021	4461	41
H22A	7277	5083	2270	28
H23A	7048	454	2173	53
H23B	6081	2136	2064	53
H23C	6645	1869	2496	53
H24A	8227	4835	1732	32
H24B	7704	2470	1652	32
H25A	6514	6460	1618	34
H25B	5975	4097	1549	34
H26A	7347	5945	1079	27
H26B	6779	3618	1007	27
H28A	6307	9363	926	46
H28B	5486	8736	1199	46
H28C	5056	9249	762	46
H29A	4138	5644	669	40
H29B	4535	4976	1102	40
H29C	4798	3432	770	40
H3A	5960(30)	4900(30)	379(11)	44(12)
H1WA	4740(20)	7140(70)	63(8)	43(12)
H1WB	3800(30)	6370(50)	-107(12)	54(14)

Table A1.10.9. Atomic occupancy for **102**.

Atom	Occupancy	Atom	Occupancy	Atom	Occupancy
O1AA	0.5	O1AB	0.5	O2AA	0.5
O2AB	0.5	C1B	0.5	C1C	0.5
H1CA	0.5	H1CB	0.5	H1CC	0.5
C1D	0.5	C1E	0.5	H1EA	0.5
H1EB	0.5	H1EC	0.5	H3AB	0.5
H3AA	0.5				

A1.11. Crystal structure data of Synthesis of of 5α-cholestan-3-one ethylene ketal, 105.

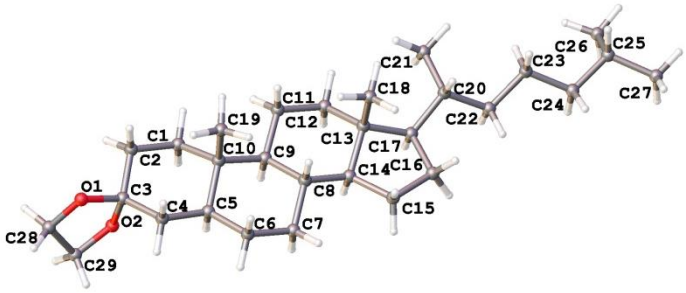

Figure A1.11. One Structure from the unit cell of **105**, determined by X-ray diffraction of a single crystal.

Table A1.11.1. Crystal data and structure refinement for **105**.

Empirical formula	$C_{29}H_{50}O_2$
Formula weight	430.69
Temperature (K)	120
Crystal system	monoclinic
Space group	$P2_1$
a (Å)	15.1002(8)
b (Å)	10.1140(5)
c (Å)	33.9511(17)
α (°)	90
β (°)	95.295(3)
γ (°)	90
Volume (Å^3)	5163.0(5)
Z	8
ρ_{calc}g (cm^3)	1.108
μ (mm^{-1})	0.503
F(000)	1920
Crystal size (mm^3)	0.29 × 0.24 × 0.015
Radiation	CuKα (λ = 1.54178)
2Θ range for data collection (°)	5.228 to 139.998
Index ranges	$-18 \le h \le 18$, $-12 \le k \le 10$, $-41 \le l \le 41$
Reflections collected	73079
Independent reflections	17883 [R_{int} = 0.0929, R_{sigma} = 0.0903]
Data/ restraints/ parameters	17883/25/1142
Goodness-of-fit on F^2	1.025
Final R indexes [I > = 2σ (I)]	R_1 = 0.0712, wR_2 = 0.1485
Final R indexes [all data]	R_1 = 0.1214, wR_2 = 0.1708
Largest diff. peak/ hole (e Å^{-3})	0.33/-0.33
Flack parameter	0.0(3)

Table A1.11.2. Fractional atomic coordinates (×10^4) and equivalent isotropic displacement parameters (Å^2×10^3) for **105**. U_{eq} is defined as 1/3 of the trace of the orthogonalised U_{IJ} tensor.

Atom	*x*	*y*	*z*	U(eq)
O1	4484(2)	8411(4)	2558.3(10)	41.1(10)
O2	4310(2)	9674(4)	3105.8(10)	35.0(9)
C1	5495(3)	7772(5)	3598.4(14)	26.9(11)
C2	4952(3)	7513(5)	3200.6(14)	33.6(12)
C3	4894(3)	8733(5)	2943.2(14)	31.5(12)
C4	5791(3)	9354(5)	2903.8(14)	31.4(12)
C5	6312(3)	9582(5)	3308.1(13)	25.3(11)

C6	7190(3)	10298(5)	3274.3(14)	33.1(12)
C7	7658(3)	10603(5)	3677.6(13)	28.4(11)
C8	7790(3)	9380(5)	3938.5(13)	23.7(11)
C9	6894(3)	8668(5)	3968.1(13)	23.5(11)
C10	6430(3)	8296(5)	3557.0(13)	24.6(11)
C11	6993(3)	7504(5)	4262.3(14)	29.8(12)
C12	7447(3)	7894(5)	4670.7(13)	26.0(11)
C13	8349(3)	8543(5)	4638.6(13)	23.3(11)
C14	8193(3)	9720(5)	4352.1(13)	22.9(10)
C15	9067(3)	10486(5)	4399.5(14)	28.8(11)
C16	9377(3)	10330(5)	4841.2(15)	32.9(12)
C17	8755(3)	9280(5)	5013.9(13)	24.3(11)
C18	9017(3)	7548(5)	4496.7(14)	31.5(12)
C19	6974(3)	7242(5)	3351.1(15)	31.5(12)
C20	3645(4)	9053(6)	2507.4(17)	43.9(15)
C21	3774(4)	10207(6)	2780.4(17)	50.0(16)
C22	9238(3)	8524(5)	5365.7(13)	26.9(11)
C23	9443(3)	9510(5)	5708.8(14)	33.7(12)
C24	9987(4)	8989(6)	6076.6(15)	36.2(13)
C25	10186(4)	10085(5)	6382.0(15)	38.2(13)
C26	10640(3)	9641(5)	6780.2(14)	34.3(12)
C27	10744(4)	10811(6)	7064.2(16)	46.9(15)
C28	11534(4)	8993(7)	6740.8(19)	54.5(17)
C29	8720(3)	7342(5)	5502.4(15)	32.3(12)
O1A	7652(3)	7673(4)	2025.7(12)	57.3(12)
O2A	7119(3)	9584(4)	1725.5(11)	49.4(11)
C1A	6657(3)	8033(6)	970.5(15)	35.3(13)
C2A	7348(3)	7719(7)	1319.1(15)	45.6(15)
C3A	7039(4)	8165(6)	1707.6(16)	43.3(14)
C4A	6112(3)	7723(5)	1768.3(15)	36.9(13)
C5A	5454(3)	8022(5)	1413.7(14)	29.2(11)
C6A	4510(3)	7625(5)	1488.5(14)	31.6(12)
C7A	3838(3)	8008(5)	1145.7(13)	28.6(11)
C8A	4091(3)	7452(5)	751.1(13)	23.7(10)
C9A	5043(3)	7872(5)	678.8(13)	23.8(11)
C10A	5736(3)	7438(5)	1020.5(14)	27.1(11)
C11A	5279(3)	7450(5)	266.6(13)	28.5(11)
C12A	4580(3)	7798(5)	-72.4(13)	27.4(11)
C13A	3661(3)	7272(4)	4.5(13)	23.3(10)
C14A	3450(3)	7870(5)	405.0(13)	24.4(11)
C15A	2463(3)	7608(5)	423.5(14)	29.2(11)
C16A	2065(3)	7670(5)	-9.1(14)	30.8(12)
C17A	2851(3)	7778(5)	-271.0(14)	26.8(11)
C18A	3655(3)	5755(5)	9.5(14)	25.5(11)
C19A	5812(4)	5925(5)	1032.0(15)	35.8(13)
C20A	8044(4)	8743(8)	2230.6(19)	64(2)
C21A	7481(4)	9926(7)	2108.5(17)	54.0(17)
C22A	2637(3)	7128(5)	-678.2(14)	27.5(11)
C23A	1812(3)	7770(5)	-893.1(14)	33.1(12)
C24A	1508(3)	7175(6)	-1295.7(15)	40.2(14)
C25A	595(3)	7659(7)	-1459.9(16)	44.7(15)
C26A	321(3)	7287(6)	-1883.3(16)	42.6(14)
C27A	826(4)	8080(8)	-2170.2(19)	68(2)
C28A	-672(4)	7491(10)	-1983(2)	84(3)
C29A	3409(3)	7151(5)	-938.4(14)	30.9(12)
O1B	5585(2)	2843(4)	2435.0(9)	38.5(9)
O2B	5703(2)	4035(4)	1871.9(10)	35.0(9)
C1B	4556(3)	1994(5)	1409.7(14)	26.6(11)
C2B	5106(3)	1821(5)	1810.6(15)	32.1(12)
C3B	5159(3)	3096(5)	2048.5(14)	30.6(12)

C4B	4254(3)	3707(5)	2077.7(13)	28.0(11)
C5B	3715(3)	3837(5)	1676.3(13)	24.8(11)
C6B	2815(3)	4499(5)	1712.0(14)	31.0(12)
C7B	2317(3)	4729(5)	1306.7(14)	27.7(11)
C8B	2218(3)	3472(5)	1055.3(13)	23.3(10)
C9B	3133(3)	2796(5)	1033.2(13)	21.6(10)
C10B	3609(3)	2512(5)	1448.2(13)	22.8(10)
C11B	3049(3)	1600(5)	756.1(13)	25.4(11)
C12B	2585(3)	1917(5)	344.2(13)	25.1(11)
C13B	1669(3)	2541(4)	367.7(13)	23.3(10)
C14B	1812(3)	3762(4)	639.3(13)	22.1(10)
C15B	923(3)	4492(5)	585.9(14)	29.3(12)
C16B	610(3)	4279(5)	145.9(14)	28.6(11)
C17B	1239(3)	3226(5)	-16.3(13)	23.1(10)
C18B	1016(3)	1540(5)	520.6(14)	29.7(11)
C19B	3090(3)	1480(5)	1666.7(14)	31.6(12)
C20B	6407(4)	3522(7)	2470.3(17)	53.0(17)
C21B	6559(4)	3908(7)	2061.3(19)	61(2)
C22B	769(3)	2417(5)	-354.3(13)	25.2(11)
C23B	508(3)	3342(5)	-707.2(14)	31.1(12)
C24B	-49(4)	2732(5)	-1053.8(14)	37.7(13)
C25B	-219(4)	3628(6)	-1405.3(15)	49.2(16)
C26B	-668(7)	3256(9)	-1804(3)	64(5)
C26K	-860(6)	2986(8)	-1723(3)	30(3)
C27B	-381(5)	1856(8)	-1922(2)	87(3)
C28B	-1652(7)	3191(13)	-1722(4)	58(4)
C28K	-1157(10)	3938(14)	-2065(4)	74(5)
C29B	1317(3)	1249(5)	-482.8(15)	31.9(12)
O1C	2485(3)	3571(5)	2963.7(12)	64.2(13)
O2C	2989(3)	5463(4)	3286.6(11)	51.0(11)
C0AA	7147(3)	3737(5)	5310.9(16)	35.1(13)
C1C	3412(4)	3878(6)	4034.5(15)	43.2(15)
C2C	2736(4)	3568(7)	3680.3(16)	54.5(18)
C3C	3061(4)	4046(6)	3295.7(17)	49.1(16)
C4C	3991(4)	3616(6)	3241.9(15)	47.6(16)
C5C	4644(4)	3903(5)	3603.3(14)	35.9(13)
C6C	5592(4)	3529(5)	3533.7(16)	43.7(15)
C7C	6236(4)	3908(6)	3885.2(16)	42.4(14)
C8C	5974(3)	3335(5)	4277.0(15)	32.7(12)
C9C	5011(3)	3731(5)	4337.8(14)	30.8(12)
C10C	4337(4)	3294(5)	3990.1(15)	34.9(13)
C11C	4751(3)	3293(5)	4745.4(14)	33.1(12)
C12C	5429(3)	3671(5)	5090.7(15)	33.8(13)
C13C	6367(3)	3191(5)	5026.8(15)	30.4(12)
C14C	6591(3)	3784(5)	4628.3(16)	34.1(13)
C15C	7587(3)	3559(6)	4619.9(17)	42.1(15)
C16C	7952(3)	3656(6)	5058.4(17)	42.3(14)
C18C	6408(4)	1664(5)	5023.6(16)	36.7(13)
C19C	4280(5)	1776(6)	3967.4(17)	54.7(17)
C20C	1978(5)	4647(8)	2807(2)	66(2)
C21C	2573(5)	5812(7)	2911.3(19)	64.2(19)
C22C	7357(3)	3097(6)	5717.1(16)	38.3(13)
C23C	8148(4)	3803(7)	5948.2(18)	50.8(16)
C24C	8432(5)	3179(8)	6337(3)	88(3)
C25C	9301(5)	3660(7)	6553(3)	82(2)
C26C	9336(4)	5107(7)	6648(2)	77(2)
C27C	8586(7)	5679(13)	6874(3)	102(4)
C27K	8730(20)	4770(40)	6980(8)	102(4)
C28C	10234(5)	5384(10)	6893(2)	99(3)
C29C	6555(3)	3070(6)	5965.5(16)	41.8(14)

Table A1.11.3. Anisotropic displacement parameters ($Å^2 \times 10^3$) for **105**. The Anisotropic displacement factor exponent takes the form: $-2\pi^2[h^2a^{*2}U_{11}+2hka^*b^*U_{12}+\ldots]$.

Atom	U_{11}	U_{22}	U_{33}	U_{23}	U_{13}	U_{12}
O1	39(2)	55(3)	28(2)	-8.9(18)	-5.6(17)	6.7(18)
O2	33(2)	44(2)	28(2)	-0.1(16)	2.7(16)	9.4(17)
C1	29(3)	24(3)	29(3)	3(2)	2(2)	-1(2)
C2	35(3)	38(3)	27(3)	-1(2)	-2(2)	-5(2)
C3	33(3)	41(3)	20(3)	-1(2)	-1(2)	8(2)
C4	39(3)	34(3)	21(3)	2(2)	3(2)	3(2)
C5	28(3)	22(3)	27(3)	-1(2)	8(2)	1(2)
C6	38(3)	34(3)	27(3)	7(2)	4(2)	-1(2)
C7	29(3)	29(3)	28(3)	6(2)	6(2)	-7(2)
C8	26(3)	22(3)	24(3)	2(2)	5(2)	0(2)
C9	23(3)	22(3)	25(3)	3(2)	4(2)	0(2)
C10	27(3)	24(3)	23(3)	-1(2)	6(2)	2(2)
C11	29(3)	27(3)	33(3)	7(2)	1(2)	-4(2)
C12	27(3)	23(3)	27(3)	9(2)	0(2)	-3(2)
C13	24(3)	21(3)	24(3)	0(2)	2(2)	2(2)
C14	23(2)	21(3)	25(3)	2(2)	6(2)	1(2)
C15	27(3)	26(3)	33(3)	1(2)	5(2)	-5(2)
C16	25(3)	34(3)	39(3)	-1(2)	-1(2)	-3(2)
C17	22(2)	23(3)	28(3)	-3(2)	2(2)	4(2)
C18	35(3)	29(3)	31(3)	-3(2)	2(2)	6(2)
C19	33(3)	31(3)	32(3)	-4(2)	4(2)	3(2)
C20	44(3)	45(4)	41(3)	3(3)	-11(3)	5(3)
C21	50(4)	49(4)	48(4)	-3(3)	-9(3)	11(3)
C22	29(3)	29(3)	22(3)	0(2)	0(2)	2(2)
C23	40(3)	29(3)	31(3)	2(2)	-1(2)	-1(2)
C24	41(3)	36(3)	31(3)	-3(2)	-2(2)	0(2)
C25	49(3)	36(3)	29(3)	-1(2)	-1(3)	-1(3)
C26	38(3)	38(3)	25(3)	3(2)	-2(2)	-4(2)
C27	60(4)	49(4)	30(3)	-6(3)	-3(3)	-8(3)
C28	47(4)	52(4)	61(4)	-14(3)	-9(3)	6(3)
C29	38(3)	28(3)	31(3)	3(2)	1(2)	1(2)
O1A	64(3)	59(3)	45(3)	8(2)	-22(2)	8(2)
O2A	53(3)	50(3)	42(2)	4(2)	-7(2)	-7(2)
C1A	31(3)	45(3)	29(3)	5(2)	0(2)	4(2)
C2A	32(3)	67(4)	36(3)	-1(3)	-7(3)	5(3)
C3A	48(4)	45(4)	35(3)	6(3)	-11(3)	3(3)
C4A	47(3)	34(3)	28(3)	2(2)	-3(3)	7(3)
C5A	36(3)	26(3)	25(3)	0(2)	0(2)	2(2)
C6A	47(3)	26(3)	22(3)	-4(2)	7(2)	-1(2)
C7A	32(3)	29(3)	25(3)	-6(2)	7(2)	-2(2)
C8A	32(3)	17(2)	23(3)	-3.2(19)	8(2)	-1(2)
C9A	28(3)	17(3)	26(3)	0(2)	4(2)	1(2)
C10A	32(3)	23(3)	26(3)	2(2)	1(2)	4(2)
C11A	26(3)	33(3)	27(3)	-2(2)	5(2)	-2(2)
C12A	30(3)	29(3)	24(3)	-1(2)	6(2)	-2(2)
C13A	26(3)	19(3)	26(3)	-3(2)	7(2)	-4(2)
C14A	33(3)	14(2)	27(3)	-2.3(19)	8(2)	2(2)
C15A	28(3)	31(3)	29(3)	-7(2)	7(2)	0(2)
C16A	26(3)	36(3)	31(3)	-1(2)	6(2)	-3(2)
C17A	31(3)	21(3)	29(3)	-3(2)	4(2)	-1(2)
C18A	29(3)	24(3)	23(3)	-2(2)	4(2)	2(2)
C19A	49(3)	30(3)	27(3)	-1(2)	0(2)	12(2)
C20A	54(4)	91(6)	43(4)	-17(4)	-15(3)	6(4)
C21A	56(4)	65(5)	40(4)	5(3)	2(3)	-20(3)
C22A	28(3)	27(3)	27(3)	-2(2)	3(2)	2(2)
C23A	32(3)	38(3)	30(3)	-5(2)	3(2)	9(2)

C24A	37(3)	49(4)	34(3)	-6(3)	-1(2)	5(3)
C25A	34(3)	65(4)	34(3)	-4(3)	-1(3)	11(3)
C26A	37(3)	50(4)	41(3)	0(3)	2(3)	4(3)
C27A	71(5)	86(6)	48(4)	18(4)	11(4)	2(4)
C28A	42(4)	138(8)	67(5)	-24(5)	-12(4)	19(5)
C29A	34(3)	31(3)	28(3)	-2(2)	3(2)	-3(2)
O1B	36(2)	52(3)	25.5(19)	9.0(17)	-6.9(16)	-5.4(18)
O2B	27.9(19)	40(2)	36(2)	13.1(17)	0.0(16)	-4.6(16)
C1B	25(3)	28(3)	26(3)	0(2)	-1(2)	2(2)
C2B	27(3)	34(3)	35(3)	8(2)	-1(2)	6(2)
C3B	32(3)	35(3)	25(3)	10(2)	1(2)	0(2)
C4B	31(3)	31(3)	21(3)	-1(2)	1(2)	-3(2)
C5B	29(3)	23(3)	23(3)	3(2)	2(2)	-2(2)
C6B	34(3)	32(3)	27(3)	-10(2)	4(2)	1(2)
C7B	27(3)	24(3)	31(3)	-4(2)	-1(2)	8(2)
C8B	21(2)	24(3)	25(3)	-1(2)	6(2)	2(2)
C9B	20(2)	22(3)	23(2)	2.2(19)	6(2)	2.6(19)
C10B	24(3)	21(3)	23(3)	2(2)	-1(2)	1(2)
C11B	26(3)	23(3)	27(3)	-5(2)	-2(2)	7(2)
C12B	26(3)	24(3)	25(3)	-2(2)	3(2)	7(2)
C13B	21(2)	20(3)	28(3)	1(2)	1(2)	-2(2)
C14B	21(2)	17(2)	28(3)	1(2)	4(2)	0.1(19)
C15B	22(3)	30(3)	36(3)	-1(2)	1(2)	4(2)
C16B	25(3)	28(3)	33(3)	0(2)	-2(2)	3(2)
C17B	26(3)	20(3)	24(3)	4(2)	2(2)	-2(2)
C18B	34(3)	26(3)	29(3)	1(2)	2(2)	-4(2)
C19B	39(3)	29(3)	27(3)	5(2)	1(2)	-2(2)
C20B	36(3)	83(5)	39(4)	-2(3)	-4(3)	-10(3)
C21B	37(3)	72(5)	70(5)	30(4)	-19(3)	-12(3)
C22B	26(3)	26(3)	24(3)	2(2)	3(2)	-3(2)
C23B	44(3)	25(3)	24(3)	1(2)	4(2)	2(2)
C24B	45(3)	37(3)	28(3)	6(2)	-7(2)	-2(3)
C25B	65(4)	47(4)	33(3)	5(3)	-4(3)	17(3)
C27B	108(7)	91(6)	59(5)	-26(4)	-12(4)	20(5)
C28B	48(8)	50(8)	72(9)	8(7)	-21(7)	-13(6)
C28K	87(11)	73(10)	54(9)	27(8)	-34(8)	-9(8)
C29B	36(3)	26(3)	32(3)	1(2)	-5(2)	-1(2)
O1C	88(4)	68(3)	34(2)	-11(2)	-7(2)	-35(3)
O2C	60(3)	53(3)	39(2)	-10(2)	-3(2)	-9(2)
C0AA	33(3)	24(3)	51(4)	-4(2)	17(3)	2(2)
C1C	47(4)	55(4)	28(3)	-6(3)	7(3)	-14(3)
C2C	53(4)	69(5)	41(4)	-3(3)	5(3)	-26(3)
C3C	65(4)	46(4)	36(3)	-13(3)	2(3)	-23(3)
C4C	82(5)	32(3)	31(3)	-7(2)	19(3)	-12(3)
C5C	55(4)	26(3)	29(3)	-7(2)	16(3)	-6(3)
C6C	70(4)	30(3)	36(3)	2(2)	34(3)	5(3)
C7C	53(4)	31(3)	48(4)	7(3)	30(3)	5(3)
C8C	43(3)	21(3)	38(3)	2(2)	25(3)	1(2)
C9C	37(3)	24(3)	33(3)	-2(2)	13(2)	0(2)
C10C	51(3)	23(3)	33(3)	-5(2)	17(3)	-10(2)
C11C	31(3)	39(3)	31(3)	2(2)	15(2)	-3(2)
C12C	38(3)	32(3)	34(3)	-4(2)	15(2)	0(2)
C13C	32(3)	22(3)	39(3)	1(2)	18(2)	4(2)
C14C	36(3)	20(3)	50(3)	-2(2)	23(3)	3(2)
C15C	40(3)	31(3)	60(4)	5(3)	28(3)	3(3)
C16C	35(3)	33(3)	62(4)	-3(3)	19(3)	0(2)
C18C	45(3)	29(3)	38(3)	2(2)	13(3)	-1(2)
C19C	90(5)	36(4)	40(4)	-6(3)	17(3)	-24(3)
C20C	61(4)	96(6)	39(4)	-9(4)	1(3)	-19(4)
C21C	78(5)	62(5)	52(4)	-7(4)	2(4)	9(4)

C22C	34(3)	35(3)	47(3)	-6(3)	11(3)	5(2)
C23C	32(3)	62(4)	59(4)	-6(3)	7(3)	-2(3)
C24C	78(6)	65(5)	113(7)	14(5)	-32(5)	2(4)
C25C	62(5)	77(6)	105(7)	-5(5)	-8(4)	7(4)
C26C	74(5)	59(5)	103(6)	-8(4)	32(5)	1(4)
C28C	78(6)	117(8)	98(7)	-13(6)	-17(5)	-32(6)
C29C	40(3)	41(3)	46(3)	6(3)	9(3)	1(3)

Table A1.11.4. Bond lengths for **105**.

Atom	Atom	Length (Å)	Atom	Atom	Length (Å)
O1	C3	1.430(6)	O2B	C3B	1.424(6)
O1	C20	1.420(6)	O2B	C21B	1.396(6)
O2	C3	1.441(6)	C1B	C2B	1.538(6)
O2	C21	1.415(6)	C1B	C10B	1.540(6)
C1	C2	1.536(6)	C2B	C3B	1.520(7)
C1	C10	1.528(6)	C3B	C4B	1.511(7)
C2	C3	1.510(7)	C4B	C5B	1.527(6)
C3	C4	1.510(7)	C5B	C6B	1.529(6)
C4	C5	1.535(6)	C5B	C10B	1.549(7)
C5	C6	1.525(6)	C6B	C7B	1.523(6)
C5	C10	1.553(6)	C7B	C8B	1.530(6)
C6	C7	1.514(6)	C8B	C9B	1.550(6)
C7	C8	1.524(6)	C8B	C14B	1.516(6)
C8	C9	1.545(6)	C9B	C10B	1.548(6)
C8	C14	1.517(6)	C9B	C11B	1.530(6)
C9	C10	1.549(6)	C10B	C19B	1.536(6)
C9	C11	1.542(6)	C11B	C12B	1.539(6)
C10	C19	1.551(6)	C12B	C13B	1.528(6)
C11	C12	1.540(6)	C13B	C14B	1.544(6)
C12	C13	1.525(6)	C13B	C17B	1.564(6)
C13	C14	1.542(6)	C13B	C18B	1.537(6)
C13	C17	1.553(6)	C14B	C15B	1.529(6)
C13	C18	1.534(6)	C15B	C16B	1.540(6)
C14	C15	1.527(6)	C16B	C17B	1.561(6)
C15	C16	1.538(6)	C17B	C22B	1.530(6)
C16	C17	1.567(7)	C20B	C21B	1.481(8)
C17	C22	1.544(6)	C22B	C23B	1.543(6)
C20	C21	1.493(8)	C22B	C29B	1.529(7)
C22	C23	1.543(7)	C23B	C24B	1.514(7)
C22	C29	1.524(7)	C24B	C25B	1.501(7)
C23	C24	1.523(7)	C25B	C26B	1.506(8)
C24	C25	1.528(7)	C25B	C26K	1.527(7)
C25	C26	1.526(7)	C26B	C27B	1.544(7)
C26	C27	1.525(7)	C26B	C28B	1.540(7)
C26	C28	1.518(7)	C26K	C27B	1.542(7)
O1A	C3A	1.445(6)	C26K	C28K	1.542(7)
O1A	C20A	1.389(8)	O1C	C3C	1.441(6)
O2A	C3A	1.442(7)	O1C	C20C	1.407(8)
O2A	C21A	1.407(7)	O2C	C3C	1.437(7)
C1A	C2A	1.537(7)	O2C	C21C	1.412(7)
C1A	C10A	1.539(7)	C0AA	C13C	1.554(7)
C2A	C3A	1.507(8)	C0AA	C16C	1.553(7)
C3A	C4A	1.501(8)	C0AA	C22C	1.530(7)
C4A	C5A	1.519(6)	C1C	C2C	1.537(7)
C5A	C6A	1.524(7)	C1C	C10C	1.536(8)
C5A	C10A	1.555(7)	C2C	C3C	1.516(8)
C6A	C7A	1.522(6)	C3C	C4C	1.498(8)
C7A	C8A	1.534(6)	C4C	C5C	1.529(7)

C8A	C9A	1.541(6)	C5C	C6C	1.521(7)
C8A	C14A	1.512(6)	C5C	C10C	1.559(7)
C9A	C10A	1.552(6)	C6C	C7C	1.517(7)
C9A	C11A	1.536(6)	C7C	C8C	1.536(7)
C10A	C19A	1.535(7)	C8C	C9C	1.540(6)
C11A	C12A	1.530(6)	C8C	C14C	1.514(7)
C12A	C13A	1.530(6)	C9C	C10C	1.550(7)
C13A	C14A	1.548(6)	C9C	C11C	1.538(6)
C13A	C17A	1.556(6)	C10C	C19C	1.540(7)
C13A	C18A	1.535(6)	C11C	C12C	1.532(6)
C14A	C15A	1.521(6)	C12C	C13C	1.532(6)
C15A	C16A	1.536(6)	C13C	C14C	1.546(7)
C16A	C17A	1.551(6)	C13C	C18C	1.546(7)
C17A	C22A	1.538(6)	C14C	C15C	1.524(7)
C20A	C21A	1.504(9)	C15C	C16C	1.542(8)
C22A	C23A	1.529(6)	C20C	C21C	1.504(9)
C22A	C29A	1.527(6)	C22C	C23C	1.542(7)
C23A	C24A	1.525(7)	C22C	C29C	1.539(7)
C24A	C25A	1.520(7)	C23C	C24C	1.491(9)
C25A	C26A	1.507(7)	C24C	C25C	1.522(9)
C26A	C27A	1.520(8)	C25C	C26C	1.498(7)
C26A	C28A	1.520(7)	C26C	C27C	1.539(6)
O1B	C3B	1.430(6)	C26C	C27K	1.551(7)
O1B	C20B	1.415(6)	C26C	C28C	1.550(6)

Table A1.11.5. Bond angles for **105**.

Atom	Atom	Atom	Angle (°)	Atom	Atom	Atom	Angle (°)
C20	O1	C3	108.2(4)	C3B	C2B	C1B	111.8(4)
C21	O2	C3	106.2(4)	O1B	C3B	C2B	109.4(4)
C10	C1	C2	113.7(4)	O1B	C3B	C4B	110.2(4)
C3	C2	C1	111.6(4)	O2B	C3B	O1B	106.1(4)
O1	C3	O2	105.8(4)	O2B	C3B	C2B	110.3(4)
O1	C3	C2	109.9(4)	O2B	C3B	C4B	108.4(4)
O1	C3	C4	109.2(4)	C4B	C3B	C2B	112.2(4)
O2	C3	C2	108.9(4)	C3B	C4B	C5B	112.8(4)
O2	C3	C4	110.1(4)	C4B	C5B	C6B	111.8(4)
C2	C3	C4	112.7(4)	C4B	C5B	C10B	113.1(4)
C3	C4	C5	111.9(4)	C6B	C5B	C10B	111.5(4)
C4	C5	C10	112.6(4)	C7B	C6B	C5B	111.3(4)
C6	C5	C4	112.4(4)	C6B	C7B	C8B	113.1(4)
C6	C5	C10	112.4(4)	C7B	C8B	C9B	110.6(4)
C7	C6	C5	111.4(4)	C14B	C8B	C7B	111.7(4)
C6	C7	C8	112.6(4)	C14B	C8B	C9B	109.0(4)
C7	C8	C9	110.3(4)	C10B	C9B	C8B	112.2(4)
C14	C8	C7	111.9(4)	C11B	C9B	C8B	110.8(4)
C14	C8	C9	108.9(4)	C11B	C9B	C10B	114.7(4)
C8	C9	C10	112.4(4)	C1B	C10B	C5B	106.4(4)
C11	C9	C8	111.4(4)	C1B	C10B	C9B	110.0(4)
C11	C9	C10	114.0(4)	C9B	C10B	C5B	108.2(4)
C1	C10	C5	106.2(4)	C19B	C10B	C1B	109.2(4)
C1	C10	C9	110.3(4)	C19B	C10B	C5B	112.3(4)
C1	C10	C19	109.6(4)	C19B	C10B	C9B	110.6(4)
C9	C10	C5	107.9(4)	C9B	C11B	C12B	113.5(4)
C9	C10	C19	111.1(4)	C13B	C12B	C11B	112.2(4)
C19	C10	C5	111.7(4)	C12B	C13B	C14B	106.5(4)
C12	C11	C9	113.3(4)	C12B	C13B	C17B	116.6(4)
C13	C12	C11	111.9(4)	C12B	C13B	C18B	111.0(4)
C12	C13	C14	107.0(4)	C14B	C13B	C17B	99.6(4)
C12	C13	C17	115.9(4)	C18B	C13B	C14B	112.6(4)

C12	C13	C18	111.0(4)	C18B	C13B	C17B	110.1(4)
C14	C13	C17	99.9(4)	C8B	C14B	C13B	115.1(4)
C18	C13	C14	112.0(4)	C8B	C14B	C15B	118.6(4)
C18	C13	C17	110.5(4)	C15B	C14B	C13B	104.1(4)
C8	C14	C13	115.7(4)	C14B	C15B	C16B	103.6(4)
C8	C14	C15	118.8(4)	C15B	C16B	C17B	107.2(4)
C15	C14	C13	104.2(4)	C16B	C17B	C13B	103.1(4)
C14	C15	C16	103.5(4)	C22B	C17B	C13B	121.1(4)
C15	C16	C17	107.2(4)	C22B	C17B	C16B	112.0(4)
C13	C17	C16	102.9(4)	O1B	C20B	C21B	105.0(4)
C22	C17	C13	121.3(4)	O2B	C21B	C20B	103.9(5)
C22	C17	C16	111.6(4)	C17B	C22B	C23B	109.0(4)
O1	C20	C21	102.6(4)	C29B	C22B	C17B	113.7(4)
O2	C21	C20	102.6(5)	C29B	C22B	C23B	110.7(4)
C23	C22	C17	108.1(4)	C24B	C23B	C22B	116.1(4)
C29	C22	C17	113.9(4)	C25B	C24B	C23B	114.4(5)
C29	C22	C23	110.5(4)	C24B	C25B	C26B	126.5(6)
C24	C23	C22	116.8(4)	C24B	C25B	C26K	110.9(6)
C23	C24	C25	111.3(4)	C25B	C26B	C27B	110.4(6)
C26	C25	C24	115.6(5)	C25B	C26B	C28B	102.0(7)
C27	C26	C25	110.1(5)	C28B	C26B	C27B	107.8(9)
C28	C26	C25	112.3(5)	C25B	C26K	C27B	109.4(6)
C28	C26	C27	110.5(5)	C25B	C26K	C28K	112.9(8)
C20A	O1A	C3A	108.7(5)	C27B	C26K	C28K	104.4(9)
C21A	O2A	C3A	107.9(4)	C20C	O1C	C3C	107.8(5)
C2A	C1A	C10A	113.0(4)	C21C	O2C	C3C	107.2(5)
C3A	C2A	C1A	111.7(5)	C16C	C0AA	C13C	103.0(4)
O1A	C3A	C2A	108.8(5)	C22C	C0AA	C13C	119.4(4)
O1A	C3A	C4A	109.7(5)	C22C	C0AA	C16C	111.6(4)
O2A	C3A	O1A	105.4(4)	C10C	C1C	C2C	112.9(5)
O2A	C3A	C2A	107.6(5)	C3C	C2C	C1C	111.3(5)
O2A	C3A	C4A	111.4(5)	O1C	C3C	C2C	110.3(5)
C4A	C3A	C2A	113.5(5)	O1C	C3C	C4C	108.2(5)
C3A	C4A	C5A	112.5(4)	O2C	C3C	O1C	106.1(5)
C4A	C5A	C6A	111.7(4)	O2C	C3C	C2C	107.9(5)
C4A	C5A	C10A	113.2(4)	O2C	C3C	C4C	110.9(5)
C6A	C5A	C10A	112.2(4)	C4C	C3C	C2C	113.2(5)
C7A	C6A	C5A	111.9(4)	C3C	C4C	C5C	112.9(4)
C6A	C7A	C8A	111.9(4)	C4C	C5C	C10C	112.5(4)
C7A	C8A	C9A	110.4(4)	C6C	C5C	C4C	112.0(4)
C14A	C8A	C7A	112.5(4)	C6C	C5C	C10C	113.0(4)
C14A	C8A	C9A	109.8(4)	C7C	C6C	C5C	111.0(4)
C8A	C9A	C10A	112.2(4)	C6C	C7C	C8C	112.9(5)
C11A	C9A	C8A	111.5(4)	C7C	C8C	C9C	109.9(4)
C11A	C9A	C10A	113.9(4)	C14C	C8C	C7C	112.3(4)
C1A	C10A	C5A	105.6(4)	C14C	C8C	C9C	109.7(4)
C1A	C10A	C9A	111.1(4)	C8C	C9C	C10C	112.7(4)
C9A	C10A	C5A	108.4(4)	C11C	C9C	C8C	111.6(4)
C19A	C10A	C1A	109.0(4)	C11C	C9C	C10C	113.6(4)
C19A	C10A	C5A	112.5(4)	C1C	C10C	C5C	105.9(5)
C19A	C10A	C9A	110.2(4)	C1C	C10C	C9C	110.8(4)
C12A	C11A	C9A	114.8(4)	C1C	C10C	C19C	109.9(5)
C11A	C12A	C13A	111.5(4)	C9C	C10C	C5C	107.7(4)
C12A	C13A	C14A	106.1(4)	C19C	C10C	C5C	111.8(4)
C12A	C13A	C17A	117.2(4)	C19C	C10C	C9C	110.6(5)
C12A	C13A	C18A	110.9(4)	C12C	C11C	C9C	114.2(4)
C14A	C13A	C17A	100.7(4)	C11C	C12C	C13C	111.9(4)
C18A	C13A	C14A	112.2(4)	C12C	C13C	C0AA	117.2(4)
C18A	C13A	C17A	109.3(4)	C12C	C13C	C14C	106.3(4)
C8A	C14A	C13A	113.8(4)	C12C	C13C	C18C	110.8(4)

C8A	C14A	C15A	118.6(4)	C14C	C13C	C0AA	101.0(4)
C15A	C14A	C13A	104.5(4)	C18C	C13C	C0AA	109.4(4)
C14A	C15A	C16A	104.6(4)	C18C	C13C	C14C	111.7(4)
C15A	C16A	C17A	107.4(4)	C8C	C14C	C13C	113.9(4)
C16A	C17A	C13A	103.5(4)	C8C	C14C	C15C	118.5(4)
C22A	C17A	C13A	119.2(4)	C15C	C14C	C13C	104.7(4)
C22A	C17A	C16A	112.1(4)	C14C	C15C	C16C	103.8(4)
O1A	C20A	C21A	106.2(5)	C15C	C16C	C0AA	107.9(4)
O2A	C21A	C20A	102.7(5)	O1C	C20C	C21C	103.0(5)
C23A	C22A	C17A	110.0(4)	O2C	C21C	C20C	102.9(6)
C29A	C22A	C17A	113.9(4)	C0AA	C22C	C23C	110.4(5)
C29A	C22A	C23A	110.5(4)	C0AA	C22C	C29C	113.2(4)
C24A	C23A	C22A	115.1(4)	C29C	C22C	C23C	109.9(5)
C25A	C24A	C23A	112.9(4)	C24C	C23C	C22C	113.6(6)
C26A	C25A	C24A	115.4(5)	C23C	C24C	C25C	117.1(7)
C25A	C26A	C27A	111.7(5)	C26C	C25C	C24C	115.3(6)
C25A	C26A	C28A	110.9(5)	C25C	C26C	C27C	117.5(8)
C27A	C26A	C28A	109.2(6)	C25C	C26C	C27K	86.1(17)
C20B	O1B	C3B	107.9(4)	C25C	C26C	C28C	107.7(6)
C21B	O2B	C3B	106.9(4)	C27C	C26C	C28C	108.1(7)
C2B	C1B	C10B	113.2(4)	C28C	C26C	C27K	101.0(15)

Table A1.11.6. Torsion angles for **105.**

A	B	C	D	Angle (°)	A	B	C	D	Angle (°)
O1	C3	C4	C5	-173.6(4)	O2B	C3B	C4B	C5B	71.7(5)
O1	C20	C21	O2	-37.3(6)	C1B	C2B	C3B	O1B	173.2(4)
O2	C3	C4	C5	70.6(5)	C1B	C2B	C3B	O2B	-70.4(5)
C1	C2	C3	O1	172.6(4)	C1B	C2B	C3B	C4B	50.5(5)
C1	C2	C3	O2	-71.9(5)	C2B	C1B	C10B	C5B	57.2(5)
C1	C2	C3	C4	50.6(6)	C2B	C1B	C10B	C9B	174.2(4)
C2	C1	C10	C5	57.5(5)	C2B	C1B	C10B	C19B	-64.3(5)
C2	C1	C10	C9	174.1(4)	C2B	C3B	C4B	C5B	-50.3(5)
C2	C1	C10	C19	-63.4(5)	C3B	O1B	C20B	C21B	-13.9(6)
C2	C3	C4	C5	-51.2(6)	C3B	O2B	C21B	C20B	-32.3(6)
C3	O1	C20	C21	25.8(6)	C3B	C4B	C5B	C6B	-178.1(4)
C3	O2	C21	C20	35.1(6)	C3B	C4B	C5B	C10B	55.0(5)
C3	C4	C5	C6	-175.9(4)	C4B	C5B	C6B	C7B	175.2(4)
C3	C4	C5	C10	55.8(5)	C4B	C5B	C10B	C1B	-56.4(5)
C4	C5	C6	C7	175.7(4)	C4B	C5B	C10B	C9B	-174.6(4)
C4	C5	C10	C1	-57.3(5)	C4B	C5B	C10B	C19B	63.1(5)
C4	C5	C10	C9	-175.5(4)	C5B	C6B	C7B	C8B	53.7(5)
C4	C5	C10	C19	62.2(5)	C6B	C5B	C10B	C1B	176.5(4)
C5	C6	C7	C8	54.2(6)	C6B	C5B	C10B	C9B	58.3(5)
C6	C5	C10	C1	174.5(4)	C6B	C5B	C10B	C19B	-64.0(5)
C6	C5	C10	C9	56.3(5)	C6B	C7B	C8B	C9B	-52.1(5)
C6	C5	C10	C19	-66.0(5)	C6B	C7B	C8B	C14B	-173.8(4)
C6	C7	C8	C9	-54.0(5)	C7B	C8B	C9B	C10B	54.8(5)
C6	C7	C8	C14	-175.4(4)	C7B	C8B	C9B	C11B	-175.6(4)
C7	C8	C9	C10	56.2(5)	C7B	C8B	C14B	C13B	-178.7(4)
C7	C8	C9	C11	-174.5(4)	C7B	C8B	C14B	C15B	-54.6(6)
C7	C8	C14	C13	179.8(4)	C8B	C9B	C10B	C1B	-173.4(4)
C7	C8	C14	C15	-55.1(6)	C8B	C9B	C10B	C5B	-57.5(5)
C8	C9	C10	C1	-172.1(4)	C8B	C9B	C10B	C19B	65.9(5)
C8	C9	C10	C5	-56.6(5)	C8B	C9B	C11B	C12B	52.4(5)
C8	C9	C10	C19	66.1(5)	C8B	C14B	C15B	C16B	-165.5(4)
C8	C9	C11	C12	52.1(5)	C9B	C8B	C14B	C13B	58.8(5)
C8	C14	C15	C16	-166.0(4)	C9B	C8B	C14B	C15B	-177.1(4)
C9	C8	C14	C13	57.5(5)	C9B	C11B	C12B	C13B	-55.3(5)
C9	C8	C14	C15	-177.4(4)	C10B	C1B	C2B	C3B	-56.1(6)

C9	C11	C12	C13	-55.0(5)	C10B	C5B	C6B	C7B	-57.0(5)
C10	C1	C2	C3	-55.8(6)	C10B	C9B	C11B	C12B	-179.3(4)
C10	C5	C6	C7	-56.0(5)	C11B	C9B	C10B	C1B	59.1(5)
C10	C9	C11	C12	-179.5(4)	C11B	C9B	C10B	C5B	175.0(4)
C11	C9	C10	C1	59.9(5)	C11B	C9B	C10B	C19B	-61.7(5)
C11	C9	C10	C5	175.5(4)	C11B	C12B	C13B	C14B	55.0(5)
C11	C9	C10	C19	-61.8(5)	C11B	C12B	C13B	C17B	165.1(4)
C11	C12	C13	C14	55.1(5)	C11B	C12B	C13B	C18B	-67.8(5)
C11	C12	C13	C17	165.5(4)	C12B	C13B	C14B	C8B	-59.4(5)
C11	C12	C13	C18	-67.4(5)	C12B	C13B	C14B	C15B	169.0(4)
C12	C13	C14	C8	-59.1(5)	C12B	C13B	C17B	C16B	-153.7(4)
C12	C13	C14	C15	168.6(4)	C12B	C13B	C17B	C22B	80.2(5)
C12	C13	C17	C16	-154.4(4)	C13B	C14B	C15B	C16B	-36.1(5)
C12	C13	C17	C22	80.0(5)	C13B	C17B	C22B	C23B	-173.8(4)
C13	C14	C15	C16	-35.6(5)	C13B	C17B	C22B	C29B	-49.9(6)
C13	C17	C22	C23	-172.3(4)	C14B	C8B	C9B	C10B	177.9(4)
C13	C17	C22	C29	-49.0(6)	C14B	C8B	C9B	C11B	-52.4(5)
C14	C8	C9	C10	179.4(4)	C14B	C13B	C17B	C16B	-39.7(4)
C14	C8	C9	C11	-51.3(5)	C14B	C13B	C17B	C22B	-165.8(4)
C14	C13	C17	C16	-40.0(4)	C14B	C15B	C16B	C17B	10.2(5)
C14	C13	C17	C22	-165.6(4)	C15B	C16B	C17B	C13B	18.8(5)
C14	C15	C16	C17	9.6(5)	C15B	C16B	C17B	C22B	150.5(4)
C15	C16	C17	C13	19.3(5)	C16B	C17B	C22B	C23B	64.2(5)
C15	C16	C17	C22	151.0(4)	C16B	C17B	C22B	C29B	-171.8(4)
C16	C17	C22	C23	66.2(5)	C17B	C13B	C14B	C8B	179.0(4)
C16	C17	C22	C29	-170.5(4)	C17B	C13B	C14B	C15B	47.5(4)
C17	C13	C14	C8	179.8(4)	C17B	C22B	C23B	C24B	-173.9(4)
C17	C13	C14	C15	47.5(4)	C18B	C13B	C14B	C8B	62.4(5)
C17	C22	C23	C24	-175.3(4)	C18B	C13B	C14B	C15B	-69.1(5)
C18	C13	C14	C8	62.7(5)	C18B	C13B	C17B	C16B	78.7(4)
C18	C13	C14	C15	-69.5(5)	C18B	C13B	C17B	C22B	-47.4(6)
C18	C13	C17	C16	78.2(4)	C20B	O1B	C3B	O2B	-5.5(5)
C18	C13	C17	C22	-47.4(6)	C20B	O1B	C3B	C2B	113.5(5)
C20	O1	C3	O2	-4.9(5)	C20B	O1B	C3B	C4B	-122.7(5)
C20	O1	C3	C2	112.5(5)	C21B	O2B	C3B	O1B	24.1(6)
C20	O1	C3	C4	-123.4(5)	C21B	O2B	C3B	C2B	-94.3(5)
C21	O2	C3	O1	-19.6(5)	C21B	O2B	C3B	C4B	142.5(5)
C21	O2	C3	C2	-137.7(4)	C22B	C23B	C24B	C25B	-174.8(4)
C21	O2	C3	C4	98.3(5)	C23B	C24B	C25B	C26B	173.3(6)
C22	C23	C24	C25	176.7(4)	C23B	C24B	C25B	C26K	-174.3(5)
C23	C24	C25	C26	173.6(4)	C24B	C25B	C26B	C27B	-38.9(12)
C24	C25	C26	C27	-176.3(5)	C24B	C25B	C26B	C28B	75.5(9)
C24	C25	C26	C28	60.1(7)	C24B	C25B	C26K	C27B	-72.1(9)
C29	C22	C23	C24	59.4(6)	C24B	C25B	C26K	C28K	172.1(9)
O1A	C3A	C4A	C5A	-171.1(4)	C29B	C22B	C23B	C24B	60.4(6)
O1A	C20A	C21A	O2A	-28.0(6)	O1C	C3C	C4C	C5C	-172.2(5)
O2A	C3A	C4A	C5A	72.5(6)	O1C	C20C	C21C	O2C	-36.3(6)
C1A	C2A	C3A	O1A	171.7(5)	O2C	C3C	C4C	C5C	71.8(6)
C1A	C2A	C3A	O2A	-74.5(6)	C0AA	C13C	C14C	C8C	175.5(4)
C1A	C2A	C3A	C4A	49.3(7)	C0AA	C13C	C14C	C15C	44.5(5)
C2A	C1A	C10A	C5A	58.2(6)	C0AA	C22C	C23C	C24C	-176.2(6)
C2A	C1A	C10A	C9A	175.5(4)	C1C	C2C	C3C	O1C	171.3(5)
C2A	C1A	C10A	C19A	-62.9(6)	C1C	C2C	C3C	O2C	-73.3(7)
C2A	C3A	C4A	C5A	-49.2(7)	C1C	C2C	C3C	C4C	49.8(7)
C3A	O1A	C20A	C21A	15.7(7)	C2C	C1C	C10C	C5C	58.8(6)
C3A	O2A	C21A	C20A	29.7(6)	C2C	C1C	C10C	C9C	175.4(5)
C3A	C4A	C5A	C6A	-177.4(4)	C2C	C1C	C10C	C19C	-62.1(6)
C3A	C4A	C5A	C10A	54.9(6)	C2C	C3C	C4C	C5C	-49.6(7)
C4A	C5A	C6A	C7A	176.1(4)	C3C	O1C	C20C	C21C	28.1(6)
C4A	C5A	C10A	C1A	-57.7(5)	C3C	O2C	C21C	C20C	30.9(7)

C4A	C5A	C10A	C9A	-176.9(4)	C3C	C4C	C5C	C6C	-176.8(5)
C4A	C5A	C10A	C19A	61.1(6)	C3C	C4C	C5C	C10C	54.7(6)
C5A	C6A	C7A	C8A	54.5(5)	C4C	C5C	C6C	C7C	176.1(4)
C6A	C5A	C10A	C1A	174.8(4)	C4C	C5C	C10C	C1C	-57.5(5)
C6A	C5A	C10A	C9A	55.6(5)	C4C	C5C	C10C	C9C	-176.1(4)
C6A	C5A	C10A	C19A	-66.4(5)	C4C	C5C	C10C	C19C	62.2(6)
C6A	C7A	C8A	C9A	-54.5(5)	C5C	C6C	C7C	C8C	54.2(6)
C6A	C7A	C8A	C14A	-177.7(4)	C6C	C5C	C10C	C1C	174.5(4)
C7A	C8A	C9A	C10A	56.7(5)	C6C	C5C	C10C	C9C	56.0(5)
C7A	C8A	C9A	C11A	-174.1(4)	C6C	C5C	C10C	C19C	-65.8(6)
C7A	C8A	C14A	C13A	-177.3(4)	C6C	C7C	C8C	C9C	-54.3(6)
C7A	C8A	C14A	C15A	-53.7(6)	C6C	C7C	C8C	C14C	-176.7(4)
C8A	C9A	C10A	C1A	-172.1(4)	C7C	C8C	C9C	C10C	56.4(6)
C8A	C9A	C10A	C5A	-56.5(5)	C7C	C8C	C9C	C11C	-174.5(4)
C8A	C9A	C10A	C19A	67.0(5)	C7C	C8C	C14C	C13C	-178.1(4)
C8A	C9A	C11A	C12A	48.4(5)	C7C	C8C	C14C	C15C	-54.2(6)
C8A	C14A	C15A	C16A	-160.3(4)	C8C	C9C	C10C	C1C	-171.9(4)
C9A	C8A	C14A	C13A	59.2(5)	C8C	C9C	C10C	C5C	-56.5(5)
C9A	C8A	C14A	C15A	-177.2(4)	C8C	C9C	C10C	C19C	66.0(6)
C9A	C11A	C12A	C13A	-53.5(5)	C8C	C9C	C11C	C12C	49.1(6)
C10A	C1A	C2A	C3A	-55.9(7)	C8C	C14C	C15C	C16C	-160.7(4)
C10A	C5A	C6A	C7A	-55.7(5)	C9C	C8C	C14C	C13C	59.4(5)
C10A	C9A	C11A	C12A	176.6(4)	C9C	C8C	C14C	C15C	-176.8(4)
C11A	C9A	C10A	C1A	60.0(5)	C9C	C11C	C12C	C13C	-53.4(6)
C11A	C9A	C10A	C5A	175.6(4)	C10C	C1C	C2C	C3C	-56.5(7)
C11A	C9A	C10A	C19A	-60.9(5)	C10C	C5C	C6C	C7C	-55.7(6)
C11A	C12A	C13A	C14A	56.9(5)	C10C	C9C	C11C	C12C	177.8(4)
C11A	C12A	C13A	C17A	168.3(4)	C11C	C9C	C10C	C1C	60.0(6)
C11A	C12A	C13A	C18A	-65.3(5)	C11C	C9C	C10C	C5C	175.4(4)
C12A	C13A	C14A	C8A	-62.3(5)	C11C	C9C	C10C	C19C	-62.2(6)
C12A	C13A	C14A	C15A	166.7(4)	C11C	C12C	C13C	C0AA	168.3(4)
C12A	C13A	C17A	C16A	-152.8(4)	C11C	C12C	C13C	C14C	56.3(5)
C12A	C13A	C17A	C22A	81.9(5)	C11C	C12C	C13C	C18C	-65.2(6)
C13A	C14A	C15A	C16A	-32.2(5)	C12C	C13C	C14C	C8C	-61.6(5)
C13A	C17A	C22A	C23A	179.3(4)	C12C	C13C	C14C	C15C	167.4(4)
C13A	C17A	C22A	C29A	-56.1(6)	C13C	C0AA	C16C	C15C	19.3(5)
C14A	C8A	C9A	C10A	-178.6(4)	C13C	C0AA	C22C	C23C	-179.6(4)
C14A	C8A	C9A	C11A	-49.4(5)	C13C	C0AA	C22C	C29C	-55.8(6)
C14A	C13A	C17A	C16A	-38.3(4)	C13C	C14C	C15C	C16C	-32.4(5)
C14A	C13A	C17A	C22A	-163.6(4)	C14C	C8C	C9C	C10C	-179.6(4)
C14A	C15A	C16A	C17A	7.5(5)	C14C	C8C	C9C	C11C	-50.5(6)
C15A	C16A	C17A	C13A	19.6(5)	C14C	C15C	C16C	C0AA	7.7(6)
C15A	C16A	C17A	C22A	149.4(4)	C16C	C0AA	C13C	C12C	-153.2(4)
C16A	C17A	C22A	C23A	58.2(5)	C16C	C0AA	C13C	C14C	-38.2(5)
C16A	C17A	C22A	C29A	-177.1(4)	C16C	C0AA	C13C	C18C	79.6(5)
C17A	C13A	C14A	C8A	175.0(4)	C16C	C0AA	C22C	C23C	60.3(6)
C17A	C13A	C14A	C15A	44.1(4)	C16C	C0AA	C22C	C29C	-175.9(5)
C17A	C22A	C23A	C24A	-177.7(4)	C18C	C13C	C14C	C8C	59.4(6)
C18A	C13A	C14A	C8A	58.9(5)	C18C	C13C	C14C	C15C	-71.6(5)
C18A	C13A	C14A	C15A	-72.0(5)	C20C	O1C	C3C	O2C	-9.8(6)
C18A	C13A	C17A	C16A	80.0(4)	C20C	O1C	C3C	C2C	106.8(6)
C18A	C13A	C17A	C22A	-45.3(5)	C20C	O1C	C3C	C4C	-128.8(5)
C20A	O1A	C3A	O2A	2.4(6)	C21C	O2C	C3C	O1C	-14.3(6)
C20A	O1A	C3A	C2A	117.6(6)	C21C	O2C	C3C	C2C	-132.4(5)
C20A	O1A	C3A	C4A	-117.7(6)	C21C	O2C	C3C	C4C	103.0(5)
C21A	O2A	C3A	O1A	-21.0(6)	C22C	C0AA	C13C	C12C	82.5(6)
C21A	O2A	C3A	C2A	-137.1(5)	C22C	C0AA	C13C	C14C	-162.5(4)
C21A	O2A	C3A	C4A	97.9(5)	C22C	C0AA	C13C	C18C	-44.7(6)
C22A	C23A	C24A	C25A	168.9(5)	C22C	C0AA	C16C	C15C	148.7(5)
C23A	C24A	C25A	C26A	170.4(5)	C22C	C23C	C24C	C25C	169.8(6)

C24A	C25A	C26A	C27A	-73.0(7)	C23C	C24C	C25C	C26C	58.9(11)
C24A	C25A	C26A	C28A	165.0(6)	C24C	C25C	C26C	C27C	53.4(12)
C29A	C22A	C23A	C24A	55.7(6)	C24C	C25C	C26C	C27K	75.3(16)
O1B	C3B	C4B	C5B	-172.6(4)	C24C	C25C	C26C	C28C	175.6(7)
O1B	C20B	C21B	O2B	28.4(7)	C29C	C22C	C23C	C24C	58.3(7)

Table A1.11.7. Hydrogen atom coordinates ($Å \times 10^4$) and isotropic displacement parameters ($Å^2 \times 10^3$) for **105**.

Atom	*x*	*y*	*z*	U(eq)
H1A	5172	8420	3750	32
H1B	5541	6938	3752	32
H2A	5234	6789	3060	40
H2B	4345	7225	3249	40
H4A	5706	10211	2764	38
H4B	6140	8771	2742	38
H5	5940	10188	3457	30
H6A	7580	9740	3124	40
H6B	7075	11132	3126	40
H7A	7304	11262	3812	34
H7B	8245	11001	3644	34
H8	8202	8762	3815	28
H9	6496	9324	4084	28
H11E	6396	7140	4296	36
H11F	7345	6796	4149	36
H12E	7058	8514	4800	31
H12F	7527	7095	4839	31
H14	7746	10297	4468	27
H15E	8973	11429	4329	35
H15F	9506	10104	4232	35
H16E	9335	11185	4980	39
H16F	10003	10028	4875	39
H17	8259	9781	5121	29
H18G	8825	7275	4225	47
H18H	9049	6772	4670	47
H18I	9605	7962	4504	47
H19G	7587	7555	3342	47
H19H	6703	7095	3081	47
H19I	6977	6412	3500	47
H20E	3164	8467	2584	53
H20F	3505	9343	2230	53
H21E	4080	10943	2656	60
H21F	3198	10529	2861	60
H22	9816	8193	5283	32
H23E	9765	10272	5607	40
H23F	8871	9847	5789	40
H24E	10553	8616	6001	43
H24F	9654	8271	6195	43
H25G	10569	10752	6268	46
H25H	9620	10526	6428	46
H26	10247	8975	6894	41
H27M	11086	11510	6948	70
H27N	11057	10523	7315	70
H27O	10155	11150	7112	70
H28J	11448	8195	6578	82
H28K	11809	8753	7004	82
H28L	11921	9612	6615	82
H29G	8153	7646	5589	48
H29H	9068	6904	5723	48
H29I	8606	6718	5283	48

H1AA	6872	7686	724	42
H1AB	6599	9004	943	42
H2AA	7459	6755	1329	55
H2AB	7915	8166	1277	55
H4AA	5916	8173	2004	44
H4AB	6115	6760	1820	44
H5A	5449	9005	1381	35
H6AA	4487	6657	1529	38
H6AB	4348	8060	1733	38
H7AA	3802	8984	1128	34
H7AB	3244	7671	1197	34
H8A	4078	6465	768	28
H9A	5046	8861	680	29
H11G	5848	7874	215	34
H11H	5374	6482	267	34
H12G	4757	7415	-322	33
H12H	4550	8770	-104	33
H14A	3516	8849	380	29
H15G	2193	8289	585	35
H15H	2365	6727	539	35
H16G	1670	8448	-51	37
H16H	1713	6863	-78	37
H17A	2951	8740	-318	32
H18J	4090	5436	220	38
H18K	3811	5420	-246	38
H18L	3061	5440	58	38
H19J	5218	5537	1033	54
H19K	6179	5656	1272	54
H19L	6089	5617	799	54
H20G	8661	8871	2161	77
H20H	8058	8598	2519	77
H21G	7008	10062	2288	65
H21H	7847	10738	2105	65
H22A	2490	6181	-632	33
H23G	1317	7703	-722	40
H23H	1936	8722	-929	40
H24G	1946	7401	-1485	48
H24H	1493	6200	-1271	48
H25I	147	7304	-1292	54
H25J	583	8635	-1438	54
H26D	457	6329	-1918	51
H27P	641	9008	-2165	102
H27Q	697	7726	-2438	102
H27R	1466	8016	-2092	102
H28M	-1001	6961	-1803	125
H28N	-838	7216	-2256	125
H28O	-817	8428	-1953	125
H29J	3576	8069	-987	46
H29K	3228	6718	-1191	46
H29L	3919	6681	-805	46
H1BA	4517	1132	1271	32
H1BB	4868	2618	1246	32
H2BA	4833	1122	1964	39
H2BB	5715	1531	1766	39
H4BA	4330	4594	2199	34
H4BB	3918	3155	2253	34
H5B	4057	4441	1513	30
H6BA	2451	3932	1872	37
H6BB	2908	5356	1850	37
H7BA	2639	5402	1164	33

H7BB	1719	5083	1342	33
H8B	1819	2846	1183	28
H9B	3514	3451	907	26
H11A	2710	899	879	31
H11B	3651	1250	725	31
H12A	2961	2532	206	30
H12B	2518	1093	187	30
H14B	2249	4336	516	27
H15A	1001	5444	647	35
H15B	493	4112	758	35
H16A	642	5119	-2	34
H16B	-12	3961	116	34
H17B	1726	3726	-131	28
H18A	1214	1302	795	45
H18B	996	744	355	45
H18C	422	1934	510	45
H19A	2465	1748	1660	47
H19B	3345	1417	1942	47
H19C	3130	618	1538	47
H20A	6891	2940	2585	64
H20B	6377	4313	2641	64
H21A	6887	4756	2058	73
H21B	6899	3219	1933	73
H22B	209	2056	-261	30
H23A	177	4102	-610	37
H23B	1061	3693	-804	37
H24A	254	1925	-1137	45
H24B	-628	2459	-965	45
H25C	350	3826	-1516	59
H25D	-474	4472	-1321	59
H25A	369	3988	-1456	59
H25B	-564	4382	-1313	59
H26B	-563	3928	-2011	77
H26K	-1392	2634	-1603	36
H27D	-793	1444	-2127	131
H27E	132	2212	-2044	131
H27F	-180	1194	-1723	131
H27A	-678	1629	-2182	131
H27B	265	1835	-1934	131
H27C	-549	1216	-1726	131
H28A	-2009	2856	-1956	87
H28B	-1859	4077	-1658	87
H28C	-1716	2597	-1498	87
H28D	-1463	4699	-1961	111
H28E	-1563	3476	-2261	111
H28F	-635	4243	-2191	111
H29A	1864	1578	-583	48
H29B	970	754	-692	48
H29C	1469	667	-256	48
H0AA	7026	4695	5356	42
H1CA	3465	4849	4065	52
H1CB	3188	3520	4278	52
H2CA	2633	2602	3665	65
H2CB	2162	4001	3719	65
H4CA	4196	4076	3009	57
H4CB	3992	2655	3187	57
H5C	4641	4884	3641	43
H6CA	5627	2564	3488	52
H6CB	5763	3984	3294	52
H7CA	6262	4883	3906	51

H7CB	6838	3588	3840	51
H8C	6003	2349	4261	39
H9C	4999	4719	4339	37
H11C	4170	3693	4789	40
H11D	4675	2321	4744	40
H12C	5245	3281	5338	41
H12D	5436	4645	5122	41
H14C	6507	4761	4650	41
H15C	7854	4244	4460	51
H15D	7708	2677	4510	51
H16C	8329	4453	5101	51
H16D	8318	2869	5135	51
H18D	5982	1322	4813	55
H18E	6258	1322	5279	55
H18F	7010	1378	4977	55
H19D	4881	1404	3978	82
H19E	3944	1516	3719	82
H19F	3978	1442	4191	82
H20C	1411	4722	2931	79
H20D	1847	4563	2517	79
H21C	3016	5929	2716	77
H21D	2224	6636	2925	77
H22C	7538	2161	5673	46
H23C	8658	3808	5785	61
H23D	7981	4734	5993	61
H24C	8483	2214	6295	106
H24D	7953	3317	6514	106
H25E	9410	3158	6803	99
H25F	9791	3451	6388	99
H26A	9116	5752	6438	93
H26C	9337	5601	6393	93
H27G	8041	5685	6705	153
H27H	8732	6565	6958	153
H27I	8517	5137	7101	153
H27J	8526	5571	7094	153
H27K	9075	4272	7180	153
H27L	8233	4259	6874	153
H28G	10288	4814	7128	149
H28H	10257	6312	6976	149
H28I	10725	5200	6732	149
H29D	6351	3975	6006	63
H29E	6731	2659	6222	63
H29F	6072	2557	5826	63

Table A1.11.8. Atomic occupancy for **105**.

Atom	Occupancy	Atom	Occupancy	Atom	Occupancy
H25C	0.5	H25D	0.5	H25A	0.5
H25B	0.5	C26B	0.5	H26B	0.5
C26K	0.5	H26K	0.5	H27D	0.5
H27E	0.5	H27F	0.5	H27A	0.5
H27B	0.5	H27C	0.5	C28B	0.5
H28A	0.5	H28B	0.5	H28C	0.5
C28K	0.5	H28D	0.5	H28E	0.5
H28F	0.5	H26A	0.25	H26C	0.75
C27C	0.75	H27G	0.75	H27H	0.75
H27I	0.75	C27K	0.25	H27J	0.25
H27K	0.25	H27L	0.25		

A1.12. Crystal structure data for Lanosterol acetate, 112.

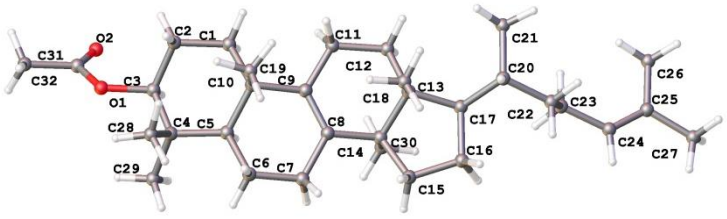

Figure A1.12. One Structure from the unit cell of **112**, determined by X-ray diffraction of a single crystal.

Table A1.12.1. Crystal data and structure refinement for **112.**

Empirical formula	$C_{32}H_{52}O_2$
Formula weight	468.73
Temperature (K)	120
Crystal system	orthorhombic
Space group	$P2_12_12_1$
a (Å)	7.4344(3)
b (Å)	10.6700(4)
c (Å)	35.6268(12)
α (°)	90
β (°)	90
γ (°)	90
Volume (Å^3)	2826.10(18)
Z	4
ρ_{calc}g (cm^3)	1.102
μ (mm^{-1})	0.498
F(000)	1040
Crystal size (mm^3)	0.28 × 0.13 × 0.04
Radiation	CuKα (λ = 1.54178)
2Θ range for data collection (°)	9.662 to 139.954
Index ranges	$-7 \le h \le 8$, $-13 \le k \le 13$, $-43 \le l \le 43$
Reflections collected	32533
Independent reflections	5203 [R_{int} = 0.0571, R_{sigma} = 0.0361]
Data/ restraints/ parameters	5203/0/317
Goodness-of-fit on F^2	1.059
Final R indexes [I> = 2σ (I)]	R_1 = 0.0446, wR_2 = 0.0973
Final R indexes [all data]	R_1 = 0.0550, wR_2 = 0.1045
Largest diff. peak/ hole (e Å^{-3})	0.32/-0.18

Table A1.12.2. Fractional atomic coordinates (×10^4) and equivalent isotropic displacement parameters (Å^2×10^3) for **112**. U_{eq} is defined as 1/3 of the trace of the orthogonalised U_{IJ} tensor.

Atom	*x*	*y*	*z*	U(eq)
O1	7801(3)	7480.1(19)	4430.4(5)	29.6(5)
O2	5621(3)	6058(2)	4536.5(6)	51.1(6)
C1	5564(3)	8048(3)	3494.6(7)	23.3(6)
C2	5911(4)	8180(3)	3916.8(7)	26.1(6)
C3	7496(4)	7371(3)	4026.2(7)	24.7(6)
C4	9264(4)	7708(3)	3827.5(7)	23.0(6)
C5	8864(3)	7696(2)	3396.8(7)	18.7(6)
C6	10522(4)	8033(3)	3161.6(7)	24.0(6)
C7	10236(3)	7772(3)	2748.6(8)	26.2(6)
C8	8344(3)	7885(2)	2612.4(7)	17.9(5)

C9	6932(3)	8123(2)	2839.2(7)	17.8(5)
C10	7203(3)	8441(2)	3256.9(7)	19.7(6)
C11	5036(3)	8198(3)	2689.7(7)	21.1(6)
C12	4741(3)	8027(3)	2263.9(7)	22.5(6)
C13	6429(3)	8347(2)	2037.3(7)	19.1(6)
C14	8019(3)	7574(2)	2203.8(7)	19.6(6)
C15	9529(4)	7861(3)	1923.4(7)	24.5(6)
C16	8553(4)	7866(3)	1538.6(8)	26.8(6)
C17	6496(4)	7941(3)	1618.3(7)	23.1(6)
C18	10046(4)	8952(3)	3969.1(8)	29.3(6)
C19	10631(4)	6662(3)	3917.7(8)	31.5(7)
C20	7388(4)	9882(2)	3274.2(8)	26.0(6)
C21	6775(4)	9762(2)	2069.6(8)	23.8(6)
C22	7673(4)	6145(2)	2195.5(8)	27.6(6)
C23	5491(4)	8713(3)	1319.0(7)	26.3(6)
C24	3461(4)	8786(3)	1392.7(8)	35.2(7)
C25	5840(4)	8183(3)	921.6(8)	34.3(7)
C26	5276(6)	6831(4)	854.1(8)	49.2(9)
C27	5662(6)	6410(4)	456.4(10)	57.4(11)
C28	4497(6)	6091(4)	193.5(10)	59.9(11)
C29	2513(7)	5951(4)	251.4(12)	70.9(13)
C30	5126(7)	5792(4)	-197.9(10)	75.4(14)
C31	6736(4)	6776(3)	4652.8(8)	36.0(7)
C32	7125(5)	7013(4)	5059.5(8)	46.5(9)

Table A1.12.3. Anisotropic displacement parameters ($Å^2 \times 10^3$) for **112**. The anisotropic displacement factor exponent takes the form: $-2\pi^2[h^2a^{*2}U_{11}+2hka^*b^*U_{12}+\ldots]$.

Atom	U_{11}	U_{22}	U_{33}	U_{23}	U_{13}	U_{12}
O1	26.4(10)	43.4(12)	19.1(9)	4.7(9)	1.6(8)	-2.4(9)
O2	53.3(15)	63.9(16)	36.1(12)	7.7(12)	11.1(12)	-21.8(14)
C1	17.2(13)	33.6(15)	19.0(13)	-0.6(12)	2.9(10)	0.3(12)
C2	19.5(14)	39.3(17)	19.5(13)	-1.3(13)	4.1(10)	-0.8(12)
C3	24.6(14)	31.8(15)	17.6(13)	0.9(12)	1.0(11)	-3.4(12)
C4	17.1(13)	28.6(15)	23.4(14)	2.2(12)	-0.4(10)	-0.1(11)
C5	15.4(13)	21.3(13)	19.4(13)	0.4(11)	0.3(9)	-0.7(10)
C6	15.8(13)	32.9(15)	23.4(13)	4.3(12)	0.4(10)	-1.5(12)
C7	15.7(14)	37.1(16)	25.7(14)	3.0(12)	4.2(10)	0.4(12)
C8	16.6(13)	15.0(12)	22.0(13)	1.4(10)	0.8(10)	1(1)
C9	16.3(13)	16.1(12)	21.1(13)	0.1(11)	0.5(10)	-0.5(10)
C10	15.9(13)	21.9(13)	21.2(13)	-0.5(11)	1.3(10)	0.5(10)
C11	15.5(13)	25.0(13)	22.8(13)	1.6(12)	2.2(10)	1.6(11)
C12	15.8(13)	31.6(15)	20.2(13)	-1.4(12)	1.5(10)	-0.8(11)
C13	16.1(13)	20.7(14)	20.4(13)	-2.2(11)	0.2(10)	-0.7(10)
C14	16.6(13)	19.9(13)	22.3(13)	-1.6(11)	5.4(10)	2(1)
C15	18.9(14)	29.6(15)	24.9(14)	0.5(12)	7.0(11)	1.4(12)
C16	24.6(14)	31.9(16)	23.8(14)	-0.7(12)	6.5(12)	-0.3(12)
C17	22.6(14)	26.4(15)	20.4(13)	-1.0(12)	4.5(11)	-3.8(12)
C18	25.8(15)	40.1(16)	22.0(14)	1.9(13)	-4.1(11)	-7.5(13)
C19	24.4(15)	44.2(18)	26.0(14)	10.0(13)	1.4(12)	8.0(14)
C20	30.8(16)	22.6(14)	24.5(14)	-2.7(12)	-4.2(12)	3.0(12)
C21	25.2(15)	23.5(14)	22.8(14)	0.6(11)	0.4(11)	2.2(11)
C22	33.7(16)	22.6(14)	26.5(14)	-1.5(12)	4.5(12)	2.0(12)
C23	26.5(15)	30.1(15)	22.4(13)	4.0(12)	-0.1(12)	-1.4(12)
C24	26.9(16)	52(2)	26.4(15)	5.9(15)	-2.6(13)	3.1(14)
C25	33.8(17)	47.2(19)	21.8(14)	5.0(14)	1.3(12)	-4.0(15)
C26	64(2)	57(2)	26.9(16)	-8.6(16)	0.7(15)	-17(2)
C27	67(3)	72(3)	32.9(18)	-15.9(19)	0.9(18)	-4(2)
C28	78(3)	64(3)	38(2)	-6.9(19)	-12(2)	5(2)

C29	91(4)	64(3)	58(3)	1(2)	-24(2)	-6(3)
C30	115(4)	76(3)	36(2)	-17(2)	-22(2)	18(3)
C31	34.3(17)	45.8(19)	27.9(16)	6.6(14)	8.4(13)	2.7(16)
C32	44(2)	71(3)	23.9(16)	9.7(17)	7.5(14)	1.2(18)

Table A1.12.4. Bond lengths for **112**.

Atom	Atom	Length (Å)	Atom	Atom	Length (Å)
O1	C3	1.462(3)	C11	C12	1.544(3)
O1	C31	1.349(4)	C12	C13	1.530(3)
O2	C31	1.203(4)	C13	C14	1.559(4)
C1	C2	1.533(4)	C13	C17	1.555(3)
C1	C10	1.542(3)	C13	C21	1.536(4)
C2	C3	1.512(4)	C14	C15	1.533(3)
C3	C4	1.535(4)	C14	C22	1.547(4)
C4	C5	1.563(3)	C15	C16	1.551(4)
C4	C18	1.534(4)	C16	C17	1.557(4)
C4	C19	1.544(4)	C17	C23	1.541(4)
C5	C6	1.533(3)	C23	C24	1.533(4)
C5	C10	1.551(3)	C23	C25	1.546(4)
C6	C7	1.513(4)	C25	C26	1.521(5)
C7	C8	1.493(4)	C26	C27	1.514(4)
C8	C9	1.348(3)	C27	C28	1.321(5)
C8	C14	1.512(3)	C28	C29	1.497(6)
C9	C10	1.539(3)	C28	C30	1.505(5)
C9	C11	1.509(3)	C31	C32	1.499(4)
C10	C20	1.546(4)			

Table A1.12.5. Bond angles for **112**.

Atom	Atom	Atom	Angle (°)	Atom	Atom	Atom	Angle (°)
C31	O1	C3	116.3(2)	C13	C12	C11	112.1(2)
C2	C1	C10	112.4(2)	C12	C13	C14	107.6(2)
C3	C2	C1	109.4(2)	C12	C13	C17	118.1(2)
O1	C3	C2	109.2(2)	C12	C13	C21	108.5(2)
O1	C3	C4	107.6(2)	C17	C13	C14	101.2(2)
C2	C3	C4	114.5(2)	C21	C13	C14	111.4(2)
C3	C4	C5	106.8(2)	C21	C13	C17	109.9(2)
C3	C4	C19	107.4(2)	C8	C14	C13	111.8(2)
C18	C4	C3	112.1(2)	C8	C14	C15	117.8(2)
C18	C4	C5	113.7(2)	C8	C14	C22	105.2(2)
C18	C4	C19	107.9(2)	C15	C14	C13	101.6(2)
C19	C4	C5	108.9(2)	C15	C14	C22	107.8(2)
C6	C5	C4	112.5(2)	C22	C14	C13	112.8(2)
C6	C5	C10	110.2(2)	C14	C15	C16	103.5(2)
C10	C5	C4	117.6(2)	C15	C16	C17	107.4(2)
C7	C6	C5	112.1(2)	C13	C17	C16	102.8(2)
C8	C7	C6	115.7(2)	C23	C17	C13	120.0(2)
C7	C8	C14	116.4(2)	C23	C17	C16	112.2(2)
C9	C8	C7	123.6(2)	C17	C23	C25	110.9(2)
C9	C8	C14	119.6(2)	C24	C23	C17	112.7(2)
C8	C9	C10	121.3(2)	C24	C23	C25	109.9(2)
C8	C9	C11	121.7(2)	C26	C25	C23	116.4(2)
C11	C9	C10	116.8(2)	C27	C26	C25	112.1(3)
C1	C10	C5	108.3(2)	C28	C27	C26	128.0(4)
C1	C10	C20	108.6(2)	C27	C28	C29	125.1(4)
C9	C10	C1	111.6(2)	C27	C28	C30	120.5(4)
C9	C10	C5	107.6(2)	C29	C28	C30	114.4(4)
C9	C10	C20	105.6(2)	O1	C31	C32	111.1(3)
C20	C10	C5	115.2(2)	O2	C31	O1	123.9(3)

C9	C11	C12	118.3(2)	O2	C31	C32	125.0(3)

Table A1.12.6. Torsion angles for **112**.

A	B	C	D	Angle (°)	A	B	C	D	Angle (°)
O1	C3	C4	C5	-175.3(2)	C11	C9	C10	C5	151.6(2)
O1	C3	C4	C18	-50.2(3)	C11	C9	C10	C20	-84.8(3)
O1	C3	C4	C19	68.0(3)	C11	C12	C13	C14	52.8(3)
C1	C2	C3	O1	-178.9(2)	C11	C12	C13	C17	166.4(2)
C1	C2	C3	C4	60.4(3)	C11	C12	C13	C21	-67.8(3)
C2	C1	C10	C5	53.5(3)	C12	C13	C14	C8	-60.2(3)
C2	C1	C10	C9	171.7(2)	C12	C13	C14	C15	173.3(2)
C2	C1	C10	C20	-72.3(3)	C12	C13	C14	C22	58.1(3)
C2	C3	C4	C5	-53.7(3)	C12	C13	C17	C16	-155.9(2)
C2	C3	C4	C18	71.4(3)	C12	C13	C17	C23	78.8(3)
C2	C3	C4	C19	-170.3(2)	C13	C14	C15	C16	-39.0(3)
C3	O1	C31	O2	2.3(4)	C13	C17	C23	C24	-59.7(3)
C3	O1	C31	C32	-177.5(3)	C13	C17	C23	C25	176.6(2)
C3	C4	C5	C6	179.4(2)	C14	C8	C9	C10	179.9(2)
C3	C4	C5	C10	49.9(3)	C14	C8	C9	C11	-5.4(4)
C4	C5	C6	C7	168.6(2)	C14	C13	C17	C16	-38.8(3)
C4	C5	C10	C1	-50.8(3)	C14	C13	C17	C23	-164.1(2)
C4	C5	C10	C9	-171.5(2)	C14	C15	C16	C17	14.8(3)
C4	C5	C10	C20	71.0(3)	C15	C16	C17	C13	15.2(3)
C5	C6	C7	C8	29.9(3)	C15	C16	C17	C23	145.5(2)
C6	C5	C10	C1	178.6(2)	C16	C17	C23	C24	179.6(3)
C6	C5	C10	C9	57.9(3)	C16	C17	C23	C25	55.9(3)
C6	C5	C10	C20	-59.6(3)	C17	C13	C14	C8	175.4(2)
C6	C7	C8	C9	-4.2(4)	C17	C13	C14	C15	48.8(2)
C6	C7	C8	C14	-177.5(2)	C17	C13	C14	C22	-66.4(3)
C7	C8	C9	C10	6.8(4)	C17	C23	C25	C26	59.7(4)
C7	C8	C9	C11	-178.5(2)	C18	C4	C5	C6	55.3(3)
C7	C8	C14	C13	-149.4(2)	C18	C4	C5	C10	-74.2(3)
C7	C8	C14	C15	-32.3(3)	C19	C4	C5	C6	-65.0(3)
C7	C8	C14	C22	87.8(3)	C19	C4	C5	C10	165.5(2)
C8	C9	C10	C1	-152.1(2)	C21	C13	C14	C8	58.6(3)
C8	C9	C10	C5	-33.5(3)	C21	C13	C14	C15	-67.9(3)
C8	C9	C10	C20	90.1(3)	C21	C13	C14	C22	176.9(2)
C8	C9	C11	C12	-1.5(4)	C21	C13	C17	C16	79.0(3)
C8	C14	C15	C16	-161.5(2)	C21	C13	C17	C23	-46.4(3)
C9	C8	C14	C13	37.0(3)	C22	C14	C15	C16	79.9(3)
C9	C8	C14	C15	154.2(2)	C23	C25	C26	C27	179.5(3)
C9	C8	C14	C22	-85.7(3)	C24	C23	C25	C26	-65.6(4)
C9	C11	C12	C13	-24.0(3)	C25	C26	C27	C28	-114.7(5)
C10	C1	C2	C3	-59.3(3)	C26	C27	C28	C29	-6.9(8)
C10	C5	C6	C7	-58.1(3)	C26	C27	C28	C30	175.2(4)
C10	C9	C11	C12	173.4(2)	C31	O1	C3	C2	80.9(3)
C11	C9	C10	C1	33.0(3)	C31	O1	C3	C4	-154.3(2)

Table A1.12.7. Hydrogen atom coordinates (Å×10^4) and isotropic displacement parameters (Å^2×10^3) for **112**.

Atom	*x*	*y*	*z*	U(eq)
H1A	4519	8573	3424	28
H1B	5258	7165	3438	28
H2A	6166	9067	3979	31
H2B	4831	7917	4059	31
H3	7198	6479	3967	30
H5	8600	6801	3335	22
H6A	10803	8933	3196	29

H6B	11566	7543	3252	29
H7A	10995	8358	2603	31
H7B	10665	6912	2695	31
H11A	4540	9025	2761	25
H11B	4312	7554	2821	25
H12A	4393	7148	2213	27
H12B	3740	8574	2181	27
H15A	10472	7206	1931	29
H15B	10084	8686	1976	29
H16A	8838	7092	1397	32
H16B	8943	8596	1388	32
H17	6017	7067	1605	28
H18A	11115	9166	3821	44
H18B	10380	8867	4234	44
H18C	9144	9615	3942	44
H19A	10213	5869	3810	47
H19B	10746	6574	4190	47
H19C	11804	6880	3810	47
H20A	8524	10135	3157	39
H20B	7378	10156	3537	39
H20C	6381	10271	3140	39
H21A	7032	9976	2332	36
H21B	5709	10222	1985	36
H21C	7807	9991	1913	36
H22A	6599	5951	2344	41
H22B	8713	5705	2301	41
H22C	7486	5873	1936	41
H23	5977	9586	1326	32
H24A	2997	7945	1446	53
H24B	2855	9126	1171	53
H24C	3235	9333	1608	53
H25A	5201	8719	738	41
H25B	7143	8254	868	41
H26A	5926	6279	1032	59
H26B	3972	6745	905	59
H27	6895	6371	387	69
H29A	1869	6373	47	106
H29B	2173	6328	492	106
H29C	2197	5059	253	106
H30A	4569	6375	-376	113
H30B	4781	4931	-262	113
H30C	6438	5874	-211	113
H32A	7902	6346	5157	70
H32B	5995	7025	5201	70
H32C	7734	7823	5087	70